# IGD

Intercontinental Geoinformation Days

# Proceedings Book of the 1st Intercontinental Geoinformation Days

25-26 November 2020 / Mersin, TURKEY

*Mersin University - Engineering Faculty - Department of Geomatics Engineering*

http://igd.mersin.edu.tr/2020/

ISBN: 978-605-7839-55-8

# The proceedings of the

# 1st Intercontinental Geoinformation Days

**Editor-in-Chief**

Prof. Dr. Murat YAKAR

**Editors**

Prof. Dr. İsmail ŞANLIOĞLU

Assoc. Prof. Dr. Erdinç AVAROĞLU

Asst. Prof. Dr. Muzaffer Can İBAN

Asst. Prof. Dr. Ali ULVİ

Asst. Prof. Dr. Osman ORHAN

Asst. Prof. Dr. Lütfiye KUŞAK

Asst. Prof. Dr. Fatma BÜNYAN ÜNEL

Res. Asst. Aydın ALPTEKİN

Res. Asst. Abdurahman Yasin YİĞİT

Res. Asst. Mehmet Özgür ÇELİK

Eng. Engin KANUN

ISBN: 978-605-7839-55-8

Mersin, 2020

## HONOR BOARD

**Ali İhsan SU** - Governor of Mersin Province
**Vahap SEÇER** - Mayor of Mersin Metropolitan Municipality
**Prof. Dr. Ahmet ÇAMSARI** - Rector of Mersin University
**Prof. Dr. Orhan AYDIN** - Rector of Tarsus University
**Mehmet Zeki ADLI** – Director of Turkish Land Registry and Cadastre
**Prof. Dr. Rudolf STAIGER** - FIG President
**Prof. Dr. Christian HEIPKE** - ISPRS President
**Prof. Dr. Chryssy POTSIOU** - FIG President (2015-2018)
**Prof. Dr. Haluk ÖZENER –** Boğaziçi University Director of Kandilli Observatory
**Dr. Orhan ERCAN** - FIG Vice President

## EXECUTIVE COMMITTEE

**Prof. Dr. Abdurrahman EYMEN** - Erciyes University
**Prof. Dr. Alexander SAGAYDAK** – State University of Land Use Planning, Russia
**Prof. Dr. Alias Abdul RAHMAN** - Universiti Teknologi Malaysia (UTM), Malaysia
**Prof. Dr. Aydın ÜSTÜN** - Kocaeli University
**Prof. Dr. Bülent BAYRAM** – Yıldız Technical University
**Prof. Dr. Çetin CÖMERT** - Karadeniz Technical University
**Prof. Dr. Dursun Zafer ŞEKER** - Istanbul Technical University
**Prof. Dr. Erkan BEŞDOK** - Erciyes University
**Prof. Dr. Ferruh YILDIZ** - Konya Technical University
**Prof. Dr. Fevzi KARSLI** - Karadeniz Technical University
**Prof. Dr. Füsun BALIK ŞANLI** – Yıldız Technical University
**Prof. Dr. Hacı Murat YILMAZ** - Aksaray University
**Prof. Dr. Hediye ERDOĞAN** - Aksaray University
**Prof. Dr. Haluk ÖZENER** - Boğaziçi University
**Prof. Dr. Hande DEMİREL** – Istanbul Technical University
**Prof. Dr. Mevlüt YETKİN** - İzmir Katip Çelebi University
**Prof. Dr. Mustafa YANALAK** – Istanbul Technical University
**Prof. Dr. Nebiye MUSAOĞLU** – Istanbul Technical University
**Prof. Dr. Niyazi ARSLAN** - Çukurova University
**Prof. Dr. Reha Metin ALKAN** - Istanbul Technical University
**Prof. Dr. Sebahattin BEKTAŞ** - Ondokuz Mayıs University
**Prof. Dr. Tahsin YOMRALIOĞLU** - Beykent University
**Prof. Dr. Tayfun ÇAY** - Konya Technical University
**Prof. Dr. Tamer BAYBURA** - Afyon Kocatepe University
**Prof. Dr. Tarık TÜRK** - Cumhuriyet University
**Prof. Dr. Taşkın KAVZOĞLU** - Gebze Technical University
**Prof. Dr. Uğur DOĞAN** - Yıldız Technical University
**Prof. Dr. Yasemin ŞİŞMAN** – Ondokuz Mayıs University
**Assoc. Prof. Dr. Anargha DHORDE** - Nowrosjee Wadia College, India
**Assoc. Prof. Dr. Aziz ŞİŞMAN** - Ondokuz Mayıs University
**Assoc. Prof. Dr. Bihter EROL** – Istanbul Technical University
**Assoc. Prof. Dr. Cevdet Coşkun AYDIN** - Hacettepe University
**Assoc. Prof. Dr. Erol YAVUZ** - Uşak University
**Assoc. Prof. Dr. Fatih DÖNER** - Gümüşhane University
**Assoc. Prof. Dr. Fatih POYRAZ** - Cumhuriyet University
**Assoc. Prof. Dr. Halil AKINCI** - Artvin Çoruh University
**Assoc. Prof. Dr. Murat UYSAL** - Afyon Kocatepe University
**Assoc. Prof. Dr. Özgün AKÇAY** - Çanakkale Onsekiz Mart University
**Assoc. Prof. Dr. Serdar EROL** – Istanbul Technical University
**Assoc. Prof. Dr. Şükran YALPIR** – Konya Technical University
**Assoc. Prof. Dr. Uğur AVDAN** - Eskişehir Technical University
**Assoc. Prof. Dr. Zaide DURAN** – Istanbul Technical University
**Asst. Prof. Dr. Berk ANBAROĞLU** - Hacettepe University
**Asst. Prof. Dr. Kemal ÇELİK** - Gümüşhane University
**Asst. Prof. Dr. Mahmut Oğuz SELBESOĞLU** – Istanbul Technical University
**Asst. Prof. Dr. Mustafa Utkan DURDAĞ** - Artvin Çoruh University
**Asst. Prof. Dr. Mustafa ÜSTÜNER** - Artvin Çoruh University
**Asst. Prof. Dr. Nizar POLAT** - Harran University
**Asst. Prof. Dr. Osman Sami KIRTILOĞLU** - İzmir Katip Çelebi University
**Asst. Prof. Dr. Süleyman Sefa BİLGİLİOĞLU** - Aksaray University
**Asst. Prof. Dr. Serdar BİLGİ** - Istanbul Technical University
**Asst. Prof. Dr. Tae-Suk BAE**- Sejong University, Republic of Korea
**Dr. Abdul-Lateef BALOGUN** - Universiti Teknologi PETRONAS (UTP), Malaysia
**Dr. Olalekan Adekunle ISIOYE** - Ahmadu Bello University, Nigeria
**Dr. Eng. Colonel Altan YILMAZ** - Turkish Gen. Directorate of Mapping
**Res. Asst. Dr. Erman ŞENTÜRK** - Kocaeli University

**International Association of Turkish Literature Culture Education (TEKE Derneği)**
**Prof. Dr. Cengiz ALYILMAZ –Bursa Uludağ University**
**Assoc. Prof. Dr. Onur ER – Düzce University**
**Assoc. Prof. Dr. Faruk POLATCAN – Sinop University**
**Assoc. Prof. Dr. Beyhan KOCADAĞİSTAN – Atatürk University**
**Dr. İsmail ÇOBAN – Artvin Çoruh University**

ORGANIZING COMMITTEE
**Mersin University - Faculty of Engineering - Department of Geomatics Engineering**
**Prof. Dr. Murat YAKAR** - Conference Chairman - Head of Department
**Asst. Prof. Dr. Muzaffer Can İBAN** - Conference Secretary
**Prof. Dr. İsmail ŞANLIOĞLU**
**Assoc. Prof. Dr. Erdinç AVAROĞLU**
**Asst. Prof. Dr. Ali ULVİ**
**Asst. Prof. Dr. Fatma BÜNYAN ÜNEL**
**Asst. Prof. Dr. Lütfiye KUŞAK**
**Asst. Prof. Dr. Osman ORHAN**
**Dr. Hakan DOĞAN –** Turkish State Meteorological Service
**Lect. Atilla KARABACAK**
**Lect. Şafak FİDAN**
**Res. Asst. Abdurahman Yasin YİĞİT**
**Res. Asst. Aydın ALPTEKİN**
**Res. Asst. Mehmet Özgür ÇELİK**
**Res. Asst. Semih KAHVECİ**
**Eng. Binnaz SARI**
**Eng. Engin KANUN**
**Eng. Ganime Melike OĞUZ**
**Eng. İldeniz Leyla ÖZTÜRK**
**Eng. Seda Nur Gamze HAMAL**
**Eng. Veli YILDIZ**
**Eng. Şafak BOZDUMAN**
**Urb. Plan. Bilal ÖZAY**
**Urb. Plan. Ezgi ŞAHİN**

Ladies, gentlemen and distinguished guests,

My name is Murat YAKAR and I am the chair of Intercontinental Geoinformation Days. It is my honour this morning to welcome you all.

It is a great pleasure for me to declare open the first Intercontinental Geoinformation Days and to welcome the participants from all over the world who participated here to exchange experience and work together for two days on field of geoinformation and their applications.

I first wish to extend to you the greetings of the Governor of Mersin Province, Metropolitan Mayor of Mersin and the rector of Mersin University. I wish to thank them for their support.

This 2-days-long conference offers online technical sessions and workshops. The technical programme consists of 67 presentations within the fields of surveying, remote sensing, photogrammetry, land administration, cartography, GIS and geodesy, including best practice and new research.

As the novel coronavirus outbreak shutters businesses and disrupts everyday life for billions around the globe, massive annual conferences and small society meetings alike have moved online. This new format poses numerous technical and organizational challenges, but it also offers opportunities—for reaching wider audiences, reducing the carbon footprint of meeting travel, and improving diversity and equity.

As a way to support our research community and to advance its scholarship during the COVID-19 pandemic, we decided to waive all registration fees for the virtual conference, cover the administrative and setup cost of hosting the conference virtually as well as the publishing and copy-editing costs of the conference proceedings.

The Intercontinental Geoinformation Days has gotten an enthusiastic response from colleagues from all around the World. And we are pleased with the positive response that this event has gotten dozens of contributions from experts in the field. The number of submitted papers is more than the level we had expected. So, I would like to thank you for your valuable contributions and kind support.

Our team is now considering to make this event traditionalized and the second IGD event is planned to be organized in May 2021. The organization committee will publish the details of the next event in the following months.

Before closing, I have to extend further thanks to academic staff of Mersin University Department of Geomatics Engineering who greatly helped in organising the conference. I sincerely hope that this conference will achieve its objectives and make great progress through wide ranging discussions.

Let me now close by wishing you a delightful and stimulating event.

**Prof. Dr. Murat YAKAR**

| | 25 November 2020 - Wednesday |
|---|---|
| 09:30-10:00 | Opening |
| 10:00-11:00 | Photogrammetry and Remote Sensing - 1 |
| | **Documentation of centennial structures in Istanbul via Terrestrial Laser Scanning technology**<br>*H. Onur Yılmaz*, Maryna Batur, Haluk Özener*<br>**A Comparative Analysis of Speeded Up Robust Features (SURF) and Harris Algorithms in Point Cloud Generation**<br>*Ramazan Alper Kuçak*, İrem Yakar, Serdar Bilgi, Serdar Erol, Adalet Dervişoğlu*<br>**Effects of Orthophoto Band Combinations on Semantic Segmentation**<br>Esra Altınoluk*, Özgün Akçay, Ahmet Cumhur Kınacı, Emin Özgür Avşar, Ahmet Batuhan Polat, Umut Aydar<br>**A Review on the Usability of Mobile Phone-based Close-Range Photogrammetry, Terrestrial Laser Scanning and UAVs in Traffic Accident Modeling**<br>*İrem Yakar*, Engin Kanun, Ganime Melike Oğuz, Şafak Bozduman, Serdar Bilgi, Kamil Karataş*<br>**Assessment of shoreline change and its relation with Mangrove vegetation: A case study over North Konkan region of Raigad, Maharashtra, India**<br>*Barnali Das*, Anargha Dhorde*<br>**Bathymetry Analysis with Use of Sentinel-2 Images**<br>*Hakan Uzakara*, Nusret Demir* |
| 11:00-11:15 | Break |
| 11:15-12:15 | Surveying and Geodesy - 1 |
| | **On The Third Dimension In Robustness Analysis**<br>*Mevlüt Yetkin*, Muhammed Ali Aytemür, Ömer Bilginer*<br>**Using Interquartile Range to Detect TEC Perturbations Associated with A Tropical Cyclone Crossing through The South China Sea**<br>*Mohamed Freeshah*, Xiaohong Zhang, Xiaodong Ren*<br>**Ionospheric TEC Prediction Performance of ARIMA and LSTM Methods in Different Space Weather Conditions**<br>*Erman Şentürk*<br>**Exploring the Usability and Suitability of Smartphone Apps for Precise and Rapid Mapping Applications**<br>*Lukman Abdulmumin*, Olalekan Adekunle Isioye, Swafiyudeen Bawa, Ahmed Muhammed*<br>**Deep Learning-Based Ionospheric TEC Prediction Approach**<br>*İsmail Demiryege*, Mustafa Ulukavak*<br>**Necmettin Erbakan University Continuously Operating Reference Station**<br>*Omer Faruk Atiz*, Salih Alcay, Sermet Ogutcu, Ibrahim Kalayci* |
| 12:15-13:15 | Lunch Break |
| 13:15-14:30 | Geographic Information Systems and Cartography - 1 |
| | **Minimum spanning tree detection on raster data**<br>*Murat Çalışkan, Berk Anbaroğlu**<br>**Realization to Web Based with Turf.JS Library of Spatial Analysis in Open Source Softwares**<br>*Halil Ibrahim Onyil*, Mehmet Yilmaz*<br>**Groundwater Quality Dependence on the Spatial Proximity of Geo-located Dumpsites in Samaru-Nigeria**<br>*Terwase Tosin Youngu*, Yahaya Abbas Aliyu, Adamu Bala, Samuel Azua, Aliyu Zailani Abubakar, Samuel Enyinna Akpa*<br>**Creating a Land Cover Change Simulation Model with SLEUTH, The Case of Istanbul Province**<br>*Ahmet Emir Yakup*, Ismail Ercument Ayazli*<br>**Evaluation of the change of Istanbul Anatolian Side land surface temperature values with CORINE data**<br>*Lütfiye Kuşak*, Ufuk Fatih Küçükali*<br>**Financial Analyses of ODHCs in Turkey in terms of Profitability**<br>*Elif Akyel*, Özşen Çorumluoğlu*<br>**Landfill Site Selection Literature Review: for Bodrum District**<br>*Cansu Nehteparov*, Emin Özgür Avşar* |
| 14:30-14:45 | Break |
| 14:45-16:15 | Land Administration, Cadastre and Land Use - 1 |
| | **Agricultural Land Consolidation (Russian Case Study)**<br>*Alexander Sagaydak*, Anna Sagaydak*<br>**Identification and analysis of parcel-based plan amendment types: the case of Istanbul**<br>*Ahmet Yılmaz*, Nur Saral, Leyla Güneş, Şeval Yanar, Pelin Ballı*<br>**Land readjustment method: Professional merit in determining implementation boundary**<br>*Halil Burak Akdeniz*, Şaban İnam*<br>**GeoValueIndex Definition for Valuation of Public Property Assets**<br>*Fatma Bunyan Unel*, Lutfiye Kusak, Murat Yakar*<br>**Agricultural land use and GHG emission in India and Turkey: a comparative trend analysis**<br>*Mohd Kamil Vakil*<br>**A House Valuation with Multiple Regression Analysis and Artificial Neural Networks**<br>*Mehmet Emin Tabar*, Aslan Cihat Basara, Yasemin Sisman*<br>**Four Dimensional Cadastre Design**<br>*Tayfun Çay, Hasan Çevik**<br>**Professional merit and ethics in choosing the development plan implementation method**<br>*Şaban İnam*, Halil Burak Akdeniz* |
| 16:15-16:30 | Break |
| 16:30-17:30 | Photogrammetry and Remote Sensing - 2 |
| | **An investigation of supervised LCLU classification performance over UAV based orthophoto**<br>*Nizar Polat, Yunus Kaya**<br>**Data Fusion of Unmanned Aerial Vehicle (UAV)-Based Photogrammetry and Close-Range Photogrammetry in Historical Sites Monitoring**<br>*İrem Yakar*, Seda Nur Gamze Hamal, İldeniz Leyla Öztürk, Mehmet Özgür Çelik, Serdar Bilgi*<br>**Ecological Appraisal of Urban Heat Island in Zaria, Nigeria**<br>*Ebenezer Akomolafe*, Olalekan Isioye, Wilson Labija*<br>**Road Surface Extraction from MLS-Based Point Clouds**<br>*Mustafa Zeybek*, Serkan Biçici*<br>**Spatial Accuracy Analysis of Sentinel-1 SAR Satellite Images by Comparing Maps**<br>*Tevfik Fikret Horzum*, Nusret Demir, Ali Kılçık*<br>**Comparison of NDT and ICP Method's Point Cloud Registration Performance**<br>*Ramazan Alper Kuçak*, Mahmut Oğuz Selbesoğlu, Serdar Erol* |

| 26 November 2020 - Thursday | |
|---|---|
| **09:30-10:00** | **Smart Cities** |
| | **Industry 4.0, Smart Cities and Urban Transformation**<br>*Yüksel Boz*, Tayfun Çay*<br>**Understanding Mobility as a Service: A Literature Review**<br>*Ömer Akın*, Hande Demirel*<br>**Smart Mobility Recommendations in Multimodal Transport for Local Authorities**<br>*Hatice Gül Önder*, Mustafa Ulukavak* |
| **10:00-11:00** | **Photogrammetry and Remote Sensing - 3** |
| | **Training data development strategy for applying deep learning in remote sensing applications**<br>*Vaibhav Katiyar*, Masahiko Nagai*<br>**Spatiotemporal analysis of land-use changes in a metropolitan city in Malaysia using geospatial techniques**<br>*Abdulwaheed Tella*, Abdul-lateef Balogun, Asmau Balogun*<br>**Remote Sensing Image Fusion Using Transform Domain Based on Optimization Algorithms**<br>*Asan Ihsan Abas*, Nurdan Akhan Baykan*<br>**Land Use and Shoreline Dynamics in Lagos State, Nigeria**<br>*Swafiyudeen Bawa*, Adamu Bala, Abubakar Sadiq Sani*<br>**Indoor navigation application using augmented reality technology**<br>*Salih Hamdi Çalık*, Fatih Gülgen*<br>**An investigation of Triangular Greenness Index performance in vegetation detection**<br>*Nizar Polat* |
| **11:00-11:15** | **Break** |
| **11:15-12:15** | **Surveying and Geodesy - 2** |
| | **GPS-IR for accurate tide gauge measurement at South Beach, Oregon, United States**<br>*Kutubuddin Ansari*, Tae-Suk Bae*<br>**Comparison of Static PPP Performance of CSRS-PPP Float and Trimble RTX-PP Services**<br>*Bilal Mutlu*, Serdar Erol, Reha Metin Alkan*<br>**Long Short Term Memory (LSTM) Network Models for Ionospheric Anomalies Detection: A Case Study for Mw=7.7 Awaran, Pakistan Earthquake**<br>*Mohd Saqib*, Sanjeev Anand Sahu, Erman Şentürk*<br>**Precipitable Water Vapour Retrieval and Analysis over Nigeria from Ground and Spaced-based GNSS Observations**<br>*Olalekan Isioye*, Mefe Moses, Usman Ibrahim Sai, Ebenezer Ayobami Akomolafe*<br>**Detecting Outliers With The Least Trimmed Squares**<br>*Hasan Dilmaç*, Yasemin Şişman*<br>**Analysis of the contribution of the multi-GNSS to long-distance RTK**<br>*Ceren Konukseven*, Omer Faruk Atiz, Salih Alcay, Sermet Ogutcu* |
| **12:15-13:15** | **Lunch Break** |
| **13:15-14:45** | **Geographic Information Systems and Cartography - 2** |
| | **Using a 3D city model for monitoring flash flood risks in Salalah (Oman)**<br>*Khalid Al Kalbani*, Alias Abdul Rahman*<br>**Cloud Based Disaster Management and Monitoring Information System**<br>*Mohd Mustaqeem*, Sani Hasan, Mohd Saqib, Abdullah Talib*<br>**The Application of GIS in the Selection of Suitable Areas for Afforestation of Konya**<br>*Ceren Yağcı*, Fatih İşcan*<br>**Identifying equality and accessibility to health centers via Spatial Information Science**<br>*Ömer Akın*, Hande Demirel*<br>**Investigation of Pedestrian Accessibility to Schools: A case study of Rize**<br>*Sabire Edanur Mamat*, Aziz Şişman*<br>**Creation Of Wind Speed Maps Of Kirklareli City**<br>*Celal Bıçakcı*, Kamil Karataş, Selim Serhan Yıldız*<br>**Developing an Algorithm on the Reporting Of Outages in the Electricity Distribution System with GIS Integration**<br>*Ahmet Ünverdi*, Aziz Şişman*<br>**GIS-Based Landslide Susceptibility Mapping Using Frequency Ratio and AHP Methods**<br>Aslan Cihat Başara*, Mehmet Emin Tabar , Yasemin Şişman |
| **14:45-15:00** | **Break** |
| **15:00-16:00** | **Surveying and Geodesy - 3** |
| | **Tropopause Height Variabilities Derived from COSMIC GNSS Radio Occultation Observations over Nigeria**<br>*Olalekan Isioye*, Mefe Moses, Usman Ibrahim Sai, Ebenezer Ayobami Akomolafe*<br>**A Study on Comparison of Observed and Derived Gravity Data**<br>*Serkan Doğanalp*<br>**The Accuracy Assessment of Terrestrial and Mobile Lidar Systems for 3D Modeling**<br>*Ramazan Alper Kuçak*, Serdar Erol, Mehmet İşiler*<br>**Identifying the best fitting 3D deformation model using information criteria**<br>*Alaz Andaç Ortaköy*, Cüneyt Aydın*<br>**An experimental study on the effect of antenna orientation on GNSS-IR**<br>Cemali Altuntaş*, Nursu Tunalıoğlu |
| **16:00-16:15** | **Break** |
| **16:15-17:15** | **Photogrammetry and Remote Sensing - 4** |
| | **UAVs and Photogrammetry**<br>*Imole Favour Okediji*<br>**UAV Based 3D Modeling of Ancient Quarry Nearby the Göbeklitepe**<br>*Nizar Polat, Mustafa Ulukavak, Abdulkadir Memduhoğlu, Halil İbrahim Şenol*, Yunus Kaya*<br>***UAV Based Crop Monitoring***<br>*Mustafa Özkan*, Nizar Polat*<br>***Using of Hybrid Data Acquisition Techniques for Cultural Heritage a Case Study of Pompeiopolis***<br>*Seda Nur Gamze Hamal*, Binnaz Sarı, Ali Ulvi*<br>**Modeling of Adamkayalar Reliefs with Current Techniques**<br>*İldeniz Leyla Öztürk*, Mehmet Özgür Çelik, Erkan Baygül*<br>**Documentation of complex structure using unmanned aerial vehicle (UAV) photogrammetry method and terrestrial laser scanner (TLS)**<br>Binnaz Sarı*, Seda Nur Gamze Hamal, Ali Ulvi |

**CONTENTS** **Page**

## Photogrammetry and Remote Sensing – 1

**Documentation of centennial structures in Istanbul via Terrestrial Laser Scanning technology**

*H. Onur Yılmaz*, Maryna Batur, Haluk Özener*

**A Comparative Analysis of Speeded Up Robust Features (SURF) and Harris Algorithms in Point Cloud Generation**

*Ramazan Alper Kuçak*, İrem Yakar, Serdar Bilgi, Serdar Erol, Adalet Dervişoğlu*

**Effects of Orthophoto Band Combinations on Semantic Segmentation**

Esra Altınoluk*, Özgün Akçay, Ahmet Cumhur Kınacı, Emin Özgür Avşar, Ahmet Batuhan Polat, Umut Aydar

**A Review on the Usability of Mobile Phone-based Close-Range Photogrammetry, Terrestrial Laser Scanning and UAVs in Traffic Accident Modeling**

*İrem Yakar*, Engin Kanun, Ganime Melike Oğuz, Şafak Bozduman, Serdar Bilgi, Kamil Karataş*

**Assessment of shoreline change and its relation with Mangrove vegetation: A case study over North Konkan region of Raigad, Maharashtra, India**

*Barnali Das*, Anargha Dhorde*

**Bathymetry Analysis with Use of Sentinel-2 Images**

*Hakan Uzakara*, Nusret Demir*

Intercontinental Geoinformation Days

http://igd.mersin.edu.tr/2020/

# Documentation of centennial structures in Istanbul via Terrestrial Laser Scanning technology

**Onur Yılmaz*[1], Maryna Batur[1], Haluk Özener[1]**

[1]*Boğaziçi University, Kandilli Observatory and Earthquake Research Institute, Department of Geodesy, Istanbul, Turkey*

**Keywords**
Point Cloud
Terrestrial Laser Scanning
Cultural Heritage
3D Documentation
Architectural Drawings

**ABSTRACT**

Historical buildings are the most important structures of cultural heritages, as they carry a long history and reflects the culture of the nation. In Turkey, some historical structures are more than 1500 years old and they were significantly damaged through natural disasters, wars, weather changes, human negligence, and effects of decay. It is an essential issue that concerns the protection of these cultural heritages for our descendants. This paper examines the importance of cultural heritage documentation via Terrestrial Laser Scanning (TLS) technology, which allows acquiring data accurately and in a short period of time. Based on a 3-dimensional (3D) data in form of point cloud, it is possible to construct 3D model of the structure, create an accurate digital archive and orthophotos, which can be used in further restoration works. This paper provides two case studies from Istanbul (Turkey). As the result of this study, 3D point cloud models, orthophotos, and façade drawings of the structures were produced.

## 1. INTRODUCTION

3D documentation of historical structures has been well recognized over recent years and it became more and more pragmatic to preserve them digitally. TLS provides a geospatial database which a third party can use for restoration, risk assessment, maintenance and addressing the need for the sustainability of existing building.

Laser scanning method has been successfully used in many applications concerning the documentation studies until today. In (Safkan et al. 2014), the side of Istanbul Technical University Foreign Languages Academy was scanned with a TLS in order to create an architectural documentation. Whiting this framework, architectural drawings were created in CAD software based on the point cloud data. 3D modelling of cultural heritage using LiDAR is shown in (Alionescu et al. 2018) on the example of Timisoara city in Romania. The comparison of TLS technology is made, and classic photogrammetric method is applied in the study (Kıvanç 2019). The author stated the advantages and disadvantages of both methods compared to each other. In (Vasilakos et al. 2018), the aim of the study was to compare the hand-held DSLR camera with the ground laser scanning tool, and to assess the post-earthquake building damage and structural deformations. As the study area, the affected town of Vrisa was selected after the earthquake of Mw 6.3 in Greece. In the study (Uray et al. 2015), 3D digital data of Diyarbakir Castle and its walls were created using TLS. It was observed that TLS technology has become an increasingly preferred measurement technique for the 3D documentation, and it offers more information and rich content compared to classical surveying techniques. In the framework of (Lepere and Lemmens 2019), 4 different iconic structures in Paris, Syria, Pagoda and Alaska were documented using TLS. (Ulvi et al. 2020) used point cloud data to create a 3D model of the Red Church located within the borders of Aksaray province by digital photogrammetry technique.

In this study, 3D documentation of two case studies was carried out using TLS technology. The first case study is almost 150 years old building of 1st Men's Dormitory of Boğaziçi University, and the second case study is a part of Istanbul Walls which are 1500 years old. As a consequence, a 3D point cloud model was created by processing the data. Furthermore, the CAD drawings of façade were created based on orthophotos.

## 2. STUDY AREA

This paper provides two case studies from Istanbul, Turkey: the first case study is the 1st Men's Dormitory of

* **Corresponding Author**

*(onur.yilmaz@boun.edu.tr) ORCID ID 0000 – 0002 – 0436 – 5109
(maryna.batur@boun.edu.tr) ORCID ID 0000 – 0001 – 9284 – 8858
(ozener@boun.edu.tr) ORCID ID 0000 – 0003 – 2531 – 3030

**Cite this study**

Yılmaz O, Batur M & Ozener H (2020). Documentation of centennial structures in Istanbul via Terrestrial Laser Scanning technology. Intercontinental Geoinformation Days (IGD), 1-4, Mersin, Turkey

Boğaziçi University and the second case study is the Land Walls, which can be seen in Fig. 1.

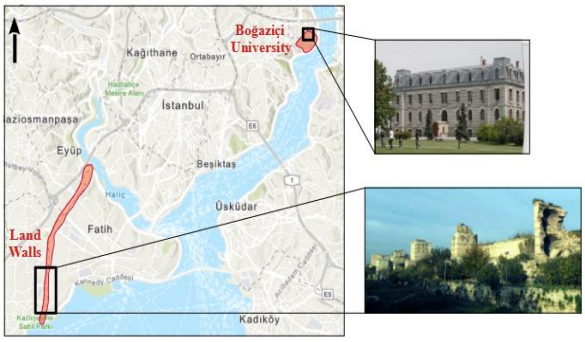


**Figure 1.** Location of Land Walls and Boğaziçi University on the Istanbul map

### 2.1. Case Study Area 1

The 1st Men's Dormitory is the oldest building of Boğaziçi University (located at South Campus) that has served as a men's dorm since 1871. It is also known as Hamlin Hall, named after Dr. C. Hamlin, who was the first President of Robert College.

### 2.2. Case Study Area 2

Being a part of Roman, Byzantine, Latin, and Ottoman Empires, the Land Walls of Istanbul have a significant historical value at the present time. This structure was built in 413 A.D. for the defensive purposes and it is located on the Historical Peninsula of Istanbul. The length of Land Walls is approximately 7.5 km. Today, this structure is a part of Historic Areas of Istanbul and has been added into the UNESCO World Heritage List.

## 3. MATERIALS AND METHODS

### 3.1. Terrestrial Laser Scanner Used in Application

The main focus of the study is to perform the 3D documentation of two historical structures using TLS technology. For this, TLS FARO Focus 330 HDR was chosen, which technical specifications are shown in Table 1. A number of studies were carried out using FARO instrument and they proved that this TLS is one of the most profitable for scanning the historical structures (Uray et al. 2015; Redweik et al. 2020; Hepyörük 2015; Temizer et al. 2013).

**Table 1.** Performance specifications of FARO Focus 330 HDR

| | |
|---|---|
| Type | Phase-based |
| Scanning range | 0.6 – 300 m indoor and outdoor scanning |
| Speed of measurement | 122,000/244,000/488,000/ 976,000 |
| Field of view | Vertical $300^0$ Horizontal $360^0$ |
| Range error | ± 2mm |
| Ambient temperature | 5 – $40^0$ C |
| Laser class | Laser class 1 |
| Wavelength of laser | 1550 nm |
| Beam divergence | Typical 0.19 mrad ($0.011^0$) |

### 3.2. Methodology

The methodology of the current study was organized according to the flowchart shown in Fig. 2.

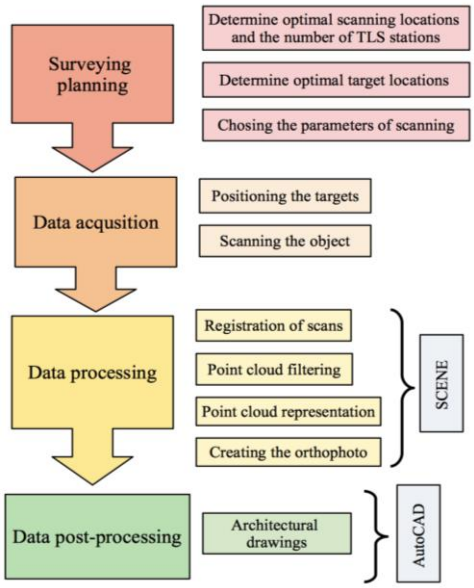


**Figure 2.** Workflow of TLS application in 3D documentation

#### 3.2.1. 1st Men's Dormitory of Boğaziçi University

The 1st Men's Dormitory of Boğaziçi University is located at the South Campus, which is usually very crowded. However, due to pandemic of COVID-19 there were not any obstructions, such as parking cars or crowds of passing people, that may prevent from clean sight of view. Two walls of the structure were fully accessible for scanning: the north-west and the north-east walls. The wall lying on the south-east were visually obstructed by tress and the south-west wall was only accessible through a narrow passage. 18 scans were used in order to capture the structure in detail and scanning was performed from approximately 10 m from the structure. One station was located on the roof of a nearby building. Fig. 3 shows the configuration of scanning in relation of building.

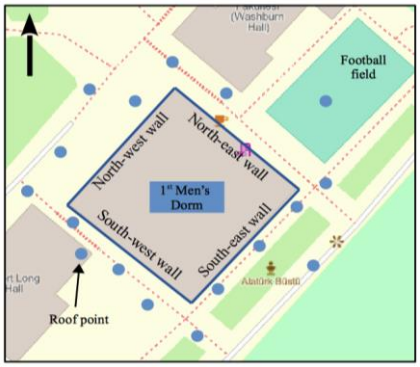


**Figure 3.** Sketch showing the study building and TLS' positions

The scanning resolution was chosen as 1/4 meaning that the total number of scan points is 43.7 MPns with

point distance of 6.1 mm on 10 m, and quality was chosen as 1x, which means that every point was fired 1 time by a laser beam. These settings are required for 3D documentation (Redweik et al. 2020). It took approximately 10 minutes to scan the structure from one each station, that makes 3 hours in total.

Due to the size of the building (the perimeter is almost 140 meters), it was decided not to use any targets and all scans were registered together using cloud-to-cloud registration method resulting in mean point error of 4.7 mm. After the registration process, redundant data outside the building were removed and 3D model of point cloud was created.

### 3.2.2. Istanbul Land Walls

In this study, a part of Land Walls (approximately 200 m) was scanned for the documentation purposes. In the first step, area to be surveyed was analyzed. In front of walls there was a gardening zone and it was decided to perform scanning from sidewalk that is approximately 40 m away from the structure. Land Walls were scanned from 8 positions using spherical targets. The scanning parameters were chosen the same as for the previous study: resolution 1/4 and quality 1x. Fig. 4 shows the study area and the scanning geometry.

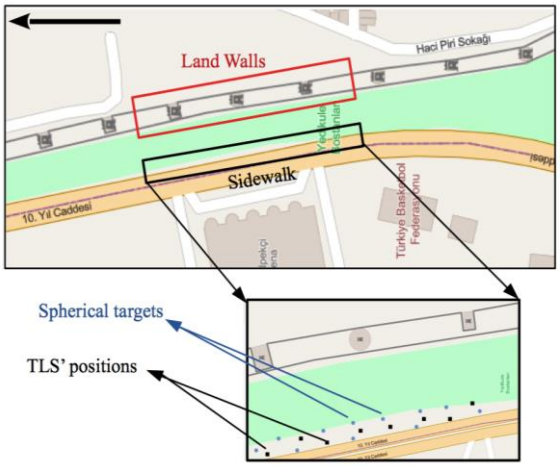


**Figure 4.** Sketch showing the study area, TLS' and targets' positions

In order to register scans together the target-based method was implemented. The mean distance error and the mean horizontal error were 0.8 mm, and the mean vertical error was equal to 0.1 mm. After the registration, data was cleaned from unnecessary points and then 3D point cloud model was made. These processes were done in the SCENE software, which is a manufacturer software delivered with the scanner.

## 4. RESULTS AND DISCUSSIONS

### 4.1. 1st Men's Dormitory of Boğaziçi University

As the results of this study, a 3D point cloud model with more than 400,000,000 points was obtained which is shown in Fig. 5.

**Figure 5.** 3D point cloud model of the 1st Men's Dormitory buildings

Orthophoto images of building façade served as a base for architectural drawings, which were done in AutoCAD software and can be seen in Fig. 6.

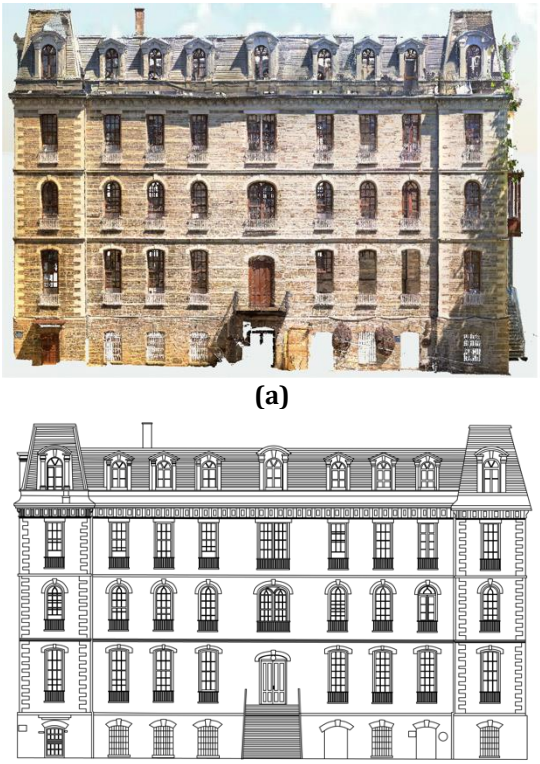

**(a)**

**(b)**

**Figure 6.** The deliverables of the TLS surveying: **(a)** an orthophoto of façade of the 1st Men's Dormitory building; **(b)** an architectural drawing of the 1st Men's Dormitory building drawn over the orthophoto

### 4.2. Istanbul Land Walls

In total, more than 500,000,000 points were involved in the 3D point cloud model, which is shown in Fig. 7.

Orthophoto images obtained from the point cloud data allow for mm accuracy and preserve all details of the façade. In the current study, orthophotos were created in SCENE software and then transferred in AutoCAD environment, where, in its turn, they were scaled at 1:1 scale. Fig. 8a and 8b shows the orthophoto and the CAD drawings respectively for the tower of Istanbul Land Walls.

**Figure 7.** 3D point cloud of the part of Istanbul Land Walls

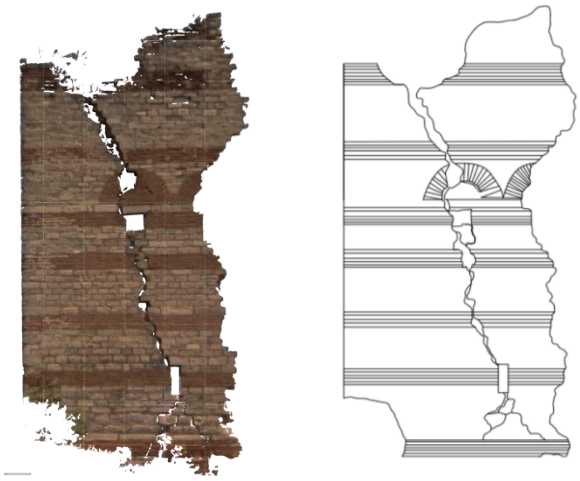

**(a)** **(b)**

**Figure 8.** The deliverables of the TLS surveying: **(a)** an orthophoto of Land Walls' Tower; **(b)** an architectural drawing of Land Walls' Tower drawn over the orthophoto

## 5. CONCLUSION

In this paper, we performed a 3D documentation of two heritages that has a historical meaning for Istanbul. For this purpose, TLS was used, and this instrument showed itself as a good tool that allows for the dense point cloud acquisition and can provide an accurate realistic orthophoto image of the scanned object.

We have devised a clear methodology for the entire work and suggest that careful attention must be paid while planning work. To be more precise, surveyed area must be carefully studied in order to avoid mistakes during the data acquisition. We believe that our method could be used as guideline in the field of 3D documentation concerning historical structures.

## ACKNOWLEDGEMENT

This study is supported by Scientific Research Projects of Boğaziçi University no. 20TP4.

## REFERENCES

Alionescu A, Herban S, Vilceanu C B (2018). 3D modelling of cultural heritage objective in Timisoara using precise LiDAR. International Conference of Numerical Analysis and Applied Mathematics (ICNAAM 2018) AIP Conf. Proc. 2116, 370002-1-37002-5; https://doi.org/10.1063/1.5114375

Hepyörük G (2015) Tarihi ve kültürel varlıkların belgelendirilmesi ve üç boyutlu modelinin oluşturulmasında yersel lazer tarayıcıların kullanım olanaklarının araştırılması ve Karacabey Türbesi (Ankara) örneği. Doktora Tezi, Selçuk Üniversitesi, Konya.

Kıvanç H (2019) Kültürel miras belgeleme çalışmalarında fotogrametrik yöntem ile yersel lazer tarama yönteminin karşılaştırılması. Yüksek Lisans Tezi, Konya Teknik Üniversitesi, Konya.

Lepere G & Lemmens M (2019). Laser scanning of damaged historical icons. GIM International – The Worldwide Magazine for Geomatics, Vol: 33 Issue: 6, 19-21.

Redweik P, Blasco J J de Sanjose, Sanchez-Fernandez M, Atkinson A D, Martinez Corrales L F (2020). Tower of Belem (Lisbon) – Status Quo 3D documentation and material origin Determination. Sensors, 20(8), 2355.

Safkan S, Hamarat H, Duran Z, Aydar U, Çelik M F (2014). Yersel Lazer Tarama yönteminin mimari belgelemede kullanılması. V. Uzaktan Algılama ve Coğrafi Bilgi Sistemleri Sempozyumu (UZAL-CBS 2014), 14-17 Ekim 2014, İstanbul, Turkey.

Temizer T, Nemli G, Ekizce E, Ekizce A, Demir S, Bayram B, Yilmaz H F (2013). 3D documentation of a historical monument using terrestrial laser scanning case study: Byzantine Water Cistern, Istanbul. The International Archives of the Photogrammetry, Remote Sensing and Spatial Information Sciences, 5, W2.

Ulvi A, Yakar M Y, Kaya Y (2020). İha ve yersel fotogrametrik teknikler kullanarak Aksaray Kızıl Kilisenin 3B modelinin ve nokta bulutunun elde edilmesi. Geomatik Dergisi, Cilt 5, Sayı 1, 22-30.

Uray F, Metin A, Varlik A (2015). 3D architectural surveying of Diyarbakir Wall's Ulu Beden Tower with terrestrial laser scanner. Procedia Earth and Planetary Science, Vol. 15, 73-78.

Vasilakos C, Chatzistamatis S, Roussou O, Soulakellis N (2018). Terrestrial photogrammetry vs laser scanning for rapid earthquake damage assessment. The International Archives of the Photogrammetry, Remote Sensing and Spatial Information Sciences, Volume XLII-3/W4, GeoInformation for Disaster Management (Gi4DM), 18-21 March 2018, Istanbul, Turkey.

Intercontinental Geoinformation Days

http://igd.mersin.edu.tr/2020/

# A Comparative Analysis of Speeded Up Robust Features (SURF) and Harris Algorithms in Point Cloud Generation

**Ramazan Alper Kucak[1], İrem Yakar*[1], Serdar Bilgi[1], Serdar Erol[1], Adalet Dervisoglu[1]**

[1]*İstanbul Technical University, Faculty of Civil Engineering, Department of Geomatics Engineering, Istanbul, Turkey*

**Keywords**
Structure from Motion
Photogrammetry
SURF Algorithm
BRISK Algorithm
Harris Algorithm

**ABSTRACT**

The precise documentation and preservation of cultural heritage elements are of fundamental importance since they represent a social, historical and cultural improvement of societies throughout history. There have been different documentation techniques from past to present such as classical architectural drawing methods, classical surveying methods, terrestrial photogrammetry and aerial photogrammetry, etc. Photogrammetry emerges as a popular method with the developing technology. On the other hand, different evaluation techniques have been evolved to evaluate the collected photogrammetric data especially with the improvements in computer vision technologies. In this aspect, Structure from Motion (SfM) became a widely used approach for producing a 3D view from photogrammetric images. This paper presents the comparison of point clouds produced by Speeded Up Robust Features (SURF) and Harris Algorithms. The point cloud production was carried out in MATLAB environment. 20 images at total captured by Nikon Coolpix A10 digital camera were used for the point cloud generation. Therefore, the resulted points clouds were investigated comparatively.

## 1. INTRODUCTION

Cultural heritage according to UNESCO can be described as the product and the process that provides societies with rich resources that are transmitted from the past, created in the present, and endowed for the benefit of future generations. It consists of three parts: tangible, natural, and intangible heritage. Tangible cultural heritage refers to monuments such as sculptures, paintings, structures of an archeological nature, historical buildings, archeological sites, etc.

The management of these tangible cultural heritage elements is crucial due to cultural and social elements that they contain besides their historical importance. In this context, modeling the historical monuments in a detailed way is a key point in terms of protecting these features and ensuring intergenerational transmission. Many different techniques have been used throughout history ranging from classical surveying methods to photogrammetry etc. for acquiring and evaluating data. In this context; photogrammetric techniques have become highly preferred for documenting the tangible cultural heritage compared with the classical methods.

Photogrammetry is a method that relies on the determination of the 3-dimensional (3D) geometry of objects by measuring and analyzing the 2-dimensional (2D) images. Usually, it is divided into two categories as close-range photogrammetry and aerial photogrammetry. In close-range photogrammetry, images are acquired from the locations near or on the surface of the earth. The close-range photogrammetric data provide detailed dimensional information of objects. In contrast, aerial photogrammetric data are collected via overhead shots from an aircraft and provides land use details (Jiang et al. 2008).

On the other hand, there are various approaches and innovations for the evaluation of photogrammetric data. Especially with the developing computer vision technology, different approaches have been developed for the production of 3D models from 2D photogrammetric images. These approaches usually are based on key point detection and descriptor algorithms. The most used of these algorithms can be sorted as SURF (Bay et al. 2008), Harris (Harris, C. G., & Stephens, M.,1988), Shift (Lowe 2004), BRISK ( Leutenegger et al. in 2011), AGAST (Mair et al., 2010), etc.

* **Corresponding Author**

(kucak15@itu.edu.tr) ORCID ID 0000 - 0002 - 1128 - 1552
* (yakari@itu.edu.tr) ORCID ID 0000 – 0002 – 7823 – 9674
(bilgi@itu.edu.tr) ORCID ID 0000 – 0002 – 8396 – 3202
(erol@itu.edu.tr) ORCID ID 0000 – 0002 – 7100 - 8267
(adervisoglu@itu.edu.tr) ORCID ID 0000 – 0001 – 7455 – 4282

**Cite this study**

Kucak A., Yakar İ., Bilgi S., Erol S & Dervisoglu A. (2020). A Comparative Analysis of Speeded Up Robust Features (SURF) and Harris Algorithms in Point Cloud Generation. Intercontinental Geoinformation Days (IGD), 5-8, Mersin, Turkey

It is possible to say the following determinations in the literature research about the algorithms. SURF algorithm is fast in the image matching process, but it is not enough in the feature point extraction (Cheng et al. 2017). However, the Harris Algorithm is an efficient corner detection algorithm, but it cannot enough the issue of scale (Cheng et al. 2017). Binary Robust Invariant Scalable Keypoints (BRISK) is presented by Leutenegger et al. in 2011. The corners are detected by the use of the AGAST algorithm. Filtering is realized with the FAST Corner score while determining the maxima in the scale-space pyramid. The BRISK algorithm is constructed as a binary string to provide illumination invariance. BRISK features are scale and rotation invariant while it has limited affine invariance (Tareen and Saleem 2018).

In addition, Structure from Motion (SfM) is one of the widely used methods for 3D modeling in computer vision software packages (Aicardi et al. 2018). Despite that SfM generally uses computer sciences, it relies on photogrammetry (Kuçak et al. 2017; Jebara et al. 1999). In this study; using SURF and Harris Algorithms in MATLAB environment, point clouds were produced with the SfM technique. The results were examined comparatively.

## 2. METHOD

### 2.1 Structure from Motion (SfM)

In the traditional photogrammetric approach; the 3D location and pose of the camera(s) or 3D coordinates of various control points are necessary to determine scene triangulation and to reconstruct the related object. Nevertheless, the Structure from Motion (SfM) method determines the camera pose and scene geometry simultaneously by the use of bundle adjustment which relies on matching features in adjacent overlapping images (Westoby et al. 2012). The initial estimation of camera positions and object coordinates can be done by tracking common features on adjacent images. Then, these positions and coordinates are refined iteratively by the use of non-linear least-squares minimization (Snavely 2008). The SfM approach basically stands for the images taken from a moving sensor. Thus, the method is most proper where the image pairs have a high degree of overlap. In such cases, the scene would be viewed from a wide range of positions that provide a fully three-dimensional structure (Westoby et al. 2012).

SfM Method is based on the epipolar geometry since it relies basically on the photogrammetric approach.

The intersection of epipolar line as well as COP1, COP2, and P points are illustrated in "Fig.1". Suppose that $P_1(u_1, v_1, 1)$ and $P_2$ $(u_2, v_2, 1)$ are the projection of an individual point in two different images. The point $P_2$ which is the projection of point $P_1$ in a single image is limited with the corresponding epipolar plane.

The fundamentals of epipolar geometry are as follows:

$$P_1^T F P_2 = 0 \qquad \textbf{(1)}$$

Equation 1 represents a least-squares minimization where; F is the fundamental matrix with 9 parameters that are restrained to have rank 2 ($\|F\| = 0$). Also, the matrix specifies an epipolar line from an image for a point in an image. These perspective projections constitute the basics of SfM algorithms (Kuçak et al. 2017; Jebara et al. 1999).

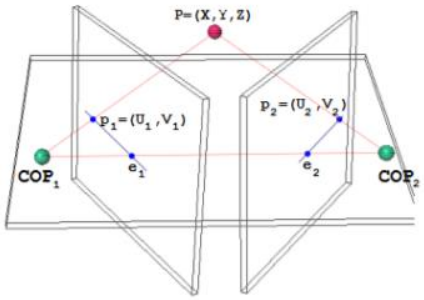


**Figure 1.** Epipolar Geometry (Jebara et al. 1999)

### 2.2 Speeded Up Robust Features (SURF)

The Speeded Up Robust Features (SURF) algorithm was presented by Bay et al. 2008. The method is basically based on Gaussian scale-space analysis. SURF relies on the determinant of the Hessian Matrix. The detector improves the feature-detection speed by utilizing integral images. Each feature in a specific neighborhood is described with a distribution of Haar wavelet in the 64 bin descriptor of SURF. The SURF features are rotation and scale-invariant. The descriptor of 128 bin values can be used to deal with the large changes in viewpoints. Hessian Matrix was given in Equation 2:

$$H(x,\sigma) = \left[L_{xx}(x,\sigma)\ L_{xy}(x,\sigma)\ L_{xy}(x,\sigma)\ L_{yy}(x,\sigma)\right] \quad (2)$$

Where; "Lxx(x,σ): the convolution of Gaussian second-order derivative with the image "I" in point "x", as well as "Lxy(x, σ)" and "Lyy (x, σ)" (Tareen and Saleem 2018).

### 2.3. Harris Algorithm

Harris and Stephens have presented the Harris detector in 1988. It basically specifies the corner points in an image. The gradient of an image is estimated for each pixel. Then, the correlation matrix is obtained. The robustness of the detection is improved by smoothing the elements in the matrix with Gaussian function. Equation 3 is used for calculating the response of each pixel. The pixel is considered a corner, only when both eigenvalues $\lambda_1$ and $\lambda_2$ are large (Kok and Rajendran 2018).

$$H = \lambda_1 \lambda_2 - k * (\lambda_1 + \lambda_2)^2 \quad (3)$$

## 3. RESULTS

Image registration can be defined as matching, aligning and overlaying multiple integral images captured from different locations. It is widely used in various vision-based applications. The registration phase can be divided into the following stages: feature detection and description, feature matching, outlier

rejection, and image reconstruction. The selection of feature detector-descriptor plays an important role in registration since the timing and accuracy are affected by the computational capability and robustness of the selected detector-descriptor. Hence, it is crucial to choose the most proper detector-descriptor in feature-matching applications (Tareen and Saleem 2018).

In this study, SURF, Harris and BRISK Algorithms were performed on MATLAB environment and resulted in point clouds were examined comparatively.

SURF detects the points based on integral images and the Hessian matrix. The matrix approximates the Gaussian second-order derivative with box filters. The second phase of SURF is the orientation assignment. A circular region is constructed around the detected point, to determine orientation. Then, interest point descriptors are constructed by computing Haar wavelet responses and by extracting square windows around the points. On the other hand, the calculation of each pixel gradient is the basis of the Harris corner detector algorithm. The pixel is determined as a corner if the absolute gradient values in 2 directions are both great (Dawood et al. 2012).

The images used in the study were captured by using Nikon Coolpix A10 digital camera featured a 16.1 megapixel 1/2.3" CCD sensor. 20 images that belong to one facade of the monument were used during the study.

The selected monument for 3D reconstruction is the Fountain of Ahmed III (Figure 2). This fountain was built in 1729 by the Sultan Ahmet III, upon the proposal of the grand vizier Nevşehirli Damat İbrahim Pasha. It is located in front of the Bab-ı Hümayun gate of Topkapı Palace in the Fatih district of Istanbul.

**Figure 2.** The selected monument for 3D reconstruction

The camera calibration was performed in MATLAB environment by using 12 images at total of MATLAB camera calibration checkerboard captured with Nikon Coolpix A10 digital camera as shown in figure 3.

14.635 key points have been used while aligning the photos in the SURF detector. 1143 key points have been used in the same phase in the Harris detector (Figure 4 & 5). On the other hand, the BRISK Algorithm with the same properties was not successful in aligning the photos since it could not find any key points.

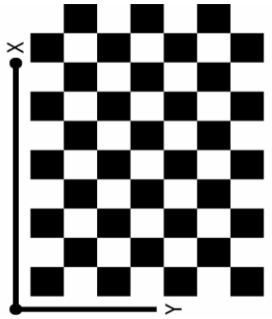


**Figure 3.** MATLAB camera calibration checkerboard

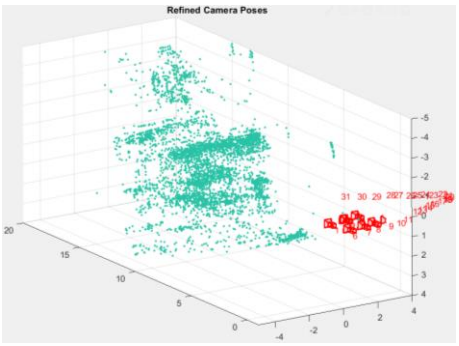


**Figure 4.** The refined camera poses in the SURF Algorithm


**Figure 5.** The refined camera poses in Harris Algorithm

In feature matching, ORB (Oriented FAST and Rotated BRIEF) (Rublee, E., et al., 2011) and BRIEF descriptors were used. The Hamming distance was used for the comparison of binary features. In this aspect, an operation in collaboration with a bit count on the result was performed to compute the binary data. The distance between the pairs of binary features could be computed effectively. On the other hand, performing a linear search for matching can be useful only for small datasets. The solution in such cases would be changing the linear search with an approximate matching algorithm (Muja and Lowe 2012).

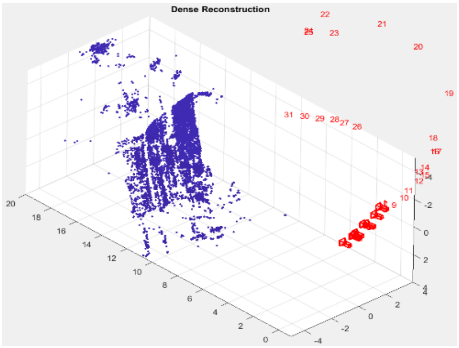


**Figure 6**. Dense reconstruction in SURF algorithm.

The resulted dense cloud in figure 6 in the SURF Algorithm belongs to one facade of the monument was exported ".ply" file format and imported to Cloud compare software, as shown in figure 7.

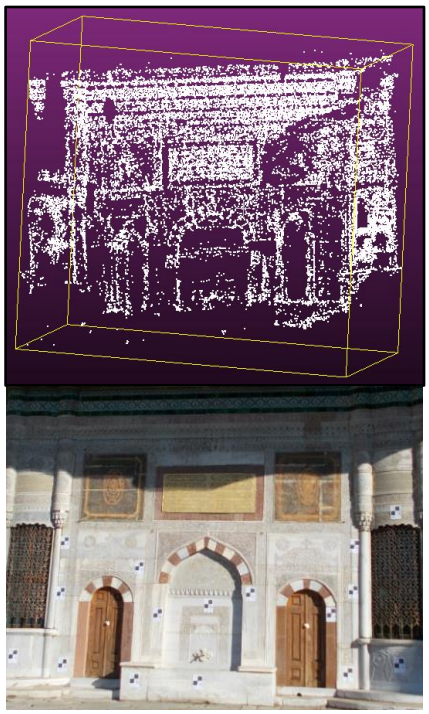

**Figure 7**. Resulted point cloud in Cloud Compare Software

## 4. DISCUSSION & CONCLUSION

In this study; using SURF and Harris in a MATLAB environment, point clouds were produced using the SfM Technique. The results were examined comparatively. It was found that that the number of incorrect points in Harris Algorithm was larger in comparison with the SURF Algorithm while the number of dense points was less. The integrity and representation of the point cloud obtained by the Harris Algorithm were also weak. The dense point cloud can be obtained by using different key point detection algorithms in the MATLAB environment. Also, more precise work could be obtained by changing the limit values in SURF and Harris Algorithms.

Different algorithms can be tried for point cloud studies in future studies and more precise 3D models can be produced. Besides, an SfM Algorithm with different detection and descriptor with the experiences gained here; It will be tested in the production of point clouds in C++ or Python environment in future research.

## REFERENCES


Aicardi I, Chiabrando F, Lingua, A M & Noardo F (2018). Recent trends in cultural heritage 3D survey: The photogrammetric computer vision approach. Journal of Cultural Heritage, 32, 257-266.

Bay, H., Ess, A., Tuytelaars, T., & Van Gool, L. (2008). Speeded-up robust features (SURF). Computer vision and image understanding, 110(3), 346-359.

Cheng C, Wang X & Li X (2017). UAV image matching based on surf feature and Harris Corner Algorithm. 4th International Conference on Smart and Sustainable City (ICSSC 2017).

Dawood M, Cappelle C, El Najjar M E, Khalil M & Pomorski D (2012, October). Harris, SIFT and SURF features comparison for vehicle localization based on virtual 3D model and camera. In 2012 3rd International Conference on Image Processing Theory, Tools and Applications (IPTA), pp. 307-312. IEEE.

Harris, C. G., & Stephens, M. (1988, August). A combined corner and edge detector. In *Alvey vision conference* (Vol. 15, No. 50, pp. 10-5244).

Jebara T, Azarbayejani A &Pentland A (1999). 3D structure from 2D motion. IEEE Signal Processing Magazine, 3D and Stereoscopic Visual Communication, Vol. 16., 66-84.

Jiang R, Jáuregui D V & White K R (2008). Close-range photogrammetry applications in bridge measure-ment: Literature review. Measurement, 41(8), 823-834.

Kok K Y& Rajendran P (2018). Validation of Harris Detector and Eigen Features Detector. In IOP Conference Series: Materials Science and Engineering, Vol. 370, No.1, IOP Publishing.

Leutenegger, S., Chli, M., & Siegwart, R. Y. (2011, November). BRISK: Binary robust invariant scalable keypoints. In 2011 International conference on computer vision (pp. 2548-2555). IEEE.

Lowe D G (2004). Distinctive image features from scale-invariant keypoints. International journal of computer vision, 60(2), 91-110.

Mair, E., Hager, G. D., Burschka, D., Suppa, M. and Hirzinger, G., 2010. Adaptive and generic corner detection based on the accelerated segment test. In: Computer Vision ECCV2010, Springer, pp. 183–196.

Muja M & Lowe D G (2012). Fast matching of binary features. In 2012 9th conference on computer and robot vision (pp. 404-410). IEEE.

Kuçak R A, Özdemir E & Erol S (2017). The segmentation of point clouds with K-means and ANN (Artifical Neural Network). The International Archives of Photogrammetry, Remote Sensing and Spatial Information Sciences, 42, 595.

Snavely, N., 2008. Scene reconstruction and visualization from Internet photo collections, unpublished PhD thesis, University of Washington, USA.

Tareen, S.A.K., & Saleem, Z. (2018, March). A comparative analysis of SIFT, SURF, kaze, akaze, ORB, and BRISK. In 2018 International conference on computing, mathematics and engineering technologies (iCoMET) (pp. 1-10). IEEE.

Westoby, M. J., Brasington, J., Glasser, N. F., Hambrey, M. J., & Reynolds, J. M. (2012). 'Structure-from-Motion' Photogrammetry: A low-cost, effective tool for geoscience applications. Geomorphology, Vol. 179, 300-314.

Intercontinental Geoinformation Days

http://igd.mersin.edu.tr/2020/

# Effects of Orthophoto Band Combinations on Semantic Segmentation

**Esra Altınoluk*[1], Özgün Akçay[2], Ahmet Cumhur Kınacı [3], Emin Özgür Avşar [2], Ahmet Batuhan Polat [2], Umut Aydar [2]**

[1]Çanakkale Onsekiz Mart University, Institute of Graduate Education, Geographic Information Technologies, Çanakkale, Turkey
[2]Çanakkale Onsekiz Mart University, Faculty of Engineering, Department of Geomatics Engineering, Çanakkale, Turkey
[3]Çanakkale Onsekiz Mart University, Faculty of Engineering, Department of Computer Engineering, Çanakkale, Turkey

**Keywords**
Deep learning
Remote sensing
Classification
CNN
DeepLabv3

**ABSTRACT**

Recently classify of the high resolution orthophotos using the convolutional neural network (CNN), which is the popular architecture of image classification applications with deep learning. In this study, trainings were carried out using the DeepLabv3 architecture based on the CNN network named ResNet. Potsdam dataset was selected as the study region, which is presented as an open data set by the International Society for Photogrammetry and Remote Sensing (ISPRS).A total of 2112 images were used, 352 of this images used for verification and another 352 images used for test data. It has been trained with five different spectral band combinations: RG (red-green), RB (red-blue), GB (green-blue), RGB (red-green-blue) and IRRG (infrared-red-green). After the trainings,the classification success was compared on the test data. RG, RB, GB, RGB, IRRG band combinations produced, %91, %85, %91, %92, %91 training accuracy rates, respectively. Results demonstrate that, using different band combinations on trainings give us different accuracy.

## 1. INTRODUCTION

Remote sensing systems are an important data source that enables us to access up-to-date information about the earth. However, in line with the technological developments in recent years, interest in the production of high-resolution aerial images and analysis of these images is increasing. In the literature, land use / land cover detection from high-resolution aerial images (Castelluccio et al. 2015; Zhang and Zhu 2011) is one of the most common research topics and is carried out by classification process.

Classification in remote sensing means labeling each object in the image to its class. The traditional pixel-based classification method uses the spectral properties of pixels. However, the heterogeneous pixels of high-resolution aerial images negatively affect the classification results. For this reason, instead of using individual pixels, objects called segments were formed by grouping neighboring pixels with similar spectral properties, and an object-based classification method, which is used in spatial information as well as spectral content, was developed (Blaschke 2010; Veljanovski et al. 2011). Although these methods achieved important results in classification applications, the increasing resolution of the images and the more detailed information content could not achieve the desired success. Algorithms such as random forest (Breiman 2001), support vector machines (Cortes and Vapnik 1995), artificial neural networks (Foody 1996) etc. have been developed in order to overcome these weaknesses and increase classification accuracy. However, in order to use the mentioned methods, feature extraction that requires a lot of time and expertise should be done (Arel et al. 2010). On the other hand, deep learning, which emerged with the development of artificial neural networks, learned from the data itself without the need for feature extraction and overcome these problems and achieved significant success.

Deep learning is a hierarchical learning method that analyzes input data from simple to complex with the help of numerous nonlinear layers (Altınoluk et al. 2019; Lecun et al. 2015). For example; in image analysis, the first layers define the edges, while the next layers can define concepts such as numbers, letters or human faces.

*Corresponding Author

*(esraltnoluk@gmail.com) ORCID ID 0000-0002-4688-2366
(akcay@comu.edu.tr) ORCID ID 0000-0003-0474-7518
(cumhur.kinaci@comu.edu.tr.) ORCID ID 0000-0002-8832-5453
(ozguravsar@comu.edu.tr) ORCID ID 0000-0002-3804-1209
(abpolat@comu.edu.tr) ORCID ID 0000-0002-7495-1998
(umutaydar@comu.edu.tr) ORCID ID 0000-0002-3987-6435

Cite this study

Altınoluk E, Akçay Ö, Kınacı A C, Avşar Ö, Polat A B & Aydar U (2020). Effects of Orthophoto Band Combinations on Semantic Segmentation. Intercontinental Geoinformation Days (IGD), 9-12, Mersin, Turkey

Convolutional Neural Network (CNN), which is the most popular architecture of deep learning, is generally used in studies such as object recognition and image classification (Krizhevsky et al. 2012). Examples of these network structures that have achieved significant success in classification studies are LeNet(LeCun et al. 1989; LeCun et al. 1998), Alexnet (Krizhevsky et al. 2012), VGGNet (Simonyanand Zisserman 2014), GoogleNet (Szegedy et al. 2015) and ResNet (He et al. 2016).Recently, a series of DeepLab have been proposed based on the theory of atrous convolution(Yu and Koltun et al. 2015). The proposed scheme using DeepLabv3+ semantic segmentation algorithm can fully utilize the spatial–spectral and context information of images as well as recognize the spatial geometric relationship between intraclass and interclass of the ground objects(Zhang et al. 2020).

In this study, it is aimed to train ResNet-based DeepLabv3 deep learning network architecture with five different spectral band combinations, namely RG, RB, GB, RGB and IRRG, using the high resolution ISPRS-Potsdam data set for land use and land cover classification. In this context, the performance of the DeepLabv3 neural network was examined and the classification accuracies were analyzed. In addition to RGB input data, which is widely used in deep learning, the contribution of IRRG data with infrared band is use for network training is among the research questions.

## 2. METHOD

ResNet based DeepLabv3 architecture was trained with RG, RB, GB, RGB and IRRG combinations of ISPRS-Potsdam dataset as a solution to the classification problem of high-resolution remote sensing data. Using the obtained models, segmentation maps were produced from the images and success rates were calculated.

### 2.1. Dataset

The Potsdam data set produced by ISPRS for the 2D Semantic Labeling Contest and presented as an open data set was used in the study. There are 6 categories in the data set: impervious surfaces (white), building (blue), low vegetation (cyan), tree (green), car (yellow) andclutter (red). The Potsdam dataset contains 38 high resolution true orthophotos; the size of each photo is 6000x6000 pixels. Fig. 1 shows an example of ISPRS-Potsdam images.

Dataset preprocessing was carried out with Matlab, training and testing of DeepLabv3 was performed using Tesla K80 and T4 GPU, which is available via Google Colaboratory, using Tensorflow version 1.15.2.


**Figure 1.** ISPRS-Potsdam orthophoto examples

In the training of the DeepLabv3neural network, RG, RB, GB and IRRG band combinations were used to investigate whether different band combinations contribute to the RGB data as well. Training data for each band combinations cover the same area.

Data slicing (Liu et al. 2018) was used in the preprocessing phase of the data. Since high resolution data will be difficult to transmit directly to the model due to GPU memory limit, 4 orthophotos selected for network training were sliced in 400x400 size and 30% overlap ratio.

Fig 2 shows sample data of 400x400 sizes RGB, IRRG, ground truth, RG, RB and GB used in training. DeepLabv3 neural network used in the study; it was trained with a total of 1760 images, including 1408 training (80%) and 352 verification data (20%) for five different spectral band combinations. The performance of the trained models was measured with 352 test data.

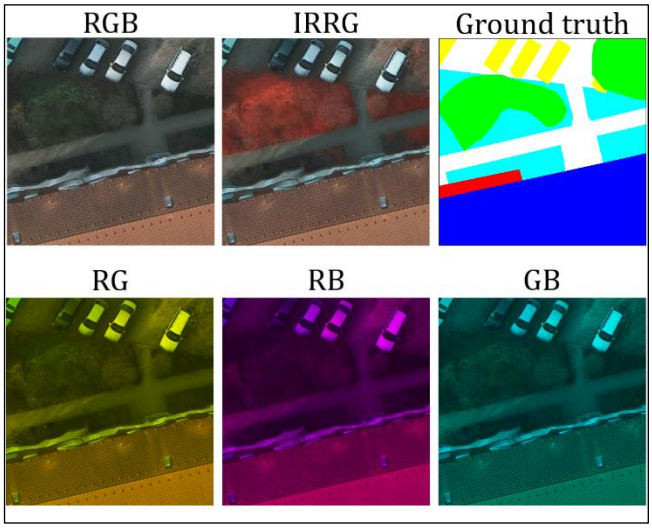


**Figure 2.** Sample RGB, IRRG, ground truth, RG, RB and GB data used in training

### 2.2. DeepLabv3

DeepLabv3 (Fig. 3) neural network is a CNN architecture developed for use in semantic segmentation applications (Chen et al. 2017b). This network, developed on the basis of the ResNet network structure, includes 4 ResNet blocks, atrous spatial pyramid pooling (ASPP) and global average pooling (GAP).

Atrous convolution, located in ResNet 4th block and ASPP, expands the field of view of the filter by a certain rate (r-1 number 0 is added) and provides more dense feature maps with fewer parameters than the classical convolution (Ratul et al. 2019; Wang et al. 2019).

GAP converts the feature map of size h (height) x w (width) x d (depth) into 1 x 1 x d. This process, which is used to reduce the tensor size as in the pooling layer, takes the average of each feature map and thus prevents the model from over learning (Lin et al. 2014).

ASPP, which first appeared in the DeepLabv2 (Chen et al. 2017a) architecture, this module applies different rates of atrous convolution (r = 6, 12, 18) operations in parallel, as well as global average pooling. In this way, feature maps with different levels of detail are produced. Classical convolution with 1x1 filter is applied by

combining the feature maps produced as a result of GAP and each atrous convolution.

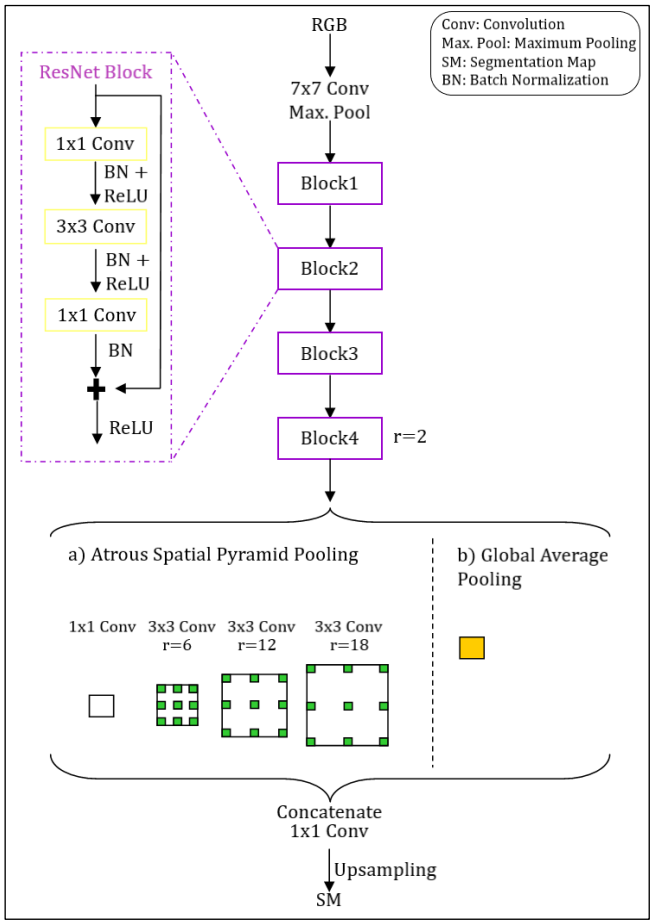


**Figure 3.** DeepLabv3 architecture

## 3. RESULTS

### 3.1. Training the DeepLabv3

DeepLabv3; for each spectral band combination, 40 epochs, 4 mini-batch sizes, Adam optimization algorithm and ResNet-50 weights were trained with using transfer learning. As a result of the trainings, the accuracy of the RG 0.91, RB 0.85, GB 0.91, RGB 0.92, IRRG 0.91 model was achieved. The training took 6 hours for RG and RB data, 6.5 hours for GB data, 9 hours for RGB data, and 9.5 hours for IRRG data.

### 3.2. Testing the DeepLabv3

DeepLabv3 models were tested with 352 test data which using RG images 30th epoch, RB images9th epoch, GB images32th epoch, RGB images38th epoch and IRRG images20th epoch weights. For the evaluation of segmentation maps produced from DeepLabv3 models, precision, precision and f-score were calculated (Table 1). The accuracy of the tested models are 0.77, 0.76, 0.83, 0.82, and 0.83 respectively. Segmentation maps are shown in Fig. 4.

## 4. DISCUSSION

According to the accuracy metrics, it has been observed that the orders of success between combinations are GB, IRRG, RGB, RG and RB. There is a difference of approximately 1% between the test accuracy of models trained with GB, IRRG and RGB data. In addition to having similar results, it has been observed that the GB combination is quite successful in impervious surface, building and car classes. It has been observed that RGB has low vegetation and IRRG is better in tree class than other combinations.

When the classification results were examined, it was concluded that the DeepLabv3 architecture trained with GB, RGB and IRRG data gave successful results in general. In addition, the red and infrared bands are thought to have an accuracy-enhancing effect on low vegetation.

**Table 1.** Accuracy metrics for each class

| | | İmp surf. | Building | Low veg. | Tree | Car | Clutter |
|---|---|---|---|---|---|---|---|
| Precision | RG | 0.78 | 0.87 | 0.68 | 0.82 | 0.80 | 0.14 |
| | RB | 0.73 | 0.94 | 0.61 | 0.84 | 0.61 | 0.34 |
| | GB | 0.83 | 0.93 | 0.71 | 0.84 | 0.82 | 0.37 |
| | RGB | 0.82 | 0.94 | 0.70 | 0.83 | 0.72 | 0.26 |
| | IRRG | 0.83 | 0.95 | 0.71 | 0.81 | 0.81 | 0.32 |
| Recall | RG | 0.74 | 0.91 | 0.70 | 0.70 | 0.67 | 0.31 |
| | RB | 0.71 | 0.78 | 0.85 | 0.74 | 0.66 | 0.27 |
| | GB | 0.80 | 0.92 | 0.83 | 0.76 | 0.73 | 0.27 |
| | RGB | 0.78 | 0.90 | 0.84 | 0.78 | 0.73 | 0.22 |
| | IRRG | 0.78 | 0.90 | 0.83 | 0.82 | 0.70 | 0.27 |
| F-Score | RG | 0.76 | 0.89 | 0.69 | 0.76 | 0.73 | 0.19 |
| | RB | 0.72 | 0.85 | 0.71 | 0.78 | 0.63 | 0.30 |
| | GB | 0.81 | 0.93 | 0.76 | 0.80 | 0.78 | 0.31 |
| | RGB | 0.80 | 0.92 | 0.77 | 0.80 | 0.72 | 0.24 |
| | IRRG | 0.80 | 0.92 | 0.77 | 0.82 | 0.75 | 0.29 |

## 5. CONCLUSION

In the study, classification success of high resolution orthophotos using DeepLabv3 architecture was investigated and five different data structures of ISPRS-Potsdam data set were used in line with this goal.

As a result, the neural network trained with GB, IRRG and RGB data performed better than the RG and RB neural networks. When we look at the in-class performances, it is seen that GB gives better results in determining the impermeable surface, building, car and clutter, RGB in determining low vegetation class and IRRG in determining the tree class, albeit with slight differences. In general, the higher accuracy of building class compared to other classes are thought to be due to the fact that it is more intense in the data set. In particular, clutter class, which has the least density and is difficult to distinguish in the data set, has the lowest accuracy.

This study, conducted using Google Colaboratory, could not increase training data due to time and memory limitations. Therefore, it is predicted that it can perform a higher performance than the results obtained with more training data and a more powerful GPU. Generally; when all the obtained results were evaluated, it was concluded that using deep learning algorithms and GB,

RGB and IRRG data structures, land use and land detection classification can be made.

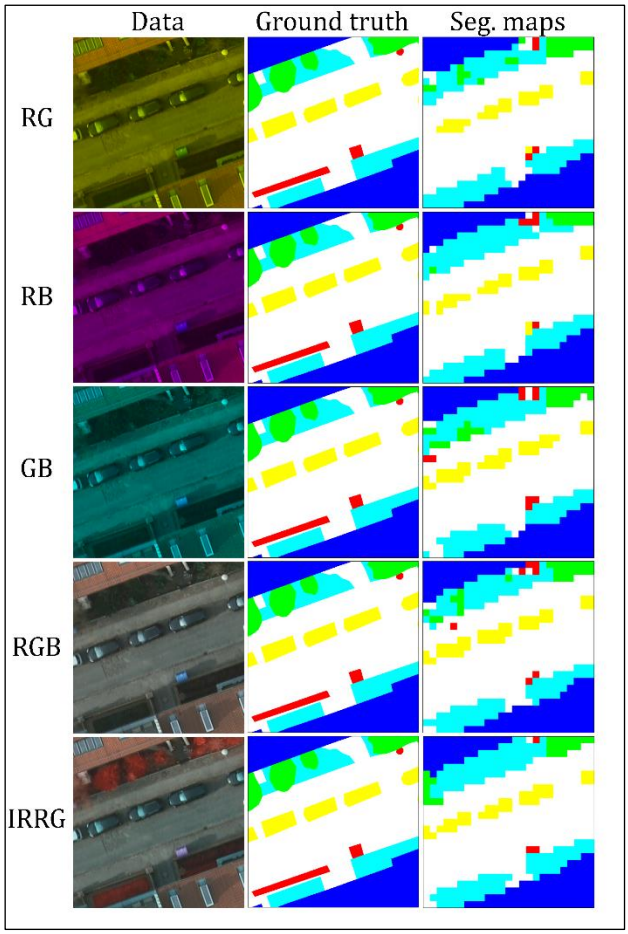


**Figure 4.** Segmentation maps examples

**ACKNOWLEDGEMENT**

This research was supported by The Scientific and Technological Research Council of Turkey (TÜBİTAK), Project No: 119Y363

**REFERENCES**

Altinoluk E, Akçay Ö, Avşar E Ö, Aydar U (2019). Recent Approaches in Segmentation Analysis with Deep Learning Methods. X. TUFUAB Teknik Sempozyumu, 20-25, Aksaray, Türkiye.

Arel I, Rose D C, & Karnowski T P (2010). Deep machine learning-a new frontier in artificial intelligence research [research frontier]. IEEE computational intelligence magazine, 5(4), 13-18.

Blaschke T (2010). Object based image analysis for remote sensing. ISPRS journal of photogrammetry and remote sensing, 65(1), 2-16.

Breiman L (2001). Random forests. Machine learning, 45(1), 5-32.

Castelluccio M, Poggi G, Sansone C & Verdoliva L (2015). Land use classification in remote sensing images by convolutional neural networks. arXiv preprint arXiv:1508.00092.

Chen L C, Papandreou G, Kokkinos I, Murphy K & Yuille A L (2017a). Deeplab: Semantic image segmentation with deep convolutional nets, atrous convolution, and fully connected crfs. IEEE transactions on pattern analysis and machine intelligence, 40(4), 834-848.

Chen L C, Papandreou G, Schroff F, Adam H (2017b). Rethinking Atrous Convolution for Semantic Image Segmentation. arXiv preprint arXiv:1706.05587.

Cortes C & Vapnik V (1995). Support-vector networks. Machine learning, 20(3), 273-297.

Foody G M (1996). Relating the land-cover composition of mixed pixels to artificial neural network classification output. Photogrammetric engineering and remote sensing, 62(5), 491-498.

He K, Zhang X, Ren S & Sun J (2016). Deep residual learning for image recognition. In Proceedings of the IEEE conference on computer vision and pattern recognition, 770-778.

Krizhevsky A, Sutskever I & Hinton G E (2012). ImageNet Classification with Deep Convolutional Neural Networks. Advances in Neural Information Processing Systems 25 (NIPS 2012), 1097-1105.

LeCun Y, Bengio Y & Hinton G (2015). Deep Learning. Nature, 521(7553), 436.

LeCun Y, Boser B, Denker J S, Henderson D, Howard R E, Hubbard W & Jackel L D (1989). Backpropagation applied to handwritten zip code recognition. Neural computation, 1(4), 541-551.

LeCun Y, Bottou L, Bengio Y, Haffner P (1998). Gradient-Based Learning Applied to Document Recognition. Proceedings of the IEEE, 86(11), 2278-2324.

Lin M, Chen Q, & Yan S (2014). Network In Network. arXiv preprint arXiv:1 312.4400.

Liu Y, Ren Q, Geng J, Ding M & Li J (2018). Efficient Patch-wise Semantic Segmentation for Large-scale Remote Sensing Images. Sensors, 18(10), 3232.

Ratul M A R, Mozaffari M H, Parimbelli E & Lee W (2019). Atrous Convolution with Transfer Learning for Skin Lesions Classification. *BioRxiv*, 746388.

Simonyan K & Zisserman A (2014). Very deep convolutional networks for large-scale image recognition. arXiv preprint arXiv:1409.1556.

Szegedy C, Liu W, Jia Y, Sermanet P, Reed S, Anguelov D & Rabinovich A (2015). Going deeper with convolutions.In Proceedings of the IEEE conference on computer vision and pattern recognition.

Veljanovski T, Kanjir U & Ostir K (2011). Object-based image analysis of remote sensing data. Geodetski vestnik, 55(4), 678-688.

Wang Y, Liang B, Ding M, Li J (2019). Dense Semantic Labeling with Atrous Spatial Pyramid Pooling and Decoder for High-Resolution Remote Sensing Imagery. Remote Sensing, 11(1), 20.

Zhang R & Zhu D (2011). Study of land cover classification based on knowledge rules using high-resolution remote sensing images. Expert Systems with Applications, 38(4), 3647-3652.

Yu F & Koltun V (2015). Multi-scale context aggregation by dilated convolutions, arXiv: 1511.07122.

Zhang Z, Huang J, Jiang T, Sui B K & Pan X L (2020). Semantic segmentation of very high-resolution remote sensing image based on multiple band combinations and patchwise scene analysis. J. Appl. Remote Sens., 14, 016502.

Intercontinental Geoinformation Days

http://igd.mersin.edu.tr/2020/

# A Review on the Usability of Mobile Phone-based Close-Range Photogrammetry, Terrestrial Laser Scanning and UAVs in Traffic Accident Modeling

**İrem Yakar*[1], Engin Kanun [2], Ganime Melike Oğuz [3], Şafak Bozduman[2], Serdar Bilgi[1], Kamil Karataş[3]**

[1]*Istanbul Technical University, Faculty of Civil Engineering, Geomatics Engineering Department, Istanbul, Turkey*
[2]*Mersin University, Faculty of Engineering, Geomatics Engineering Department, Mersin, Turkey*
[3]*Aksaray University, Faculty of Engineering, Geomatics Engineering Department, Aksaray, Turkey*

**Keywords**
Traffic Accident Modeling
Photogrammetry
Laser Scanning
UAV

**ABSTRACT**

Fast, detailed and accurate three-dimensional (3D) documentation of traffic accident scenes are crucial since it provides data for traffic accident reconstruction which allows determining the vehicle speed, examining the nature of the collision, and affording evidence in court cases. There are various documentation techniques such as classical drawing techniques, photogrammetry, laser scanning etc. The modern methods have become more preferable compared with the classical drawing methods along with the developing technology. In this aspect, 3D models emerge as a solution for fast and detailed documentation of traffic accidents. In addition, deformations can be determined more accurately by using these models in comparison with the classical methods. In this study, three different models were produced by using mobile phone-based photogrammetry, UAV photogrammetry and terrestrial laser scanning. Then, each model was examined comparatively in terms of completeness, visual representation, time efficiency and metric accuracy. In addition, the usability of mobile-phones as a fast and low-cost tool for 3D modeling was also examined in terms of incident modeling.

## 1. INTRODUCTION

The number of fatal traffic accidents increases as a result of the rise in vehicle numbers and car speeds. This situation causes some challenges such as taking substantial time for officers to record the evidence and important scene characteristics after a traffic accident (Du et al., 2009). Today, spatial analysis of traffic accidents is mostly based on visual examinations. Hence, it highly depends on the observer (Sabel et al., 2005). Providing data for traffic accident reconstruction which allows determining the vehicle speed, examining the nature of the collision, and affording evidence in court cases are important. Hence having a fast and accurate examination method is necessary (Du et al., 2009). In addition to this; in terms of evaluating the performance of safety systems, determining the deformations on cars after traffic accidents is really crucial (Kullgren, Lie, & Tingvall, 1994).

Therefore, a fast examination of traffic accidents has been gained more attention along with the developing technology.

The developments in technology result in easy and fast data collecting along with the opportunity to store the collected data in computer systems. Incident reporting systems are started to be widely used by analysts due to its huge ability of data mine in addition to the aim of reducing the accident rate (Cassidy et al.,2003; Sabel et al., 2005).

In this case, close range photogrammetry, UAV photogrammetry and terrestrial laser scanning offer quick solutions for traffic accident documentation.

* **Corresponding Author**

*(yakari@itu.edu.tr) ORCID ID 0000 – 0002 – 7823 – 9674
(ekanun@mersin.edu.tr) ORCID ID 0000– 0002 – 2369 – 5322
(ganime.melike.oguz@asu.edu.tr) ORCID ID 0000 – 0003 – 0241 – 6870
(bozduman19@itu.edu.tr) ORCID ID 0000 – 0003 – 0359 – 9090
(bilgi@itu.edu.tr) ORCID ID 0000 – 0002 – 8396 – 3202
(kkaratas@aksaray.edu.tr) ORCID ID 0000 – 0001 – 5174 – 7153

**Cite this study**

Yakar I, Kanun E , Oguz G.M, Bozduman S, Bilgi S, Karatas K. (2020). A Review on the Usability of Mobile Phone-based Close-Range Photogrammetry, Terrestrial Laser Scanning and UAVs in Traffic Accident Modeling. Intercontinental Geoinformation Days (IGD), 13-16, Mersin, Turkey

Close range photogrammetry is a valuable tool for 3D modelling with its long history. In recent years, there have been many important changes and growth in the close range photogrammetric measurement area (Fraser & Hanley, 2004). In this aspect, mobile phones emerge as a tool for fast and low-cost data acquisition. However, the resulted 3D model needs to be examined whether it can provide sufficient models or not in traffic accident modeling.

On the other hand, UAV-based photogrammetry has gained popularity since the remotely controlled drones offer various capabilities for autonomous flying. UAV-based photogrammetry can be used in wide range of applications such as topographic mapping, environmental monitoring, archeological surveys, etc. In general, obtained images are processed by the use of SfM Software, which automatically produces point clouds (Luhmann, 2019).

In addition, 3D models obtained by using terrestrial laser scanners are useful for obtaining accurate, detailed and reliable information about the object to be scanned.

The laser scanners are capable of producing realistic models by using color information which can be obtained either from sensor or from a digital camera. On the other hand, the surface light is effective on the resulted data. In this case, the surface to be scanned plays an important role in the produced 3D model modeling (Godin et al., 2001).

In this study, usability of 3D models obtained by the use of mobile phone-based photogrammetry, UAV photogrammetry and terrestrial laser scanning were examined comparatively. The processes of the close range photogrammetric images were made in ContextCapture Software while UAV images were processed in Agisoft Photoscan Software. Faro Scene Software was used in order to generate 3D point cloud from terrestrial scans.

## 2. METHOD

Since the aim of the study was the production and comparison of close range photogrammetry, UAV-based photogrammetry and terrestrial laser scanning, different data acquisition techniques were carried out.

### 2.1. Close-Range Photogrammetric Survey

Close-range photogrammetric survey consists of two phases such as field work and office work. During the field work, photogrammetric images were captured in order to reconstruct the accident in 3D. Digital images of survey area (A test area closed to traffic at Mersin University Stadium) were acquired by using Apple Iphone 6s mobile phone during the field work. The mobile phone has a 12 Megapixel camera with a 1/3" sensor size and focal length of f/2.2, 29mm. 92 images at total were captured. As the next step of field work, 4 Ground Control Points (GCPs) were established on the ground and were measured with Topcon HiPer Sr GNSS receiver in ITRF-96 datum, UTM projection, GRS80 ellipsoid, 2005.0 epoch, 3-degree zone-33, in Continuously Operating GNSS Kinematic Reference Stations (CORS-TR) System. 31 detail points respectively consisting of targets pasted on the vehicles and specific points selected on the vehicles (corners etc.) were measured in reflectorless mode with Topcon GM series total station (Figure 1). In the office work phase, 3D coordinates of the detail points on the vehicles were computed on the Netcad software by the use of measured four GCPs and total station data. This process allowed to bring both close range photogrammetric and UAV model in common reference system. Thereby, integrating two models would be possible in case of some data is missing in other model. The 3D coordinates of the 15 of measured control points were used for geo-referencing the 3D model.

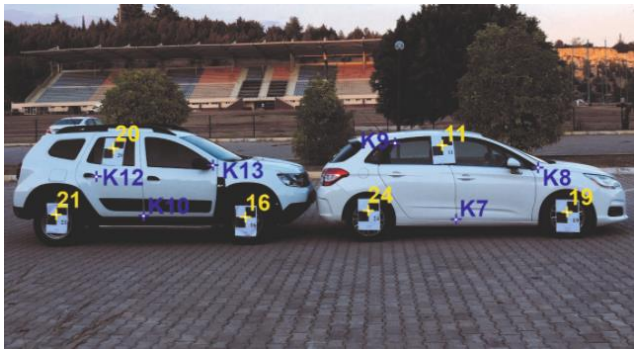


**Figure 1.** Details point on the one facade of the scene

During the office phase of the study, 73 of the images were processed in Bentley's Context Capture Software. Thus, point cloud and textured model were produced of the traffic accident scene (Figure 2).

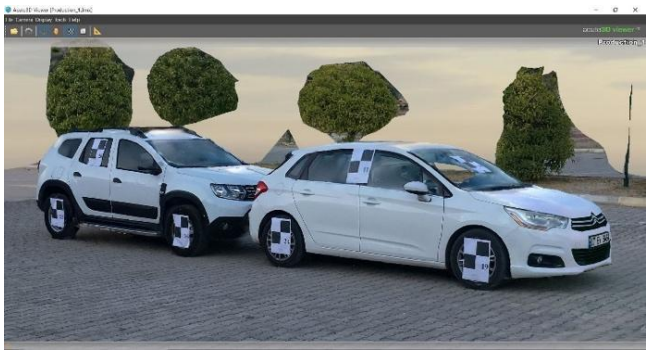

**Figure 2.** Textured model obtained by the use of close range photogrammetric images

### 2.2. UAV-Based Photogrammetric Survey

UAV-based photogrammetry is divided in two phases such as field and office work as well as the close-range photogrammetric survey. Parrot Anafi UAV was used for the UAV-based photogrammetric survey. It has a 4K HDR camera with a 180º inclined gimbal. The images were captured in two flight plans, one in circular and other in double grid mission by using Pix4DCapture. 168 images at total were captured in UAV-based photogrammetric survey. Then, the established four ground control points were measured in ITRF-96 datum, UTM projection, GRS80 ellipsoid, 2005.0 epoch, 3-degree zone-33 (Figure 3).

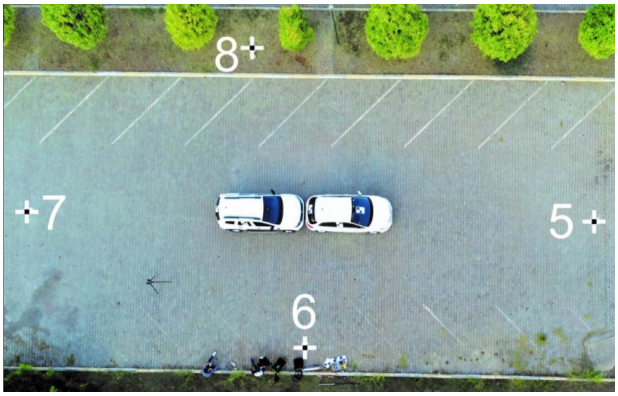


**Figure 3.** Established four GCPs

These GCPs were later used for geo-referencing the UAV-based point cloud in order to bring it in common reference system with the point cloud obtained by the use of close-range photogrammetry. During the office work, 164 images were processed in Agisoft Photoscan Software for producing 3D point cloud. Then, textured model of the traffic accident scene was obtained (Figure 4 & 5).

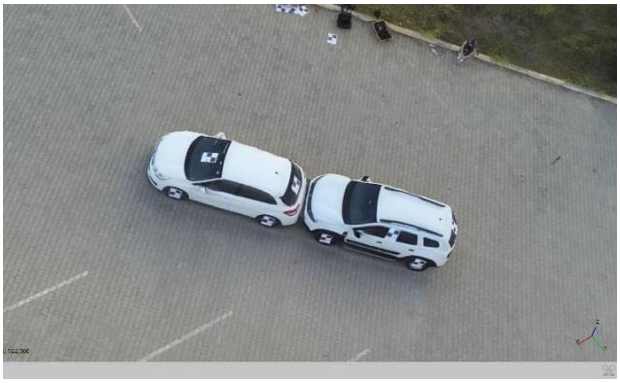

**Figure 4.** Textured model obtained by the use of UAV images

**Figure 5.** Textured model obtained by the use of UAV images

### 2.3. Terrestrial Laser Scanning

10 scans around the traffic accident scene were performed by using Faro Focus$^S$ 350 scanner in the field. Then, the data acquired during the field work was processed in Faro Scene Software. Target based registration was performed in data processing phase. After registration; coloration, reflectance threshold and distance filter options were used in order to arrange the data. Thus, a meaningful point data set was obtained for 3D model production. Noise reduction was also performed in order to avoid redundant data. The resulted point cloud is shown in figure 6.

**Figure 6.** Point cloud obtained by terrestrial laser scanning

## 3. ACCURACY ASSESSMENT

In order to define the metric performance of each model; 10 distances between selected detail points were compared with the distances calculated by using the 3D coordinates obtained from GNSS and total station data (Figure 7, 8 & 9).

| Close-Range Photogrammetry | | | | |
|---|---|---|---|---|
| Points | Model Distance | Ground Truth | V | VV |
| | [m] | [m] | *[cm]* | [cm²] |
| (K1-K2) | 1.327 | 1.378 | 5.13 | 26.30 |
| (K2-K3) | 1.036 | 1.138 | 10.12 | 102.36 |
| (K3-K4) | 1.285 | 1.372 | 8.66 | 75.05 |
| (K4-K5) | 1.183 | 1.285 | 10.16 | 103.19 |
| (K5-K6) | 0.484 | 0.522 | 3.74 | 13.99 |
| (K10-K11) | 0.904 | 0.970 | 6.67 | 44.48 |
| (21-20) | 1.111 | 1.175 | 6.41 | 41.15 |
| (16-24) | 1.593 | 1.687 | 9.44 | 89.05 |
| (24-11) | 1.278 | 1.357 | 7.82 | 61.11 |
| (11-19) | 1.719 | 1.824 | 10.54 | 111.00 |
| | | | RMS = ± 8.61 cm | |

**Figure 7.** Accuracy assessment of close range photogrammetric model

| UAV Photogrammetry | | | | |
|---|---|---|---|---|
| Points | Model Distance | Ground Truth | V | VV |
| | [m] | [m] | *[cm]* | [cm²] |
| (K1-K2) | 1.361 | 1.378 | 1.71 | 2.92 |
| (K2-K3) | 1.173 | 1.138 | 3.53 | 12.43 |
| (K3-K4) | 1.361 | 1.372 | 1.08 | 1.16 |
| (K4-K5) | 1.243 | 1.285 | 4.19 | 17.56 |
| (K5-K6) | 0.532 | 0.522 | 1.02 | 1.05 |
| (K10-K11) | 0.991 | 0.970 | 2.07 | 4.31 |
| (21-20) | 1.172 | 1.175 | 0.27 | 0.07 |
| (16-24) | 1.674 | 1.687 | 1.25 | 1.56 |
| (24-11) | 1.336 | 1.357 | 2.09 | 4.38 |
| (11-19) | 1.805 | 1.824 | 1.93 | 3.72 |
| | | | RMS = ± 2.34 cm | |

**Figure 8.** Accuracy assessment of UAV-based photogrammetric model

| Laser Scanning | | | | |
|---|---|---|---|---|
| Points | Model Distance | Ground Truth | V | VV |
| | [m] | [m] | [cm] | [cm²] |
| (K1-K2) | 1.305 | 1.378 | 7.26 | 52.77 |
| (K2-K3) | 1.079 | 1.138 | 5.84 | 34.14 |
| (K3-K4) | 1.341 | 1.372 | 3.10 | 9.60 |
| (K4-K5) | 1.273 | 1.285 | 1.16 | 1.35 |
| (K5-K6) | 0.540 | 0.522 | 1.84 | 3.38 |
| (K10-K11) | 0.981 | 0.970 | 1.08 | 1.18 |
| (21-20) | 1.220 | 1.175 | 4.52 | 20.47 |
| (16-24) | 1.679 | 1.687 | 0.81 | 0.65 |
| (24-11) | 1.396 | 1.357 | 3.96 | 15.68 |
| (11-19) | 1.776 | 1.824 | 4.81 | 23.12 |
| | | | RMS = ± 4.25cm | |

**Figure 9.** Accuracy assessment of laser scanning model

## 4. RESULTS

In this study, three point clouds obtained by using mobile-phone-based close range photogrammetry, UAV photogrammetry and terrestrial laser scanning were examined in terms of completeness, visual representation, time efficiency and metric accuracy. In terms of completeness and visual representation; terrestrial laser scanner point cloud and close-range photogrammetric point cloud may have some missing data at the roof of the vehicles since the view may not be seen clearly depending on the elevation which the data are acquired from. On the other hand, UAV-photogrammetry provides a complete 3D model since it can acquire data both from above and around the accident scene. However, the facades of the vehicles were more realistically reconstructed in close range photogrammetry. Based on the results, it is observed that; UAV photogrammetry is more suitable for obtaining a complete 3D model. In this case, the missing data in close-range photogrammetric point cloud and laser scanner point cloud can be completed by integrating the UAV point cloud since all models are in the same coordinate system. In terms of time efficiency, capturing images for close range photogrammetry and UAV photogrammetry both took approximately 15 minutes, while laser scanning process took approximately 1 hour in the field. Data processing time for all three methods was approximately 4 hours. Since acquiring data after a traffic accident in the fastest way possible is crucial, it is seen that; UAV-photogrammetry and close range photogrammetry are more time-efficient in comparison with the terrestrial laser scanning. On the other hand, metric accuracy of obtained models were also examined. In this term, 10 distances were compared with the ground truth data obtained by using total station and GNSS measurements. Mobile phone-based close range photogrammetry provides ± 8.61 cm accuracy model, while UAV photogrammetry is ± 2.34 cm accurate and terrestrial laser scanning is ± 4.25 cm accurate. However, the resolution of the camera plays an important role in geo-referencing the close range photogrammetric data. The results would be better if a higher resolution camera can be used.

## 5. CONCLUSION

There are various factors for evaluating the performance of obtained models in terms of traffic accident modeling. These factors can be listed as follows: completeness, visual representation, time efficiency and metric accuracy. It is seen that each method has its own advantages and disadvantages. Photogrammetric methods are more suitable for faster data acquisition in the field while data processing times are close to each other. On the other hand, UAV photogrammetry provides a complete model in a short time. In this context, there would be some missing data in the roof of the vehicles in use of close range photogrammetry and terrestrial laser scanning. But, both methods are successful in representing the facades of the vehicles. In terms of metric accuracy, the methods can be ranked in following order: UAV photogrammetry, laser scanning and close range photogrammetry.

In addition, it is seen that mobile phones can be used as a fast and low cost data acquisition tool for traffic accident modeling

In future studies, the usability of fusion models generated by using all methods can be investigated in terms of traffic accident modeling.

## REFERENCES

Cassidy, D., Carthy, J., Drummond, A., Dunnion, J., & Sheppard, J. (2003). The use of data mining in the design and implementation of an incident report retrieval system. Paper presented at the IEEE Systems and Information Engineering Design Symposium, 2003.

Du, X., Jin, X., Zhang, X., Shen, J., & Hou, X. (2009). Geometry features measurement of traffic accident for reconstruction based on close-range photogrammetry. Advances in Engineering Software, 40(7), 497-505.

Fraser, C., & Hanley, H. (2004). Developments in close-range photogrammetry for 3D modelling: the iWitness example. Paper presented at the Presented paper, International Workshop: Processing and Visualization using High-Resolution Imagery, Pitsanulok.

Godin, G., Rioux, M., Beraldin, J. A., Levoy, M., Cournoyer, L., & Blais, F. (2001). An assessment of laser range measurement of marble surfaces. Paper presented at the Conference on Optical 3D Measurement Techniques.

Kullgren, A., Lie, A., & Tingvall, C. (1994). Photogrammetry for documentation of vehicle deformations—A tool in a system for advanced accident data collection. Accident Analysis & Prevention, 26(1), 99-106.

Sabel, C. E., Kingham, S., Nicholson, A., & Bartie, P. (2005). Road traffic accident simulation modelling-a kernel estimation approach. Paper presented at the The 17th annual colloquium of the spatial information research Centre University of Otago, Dunedin, New Zealand.

Intercontinental Geoinformation Days

http://igd.mersin.edu.tr/2020/

# Assessment of shoreline change and its relation with Mangrove vegetation: A case study over North Konkan region of Raigad, Maharashtra, India

**Barnali Das*[1], Anargha Dhorde [1]**

[1]*Nowrosjee Wadia College, Geography, Pune, India*

**Keywords**
Shoreline Change
DSAS
Mangroves
Remote sensing

**ABSTRACT**

Shorelines, in response to accretion and denudation, are dynamic in nature. Vulnerability of Sea Level Rise varies from place to place with 20th century observing greatest threat to it. Mangroves along the shore, are the one to first sustain this impact of SLR. In the present study an attempt has been made to understand the relation between shoreline changes with mangrove habitat through remote sensing data and geospatial technique. Shoreline change rate has been calculated for the years 2000, 2012 and 2019, in Digital Shoreline Analysis System by End Point Rate. Change analysis indicates that in last 20 years erosion dominated the study area with an average rate of -0.02m/yr. During 2000 to 2012, relatively higher erosional rates (-0.35m/yr) were observed. While from 2012 to 2019 accretion process dominated this area with a rate of 0.43m/yr. Sonakothakar, Mothe Bhal and Dadar with denudational trends have observed landward progradation of mangroves whereas, at Aware, a zone of over accretion exhibited a seaward progradation of mangroves. This type of integrated study not only will help to understand active process over the shore but also will help to conserve mangrove habitat. Such regional scale studies should be carried out before implementing any coastal conservation projects.

## 1. INTRODUCTION

Shorelines are dynamic in nature and often respond to the changes in sea level. Global mean sea level (GMSL) was envisaged to be accelerating at considerable rate during 19th century with a further leap in its rate in 20th century (Church and White 2006). The speed of GMSL rise during 1900 to 2009 was estimated about 1.7 ± 0.2 mm/year which raise up to 3.2 ± 0.4mm/year at the end of 20th century (Mimura 2013). Vulnerability of Sea Level Rise (SLR) varies from place to place, with developing countries being much more susceptible to it (Wheeler and Yan 2009). In the Indian scenario east coast are much more vulnerable to erosion as compared to west coast, however, 36% of Maharashtra coast is under the process of erosion (Mohanty et al. 2017).

Mangroves thrive on mudflats along the shore. Mangrove habitat is considered as a boon to mankind. However, mangrove habitat is under continuous threat of shoreline change. It was observed that during early Holocene period there was high SLR to which mangroves were able to withstand the effect however, this characteristic of withstanding varies time to time and from place to place (Woodroffe 1990). At paces resilient nature of mangroves was noted that was attributed to the anthropogenic pressure and physiographic settings (Nitto et al. 2014). However, certain studies have shown that mangrove ecosystem is very dynamic in nature and they can even migrate landward in order to balance with SLR (McLeod and Salm 2006). Mangrove forest structure exhibits an interesting pattern of transition from seaward fringe to land ward, with healthy strong tree near the sea to dwarf forest far inland (Feller 2015).

SLR has eroded considerable parts of coast, wetlands and mudflats in India (Dwivedi and Sharma 2005). However, mangroves act as a stabilizer and protector to SLR, deforestation to which may boost up erosion rate like Alibag coast in Maharashtra (Vidya et al. 2015).

* **Corresponding Author**

*(barnali25das@gmail.com) ORCID ID 0000-0002-6103-4656
(e-mail) ORCID ID 0000- 0002 – 5678 - 7397

**Cite this study**

Das B & Dhorde A (2020). Assessment of shoreline change and its relation with Mangrove vegetation: A case study over North Konkan region of Raigad, Maharashtra, India. Intercontinental Geoinformation Days (IGD), 17-20, Mersin, Turkey

Over last two decades it has been observed that mangroves in the study area have increased profusely. Impact of changing shoreline on mangrove vegetation needs to be addressed. Thus, present study aims at understanding the relation of mangrove growth with shoreline change. The specific objectives set are i) Detecting the changes in Shoreline and ascertaining the zones of denudation and accretion and ii) assessing the growth/decline in mangroves within the selected patches.

## 2. STUDY AREA

Raigad district is located on the west coast of Maharashtra, India. This coast is intertwined by rocky and sandy coast. A number of creeks are also observed to have developed marsh ecosystem at places. Within these belts of mudflats and marshes, lining the creeks, clusters of Mangrove patches are observed. Various local newspaper articles cited that in the last two decades these mangrove clusters, especially along the northern Raigad, has shown exponential growth. A few patches of mangroves from the North Raigad region are selected for the present study(Fig 1). The study area extends between 18° 53' 12.28"N and 18° 45' 16.2"N latitudes, and 72° 52' 14"E and 73° 1' 42.2"E longitudes. In Raigad there are 11 true mangrove species and 15 mangrove associates (Mhatre et al. 2013).

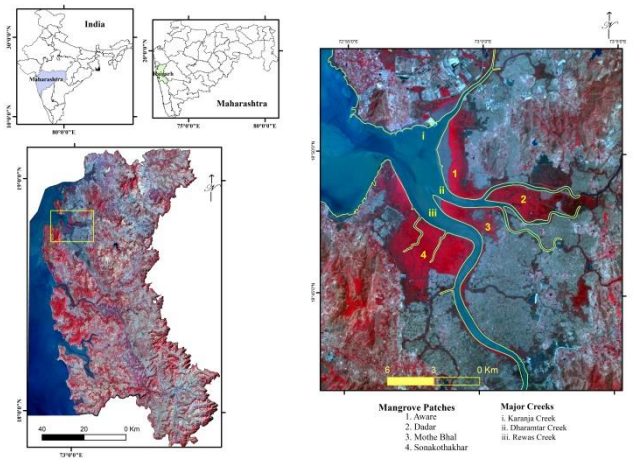


**Figure 1.** Location map

## 3. DATA & METHOD

### 3.1. Data Base

Present work depends on secondary data, in the form of satellite images were retrieved first. Since shorelines are highly dynamic and exposure of mangroves depends upon the tidal conditions, the level and condition of tides during the process of capturing the satellite images has to be taken into consideration. Table 1 presents the dates and tidal condition selected for retrieving the satellite images.

**Table 1**: Detail of Dates selected and Tide condition for each scene

| Date & Year | Satellite & Sensor | Approx. Satellite Pass time | Time | Tide Level | Tide Stage |
|---|---|---|---|---|---|
| 13/04/2000 | Landsat 7 TM (Level II) | 10:37am | 12:29pm | 0.72 | Ebbing |
| 04/04/2012 | Landsat 7 TM (Level I) | 10:37am | 11:13am | 1.40 | Ebbing |
| 25/03/2019 | Landsat 8 OLI (Level II) | 10:37am | 10:58am | 0.96 | Ebbing |

### 3.2. Image processing

Image pre-processing was carried out for all the images wherein the images were subjected to geometric and radiometric corrections. The image of 2012 was processed for image correction as it had a problem of scan line error. This problem was fixed with the help of Landsat toolbox plugin in ArcGIS. Image post processing was carried out over the images for layer stacking and obtaining certain indices which were essential for further analysis. Normalized Difference Vegetation Index (NDVI), Normalized Difference Moisture Index (NDMI), Tasseled Cap (TC), and Normalized Difference Water Index (NDWI) were computed in ERDAS Imagine. Along with these indices, image segmentation was performed in eCognision. In order to delineate the shoreline and obtain the erosional and depositional rates along the shoreline, Digital Shoreline Analysis System (DSAS) was employed.

### 3.3. Shoreline Extraction and Rates calculation

The general methodology adopted for the present study is outlined in figure 2. Shorelines were extracted through the DSAS program by employing band combinations of NDVI-TC band, NDMI-TC band and NDWI. These were then compared with the manually digitized shorelines to obtain the deviation statistics (table 2). Shoreline with minimum deviation in respective year was taken into consideration for further work of change detection analysis. Rates of changes along the selected stretches of shoreline were obtained in the DSAS software. DSAS employ several perpendicular transect from a baseline (in this study 150m away from the extracted shoreline) and records point of intersection between transect and shorelines for different years. DSAS automatically calculate several statistical methods for shoreline change viz. End Point Rate (ERP), Jackknife Rate (JKR), Linear Regression Rate (LRR), Shoreline Change Envelope (SCE), Net Shoreline Movement (NSM), Least Median of Square (LMS) and Weighted Linear Regression (WLR). All these methods have some advantages and disadvantages. In the present study shoreline change by ERP rate is taken into consideration as for relatively small data it gives good results (Esmail et al., 2019). Moreover it shows normal distribution and is simple and universally prevalent method (Nassar, 2018).

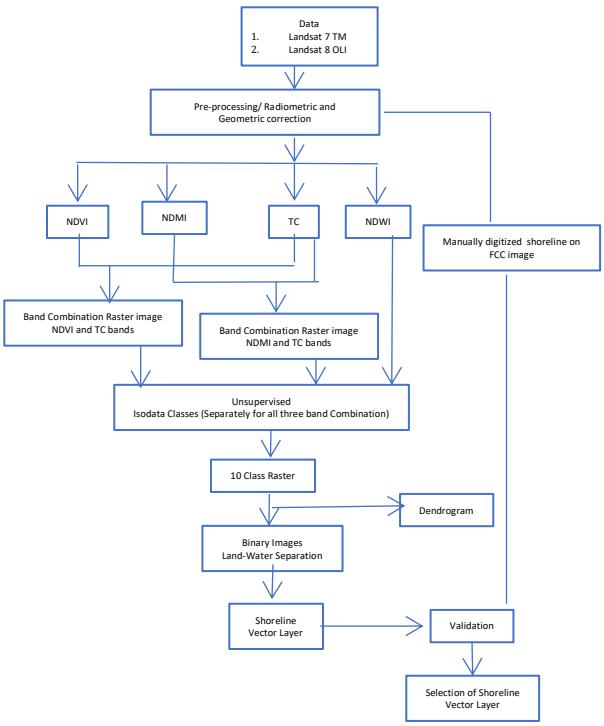


**Figure 2.** Methodology

**Table 2.** Within pair difference between manually created shoreline and other methods

| Method | Deviation from Manually Digitized Shoreline | | |
|---|---|---|---|
| | 2000 | 2012 | 2019 |
| NDWI | Min = 0.62<br>Mean=210.85<br>Max=999.18 | Min = 0.17<br>Mean=256.38<br>Max=998.28 | Min = 0.06<br>Mean=324.86<br>Max=999.73 |
| NDVI_TC | Min = 0.23<br>Mean=243.3<br>Max=998.47 | Min = 0.00<br>Mean=236.50<br>Max=999.83 | Min = 0.14<br>Mean=151.20<br>Max=997.78 |
| NDMI_TC | Min = 0.54<br>Mean=339.77<br>Max=999.64 | Min = 0.32<br>Mean=386.98<br>Max=999.73 | Min = 0.03<br>Mean=143.40<br>Max=998.91 |

### 3.4. Image Segmentation

Image segmentation process has been applied on False Color Composite (FCC) and NDVI image, to delineate mangrove patches in eCognition software. Scale parameter of 1, shape factor of 0.1 and compactness of 0.5 has been assigned to generate vector layer of mangrove. This vector layers, for individual patches are used to extract NDVI data. Ground control points (GCPs) collected through field visit from mangrove patches are used for proper delineation and segmentation of patches.

## 4. RESULTS & DISCUSSION

Shoreline change analysis for the present study has been carried over a span of 20 years ranging from 2000 to 2019. A time sectional analysis was also attempted between 2000 to 2012 and 2012 to 2019. Change detection analysis of the study area indicated that the shoreline has undergone both accretion and denudation process in last 20 years. Transects demarcated for accretion and denudation rates, indicates that almost 70.99% of the area has undergone erosion during the entire study period (2000 to 2019). While, almost 71.41% (2000 to 2012) and 67.79% (2012 to 2019) of the transects were subjected to erosion. However, during 2012 to 2019 it was observed that although 67.79% area was under erosion but the rate of erosion was relatively less than the rate of accretion.

Change analysis indicated that in the last 20 years erosion process dominated over the study area with an average rate of -0.02m/yr. During 2000 to 2012, erosion rate was high with -0.35m/yr whereas, from 2012 to 2019 accretion process dominated over denudation with a rate of 0.43m/yr (Fig 3). Overlay of extracted NDVI for mangrove patches clearly depicts that mangrove colony have undergone changes. In the regions of denudation like Sonakothakar, Mothe Bha and Dadar, it was observed that there is landward progradation of mangrove habitat whereas accretion dominated over Aware region with no major landward progradation but a seaward progradation was observed. This is mainly due to the stable shoreline as a result of accretion. NDVI values overall have risen from 0.6 to 0.8 during 2000 to 2019. However, steady inter patch transformation was observed during the time with major part of the patch reaching towards higher NDVI values. This leap in NDVI values during the time span indicates the healthy status of mangrove vegetation. Mangroves are salt tolerant species. Inland shift of shoreline often leads to saltwater penetration through soil and creeks, in such cases, mangroves then acts as a feeder to salinity (Prerna et al. 2015; Lambs et al. 2015) which is reflected in their overall health status. Minor decline of the mangroves was also observed in the study area it is only because of anthropogenic pressure over the region.

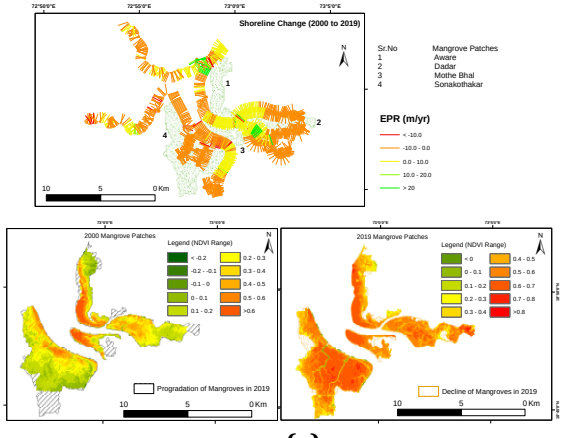


**(a)**

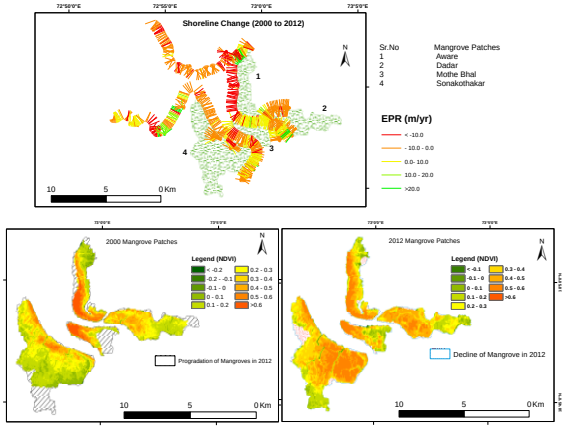


**(b)**

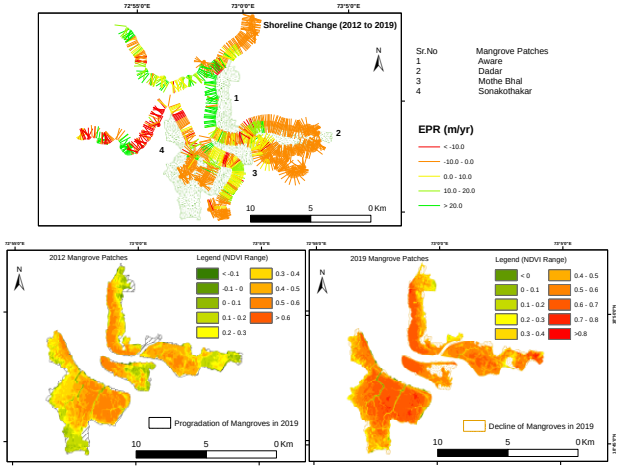


**(C)**

**Figure 3**: Shoreline change and Mangrove spatial extent transformation during **(a)** 2000-2019, **(b)** 2000-2012 and **(c)** 2012-2019

## 5. CONCLUSION

The present study concludes that shoreline over north Konkan region is under immense impact of shoreline change with processes of accretion and denudation varying from time to time. Process of erosion increased over Sonakothakar, Mothe Bha and Dadar whereas Aware observed accretion. This change has direct relation with mangrove habitat. Areas with denudation clearly witnessed an inland extension of mangrove vegetation over time whereas seaward progradation of mangroves was observed in the areas dominated by accretion processes. Over the time span, whether erosion or deposition zone, mangrove NDVI values exhibited an increasing trend indicating overall good health of the species. With intensified effect of climate change, sea level ought to increase, leading landward migration of mangroves (Gilman 2008). This type of integrated study not only will help to understand active process over the shore but also will help to conserve mangrove habitat. Such regional scale studies should be carried out before implementing any coastal conservation projects.

## REFERENCES


Church J & White N (2006). A 20th century acceleration in global sea-level rise. Geophysical Research Letters, VOL. 33, L01602, doi:10.1029/2005GL024826

Dasgupta S, Laplante B, Meisner C, Wheeler D & Yan J (2009). The impact of sea level rise on developing countries: a comparative analysis. Climatic Change, 93:379–388, DOI 10.1007/s10584-008-9499-5

Dwivedi D N & Sharma VK (2005). Analysis of Sea Level Rise and its Impact on Coastal Wetlands of IndiaProceedings of the 14th Biennial Coastal Zone Conference, New Orleans, Louisiana.

Eric L. Gilman E L, Ellison J, Duke N C & Field C (2008). Threats to mangroves from climate change and adaptation options.Aquatic Botany, doi:10.1016/j.aquabot.2007.12.009

Esmaila M, Mahmoda W E & Fatha H (2019). Assessment and prediction of shoreline change using multi-temporal satellite images and statistics: Case study of Damietta coast, Egypt. Applied Ocean Research, 82 274–282

Feller I C, Lovelock C E, McKee K L & Thompson R (2005) Variation in Mangrove Forest Structure and Sediment Characteristics in Bocas del Toro Panama. Caribbean Journal of Science · 41(3), 456-464.

Lambs L., Bompy F., Imbert D., Corenblit D., & Dulormne M. (2015). "Seawater and Freshwater Circulations through Coastal Forested Wetlands on a Caribbean Island" Water 7: 4108-4128, doi:10.3390/w7084108

McLeod E & Salm R V (2006) Managing Mangroves for Resilience to Climate Change Gland, Switzerland, IUCN

Mhatre K., Singh R., Cerejo S., & Shinde R. (2013). "Diversity of Mangroves in Raigad District, Maharashtra and need for their conservation". International Journal of Environmental Sciences Vol 2(4): pp 205-209. ISSN 2249-2127.

Mimura N (2013). Review Sea-level rise caused by climate change and its implications for society. Proceedings of Japan Academy, doi: 10.2183/pjab.89.281

Mohanty P C, Mahendra R S, Nayak R K & Kumar T S (2017). Impact of sea level rise and coastal slope on shoreline change along the Indian coast Natural Hazards, 89:1227–1238. DOI: 10.1007/s11069-017-3018-9

Nassar K, Mahmod W E, Fath H, Masria A, Nadaoka K & Negm N (2018). Shoreline change detection using DSAS technique: Case of North Sinai coast, Egypt. Marine Georesources & Geotechnology, DOI: 10.1080/1064119X.2018.1448912

Nitto D D, Neukermans G, Koedam N, Defever H, Pattyn F, Kairo J G & Dahdouh-Guebas F (2014) Mangroves facing climate change: landward migration potential in response to projected scenarios of sea level rise. Biogeosciences, 11, 857–871. doi:10.5194/bg-11-857-2014

Prerna R., Naidu V. S., Sukumaran S., & Gajbhiye S. N. (2015). "Observed decadal changes in extent of mangroves and coral reefs in southern Gulf of Kachchh using principal component analysis and geo-spatial techniques: a case study ". J Coast Conservation 19:257–267, DOI 10.1007/s11852-015-0385-9

Vidya, Biradar R S, Inamdar A B, Srivastava S & Pikle M (2015) Assessment of shoreline changes of Alibag coast (Maharashtra, India) using remote sensing and GIS. Journal of Marine Biology, 57 (2)

Woodroffe C D(1990). The impact of sea-level rise on mangrove shorelines. Progress in Physical Geography, 14, 483–520, 1990.

Intercontinental Geoinformation Days

http://igd.mersin.edu.tr/2020/

# Bathymetry analysis with use of Sentinel-2 images

**Hakan Uzakara** [*1], **Nusret Demir** [1]

[1]*Akdeniz University, Faculty of Science, Department of Space Sciences and Technologies, Antalya, Turkey*

**Keywords**
Remote sensing
Bathymetry
LIDAR
Sentinel-2

**ABSTRACT**

Bathymetry is described as Sea and Ocean depth measurements, and performed by many methods. Traditional methods, which are still used from the past to the present, have been replaced by modern methods with the development of technology. Sonar systems, LIDAR and remote sensing systems are listed as examples of these modern methods. The use of acoustic systems or LIDAR, are not economical in terms of both time and cost. In this study, remote sensing methods are investigated in order to minimize the time and cost. It is aimed to extract the information about bathymetry with use of free of charge satellite images. As input data, Sentinel-2 satellite images of the study area and reference bathymetry points from predefined locations, were used. Band ratio and multi-band methods are used, and the results were evaluated.

## 1. INTRODUCTION

Remote sensing is a science that provides information about the natural and artificial objects of the earth and evaluates them, without physical contact with the objects by using several platforms including satellites. It provides fast and economical solutions for many cases including land use, agriculture and marine studies etc..

In the literature, bathymetry are generally obtained from sonar devices, lidar data and satellite images. Although satellite-derived bathymetry does not have sonar or lidar accuracy, its large field capability, low cost and allowing analysis for areas where are not contacted easily (Gao 2009). To overcome the difficulties and disadvantages of these traditional methods, satellite-based remote sensing techniques have been developed (Pacheco et al. 2015) Basically, satellite-derived bathymetry is based on the relationship between reflected energy and water depth. For each pixel of the satellite image, there is a statistical relationship between the amount of energy detected by the sensor and the depth of the water at that pixel location. This relationship can be utilized with various calculation algorithms (Kumari and Ramesh 2020). Most of these algorithms require reference points which include about the depth (Jawak and Luis 2015).

Satellite images have different spatial resolution (+100 m - 31 cm). Only images with a resolution higher than 30 m are suitable since bathymetry derived from satellite images are based on average depth per pixel (Bailly du Bois 2011). High resolution (less than a few meters) satellites such as WorldVIEW-2 and RapidEye for deriving bathymetry from satellite images, medium resolution (10 - 30 m) satellites such as Landsat-8 and Sentinel-2, 3 are increasingly being tested for bathymetry analysis of shallow regions (Caballero and Stumpf 2019) (Stumpf et al. 2003). The spatial and spectral resolution of satellite images used in bathymetry analyzes, satellite viewing angle, atmospheric effects, tidal level, sunlight and vegetation affect the accuracy. Some of these effects can be overcome by preciese selection of satellite images and image processing (Kumari and Ramesh 2020). In this study, bathymetry analysis was performed with free use of Sentinel-2 images, which are freely available thorugh ESA Copernicus program.

## 2. METHOD

### 2.1. Study Area

The study area has been selected from the coastal zone of the city of Los Angeles in the state of California, USA. The coordinates of the study area are located at latitudes North = 33.747, West = 118.412, South = 33.62, East = 118.285.

* **Corresponding Author**

*(hakanuzakara@gmail.com) ORCID ID 0000 – 0001 – 9985 – 832X
(nusretdemir@akdeniz.edu.tr) ORCID ID 0000 – 0002 – 8756 – 7127

**Cite this study**

Uzakara H & Demir N (2020). Bathymetry analysis with use of Sentinel-2 images. Intercontinental Geoinformation Days (IGD), 21-24, Mersin, Turkey

**Figure 1.** Study area

As a result of preliminary analysis in the region, it has been determined that there is a large amount of chlorophyll and similar structures in areas up to 10 meters from the shore. Since these cause deviations in spectral reflections, regions with a depth of 10 meters to 30 meters were chosen as the study area.

### 2.2. Materials

Sentinel-2 satellite images of the study area were downloaded from ESA's Copernicus platform. Sentinel-2 MSI is a polar-orbit, multispectral high-resolution satellite that aims to perform field analyzes such as vegetation, soil and water cover areas. Sentinel-2A started operations on June 23, 2015, and Sentinel 2B on March 7, 2017.

**Table 1.** Sentinel-2 satellite band features

| Band | Name | Central wavelength (nm) | Spatial resolution (m) |
|---|---|---|---|
| | Aerossol | | |
| 1 | | 443 | 60 |
| 2 | Blue | 490 | 10 |
| 3 | Green | 560 | 10 |
| 4 | Red | 665 | 10 |
| 5 | Red Edge 1 | 705 | 20 |
| 6 | Red Edge 2 | 740 | 20 |
| 7 | Red Edge 3 | 783 | 20 |
| 8 | NIR | 842 | 10 |
| 9 | Cirrus | 945 | 60 |
| 10 | SWIR 1 | 1380 | 60 |
| 11 | SWIR2 | 1610 | 20 |
| 12 | Red Edge 4 | 2190 | 20 |

Reference bathymetry data of the analysis area was obtained from TCarta Global Bathymetry GIS Data site at 10m resolution.

### 2.3 Method

The analysis is directly dependent on solar radiation. Absorption, scattering and reflection occur when solar radiation reaches the water surface. The energy of the light entering the water body will be reflected from the base and reach the sensor. Depth estimation can be made as a function of light reflected from underwater using bands of different wavelengths. Depth was estimated using different band combinations in the study. Different combinations were obtained by using blue, green and red spectral bands. The interaction of each band with the water column has different reflection properties, which is an important factor in improving accuracy in depth estimation.

#### 2.3.1 Dual band ratio method

The bottom reflectance of the two bands does not change with the type of substrate. This can eliminate the influence of water type and the ratio of the two bands can be used to calculate water depth (Chen et al. 2019; Bramante et al. 2012).

$$Z = m_0 * \frac{ln\ ln\left(R_w(\lambda i)\right)}{ln(R_w(\lambda j))} - m_1 \quad (1)$$

Equation (1) λi and λj are the reflection values of the bands. For the equation to be positive in all conditions, n is a constant number. The reference bathymetric depths will be written instead of z and the m1 and m0 coefficients will be found. By using the coefficients found, a depth estimation is aimed for areas of unknown depth. This method is based on the absorption of each tape into a different body of water. These different absorptions create a ratio between the bands. These rates theoretically increase as the depth increases.

#### 2.3.2 Multi band method

The multi-band model represents more than one aspect of water depth (Stumpf et al. 2003). Z reference depth values, spectral reflection values of the $R_n$ n band, a are indeterminate coefficients.

$$Z = a_0 + a_1 ln(R_1) + a_2 ln(R_2) + \ldots . + a_n ln(R_n) \quad (2)$$

The above equation calculates unknown coefficients $a_n$ by multiple regression analysis, using $R_n$ bands against reference depth values.

#### 2.3.3 Accuracy Evaluation

The results obtained from both models were evaluated with absolute error ($D_a$), relative error ($D_b$) and RMSE ($D_c$).

$$D_a = \frac{|z_1 - z_2|}{n} \quad (3)$$

$$D_b = \frac{\sum_1^n \left|\frac{z_1 - z_2}{z_1}\right|}{n} \quad (4)$$

$$D_c = \sqrt{\frac{\sum_1^n (z_1 - z_2)^2}{n}} \quad (5)$$

$z_1$ represents the actual depth value, $z_2$ represents the calculated depth value n and the sample size.

## 3. RESULTS

Correlation analysis was performed between reference bathymetry values and band combinations to determine the most appropriate method and band

combination. Table 2 below shows the calculated correlation coefficients.

In the multi-band model, the best correlation was obtained with the combination of blue, green and red bands. In the double band ratio model, the lowest is obtained from the ratio of blue band to green band. In general, it is seen that the correlation coefficients are significant. Equation 1. regression analysis and Equation 2. As a result of multiple regression analysis, the depth estimation of the analysis area was made by calculating the m and a coefficients.

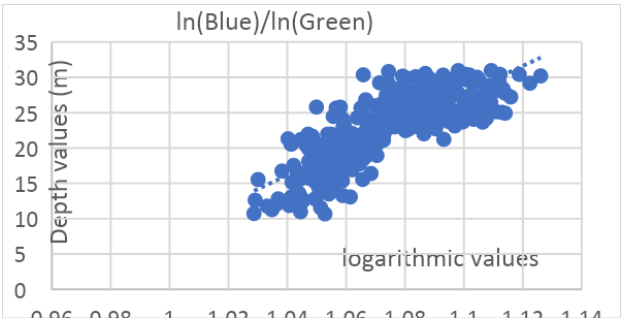


**Figure 2**. Band rate distribution

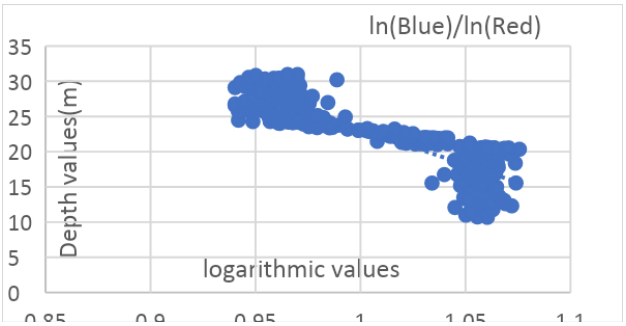


**Figure *4*.** Band rate distribution

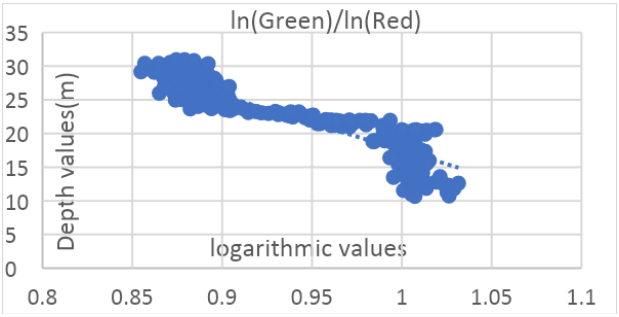


**Figure *5*.** Band rate distribution

As shown in Figures 3, 4, 5, the (blue) / ln (green) band ratio values fit better along the regression line compared to the other graphs. In ln (blue) / ln (red) and ln (green) / ln (red) band combinations, scattering from the regression line is observed in regions with a depth of 10 to 15 meters and 25 to 30 meters. . The factors causing these scattering are the fact that the red spectral band has more absorption in the water column than the other bands, resulting in a narrower spectral reflection values. This narrow spectral reflection range is thought to cause scattering in the regression line in combinations with the red band.

Using the coefficients calculated by regression analysis, Equation 1 and Equation 2 depth estimation was made at points of unknown depth.

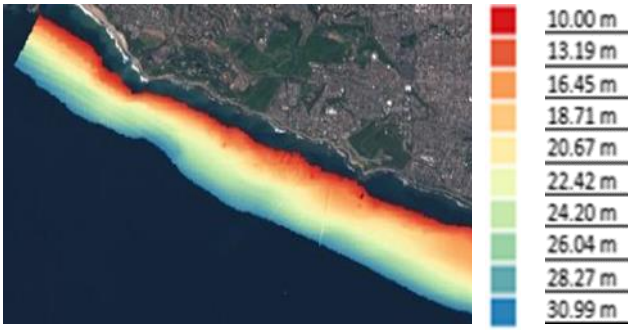


**Figure 3.** Reference bathymetry map of the study area

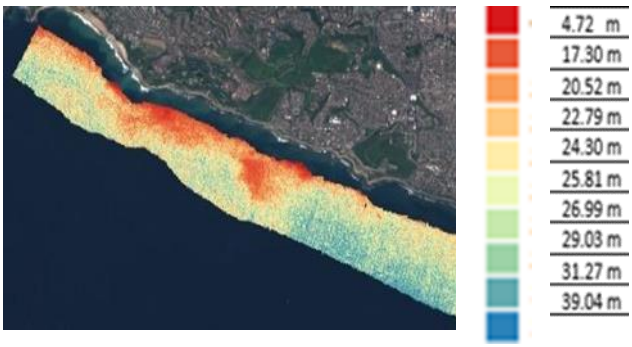


**Figure 4.** ln (blue) / ln (green) forecast bathymetry map

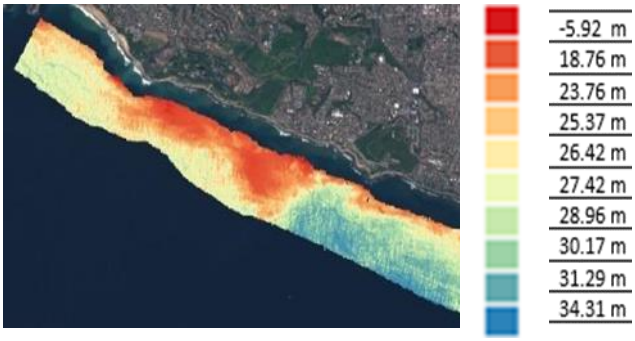


**Figure 5.** ln (green) + ln (blue) + ln (red) forecast bathymetry map

It has been observed that the estimated bathymetry maps generally have values close to each other. The best correlation was obtained from multiple regression analysis with a combination of blue, green, and red bands. The lowest correlation was calculated from the ratio of the blue band to the green band. The error from the blue, green and red band combination with the best correlation is higher than the error from the ratio of the blue band to the green band with the lowest correlation (Table 2). The reason for this error is the changes in the spectral reflection of the red band associated with the water column.

**Table 2.** Correlation and error of band groups

| Models | Dual band ratio method | | | Multi band method | |
|---|---|---|---|---|---|
| | ln(blue)/ ln(green) | ln(blue) / ln(red) | ln(green)/ ln(red) | ln(blue) / ln(green) | ln(blue)+ ln(green)+ ln(red) |
| Correlation | 0.802 | -0.884 | -0.913 | 0.966 | 0.968 |
| Absolute error | 5.364 | 5.429 | 5.431 | 5.607 | 5.951 |
| Relative error(%) | 30.199 | 32.883 | 32.233 | 32.913 | 34.669 |
| RMSE | 6.565 | 6.835 | 6.722 | 6.909 | 7.305 |

## 4. DISCUSSION

This study demonstrates the potential of Sentinel-2 satellite images to predict bathymetry at 10 m spatial resolution for Los Angeles coastal regions in low turbidity conditions. Batimetry products derived from satellites can be obtained in both models. Several researchers report that the methods are successful in shallow water areas of approximately 15 m (Kerr and Purkis 2018)

Bathymetry data derived from satellites can be used as reference data in remote areas, hard-to-reach areas or areas not drilled. Therefore, bathymetry can be considered as a potential technology in areas where research is not conducted or is insufficient.

The red band at 665nm (B04) has a narrow reflection range as a result of its interaction in the water column. This caused more scattering than other band combinations (Figure 4.) in regions with depths of 10 m and 15m and 25 m and 30m, resulting in outliers.

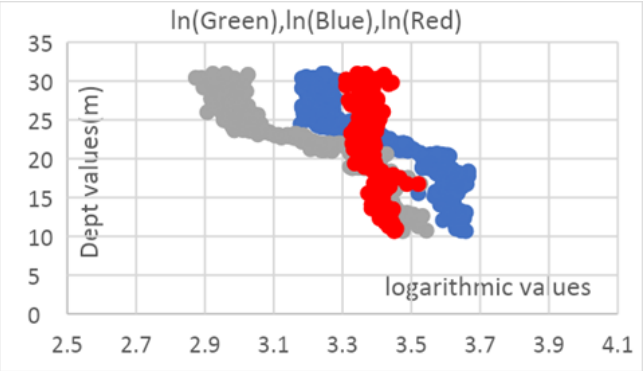


**Figure 9.** Logarithmic reflections of blue, green, red bands

## 5. CONCLUSION

In this study, Sentinel-2 demonstrates the ability to produce bathymetric maps with 10 m resolution with satellite images. The methods showed satisfactory results in shallow and less turbid waters. In band combinations with red band, it has been observed that the interaction of the red band with the water column causes more errors than the other combinations.

## ACKNOWLEDGEMENT

This work has been supported by General Directorate of Mapping Turkey. Authors acknowledge the datasets provided by Sentinel Copernicus and TCARTA.

## REFERENCES

Bailly du Bois P (2011). Automatic calculation of bathymetry for coastal hydrodynamic models. Computers & Geosciences, *37*(9), 1303-1310. https://doi.org/10.1016/j.cageo.2010.11.018

Bramante J F, Raju D K & Sin T M (2012). Multispectral derivation of bathymetry in Singapore's shallow, turbid waters. International Journal of Remote Sensing, *34*, 2070-2088. https://doi.org/10.1080/01431161.2012.734934

Caballero I & Stumpf P R (2019). Retrieval of nearshore bathymetry from Sentinel-2A and 2B satellites in South Florida coastal waters. Estuarine, Coastal and Shelf Science, *226*, 106-277. https://doi.org/10.1016/j.ecss.2019.106277

Chen B, Yang Y X D & Huang E (2019). A dual band algorithm for shallow water depth retrieval from high spatial resolution imagery with no ground truth. ISPRS Journal of Photogrammetry and Remote Sensing, *151*, 1-13. https://doi.org/10.1016/j.isprsjprs.2019.02.012

Gao J (2009). Bathymetric mapping by means of remote sensing: Methods, accuracy and limitations. Progsress in Physical Geography, *33*(1), 103-116.

Jawak S D & Luis A J (2015). Spectral Information Analysis for the Semiautomatic Derivation of Shallow Lake Bathymetry Using High-resolution Multispectral Imagery: A Case Study of Antarctic Coastal Oasis and Aquatic Procedia, *4*, 1331-1338. https://doi.org/10.1016/j.aqpro.2015.02.173

Kerr J M & Purkis S (2018). An algorithm for optically-deriving water depth from multispectral imagery in coral reef landscapes in the absence of ground-truth data. Remote Sensing of Environment, *210*, 307-324. https://doi.org/10.1016/j.rse.2018.03.024

Kumari P & Ramesh H (2020). Remote sensing image based nearshore bathymetry extraction of Mangaluru coast for planning coastal reservoir. Sustainable Water Resource Development Using Coastal Reservoirs, 247-265. https://doi.org/10.1016/B978-0-12-818002-0.00013-7

Pacheco A, Horta J, Loureiro C & Ferreira Ó (2015). Retrieval of nearshore bathymetry from Landsat 8 images: A tool for coastal monitoring in shallow waters. Remote Sensing of Environment, 102-116. https://doi.org/10.1016/j.rse.2014.12.004

Stumpf P R, Holderied K & Sinclair M (2003). Determination of water depth with high-resolution satellite imagery over variablebottom types. Limnol and Oceanog, *48*(1), 547-556. https://doi.org/10.4319/lo.2003.48.1_part_2.0547

## Surveying and Geodesy – 1

**On The Third Dimension In Robustness Analysis**

*Mevlüt Yetkin*, Muhammed Ali Aytemür, Ömer Bilginer*

**Using Interquartile Range to Detect TEC Perturbations Associated with A Tropical Cyclone Crossing through The South China Sea**

*Mohamed Freeshah*, Xiaohong Zhang, Xiaodong Ren*

**Ionospheric TEC Prediction Performance of ARIMA and LSTM Methods in Different Space Weather Conditions**

*Erman Şentürk*

**Exploring the Usability and Suitability of Smartphone Apps for Precise and Rapid Mapping Applications**

*Lukman Abdulmumin*, Olalekan Adekunle Isioye, Swafiyudeen Bawa, Ahmed Muhammed*

**Deep Learning-Based Ionospheric TEC Prediction Approach**

*İsmail Demiryege*, Mustafa Ulukavak*

**Necmettin Erbakan University Continuously Operating Reference Station**

*Omer Faruk Atiz*, Salih Alcay, Sermet Ogutcu, Ibrahim Kalayci*

Intercontinental Geoinformation Days

http://igd.mersin.edu.tr/2020/

# On the third dimension in robustness analysis

**Mevlüt Yetkin** [*1], **Muhammed Ali Aytemür** [1], **Ömer Bilginer** [1]

[1]*Izmir Katip Celebi University, Faculty of Engineering and Architecture, Department of Geomatics Engineering, Izmir, Turkey*

**Keywords**
Reliability
Robustness
Strain
Levelling network

**ABSTRACT**

Robustness analysis is a combination of Baarda's classical reliability analysis and geometrical strength analysis that is based on strain. It measures the ability of a geodetic network to oppose deformations caused by the maximum undetectable biases that are obtained from internal reliability analysis. The virtual deformations originated from undetected biases might be portrayed as displacements. The application of robustness analysis to geodetic networks depends on the dimension of the network. There are some discrepancies among the robustness analysis of levelling networks, horizontal control networks and three-dimensional networks. As well known, heights can be determined precisely in a levelling network using trigonometric heighting or differential leveling methods. Nevertheless, horizontal coordinates are generally approximately known in these types of networks. Therefore, it is needed to concentrate on the vertical displacements. In the present study, we discuss the robustness analysis of one-dimensional networks. Furthermore, some numerical examples are given.

## 1. INTRODUCTION

Traditionally, the quality of a geodetic network is measured by precision, reliability and economy. Additionally, sensitivity for deformation monitoring networks may be considered. On the other hand, as an augmentation of Baarda's reliability criterion, robustness analysis combines the criteria of reliability and geometrical strength. It is based on strain technique and measures the network ability to resist virtual deformations caused by the maximum undetectable biases. Robustness primitives, displacements and strain invariants are calculated in order to evaluate the robustness of each network point (Krakiwsky et al., 1993).

Outliers may deteriorate the least squares method's results. So, they should be determined and eliminated using an appropriate technique such as Baarda's data snooping approach. However, Baarda's test may not be successful for outlier diagnosis. There are two reasons for this: 1) insufficiently controlled observations, i.e., low redundancy numbers and 2) the effect of the power of the test, i.e., type II error. The influence of undetected biases may be evaluated using reliability analysis. Nevertheless, classical reliability analysis is dependent upon the choice of network datum. Since robustness analysis only reflects the network geometry, it is preferred (Vaníček et al., 2001; Berber, 2006).

Robustness analysis method was first developed by using Baarda's classical reliability criteria analysis approach that is based on one single outlier. However, Knight et al., (2010) presented the reliability criteria that should be used in the case of multiple outliers. Thereupon, Yetkin and Berber (2013) changed the robustness analysis by using the reliability criteria developed for multiple outliers. Naturally, the robustness of the network gets worse as the number of outliers increases.

The application of robustness analysis depends on the dimension of the network. It is generally applied to 2D networks, i.e., horizontal control networks and 3D networks such as GPS networks. However, 1D networks that are measured utilizing trigonometric levelling or geometric levelling techniques have a crucial role in Geomatics Engineering. They are vital tools to determine vertical deformations. For example, these methods may be applied in monitoring vertical crustal movements. But, undetected biases in observations may cause

* **Corresponding Author**

*(mevlut.yetkin@ikcu.edu.tr) ORCID ID 0000 – 0003 – 3438 – 1801
(m.aliaytemur@gmail.com) ORCID ID 0000 – 0002 – 2819 – 5706
(omer.bilginer@ikcu.edu.tr) ORCID ID 0000 – 0001 – 5789 – 7929

**Cite this study**

Yetkin M, Aytemür M. A & Bilginer Ö (2020). On The Third Dimension In Robustness Analysis. Intercontinental Geoinformation Days (IGD), 25-27, Mersin, Turkey

improper deformation interpretation. Thus, the robustness of a 1D network should be assessed using robustness analysis. In this paper, robustness analysis of 1D networks have been studied and some numerical computations have been performed.

## 2. ROBUSTNESS ANALSIS OF 1D NETWORKS

The displacements in the vertical direction should be considered in a 1D network. The displacement of a point $P_i$ is

$$\Delta x_i = [\Delta z_i] = [w_i] \quad (1)$$

where $w_i$ is the displacement in the z direction. It is external reliability criterion. Then, the tensor gradient with respect to position (strain matrix) is

$$E_i = \left[\frac{\partial w_i}{\partial z}\right] \quad (2)$$

The estimation of the strain matrix $E_i$ can be found in Berber (2006). It should be noted that only dilation may be defined in a 1D network. The remaining robustness primitives cannot be calculated. Dilation shows deformation (or robustness) in expansion. Some problematic cases for a 1D network should be taken into account (Berber, 2006). In robustness analysis, one may move from displacement field (external reliability) to strain field (strain matrix). However, it is possible to move from strain field to displacement field. Thus, vertical displacements for each point in the network can be computed using this procedure. The details of the computation of displacements may be found in Berber (2006).

## 3. NUMERICAL RESULTS

Three examples are given to illustrate the application of robustness analysis to the 1D networks.

**Case I:** Dilations are computed in a geometric levelling network. The network includes 4 points and 6 observations. The datum of the network is provided by minimal constraints, i.e., only one point (A) is fixed (Ghilani, 2010). The non-centrality parameter $\delta_0$ is 3.61 ($\alpha_0 = 0.05, \beta = \beta_0 = 0.05$). The redundancy numbers, internal reliability (MDB: Minimal Detectable Bias) and external reliability criteria are shown in Table 1, Table 2, and Table 3, respectively. The external reliability are for points B, C and, respectively.

**Table 1.** Redundancy number

| Observation Number | Redundancy Number |
|---|---|
| 1 | 0.6549 |
| 2 | 0.3294 |
| 3 | 0.5092 |
| 4 | 0.1877 |
| 5 | 0.4326 |
| 6 | 0.8862 |
| | ∑=3 |

**Table 2.** Internal reliability (m)

| Observation Number | MDB |
|---|---|
| 1 | 0.0265 |
| 2 | 0.0252 |
| 3 | 0.0253 |
| 4 | 0.0250 |
| 5 | 0.0220 |
| 6 | 0.0460 |

**Table 3.** External reliability (m)

| 1 | 2 | 3 | 4 | 5 | 6 |
|---|---|---|---|---|---|
| 0.0092 | -0.0053 | -0.0038 | -0.0148 | -0.0097 | 0.0029 |
| 0.0067 | 0.0116 | -0.0108 | -0.0159 | -0.0046 | 0.0052 |
| 0.0040 | 0.0006 | 0.0016 | -0.0203 | 0.0027 | 0.0018 |

The dilations are shown in Table 4. The geometry of the network is highly uniform. Thus, dilations for any observation is the same in each point.

**Table 4.** Dilations of points for 6 observations (ppm)

| Observation Number | B | C | D |
|---|---|---|---|
| 1 | 492.025 | 492.025 | 492.025 |
| 2 | 562.423 | 562.423 | 562.423 |
| 3 | -681.396 | -681.396 | -681.396 |
| *4* | *-961.068* | *-961.068* | *-961.068* |
| 5 | -433.238 | -433.238 | -433.238 |
| 6 | 325.765 | 325.765 | 325.765 |

As can be seen from Table 4, the maximum dilation is due to observation 4. It has lowest redundancy number (See Table 1). Accordingly, it causes maximum deformation in the network. Furthermore, it has the lowest standard deviation.

**Case II:** Robustness analysis has been performed in a geometric levelling network for multiple outliers. The network has 5 points and 6 observations. There are two fixed points. The data (standard deviations of observations, internal and external reliability criteria) of the network can be found in Knight et al., (2010). The computed dilations for one undetectable bias are shown in Table 5.

**Table 5.** Dilations of points for one undetected outlier (ppm)

| Observation Number | P2 | P3 | P5 |
|---|---|---|---|
| 1 | 2985.47 | 4440.24 | 227.48 |
| 2 | -1941.50 | -2598.61 | 6693.15 |
| *3* | *22453.21* | *33662.08* | *6693.15* |
| 4 | 3541.19 | 6021.11 | 551.30 |
| 5 | 4046.08 | 4550.73 | 4851.85 |
| 6 | 1694.88 | 2902.87 | 2006.79 |

The observation 3 has largest controllability value (see Knight et al., 2010). Therfore, it led to the maximum dilation.

As known from Knight et al., (2010), the external reliability values for some observation pairs are infinite. If we use these reliability analysis results then maximum dilation will be infinite. Thus, the network is not robust. The network is broken due to two undetected biases.

**Case III:** Robustness analysis of a trigonometric levelling network has been performed. The network consists of 4 points and 5 observations. The data of the network can be found in Demirel (2005). The redundancy numbers and internal reliability criteria are shown in Table 6. On the other hand, external reliability criteria are shown in Table 7.

**Table 6.** Redundancy numbers, standard deviations and internal reliability

| Redundancy Number | Standard Deviation (mgon) | MDB (mgon) |
|---|---|---|
| 0.7763 | 1.5 | 6.1458 |
| 0.8478 | 1.5 | 5.8809 |
| 0.7573 | 1.5 | 6.2226 |
| 0.3914 | 0.75 | 4.3279 |
| 0.2272 | 0.75 | 5.6803 |
| ∑=3 | | |

**Table 7.** External reliability (cm)

| 1 | 2 | 3 | 4 | 5 |
|---|---|---|---|---|
| 7.7447 | 3.6659 | 8.1684 | -10.7915 | 15.4327 |
| 3.7727 | -1.5609 | 3.9791 | 4.5948 | 22.3509 |

Dilations of points 32 and 34 are shown in Table 8.

**Table 8.** Dilations (ppm)

| Observation Number | 32 | 34 |
|---|---|---|
| 1 | 3977.60 | 7991.92 |
| 2 | 6567.96 | 8428.07 |
| 3 | 4195.21 | 8429.15 |
| *4* | *-19334.31* | *-24810.00* |
| 5 | -12839.57 | -4662.83 |

Displacements of points 32 and 34 are shown in Table 9.

**Table 9.** Displacements (cm)

| Observation Number | 32 | 34 |
|---|---|---|
| 1 | 2.0 | -1.0 |
| 2 | 2.6 | -2.0 |
| 3 | 2.2 | -4.05 |
| *4* | *-7.5* | *5.86* |
| 5 | 0.94 | 2.58 |

As can be seen from Table 8 and 9 maximum dilation and displacement are due to observation 4. It may be remedied by improving the network geometry and/or observational accuracy.

## 4. CONCLUDING REMARKS

Dilation and vertical displacement of any point in a levelling network are computed for each observation utilizing robustness analysis. The maximum of these is kept as the robustness criterion at that point. If we have calculated the displacements, we can make an evaluation by comparing with threshold values. However, the calculation of threshold values is not included in this study. Certainly, we can refer to traditional precision analysis for threshold values. This subject may be recommended as a future work.

The network geometry (redundancy numbers) and the accuracies of the observations play a crucial role in the network robustness. Additionally, the number of undetected outliers affects the robustness analysis results. The robustness of the network naturally worsens as the number of outliers that cannot be determined increases.

## REFERENCES

Berber M., (2006). Robustness analysis of geodetic networks, Technical Report No. 242, Department of Geodesy and Geomatics Engineering, University of New Brunswick, Fredericton, NB, Canada.

Demirel H., (2005), Dengeleme Hesabı, YTÜ, İnşaat Fakültesi, Sayı: İN.JFM-2005.001.

Ghilani C.D., 2010. Adjustment Computations Spatial Data Analysis, Fifth Edition, Wiley.

Knight, N.L.; Wang, J.;, & Rizos, C. (2010). Generalized measures of reliability for multiple outliers. Journal of Geodesy, 84(10), 625-635.

Krakiwsky, E. J., Vaníček, P. & Szabo,D. (1993). Further development and testing of robustness analysis. Contract rep 93-001, Geodetic Survey Division, Geomatics Canada, Ottowa.

Vaníček, P., Craymer, M. R., & Krakiwsky, E. J. (2001). Robustness analysis of geodetic horizontal networks. Journal of Geodesy, Berlin, 75,199-209.

Yetkin,M. & Berber M., (2013). Robustness analysis using the measure of external reliability for multiple outliers. Survey Review, 45, 215-219.

Intercontinental Geoinformation Days

http://igd.mersin.edu.tr/2020/

# Using Interquartile Range to Detect TEC Perturbations Associated with A Tropical Cyclone Crossing through The South China Sea

**Mohamed Freeshah** [*1,4,5], **Xiaohong Zhang** [2,3,4], **Xiaodong Ren** [2]

[1] *Wuhan University, State Key Laboratory of Information Engineering in Surveying, Mapping and Remote Sensing, Wuhan 430079, China*
[2] *Wuhan University, School of Geodesy and Geomatics, Wuhan 430079, China*
[3] *Key Laboratory of Geospace Environment and Geodesy, Ministry of Education, 129 Luoyu Road, Wuhan 430079, China*
[4] *Collaborative Innovation Center for Geospatial Technology, 129 Luoyu Road, Wuhan 430079, China*
[5] *Benha University, Faculty of Engineering at Shoubra, Surveying Engineering Department, Cairo, Egypt*

**Keywords**
GNSS
Ionosphere
Mangkhut
Interquartile Range
Total electron content

**ABSTRACT**

In this paper, we investigate the highest amplitude ionospheric variations, maximum sustained wind speed, and typhoon cloud during an extremely powerful tropical cyclone (TC) crossing through the South China Sea in September 2018 that caused extensive damage in Guam, the Philippines, and South China. Regional Ionosphere Maps (RIMs) were created through Hong Kong SatRef and IGS data around the Mangkhut Typhoon. RIMs are utilized to analyze the ionospheric response over the maximum wind speed points (maximum spots) after taking the solar-terrestrial environment and geomagnetic storm indices into consideration. The total electron content (TEC) time sequences over the maximum spots are detected by the method of interquartile range method (IQR) during super typhoon Mangkhut. The research findings indicating that significant ionospheric variations are detected over the maximum spots during the powerful typhoon within a few hours before the extreme wind speed. All the ionospheric variations are positive values. The infrared satellite snapshots confirmed that the maximum ionospheric perturbations do not coincide with the center of the storm but are detected in the area close to the typhoon edges. The possible ionospheric response mechanism is based on strong convective cells which create the gravity waves over TCs.

## 1. INTRODUCTION

Solar radiation and geomagnetic storms play a crucial role in the dynamic regime of the ionosphere (Sojka et al, 1981). However, some ionospheric perturbations should be interpreted by tropospheric activities (Chane-ming et al., 2002); (Guha et al., 2016). In 1960, the theoretical studies of atmospheric acoustic gravity waves (AGWs) have been indicated that the ionosphere could respond to severe weather activities for instance lightning, cyclones, tornadoes, and hurricanes (Hine, 1960).

For the first time, (Bauer, 1958) has reported the findings of the ionospheric response to typhoon passage where the F2 layer's critical frequency was increased when the typhoon getting close to the High-Frequency (HF) Radio station. The electric field and ion oscillation in a studied region would enhance according to the strength of the cyclone, and this depends on charged aerosols and droplets (Isaev et al., 2010, 2002). On the same side, (Sorokin et al., 2005; Pulinets et al., 2000) have reinforced that an ionospheric plasma irregularity may be generated over the regions of powerful synoptic perturbations for the electric fields.

Recently, the Global Navigation Satellite System (GNSS) has a fast development and the number of GNSS receivers has been increased globally and domestically. The ionospheric response to typhoon could be studied by using GNSS sounding and calculating the total electron content (TEC) through ground GNSS station. Although the highest amplitudes of TEC variation have been recorded during the cyclone's maximum wind speed (maximum spot) (Polyakova and Perevalova, 2013). Many previous studies have been concentrated more on ionospheric variations associated with TCs on the day of typhoon landfall (Guha et al., 2016; Jun Chen et al., 2020; Song et al., 2019). W. Li et al., 2017 have used the TEC

* **Corresponding Author**

*(mohamedfreeshah@whu.edu.cn) ORCID ID 0000-0003-3539-7450
(xhzhang@sgg.whu.edu.cn) ORCID ID xxxx-xxxx-xxxx-xxxx
(renxiaodongfly@gmail.com) ORCID ID xxxx-xxxx-xxxx-xxxx

**Cite this study**

Freeshah M, Zhang X and Ren X (2020). Using Interquartile Range to Detect TEC Perturbations Associated with A Tropical Cyclone Crossing through The South China Sea. Intercontinental Geoinformation Days (IGD), 28-31, Mersin, Turkey

maps from the Center for Orbit Determination in Europe (CODE) to detect the ionospheric disturbances during the passing of powerful TC's. The produced TEC maps from CODE have a limited spatial resolution of 2.5 degrees in latitude versus 5 degrees in longitude, moreover, it depends mainly on IGS stations.

In this study, we produced the ionosphere maps with a spatial grid 0.2*0.4 degree in latitude and longitude, respectively, with 2 hrs as a temporal resolution by using dense CORS in Hong Kong and IGS stations around the typhoon. Besides, the interquartile range method was used for checking possible TEC disturbances over maximum spots.

## 2. DATA AND METHODS

### 2.1. Space and Mangkhut data

We collected the GNSS observations from IGS and the Hong Kong Satellite Positioning Reference Station Network (SatRef) in the area around the typhoon. the F10.7 cm is an indicator of solar activity, the Disturbance storm-time (Dst), and Kp indices were obtained from NASA OmniWeb Data Explorer. The infrared (IR) satellite snapshots of typhoon Mangkhut's cloud system were selected for certain moments from the Cooperative Institute for the Meteorological Satellite Studies / University of Wisconsin-Madison.

### 2.2. Calculation of STEC, VTEC, and RIMs

We derived the Slant TEC (STEC) along the line of sight from GNSS constellation satellites to GNSS receivers through Carrier-to-Code Leveling (CCL) method for more details we can refer to (Freeshah et al., 2020; Z. Li et al., 2014). We can express the ionospheric delay in length unit and TEC as a function in ƒ frequency (f1 = 1575.42 MHz, f2 =1227.60 MHz) through the next equation:

$$TEC = \frac{I.f^2}{40.31 \times 10^{16}} \quad (1)$$

where $I$ is the ionospheric delay along a specific line of sight (LOS). According to the modeling-hypothesis of a single shell layer where the 2D modeling process assumes that the total free electrons of the whole ionosphere are concentrated in a thin layer at the elevation with the max electron density (Sidorenko and Vasenina, 2016). The slant TEC value along the LOS at the Ionospheric Pierce Point (IPP) can be converted into the corresponding vertical TEC (VTEC) by using a common ionospheric mapping-function (MF).

$$VTEC = cos\ cos\left[arcsin\ arcsin\left(\frac{R}{R+H} sinz\right)\right] STEC \quad (2)$$

where R represents the average radius of the earth, H denotes the altitude of the ionospheric shell layer, z stands for the satellite zenith angle at the receiver. A dot should be placed after the figure number. We have created a high resolution regional ionospheric maps (RIMs) of 0.2*0.4 degree in latitude and longitude, respectively, around the area of typhoon by the Spherical Harmonics expansion.

To reduce the multipath effect error, the elevation cutoff angle was set to be 15 degrees, besides, the term of windup has been adjusted by orbital information and coordinates of each station.

To discover the possible anomalous signals of the TEC variations, the TEC sequences of 10 days before 11st of September 2018 where the tropical cyclone was classified as Super Typhoon according to HKO, was used as window length to calculate the upper quartile, lower quartile, and median, denoted as QU, QL, and M, respectively, for more details we can refer to (W. Li et al., 2017). During the process of data analysis, the values of TECs over the two maximum spots at the same time are extracted from the RIMs.

The TECs have values outside corresponding to upper or lower boundaries are regarded as abnormal signals where it can be positive or negative anomalies, respectively. The TEC anomalies can last for six hours at least (W. Li et al., 2017). The TEC time series were analyzed for the next seven days (from Doy254-Doy260) during Super Typhoon Mangkhut over the two maximum spots.

## 3. RESULTS

According to the recorded data for the Maximum sustained-wind near the center of the Mangkhut, there are two points with maximum wind speed at all. Figure 1 shows the maximum wind speed is 250 km/hr over the positions (17.7 N, 123.2 E) at 23:00 HKT on 14 September 2018 and (18.0 N, 122.3 E) at 02:00 HKT on 15 September 2018.

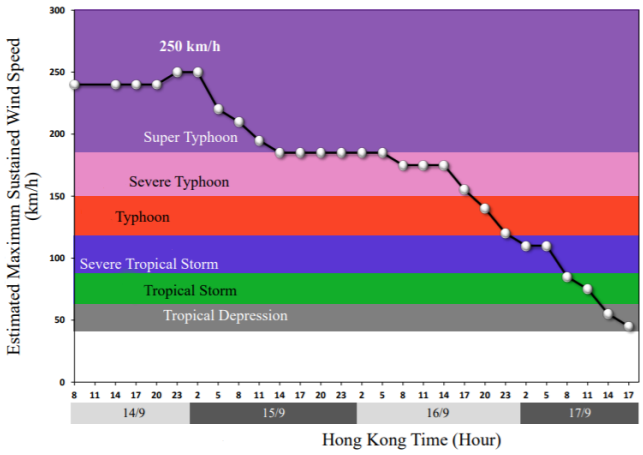


**Figure 1.** Air intensity from Sep 14th -17th with colors representing the typhoon classification

To distinguish whether the space weather impacts on TEC deviations during the typhoon, the F10.7, the Disturbance storm-time (Dst), and geomagnetic Kp indices have been investigated before analyze TEC variations associated with typhoons. Figure 2 shows no existence of a strong solar activity or geomagnetic activity. There is a low geomagnetic activity (Kp≤4), except on the Doy257 Kp≤4.3, Doy253 Kp≤5, and the Doy254 that has the highest value of Kp ≤ 6, indicating a moderate geomagnetic activity, Doy254 was excluded from the IQR window length to skip the variation based on geomagnetic activity.

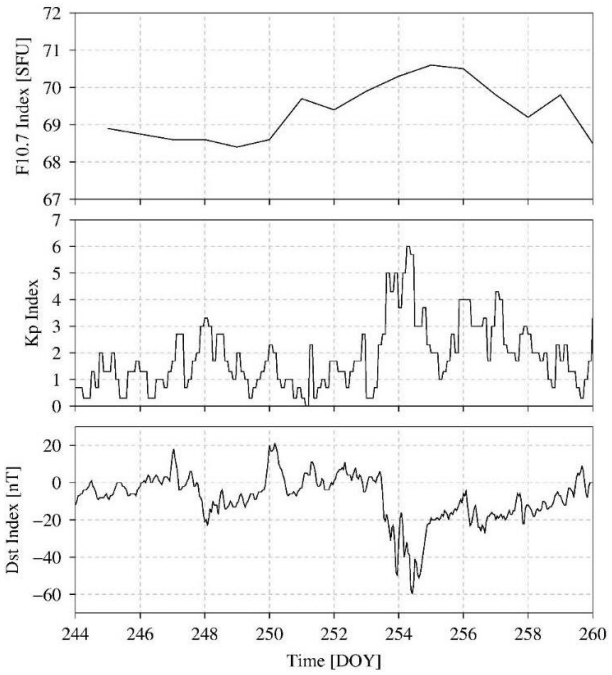


**Figure 2.** F10.7, Kp, and Dst indices in the period from DOY 244 to DOY 260 of 2018

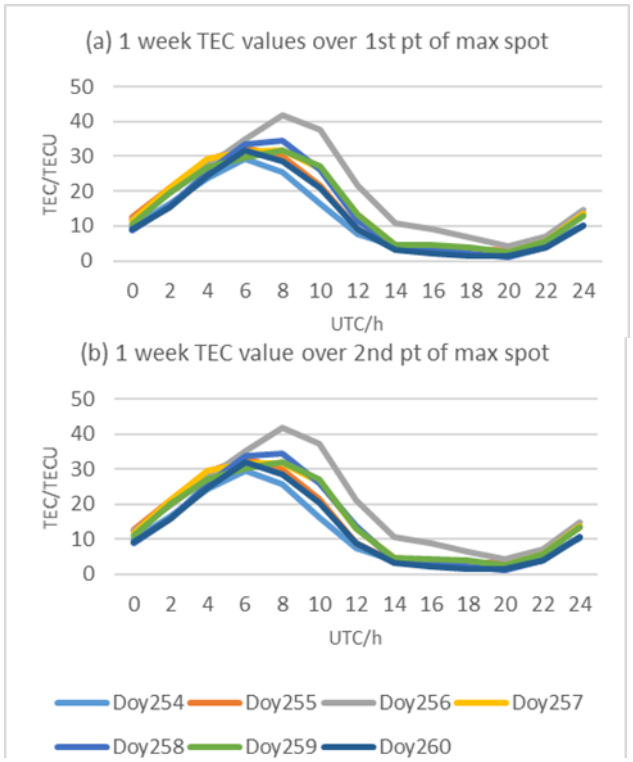


**Figure 3.** (a) and (b) TEC values over 1st and 2nd maximum spots of the Mangkhut, from Sep 11 to Sep 17

Figure 3 shows the TEC time series values for 24 hrs/week over the 1st and 2nd max spots during the typhoon. The range of 34.55-1.2 TECU was maintained for most of the time during the typhoon except for Doy256 where the range increased significantly to become 41.9-4.2 TECU, Figure 3(a). For Doy256, TEC gradually increased to the maximum value of about 8 am UT, then TEC gradually decreased. As shown in Figure 3(b), the range of 34.6-1.25 TECU was maintained for most of the time during the typhoon except for Doy256 where the range increased significantly to become 42.05-4.35 TECU. For Doy256, TEC gradually increased to the maximum value of about 8 am UT, then TEC gradually decreased.

To verify the previous TEC variations on Doy 256, parameters of interquartile range method UQ, MQ, LQ, and IQR were calculated from the 10 days before the Mangkhut typhoon (from Doy244-Doy253). l1 and l2 can be calculated by taking twice the IQR as a tolerance (~2.7 standard deviations), where l1 and l2 are the lower and upper boundaries, respectively. Figure. 4 shows the TEC time series of Doy256 in gray color versus the lower and upper boundaries in blue and orange colors, respectively. Figure. 4(a) and (b) show significantly increased in TEC over the 2 maximum wind speed points last about 6–14 UT. The lower and upper boundaries used to discriminate the ionospheric anomalies response to typhoon depend on the IQR through the 10 previous days before the cyclone converted into a super typhoon. It is worth indicating that the ionospheric disturbances showed in Figure 4 is a positive value and agree with the general behavior in Figure 3.

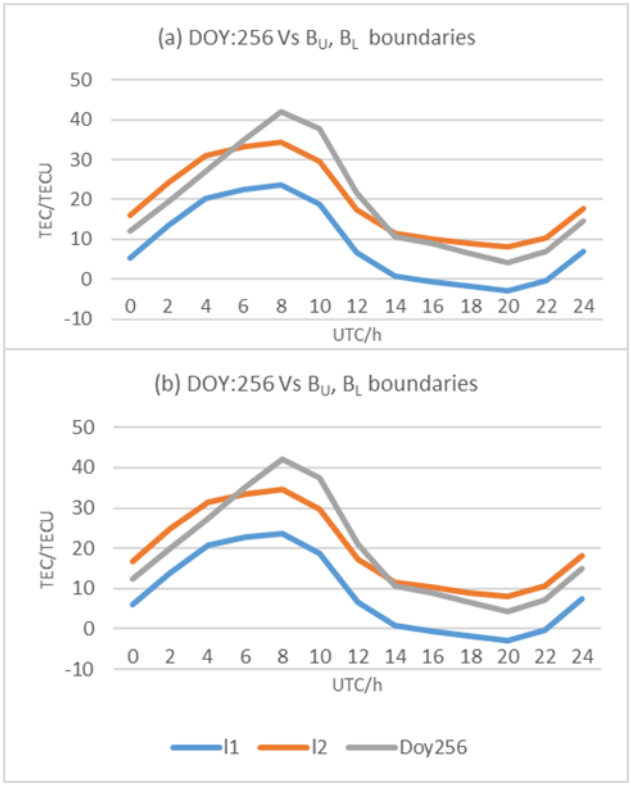


**Figure 4.** (a) and (b) TEC lower and upper boundaries (l1 and l2, respectively) of the IQR method versus the TEC sequences of Doy256

## 4. DISCUSSION

(Polyakova and Perevalova, 2013; W. Li et al., 2017) have shown that during the day of the maximum wind speed value over the TC, the highest amplitude of TEC variation was observed. In contrast, the current study showing that the highest TEC variation amplitude was observed on September 13 (Doy256) when the wind speed in the TC had a second-highest value. To interpret the possible reasons, the infrared satellite snapshots of typhoon cloud at 4 selected time instances are depicted in Figure 5. The red triangle shows the maximum spots.

The panels (a) to (d) show the position and tracking of the Typhoon direction from southeast to northwest and ended on 16th September (panel (d)). Panel (b) shows an instance on 13th September where the maximum spot is far away from the typhoon's center (eye) and more close to the edge of the typhoon, meanwhile, panel (c) shows the maximum spot close to the typhoon's eye on September 14 (the day of maximum wind speed), that could explain why the highest TEC variations have happened in the second-highest wind speed where the magnitude of the ionospheric perturbation is depending on the distance away/close from the typhoon (Jun Chen et al., 2020). This implies that ionospheric perturbations in the eye of the storm are fewer than those at the edges of cyclones (W. Li et al., 2017).

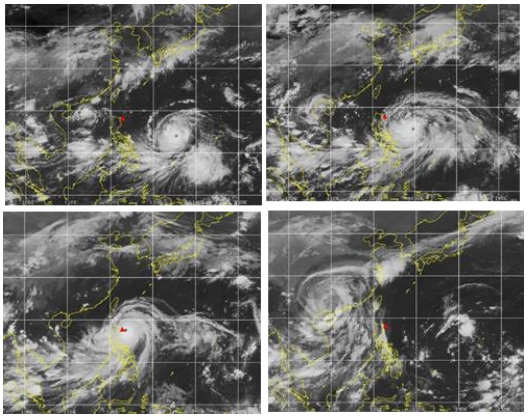

**Figure 5.** IR satellite snapshots of typhoon cloud at 4-time instances, the red triangle denotes maximum spots, (a): 04:30/12 (UTC); (b) 07:30/13; (c) m, (d) 22:30/16

**REFERENCES**


Bauer, S. J. (1958). Correlations between tropospheric and ionospheric parameters. Geofisica Pura e Applicata, 40, 235–240. https://doi.org/https://doi.org/10.1007/BF0198131

Chane-ming, F., Roff, G., Robert, L., & Leveau, J. (2002). Gravity wave characteristics over Tromelin Island during the passage of cyclone Hudah. Geophysical Research Letters, 29(6). https://doi.org/http://dx.doi.org/10.1029/2001G013286

Freeshah, M., Zhang, X., Chen, J., Zhao, Z., Osama, N., Sadek, M., & Twumasi, N. (2020). Detecting Ionospheric TEC Disturbances by Three Methods of Detrending through Dense CORS During A Strong Thunderstorm. Annals of Geophysics. In Press

Guha, A., Paul, B., Chakraborty, M., & De, B. K. (2016). Tropical cyclone effects on the equatorial ionosphere: First result from the Indian sector. Journal of Geophysical Research: Space Physics, 121, 5764–5777. https://doi.org/10.1002/2016JA022363.

Hine, C. O. (1960). Internal atmospheric gravity waves at ionospheric heights. Canadian Journal of Physics, 38(11).

Jun Chen, Xiaohong Zhang, Xiaodong Ren, Jincheng Zhang, Mohamed Freeshah, & Zhibo Zhao. (2020). Ionospheric disturbances detected during a typhoon based on GNSS phase observations: A case study for typhoon Mangkhut over Hong Kong. Advances in Space Research, In press. https://doi.org/https://doi.org/10.1016/j.asr.2020.06.006

Li, W., Yue, J., Yang, Y., Li, Z., Guo, J., Pan, Y., & Zhang, K. (2017). Analysis of ionospheric disturbances associated with powerful cyclones in East Asia and North America. Journal of Atmospheric and SolarTerrestrial Physics, 161(June), 43–54. https://doi.org/10.1016/j.jastp.2017.06.012

Li, Z., Yuan, Y., Fan, L., Huo, X., & Hsu, H. (2014). Determination of the Differential Code Bias for Current BDS Satellites. IEEE Transactions on Geoscience and Remote Sensing, 52(7), 3968–3979. https://doi.org/10.1109/TGRS.2013.2278545

N. V. Isaev, V. M. Kostin, G. G. Belyaev, O. Ya. Ovcharenko, & E. P. Trushkina. (2010). Disturbances of the topside ionosphere caused by typhoons. Geomagnetism and Aeronomy, 50, 243–255. https://doi.org/https://doi.org/10.1134/S001679321002012X

N. V. Isaev, V. M. Sorokin, V. M. Chmyrev, O. N. Serebryakova, & A. K. Yashchenko. (2002). Disturbance of the Electric Field in the Ionosphere by Sea Storms and Typhoons. Geomagnetism and Aeronomy, 40(5), 638–643.

Polyakova, A. S., & Perevalova, N. P. (2013). Comparative analysis of TEC disturbances over tropical cyclone zones in the North-West Pacific Ocean. Advances in Space Research, 52(2013), 1416–1426. https://doi.org/10.1016/j.asr.2013.07.029

S. A. Pulinets, K. A. Boyarchuk, V. V. Hegai, V. P. Kim, & A. M. Lomonosov. (2000). Quasielectrostatic model of atmosphere-thermosphere-ionosphere. Advances in Space Research, 26(8), 1209–1218.https://doi.org/https://doi.org/10.10-16/S0273-1177(99)01223-5

Sidorenko, K. A., & Vasenina, A. A. (2016). Ionospheric parameters estimation using GLONASS / GPS data. Advances in Space Research, 57, 1881–1888. https://doi.org/10.1016/j.asr.2016.01.025

Sojka, J. J., Raitt, W. J., & Schunk, R. W. (1981). Theoretical predictions for ion composition in the high-latitude winter F-region for solar minimum and low magnetic activity. J. Geophys. Res., 86, 2206– 2216. https://doi.org/https://doi.org/10.1029/JA086iA04p02206

Song, Q., Ding, F., Zhang, X., Liu, H., Mao, T., Zhao, X., & Wang, Y. (2019). Medium-Scale Traveling Ionospheric Disturbances Induced by Typhoon Chan-hom Over China. Journal of Geophysical Research: Space Physics, 124(3), 2223–2237. https://doi.org/10.1029/2018JA026152

Sorokin, V. M., Isaev, N. V, Yaschenko, A. K., Chmyrev, V. M., & Hayakawa, M. (2005). Strong DC electric field formation in the low latitude ionosphere over typhoons. Atmospheric and Solar-Terrestrial Physics, 67(2005), 1269–1279. https://doi.org/10.1016/j.jastp.2005.06.014

Intercontinental Geoinformation Days

http://igd.mersin.edu.tr/2020/

# Ionospheric TEC Prediction Performance of ARIMA and LSTM Methods in Different Space Weather Conditions

**Erman Şentürk**[*1]

[1]*Kocaeli University, Faculty of Engineering, Department of Geomatics, Kocaeli, Turkey*

**Keywords**
ARIMA
Geomagnetic Storm
Ionosphere
LSTM
TEC Prediction

**ABSTRACT**

The ionosphere has some temporal regular changes under the dominant control of the Sun. The stationary structure of the ionospheric time series (e.g. TEC, foF2) allows it to be modeled on a specific time. In this study, we tested the performance of the artificial intelligent (AI) techniques e.g. a machine learning-based method, autoregressive integrated moving average (ARIMA), and a deep learning-based method, long short-term memory (LSTM) network to the prediction of Total Electron Content (TEC) values. The TEC data of six different locations in low, middle, and high latitudes were selected from the Center for Orbit Determination in Europe – Global Ionosphere Maps (CODE-GIMs). To show the performance of the proposed methods during quiet space weather and a severe geomagnetic storm, we trained the 60 days TEC data (24 data points in one day) and forecasted the TEC data of the subsequent five days by fitted models with optimal hyperparameters. The forecasted TEC values were compared with observed TEC through some statistical metrics (RMS, MAE). The results indicated that the LSTM is more successful in TEC prediction than ARIMA. This study brings new insights into the AI techniques in the ionospheric TEC prediction.

## 1. INTRODUCTION

The ionosphere is a three-dimensional dispersive medium atmosphere layer whose primary driver is the Sun. The layer locates above approximately 50-1000 km from the Earth's surface and includes molecules with potential for photoionization. When molecules are exposed to light energy emitted from the Sun, their components are divided into atoms, which are negative electrons and positive ions. Negatively charged electrons affect the propagation of electromagnetic signals traveling between the earth and space.

The number of free electrons is described by the Total Electron Content (TEC) parameter. The TEC describes the number of free electrons in a cylinder with a 1 $m^2$ base area throughout the line-of-sight (LOS). The unit of the TEC (TECU) is equal to $10^{16}$ electron/$m^2$. TEC values have periodic temporal and spatial variations such as the diurnal, 27-day, seasonal, semi-annual, annual, and 11-year under control of the Sun (Vaishnav et al., 2019).

The TEC also increase/decrease due to space weather events such as solar winds, solar flares, geomagnetic storms (Bagiya et al., 2009), earthquakes (Şentürk et al., 2019), tsunamis (Occhipinti et al., 2013), volcanic eruptions (Dautermann et al., 2009), hurricanes/typhoons (Chen et al., 2020) and anthropogenic events (Lin et al., 2017). These events generally cause non-secular changes and affect the regular change of TEC variation.

There are some traditional time series analysis methods to modeling the TEC time series, but these methods are not adequate to simulation the previous TEC observation and the pattern that is far away from forecasting-initial-point, as any artificial intelligence (AI) algorithms. However, AI method such as ARIMA and LSTM learns the trend, seasonality, and residuals patterns in the TEC time series and successfully forecasting TEC values for a short period. Some AI-based methods were previously utilized to forecast ionospheric parameters (McKinnell and Poole, 2004; Athieno et al., 2017; Sai Gowtam and Tulasi Ram, 2017; Srivani et al., 2019; Kaselimi et al., 2020; Ruwali et al., 2020).

In this study, we discussed the advantages and disadvantages of the ARIMA and LSTM methods for ionospheric TEC forecasting. For this purpose, TEC data of CODE-GIMs were obtained in low, middle, and high latitudes of the hemispheres during quiet space weather and geomagnetic storm. The forecasting performance of the methods was compared using some statistical metrics.

* **Corresponding Author**

* (erman.senturk@kocaeli.edu.tr) ORCID ID 0000-0002-0833-7113

**Cite this study**

Şentürk E (2020). Ionospheric TEC Prediction Performance of ARIMA and LSTM Methods in Different Space Weather Conditions. Intercontinental Geoinformation Days (IGD), 32-35, Mersin, Turkey

## 2. METHOD

We have fitted two models to forecast TEC values; the ARIMA and LSTM. The ARIMA is a statistical, traditional, machine learning approach while LSTM is a more advanced version of a special kind of Artificial Neural Network (ANN) named Recurrent Neural Network (RNN). We split our analysis into three divisions: (1) data collection and pre-processing, (2) formulation of the models, and (3) implementations which are the following:

### 2.1. Data Collection and Pre-processing

The TEC time series of $75^0$N-S (high latitude), $45^0$N-S (middle latitude), and $15^0$N-S (low latitude) at prime meridian were obtained from GIMs produced by the CODE. These GIMs are gridded between $\pm 87.5^0$ N-S and $\pm 180^0$ W-E with a $2.5^0$x$5^0$ spatial resolution, respectively, and with a 1-hour temporal resolution. The gridded TEC values are published by files in the Ionosphere Map Exchange Format (IONEX), which is freely available in ftp://cddis.gsfc.nasa.gov/gps/products/ionex/.

We selected the TEC data at a two-time interval for quiet space weather (from February 27 to May 01, 2020) and a geomagnetic storm (from June 28 to August 31, 2018). The geomagnetic storm is identified by the disturbance storm-time (Dst) index which decreased to -174 nT on August 26, 2018. This Dst value indicates a severe geomagnetic storm. Also, the quiet space weather period is decided by threshold values of Dst > -20 nT, solar radio flux (F10.7) < 90 sfu. The indices are available at https://omniweb.gsfc.nasa.gov/form/dx1.html.

### 2.2. Model formulation

#### 2.2.1. Autoregressive Integrated Moving Average (ARIMA)

ARIMA is a time series model based on traditional statistical concepts and integration of two methods: Auto Regression (AR), and Moving Average (MA).

An ARIMA model can be defined as three parameters: (1) p is the number of autoregressive terms, (2) d is the number of nonseasonal differences needed for stationarity, and (3) q is the number of moving averages.

Jenkins and Box proposed a method to get the order of ARIMA using the autocorrelation function (ACF) and the partial autocorrelation function (PACF) of the sample data (Bartholomew, 2020). The parameters, q calculates using ACF plot and p obtains from the PACF plot.

We can formulate ARIMA (p, d, q) as follows:

$$Y_t = \delta + \alpha_1 Y_{t-1} + \alpha_2 Y_{t-2} + \alpha_3 Y_{t-3} + \cdots + \alpha_p Y_{t-p} + \varepsilon_t - \theta_1 \varepsilon_{t-1} - \theta_2 \varepsilon_{t-2} - \theta_3 \varepsilon_{t-3} - \cdots - \theta_q \varepsilon_{t-q} \quad (1)$$

where $\delta$ is a constant, $Y_t$ is linear combinations of the previous time-series terms with the coefficients $\alpha_1, \alpha_2, \alpha_3, \ldots, \alpha_p$ and $\varepsilon_t$ is a random shock at time t.

#### 2.2.2. Long Short Term Memory (LSTM) Network

Time series is a very special type of data in which dependent and independent variables are the same, and the target attribute depends on its previous observations rather than on the independent variables.

TEC variation has the same daily min-max values with little erratum but this erratum becomes high during any special events (e.g. magnetic storms, solar activity, or earthquakes). Traditional ANN is advanced enough to capture and learn the irregularity in the TEC data and forecast upcoming value but being a time series data it is highly correlated with the previous terms. So, RNN is used to pass previous learning to the adjacent nodes. Although RNN predicts well, it does not have any memory power to keep within whatever it has learned from the nodes that are far away from the current node. This problem is also known as a vanishing gradient problem. LSTM comes into existence to overcome the problem of the vanishing gradient. The special architectures of the LSTM-RNN network (Fig. 1) made it possible to keep those learning within the network and forecast based on these learning.

LSTM networks have four components: Cell State, Input Gate, Forget Gate, and Output Gate (Fig.1b).

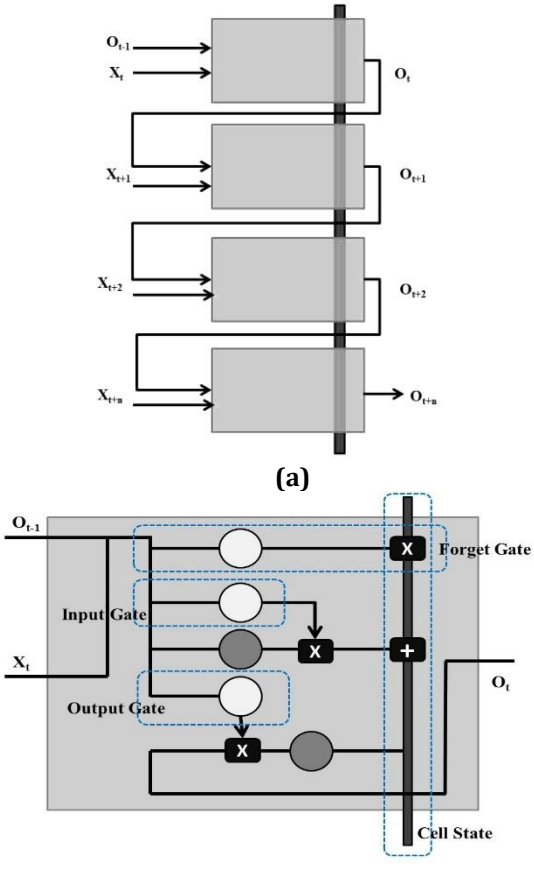


**Figure 1.** The architecture of LSTM. (a) The complete connected architecture of LSTM-RNN, (b) One-single-node representation of LSTM-RNN.

### 2.3. Implementations

We have split our dataset into two-part; training dataset and test dataset. The training data for quiet space weather include 60 days from Feb 27 to Apr 26, 2020, and test data includes the subsequent 5 days between Apr 27 and May 1, 2020. Also, the training data for geomagnetic storm includes 60 days from Jun 28 to Aug

26, 2018, and test data includes 5 days on Aug 27-31, 2018.

ARIMA and LSTM models were implemented in the MATLAB R2019b using Econometrics and Deep Learning Toolboxes.

Two statistical metrics employed to evaluate the performance of the proposed models; Maximum Absolute Error (MAE) and Root Mean Square (RMS) error.

$$MAE = \max(|TEC_{Forecast} - TEC_{Observed}|) \quad (2)$$

$$RMS = \sqrt{\frac{1}{n}\sum_{i=1}^{n}(TEC_{Forecast}\text{-}TEC_{Observed})^2} \quad (3)$$

## 3. RESULTS

In this section, we showed our ARIMA and LSTM results only at 15⁰ N and 45⁰ S for both quiet space weather and geomagnetic storm, respectively.

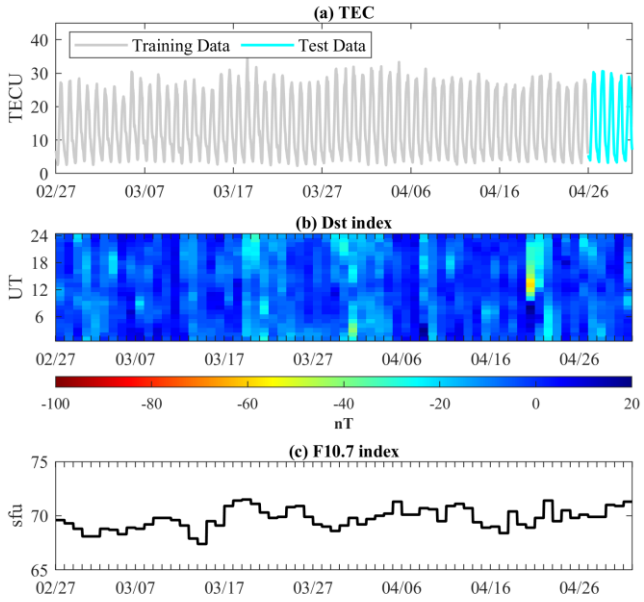


**Figure 2.** (a) TEC time series at 15⁰ N, (b) Dst index, (c) F10.7 index from Feb 27 to May 1, 2020. The gray and cyan lines indicate training and test data, respectively.

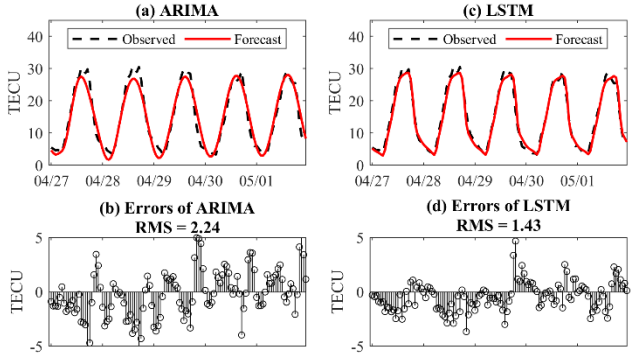


**Figure 3.** (a-c) Observed TEC at 15⁰ N and Forecast TEC calculated by ARIMA and LSTM methods (b-d) Errors from Apr 27 to May 1, 2020.

In Fig. 2, we showed the time series of TEC, Dst, and F10.7 for the quiet space weather period. The Dst values range between -59 nT and 20 nT and F10.7 values range between 67.4-71.5 sfu. These values indicate quiet space weather for ionospheric variation except for Apr 20, 2020. A moderate geomagnetic storm (Dst < -50 nT between 11-13 UT) occurred on the relevant day.

In Fig. 3, we showed the observed TEC, forecast TEC, and RMS errors of proposed methods for the quiet space weather period. We forecasted TEC values with an accuracy of 2.24 and 1.43 TECU for ARIMA and LSTM methods, respectively.

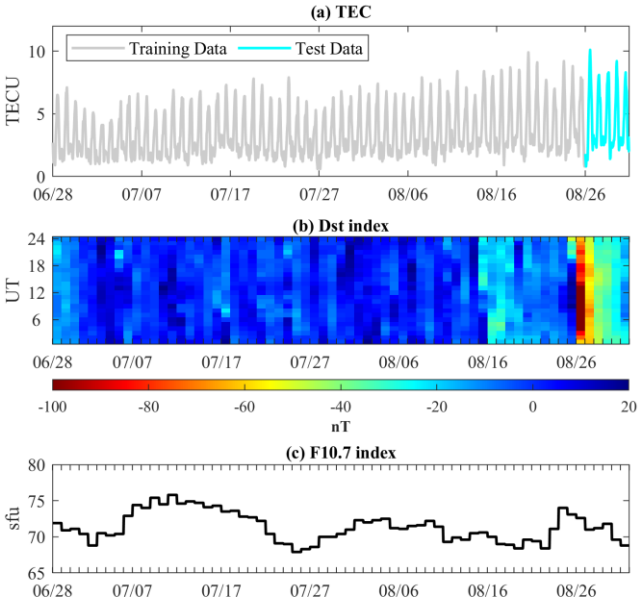


**Figure 4.** (a) TEC time series at 45⁰ S, (b) Dst index, (c) F10.7 index from Jun 28 to Aug 31, 2018. The gray and cyan lines indicate training and test data, respectively.

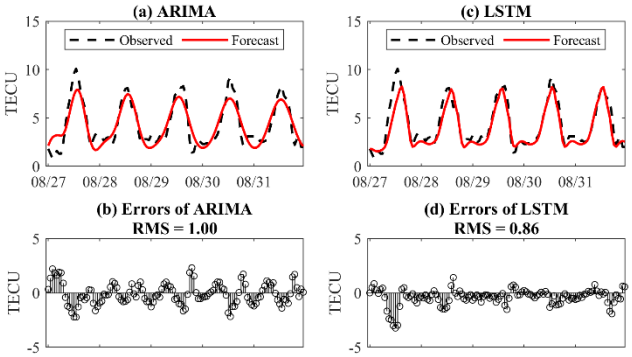


**Figure 5.** (a-c) Observed TEC at 45⁰ S and Forecast TEC calculated by proposed methods (b-d) Errors from Aug 27 to Aug 31, 2020.

In Fig. 4, we showed the time series of TEC, Dst, and F10.7 for the geomagnetic storm period. The Dst values range between -174 nT and 21 nT and F10.7 values range between 67.9-75.8 sfu. The F10.7 values indicate quiet space weather for ionospheric variation in training data but the Dst value of -174 nT indicates a severe geomagnetic storm on August 26, 2018 (in test data).

In Fig. 5, we showed the observed TEC, forecast TEC, and RMS errors of proposed methods for the geomagnetic storm period. We forecasted TEC values with an accuracy of 1.00 and 0.86 TECU for ARIMA and LSTM methods, respectively.

We also showed the RMS and MAE values of proposed methods for other locations in Table 1.

**Table 1.** RMS and MAE values (in TECU) of proposed methods for quiet space weather and geomagnetic storm

| Locations | Quiet Space Weather | | | | Geomagnetic Storm | | | |
|---|---|---|---|---|---|---|---|---|
| | ARIMA | | LSTM | | ARIMA | | LSTM | |
| | RMS | MAE | RMS | MAE | RMS | MAE | RMS | MAE |
| 75⁰ N | 0.61 | 1.25 | 0.88 | 2.95 | 0.96 | 2.95 | 0.95 | 2.60 |
| 45⁰ N | 1.28 | 2.67 | 1.05 | 3.15 | 1.12 | 2.56 | 1.13 | 2.66 |
| 15⁰ N | 2.24 | 6.22 | 1.43 | 4.66 | 3.77 | 11.24 | 2.90 | 9.42 |
| 15⁰ S | 2.28 | 5.56 | 1.46 | 4.03 | 2.48 | 5.46 | 2.76 | 9.34 |
| 45⁰ S | 1.71 | 6.60 | 0.80 | 2.57 | 1.00 | 2.30 | 0.86 | 3.23 |
| 75⁰ S | 0.85 | 1.88 | 0.83 | 1.84 | 1.29 | 3.41 | 1.38 | 3.79 |

## 4. CONCLUSION

In this study, the TEC data of six different locations were used to analyze the prediction performance of ARIMA and LSTM methods in different locations and space weather conditions.

We showed that both ARIMA and LSTM are successful for forecasting ionospheric TEC, but LSTM is more accurate than the ARIMA model. While LSTM produced better results especially in the low and middle latitudes, there was no significant difference between both methods in the high latitudes. Also, both methods generally predicted TEC values with lower RMS in the quiet space weather period than the geomagnetic storm period.

In the study, we have seen the capabilities and abilities of the AI-based models in forecasting the TEC time series. We showed that deep learning methods provide more accurate forecasting TEC data.

## ACKNOWLEDGEMENT

The author is thankful to the CODE for providing the GIMs, and NASA for providing the space weather indices.

## REFERENCES

Athieno, R., Jayachandran, P. T., & Themens, D. R. (2017). A neural network-based foF2 model for a single station in the polar cap. Radio Science, 52(6), 784-796.

Bagiya, M. S., Joshi, H. P., Iyer, K. N., Aggarwal, M., Ravindran, S., & Pathan, B. M. (2009). TEC variations during low solar activity period (2005–2007) near the equatorial ionospheric anomaly crest region in India. Annales Geophysicae, 27(3), 1047-1057.

Bartholomew D. J. (2020). Time Series Analysis Forecasting, Operational Research Quarterly, 22(2), 199-201.

Chen, J., Zhang, X., Ren, X., Zhang, J., Freeshah, M., & Zhao, Z. (2020). Ionospheric disturbances detected during a typhoon based on GNSS phase observations: A case study for typhoon Mangkhut over Hong Kong. Advances in Space Research, 66(7), 1743-1753.

Dautermann, T., Calais, E., Lognonné, P., & Mattioli, G. S. (2009). Lithosphere-atmosphere-ionosphere coupling after the 2003 explosive eruption of the Soufriere Hills Volcano, Montserrat. Geophysical Journal International, 179(3), 1537-1546.

Kaselimi, M., Voulodimos, A., Doulamis, N., Doulamis, A., & Delikaraoglou, D. (2020). A Causal Long Short-Term Memory Sequence to Sequence Model for TEC Prediction Using GNSS Observations. Remote Sensing, 12(9), 1354.

Lin, C. C., Shen, M. H., Chou, M. Y., Chen, C. H., Yue, J., Chen, P. C., & Matsumura, M. (2017). Concentric traveling ionospheric disturbances triggered by the launch of a SpaceX Falcon 9 rocket. Geophysical Research Letters, 44(15), 7578-7586.

McKinnell, L. A., & Poole, A. W. (2004). Predicting the ionospheric F layer using neural networks. Journal of Geophysical Research: Space Physics, 109(A8).

Occhipinti, G., Rolland, L., Lognonné, P., & Watada, S. (2013). From Sumatra 2004 to Tohoku-Oki 2011: The systematic GPS detection of the ionospheric signature induced by tsunamigenic earthquakes. Journal of Geophysical Research: Space Physics, 118(6), 3626-3636.

Ruwali, A., Kumar, A. S., Prakash, K. B., Sivavaraprasad, G., & Ratnam, D. V. (2020). Implementation of Hybrid Deep Learning Model (LSTM-CNN) for Ionospheric TEC Forecasting Using GPS Data. IEEE Geoscience and Remote Sensing Letters. DOI: 10.1109/LGRS.2020.2992633

Sai Gowtam, V., & Tulasi Ram, S. (2017). An Artificial Neural Network-Based Ionospheric Model to Predict NmF2 and hmF2 Using Long-Term Data Set of FORMOSAT-3/COSMIC Radio Occultation Observations: Preliminary Results. Journal of Geophysical Research: Space Physics, 122(11), 11-743.

Srivani, I., Prasad, G. S. V., & Ratnam, D. V. (2019). A deep learning-based approach to forecast ionospheric delays for GPS signals. IEEE Geoscience and Remote Sensing Letters, 16(8), 1180-1184.

Şentürk, E., Livaoğlu, H., & Çepni, M. S. (2019). A Comprehensive Analysis of Ionospheric Anomalies before the Mw 7.1 Van Earthquake on 23 October 2011. The Journal of Navigation, 72(3), 702-720.

Vaishnav, R., Jacobi, C., & Berdermann, J. (2019). Long-term trends in the ionospheric response to solar extreme-ultraviolet variations. In Annales Geophysicae, 37(6), 1141-1159.

Intercontinental Geoinformation Days

http://igd.mersin.edu.tr/2020/

# Exploring the Usability and Suitability of Smartphone Apps for Precise and Rapid Mapping Applications

**Lukman Abdulmumin** [*1], **Olalekan Adekunle Isioye** [1], **Swafiyudeen Bawa**[1], **Ahmed Muhammed**[1]

[1]*Ahmadu Bello University, Faculty of Environmental Design, Department of Geomatics, Zaria, Nigeria*

**Keywords**
Smartphones
Global Navigation Satellite System (GNSS)
Global Positioning System (GPS)
Positioning Accuracy

**ABSTRACT**

This study explored the usability and suitability of freely available smartphone positionig apps for precise and rapid mapping applications. The study takes eight smartphone applications (GPS Data, Geo-location, Map coordinate, My GPS location, Mobile Topographer, Super GEO GPS, UTM GEOMAP and GNSS logger Application) and Garmin Map76s handheld GPS into consideration with observations from Hi-Target V30 GNSS receiver as basis for comparison. Eleven stations distributed all over the main Campus of Ahmadu Bello University in Nigeria were used for the study. The study treated Garmin Map76s and seven smartphone applications (GPS Data, Geo-location, Map coordinate, My GPS location, Mobile Topographer, Super GEO GPS, and UTM GEOMAP) first. Garmin Map76s turns out to be the best with an RMSE value less than 0.3m on both easting and northing components. UTM GEOMAP gave the best result among the seven smartphone applications with and RMSE value of 0.3m on both easting and northing. The GNSS logger application used on a Samsung galaxy S9+ was later treated separately and compared its performance alongside the Hi-Target V30 observation. The application performed well at most of the stations but showed less precision to the Hi-Target V30 observation but assumably better than the oyther positioning apps.

## 1. INTRODUCTION

Numerous applications in surveying and mapping have been made easier and more exact because of the advent of the Global Navigation Satellite System (GNSS), and along these lines, the interest for utilizing forefront GNSS strategies in surveying and mapping applications have become imperative. GNSS is one of the most creative and useful advances created as of late. Since its origin, it has developed to give overall all-weather navigation as well as exact position assurance capacities to all users particularly for surveying and geodetic applications (Isioye et al. 2018).

The GNSS receivers in smartphones normally belong to the family of 'high-sensitivity' receivers that are equipped for receiving GNSS signals with a power ratio under −150 dBm which is higher than that of a typical receiver (around −130 dBm) (Tomaštík et al., 2020). The Assisted-GPS function of a smartphone utilizes the capacity of the smartphones to connect with the Web to determine data about satellite signals, which ought to be accessible in the estimated area of the smartphone. Hence, the receiver doesn't need to look through every single imaginable signal and the time to First Fix can be lessened. Generally, mid-and high-level smartphone GNSS receivers can get signals from different satellite systems. There are receivers equipped for getting signals from all systems operational at a global scale including GPS (USA), GLONASS (Russia), Galileo (EU), Beidou (China) just as Regional systems, like QZSS of Japan and IRNSS of India (Tomaštík et al., 2020). Many usable satellites offer better positioning.

The GNSS antenna contained within the smartphone uses linear polarization, making it especially liable to multipath effects resulting from GNSS signals bouncing off the ground or nearby surfaces before reaching the antenna (Schwieger and Gläser 2005). In the process of computing the observations, the GNSS receiver must discriminate between the direct signal and the reflected ones, resulting in noisier and possibly biased measurements. More often than not the accuracy of positioning apps in the smartphone are degraded by these conditions.

It is a well-known fact that the accuracy of smartphone apps for the survey is very low compared to the geodetic grade receiver. Many studies have focused on the evalaution of the performances of smartphones apps ( see, Bauer 2013; Hwang et al., 2012; Lee et al., 2017; Merry and Bettinger, 2019; Paziewski, 2020; Schaefer and Woodyer, 2015; Szot et al. 2019; Tomastík et al., 2017; Tomaštík et al., 2020).

* **Corresponding Author**

*(labdulmumin54@gmail.com) ORCID ID 0000–0003– 0750–3914
(olalekanisioye@gmail.com) ORCID ID 0000-0001-5734-5374
(bswafiyudeen@gmail.com) ORCID ID 0000-0002-2384-9432

**Cite this study**

Abdulmumin L, Isioye O. A, Bawa S, & Muhammed A (2020). Exploring the Usability and Suitability of Smartphone Apps for Precise and Rapid Mapping Applications. Intercontinental Geoinformation Days (IGD), 36-39, Mersin, Turkey

This study aims to explore the usability and suitability of smartphone applications for precise and rapid mapping applications.

## 2. METHOD

Data used for this study were obtained from a geodetic grade GNSS receiver (Hi-Target V30), Garmin Map76s (handheld GPS) and eight Android Smartphone Applications (GPS Data, Geo-location, Map coordinate, My GPS location, Mobile Topographer, Super GEO GPS, UTM GEOMAP and GNSS logger Apps of Samsung S9+) stationed over 11 stations distributed all over the Ahmadu Bello University (ABU) Main Campus, Zaria. Each smartphone application was allowed to observe for a period of 20 minutes. The Fig.1 shows the distibution of the stations within the ABU main campus.


**Figure 1**. Distribution of Eleven Verification Stations within the Campus of ABU

Observations from seven smartphone applications and the Garmin Map76s were in direct coordinates. On the contrary, those obtained from the geodetic grade receiver and the GNSS logger application of Samsung galaxy S9+ were in Receiver Independent Exchange format (RINEX) files which were further processed in order to obtain the respective coordinates of individual stations. The Hi-Geomatics Office (HGO) and GNSS analysis window software were respectively used to accomplish the task.

Results from Garmin Map76s and seven smartphone applications (i.e. GPS Data, Geo-location, Map coordinate, My GPS location, Mobile Topographer, Super GEO GPS, and UTM GEOMAP) were treated separately. The GNSS logger Apps of Samsung S9+ was also treated alone.

Basic statistical analysis of calculating the Root Mean Square Error (RMSE) was carried out to check the suitability of the smartphone apps for mapping. The mean coordinate errors were determined as in equations 1&2.

$$\text{RMSE}_E = \sqrt{\sum_{i=1}^{n} \frac{\Delta Ei^2}{n}} \quad (1)$$

$$\text{RMSE}_N = \sqrt{\sum_{i=1}^{n} \frac{\Delta Ni^2}{n}} \quad (2)$$

Where $\Delta Ei, \Delta Ni$ are the differences between the GNSS acquired and the reference (true) coordinates, and $n$ is the number of points in the set.

Root Mean Square Error $\text{RMSE}_{EN}$ in coordinate was calculated. This is a characteristic of point sets accuracy and is one of the most common accuracy measures in geodesy. The $\text{RMSE}_{EN}$ is calculated as in Equation 3;

$$RMSE_{EN} = \sqrt{(RMSE_E)^2 + (RMSE_N)^2} \quad (3)$$

## 3. RESULTS

The coordinates of these stations were obtained and were converted to equivalent Universal Traverse Mercator (UTM) coordinate system with projection on the WGS 84 ellipsoid. The coordinates of the stations used in this study as obtained from the Hi-Target V30 geodetic grade receiver is presented in Table 1. In addition, all coordinates were converted to UTM system for easy comparison.

To compare accuracy of the eight smartphone applications and Garmin Map76s, the coordinates of the stations obtained from Hi-Target V30 were processed and taken as reference. The coordinate differences of each smartphone application and Garmin Map76s subtracted from reference coordinates of all the stations and RMSEE, $\text{RMSE}_N$, and $\text{RMSE}_{EN}$ have been computed by Equations (1)– (3). The combined results of the performance measures ($\text{RMSE}_E$, $\text{RMSE}_N$, and $\text{RMSE}_{EN}$) for the seven-smartphone applications is presented in Table 2 for observations at all the stations.

**Table 1.** Observed Stations from Hi-Target V30

| POINT ID | E (m) | N (m) | H (m) |
|---|---|---|---|
| **ABU2011** | 352459.943 | 1233203.374 | 692.1641 |
| **ABU2014** | 352696.679 | 1233424.392 | 690.7929 |
| **ABU2015** | 352846.384 | 1233659.501 | 694.9549 |
| **ABUBARDA 2548** | 352349.3366 | 1233363.464 | 692.9329 |
| **GSES21** | 352527.038 | 1233238.586 | 689.6248 |
| **ABU GEOM 2588** | 352409.461 | 1232991.232 | 688.8541 |
| **ABU2550** | 351837.6957 | 1233262.782 | 689.361 |
| **ABU2020** | 352233.2777 | 1233064.653 | 687.4559 |
| **ABU FOUNTAIN** | 353260.047 | 1233089.818 | 692.3665 |
| **ABU2053** | 352229.518 | 1233058.154 | 694.1548 |
| **ABU 2018** | 352915.937 | 1232591.472 | 684.357 |

The result for the Garmin Map76s and the seven smartphone applications shows that Garmin Map76s has the best RMSE value of typically less than 0.3 m. UTM GEOMAP, My GPS Location and Super Geo GPS amongst the seven smartphone applications were the best with 0.3, 0.4 and 0.4m respectively in both easting and nothing components. On the contrary, Map Coordinates gave the worst result with RMSE value of about 0.6m on both axes.

Figure 1 is a plot of the different performance measures RMSE of the seven smartphone applications and Garmin Map76s. The Fig.2 and table 2 presents the results.

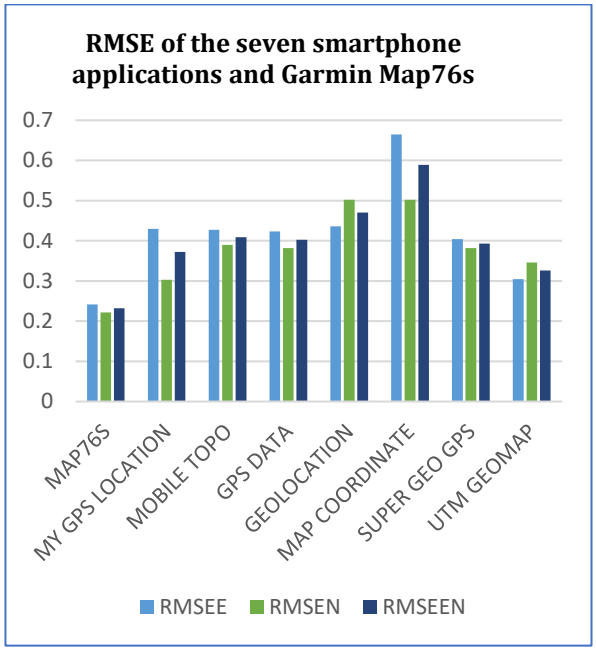


**Figure 2.** RMSE of the Seven-Smartphone Applications with Garmin Map76s

On the other hand, the result for the GNSS logger smartphone application used on Samsung galaxy S9+ on these 11 stations shows that the application performs best on the station ABU2020 with an RMSE value of roughly 0.2m on easting, northing and height. The application performs to the lowest at stations ABU2014, ABU FOUNTAIN and BARDA 2550 with RMSE value of 0.6, 0.7 and 0.5m respectively on easting, northing and height. This can be attributed to the effect of multipath because of high rising structures and vegetation cover. Table 3 shows the RMSE values obtained on all stations. Fig. 3 is a plot of the different performance measures RMSE on all stations using the GNSS logger application.

## 4. DISCUSSION

Based on the findings of this study, Fig. 2 shows that Garmin Map76s has the best result and hence above all the remaining seven smartphone application in the pecking order. In its absence, UTM GEOMAP can be used as a substitute because of its performance. My GPS Location and Super Geo GPS also did very well and can be used in carrying out a precise and rapid mapping exercise.

GNSS logger application as seen in Fig. 3 showed good performance on the station ABU2020. However, it gave some bad result as seen in stations ABU2014, ABU FOUNTAIN, and BARDA 2550. As stated earlier, this performance was attributed to multipath effect and also very short reception time. With advancement in technology, the smartphone applications might be improved to make GNSS observations better. For the better the accuracy, the more they will be accepted into surveying and geodesy activities (such as precise and rapid mapping).

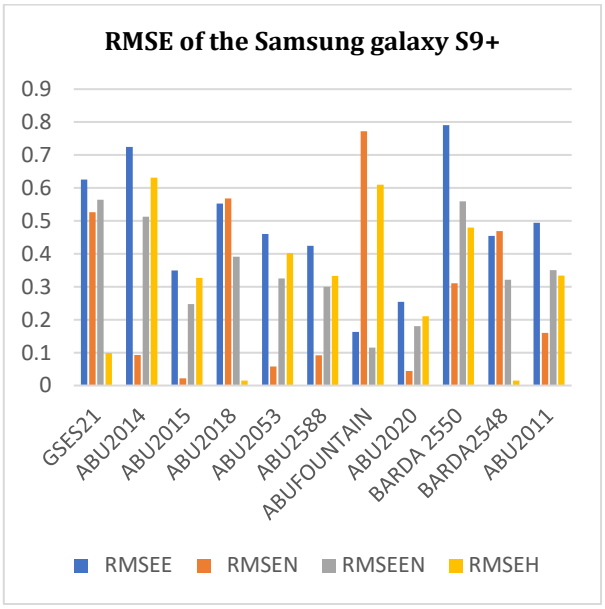


**Figure 3.** RMSE on all stations using the GNSS logger application

## 5. CONCLUSION

The study tests the usability and suitability of the use of smartphone applications for precise and rapid mapping. The first set of applications used are the Garmin Map76s, UTM GEO MAP, MY GPS LOCATION, SUPER GEO GPS, GPS DATA, MOBILE TOPO and GEO LOCATION. Garmin Map76s performs better than all the smartphone applications. UTM GEO MAP amongst the smartphone applications gave the best result. On the other hand, GNSS logger application that gives observations in RINEX file format was also used and its results compared to the Hi-Target V30 geodetic grade receiver. It performs well on station ABU2020 but was bad on other stations due to multipath effects. The results clearly point out to UTM GEO MAP as the best smartphone application used in this study.

**Table 2.** RMSE of the seven smartphone applications and Garmin Map76s

| APPLICATIONS | E (m) | N (m) | $E^2$ | $N^2$ | $RMSE_E$ | $RMSE_N$ | $RMSE_{EN}$ |
|---|---|---|---|---|---|---|---|
| **MAP76s** | 1.935 | 1.779 | 3.745 | 3.166 | 0.242 | 0.222 | 0.232 |
| **MY GPS LOCATION** | 3.444 | 2.425 | 11.860 | 5.880 | 0.430 | 0.303 | 0.372 |
| **MOBILE TOPO** | 3.417 | 3.119 | 11.673 | 9.731 | 0.427 | 0.390 | 0.409 |
| **GPS DATA** | 3.385 | 3.056 | 11.459 | 9.337 | 0.423 | 0.382 | 0.403 |
| **GEOLOCATION** | 3.485 | 4.013 | 12.146 | 16.108 | 0.436 | 0.502 | 0.470 |
| **MAP COORDINATE** | 5.320 | 4.015 | 28.299 | 16.121 | 0.665 | 0.502 | 0.589 |
| **SUPER GEO GPS** | 3.233 | 3.060 | 10.451 | 9.361 | 0.404 | 0.382 | 0.393 |
| **UTM GEOMAP** | 2.443 | 2.766 | 5.970 | 7.651 | 0.305 | 0.346 | 0.326 |

**Table 3.** RMSE on station using the GNSS logger application

| STATIONS | E (m) | N (m) | H (m) | $E^2$ | $N^2$ | $RMSE_E$ | $RMSE_N$ | $RMSE_{EN}$ | $RMSE_H$ |
|---|---|---|---|---|---|---|---|---|---|
| **GSES21** | 2.074 | 1.745 | 0.329 | 4.301 | 3.045 | 0.625 | 0.526 | 0.564 | 0.099 |
| **ABU2014** | 2.404 | 0.31 | 2.094 | 5.779 | 0.096 | 0.725 | 0.093 | 0.513 | 0.631 |
| **ABU2015** | 1.159 | 0.074 | 1.085 | 1.343 | 0.005 | 0.349 | 0.022 | 0.247 | 0.327 |
| **ABU2018** | 1.834 | 1.884 | 0.05 | 3.364 | 3.549 | 0.553 | 0.568 | 0.391 | 0.015 |
| **ABU2053** | 1.524 | 0.191 | 1.333 | 2.323 | 0.036 | 0.460 | 0.058 | 0.325 | 0.402 |
| **ABU2588** | 1.407 | 0.304 | 1.103 | 1.980 | 0.092 | 0.424 | 0.092 | 0.300 | 0.333 |
| **ABUFOUNTAIN** | 0.539 | 2.562 | 2.023 | 0.291 | 6.564 | 0.163 | 0.772 | 0.115 | 0.610 |
| **ABU2020** | 0.843 | 0.145 | 0.698 | 0.711 | 0.021 | 0.254 | 0.044 | 0.180 | 0.210 |
| **BARDA 2550** | 2.623 | 1.032 | 1.591 | 6.880 | 1.065 | 0.791 | 0.311 | 0.559 | 0.480 |
| **BARDA2548** | 1.506 | 1.555 | 0.049 | 2.268 | 2.418 | 0.454 | 0.469 | 0.321 | 0.015 |
| **ABU2011** | 1.64 | 0.531 | 1.109 | 2.690 | 0.282 | 0.494 | 0.160 | 0.350 | 0.334 |

## REFERENCES


Bauer C (2013). On the (in-)accuracy of GPS measures of smartphones: a study of running tracking applications. *11th International Conference on Advances in Mobile Computing &Multimedia (MoMM2013)*, (pp. 335-340). Vienna, Austria.

Hwang J, Yun H, Suh Y, Cho J & Lee D (2012). Development of an RTK-GPS positioning application with an improved position error model for smartphones. *Sensors (Switzerland)*, *12*(10), 12988–13001. https://doi.org/10.3390 /s121012988.

Isioye O A, Moses, M & Abdulmumin L (2019). Comparative Study of Some Online GNSS Post-Processing Services at Selected Permanent GNSS Sites in Nigeria. In *Accuracy of GNSS Methods* (p. 19). IntechOpen. https://doi.org/10.5772/ intechopen.79924

Lee A M, Majhi S & Mukherjee A (2017). Utilizing smartphones for geospatial data collection and construction set out surveying. *Mechanics of Structures and Materials: Advancements and Challenges - Proceedings of the 24th Australasian Conference on the Mechanics of Structures and Materials, ACMSM24 2016*, *December*, 1559–1564.

Merry K & Bettinger P (2019). Smartphone GPS accuracy study in an urban environment. *PLoS ONE*, *14*(7), 1–19. Doi.org/10.1371/journal.pone.0219890

Paziewski J (2020). Recent advances and perspectives for positioning and applications with smartphone GNSS observations. *Measurement Science and Technology*, *31*(9), 1–13. https://doi.org/10.1088 /1361-6501/ab8a7d

Schaefer M & Woodyer T (2015). Assessing absolute and relative accuracy of recreation-grade and mobile phone GNSS devices: a method for informing device choice. *Area 47*, 185–196. doi:10.1111/ area.12172

Schwieger V & Gläser A (2005). Possibilities of Low Cost GPS Technology for Precise Geodetic Applications Possibilities of Low Cost GPS Technology for Precise Geodetic Applications. *From Pharaohs to Geoinformatics FIG Working Week 2005 and GSDI-8*, 1–16.

Szot T, Specht C, Specht M & Dabrowski P (2019). Comparative analysis of positioning accuracy of Samsung Galaxy smartphones in stationary measurements. *PLoS One 14*, 1-13. doi:10.1371 /journal.pone.0215562.

Tomaštík J, Chudá J, Tunák D, Chudý F & Kardoš M (2020). Advances in smartphone positioning in forests: dual-frequency receivers and raw GNSS data. *Forestry: An International Journal of Forest Research*, 1–19. https://doi.org/10.1093/forestry /cpaa032

Tomastík J, Salon K & Piroh R (2017). Horizontal accuracy and applicability of smartphone GNSS positioning in forests. *Forestry*, 187-198. doi:10.1093/forestry/cpw031

Intercontinental Geoinformation Days

http://igd.mersin.edu.tr/2020/

# Deep Learning-Based Ionospheric TEC Prediction Approach

**İsmail DEMİRYEGE*[1], Mustafa ULUKAVAK [1]**

[1]*Harran University, Engineering Faculty, Department of Geomatics Engineering, Şanlıurfa, Turkey*

**Keywords**
Deep Learning
TEC
GPS
Ionospheric Delay
LSTM

**ABSTRACT**

The ionosphere layer is an environment that causes a time delay depending on the frequencies of the radio waves of the Global Positioning System (GPS) satellites. Most ionospheric studies are performed using total electron content (TEC) changes obtained from GPS signals. Today, studies on the physical structure of the ionosphere continue in many areas such as the prediction of space weather conditions, positioning, navigation, and communication. This study aims to create a deep learning-based model for the prediction of ionospheric TEC. Artificial Neural Networks (ANN) method was used to create this model. The artificial neural network and related properties designed for this method have been prepared in the MATLAB® environment using the Deep Learning Toolbox. In this study, HRUH permanent station which is located in Harran University Campus was registered Turkey Continuously Operating Reference Station' (CORS-TR) RINEX observations are used. TEC variations were obtained from GPS observations between the years 2016 and 2019 with two hours of temporal resolution. In this study, the determination of the optimum parameters was investigated which aims to forecast ionospheric TEC variations for the first six months of 2019. In the created model, the number of iterations is selected as constant (i = 100). The minimum RMSE value is ±0.28704 TECU with parameters where the number of hidden layers is selected as 50. The RMSE value of the forecasting model which is calculated in 1 hidden layer is ± 0.47298 TECU.

## 1. INTRODUCTION

The global positioning system (GPS) is a positioning and navigation system based on satellite technology. Although GPS is widely used in various fields such as air, sea, and land navigation, it is also used in daily life, industry, research, and education. A large part of the atmospheric effects encountered in positioning caused by ionospheric effects on GPS signals. Disruptions in the ionosphere; In particular, changes caused by space weather conditions damages the radio communication system and propagation (S.-S. Tan, 2008). Therefore, it may negatively affect the communication of radio signals such as communication, navigation, and radar (S. Tan, Zhou, Guo, & Liu, 2011). Since the ionosphere plays an important role in radio communication, applications should be carried out by considering ionospheric conditions.

Total Electron Content (TEC) is defined as the total number of electrons ($10^{16}$el/m$^2$) obtained in a cross-sectional area of 1 square meter along the signal path from GPS satellites to the GPS receiver, and its unit is expressed as the total electron content unit (TECU) (Abdullah, Strangeways, & Walsh, 2009). TEC is an indication of ionospheric variability obtained from GPS signals corrected by free electrons (Yaacob, Abdullah, & Ismail, 2010). TEC is an important parameter that provides information about disturbances in the ionosphere (Chakraborty, Kumar, De, & Guha, 2014; Schmidt, Bilitza, Shum, & Zeilhofer, 2008). Complex physical interactions between the geomagnetic field and solar activities make it difficult to model and predict ionospheric effects (Xu, 2007). GPS observations, along with navigation and positioning applications, are also used to investigate the effects of ionospheric space climatic conditions (Hofmann-Wellenhof, Lichtenegger, & Collins, 1993).

In this study, the performance of the LSTM Estimated TEC model for the GPS-TEC data mentioned above for the TEC time series estimation will be evaluated. Artificial Neural Networks (ANN) models will be used to model and predict ionospheric TEC

* **Corresponding Author**

*(demiryege@hotmail.com) ORCID ID 0000-0003-3836-3328
(mulukavak@gmail.com) ORCID ID 0000-0003-2092-3075

**Cite this study**

Demiryege İ, & Ulukavak M (2020). Deep Learning-Based Ionospheric TEC Estimation Approach. Intercontinental Geoinformation Days (IGD), 40-43, Mersin, Turkey

differences using the TEC time series measured by GPS. Although NNs perform better than statistical methods, the necessity of large-input training data including TEC samples of many years and the complexity in determining synaptic weights in the training process, and the lack of standard mathematical background limiting the application of the NN model for short-term TEC estimation have been identified (Leandro & Santos, 2007; Tulunay, Senalp, Radicella, & Tulunay, 2006). For this reason, recurrent neural networks (RNNs) are designed for time series in deep learning. Long Short-Term Memory (LSTM) is a specific recurrent neural network (RNN) architecture designed to model time series and long-range dependencies (Hochreiter & Schmidhuber, 1997). From the past time series data consisting of TEC values, forward-looking GPS-TEC predictions can be made with the LSTM network model. In short, forward-looking time series and the relationship between these series can be found. In this study, the LSTM network model is applied to predict 3.5-year sequential GPS-TEC data during the 24th solar cycle.

## 2. METHOD

### 2.1. Artificial Neural Network (ANN)

Artificial Neural Network (ANN) is a method developed by simulating the cognitive learning process of the human brain (Karahan, 2015). ANN is similar to the human brain in two ways (Ataseven, 2013; Gülpınar, 2015): first, the information in ANN is obtained by the network through the learning process, then the ANN uses it to store the information of the relationship between neurons known as synaptic weights. The general purpose of ANN is the learning process. ANN learns by training and testing similar to the human brain (Karymshakov & Abdykaparov, 2012). ANN; It can reveal the relationship between learning, memorizing, and data (Özkan, 2012). ANN imitates the working principle of the human brain; It has many important features such as being able to learn from examples (learning), generalize, work with missing information, complete pattern, establish relationships (associate), perform one or more of the classification and optimization processes (Aydemir, Karaatlı, Yılmaz, & Aksoy, 2014; Öztemel, 2006).

#### 2.1.1. Long Short-Term Memory (LSTM) TEC Model

The proposed LSTM network architecture for the prediction of the TEC time series consists of 4 layers as input layers, LSTM layers, hidden layers, and output layers (Figure 1).

Each element of the input layer are vectors obtained from TEC values. LSTM has input layer [$x_t = (x_1, x_2, x_3, ..., x_n)$] and hidden layer output [$h_t = (h_1, h_2, h_3, ..., h_n)$] in the peered order. The process of these operations is done according to the following equations:

$$i_t=\sigma (W_{ix}x_t + W_{ih}h_{t-1} + b_i) \quad (1)$$

$$f_t= \sigma (W_{fx}x_t + W_{fh}h_{t-1} + b_f) \quad (2)$$

$$o_t= \sigma (W_{ox}x_t + W_{oh}h_{t-1} + b_o) \quad (3)$$

$$c_t= f_t * c_{t-1} + i_t*\tanh (W_{ox}x_t + W_{ch}h_{t-1} + b_c) \quad (4)$$

$$h_t= o_t*\tanh(c_t) \quad (5)$$

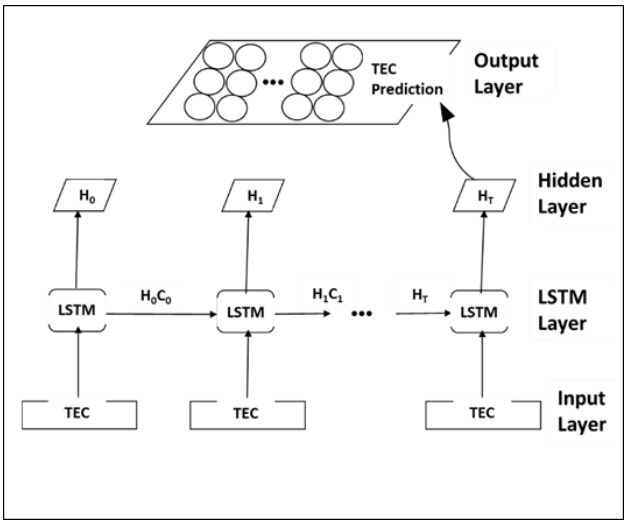


**Figure 1.** LSTM Network Architecture

The i in the formula is the input gate controlling how much of the input to each hidden unit is written into the inner state vector ($c_t$). ƒ is the discharge gate that determines how much of the previous internal state ($c_{t-1}$) is maintained. The combination of write and drain ports enables the network to control what information needs to be stored and overwritten at each step. It is the output gate and controls how much of each unit's update is preserved and is involved in storing non-relevant information of the LSTM cell. $c_t$ is the cell that learns the long dependencies of time series data. The last latent case h represents the predicted values of time series data (Sun et al., 2017).

## 3. RESULTS

In this study, an application was carried out to predict the TEC values for the first half of the year 2019 by using the TEC values obtained by using GPS observations of the HRUH station 3-years TEC changes data were used as training data in the established LSTM network. To train 3 years of data in a deep learning environment; the main parameters of the deep learning model such as the initial learning rate, the number of hidden layers, and the number of iterations were determined. The information was updated with the sigmoid function and it was ensured that the data were associated with the preceding data for the convolution of the network. Then, the training of the network was provided according to the determined parameters, and the standardization of the test data was made. Estimates of ionospheric TEC changes and squared mean errors (RMSE) were obtained for the first six months of the year 2019. The 6-month estimated TEC values were obtained through the deep learning process and these data were compared with the test data of the year 2019. After this encounter, the RMSE values were reduced by updating again over the estimated-TEC values.

In this study, the number of hidden layers was chosen as 50, and the number of iterations selected as 100. Separate and sequential deep learning processes were made 1 to 50 hidden layers. RMSE values obtained from the solutions are shown in Figure 2.

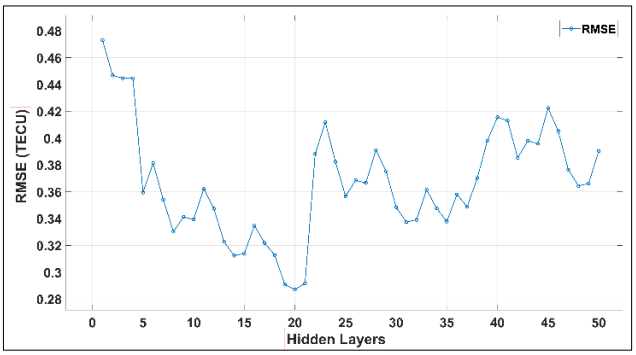


**Figure 2.** RMSE values calculated based on the number of hidden layers

In Figure 2, it is seen that as the number of hidden layers is increased, there is a decrease in the RMSE values, but there is an increase again after the 20th hidden layer value (RMSE = ±0.28704 TECU). The comparison of the estimated data with the test data and the errors between are shown in Figure 3.

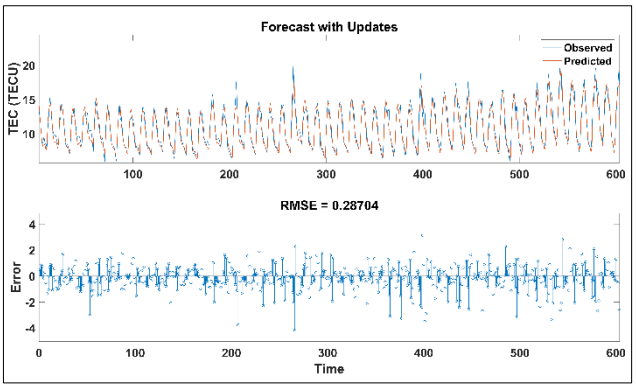


**Figure 3.** Plots of the 2019's first 48 days TEC validations

## 4. CONCLUSION

The time-series data in the installed model consists of the TEC changes between 2016-2019 with a two-hour temporal resolution. Based on these 3-year TEC data, the forecast of the TEC changes for the first 6 months of the year 2019 was investigated. In other words, the relationship between the 6-month estimated TEC time series data was investigated over the past 3-year TEC time series data.

In order to use the Deep Learning Toolbox customized in the MATLAB® environment, the computer hardware (such as video card, ram) must have the ability to perform high-capacity processing. In addition, the solution method of the selected network should be chosen to better represent the time series values. The use of the stochastic gradient descent momentum (SGDM) method for data with very long inputs is suggested as the findings of this study. The other solution method, adaptive momentum estimation (ADAM), is recommended to be used in the analysis of fewer data. The mathematical formulas and analysis forms of these 2 solution methods can be accessed from the MATLAB® Deep Learning Toolbox.

## ACKNOWLEDGEMENT

The authors would like to thank the data center that the General Directorate of Land Registry and Cadastre (TKGM) for providing the GPS recordings of Turkish CORS Network for providing the RINEX data of the HRUH permanent GNSS Station.

## REFERENCES

Abdullah, M., Strangeways, H. J., & Walsh, D. M. A. (2009). Improving ambiguity resolution rate with an accurate ionospheric differential correction. *Journal of Navigation*. doi:10.1017/S0373463308004979

Ataseven, B. (2013). YAPAY SİNİR AĞLARI İLE ÖNGÖRÜ MODELLEMESİ. *Öneri Dergisi*. Marmara Üniversitesi. doi:10.14783/od.v10i39.1012000311

Aydemir, E., Karaatlı, M., Yılmaz, G., & Aksoy, S. (2014). 112 Acil Çağrı Merkezine Gelen Çağrı Sayılarını Belirleyebilmek için Bir Yapay Sinir Ağları Tahminleme Modeli Geliştirilmesi. *Pamukkale Üniversitesi Mühendislik Bilimleri Dergisi*. Pamukkale Üniversitesi. doi:10.5505/pajes.2014.98608

Chakraborty, M., Kumar, S., De, B. K., & Guha, A. (2014). Latitudinal characteristics of GPS derived ionospheric TEC: a comparative study with IRI 2012 model. *Annals of Geophysics*, *57*(5). doi:10.4401/ag-6438

Gülpınar, V. (2015). YAPAY SİNİR AĞLARI VE SOSYAL AĞ ANALİZİ YARDIMI İLE TÜRK TELEKOMÜNİKASYON PİYASASINDA MÜŞTERİ KAYBI ANALİZİ. *Marmara Üniversitesi İktisadi ve İdari Bilimler Dergisi*. Marmara Üniversitesi.

Hochreiter, S., & Schmidhuber, J. (1997). Long Short-Term Memory. *Neural Computation*, *9*(8), 1735–1780. doi:10.1162/neco.1997.9.8.1735

Hofmann-Wellenhof, B., Lichtenegger, H., & Collins, J. (1993). *Global Positioning System. Theory and practice. Global Positioning System. Theory and practice.*

Karahan, Y. D. D. M. (2015). TURİZM TALEBİNİN YAPAY SİNİR AĞALARI YÖNTEMİYLE TAHMİN EDİLMESİ. *Süleyman Demirel Üniversitesi İktisadi ve İdari Bilimler Fakültesi Dergisi*. Süleyman Demirel Üniversitesi.

Karymshakov, K., & Abdykaparov, Y. (2012). Forecasting stock index movement with artificial neural networks: The case of Istanbul Stock Exchange. *Trakya University Journal of Social Science*, *14*, 231–242.

Leandro, R. F., & Santos, M. C. (2007). A neural network approach for regional vertical total electron content modelling. *Studia Geophysica et Geodaetica*, *51*(2), 279–292. doi:10.1007/s11200-007-0015-6

Özkan, F. (2012). Döviz Kuru Tahmininde Parasal Model ve Yapay Sinir Ağları Karşılaştırması. *A Comparison of the Monetary Model and Artificial Neural Networks in Exchange Rate Forecasting. (English)*, *3*(2), 27–29.

Öztemel, E. (2006). *Yapay Sinir Ağları. Papatya Yayıncılık*. İstanbul.

Schmidt, M., Bilitza, D., Shum, C. K., & Zeilhofer, C. (2008). Regional 4-D modeling of the ionospheric electron density. *Advances in Space Research*, *42*(4), 782–790. doi:10.1016/j.asr.2007.02.050

Sun, W., Xu, L., Huang, X., Zhang, W., Yuan, T., Chen, Z., & Yan, Y. (2017). *Forecasting of ionospheric vertical total electron content (TEC) using LSTM networks*. In *Proceedings of 2017 International Conference on Machine Learning and Cybernetics, ICMLC 2017*. doi:10.1109/ICMLC.2017.8108945

Tan, S.-S. (2008). Development and thought of compass navigation satellite system. *Yuhang Xuebao/Journal of Astronautics*, *29*, 391–396.

Tan, S., Zhou, B., Guo, S., & Liu, Z. (2011). Research on COMPASS navigation signals of China. *Zhongguo Kongjian Kexue Jishu/Chinese Space Science and Technology*, *31*, 9-14+29. doi:10.3780/j.issn.1000-758X.2011.04.002

Tulunay, E., Senalp, E. T., Radicella, S. M., & Tulunay, Y. (2006). Forecasting total electron content maps by neural network technique. *Radio Science*, *41*(4). doi:10.1029/2005RS003285

Xu, G. (2007). *GPS: Theory, algorithms and applications*. *GPS: Theory, Algorithms and Applications*. doi:10.1007/978-3-540-72715-6

Yaacob, N., Abdullah, M., & Ismail, M. (2010). GPS Total Electron Content (TEC) Prediction at Ionosphere Layer over the Equatorial Region. In *Trends in Telecommunications Technologies*. doi:10.5772/8474

Intercontinental Geoinformation Days

http://igd.mersin.edu.tr/2020/

# Necmettin Erbakan University Continuously Operating Reference Station

**Omer Faruk Atiz*[1], Salih Alcay [1], Sermet Ogutcu [1], Ibrahim Kalayci [1]**

[1]*Necmettin Erbakan University, Faculty of Engineering and Architecture, Department of Surveying Engineering, Konya, Turkey*

**Keywords**
GNSS
CORS
RTCM
NTRIP
RINEX

**ABSTRACT**

The Continuously Operating Reference Stations (CORS) are geodetic grade Global Navigation Satellite System (GNSS) receivers with permanently installed antennas, that are collecting GNSS data 24/7. Today the CORS, has vital importance in the GNSS community, whether for civilian users or researchers. Global CORS networks were established such as International GNSS Service's network. Also, most of the countries are established their own CORS networks e.g. Turkish CORS-TR. With the CORS networks, access to GNSS data for different purposes has become easier. In addition, for educational or some other research purposes it can be necessary to establish a CORS station. For this purpose, a CORS station was established at the rooftop of Necmettin Erbakan University. NEU-CORS station can track GPS, GLONASS, Galileo, BDS and SBAS satellites. The collected data is archived in the standard formats, and a real-time data stream via the Internet is provided. In this study, NEU-CORS station was introduced. The specification of the reference receiver, antenna and data formats are explained in detail. However, sample data is presented to examine the SNR (Signal to Noise Ratio), multipath and satellite visibility.

## 1. INTRODUCTION

In the last decade, the use of Global Navigation Satellite System (GNSS) has been drastically increased. With the development of new methods and algorithms, Continuously Operating Reference Station (CORS) has emerged. The CORS stations are geodetic grade GNSS receivers with permanently installed antennas. With the CORS stations, users are allowed to collect GNSS data for research or civilian purposes on 7/24. Hereby, the necessity to set a reference station is substantially eliminated. Today, CORS has become a remarkable tool for geosciences with enhanced usages such as real-time applications (Erenoglu 2017), structural health monitoring (Akpinar et al. 2017), datum defining (Altamimi and Collilieux 2009) and seismic monitoring (Bitharis et al. 2016). Global CORS networks were established for the datum consistency on a global scale such as the International GNSS Service (IGS) network. Also, most of the developed countries established their own CORS networks such as Turkish CORS-TR (Eren et al. 2009). Rizos 2008, proposed a classification between the permanent GNSS reference stations. According to this, IGS network is in Tier 1 stations, national networks are in Tier 2 stations and other regional or private reference stations are in Tier 3 (Rizos 2008).

CORS networks can provide real-time centimeter-level positioning accuracy with the Network-RTK (Real-Time Kinematic) corrections (Ogutcu 2014). Besides, the GNSS data is archived in RINEX (Receiver Independent Exchange Format) format. The collected data can be used for post-process positioning. In addition to benefits in the positioning, the monitoring of the atmosphere has been possible by estimating tropospheric wet delays (Zheng et al. 2018) or estimating total electron content (TEC) in the ionosphere layer (Nykiel et al. 2017).

Even there are many CORS networks, institutes can establish their own networks for different research purposes such as seismogeodetic networks. Also, on the university side, a CORS station can be established for educational and research purposes. Therefore, a CORS station is established at the rooftop of Necmettin Erbakan University, hereafter called NEU-CORS.

* **Corresponding Author**

*(oatiz@erbakan.edu.tr) ORCID ID 0000 – 0001 – 6180 – 7121
(salcay@erbakan.edu.tr) ORCID ID 0000 – 0001 – 5669 – 7247
(sermetogutcu@erbakan.edu.tr) ORCID ID 0000-0002-2680-1856
(ikalayci@erbakan.edu.tr) ORCID ID 0000-0003-1082-0005

**Cite this study**

Atiz O, Alcay S, Ogutcu S & Kalayci I (2020). Necmettin Erbakan University Continuously Operating Reference Station. Intercontinental Geoinformation Days (IGD), 44-47, Mersin, Turkey

In this study, NEU-CORS station is introduced in detail. The data formats and technical specifications of the station are explained. Also, as a sample, the data of DOY 290 in 2020 is presented. The sample data is examined with the SNR (Signal to Noise Ratio), multipath and satellite visibility graphics.

This paper is organized as follows. In Section 2 the main features of NEU-CORS station are given. The sample data is presented in Section 3. The discussions and conclusions are given in Section 4.

## 2. NEU-CORS STATION

The NEU-CORS station is installed at the rooftop of the Engineering and Architecture Faculty of Necmettin Erbakan University, in Konya. NEU-CORS station is managed and operated by the Department of Surveying Engineering. The location of the station is shown in Figure 1.

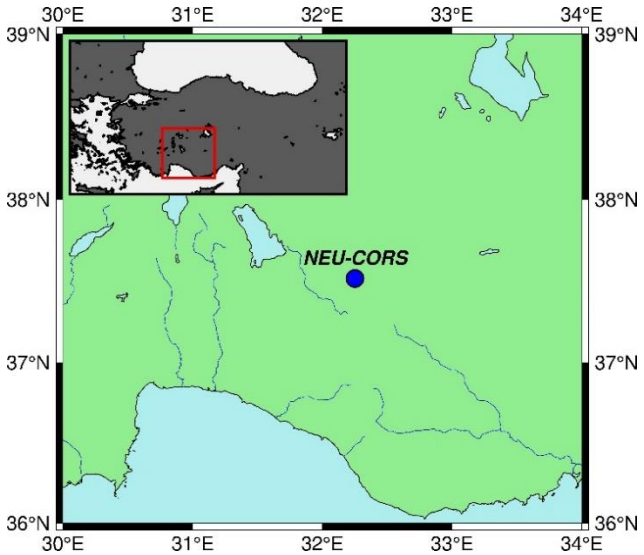


**Figure 1.** The location of NEU-CORS station

The station has a CHC N72 multifrequency GNSS receiver which can track 220 channels. CHC N72 receiver is equipped with CHC C220GR GNSS choke ring antenna. The choke ring antenna is placed on an iron pillar at the roof whereas the receiver is placed in a cabinet. A power supply and internet connection are provided to the cabinet. The cabinet and the antenna are given in Figure 2 and Figure 3, respectively.

**Figure 2.** The cabinet of NEU-CORS station

**Figure 3.** The antenna of NEU-CORS station

The receiver can provide an update rate of 1 Hz to collect GNSS data. The trackable constellations are GPS, GLONASS, BDS, Galileo and SBAS. More detailed specifications of the N72 GNSS receiver are given in Table 1 (CHC 2015).

**Table 1.** The detailed specifications of the N72 receiver

| Feature | Specification |
|---|---|
| GNSSs | GPS, GLONASS, Galileo, BDS and SBAS |
| Frequencies | GPS: L1 C/A, L2C, L2E, L5<br>GLONASS: L1 C/A, L1P, L2 C/A, L2P<br>Galileo: E1, E5a, E5b<br>BDS: B1, B2<br>SBAS: WAAS, EGNOS, MSAS |
| Channel number | 220 channels |
| Pseudorange measurement | High precision multi-correlator |
| Carrier phase measurement | Very low noise <1 mm precision in 1 Hertz |
| Positioning capacity | RTK: 8 mm + 1 ppm RMS for horizontal and 15 mm +1 ppm RMS for vertical<br>Static: 2.5 mm + 0.5 ppm RMS for horizontal and 5 mm +0.5 ppm RMS for vertical |
| Data storage | 16 GB internal storage and 1 TB external storage |
| Power | Connected to a power supply and up to 17 hours with integrated battery |
| Connections | Ethernet, Wireless and Bluetooth |
| Processor | IBMX287 450 MHz processor based on embedded Linux |

As default, the receiver is set to record data in three different modes. In recording mode 1, data is archived in CHC's binary format, so-called HCN format, with a 5 s sample interval. In recording mode 2, data is archived in RINEX 3.02 format with a 5 s sample interval. In recording mode 3, RINEX 2.11 file format is used with a 30 s sample interval. For all recording modes, the elevation cut-off angle is set to 0 degree, PDOP mask is set to 6 and GPS, GLONASS, Galileo and BDS satellites are activated. Whereas SBAS is supported, in default data recording is not used. Also, different sample interval options -up to 1 Hz- and satellite configurations can be selected. The recorded data is sent to a server and accessible via FTP (File Transfer Protocol).

The observation types obtained for each satellite system in default data recording are provided in Table 2. For the GPS system, as default P-code observation is used instead of C/A-code due to the lower noise of P-code observation. Therefore, L2P is used but L2C option can be selected instead of L2P.

**Table 2.** The measured observation types

| Satellite System | Observation Types |
|---|---|
| GPS | C1C L1C D1C S1C C2P L2P D2P S2P C5X L5X D5X S5X |
| GLONASS | C1C L1C D1C S1C C2P L2P D2P S2P |
| Galileo | C1X L1X D1X S1X C5X L5X D5X S5X C7X L7X D7X S7X C8X L8X D8X S8X |
| BDS | C1I L1I D1I S1I C7I L7I D7I S7I C6I L6I D6I S6I |

In addition to static data recording in RINEX or binary formats, real-time GNSS data format, so-called the RTCM SC-104 (The Radio Technical Commission for Maritime Services- Special Committee 104) format, can be utilized. RTCM SC-104 is a standard data format to broadcast differential corrections and raw GNSS observations (Heo et al. 2009). RTCM data is streamed via the Internet using the NTRIP (Networked Transport of RTCM via Internet Protocol). For NEU-CORS, with the NTRIP service single base RTK can be performed.

For the specific studies, apart from the default data recording, some other options can be provided on demand.

## 3. RESULTS

The NEU-CORS station is assessed in terms of observation data quality. For this purpose, sample data belong to the DOY 290 in 2020 is examined. The satellite visibilities, SNR and multipath values are derived by RTKPLOT module of RTKLIB open source software (Takasu 2013). Maximum, minimum, and mean satellite visibilities for each satellite system are given in Table 3.

**Table 3.** The satellite visibilities for DOY 290

| Satellite System | Max | Min | Mean |
|---|---|---|---|
| GPS | 14 | 7 | 10.3 |
| GLONASS | 11 | 5 | 8.2 |
| Galileo | 7 | 1 | 4.6 |
| BDS | 15 | 4 | 10.5 |

According to Table 3, average visible satellite for each constellation is above 8, except for Galileo. SNR graphics for GPS, GLONASS, Galileo and BDS satellite systems using L1 frequencies are shown in Figures 4-7.

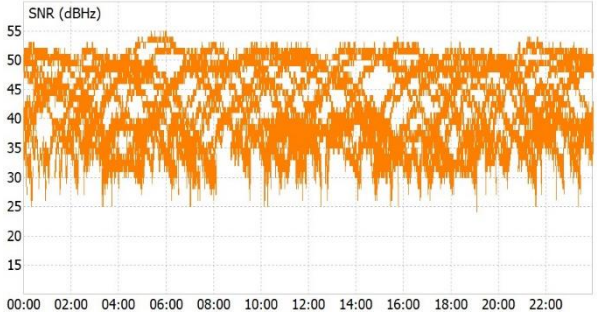


**Figure 4.** SNR (dBHz) for GPS

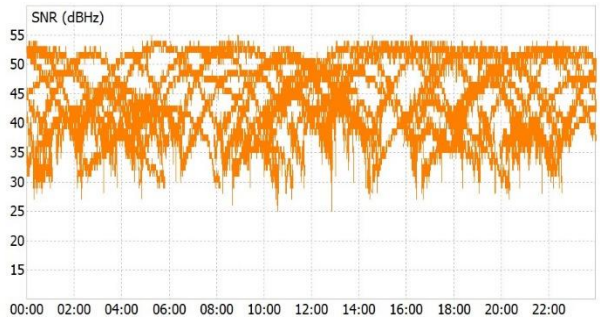


**Figure 5.** SNR (dBHz) for GLONASS

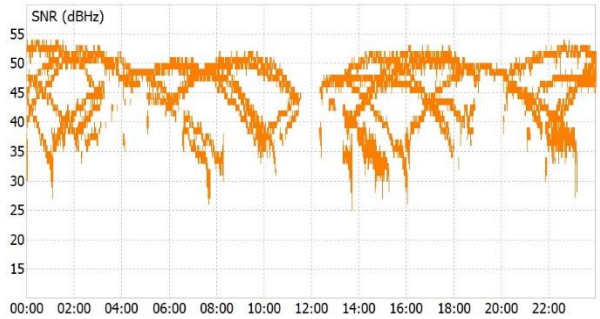


**Figure 6.** SNR (dBHz) for Galileo

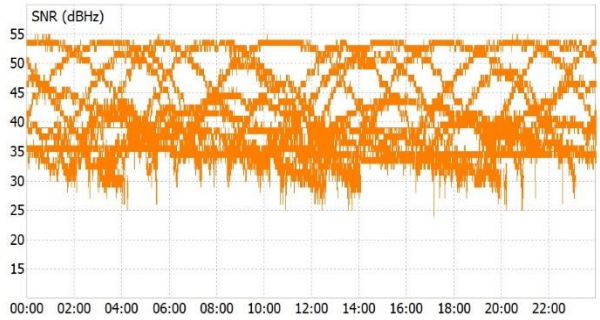


**Figure 7.** SNR (dBHz) for BDS

As seen from the Figures 4-7, the SNR values for each satellite system are similar and between 25 dBHz and 55 dBHz. The multipath values derived by RTKPLOT are provided in Figure 8-11.

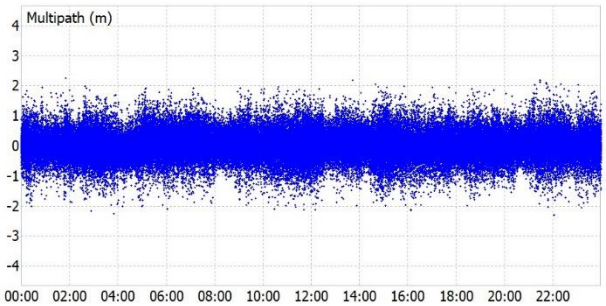


**Figure 8.** Multipath value for GPS

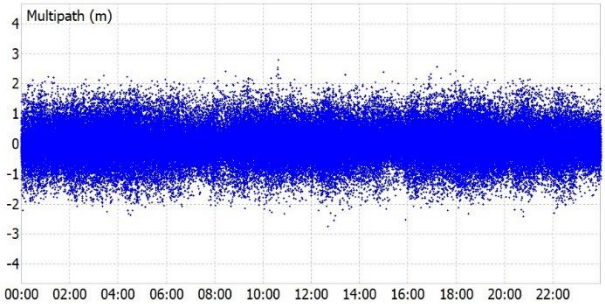


**Figure 9.** Multipath value for GLONASS

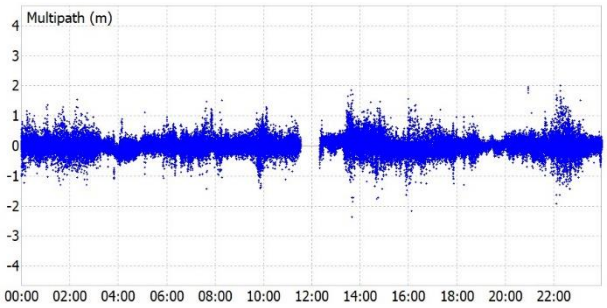


**Figure 10.** Multipath value for Galileo

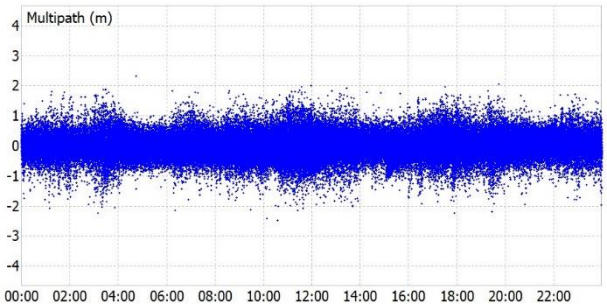


**Figure 11.** Multipath value for BDS

L1 signals of each satellite system is used for multipath plot. Galileo has the lowest multipath value whereas GLONASS has the biggest multipath value. Also, as the elevation angle and SNR value of the satellites increased the multipath decreased.

## 4. DISCUSSION AND CONCLUSION

A new continuously operating reference station (NEU-CORS) was established in Konya, Turkey. The reference station was introduced in detail and a sample data analysis was conducted. NEU-CORS station is considerable because of the multi-GNSS support. Also, the station has the ability of streaming real-time data. With this it is possible to perform RTK positioning via Internet.

Furthermore, the operators of NEU-CORS station is open to data sharing and any cooperation. Those interested can get contact with the corresponding author of this manuscript.

## ACKNOWLEDGEMENT

This work is supported by Necmettin Erbakan University Scientific Research Projects (BAP), Turkey. The project number is 171219008.

## REFERENCES

Akpinar B, Aykut N O, Dindar A A, Gürkan K & Gülal E (2017). Ağ RTK GNSS yönteminin yapı sağlığı izleme çalışmalarında kullanımı. Afyon Kocatepe Üniversitesi Fen Ve Mühendislik Bilimleri Dergisi, 17(3), 1030-1040. https://doi.org/10.5578/fmbd.66278

Altamimi Z & Collilieux X (2009). IGS contribution to the ITRF. Journal of Geodesy, 83(3-4), 375-383. https://doi.org/10.1007/s00190-008-0294-x

Altiner Y, Söhne W, Güney C, Perlt J, Wang R & Muzli M (2013). A geodetic study of the 23 October 2011 Van, Turkey earthquake. Tectonophysics, 588, 118-134. https://doi.org/10.1016/j.tecto.2012.12.005

Bitharis S, Fotiou A, Pikridas C, Rossikopoulos D, Pavlides S & Chatzipetros A (2016). The Samothrace earthquake of May 2014 and the displacements estimations using permanent GPS stations data. Bulletin of the Geological Society of Greece, 50(3), 1545-1552. https://doi.org/10.12681/bgsg.11867

CHC (2015). N72 GNSS Reference Receiver User Guide.

Eren K, Uzel T, Gulal E, Yildirim O & Cingoz A (2009). Results from a comprehensive Global Navigation Satellite System test in the CORS-TR network: Case study. Journal of Surveying Engineering, 135(1), 10-18.

Erenoglu R C (2017). A comprehensive evaluation of GNSS-and CORS-based positioning and terrestrial surveying for cadastral surveys. Survey Review, 49(352), 28-38. https://doi.org/10.1080/00396265.2015.1104093

Heo Y, Yan T, Lim S & Rizos C (2009, December). International standard GNSS real-time data formats and protocols. IGNSS Symposium 2009.

Nykiel G, Zanimonskiy Y M, Yampolski Y M & Figurski M (2017). Efficient usage of dense GNSS networks in central europe for the visualization and investigation of ionospheric TEC variations. Sensors, 17(10), 2298. https://doi.org/10.3390/s17102298

Ogutcu S (2014). Accuracy analysis of network based RTK techniques. MS Thesis, Necmettin Erbakan University, Konya (in Turkish).

Rizos C (2008). The contribution of GNSS CORS infrastructure to the mission of Modern Geodesy. In 7th Int. Symp. & Exhibition on Geoinformation.

Takasu T (2013). RTKLIB ver. 2.4.2 Manual. RTKLIB: An Open Source Program Package for GNSS Positioning, 29-49.

Zheng F, Lou Y, Gu S, Gong X & Shi C (2018). Modeling tropospheric wet delays with national GNSS reference network in China for BeiDou precise point positioning. Journal of Geodesy, 92(5), 545-560. https://doi.org/10.1007/s00190-017-1080-4

## Geographic Information Systems and Cartography – 1

**Minimum spanning tree detection on raster data**

*Murat Çalışkan, Berk Anbaroğlu**

**Realization to Web Based with Turf.JS Library of Spatial Analysis in Open Source Softwares**

*Halil Ibrahim Onyil*, Mehmet Yilmaz*

**Groundwater Quality Dependence on the Spatial Proximity of Geo-located Dumpsites in Samaru-Nigeria**

*Terwase Tosin Youngu*, Yahaya Abbas Aliyu, Adamu Bala, Samuel Azua, Aliyu Zailani Abubakar, Samuel Enyinna Akpa*

**Creating a Land Cover Change Simulation Model with SLEUTH, The Case of Istanbul Province**

*Ahmet Emir Yakup*, Ismail Ercument Ayazli*

**Evaluation of the change of Istanbul Anatolian Side land surface temperature values with CORINE data**

*Lütfiye Kuşak*, Ufuk Fatih Küçükali*

**Financial Analyses of ODHCs in Turkey in terms of Profitability**

*Elif Akyel*, Özşen Çorumluoğlu*

**Landfill Site Selection Literature Review: for Bodrum District**

*Cansu Nehteparov*, Emin Özgür Avşar*

Intercontinental Geoinformation Days

http://igd.mersin.edu.tr/2020/

# Minimum spanning tree detection on raster data

**Murat Çalışkan[1], Berk Anbaroğlu*[1]**

[1]*Hacettepe University, Faculty of Engineering, Geomatics Engineering, Ankara, Turkey*

**Keywords**
Minimum Spanning Tree
Kruskal's
Raster

**ABSTRACT**

Various real-life systems including transportation, infrastructure and social networks require the use of a graph data structure. These graphs usually consist of weighted edges, such as the distance between two intersections on a highway or the cost to establish a power line between two electricity distribution centers. Therefore, having correct weights (costs) assigned to the edges of a graph is an important issue. Assigning these weight values manually is a time-consuming task in a real-world application, since graphs may consist of thousands of edges. On the other hand, assuming distance to represent weight would over-simplify the problem, especially when a graph is representing a real-life spatial phenomenon such as modeling of infrastructure lines. Specifically, raster data should be utilized to model such real-life entities. This paper investigates the effectiveness of three different methods to determine the costs of a weighted graph when the purpose is to detect the minimum spanning tree, which is a tree structure that connects all nodes with minimum cost.

## 1. INTRODUCTION

Minimum Spanning Tree (MST) is subset of a graph, which is defined as the tree that connects all of the nodes in a graph with the lowest cost (weight). MST can be determined using different algorithms. Kruskal's Algorithm and Prim's Algorithms are two of them. Kruskal's algorithm sorts all edges based on ascending costs, and include them in order to the MST as long as they do not form a cycle and all nodes are included(Kruskal, 1956). Prim's algorithm starts with a random node and grows the MST by including the node that is reachable by the lowest available cost within the nodes that are included in the set(Prim, 1957).

Detecting a MST of a weighted graph is used extensively in network optimization studies such as creating computer circuits, telecommunication network design, delivery routing etc(Ahuja, Magnanti, Orlin, & Reddy, 1995; Dippon & Train, 2000; Mareš, 2008; Pettie & Ramachandran, 2000; Rothfarb, Frank, Kleitman, Rosenbaum, & Steiglitz, 1970). Some of these usage areas are related to Geographic Information Systems. For example; in a study, the length of the line was reduced from 66 km to 49.9 km in the Amoco East Cross oil pipeline project in Alberta-Canada(Dott, 1998). Another study was carried out for the optimization of the South Gabon oil pipeline and with this study, the total line length was reduced from 188.2 miles to 156.2 miles using the Prim's algorithm(Brimberg, Hansen, Lih, Mladenović, & Breton, 2003).

One problem while working with graph data is assigning values to the edges as weight/cost. If the number of edges is few, it can be done manually. But there are more edges to consider, the problem gets more difficult. Suppose that you have a pipeline network that consists of ten thousands of elements that is used within an urban environment. It would take a lot of time to assign a cost value to each edge. The +simple solution is to use length of the edge as cost. But this solution may not be true in every condition. As an instance, while creating an electricity transmission line; land value, slope, land use, height from sea level, type of soil etc. may also be important beside the length of the electricity line. In these kind of situations, a combination of these factors should be taken into account. Specifically, instead of discrete vector data, continuous raster data should be used to estimate the costs of edges of a graph.

* **Corresponding Author**

*(banbar@hacettepe.edu.tr) ORCID ID 0000-0003-2331-6190
(muratcaliskan@hacettepe.edu.tr) ORCID ID 0000-0003-1863-9032

**Cite this study**

Çalışkan M & Anbaroğlu B (2020). Minimum spanning tree detection on raster data. Intercontinental Geoinformation Days (IGD), 48-51, Mersin, Turkey

## 2. METHOD

This section first describes the MST and Kruskal's algorithm, and then describes the three main cost methods to estimate the costs of edges when relying on raster data.

### 2.1. Detecting MST by Kruskal's Algorithm

Graph is a data structure that consists of nodes and edges between these nodes. This structure is used for modelling the transportation systems, internet network, relationship between people in social media etc. An exemplar network consisting of 9 nodes and 13 edges is illustrated in Figure 1.

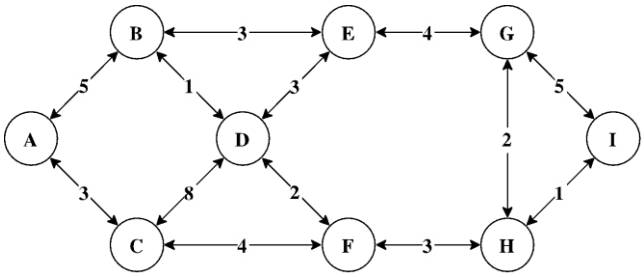


**Figure 1.** Graph Data Structure

One of the common algorithms that operate on graphs is determining the "Minimum Spanning Tree (MST)", which is defined as the tree connecting all of the nodes in a graph with the lowest cost(weight)(Degenne & Lo Seen, 2016; Graham & Hell, 1985).

In Figure 2 there is a graph consists of nodes A, B, C, D, E and F. Several spanning trees (red dotted lines), that connects all of these nodes, are illustrated. There are more than one options to connect all the nodes as seen. Among them, the one with minimum cost is called Minimum Spanning Tree Figure 2d.

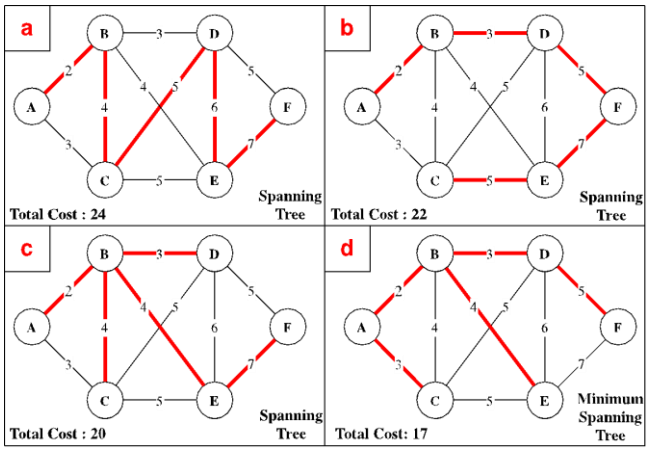


**Figure 2.** Spanning Tree and Min. Span. Tree

### 2.2. Generating MST Based on Raster

As mentioned in previous section; in some conditions it may be impossible to assign cost value to the graph manually due to large number of edges and using length of the edge as cost value may be insufficient.

In this study, we proposed a solution for this kind of situations. Our solution is; "Determining the MST, based on a cost raster" as can be seen in Figure 3. For this purpose, we created a plugin that runs on QGIS software and it is published in QGIS Plugin Repository. Using raster data to estimate cost value is also handled and explained thoroughly in Çalışkan and Anbaroğlu, 2020.

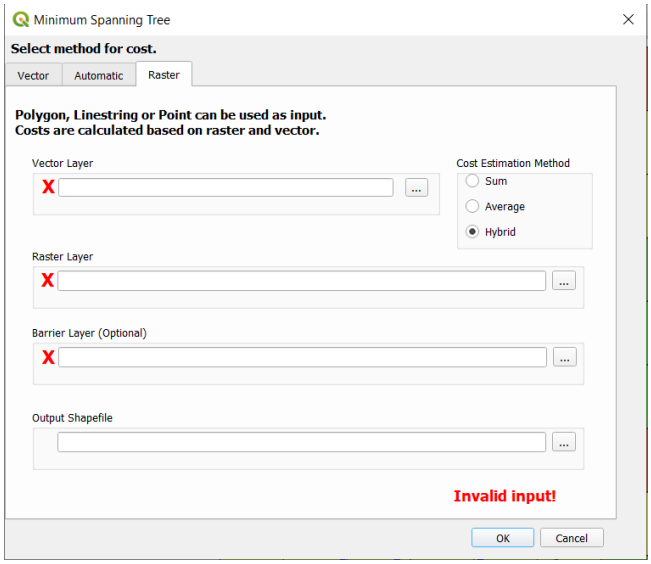


**Figure 3.** QGIS Plugin for Creating Raster Based MST

Raster, is a grid-like data type that consists of pixels. And in this method, every pixel represents the cost of its location. Therefore, a cost raster is required for edges to be able to gain the cost values. The edges get their cost/weight from corresponding pixels of the cost raster.

There are three ways for calculating the cost of the edge. First one is "summation of the pixels". In this method; the values of the pixels, that the edge intersects, are summed up and used as cost. The second one is "average of the pixels". In this method; the average of the values of the pixels, that the edge intersects, is used as cost. And the last method is "hybrid method". In this method; the average of the values of the pixels, that the edge intersects, is multiplied by the length. And the result is used as cost.

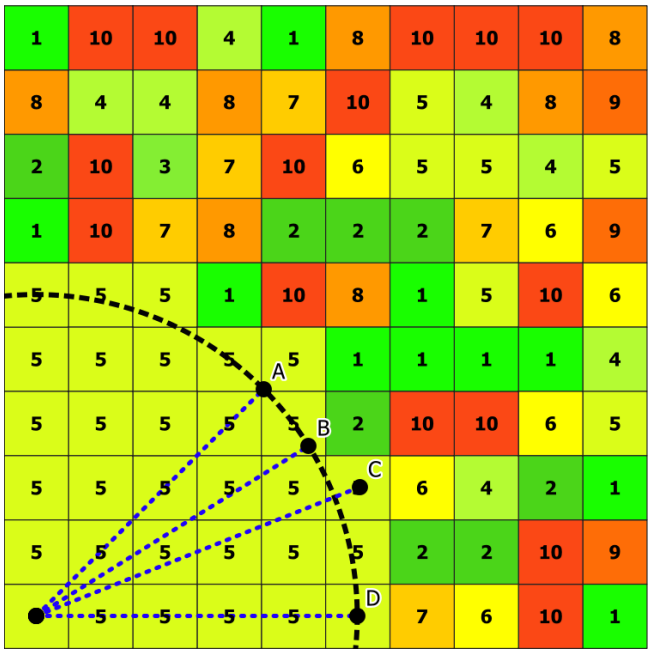


**Figure 4.** Illustration of Cost Estimation

Based on raster data illustrated in Figure 4, the associated cost values of the four edges are stated in Table 1.

**Table 1.** Cost Estimation Methods

| Edge | Distance | Average | Sum | Hybrid (Dist*Avg) |
|---|---|---|---|---|
| A | 5 | 5 | 25 | 25 |
| B | 5 | 5 | 40 | 25 |
| C | 5.5 | 5 | 40 | 27.5 |
| D | 5 | 5 | 30 | 25 |

All of these three methods can be used to gain the cost from rasters, but the hybrid method is advised for this process. Because, there are some problems about the first and the second methods. Specifically, in the first method, all the pixel values that an edge intersects are added up. In some conditions the results of this method can be wrong. For example, as seen in Figure 4, the length of edges A and B are the same and they are both in same homogenous surface. But their costs are different because of the size of the pixels.

In the second cost estimation method, average of the pixel values, that an edge intersects, are used as cost. This method isn't affected from the distance in homogenous surfaces, but this method also has some weakness in some situations. As illustrated in Table 1; edges B and C has the same cost in same homogenous surface, although their distances are different. In practical their costs are expected to be different.

In the last method, the cost is multiplication of the length of the edges and the average of the corresponding pixels. This method eliminates the errors, made in previous methods.

For the process in this study, two obligatory and one optional parameter are required. The optional parameter is barrier data. It is a restriction in the process and must be in line format. The MST cannot cross the barrier line. And the obligatory ones are; graph(vector) data and cost(raster) data. The graph data can be in point, line or polygon format. If a point data is used as input, the point features are used as nodes and edges are generated by Delaunay Triangulation. If a polygon data is used as input; at first, centroids of the polygon features are created and the rest is the same as point data. If the input is in line format, the line features are used as edges of the graph.

Cost raster must be created based on needs before the process is started. While creating the cost raster; it must be taken into account that, the higher the pixel value is, the harder it would be to pass that pixel. Restriction, is also possible via the cost raster. If some places are desired to be avoid while generating the MST, the pixels that correspond to the desired places are set as null. In this way, the edges of the MST won't be able to pass those places.

## 3. RESULTS

As an exemplar scenario for the steps, explained in Figure 5, a case study was performed and the details are explained below.

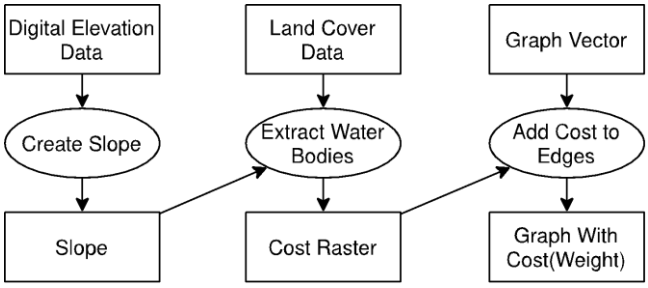


**Figure 5**. Illustrative Explanation of Gaining Cost Raster

In this example; a slope raster which is assumed to contain cost values was created. In order to create the cost raster data; first of all, Digital Elevation Model(3''≈100m) data for Turkey (from viewfinderpanoramas.org) and CORINE Land Cover data(from https://land.copernicus.eu/pan-european) were downloaded. Next, a slope raster was generated using the DEM and the water bodies are extracted from the DEM as they are thought to be restricted zones in our scenario. The resulting slope data was used as cost raster.

As graph data, the centroids of the cities, which are in point format, in Turkey was used. For barrier line, which is optional in this process, roughly drawn TANAP Natural Gas Pipeline is used(https://enerji.gov.tr/bilgi-merkezi-dogal-gaz-boru-hatlari-ve-projeleri). After all these preparations, only thing to do is to use these data as input for the plugin. In this process, it is required for all of the inputs to be in same coordinate system. The result is illustrated in Figure 6.

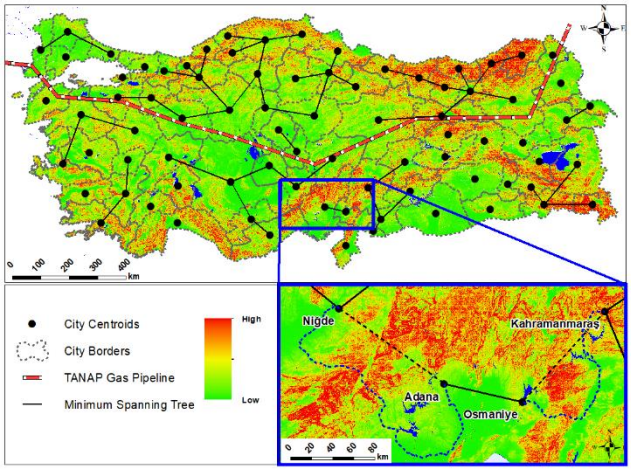


**Figure 6.** Cost Raster, City Centroids, Barrier Lines and MST in Turkey

In Figure 6; the cost raster, barrier lines, city centroids and the result MST is illustrated. It is obvious in the result that, none of the edges of the MST crosses either the barrier line or the null pixels of the raster.

## 4. DISCUSSION

In theory, all of the points (city centroids) have to be connected by a continuous line. In Figure 6, it is seen that there are some isolated points. For example, in the blue bordered area, the connection between "Niğde-Adana" and "Osmaniye-Kahramanmaraş" is missing. These cities are expected to be connected by black dotted line. They are not connected, because, there are null values (water

bodies) in the raster under those edges (Niğde-Adana, Osmaniye-K.Maraş). Since the barrier line restricts the connection of the points, it also causes these kind of disconnections.

When it is obligatory to connect these points, some other solutions have to be taken into account. If the point is not in a fully restricted area, such as island, determining a line with multiple vertices that goes around the restricted area, rather than straight line, would be an option.

In Figure 6 an alternative route is illustrated as an example in blue dotted line between Niğde-Adana and Osmaniye-K.Maraş. These lines are created based on the cost raster to minimize the cost.

## 5. CONCLUSION

In Geographic Information Systems projects, most of the time costed edges are used when working with graph based data. If the costs of the edges aren't assigned while collecting the data, or the cost parameters are changed later, new cost values should be assigned. This process is time consuming. For this kind of situations an easy and practical solution is needed.

In this study, it is aimed to find an efficient solution for adding cost to graph datasets. For this purpose, a raster based method is suggested. Thanks to newly created QGIS plugin, performing this process is also very easy to implement.

Beside being such useful, there is a problem with generating MST using graph, that consists of edges whose costs are assigned from raster. The problem is that, if there are restricted areas in the raster (null values), some disconnected points may occur. As a future work we will be investigating ways in which to connect such disconnected nodes to the MST.

## REFERENCES


Ahuja, R. K., Magnanti, T. L., Orlin, J. B., & Reddy, M. R. (1995). Applications of Network Optimization. *Network Models*, *7*(June), 1–83.

Brimberg, J., Hansen, P., Lih, K. W., Mladenović, N., & Breton, M. (2003). An oil pipeline design problem. *Operations Research*, *51*(2). https://doi.org/10.1287/opre.51.2.228.12786

Çalışkan, M., & Anbaroğlu, B. (2020). Geo-MST: A geographical minimum spanning tree plugin for QGIS. *SoftwareX*, *12*, 100553. https://doi.org/10.1016/j.softx.2020.100553

Degenne, P., & Lo Seen, D. (2016). Ocelet: Simulating processes of landscape changes using interaction graphs. *SoftwareX*. https://doi.org/10.1016/j.softx.2016.05.002

Dippon, C. M., & Train, K. E. (2000). The cost of the local telecommunication network: A comparison of minimum spanning trees and the HAI model. *Telecommunications Policy*, *24*(3), 253–262. https://doi.org/10.1016/S0308-5961(00)00009-4

Dott, D. R. (1998). Optimal network design for natural gas pipelines. *ProQuest Dissertations and Theses*, 117. https://doi.org/10.11575/PRISM/22946

Graham, R. L., & Hell, P. (1985). On the History of the Minimum Spanning Tree Problem. *Annals of the History of Computing*, *7*(1), 43–57. https://doi.org/10.1109/MAHC.1985.10011

Kruskal, J. B. (1956). On the Shortest Spanning Subtree of a Graph and the Traveling Salesman Problem. *Proceedings of the American Mathematical Society*, *7*(1), 48. https://doi.org/10.2307/2033241

Mareš, M. (2008). The saga of minimum spanning trees. *Computer Science Review*, *2*(3), 165–221. https://doi.org/10.1016/j.cosrev.2008.10.002

Pettie, S., & Ramachandran, V. (2000). An optimal minimum spanning tree algorithm. *Lecture Notes in Computer Science (Including Subseries Lecture Notes in Artificial Intelligence and Lecture Notes in Bioinformatics)*, *1853*(1), 49–60. https://doi.org/10.1007/3-540-45022-x_6

Prim, R. C. (1957). Shortest Connection Networks And Some Generalizations. *Bell System Technical Journal*. https://doi.org/10.1002/j.1538-7305.1957.tb01515.x

Rothfarb, B., Frank, H., Kleitman, D. J., Rosenbaum, D. M., & Steiglitz, K. (1970). Optimal Design of Offshore Natural-Gas Pipeline Systems. *Operations Research*. https://doi.org/10.1287/opre.18.6.992

Intercontinental Geoinformation Days

http://igd.mersin.edu.tr/2020/

# Realization of Web Based with Turf.JS Library of Spatial Analysis in Open Source Softwares

**Halil Ibrahim Onyıl**[*1] **Mehmet Yılmaz**[1]

[1]*Harran University, Geomatics Engineering Department, Sanliurfa, Turkey*

**Keywords**
Web-GIS
Spatial Analysis
WPS
Turf.JS Library

**ABSTRACT**
In this study, the analysis, process and outputs of an integrated system that will enable the spatial analysis of web-gis applications will be discussed. Desktop GIS software, spatial database, web-map server and web server will be selected from open source software. The system architecture of the problem will be analyzed and the most appropriate system architecture will be developed. System architecture consists of open source software; QGIS as desktop GIS software, PostgreSQL / PostGIS as spatial database, Turf library, alternative to Web Processing Service (WPS) service for spatial analysis, Apache Tomcat web server will be used. The urban test data prepared as a result will be subjected to spatial analysis in the study and the system's operability will be tested.

## 1. INTRODUCTION

Due to the development of open source web-based technologies day by day, its use in the map / geomatics sector is increasing daily. The spatial / spatial information perception of our profession; It has been instrumental in taking great steps in keeping up with the pace of the day; This situation also played an important role in determining the purpose and target of the study.

Open source softwares used in today's world are shown in Figure 1. These softwares are preferred because they are free, user-friendly and easily accessible.

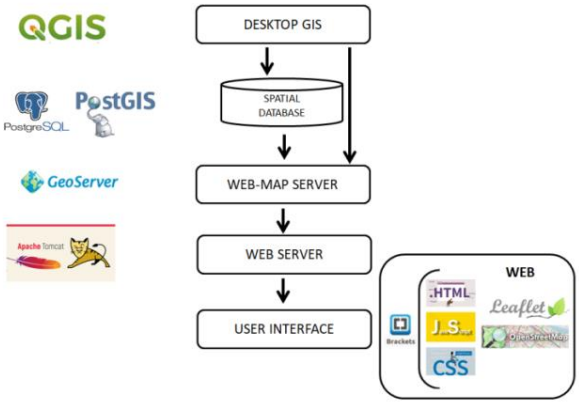


**Figure 1.** Open Source Softwares

Open source thinking has the key role on that situation in terms of being free, independent and managaeble in a manner of answering the necessities of policy makers, engineers and researches (Akın, 2020).

Spatial analysis using to perform statistical inferences, perform spatial relations of point, line and area data, It is the whole of exploratory processes that help us to understand space and geography based on spatial data.

Spatial analysis studies are important in that they provide the opportunity to evaluate spatial data under certain conditions and values and assist engineers and managers in decision-support stages. The obligation to fulfill this opportunity only through desktop GIS software, the obligation to use licensed software, and moreover, the absence of knowledge to use these software; It can restrict the possibility of spatial analysis and even make it face with the inability to make any analysis (Yilmaz, 2009). In such a situation, it seems essential for users to switch from desktop GIS software to web-based platforms.

Geographical Information Systems have some requirements including both hardware and software. With the rapid development of internet technology over time, various data can be delivered to users via web pages without any location and time problems (Guler, 2020).

* **Corresponding Author**

*[1](hibrahimonyil@gmail.com) ORCID ID 0000-0002-7916-8820
[2](yilmazmeh@harran.edu.tr) ORCID ID 0000-0003-3176-6992

**Cite this study**

Onyıl, H I, Yilmaz M (2020). Realization to Web Based of Spatial Analysis with Open Source Softwares. Intercontinental Geoinformation Days (IGD), 52-55, Mersin, Turkey

Web based applications; Many maps and platforms with a widespread use and an easy user interface provide convenience for us (Filiz, 2013). The subject of this study also offers us solutions at this point.

Spatial analysis includes a variety of techniques and processes used to understand patterns and relationships of geographic features. WPS where these processes can be performed, is a web processing service that enables the execution of spatial analysis information processing processes and the retrieval of metadata explaining their purposes and functions. With this service, spatial data can be easily analyzed and displayed on the web (Granell, 2012).

The core capabilities of the WPS server fall into two categories: The first category is process determination and process capabilities. The second category includes the ability to manage and track machining jobs. Because the processes provided by a WPS server can have varying degrees of complexity, the server must show the mode of job control capabilities allowed per transaction offer. It may be provided with the service for other service capabilities, namely secure communication and user authentication, but does not cover or limit these details unless they change the meaning of other business control capabilities (OGC, 2018).

Another spatial analysis process is the Turf.js library, which is open source code and faster and more ergonomic than the WPS service(Miller, 2019). This javascript library is user friendly thanks to its open source, free and easy use. And for software developers, it can give results in a shorter time with less code without tiring system architectures.

In this article, a user-friendly web interface will be developed with open source web technologies to facilitate the spatial analysis that is desired to be carried out. Thus, spatial / spatial analysis that will produce solutions to many different problems will be easily achieved. In addition, by introducing the WPS standard, using the alternative Turf.js library, it is aimed to share and organize / contribute data between the user and the administrator for the first time with a system architecture operation, unlike the one used until today (Miller, 2019).

The road map followed in the study is as follows. By analyzing the system of the problem, the most suitable system architecture will be developed for the system. System architecture consisting of open source software; QGIS will be used as desktop GIS software, PostgreSQL / PostGIS as spatial database, Turf.js library as an alternative to WPS service (Integrated to Geoserver) for spatial analysis operations and Apache Tomcat as web server.

The data to be used as test data in the study will primarily be prepared as geographical and verbal data in desktop GIS software. It will then be integrated into the spatial database. Then the data will be integrated into the spatial database to be created on the web server. Finally, by developing a user interface where spatial analysis can be done with web programming (HTML, CSS, JS and PHP), the work will be integrated into the web server (in localhost) environment.

## 2. METHOD

With today's dense spatial data sets, our modeling of our world has become quite complicated, and in this respect, GIS appears before us as a method and tool for reaching the determined goal. In GIS applications \ projects to be made in this respect, first of all, determining the purpose and target; will play a very important role in system analysis and shaping the system architecture. Because a goal that has not been well analyzed; It will lead to waste of time, opportunity and human resources. In this case, it will cause the projects to fail halfway and prevent the development of future projects.

Within the scope of the study, the subject of "spatial analysis" that will take place with user interface interaction of spatial data in the web environment is adopted as a theme. In this context, the study; system analysis consists of the design of the system architecture and the realization of the system.

### 2.1. System Analysis

System analysis is an area of interest that determines how the data available in the information system should be used, examines the logic of the inputs required for the system, the process of transformation, and ultimately creates a system. All information systems reach the result by going through a certain cycle (Yüregir, 2001).

Within the scope of the study, the structural and functional properties of the user, spatial data, web technologies and spatial analysis processes were examined. Thus, a system analysis flow diagram has emerged where spatial analysis can be performed. The resulting diagram is shown in Figure-2.

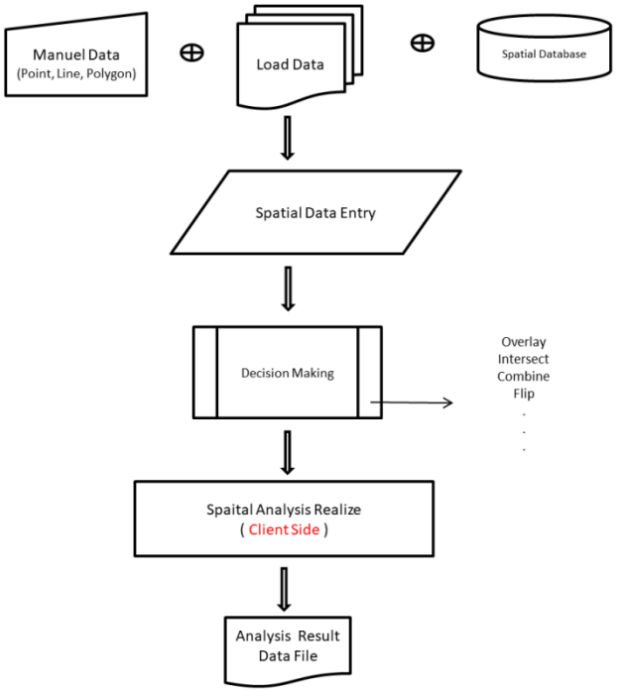


**Figure 2.** After System Analysis Flow Diagram

According to the diagram, the user can transfer data to the web environment with three different methods. Then he will be able to analyze according to the type of analysis he will choose. Finally, it can complete the process as a printout or by downloading.

### 2.2. System Architecture

System architecture, it is a conceptual model that defines the structure, behavior and formality of the system. An architectural definition; it is a standard explanation or representation of relationality, organized to support rationality about the structures and behaviors of the system.

In this application, the system architecture consists of open source software; QGIS as a desktop GIS software, PostgreSQL / PostGIS as a spatial database, Geoserver as a web-map server, WPS service for spatial analysis operations, and alternatively Turf.Js. library and finally, Apache Tomcat (in localhost) was used as the web server in the application phase of the study. The system architecture specific to this application is shown in Figure 3.

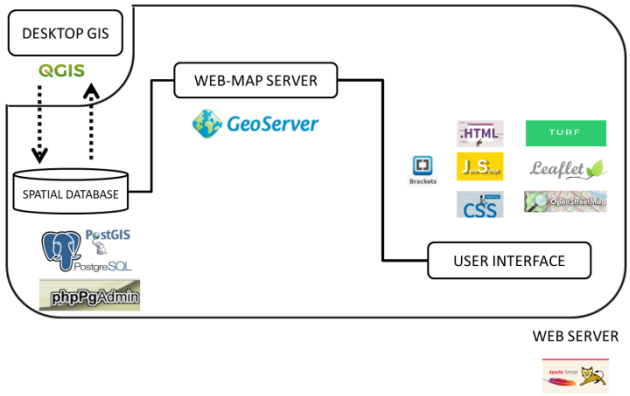


**Figure 3.** System Architecture

### 2.3. System Realization

The study consists of spatial analysis using test data after the installation and integration of open source software suitable for the system architecture.

Within the scope of the study, geographical and verbal data were prepared in QGIS desktop GIS software for database and ready data file entries. Geographical data; It was produced as a spatial data set consisting of point, line and area data. As point data, stop, lamp post data were generated. As line data, boulevard, street and street data were produced. Then, test data was imported into PostgreSQL / PostGIS spatial database.

Then, after the integration of the web-map server and Geoserver, the data was transferred to the working folder in Geoserver. By providing WPS service and Geoserver integration. Finally, the user interface where spatial analysis can be done with web programming (HTML, CSS and JS, Leaflet.js); the visual showing the steps for the application stages of the study is shown in Figure-4.

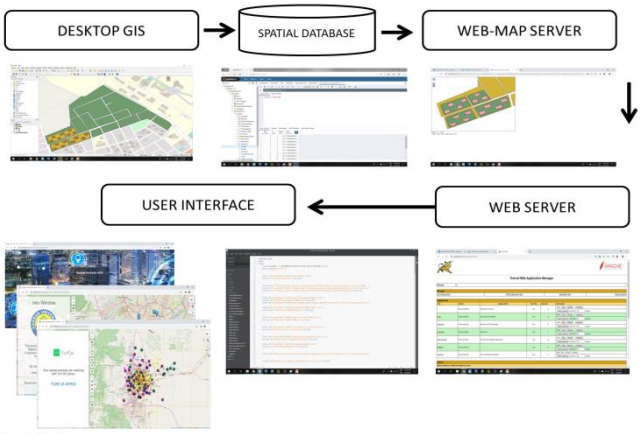


**Figure 4.** System Realization

Developed with the WPS and TURF.js library, the work was integrated into the web server (in localhost) and the spatial analysis of manual, ready-made data file and spatial database data was tested with the query and analysis performed, and the operability and usability of the system was revealed.

## 3. RESULTS

Finally, spatial analysis in web-GIS platform; the following findings were obtained by using the Turf.JS library.

- There is no software cost due to the use of open source software.
- Going beyond the classical web-gis applications, data can be entered data by the user in three different ways.
- These are manual, ready data to be transferred to the platform by drag and drop method and the use of the database. As shown in Figure 5, the possibility to enter data directly into the database from the user interface is shown.

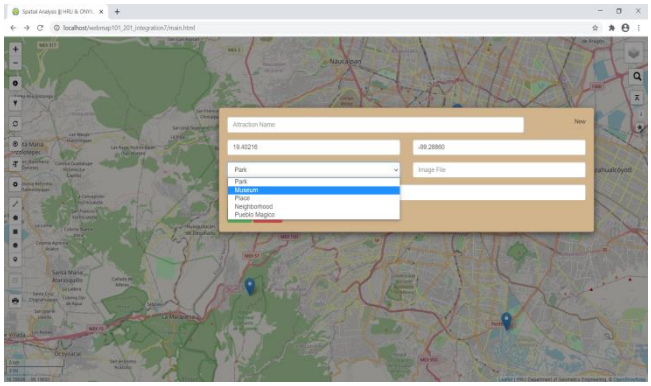

**Figure 5.** Database Data Entry

- We perform in desktop gis software, proximity, distance, area, merge, intersection, etc. Spatial analysis can be performed on the web using the Turf.JS library procedure(Miller, 2019). The results of the buffer and area calculations performed are shown in Figure 6 as an example.

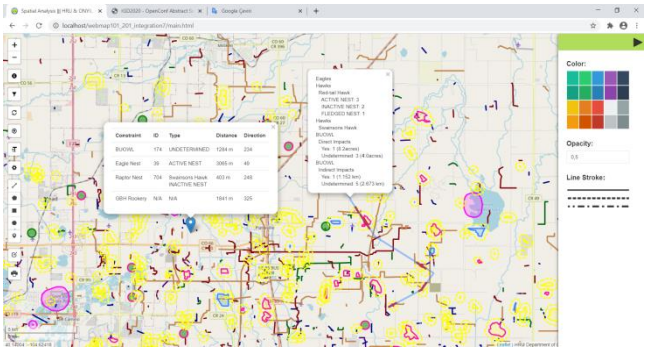

**Figure 6.** Turf.Js Library Applications(Distance, Buffer etc.)

- It is faster and more flexible than WPS services.
- Having an easy, accessible and user-friendly interface.

As a result, in the implementation phase of the study, going beyond a classical web-GIS, not only the queries but also; A platform that can offer analysis, data entry and data download has been obtained.

It is hoped that the study will shed light on new studies and contribute to our country's webGIS studies.

## 4. DISCUSSION

In Turkey, increasing web-GIS studies to be an alternative to desktop GIS applications. The use widespread of closed source software, for many institutions also beyond being a costly process cannot go. This situation, is requires open source a software revision for institution and persons.

## 5. CONCLUSION

Geographical information systems appear before us as a method and tool for reaching the target and purpose determined using spatial data. In GIS applications to be made, first of all, is required determining the purpose and target; this situation, it will play a very important role in system analysis and shaping the system architecture. Thus, during the implementation of the study, many problems to be experienced; Before working, it will be prevented.

Spatial analysis includes a variety of techniques and processes used to understand patterns and relationships of geographic features. It is essential to make these processes web-based today.

Web based applications; With many maps, platforms that are widely used and have an easy user interface provide convenience for us (Filiz, 2013).

It is a great advantage to perform spatial analysis processes with the open source, web-based Turf.js library, which is faster and more ergonomic than the WPS service. This javascript library is user friendly thanks to its open source, free and easy use (Miller, 2019).

In this context, the study is important in terms of showing that web-based spatial analysis is feasible in terms of feasibility, use and cost. It is attractive and valid for institutions and organizations to use a method that provides spatial analysis such as open source GIS software, spatial databases, web-map servers and Turf.JS library.

In the upcoming scientific process, it is foreseen that the WPS and Turf.JS library can be used in many studies, and that these possibilities and technologies can be used in virgin areas such as the last period of Polar Research and Wildlife Ecology in our country.

## REFERENCES

Akın O (2020) An Open Source Spatial Software for Transpotation Infrastructure Performance Metrics, İstanbul Technical University, M.Sc., Istanbul, Turkey.

Filiz B G (2013) Implementation of A Search and rescue monitor system based on spatial data on web based maps. MS Thesis, Turk Air Force Academy University, Istanbul (in Turkish), Turkey.

Granell C, Diaz L, Tamayo A, Huerta J (2012) Assessment of OGC Web Processing Services for REST principles. International Journal of Data Mining, Modelling and Management, Spain.

Guler E (2020) Developing A Web Based Mobile GIS Application for Soil Mapping Studies, Konya Technical University, PhD Thesis, Konya, Turkey.

OGC (2018) OGC Standarts, Internal reference number of this OGC® document: 14-065r2

Miller M (2019) Introduction to Web Programming for GIS Applications, Udemy Course Lecture Notes, Mexico.

Yuregir O H (2001) System analysis and design in informatics. ISBN: 975-85-61-05-7

Yilmaz C (2009) Developing Spatial Web Services with Free and Open Source Software. MS Thesis, Karadeniz Technical University. Trabzon, Turkey.

Intercontinental Geoinformation Days

http://igd.mersin.edu.tr/2020/

# Groundwater Quality Dependence on the Spatial Proximity of Geo-located Dumpsites in Samaru-Nigeria

**Terwase Tosin Youngu*[1], Yahaya Abbas Aliyu [1], Adamu Bala [1], Samuel Azua [1], Aliyu Zailani Abubakar [1], Samuel Enyinna Akpa [1]**

[1]*Ahmadu Bello University, Faculty of Environmental Design, Department of Geomatics, Zaria, Nigeria*

**Keywords**
Geo-location
Groundwater Quality
Solid Waste Management
Spatial Proximity
WHO

**ABSTRACT**

The coordinates of 10 solid waste dumpsites in proximity to the boreholes and wells in the Samaru community of Kaduna state, Nigeria were acquired with a GPS-enabled smartphone. In addition, 10 groundwater samples in relation to the dumpsites were collected for the testing of 11 physical and chemical parameters of water quality based on the World Health Organisation (WHO) standard limits. The results of the spatial proximity analyses carried out revealed that the requirement for locating dumpsites was not met as specified by the Environmental Protection Agency (EPA) regarding the minimum safe distance from groundwater sources. The results of the study revealed also that a majority (about 90%) of the groundwater samples met the conditions for good drinking water even with their closeness to the dumpsites. However, only Calcium, Dissolved Oxygen, and Biochemical Oxygen Demand concentrations were significantly affected ($p < 0.05$ at the 95% significance level) by the closeness of the solid waste dumpsites to the boreholes and wells with very strong ($R^2$ = 86%) and strong ($R^2$ = 79%) relationships, respectively. Suggestions were nonetheless made for investigations into other factors responsible for groundwater contamination.

## 1. INTRODUCTION

The inability to manage effectively solid waste disposal (Aibor and Olorunda, 2006; Environmental Protection Agency [EPA], 2016; New York State Department of Environmental Conservation [NYSDEC], 2016) has become an issue of great concern in different parts of the world. This is due to the fact that that wastes adversely affect the quality of our food, health, and environment (European Environment Agency [EEA], 2019). Moreover, solid waste dumpsites pollute the underground water sources thereby decreasing their quality as a result of changes to their physical and chemical characteristics (El-Salam and Abu-Zuid, 2015; Simeon, 2009).

The increased quantity of waste in a vast majority of developing countries is as a result of economic growth, industrialisation and urbanisation which is without its attendant problem of waste disposal (Ferronato and Torretta, 2019). As a matter fact, it was estimated that in 2006 the total amount of municipal solid waste (MSW) generated globally reached 2.02 billion tones, representing a 7% annual increase since 2003 (United Nations Environmental Programme [UNEP], 2007).

Arimah and Adinnu (1995) observed that the perceived environmental costs, health-related hazards, social and economic impacts associated with waste dumpsites are often not confined to the immediate environment but extend up to a few kilometres. This is one of the reasons why several research efforts have been carried out in the recent past to manage solid waste in different parts of the world (Abbas *et al.,* 2018; Akinbile and Yusoff, 2011; Pande *et al.*, 2015; Remy *et al.*, 2017; Somani *et al.,* 2019).

It is therefore against this backdrop that this study assessed the quality of groundwater due to the proximity of solid waste dumpsites in Samaru, Kaduna state-Nigeria with a view to proffering proper waste management practices. This is achieved through the identification of dumpsites in proximity to the groundwater sources in the study area and the testing of the leachate concentration from the groundwater

* **Corresponding Author**

*(terwasey2000@gmail.com) ORCID ID 0000-0003-3707-5113
(ayabbas1@yahoo.com) ORCID ID 0000-0001-8861-7109
(adamubala09@gmail.com) ORCID ID 0000-0002-9666-5722

**Cite this study**

Youngu T. T., Aliyu Y. A., Bala A, Azua S., Abubakar A. Z. & Akpa S. E. (2020). Groundwater Quality Dependence on the Spatial Proximity of Geo-located Dumpsites in Samaru-Nigeria. Intercontinental Geoinformation Days (IGD), 56 - 59, Mersin, Turkey

samples, as well as the determination of the spatial distribution of dumpsites in proximity to the groundwater sources using geospatial techniques. The locations of the dumpsites, boreholes and wells in the study area are shown in Fig. 1.

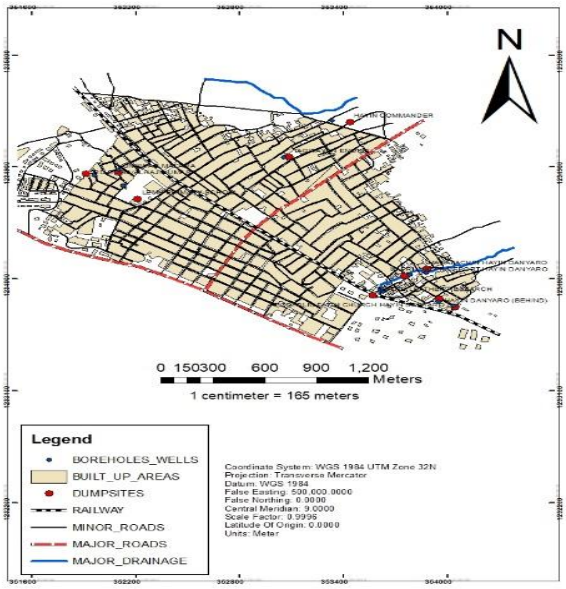


**Figure 1.** Locations of dumpsites, boreholes, and wells

## 2. METHOD

### 2.1. Planning/Reconnaissance

The planning stage involved both the office and field reconnaissance where the choice of relevant data and information (both spatial and attribute data of the dumpsites, boreholes and wells), survey method, and logistics requirements were considered. It also involved the cross-checking of the information obtained as well as determining the number of locations to be surveyed.

### 2.2. Data Acquisition

The coordinates of the dumpsite, borehole and well locations were acquired using a GPS-enabled smartphone (Tecno WX3 Pro Android Version 7.0) device with an overall average horizontal accuracy to within 13 m (95% of the time) which is consistent with the general accuracy levels observed of recreation-grade GPS receivers in urban environments (Merry and Bettinger, 2019). The attribute information of each dumpsite, borehole and well were obtained on site. Water samples of each of the 10 boreholes and wells in proximity to the dumpsites were also acquired with properly labelled water bottles for testing in the Laboratory.

### 2.3. Data Processing

The downloaded Google Earth imagery and acquired coordinates (E, N) of the existing dumpsites, boreholes and wells were imported into the ArcGIS 10.3 environment where the reference system (WGS 84, UTM zone 32N) was defined. Thereafter, the digitizing process was carried out with the creation of the dumpsite, borehole, well positions, built-up, roads, railway and drainage layers as shapefiles. The attribute information of the dumpsites, boreholes and wells were added to the attribute table linking the shapefiles in the ArcGIS environment to create the geo-database.

The collected water samples were tested for 11 (Temperature, pH, Electrical Conductivity [EC], Dissolved Oxygen [DO], Chloride, Hardness, Total Dissolved Solids [TDS], Calcium, Nitrate, Turbidity, and Biochemical Oxygen Demand [BOD]) physical and chemical properties according to the WHO (2017) standard for water quality in the Water Resources and Environmental Engineering laboratory in Ahmadu Bello University Samaru, Zaria.

## 3. RESULTS

### 3.1. Spatial Proximity of Dumpsites to Boreholes and Wells

Table 1 presents the spatial proximity of the 10 major dumpsites to the boreholes and wells under investigation in this study based on their coordinates.

**Table 1.** Proximity of dumpsites to boreholes and wells

| S/N | Dumpsite Location | Proximity (m) |
|---|---|---|
| 1 | Leather Research | 67.85 |
| 2 | Lemu Primary School | 134.86 |
| 3 | Ungwan Malawa | 20.95 |
| 4 | Alhaji Jumare | 50.28 |
| 5 | Tagwayin Engine | 31.69 |
| 6 | Hayin Commander | 103.35 |
| 7 | Behind Hayin Danyaro | 14.64 |
| 8 | Apostolic Faith Church Hayin Danyaro | 25.18 |
| 9 | Madaki Hayin Danyaro | 26.09 |
| 10 | Napri Water Depot Hayin Danyaro | 30.76 |

The result of Table 1 shows that the closest and farthest dumpsites from groundwater source (borehole or well) are found in the Ungwan Malawa and Lemu Primary School locations at 21 m and 135 m, respectively. Meanwhile, the average distance between a dumpsite and borehole or well is about 51 m. The results indicate that the reuirement set by the EPA (2016) which stipulates that dumpsites should be positioned not less than 160 m from groundwater sources have not been met.

### 3.2. Results of Physical and Chemical Analyses of Groundwater Samples

Table 2 presents the results of the analyses of pH, temperature [T (℃)], turbidity [Tb (NTU)], and electrical conductivity [EC (ms/cm)]) of water samples obtained from the boreholes and wells in proximity to the dumpsite locations (serial numbers 1 to 10 which directly relate to Table 1) against the WHO (2017) standard limits.

**Table 2.** Results of pH, temperature, turbidity, and electrical conductivity vs. WHO limits

| Dumpsite Location | pH | T (℃) | Tb (NTU) | EC (ms/cm) |
|---|---|---|---|---|
| 1 | 8.45 | 24.6 | 3.04 | 796 |
| 2 | 8.39 | 24.8 | 8.28 | 860 |
| 3 | 8.25 | 24.7 | 6.27 | 228 |
| 4 | 7.85 | 23.9 | 3.51 | 470 |
| 5 | 8.37 | 24.3 | 3.88 | 770 |
| 6 | 8.43 | 24.5 | 1.86 | 487 |
| 7 | 8.54 | 24.9 | 0.77 | 1593 |

| | | | | |
|---|---|---|---|---|
| 8 | 7.74 | 23.9 | 1.75 | 662 |
| 9 | 8.34 | 24.2 | 9.13 | 613 |
| 10 | 7.95 | 23.9 | 2.79 | 377 |
| WHO | 6.5-8.5 | Nil | 1-5 | 2500 |

The Fig. 2 displays the concentrations of Dissolved Oxygen (DO), Total Dissolved Solids (TDS), Total Hardness, Nitrate, Biochemical Oxygen Demand (BOD), Chloride, and Calcium, respectively obtained from the groundwater locations.

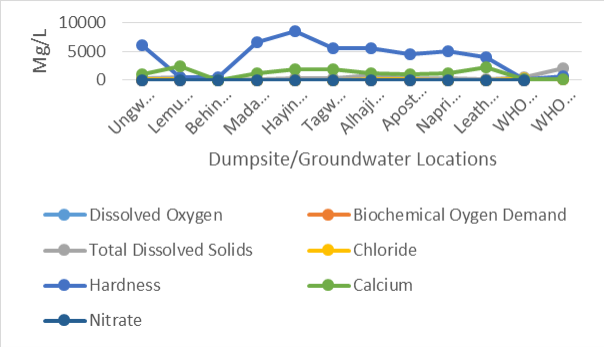


**Figure 2.** The concentrations of DO, TDS, Hardness, Nitrate, BOD, Chloride, and Calcium at groundwater locations vs. WHO standard

### 3.3. Relationship between Spatial Proximity of Dumpsites and the Physical and chemical Parameter Concentrations

It is pertinent to investigate whether there is a relationship between the proximity of the dumpsites to the boreholes and wells and whether it has significant effects on the levels of the physical and chemical constituents of the groundwater sources. Therefore, Table 3 presents the results of a multiple regression analysis carried out to verify these assumptions.

**Table 3.** The relationship and effect of proximity of dumpsites to boreholes and wells

| VIF Category | Parameter | R | R Squared | Sig. |
|---|---|---|---|---|
| I | Electrical Conductivity (ms/cm) | 0.93 | 0.86 | 0.111 |
| | Chloride (mg/l) | | | 0.236 |
| | Total Hardness (mg/l) | | | 0.109 |
| | Calcium (mg/l) | | | **0.023** |
| | Nitrate (mg/l) | | | 0.216 |
| II | pH | 0.89 | 0.79 | 0.547 |
| | Dissolved Oxygen (mg/l) | | | **0.009** |
| | Biochemical Oxygen Demand (mg/l) | | | **0.018** |
| | Temperature ($^0$C) | | | 0.950 |
| III | Total Dissolved Solids (mg/l) | 0.47 | 0.22 | 0.298 |
| | | | | 0.295 |

The multiple regression analysis was based on the Variance Inflation Factor [VIF] (Systat Software Inc., 2014) categories of the variables (physical and chemical parameters) at play. The spatial proximity of the dumpsites to the boreholes and wells formed the dependent variable while the physical and chemical parameters formed the independent variables.

## 4. DISCUSSION

The results of this study have shown that a majority (about 80%) of the solid waste dumpsites are located too close to the groundwater sources. This is an indication that most of the dumpsites did not meet the requirement set by EPA (2016) regarding the minimum distances required for their location.

A majority (90%) of the groundwater sites revealed pH values within the acceptable limit set by the WHO in 2017 for good water quality.

Only one (10%) of the groundwater sites showed that the concentration TDS was within the limit of good water quality while the levels of DO were unacceptable across all the sites. The results of the Total Hardness revealed that only a couple (20%) of the groundwater sites (Lemu Primary School and Hayin Danyaro) met the requirement set by the WHO. The concentrations of Nitrate and BOD at all the groundwater sites revealed that they were below the limit set by the WHO which is an indication of a condition acceptable for good drinking water. The concentrations of Chloride for a majority (90%) of the groundwater sites showed that they were within the acceptable limit for good water quality as set by the WHO. The results of the concentrations of Calcium revealed that only one groundwater site (Behind Hayin Danyaro) met the requirement set by the WHO.

Meanwhile, the results of the Temperature across the groundwater sites revealed that they were within the limit of being acceptable for good drinking water. However, the results of the Turbidity revealed that 60% of the groundwater sites fell within the permissible limit set by the WHO while 30% of the sites (Lemu Primary School, Behind Hayin Danyaro, Napri Water Depot Hayin Danyaro) exceeded the limit. The remaining 1% (Alhaji Jumare) fell below the limit and may be considered as acceptable. The contents of EC across the groundwater sites revealed that they were acceptable for good water quality.

The results of the study went further to reveal that only the concentrations of Dissolved Oxygen, and Biochemical Oxygen Demand were significantly influenced ($p < 0.05$ at the 95% significance level) by the closeness of the solid waste dumpsites to the boreholes and wells with very strong ($R^2$ = 86%) and strong ($R^2$ = 79%) relationships, respectively.

This study is in agreement with Akinbile and Yusoff, (2011) who reported similar findings but differs slightly from (Pande *et al.*, 2015; Remy *et al.*, 2017) regarding the contamination of the groundwater sources as a result of the proximity of the dumpsites. Moreover, it disagrees with (Abbas *et al.*, 2018; Somani *et al.*, 2019) based on the fact that the adoption of both controlled and uncontrolled conditions were prejudiced.

## 5. CONCLUSION

This study was set out to assess the quality of ten (10) major underground water sources (boreholes and

wells) in proximity to dumpsite locations in the Samaru community of Kaduna state, Nigeria.

The results revealed that the distances between the dumpsites and boreholes or wells, residential areas, and roads were far less than the minimum stipulated by the EPA regarding safe areas for locating dumpsites. The results also revealed based on the permissible limits set by the WHO that groundwater quality conditions for drinking water were met at some of the water sample sites despite the closeness of these dumpsites to the groundwater sources.

The results of the study showed that the concentrations of only three (3) (Calcium, Dissolved Oxygen, and Biochemical Oxygen Demand) out of the eleven (11) physical and chemical parameters tested were significantly affected by the proximity of the dumpsites to the groundwater sources with very strong and strong relationships, respectively.

In view of the findings of this study, it shows that the proximity of dumpsites to groundwater sources may not be the only reason for groundwater contamination perhaps other factors such as the topography or elevation, soil, slope amongst others may combine to create such a situation and would need to be investigated.

**REFERENCES**


Abbas, T., Fahad-Ullah, M., Riaz, O. & Shehzad, T. (2018). Impact of Municipal Solid Waste on Groundwater Quality in Jhang City Punjab, Pakistan. *Journal of Biodiversity and Environmental Sciences*, 12(1):134-141.

Aibor, M. S. & Olorunda, J. O. (2006). Environmental Health in the 21st Century. *A Technical Handbook of Environmental Health in the 21st Century for Professional Students*. Akure: His Mercy Publisher.

Akinbile, C. & Yusoff, M. S. (2011). Environmental Impact of Leachate Pollution on Groundwater Supplies in Akure, Nigeria. *International Journal of Environmental Science and Development*, 2. 81-86. https://doi:10.7763/IJESD.2011.V2.101

Arimah, B. & Adinnu, F. (1995). Market Segmentation and the Impact of Landfills on Residential Property Values: Empirical Evidence from an African City. *Journal of Housing and the Built Environment,* 10(2): 157-170. https://doi: 10.1007/BF02496533

El-Salam, M. M. A. & Abu-Zuid, G. I. (2015). Impact of Landfill Leachate on the Groundwater Quality: A Case Study in Egypt. *Journal of Advanced Research*, 6(4): 579–586. https://doi:10.1016/j.jare.2014.02.003

Environmental Protection Agency (2016). Environmental Guidelines: Solid Waste Landfills. August 14, 2019, www.epa.nsw.gov.au/resources/waste/solid-waste-landfill-guidelines-160259.pdf.

European Environment Agency (2019). Waste: A Problem or a Resource? May 29, 2020, https://www.eea.europa.eu/signals/signals-2014/articles/waste-a-problem-or-a-resource

Ferronato, N. & Torretta, V. (2019). Waste Mismanagement in Developing Countries: A Review of Global Issues. *International Journal of Environmental Research and Public Health*, 16(6): 1060. https://doi: 10.3390/ijerph16061060

Merry, K. & Bettinger, P. (2019). Smartphone GPS Accuracy Study in an Urban Environment. *PLoS ONE*, 14(7): e0219890. https://doi.org/10.1371/journal.pone.0219890

New York State Department of Environmental Conservation (2016). Waste Management. May 28, 2020, https://www.dec.ny.gov/chemical/292.html.

Pande, G., Alok, S. & Agrawal, S. (2015). Impacts of Leachate Percolation on Groundwater Quality: A Case Study of Dhanbad City, India*. Global Nest Journal, 17. 162-174.*

Remy, P. T., Hategekimana, F., Aphrodice, N. & Kumaran, S. G. (2017). Assessment of Leachate Effects on Groundwater and Soil from Nduba Landfill in Kigali, Rwanda. *International Journal of Engineering Research in Africa*. 33. 68-75. June 21, 2019, from 10.4028/www.scientific.net/JERA.33.68.

Simeon, O. D. (2009). Impact of Poor Solid Waste Management in Kenya on Groundwater. MSc. Thesis, University of Nairobi, Kenya.

Somani, M., Datta, M., Gupta, S., Sreekrishnan, T. R. & Gunturi, R. (2019). Comprehensive Assessment of the Leachate Quality and Its Pollution Potential from Six Municipal Waste Dumpsites of India. *Bio-resource Technology Reports*, 6. Doi:10.1016/j.biteb.2019.03.003

Systat Software Inc. (2014). Variance Inflation Factor. SigmaPlot 11.0 Statistical User Guide. http://systatsoftware.com/products/sigmaplot/.

United Nations Environmental Programme (2007). Global Waste Management Outlook. *Global Waste Management Market Report*. https://www.researchgate.net/profile/Costas_Velis/publication/283085861_Global_Waste_Management_Outlook_United_Nations_Environment_Programme_UNEP_and_International_Solid_Waste_Association_ISWA/links/5694079f08ae425c68962336.pdf

World Health Organization [WHO] (2017). Guidelines for Drinking-water Quality. https://www.who.int/water_sanitation_health/publications/drinking-water-quality-guidelines-4-including-1st-addendum/en/.

Intercontinental Geoinformation Days

http://igd.mersin.edu.tr/2020/

# Creating a Land Cover Change Simulation Model with SLEUTH, The Case of Istanbul Province

**Ahmet Emir Yakup**[*1], **İsmail Ercüment Ayazlı** [2]

[1]*Hitit University, Osmancik Vocational School, Department of Architecture and Urban Planning, Corum, Turkey*
[2]*Sivas Cumhuriyet University, Engineering Faculty, Department of Geomatics Engineering, Sivas, Turkey*

**Keywords**
Land Cover Change
Urban Growth
Change Detection
Simulation
GIS

**ABSTRACT**

Population growth leads to the growth of cities and the destruction of natural areas. Urban growth triggers changes in land cover. Determining the effects of change in land cover is necessary for sustainable urban management. For this reason, simulation applications are used extensively in planning studies. The cellular automata (CA) based simulation methods are often preferred to investigate land cover/use changes caused by urban growth. In this study, it is aimed to create a simulation model for the year 2040 in line with the ongoing urban growth trends of Istanbul by using CA-based SLEUTH model. The temporal data required by the model are generated from CORINE Land Cover data for the years 2000, 2006, 2012 and 2018. With the simulation model created, the effects of possible urban growth and land cover change in Istanbul were investigated. According to the simulation model produced, it was determined that 25% of Agricultural Land, 2% of wetlands and 14% of forests could be turned into residential areas. It is estimated that there may be 24% urban growth in Istanbul between 2018 and 2040. The results showed that the province of Istanbul is under intense urbanization pressure.

## 1. INTRODUCTION

With the population growth in the world especially after 1950, migration from rural to urban areas accelerated urbanization. (Satterthwaite 2005). This high acceleration has caused unhealthy or excessive urbanization (Saadani et al. 2020). Thus, the destruction of the environment brought along physical unplannedness, settlement irregularity, planning and management problems. With the transformation of open lands, forests and agricultural lands into residential areas, the pressure on natural resources is increasing day by day. (EEA 2016). Tourism, urbanization and industrialization in particular have accelerated the destruction of natural resources.

Many models and simulation tools have been developed by researchers to determine changes in urban growth and land cover. When researches on this subject are examined, cellular automata (CA)-based models are preferred due to their ease of calculation, simplicity of use, and their inherently spatial nature (White et al. 2004).

CA-based SLEUTH (Gigalopolis 2020b), which is used in many studies worldwide, was first applied in San Francisco and Washington-Baltimore regions (Clarke et al. 1997; Clarke and Gaydos 1998). In the following period, a series of studies were carried out in Santa Barbara to determine the technical development of the urbanization process (Candau and Clarke, 2000; Goldstein et al. 2004; Herold et al. 2003). It has been applied for the first time in Europe by Portugal's Lisbon and Porto metropolitans (E. A. Silva and Clarke 2005; E. Silva and Clarke 2002). On the other hand, SLEUTH has the highest number of applications in China. Simulations were produced under the ongoing conditions of the city or under alternative scenarios to assess the impact and extent of urbanization in rapidly growing cities such as Beijing (Yi and He 2009), Lanzhou (Xie et al. 2010), and Nanjing (Zhang et al. 2010). In the study conducted in Istanbul, it was applied for the changes in land use caused by the 3rd bridge and the main transportation networks of the city (Ayazli et al. 2015).

The SLEUTH model is divided into two sub-models as UGM (Urban Growth Model) and LCD (Land Cover Deltatron). UGM is the core module and constitutes urban growth simulations. The LCD matches the UGM if desired, simulating the land cover changes triggered by

* **Corresponding Author**

*(emiryakup@hitit.edu.tr) ORCID ID 0000 – 0002 – 1789 – 4448
(eayazli@cumhuriyet.edu.tr) ORCID ID 0000 – 0003 – 0782 – 5366

**Cite this study**

Yakup A E & Ayazlı I E (2020). Creating a Land Cover Change Simulation Model with SLEUTH, The Case of Istanbul Province. Intercontinental Geoinformation Days (IGD), 60-63, Mersin, Turkey

urban growth. In this context, LCD works integrated with UGM and is not independent.

In this study, the answers to the following questions were investigated:

- How do possible urban growth trends in Istanbul affect land cover changes?
- How does the urban growth rate change between 2018 and 2040 according to the scenario produced?
- How will the land cover of the region change in 2040 in Istanbul?

In order to create a model for this purpose, first CORINE land cover data for 2000, 2006, 2012 and 2018 were used. The input data of this model were generated using 2000, 2015 and 2018 transportation network data obtained from the Open Street Map service and digital elevation model (DEM) data obtained from the General Directorate of Mapping (HGM). Thus, an urban growth model has been prepared for 2040.

## 2. METHOD and METARIALS

### 2.1. Cellular Automata

The Cellular Automata concept consists of five basic components. These are; grid network, status, neighborhood, conversion rules and time. (Benenson and Torrens 2004). Cells are the smallest units that are adjacent to each other. Cells come together to form the grid network. Each cell has a state Depending on the state of neighboring cells, the conversion function changes the cell states. In urban modeling techniques, CA is suitable for modeling complex and dynamic natural phenomena such as urban areas (Tobler 1970).

### 2.2. SLEUTH Model

The model is a Unix-based software developed with the C language running on cellular automata. Since it is an open source software, the researchers developed the model according to local research areas.

The process of the model takes place in three main stages. These are the testing, calibration and prediction stages. In the test phase, the compliance of the input data required by the model with the model standards is questioned (Ayazli et al. 2015). If it is successful, the calibration phase is started. The calibration stage is also made in four stages as coarse, fine, final and forecast (Gigalopolis 2020a). At the calibration stage, the parameters of the model's growth rules are calculated using historical data. The five coefficient values from 0 to 100 are narrowed at each stage and reduced to a singular value (Gigalopolis 2020a). Possible singular values are investigated using the Brute Force Calibration (BFC) method according to 13 criteria. (Clarke and Gaydos 1998). With BFC, the model calculates the current situation in control years from the core year by comparing it with the regression method. In this way, the accuracy of the model is checked by calculating the regression values between the model and the calculated values.

In this study, OSM (Optimum SLEUTH Metric) was used as the calibration method. The method developed by Dietzel and Clarke is considered the most powerful of the methods used today. Coefficient ranges are selected by ranking the score values obtained from the multiplication of Compare, Pop, Edges, Clusters, Slope, X-Mean and Y-Mean criteria as in the 1st formula (Dietzel and Clarke 2007). The fact that the OSM score value is close to 1 indicates that the selected coefficient sequence represents the area with high accuracy, while the fact that it is close to 0 indicates that the area representation of the determined coefficient sequence is weak (Dietzel and Clarke 2007).

$$OSM = Compare * Pop * Edges * Clusters * Slope * X\text{-}mean * Y\text{-}mean \quad (1)$$

### 2.3. Input Data

CORINE is the land use/cover data produced by computer-aided visual interpretation method over satellite images according to the land cover/use classification in line with the standards determined by the European Environment Agency (EEA) (EEA 2020). The project, approximately 5.8 million km$^2$ area, including in Turkey, is carried out in 39 countries. It is aimed to create a standard database in all member countries (Ministry of Agriculture 2020). According to EEA criteria and classification units, changes in land cover/ land use for monitoring land via satellite images are detected using remote sensing and geographic information systems. CORINE data are served at three different classification levels (EEA 2020). The land cover data used in this study were used at the level 1 (City, Agriculture, Wetlands, Forest and Water Body).

**Table 1.** Data and sources used in the study

| Data Type | Source | Year |
|---|---|---|
| Land Use | CORINE | 2000<br>2018 |
| Urban | CORINE | 2000<br>2006<br>2012<br>2018 |
| Transportation | Open Street Map | 2000<br>2015<br>2018 |
| Slope | HGM | - |
| Hillshade | HGM | - |
| Excluded | IMM Administrative Border | - |

Urban data was obtained by subtracting residential areas from CORINE Land Cover data for four periods. Transportation data is obtained from Open Street Map, an open source and free service. Considering the routes of 1st degree importance in the region in transportation data, other routes are not included in the data. Transport data is prepared for 2000, 2015 and 2018. The slope and Hillshade data are produced from the Digital Elevation Model obtained from HGM.

## 3. RESULTS

Parameter values were determined according to the results of the calibration process for the urban simulation model of Istanbul Province. These parameters were used in the estimation phase. When the values are examined, it is concluded that the road effect of the model and urban growth are intense. According to the intervals in the calibration stages and the calculated OSM scores, the highest three coefficient information is presented in "Table 2", "Table 3" and "Table 4".

**Table 2.** Coarse calibration results

| Coefficients | Starting Ranges | | | OSM TOP 3 | | |
|---|---|---|---|---|---|---|
| | START | STEP | STOP | 1 | 2 | 3 |
| Diff | 0 | 25 | 100 | 25 | 25 | 25 |
| Breed | 0 | 25 | 100 | 1 | 100 | 100 |
| Spread | 0 | 25 | 100 | 25 | 25 | 25 |
| Slope | 0 | 25 | 100 | 75 | 75 | 75 |
| Road | 0 | 25 | 100 | 1 | 100 | 50 |

**Table 3.** Fine calibration results

| Coefficients | Starting Ranges | | | OSM TOP 3 | | |
|---|---|---|---|---|---|---|
| | START | STEP | STOP | 1 | 2 | 3 |
| Diff | 25 | 1 | 25 | 25 | 25 | 25 |
| Breed | 1 | 25 | 100 | 1 | 1 | 26 |
| Spread | 25 | 1 | 25 | 25 | 25 | 25 |
| Slope | 75 | 1 | 75 | 75 | 75 | 75 |
| Road | 0 | 25 | 100 | 76 | 51 | 1 |

**Table 4.** Final calibration results

| Coefficients | Starting Ranges | | | OSM TOP 3 | | |
|---|---|---|---|---|---|---|
| | START | STEP | STOP | 1 | 2 | 3 |
| Diff | 25 | 1 | 25 | 25 | 25 | 25 |
| Breed | 1 | 5 | 26 | 21 | 26 | 16 |
| Spread | 25 | 1 | 25 | 25 | 25 | 25 |
| Slope | 75 | 1 | 75 | 75 | 75 | 75 |
| Road | 1 | 15 | 76 | 61 | 1 | 31 |

The coefficient values obtained after the calibration process are presented in "Table 5". These values were used in the creation of the urban growth simulation model of Istanbul Province.

**Table 5.** Calculated coefficient values

| Coefficent | BEST_FIT |
|---|---|
| Diff | 25 |
| Breed | 21 |
| Spread | 25 |
| Slope | 75 |
| Road | 61 |

Change analysis was conducted between 2018 and 2040. As a result of the analysis, the rates of the land cover classes transformed into each other were calculated. Results are presented in "Table 6".

**Table 6.** Amounts of conversion to urban space

| Class | 2018-2040(ha) | % |
|---|---|---|
| Agriculture | 29,561 | 25.18 |
| Wetlands | 3 | 1.96 |
| Forest | 37,826 | 14.06 |
| Water Body | 0 | 0 |

As a result of the change analysis, an urban growth possibility of 24% in Istanbul was determined until 2040.

## 4. CONCLUSION

The rapid population growth in Istanbul and the irregular urbanization brought about by this caused unplanned land use. Therefore, the Istanbul metropolis needs an urban growth model that can describe land uses and local government decisions to assess the potential impact of growth policies. CA-based SLEUTH model has been preferred in modeling Istanbul city development due to its independent, dynamic and conforming to the basic conditions of urban growth simulation. In order to determine the urban development of the region in the model, it is necessary to determine the current situation at certain dates.

In this direction, especially given the urban growth structure of Istanbul, it is believed that the unstructured areas and their surroundings in Istanbul are under intense urbanization pressure. According to the results of the simulation model created, between 2018 and 2040, urban areas increased by 67390 hectares. Of this amount, 29561 hectares have been transformed from agricultural lands, 3 hectares from wetlands and 37826 hectares from forest lands. For this reason, whether forest and farmland will be protected will directly affect planning and local government decisions.

When developing policies that can control growth, legislators can use urban growth simulation models as a prediction. Simulation models should be produced under alternative scenarios in order to evaluate the possible effects of infrastructure projects that trigger dynamic and complex land cover changes in the metropolis of Istanbul.

## REFERENCES

Ayazli I E, Kilic F, Lauf S, Demir H & Kleinschmit B (2015). Simulating urban growth driven by transportation networks: A case study of the Istanbul third bridge. *Land Use Policy*, *49*, 332–340. https://doi.org/10.1016/j.landusepol.2015.08.016

Benenson I & Torrens P (2004). *Geosimulation: Automata-based modeling of urban phenomena*. John Wiley & Sons.

Candau J & Clarke K C (2000). Probabilistic Land Cover Transition Modeling Using Deltatrons. *2000 URISA Annual Conference, Orlando*.

Clarke K C, Hoppen S & Gaydos L (1997). A self-modifying cellular automaton model of historical urbanization in the San Francisco Bay area. *Environment and Planning B: Planning and Design*, *24*(2), 247–261. https://doi.org/10.1068/b240247

Clarke Keith C & Gaydos L J (1998). Loose-coupling a cellular automaton model and GIS: Long-term urban growth prediction for San Francisco and Washington/Baltimore. *International Journal of Geographical Information Science*, *12*(7), 699–714. https://doi.org/10.1080/136588198241617

Dietzel, C & Clarke K (2007). Toward Optimal Calibration of the SLEUTH Land Use Change Model. *T. GIS*, *11*, 29–

45. https://doi.org/10.1111/j.1467-9671.2007.01031.x

EEA (2016). *Urban Sprawl in Europe: Joint EEA-FOEN*.

EEA (2020). *CORINE land cover*. European Environment Agency.

Gigalopolis (2020a). *Project Gigalopolis Web Page*. USGS.

Gigalopolis P (2020b). *SLEUTH Applications*. USGS.

Goldstein N C, Candau J T & Clarke K C (2004). Approaches to simulating the "March of Bricks and Mortar." *Computers, Environment and Urban Systems*, *28*(1), 125–147. https://doi.org/https://doi.org/10.1016/S0198-9715(02)00046-7

Herold M, Goldstein N C & Clarke K C (2003). The spatiotemporal form of urban growth: measurement, analysis and modeling. *Remote Sensing of Environment*, *86*(3), 286–302. https://doi.org/https://doi.org/10.1016/S0034-4257(03)00075-0

Ministry of Agriculture (2020). *What's corine?* Republic Of Turkey Ministry Of Agriculture And Forestry.

Saadani S, Laajaj R, Maanan M, Rhinane H & Aaroud A (2020). Simulating spatial–temporal urban growth of a Moroccan metropolitan using CA–Markov model. *Spatial Information Research*. https://doi.org/10.1007/s41324-020-00322-0

Satterthwaite D (2005). *The Scale of Urban Change Worldwide 1950-2000 and Its Underpinnings*. International Institute for Environment and Development.

Silva E A & Clarke K C (2005). Complexity, emergence and cellular urban models: lessons learned from applying SLEUTH to two Portuguese metropolitan areas. *European Planning Studies*, *13*(1), 93–115. https://doi.org/10.1080/0965431042000312424

Silva E & Clarke K (2002). Calibration of the SLEUTH urban growth model for Lisbon and Porto, Portugal. *Computers, Environment and Urban Systems*, *26*, 525–552. https://doi.org/10.1016/S0198-9715(01)00014-X

Tobler W R (1970). A Computer Movie Simulating Urban Growth in the Detroit Region. *Economic Geography*, *46*, 234–240. https://doi.org/10.2307/143141

White R, Straatman B & Engelen G (2004). Planning scenario visualization and assessment: a cellular automata based integrated spatial decision support system. In D. G. Goodchild, M. F., & Janelle (Ed.), *Spatially integrated social science* (pp. 420–442). Oxford University Press, Inc.

Xie Y, Ma A & Wang H (2010). Lanzhou urban growth prediction based on Cellular Automata. In *2010 18th International Conference on Geoinformatics, Geoinformatics 2010*. https://doi.org/10.1109/GEOINFORMATICS.2010.5567556

Yi W & He B (2009). Applying SLEUTH for simulating urban expansion of Beijing. In *Proceedings - 2009 International Forum on Information Technology and Applications, IFITA 2009* (Vol. 2). https://doi.org/10.1109/IFITA.2009.543

Zhang Z, Jiang L, Peng R & Yin Y (2010). The spatiotemporal change of urban form in Nanjing, China: Based on SLEUTH and spatial metrics analysis. *2010 18th International Conference on Geoinformatics*, 1–5. https://doi.org/10.1109/GEOINFORMATICS.2010.5567753

Intercontinental Geoinformation Days

http://igd.mersin.edu.tr/2020/

# Evaluation of the change of Istanbul Anatolian Side land surface temperature values with CORINE data

**Lutfiye Kusak*[1], Ufuk Fatih Kucukali [2]**

[1]*Mersin University, Engineering Faculty, Geomatics Engineering Department, Mersin, Turkey*
[2]*Istanbul Aydın University, Department of Architecture, Istanbul, Turkey*

**Keywords**
LST
Impervious surfaces
Landsat 8 OLI
Sustainability
Urban planning

**ABSTRACT**

Socio-economic developments, diversity of employment opportunities, proximity to city functions such as education, health, and social services make cities the focus of people's attention. Consequently, in order to serve all functions such as industry, trade, accommodation, education, entertainment and transportation, a very dense impervious surface structures occur in cities. The increase in these uncontrolled artificial impervious areas causes changes in the urban climate and land surface temperature (LST). Remote sensing technologies have been frequently preferred in recent years to monitoring and detecting these changes quickly. In this study, using Landsat 8 OLI images, the temperature changes on the surfaces in the Anatolian Side of Istanbul, whose surface temperature values were obtained, were evaluated. In the study, LST values of Landsat 8 OLI satellite images of 23 April 2018 and 28 April 2020 were obtained and analyzed with the help of 2018 CORINE data. The Anatolian Side of Istanbul shows an intense urbanization tendency, especially in the coastal part. Special focus has been placed on the temperature changes of the impervious surfaces used in this region. It has emerged that these surfaces should be especially evaluated in planning and design studies due to their effect on city surface temperature changes.

## 1. INTRODUCTION

In the determination of surface temperatures, remote sensing technologies have been used in different scales and in many different interdisciplinary studies in recent years. There are both regional (Weng, 2001; Chen et al. 2006; Luan et al. 2020) and structure-based studies (Qiao et al. 2020; Aboelata and Sodoudi, 2020).

In addition, studies on global warming and climate change have increased remarkably today. A large part of the human population that will be most affected by these changes live in cities. This situation reveals the necessity of examining the temperature changes in cities and monitoring them in more detail within the framework of cause and effect relationships (Kusak and Kucukali, 2018). When temperature changes in cities are examined in the context of cause and effect relationships (Zhao et al. 2006; Wang et al. 2008; Deng et al. 2009; Liu et al. 2017), multiple parameters affect urban ecology with a complex network of relationships (Vlahov and Galea, 2002; Liao et al. 2017) and different ecological, physical and environmental characteristics of that area (Nacef et al. 2016; El Helew, 2018) and different anthropogenic effects (Shen et al. 2016) in each geographical area.

Morphological changes in the topography of cities, qualitative and quantitative decreases in green areas, increases in impermeable man-made surfaces such as concrete, asphalt and roof materials change the ecology of cities and create a unique microclimatic area under the influence of natural-artificial factors. The main determinant of these phenomena is urbanization and unplanned settlements and unsuitable land use. Although the relationship between land use and temperature difference has been investigated in many studies on land use and related temperature changes in cities, the choice and properties of materials used on artificial surfaces (Okeil, 2010), roof materials (Al-Obaidi et al. 2014), orientation of buildings Criteria such as their conditions and building form (O-Malley et al. 2014) and the relationship of climatic data, building sizes (Li et al. 2019), location selection of heat-discharging outdoor units of artificial ventilation elements (Kikegawa et al. 2006; Kusak and Kucukali, 2018) have also taken place in the literature as subjects of study .

There are many studies in which LST and CORINE data set were used together. The spatial distribution of surface temperature and land use (Lai et al. 2020; Alvi et al. 2019) and for the detection of cold and hot poles in

* **Corresponding Author**

*(lutfiyekusak@mersin.edu.tr) ORCID ID 0000-0002-7265-245X
(ufkucukali@aydin.edu.tr) ORCID ID 0000-0002-2715-7046

**Cite this study**

Kusak L. & Kucukali U. F. (2020). Evaluation of the change of Istanbul Anatolian Side land surface temperature values with CORINE data. Intercontinental Geoinformation Days (IGD), 64-67, Mersin, Turkey

cities (Lemus-Canovas et al. 2020) are some of these studies, LST and CORINE have been evaluated together.

Anatolian Side, or Asian Side of Istanbul, which is the region where approximately one third of the population in Istanbul lives, has experienced a rapid increase in terms of urbanization in recent years. For this reason, the region has been taken under the scrutiny in terms of urban planning, and the surface temperature changes of the land, especially in the last two years, are evaluated in this study. The obtained findings were interpreted in terms of urban planning with the CORINE data set.

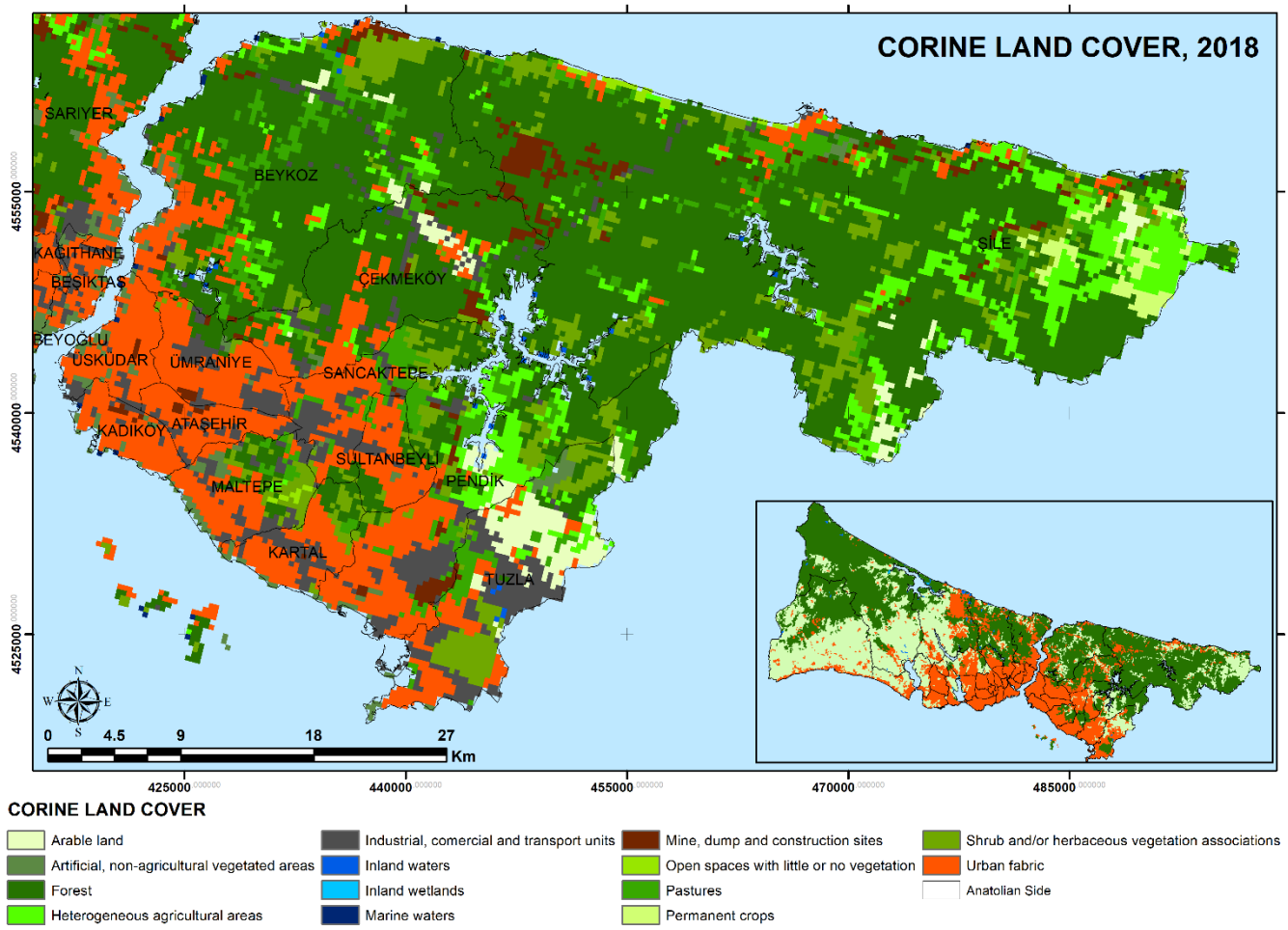


Figure 1. CORINE Land Cover (2018), Anatolian Side, Istanbul

## 2. MATERIALS AND METHOD

### 2.1. Study Area

Istanbul Anatolian Side has been studied as the study area. Anatolian Side is the eastern half of the city of Istanbul, located east of Bosphorus and geographically on the Asian mainland. Consisting of 38 districts in total, 14 districts of Istanbul are on the Anatolian side. Another airport in Istanbul, which also provides international transportation like Sabiha Gökçen Airport, is on this side. With the recent migrations and urbanization, the population on the Anatolian Side has reached approximately 4.3 million according to 2019 data. 1/3 of the population of Istanbul lives here. The increase in the population has led to an increase in residential areas, as well as an increase in places such as shopping centers where people can spend their daily time. Urbanization and gigantic structures have led to an increase in impermeable surfaces in the area, which was mostly green areas (Figure 1).

All these changes have brought about a change in the city temperature.

### 2.2. Data

In the study, April 23, 2018 and April 28, 2020 Landsat 8 OLI images were used to obtain LST values. Using Landsat 8 OLI images, the April 23, 2018 and April 28, 2020 images were prepared by the EROS Science Processing Architecture (ESPA) on-demand interface that provides Landsat higher-level science data products, including Climate Data Records (top of atmosphere (TOA) reflectance, brightness temperature, and spectral index which is NDVI. Additionally, 2018 CORINE data set was employed to interpret the relationship between LST and land use.

### 2.3. Methods

In the study, first LST values were obtained and then evaluations were made with the analyzed CORINE data.

The LST values are calculated using brightness temperature (BT) values. As the file prepared by ESPA contains TOA reflectance, BT, and surface reflectance NDVI, these steps were omitted. LST based on satellite brightness temperature (BT) was computed using the

following equation Eq. (1). Therefore, emissivity values are also defined in the study.

$$LST = \frac{BT}{1+(\lambda+\frac{BT}{\alpha})lnln\ \varepsilon} \quad (1)$$

BT is the effective at satellite temperature in Kelvin, λ is the wavelength of the emitted radiance in meters, α=1.438 x 10-2mK, and ε is the surface emissivity.

Since each object has a emissivity, the relationship between land cover and emissivity has been studied for many years (Van de Griend and Owe 1993; Valor and Caselles, 1996).

NDVI-based studies have been developed for the use of the obtained values in satellite images and land cover classes and emissivity values have been defined (Sobrino et al. 2004; Stathopoulou and Cartalis 2007; Tang et al. 2015).

In this study, the method used in the previous study (Kusak and Kucukali, 2018) and developed by Shen was preferred in LST calculation. Here, emissivity values of 0.9923 for water areas, 0.923 for urban impervious and bare soil areas, and 0.986 for vegetation areas are accepted. The formula in Eq. (2) for mixed areas is also used (Shen et al. 2016).

$$\varepsilon = 1.0094 + 0.047\ ln\ ln\ (NDVI) \quad (2)$$

## 3. RESULTS

The CORINE 2018 data set was cut for the Anatolian Side of Istanbul and evaluated using ArcGIS 10.5. According to the results of the evaluation, it has been determined that 23.02% of these areas are artificial surfaces, 30.02% are agricultural areas, 46.38% are forest and semi-natural areas and the remaining areas are wetlands or water bodies.

In addition, the percentage distributions of temperature values for 2018 and 2020 in these areas were calculated and these results are presented (Table 1). LST values were divided into 5 different classes as <25°C, 25-30°C, 30-35°C, 35-40°C and> 40°C. Using the 2018 CORINE data, the areal distributions of LST values classified for 4 main areas were calculated and then their percentage values were obtained. Although there was a decrease in regions higher than 40 degrees in 4 different regions, it was ignored because it was meaningless in the percentage presentation in the table.

When the evaluation is made between 2018 and 2020, it is seen that the regions with surface temperature values less than 25 °C in total have increased. In addition, there is a decrease in surface temperature values on artificial surfaces.

In the comparison made using satellite images dated 23 April 2018 and 28 April 2020, it is thought that the temporary closure measures experienced in many sectors and sub-sectors due to the COVID-19 pandemic experienced worldwide are effective.

**Table 1**. Land Surface Temperature (LST) (%)

| | 2018 | 2020 | 2018 | 2020 | 2018 | 2020 | 2018 | 2020 |
|---|---|---|---|---|---|---|---|---|
| | <25 °C | | 25-30 °C | | 30-35 °C | | 35-40 °C | |
| Total Surface | 58.27 | 72.82 | 38.94 | 24.49 | 2.77 | 2.67 | 0.02 | 0.02 |
| Artificial Surface | 4.33 | 5.85 | 18.98 | 17.43 | 2.59 | 2.61 | 0.02 | 0.02 |
| Agricultural Area | 7.59 | 12.49 | 8.75 | 3.88 | 0.07 | 0.03 | 0.00 | 0.00 |
| Forest and Seminatural Areas | 46.28 | 54.40 | 11.18 | 3.15 | 0.11 | 0.02 | 0.00 | 0.00 |
| Wetlands and Water Bodies | 0.08 | 0.08 | 0.04 | 0.03 | 0.00 | 0.00 | 0.00 | 0.00 |

## 4. DISCUSSION

LST values were calculated for the Anatolian side of Istanbul, which is an important region that has an intense urbanization phenomenon, urban development and growth dynamics, which covers a large area and should be kept under constant observation after the 1950s, and analyzed with the CORINE data set, and the results were discussed. Accordingly, cooling is observed in artificial areas in 2020. As emphasized before, the pandemic is thought to be effective in this. However, it should be observed whether this effect is permanent or temporary.

## 5. CONCLUSION

Remote sensing technologies have been used for a long time to monitor surface temperature changes in cities. The fact that remote sensing technologies have high resolutions in terms of spatial, temporal and spectral means that these technologies are preferred. In spite of their sensitivity, studies conducted with local methods at the city scale are long-term and costly. In addition, since climate change is a global phenomenon, its impact area includes wide areas beyond the scale of the building. In this study, it is suggested to benefit from easy, fast and cost-reducing supports to identify and monitor all these processes from urban planning to building production scale. For this purpose, Landsat 8 OLI satellite images and existing CORINE data set were used. In future studies, UAVs with thermal and multispectral sensor support can be used to examine smaller areas. In this way, problem areas can be focused and monitored.

## REFERENCES

Aboelata, A., & Sodoudi, S. (2020). Evaluating the effect of trees on UHI mitigation and reduction of energy usage in different built up areas in Cairo. Building and Environment, 168, 106490.

Al-Obaidi, K. M., Ismail, M., & Rahman, A. M. A. (2014). Passive cooling techniques through reflective and radiative roofs in tropical houses in Southeast Asia: A literature review. Frontiers of Architectural Research, 3(3), 283-297.

Alvi, U., Suomi, J., Almalla, R., & Käyhkö, J. (2019, January). A cost-efficient method for deriving spatially

continuous urban air temperatures using Landsat 8 and open land use-land cover data. In Geophysical Research Abstracts (Vol. 21).

Chen, X. L., Zhao, H. M., Li, P. X., & Yin, Z. Y. (2006). Remote sensing image-based analysis of the relationship between urban heat island and land use/cover changes. Remote sensing of environment, 104(2), 133-146.

Deng, J. S.,Wang, K., Hong, Y., andQi, J. G. (2009). Spatio-temporal dynamics and evolution of land use change and landscape pattern in response to rapid urbanization. Landscape and urban planning, 92(3-4), 187-198.

El Helew, W. K. (2018). Evaluation of dynamic interaction of surface thermal temperature changes with agricultural development aocesses ubder climate change conditions of egypt. Misr Journal of Agricultural Engineering, 35(4), 1533-1548.

Kikegawa, Y., Genchi, Y., Kondo, H., & Hanaki, K. (2006). Impacts of city-block-scale countermeasures against urban heat-island phenomena upon a building's energy-consumption for air-conditioning. Applied Energy, 83(6), 649-668.

Kuşak, L.,& Küçükali, U. F. (2018). Outlier detection of land surface temperature: Küçükçekmece region. International Journal of Engineering and Geosciences, 4(1), 1-7.

Lai, S., Leone, F., & Zoppi, C. (2020). Spatial Distribution of Surface Temperature and Land Cover: A Study Concerning Sardinia, Italy. Sustainability, 12(8), 3186.

Lemus-Canovas, M., Martin-Vide, J., Moreno-Garcia, M. C., & Lopez-Bustins, J. A. (2020). Estimating Barcelona's metropolitan daytime hot and cold poles using Landsat-8 Land Surface Temperature. Science of the Total Environment, 699, 134307.

Li, X., Zhou, Y., Yu, S., Jia, G., Li, H., & Li, W. (2019). Urban heat island impacts on building energy consumption: A review of approaches and findings. Energy, 174, 407-419.

Liao, J.,Jia, Y., Tang, L., Huang, Q., Wang, Y., Huang, N., and Hua, L. (2017). Assessment of urbanization induced ecological risks in an area with significant ecosystem services based on land use/cover change scenarios. International Journal of Sustainable Development and World Ecology, 1-10.

Liu, Y.,Chen, Z. M., Xiao, H., Yang, W., Liu, D., and Chen, B. (2017). Driving factors of carbondioxide emissions in China: an empirical study using 2006-2010 provincial data. Frontiers of Earth Science, 11(1), 156161.

Luan, X. L., Yu, Z., Zhang, Y., Wei, S., Miao, X., Huang, Z. Y., & Xu, C. (2020). Remote sensing and social sensing data reveal scale-dependent and system-specific strengths of urban heat island determinants. Remote Sensing, 12(3), 391.

Nacef, L.,Bachari, N. E. I., Bouda, A., &Boubnia, R. (2016). "Variability and decadal evolution of temperature and salinity in the Mediterranean Sea surface". International Journal of Engineering and Geosciences, 1(1), 20-29.

O'Malley, C., Piroozfarb, P. A., Farr, E. R., & Gates, J. (2014). An investigation into minimizing urban heat island (UHI) effects: A UK perspective. Energy Procedia, 62(0), 72-80.

Okeil, A. (2010). A holistic approach to energy efficient building forms. Energy and buildings, 42(9), 1437-1444.

Qiao, Z., Liu, L., Qin, Y., Xu, X., Wang, B., & Liu, Z. (2020). The impact of urban renewal on land surface temperature changes: a case study in the main city of Guangzhou, China. Remote Sensing, 12(5), 794.

Shen, H., Huang, L., Zhang, L., Wu, P., & Zeng, C. (2016). Long-term and fine-scale satellite monitoring of the urban heat island effect by the fusion of multi-temporal and multi-sensor remote sensed data: A 26-year case study of the city of Wuhan in China. Remote Sensing of Environment, 172, 109-125.

Shen, H., Huang, L., Zhang, L., Wu, P., and Zeng, C. (2016). Long-term and fine-scale satellite monitoring of the urban heat island effect by the fusion of multi temporal and multi-sensor remote sensed data: A 26year case study of the city of Wuhan in China. Remote Sensing of Environment, 172, 109-125.

Sobrino, J. A., Jiménez-Muñoz, J. C., & Paolini, L. (2004). Land surface temperature retrieval from LANDSAT TM 5. Remote Sensing of environment, 90(4), 434-440.

Stathopoulou, M., & Cartalis, C. (2007). Daytime urban heat islands from Landsat ETM+ and Corine land cover data: An application to major cities in Greece. Solar Energy, 81(3), 358-368.

Tang, B. H., Shao, K., Li, Z. L., Wu, H., & Tang, R. (2015). An improved NDVI-based threshold method for estimating land surface emissivity using MODIS satellite data. International Journal of Remote Sensing, 36(19-20), 4864-4878.

Valor, E., & Caselles, V. (1996). Mapping land surface emissivity from NDVI: Application to European, African, and South American areas. Remote sensing of Environment, 57(3), 167-184.

Van de Griend, A. A., & OWE, M. (1993). On the relationship between thermal emissivity and the normalized difference vegetation index for natural surfaces. International Journal of remote sensing, 14(6), 1119-1131.

Vlahov, D. and Galea, S. (2002). Urbanization, urbanicity, and health. Journal of Urban Health, 79(1), pp.S1-S12.

Wang, J., Da, L., Song, K., and Li, B. L. (2008). Temporal variations of surface water quality in urban, suburban and rural areas during rapid urbanization in Shanghai, China. Environmental Pollution, 152(2), 387393.

Weng, Q. (2001). A remote sensing? GIS evaluation of urban expansion and its impact on surface temperature in the Zhujiang Delta, China. International journal of remote sensing, 22(10), 1999-2014.

Zhao, S., Da, L., Tang, Z., Fang, H., Song, K., and Fang, J. (2006). Ecological consequences of rapid urban expansion: Shanghai, China. Frontiers in Ecology and the Environment, 4(7), 341-346

Intercontinental Geoinformation Days

http://igd.mersin.edu.tr/2020/

# Financial analyses of ODHCs in Turkey in terms of profitability

**Elif Akyel*[1], Ozsen Corumluoglu [1]**

[1]İzmir Katip Çelebi Üniversitesi, Mühendislik ve Mimarlık Fakültesi, Harita Mühendisliği, İzmir, Türkiye

**Kewords**
Inverse Distance Weighting
Financial Performance Analysis
Oral and Dental Health Center

**ABSTRACT**

Oral and Dental Health Centers (ODHC), which occupy an important place in health services, have increased in number with the Health Transformation Program (HTP) implemented in Turkey (Islıcık & Yar, 2018). In this way, public access to dental treatment services has been facilitated and have allowed them to gain continuity. These services, which allow people to increase their well-being , contribute to the mental well-being of individuals, but also come to the fore in their therapeutic aspect. Services, whose contribution is undeniable in terms of social benefit, require quite high amounts of resources from the point of view of the country's economy. This also requires a financial performance analysis.

Dentists are one of the most important factors for ODHCs to continue their work regularly. For this reason, in the study, financial performance analyzes of existing ODHCs depending on the variable of profit per dentist were carried out with Geographical Information Systems (GIS) Inverse Distance Weighting-IDW and related maps were produced. When the GIS findings are evaluated, a more understandable result is obtained by visualizing the financial performance analysis of 128 public ODHCs, and the importance levels of the variables that affect the performance are also revealed.

## 1. INTRODUCTION

There are many service areas that people need to live their lives. Health services are also one of these areas that are needed because of their vital importance on human life.

Financial performance analysis is one of the most challenging areas for health systems and is of critical importance. A performance analysis gives businesses the opportunity to test the efficiency of their past activities. In order to ensure efficiency and productivity in the use of resources, minimizing expenses and maximizing revenues, financial performance analyzes are also closely related to politicians and decision makers. A performance analysis allows you to act consciously in decisions, work and actions to be taken (Ercan , Dayı, & Akdemir, 2013). For this reason, it is recommended that performance analysis be performed regularly for ODHCs.

In this study, data of 128 ODHCs were obtained from the Department of Statistics, Analysis, Reporting and Strategic Management of the Ministry of Health, based on the first 6 months of 2016. From the data obtained, the number of canal treatments per dentist, the number of fillings per dentist, the number of teeth extracted per dentist scaling per dentist, the number of surgical interventions per dentist and fixed prosthesis per dentist and the number of removable prostheses per dentist were the variables used in financial performance analysis as factors affecting profit per dentist. As a result of the interpolation studies carried out in the GIS which allows analysis of all these factors on a spatial basis, maps showing the financial status of the existing ODHCs were created. This study is important in terms of benefiting from GIS while performing financial performance analysis of ODHCs.

## 2. METHOD

In this study, the performance analysis of ODHCs and the spatial distributions according to several factors which are effective on the current performances of ODHCs are revealed, and the performance improvement of ODHCs have been determined by IDW. Inverse distance weight interpolation method is based on the use of inverse weighting of the distance between points

* **Corresponding Author**

*(elifakyel@outlook.com) ORCID ID 0000-0002-9355-7478
(ozsen.corumluoglu@ikcu.edu.tr) ORCID ID 0000-0002-7876-6589

**Cite this study**

Akyel E, & Çorumluoğlu Ö. (2020). Financial analyses of ODHCs in Turkey in terms of profitability, Intercontinental Geoinformation Days (IGD), 68-71, Mersin, Turkey

whose main values are known and the point to be estimated as weight (Göğsu & Hastaoğlu, 2019). Rather than point representation, the IDW technique was used because it enables the raster representation to compare this value of the factor at the points whose value is known visually much more effectively with the values of the other values of the points. In accordance with this selection, the distributions resulting from the application of the inverse distance weight interpolation method (Inverse Distance Weighting-IDW) technique were used for raster notation.

As a result of the analysis carried out in ArcGIS using the IDW method, the mathematical model of which is given below, colored maps can be created that effectively show the spatial distribution of the financial performance of the Centers. Since the weighted moving average is a widely used approach in interpolation, IDW is a preferred form in GIS analysis, although various methods including different weight functions have been used. IDW is a complete intermediate generator (interpolator) and reinforces the values of the data. The IDW estimator can be given by the following equation (Demircan, Alan, & Şensoy, 2011)

$$Z(X_0) = \frac{\sum_{1=1}^{n} z(X_i).d_{i0}^{-r}}{\sum_{i=1}^{n} d_{i0}^{-r}} \qquad (1)$$

The location $X_0$, where the predictions are made is a function of n neighboring measurements giving the number of neighboring measurements. ($z(X_i)$ ve i=1,2,…,n,); r is the exponential value that determines the assigned weight of each of the observations, and $d_{i0}$ is the distance that separates the observation location $X_i$ and the prediction location $X_0$. As the exponent grows, the assigned weight of observations far from the prediction location shrinks; increasing the denominator indicates that the forecasts are very similar to the nearest observations (Demircan, Alan, & Şensoy, 2011).

## 3. RESULTS

In the study, the financial performance analysis of the centers was carried out based on the variable profit per dentist obtained by the inclusion of income and expense items of 128 public ODHCs into the process. The IDW interpolation method was used to reveal spatial patterns of the resulting variance in the financial performance of the Centers, and maps were created that effectively revealed spatial models of the financial performance of the CentersIn this way, the pattern of financial performance of existing ODHCs in terms of profitability per dentist in the country was demonstrated by measuring. Profitability per dentist financial performance of centers visualized by interpolating them with GIS.

The variable of profit per dentist was obtained as a result of mathematical processing of the numbers of scaling treatment, root canal treatment, surgical intervention treatment, fixed prosthesis treatment, extraction and filling treatment. The variables that had the most effect on the profit variable were determined. After that the variables with the highest impact rate and the profitability variable were analyzed together and maps were created to determine the current situation. When the maps created are examined, the subsets that affect profitability and their effects on performance measurement are seen. When Scaling treatment is analyzed together with Surgical treatment, the profitability map of Turkey is formed given in Figure 1.

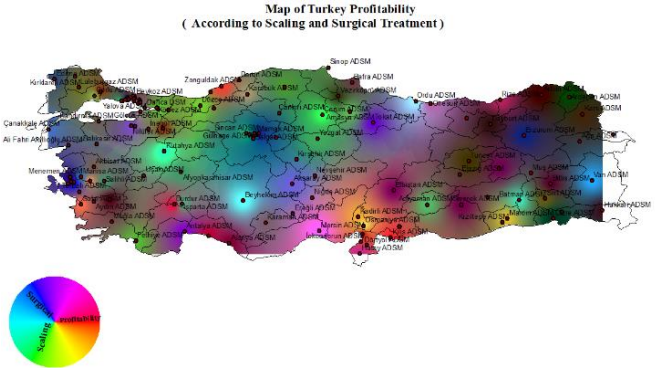


**Figure 1.** According to Scaling and Surgical Treatment

When Scaling treatment is analyzed together with Root Canal Treatment, the profitability map of Turkey is formed given in Figure 2.

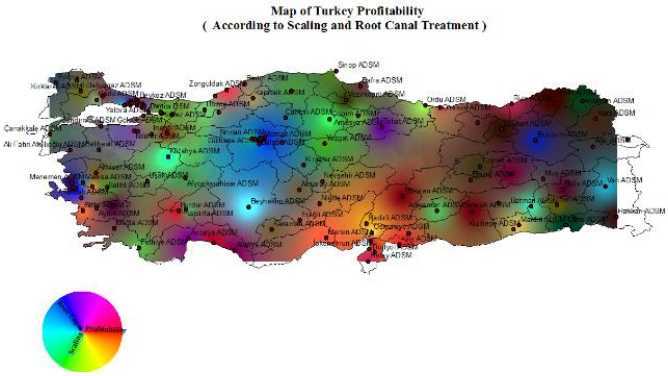


**Figure 2.** According to Scaling and Root Canal Treatment

When Scaling treatment is analyzed together with Fixed Prosthesis treatment, the profitability map of Turkey is formed given in Figure 3.

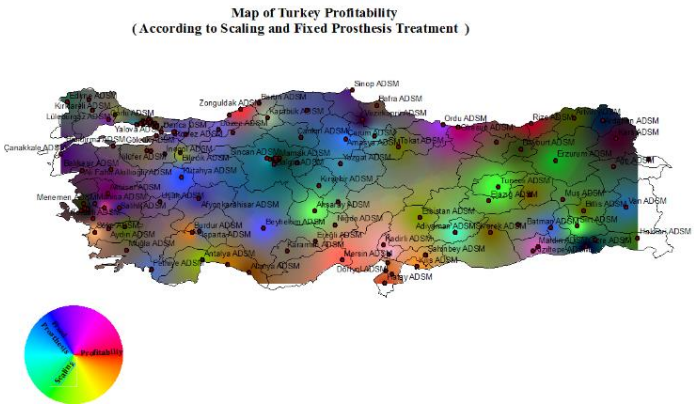


**Figure 3.** According to Scaling and Fixed Prosthesis Treatment

When Root Canal treatment is analyzed together with Surgical treatment, the profitability map of Turkey is formed given in Figure 4

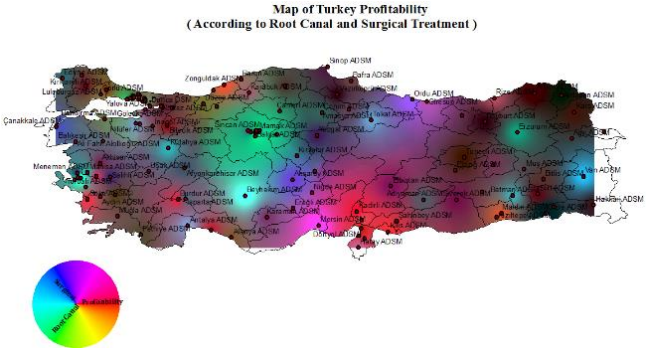


**Figure 4.** According to Root Canal and Surgical Treatment

When Root Canal treatment is analyzed together with Fixed Prosthesis treatment, the profitability map of Turkey is formed given in Figure 5.

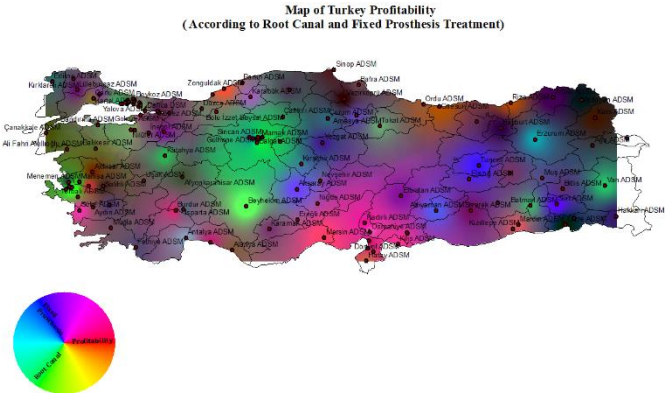


**Figure 5.** According to Root Canal and Fixed Prosthesis Treatment

## 4. CONCLUSION

Today, it is important for healthcare enterprises to evaluate their performance in order to increase their competitiveness and ensure their continuity (Samut 2014). Since areas that need to be improved can be easily identified in performance analysis, regular performance analysis is a report card for institutions. Performance analysis of ODHCs, which facilitate public access to treatment in the health sector, is important.

In this study, the financial performance assessment of 128 ODHCs in Turkey was carried out in GIS. Performance evaluation is based on the variable profit per dentist. The variables affecting profitability per dentist more; number of scaling treatments, surgical intervention treatment, root canal treatment and fixed prosthesis treatment.In addition to the profit variable per dentist, other variables with a high impact rate were taken into account during the analysis. As a result of the analysis, maps were created where the contribution of these variables on profitability can be seen.

As a result of the financial performance assessment of the centers, it is seen that there are profit centers, as well as losses. When the analyzes are evaluated, the center that has the best performance Tunceli Oral and Dental Health Center. The reason for the high performance of this center is that it is the only ODHC on a provincial basis, there isn't other public dental treatment center that the public can apply to and the socio-economic situation of the public According to the analysis results, the financial performance of 26 ODHCs is high. These centers are clustered in two points. These are Central Anatolia region and Aegean region. The reasons for the high financial performance in these regions are the intensive application of the treatments that affect the profit rate the most, the population density receiving service from the centers and the number of other ODHCs accessible in that region.In addition, the educational level of the people living in this region, the economic situation, the quality and competence of the dentists who carry out their activities in the private sector can be interpreted as other factors that affect the financial performance of the centers.

On the other hand, when the financial performance is evaluated, it is seen that 14 centers have lost. When these centers are examined, the centers with lowest financial performans among the ODHCs is found as Şırnak Dt. Nurullah Kadirhan. Cizre ODHC, located in the Cizre district of Şırnak, is recorded as the second most unprofitable center. It is possible to say that the reasons for the loss of the centers in Şırnak province are high expenditure and the socio-economic and socio-cultural situation in the region.

When the resulting clusters are evaluated, finding low-performance centers in high-performance clusters can be considered as a remarkable finding in terms of the study. It is possible to interpret that there is not competitive relationship between centers, after examining the spatial patterns that explain financial performance. The fact that the centers are financed by the state is considered to be effective in this situation.

In this study, the financial performance of ODHCs was measured and the importance of variables affecting performance was revealed. As a result of the literature review, there are only few studies on financial performans analyses on ODHC. It shows that a financial performance analysis for ODHCs that require high amounts of resource use will provide important information that can be used by individuals, institutions and organizations.

Potential population information from the centers was not taken into consideration in the study. How the financial performance changes by keeping the population information served from the centers under control is also a new research topic. Furthermore, in order to develop a holistic understanding of the financial performance of the centers, it can also be investigated how variance changes over the years. Thus, more valid findings can be obtained with the financial performance of the health system.

## REFERENCES

Demircan, M., Alan, İ., & Şensoy, S. (2011). Coğrafi Bilgi Sistemleri Kullanılarak Sıcaklık. TMMOB Harita ve Kadastro Mühendisleri. Ankara.

Ercan , C., Dayı, F., & Akdemir, E. (2013). Kamu Sağlik İşletmelerinde Finansal Performans. Asia Minor Studies, 54-71.

Göğsu, S., & Hastaoğlu, K. Ö. (2019 Nisan 25-27)Ters Mesafe Ağırlıklı Enterpolasyon Yönteminde Güç Fonksiyonu. TMMOB Harita ve Kadastro Mühendisleri Odası 17. Türkiye Harita Bilimsel ve Teknik Kurultay. Ankara.

Islıcık, S., & Yar, C. E. (2018). Kamu Ağız ve Diş Sağlığı Merkezlerinin Coğrafi Bölgelere Göre Finansal Performanslarının Değerlendirilmesi. İşletme Araştırmaları Dergisi, 184-209.

Y.P.K.Samut. (2014).İki Aşamalı Çok Kriterli Karar Verme İle Performans Değerlendirmesi:AHP ve TOPSIS Yöntemlerinin Entegrasyonu. Anadolu Üniversitesi Sosyal Bilimler Dergisi, 57-68

.

Intercontinental Geoinformation Days

http://igd.mersin.edu.tr/2020/

# Landfill site selection literature review: For Bodrum District

**Cansu Nehteparov*[1], E. Özgür Avşar [2]**

[1]Çanakkale Onsekiz Mart University, Institute of Graduate Studies, Department of Geomatics Engineering, Çanakkale, Turkey
[2]Çanakkale Onsekiz Mart University, Engineering Faculty, Department of Geomatics Engineering, Çanakkale, Turkey

**Keywords**
Solid waste
Landfill site selection
Criteria
Frequency
Analytical Hierarchy Process

**ABSTRACT**

With the rapid increase of the world's population, waste production is also increasing rapidly and these wastes must be disposed of in landfill sites under control in national-international accordance with the decrees. Nowadays, some of the waste is still disposed of in wild irregular landfill sites. As a result of these wild irregular landfill sites, it is seen that there is a need for solid waste landfill sites due to environmental pollution and health risks. One of the areas where solid waste is disposed of in wild irregular landfill sites is the Bodrum district of Muğla province. For these solid waste landfill sites to be built in suitable areas, some criteria need to be considered. In this study, the location selection criteria for solid waste landfill sites for the Bodrum district of Muğla province were determined by examining the frequency of use in the literature. Nevertheless, national-international decrees that were evaluated in criterion restrictions have also been examined.

## 1. INTRODUCTION

With the increase in the world population, waste production is also increasing. Today, some of the waste produced is still disposed of wild irregular landfill sites that cause environmental pollution and health risks. Therefore, an effective solid waste management system is needed (Özkan 2018). The wastes must be collected, disposed of, and recycled in an order determined by national and international decrees (Chabuk et al. 2016).

These landfill sites must be able to serve for long terms as well as the population of the land it will serve, waste produced per person, the assumed number of waste to be produced in the following years as calculated by the earlier years of service should be determined. Then, it should be investigated whether there are sufficient alternative areas for the construction of the calculated storage area.

Solid waste landfill site selection is a complicated process because the suitability of alternative areas should be determined by paying attention to many environmental, economic, and social criteria (Özkan 2018).

For landfill site selections to be performed efficaciously, the criteria must be determined by paying attention to national-international decrees, expert opinions, and frequency of use in literature. Additionally, the criteria may vary according to the data availability and characteristics of the relevant region.

Geographic Information System (GIS) and Multi-Criteria Decision Analysis (MCDA) should be used in landfill siting because they are powerful, integrated tools used to solve the problem of landfill site selection (Chabuk et al. 2016). Among the MCDA methods, Analytical Hierarchy Process (AHP) is the most common and popular, used to identify criteria weights using a pairwise comparison matrix (Mohammed et al. 2019).

In Muğla, Bodrum where this study uses as an application area, wild irregular landfill sites that are close to residential zones, affects the environment and human health negatively due to methane gas explosions chained by the increase in heat during the summertime.

Also, Bodrum is one of the most touristic regions of Turkey and the summer population is much higher than the winter population. Therefore, the size of the landfill site should be taken into account according to the amount of waste in the summer population.

Consequently, a solid waste landfill site appears to be needed in Bodrum.

In this study, the frequency of use of the criteria in the literature and the national-international decrees that were considered in the criterion constraints were

*Corresponding Author

*(nehteparovcansu@gmail.com) ORCID ID 0000 – 0001 – 5402 – 3038
(ozguravsar@comu.edu.tr) ORCID ID 0000 – 0002 – 3804 – 1209

Cite this study

Nehteparov C. & Avşar E. Ö. (2020). Landfill site selection literature review: For Bodrum District. Intercontinental Geoinformation Days (IGD), 72-75, Mersin, Turkey

examined. At the same time, this study will guide the criteria to be determined for future research.

## 2. METHOD

GIS and AHP are often used for the alternative landfill site selections. AHP divides the decision problems into understandable parts; each of these parts is analyzed separately and integrated in a logical manner (Rahmat et al. 2016). AHP is a method used to determine the severity of effective measures in decision making with binary comparisons. The method helps to evaluate multi-criteria decision-making problems under uncertainty by including the decision maker's experience, knowledge, and intuition in the decision. In order to find the weights of the criteria, 1-9 grades of importance are used (Avşar 2018).

The reason for determining severity grades is to determine whether the decision- decider behaves consistently when comparing criteria. Weights can be used in comparison matrices as a result of the consistency rate being less than 10%.

In this study, the frequency of use of criteria has been examined in a total of 23 sources applied in 14 different countries since 2010. These countries are; Turkey, Iraq, Serbia, Pakistan, Morocco, Egypt, Malaysia, Bangladesh, Iran, Ethiopia, Ghana, India, Italy, and Cameroon.

Frequency of use of the criteria is shown in the Fig. 1 below. The least mentioned criteria in the literature were collected under the name of the other group.

The 28 criteria examined were weighted according to their frequency of use. The weighting table was shown in Table 1.Then, taking into account the characteristics of the region, the selected 11 criteria were reweighted. The reweight table was shown in Table 2.

## 3. RESULTS

In this study, the criteria to be considered in the selection of solid waste landfill site locations were examined. Since 2010, the criteria have been examined on a total of 23 sources in 14 different countries. As Fig.1 suggests, the most commonly used criteria are; distance to roads, distance to surface waters, slope, distance to settlements, and land use/land cover. Respectively weights; 0.10, 0.09, 0.08, 0.08, 0.08.

These criteria were seen to be the most important criteria for landfill site selections. Other criteria have been seen to change according to the characteristics of the region.

For Bodrum district, 11 criteria were selected from 28 criteria. Taking into account the data obtained from the open-source and the characteristics of the region, the criteria were determined. These criteria; distance to roads, distance to surface waters, slope, distance to settlements, land use/land cover, geology, distance to protected areas, distance to airports, aspect, distance to the coastline, and population density.

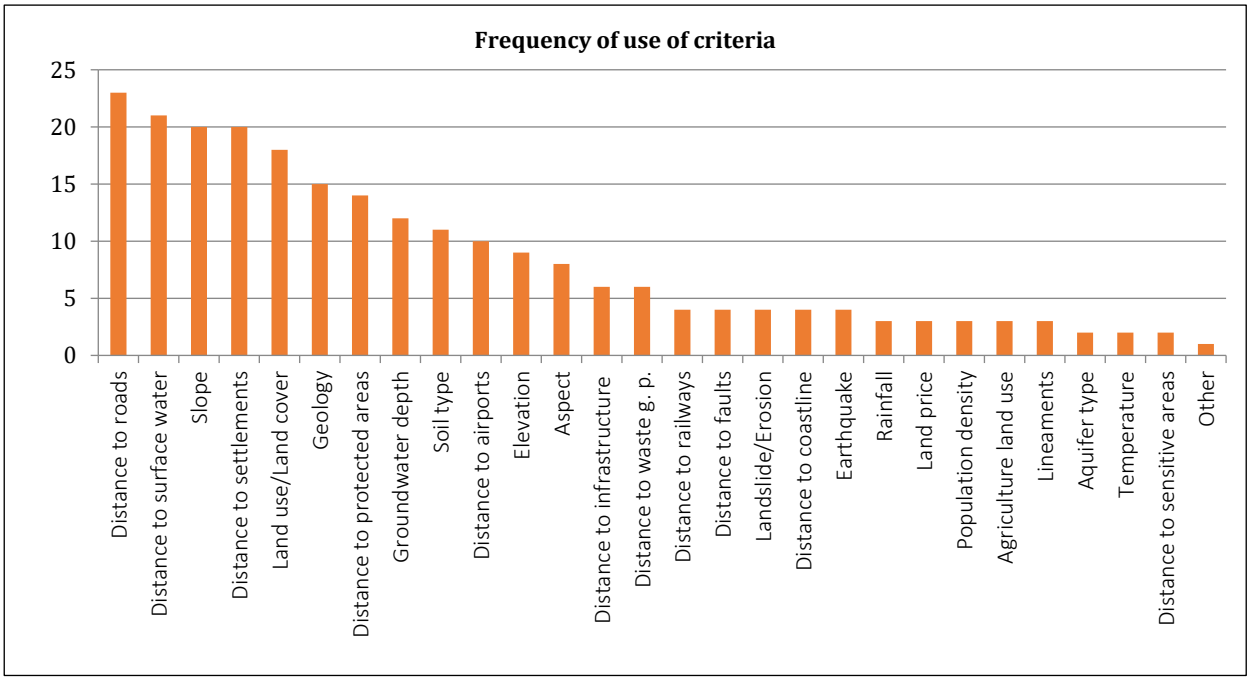


**Figure 1.** Frequency of use of criteria in literature

Other criteria are; state border, forests, snow/glacier, plantation, military areas, talwegs, landscape, borehole, flooding, nonferrous exploitation fields, and distance to industrial areas.

**Table 1.** Criteria in literature and their weight

| Criteria | Weight | Criteria | Weight | Criteria | Weight | Criteria | Weight |
|---|---|---|---|---|---|---|---|
| D.t.roads | 0.10 | G.water depth | 0.05 | D.t.railw. | 0.02 | Popul. Den. | 0.01 |
| D.t. s.water | 0.09 | Soil type | 0.05 | D.t.faults | 0.02 | Agri. l. use | 0.01 |
| Slope | 0.08 | D.t.airports | 0.04 | L.S./Eros. | 0.02 | Lineaments | 0.01 |
| D.t.settl. | 0.08 | Elevation | 0.04 | D.t.coastl. | 0.02 | Aquifer ty. | 0.01 |
| L.U./L.C. | 0.08 | Aspect | 0.03 | Earthquake | 0.02 | Temperat. | 0.01 |
| Geology | 0.06 | D.t. infrast. | 0.03 | Rainfall | 0.01 | D.t.sens. a. | 0.01 |
| D.t. prot.ar. | 0.06 | D.t.waste g. | 0.03 | Land price | 0.01 | Other | 0 |
| | | | | | | Summation | 1.00 |

Then, the 11 criteria selected were reweighted. In the reweighting for the selected 11 criteria, distance to roads, distance to surface waters, slope, distance to settlement areas, and land use/land cover criteria were found to take high weights. Respectively weights are 0.15, 0.13, 0.13, 0.13, 0.11.

**Table 2.** Determined criteria and their weight

| Criteria | Weight | Criteria | Weight | Criteria | Weight |
|---|---|---|---|---|---|
| D.t.roads | 0.15 | L.U./L.C | 0.11 | Aspect | 0.05 |
| D.t.s.w. | 0.13 | Geology | 0.10 | D.t.c.l. | 0.03 |
| Slope | 0.13 | D.t.p.a. | 0.09 | Pop.de. | 0.02 |
| D.t.settl. | 0.13 | D.t.air. | 0.06 | Sum. | 1.00 |

While examining the criteria in the literature, it was also examined whether there are national-international decrees set by the countries.

When the studies carried out in Iran were examined; in 2016, Rahmat and others ignored national decrees, while in 2019 it was observed that Barzehkar and others took into account the decrees in his study. It has also been observed that Ghana and India take into account national decrees when determining criteria restrictions. Studies conducted in other countries have observed that expert opinions, questionnaires, and national-international decrees together were taken into account in determining criteria restrictions.

## 4. DISCUSSION

These findings suggest that the first five criteria were significant according to the weightings process. The first most commonly used criterion is the distance to roads criterion. Landfill sites need to be close to roads because moving waste over long distances will increase the cost. At the same time, landfill sites should not be too close to roads and should not create visual pollution.

Therefore, it has been seen that the distance to roads criterion is one of the criteria to be considered the most. The second crucial criterion is the distance to surface water. In this criterion, landfill sites must be built away from surface waters to avoid environmental pollution. The third most commonly used criterion was the slope criterion. Building landfill sites in areas with high slopes will cost a lot of money due to excavation-filling operations.

Therefore, landfill sites should be built where the slope is low. Landfill sites should be built in areas far from settlement areas. The environment and human health should not be compromised. The fifth most widely used criterion in the literature is the land use criterion. Land use/Land cover is the fifth most widely used criterion in the literature. Landfill sites should not be built in forest areas. It can be said that these criteria are the main criteria to be considered in future studies.

When criterion restrictions were examined, it was observed that 3 out of 14 countries were bound by decrees. In the studies examined, it was observed that the researchers applied different references when determining the criteria. As a result of the reviews, it is clear that the national decrees of the countries were inadequate.

## 5. CONCLUSION

In Bodrum, wild irregular landfill sites imperil the environment and human health. Therefore, a solid waste landfill site appears to be needed in Bodrum. In this study, the frequency of use of the criteria used in the selection of solid waste storage areas in the literature for Bodrum district was examined. The 28 criteria determined as a result of the literature review were weighted according to their frequency of use. The most commonly used criteria were observed as a result of weighting. 11 criteria were determined for the Bodrum district. The criteria were determined by taking into account the characteristics of the region and the data obtained. It was observed that the criteria vary according to regional characteristics in the sources examined. At the same time, it was examined whether national-international decrees were taken into account in the criterion restrictions. It has been observed in most sources that national-international decrees were not taken into account. It is clear that national-international decrees must be taken into account for an efficient outcome. This study will guide future studies.

## REFERENCES

Aksoy E (2016). Landfill site selection of Antalya city using remote sensing and geographical information systems, MS Thesis, Akdeniz University, Antalya (in Turkish).

Alfy Z, Elhadary R & Elashry A (2010). Integrating GIS and MCDM to deal with landfill site selection. International Journal of Engineering & Technology, 33-40.

Amoah R & Kursah M (2019). Geospatial analysis of landfill site selection perspectives using geographic information systems in Bongo district, Ghana. SN Applied Sciences, 1-15. https://doi.org/10.1007/s42452-019-1273-y

Avşar M (2018). A multi goal model proposal for project acceleration. PhD Thesis, Yıldız Technical University, Istanbul (in Turkish).

Barzehkar M, Dinan N, Mazaheri S, Tayebi R & Brodie G (2019). Landfill site selection using GIS-based multi-criteria evaluation (case study: SaharKhiz Region located in Gilan Province in Iran. SN Applied Sciences,https://doi.org/10.1007/s42452-019 1109-9

Bouroumine Y, Bahi L, Ouadif L & Errouhi A (2019). Sitting MSW landfill combining GIS and Analytical Hierarchy Process (AHP), case study: Ajdir, Morocco. International Journal of Civil Engineering and Techhnology, 1113-1123.

Chabuk A, Al-Ansari N, Hussain H, Knutsson S & Pusch R (2016). Landfill siting using GIS and AHP (Analytical Hierarchy Process): a case study Al-Qasim Qadhaa, Babylon, Iraq. Journal of Civil Engineering and Architecture, 530-543. https://doi.org/10.17265/19347359/2016.05.002

Chaudhry M, Ashraf U, Ali I & Ali S (2019). GIS- Based Multi-Criteria Evaluation of Landfill Site Selection in Lahore, Pakistan. Polish Journal of Environmental Studies, 1-11. https://doi.org/10.15244/pjoes/95181

Ciritci D & Turk T (2019). Automatic determination of alternative landfill sites with analytical hierarchy process and geographical information systems: a case study in Sivas city. Journal of Geodesy and Geoinformation,61-74.https://doi.org/10.9733/JGG.2019R00601005.T

Dar S, Shah S, Wani M & Skinder S (2018). Identification of suitable landfill site based on GIS in Leh, Ladakh Region. GeoJournal, 1-15. https://doi.org/10.1007/s10708-018-9933-9

Deniz M & Topuz M (2018). Alternative landfill site selection in Uşak district by using multi-criteria decisionmaking analysis supported by geographical information systems (GIS) with analytic hierarchy process. Journal of Hitory Culture and Art Research, 544-578. https://dx.doi.org/10.7596/taksad.v7i5.1830

Gebre S & Getahun K (2020). GIS-based potential landfill site selection using MCDM-AHP modeling of Gondar Town, Ethiopia. African Geographical Review, 1-20. https://doi.org/10.1080/19376812.2020.1770105

Ghoutum A, Lebga A & Edith K (2020). Landfill site suitability selection using geospatial technology for the Yaounde Metropolitan City and its Environs: case of Soa Subdivision, Cameroon. European Scientific Journal, 95-111. https://doi.org/10.19044/esj.2020.v16n6p95

Güler D (2016). Alternative landfill site selection using analytic hierarch process and geographic information systems: a case study Istanbul, MS Thesis, Istanbul Technical University, Istanbul (in Turkish).

Islam A, Hasan M & Murshed S (2020). Selecting suitable landfill site with multi-criteria evaluation and GIS: a case of Savar upazila in Bangladesh. Arabian Journal of Geosciences, 1-15.https://doi.org/10.1007/s12517-020-05925-3

Laue J, Chabuk A, Alkaradaghi K, Ali S & Al-Ansari N (2019). Landfill site selection using MCDM Methods and GIS in the Sulaimaniyah Governorate, Iraq. Sustainability, 1-22. https://doi.org/ 10.3390/su11174530

Lokhande T & Mane S (2017). Identification of suitable landfill site alternatives using GIS- a case study. International Journal of Engineering Science and Computing, 14825-14828.

Mohammed H, Majid Z, Yamusa Y, Ariff M, Idris K & Darwin N (2019). Sanitary landfill siting using GIS and AHP. Engineering, Technology & Applied Science Research, 4100-4104.

Özkan B (2018). A GIS-based multi criteria decision analysis for the municipal solid waste landfill site selection and collection system. PhD Thesis, Eskişehir Osmangazi University, Eskişehir (in Turkish).

Rahmat Z, Niri M, Alavi N, Goudarzi G, Babaei A, Baboli Z & Hosseinzadeh M (2016). Landfill site selection using GIS and AHP: a case study: Behbahan, Iran. KSCE Journal of Civil Engineering, 1-8. https://doi.org/10.1007/s12205-016-0296-9

Randazzo L, Cusumano A, Oliveri G, Di Stefano P, Renda P, Perricone M & Zarcone G (2018). Landfill site selection for municipal solid waste by using AHP method in GIS environment: waste management decision-support in Sicily (Italy). Multidisciplinary Journal for Waste Resources & Residues, 78-88. https://doi.org/10.31025/2611-4135/2018.13656

Saaty T (2008). Decision making with the analytic hierarchy process. International Journal of Services Sciences, 83-98.

Şener S, Şener E & Karagüzel R (2010). Solid waste disposal site selection with GIS and AHP methodology: a case study in Senirkent-Uluborlu (Isparta) Basin, Turkey. Environ Monit Assess, 533-554. https://doi.org/10.1007/s10661-010-1403-x

Yıldırım Ü (2012). Determination of alternative municipal solid waste disposal sites for the city of Mersin using analytic hierarchy process and geographic information system methods, MS Thesis, Mersin University, Mersin (in Turkish)

Zelenovic T, Bajcetic R & Miloradov M (2011). GIS and the analytic hierarchy process for regional landfill site selection in transitional countries: a case study from Serbia. Environmental Management, 1-14. https://doi.org/10.1007/s00267-011-9792-3

## Land Administration, Cadastre and Land Use – 1

Intercontinental Geoinformation Days

http://igd.mersin.edu.tr/2020/

# Agricultural land consolidation (Russian case study)

**Alexander Sagaydak*[1], Anna Sagaydak[1]**

[1]*State University of Land Use Planning, Department of Agricultural Economics and Farm Management, Moscow, Russia*

**Keywords**
Agricultural Land Consolidation
Russia
Republic of Kalmykia

**ABSTRACT**

Agricultural Land Consolidation is a merging, enlargement, eliminating of mosaic land ownership and improvement of configuration as well as optimization of the size of land plots. The development of Agricultural Land Consolidation in Russia is featured by the development of agricultural holdings and the increasing size of private farms. The average size of a holding amounted to 608.2 thousand hectares in 2020. Compared to 2018 it increased by 18.6 % in 2020. The average size of a private farm was estimated at 75.2 hectares in 2018. It increased by 75.3 % compared to 1995. The development of Agricultural Land Consolidation in Russia is mostly dependent on regional land policies. The Republic of Kalmykia is located in the Southeastern edge of Europe and it is a part and federal subject of the Russian Federation. In the Republic of Kalmykia, there is a unique trend, which is in the increase in the number of private farms and their average size. In 2019, the average size of a private farm amounted to 1,056 hectares in the region. It increased by more than 1.8 times compared to 1992.

## 1. INTRODUCTION

Agricultural Land Consolidation is a merging, enlargement, eliminating of mosaic land ownership and improvement of configuration as well as optimization of the size of land plots. The specific objectives of Agricultural Land Consolidation are the following: increasing the efficiency of agricultural production; providing sustainable development of the agrarian sector; rational use of land, labor, and capital in agriculture; optimization of agricultural production structures both in territorial and production aspects; increasing the competitiveness of agricultural producers in domestic as well as foreign markets; environmental protection; development of production as well as social infrastructure in agriculture. The main functions of Agricultural Land Consolidation are the following: elimination of hunger and poverty as well as reducing the gap in living conditions and incomes between urban and rural areas. Agricultural Land Consolidation should be carried out based on the following principles: voluntariness; openness and transparency; financial and economic feasibility; taking into account the interests of the population groups involved including women and youth as well as indigenous people; step by step implementation; consideration of local conditions; state and NGO support. In theory, Agricultural Land Consolidation can be carried out as voluntary land consolidation and compulsory land consolidation. Both administrative and economic methods, for example, the development of the Agricultural Land Market could be used for Agricultural Land Consolidation. In our opinion, preference should be given to voluntary land consolidation. In that sense, the development of the Agricultural Land Market is very important for the stimulation of Agricultural Land Consolidation. However, the Agricultural Land Market in Russia is still not formed, which impedes the formation of a flexible system of land tenure and land use. Most of the Agricultural Land Market transactions are leasing of land shares now. Meantime, agricultural land selling and buying transactions as well as agricultural land mortgage transactions are limited.

## 2. METHOD

The methodology includes the study of theoretical foundations and the development of practical recommendations for improving the consolidation of agricultural land in Russia. At the same time, using statistical methods, as well as monographic surveys, trends in the development of Agricultural Land Consolidation at both the federal and regional levels were identified, which are: the concentration of land

* **Corresponding Author**

*(asagaydak@yahoo.com) ORCID ID 0000 – 0002 – 6316 –6134
(ann1806@mail.ru) ORCID ID 0000 –0003 – 4389 – 8570

**Cite this study**

Sagaydak A, Sagaydak A (2020).Agricultural land consolidation (Russian case study). Intercontinental Geoinformation Days (IGD), 76-79, Mersin, Turkey

ownership by agro-industrial holdings, as well as an increase in the average size of private farms while reducing their number. However, in the Republic of Kalmykia, which is a federal subject of the Russian Federation, unique trends have been identified in increasing the area of agricultural land, increasing the number and average size of private farms.

## 3. RESULTS

The present stage of the development of Agricultural Land Consolidation in Russia is featured by the development of agricultural holdings and the increasing size of private farms. The state and municipal-owned land amounted to 1,579.4 million hectares, or 92.2 %, private land -112.1 million hectares, or 6.6 % and land owned by legal entities – 21.0 million hectares, or 1.2 % of the total the Russian Federation territory in 2018. The size and the share of the state and municipal-owned land in the total land of the Russian Federation were not changed in 2018 compared to 2017. The private land area decreased by .8 million hectares in 2018 compared to 2017 from 112.9 million hectares to 112.1 million hectares, or by .7 %. The share of private land in the total land of the Russian Federation was not changed in 2018 compared to 2017. At the same time, the area of land owned by legal entities increased by .8 million hectares in 2018 compared to 2017 from 20.2 million hectares to 21.0 million hectares, or by 4.0 %.

The share of land owned by legal entities in the total land of the Russian Federation was not changed in 2018 compared to 2017. The state and municipal-owned agricultural land amounted to 254.8 million hectares, or 66.6 %, private land - 107.6 million hectares, or 28.2 % and land owned by legal entities – 20.0 million hectares, or 5.2 % of the total Russian Federation agricultural land in 2018. Thus, the private agricultural land area decreased by .9 million hectares in 2018 compared to 2017 from 108.5 million hectares to 107.6 million hectares, or by .8 %. At the same time, the area of agricultural land owned by legal entities increased by .8 million hectares in 2018 compared to 2017 from 19.2 million hectares to 20.0 million hectares, or by 4.2 %. Moreover, the state and municipal-owned agricultural land area decreased by .6 million hectares in 2018 compared to 2017 from 255.4 million hectares to 254.8 million hectares, or by .2 %. The share of the state and municipal-owned agricultural land in 2018 compared to 2017 decreased by .1 percentage points from 66.7 % to 66.6 % in the total agricultural land.

The share of agricultural land owned by legal entities in 2018 compared to 2017 increased by .2 percentage points from 5.0% to 5.2% in the total agricultural land. However, the share of the private owned agricultural land in 2018 compared to 2017 decreased by .1 percentage points from 28.3 % to 28.2 % in the total agricultural land. Thus, at the federal level, there is a trend of the absorption of private land by legal entities. This, in particular, is also evident in the fact that a dominant role in the Russian agricultural land use has played joint-stock companies as well as production coops. The share of joint-stock companies and partnerships in the total area of agricultural land use of parastatals compared to 2017 increased by .7 percentage points from 53.3% to 54.0% in 2018. Compared to 2017 the share of joint-stock companies and partnerships in cropland of parastatals increased by .8 percentage points from 58.6% to 59.4% in 2018.

At the same time, the share of production coops in the total area of agricultural land use of parastatals compared to 2017 decreased by .5 percentage points from 35.6% to 35.1% in 2018. Compared to 2017 the share of production coops in cropland of parastatals decreased by .7 percentage points from 31.7% to 31.0% in 2018.Thus, there is a trend of decreasing land use of production coops and increasing land use of joint-stock companies and partnerships, which also indicates further development of the Agricultural Land Consolidation by large and medium agricultural enterprises. The average size of agricultural holding amounted to 608.2 thousand hectares in 2020. Compared to 2019 it increased by 5.8 % in 2020. It varied from 380 thousand hectares to 1,047 thousand hectares in 2020.

After a boom in the first period of reform, the number of private farms has been decreased due to severe macroeconomic instability and lack of market infrastructure as well as market economy knowledge. In 2018 the number of private farms decreased by 7.6 % compared to 1995. However, the average size of agricultural land occupied by the private farm has been increased due to land consolidation. It was estimated at 75.2 hectares in 2018. Thus, it increased by 75.3 % compared to 1995.

The development of Agricultural Land Consolidation in the Russian Federation is mostly dependent on regional land policies. One of the successful examples of them is the Republic of Kalmykia Land Policy. The Republic of Kalmykia is located in the Southeastern edge of Europe and it is a part and federal subject of the Russian Federation.

In the Republic of Kalmykia, we can observe a unique trend, which is in the increase in the number of private farms and the increase in their average size. In 2019, there were 3,042 private farms in the region. The number of private farms in the Republic of Kalmykia increased in 2019 compared to 1992 by 10.4 times. The land area occupied by private farms in the region increased in 2019 compared to 1992 by 19.1 times. The average size of the private farm amounted to 1,056 hectares in the Republic of Kalmykia in 2019. It increased in 2019 compared to 1992 by 1.8 times due to land consolidation based on renting and buying of agricultural land shares. It is significantly different from the average for the Russian Federation, where an increase in the area mentioned above farms is accompanied by a reduction in their number. Here we can also observe another unique trend of increasing area of agricultural land in 2010-2019. The total area of agricultural land increased in 2019 compared to 2010 by 52.1 thousand hectares, or by .8% from 6,885.2 thousand hectares to 6,937.3 thousand hectares.

The Agricultural Land Market in the Republic of Kalmykia has been steadily developed despite the increase in the cadastral value of the land. To encourage

land consolidation, it is necessary to develop the Agricultural Land Market based on land auctions. In turn, the market price of land is the basis for Agricultural Land Taxation and mortgage transactions. Due to it, the Starting Agricultural Land Market Auction Price Model or SALAPM has been developed. In general, we can treat the Land Market Auction Price as a ratio between agricultural land rent and interest rate adjusted for income and Agricultural Land Taxation as well as the inflation rate. In this sense, it is very important to determine land tax and mortgage value based on Agricultural Land Market Value. The SALAPM looks like:

$V_a = [R_0(1+g)(1-t)]/\{[k(1-at)-g]\ (1+c)+p(1-t)\}$, where $V_a$- Starting Agricultural Land Auction Price, rubles per hectare;$V_0$ -cadastral value of agricultural land, rubles per hectare;$V_1$ - cadastral value of agricultural land adjusted for the land rent growth, rubles per hectare;$R_0$ - land rent, rubles per hectare; g-land rent growth, %;t-income tax, %;p - land tax, %;k -interest rate, %;c - transaction costs, %;a -tax adjustment coefficient, calculated as $a=R_0(1+g)/\ [\ R_0(1+g) +(V_1-V_0)]$.The values of the mentioned above indicators were taken as follows: land rent value ($R_0$) was calculated on the base of the cadastral value of agricultural land treated as $V_0$ and interest rate (k) taken as 3% and used for determination of the value; annual land rent growth (g) was estimated at 12%; transaction costs (c) were estimated at 10%; income tax (t) was taken as 20 %; agricultural land tax (p) was estimated at .3 % of cadastral land value; interest rate (k) was taken as 15.25 %. The ratio between the Starting Agricultural Land Auction Price and Agricultural Land Mortgage Value was taken as 70% (see Table 1).

**Table 1.** Agricultural Land Cadastral Values, Auction Prices, Mortgage Values, Land Tax Rates, Republic of Kalmykia, rubles/ha (draft)

| Municipalities | Cadastral Value | Auction Price | Mortgage Value | Land Tax |
|---|---|---|---|---|
| Gorodovikovskoe | 84,580 | 14,912 | 10,438 | 44.74 |
| Iki-Burulskoe | 10,760 | 1,904 | 1,332 | 5.71 |
| Ketchenerovskoe | 11,800 | 2,080 | 1,456 | 6.24 |
| Laganskoe | 2,800 | 494 | 345 | 1.48 |
| Maloderbetovskoe | 12,430 | 2,186 | 1,530 | 6.56 |
| Oktyabr'skoe | 4,200 | 740 | 518 | 2.22 |
| Priyoutnenskoe | 19,800 | 3,490 | 2,443 | 10.47 |
| Sarpinskoe | 13,570 | 2,397 | 1,678 | 7.19 |
| Tselinnoe | 10,980 | 1,939 | 1,357 | 5.82 |
| Chernozemelskoe | 2,900 | 511 | 358 | 1.53 |
| Youstinskoe | 3,150 | 546 | 382 | 1.64 |
| Yashaltinskoe | 39,050 | 6,874 | 4,812 | 20.62 |
| Yashkul'skoe | 2,440 | 2,115 | 1,481 | 6.34 |
| Average | 15,760 | 2,961 | 2,073 | 8.88 |

Land tax was calculated as .3 % of the starting auction price of agricultural land. In theory, the contract land rent rate can't be less than land tax rates. Otherwise, the landowner will not be interested to give land on lease. Therefore, it is necessary to provide at least the average level of profitability for the landowner that can be taken as 40 % compared to the rate of land tax. It is also important to implement a logical framework methodology for designing Agricultural Land Consolidation Projects. In this regard, the super goal of Agricultural Land Consolidation Projects is to implement and develop Agricultural Land Consolidation to increase the efficiency of agricultural production to eliminate hunger and food shortages as well as poverty due to the rapidly growing world population. In this regard, the modified Agricultural Land Consolidation Project Logical Framework Matrix (ALCPLFM) has been designed (see Table 2).

**Table 2.** Agricultural Land Consolidation Project Logical Framework Matrix

| Content | Verified Indicators | Narrative Summary | Assumptions |
|---|---|---|---|
| Supergoal | Increase the efficiency of agricultural production | Increasing financial and economic efficiency | Growth of land rent and price of land |
| Specific Objectives | Increase, optimization of the size and configuration of land plots, elimination of mosaic land ownership | Improving the efficiency of the use of agricultural machinery | Growth of agricultural production |
| Activities | List of land use planning work in physical terms | The volume of land use planning work in physical terms | Owners and beneficiaries of the project |
| Investments | Financing of land use planning work | The investment required for the implementation of land use planning work | Attracting outside investors to finance the project |
| Investment sources | Ensuring targeted investment financing | Lending required to provide targeted financing for the Agricultural Land Consolidation Project | The Central Bank's policy and refinishing rate. Market interest rate. Inflation rate |

## 4. DISCUSSION

There are different models of Agricultural Land Consolidation in Russia. The first of them - Nizhny Novgorod Model was intended to consolidate the land shares to create production cooperatives. However, due to the absence of post-privatization support, this task remained unfulfilled. In this regard, noteworthy Belgorod and Orel Models, which are used respectively in Belgorod and Orel regions based on buying and renting of land shares by private farms, agricultural

holdings as well as local authorities. In this regard, other economists think that only further development of agricultural holdings is necessary. But, there is concern that the development of the agricultural holdings leads to the emergence of the so-called "latifundium", which should be treated as a system of land tenure based on large private land ownership. But it does not take into account the fact that the characteristic features of real latifundium are the following:the existence of a monopoly of large private land ownership as an object of ownership in agriculture; formation of two types of monopoly on land in agriculture: monopoly on land as an object of ownership and monopoly on land as an object of economy, which are separated and do not coincide with each other; the complexity of land relations and, first of all, rental, often due to the remnants of slavery and feudalism, which is expressed, in particular, in the existence of labor and product rent; collection by the landlord land rent which is economically realizing its right of monopoly on the land as an object of private property; despite the large size of estates, inside them there were small parcels of land and therefore, the formation of unfavorable organizational and economic conditions of agricultural production; technical and technological backwardness of agriculture caused by the lack of incentives for the development of agricultural production by landlords and tenants. As a result, the development of agriculture in latifundium was slow and inefficient. At the same time, the production process in the agricultural sector was often simple or even shortened. Therefore, it would be wrong to mix latifundium and large-scale market agricultural production, agricultural holdings, which act as an important factor in agricultural development. They have, as a rule, capital-saving type of agricultural production, based on the use of advanced scientific and technological progress. Besides, it should be noted, another important difference between agricultural holding and latifundium. In agricultural holdings, a monopoly on land as an object of private ownership and a monopoly on land as an object of the economy coincide with each other. This leads to the so-called "disappearance" of land rent and thus contributes to the efficiency of agricultural production.

## 5. CONCLUSION

The following measures must be implemented to strengthen the organizational as well as institutional sustainability of Agricultural Land Consolidation development in Russia: Agricultural Land Consolidation legislation must be revised and improved both at the federal as well as regional level; the institutional framework for implementation of Agricultural Land Consolidation must be improved both at the federal as well as regional level too; the Agricultural Land Auctions must be introduced to stimulate the development of the Agricultural Land Market and Agricultural Land Consolidation in the regions of Russia; the training and retraining programs related to Agricultural Land Consolidation development issues must be introduced; the public relation campaign to strengthen people's ability to understand the role and importance of Agricultural Land Consolidation development must be initiated; the pilot projects focused on Agricultural Land Consolidation development should be launched in some of the regions of Russia to make a demonstration effect; the Agricultural Land Consolidation development experience should be collected, scrutinized and disseminated.

## ACKNOWLEDGEMENT

The authors would appreciate it if the Conference Committee could find an opportunity to accept the paper. The authors would like also to inform the Conference Committee that all ethical standards regarding the publishing of the paper have been accepted by us. Funding for the research related to the study of Agricultural Land Consolidation in Russia was carried out only at the expense of our private funds. In connection with the mentioned above, there is no conflict of interest related to the publication of the paper. We also fully accept, approve, and support the ethical standards related to the study. Due to it, we consent to the possible publication of our paper in the proceedings of the conference.

## REFERENCES

### Reports

The State (National) Report on the Status and Use of Lands in the Russian Federation in 2018(2019), Rosreestr.

The Regional Report on the Status and Use of Lands in the Republic of Kalmykia in 2019(2020), Kalmykiareestr.

Rating of the largest owners of agricultural land in Russia in May 2020 (2020), www.agroxxi.ru.

Intercontinental Geoinformation Days

http://igd.mersin.edu.tr/2020/

# Identification and analysis of parcel-based plan amendment types: The case of Istanbul

**Ahmet Yılmaz*[1], Nur Saral[1], Leyla Güneş[1], Şeval Yanar[1], Pelin Ballı[1]**

[1]*Yildiz Technical University, Faculty of Civil Engineering, Department of Geomatics Engineering, Istanbul, Turkey*

**Keywords**
Plan amendment
Land use
Development charges
Case study
Istanbul

**ABSTRACT**

Planning system in Turkey is a plan-led system typically driven by national policies through a hierarchy of plans and land-use decisions are implemented at the local level. However, high number of planning amendment reverses the hierarchy of a planning system and transfers the power to the last level. Therefore, the main aim of this article is to identify and analyze the parcel based plan amendments. The research method used to identify the types of the parcel based plan amendments is a systematic review of the municipal council reports in Istanbul as an explanatory case study and to analyze the timing, location, and spatial distributions of different types of the parcel based plan amendments. Based on the case study, six main parcel based plan amendment type is defined. By using this classification more than 2.900 proposals between the years 2014 and 2020 are analyzed and preliminary results of the types, the scope of the change, location, responsible municipality, and approval status of the parcel based plan amendments are given.

## 1. INTRODUCTION

Spatial planning is the set of governance practices for developing and implementing strategies, plans, policies and projects, and for regulating the location, timing and form of development (Healey 1997). It is important for delivering economic, social and environmental benefits via creating more stable and predictable conditions for investment and development, securing community benefits from development, and promoting a prudent use of land and natural resources for development (UNECE 2008).

Planning systems in the world are generally divided into two main systems, which are development-led discretionary systems and plan-led regulatory systems. The plan-led planning system is designed to lead the development of space in accordance with the decisions of the plan (Özkan and Türk 2016). These systems are generally known with their hierarchical structure and legally binding, certain, inflexible and rigid spatial plans.

An effective plan-led planning system should be able to implement land policies through efficient means of land use control. Therefore, a coordinated planning hierarchy should imply consistency of land-use planning policy objectives from the national to the local and neighborhood scale, in a system that enables more detailed plans to remain in line with the upper-level plans (UN-Habitat 2018)

In Turkey, the legal framework of spatial planning and physical development is provided by the Development Law No. 3194 dated 1985. Before this Law, urban planning departments were centralized government offices under the Ministry of Reconstruction and Resettlement. Their roles were to designate the land use, to preparation of land-use plans, to control the planning ordinances, to license new developments of private owners, and to locate public facilities. These privileges are decentralized and transferred to the local governments with the Development Law (Gülkan 2001). However, since the 2000s, significant changes in the planning system have led to a flexible planning system in practice, which is defined as regulatory planning system in theory (Tarakçı and Türk 2018). One change in the legal framework is realized by the establishment of the Ministry of Environment and Urbanism with the Decree Law No. 644 adopted in 2011. The Law sets forth the duties and responsibilities of the Ministry in urban planning and provides centralization of planning system. For instance, in Istanbul, Ministries have 74% of the planning authority, and Istanbul Metropolitan Municipality has 26% of the planning authority. The rates shows fragmented structure of planning, the power

*Corresponding Author

*(ayilmaz@yildiz.edu.tr) ORCID ID 0000-0002-4770-7826
[2](nurrsaral@gmail.com) ORCID ID 0000-0003-1846-9467
[3](gunesleyla123@gmail.com) ORCID ID 0000-0002-4960-3131
[4](sevvalynrr@gmail.com) ORCID ID 0000-0001-8112-765X
[5](pelin_dgal@hotmail.com) ORCID ID 0000-0002-8203-1040

Cite this study

Yılmaz A, Saral N, Güneş L, Yanar Ş & Ballı P (2020). Identification and analysis of parcel-based plan amendment types: The case of Istanbul. Intercontinental Geoinformation Days (IGD), 80-83, Mersin, Turkey

of government and centralization of planning system (Gürsoy and Edelman 2017).

Planning system in Turkey is typically driven by the national policies and through a hierarchy of plans land-use decisions are implemented at a local level. The hierarchy of the planning system is stated in the Regulation on Making Spatial Plans, which was accepted in 2014. According to the first paragraph of Article 6 of this regulation, spatial plans are prepared as Spatial Strategy Plans, Environmental Plans and Development Plans in terms of the area they cover and their purposes. The regulation defines the hierarchical system of the Turkish planning system as Spatial Strategy Plan, the Environmental Plan, the Master Plan and the Implementation Plan from upper level to lower level, respectively. The local detailed plan that provides the basis for the building permits is prepared by the municipalities in areas inside the municipal boundaries and by the governorships outside the municipal boundaries. For the coordination of the local and upper-level plans, Master and Implementation Plans have to be in accordance with the regional and environmental development plans prepared by the central government.

Master Plans are generally produced at 1/5000 scale and determine the block based land uses, zoning types, population densities and main social and technical infrastructure. Implementation Plans are produced at 1/1000 scale and show all the details of the building rights of the parcels. The implementation plans in Turkey determine the permitted usage, the amount and the characteristics of the development, therefore, has a fundamental impact on the values of land and property, which is the main driving force of planning amendments by developers and individuals.

Planning amendments or modifications of plans can be realized by two ways. Comprehensive modifications made through Revision, Partial and Additional Development Plans by public authorities and generally do not reflect the private interest. However, block or parcel based plan amendments are frequently used by landowners and developers to change the plan decisions, mainly for rent seeking via increment of the density, function or use.

Modifications in plans follow the same procedure as in the preparation and ratification of the plans and with the paradigm shift on decentralization of the planning powers in 1985, Municipal Councils becomes the only authority in the decision making of plan amendment proposals. Therefore, decentralizations of the planning powers to local governments with the Development Law resulted much easier and uncontrolled plan amendments.

One reason of the high demand in planning amendment can be that the value increase as a result of the planning decisions remain to the developers or the landowners and weak value capture tools result in plan amendments regarding value increases. Recently, as a solution to this problem, a development charge has been defined for plan amendments and rules about the development charges in plan amendments are added by the Article 12 Of The Law Amending Geographic Information Systems and Some Other Laws No.7221 as the Supplementary Article 8 of the Development Law No.3194 in 2020. In addition, the Regulation on development charges for plan amendments is published in 2020. According to the law and the regulation, parcel-based plan amendments are prohibited and for the value increase as a result of block based plan amendments, a development charge is introduced. In a block-based plan amendment, the developer or the landowner receives additional development rights or a more profitable land use in exchange for obligation to compensate in cash. The charge will be shared among the public administrations. In metropolitan municipality provinces, development charges will be shared equally among metropolitan municipality, district municipality, the Ministry of Environment and Urbanization, and the Treasury. However, if the plan amendment is approved by the Ministry of Environment and Urbanization, then the value increase will be shared between the Ministry (75%), the metropolitan municipality (15%) and the district municipality (10%). In non-metropolitan districts, development charges will be shared among the administration that approved the plan amendment (40%), the Ministry of Environment and Urbanization (30%), and the Treasury (30%). However, if the plan amendment is approved by the Ministry of Environment and Urbanization, then the development charges will be shared between the Ministry (75%) and the relevant administration (25%). In addition, if the plan amendment is approved by a public administration, then development charge will be captured by the Treasury. The revenues from development charges are planned to be used in public services such as expropriation, urban transformation and infrastructure.

Parcel based plan amendments are perceived as corruption and irregularity by the society. Therefore, prohibition of the parcel based plan amendments highlighted the need for a comprehensive evaluation on amendments realized before the prohibition. However, there are few studies analyzing parcel-based planning amendments realized in Istanbul. For instance, Altın (2006) analyze a total of 1614 plan amendments realized between the years 1990 and 2004 in Üsküdar and Şişli districts of Istanbul. Kılınç and Turk (2018) analyze a total of 10.288 plan amendment proposals between the years 2008 and 2017 in Istanbul to identify the behavior of the distribution of demand and supply of plan amendments and influencing factors. Demir (2009) analyzed a total of 159 plan amendments realized between the years 1995 and 2009 in Zeytinburnu district of Istanbul. Yavuz and Sertyesilisik (2009) analyze a total of 105 plan amendments realized between the years 2007 and 2016 in Kağıthane district of Istanbul. The main reason of scare literature on the parcel based plan amendments could be that there are no statistical data regarding plan amendments and data can only be gathered from municipal council reports, which are paper based and not spatially enabled.

Therefore, the main aim of this study is to contribute to the existing scare literature on the parcel based plan amendments, which include identification of the amendment types and analyze of the timing, location, and spatial distributions of these types. For this aim, parcel based plan amendments in Istanbul is examined as an explanatory case study. This paper has been divided into

four parts. The first part makes an introduction and provides the aim of the study. Chapter 2 identifies the methodology and the data of the case study. Chapter 3 presents the result of the case study and identifies the parcel based plan amendment types of Istanbul. Chapter 4 makes a conclusion.

## 2. METHOD AND DATA

The main aim of this paper is to identify the leading types of the parcel based plan amendments and in addition, by using this classification to analyze the timing, location, and spatial distributions of these types. For this aim, parcel based plan amendments in Istanbul is examined as an explanatory case study. Istanbul is one of the world's largest city by its population, ranking as the world's fifteenth-largest city and the largest city in Europe with a total population of around fifteen million residents in metropolitan area.

The research data in this paper is drawn from the official council decision documents of the Municipal Council of Istanbul Metropolitan Municipality. The Municipal Council is the ultimate decision-making body of the Istanbul Metropolitan Municipality. Its members come from districts within the metropolitan boundaries and chaired by Metropolitan Mayor for a term of five years. Therefore, the time period of the data set is chosen as 2014-2020 to reflect political relations and decision making in a five-year period.

This study systematically analyzed the official council decision documents of the Municipal Council of Istanbul that includes a proposal or a decision related with parcel based plan amendments. As for case study, more than 2.900 proposals between the years 2014 and 2020 are analyzed and preliminary results on the types and the scope of the parcel based plan amendments, their location and approval status, and the responsible municipality are given in the next section.

## 3. RESULTS

The main aim of this paper is to identify the types of the parcel based plan amendments and by using this classification to analyze the timing, location, and spatial distributions of these types.

For this aim, parcel based plan amendments in Istanbul is examined as an explanatory case study. In the case study, more than 2.900 plan amendment proposals between the years 2014 and 2020 are analyzed. Based on this analyze, the main types of the parcel based plan amendments, and their classification are identified as;

- Type 1. Plan amendments between social or technical infrastructure and private ownership.
    - Type 1.1. Plan amendments reducing social or technical infrastructure areas.
    - Type 1.2. Plan amendments increasing social or technical infrastructure areas.
- Type 2. Plan amendments exchanging social or technical infrastructure areas.
- Type 3. Plan amendments in protected areas or for protection purposes.
- Type 4. Plan amendments causing value increase
- Type 5. Plan amendments for applicability and efficiency of a plan.

This classification defines all types of plan changes that may occur on a parcel basis. In addition, the classification is designed by taking account the content of the data, the typology specified in the law and the research design that enables analyzing different aims. The classification of the parcel based plan amendments and preliminary results of the type-based analyses are detailed below.

### 3.1. Type 1: Plan-amendments between social or technical infrastructure and private ownership

This type of plan amendments includes conversion between social or technical infrastructure and private ownership. According to the Article 26 of the Regulation of Making Spatial Plans conducted with the official Gazette numbered 29030 and dated 14.06.2014, certain rules must be fulfilled for these types of plan amendments. As a rule, plan amendments regarding the removal, reduction or relocation of social and technical infrastructure areas cannot be made unless there is a necessity. In case of necessity, in order to make such a change an equivalent new area within the service area of these facilities should be separated. In order to question whether this rule is applied or not, plan amendments that cause a decrease and an increase in these areas are defined separately under Type 1 as Type 1.1 and Type 1.2 as detailed below.

#### 3.1.1. Type 1.1 Plan amendments reducing social or technical infrastructure areas.

The Type 1.1 includes plan amendment proposals aiming a reduction in social or technical infrastructure areas. Almost 24% of all plan amendment proposals between 2014 and 2020 includes Type 1.1 and Tuzla, Kartal, and Esenyurt are the leading districts.

#### 3.1.2. Type 1.2. Plan amendments increasing social or technical infrastructure areas

The Type 1.2 includes plan amendment proposals aiming an increase in social or technical infrastructure areas. Almost 13% of all plan amendment proposals between 2014 and 2020 includes Type 1.2 and Tuzla, Kartal, Pendik, and Sancaktepe are the leading districts.

Plan amendment proposals within the scope of Type 1.1 should additionally include Type 1.2 in order to be legal and comply with the law. However, only 25% of the Type 1.1 plan amendment proposals also include Type 1.2. Kartal, Tuzla, Esenyurt and Çekmeköy are the leading Districts containing Type 1.1 proposals without Type 1.2 within the time frame of the study.

### 3.2. Type 2: Plan amendments among social or technical infrastructure areas

The Type 2 includes plan amendment proposals between social or technical infrastructure areas as exchange. Almost 25% of all plan amendment proposals between 2014 and 2020 includes Type 1.2 and Fatih,

Tuzla, Kartal, Bağcılar, and Pendik are the leading districts.

### 3.3. Type 3: Plan amendments in protected areas or for protection purposes

The Type 3 includes the plan amendment proposals in protected areas or for protection purposes. Almost 10% of all plan amendment proposals between 2014 and 2020 includes Type 3, and Fatih is the leading district by having 75% of all Type 3 proposals.

### 3.4. Type 4: Plan amendments causing value increase

The Type 4 includes plan amendment proposals causing a value increase such as the change of density, function or use. Almost 16% of all plan amendment proposals between 2014 and 2020 includes Type 4 and Tuzla, Fatih, and Bağcılar are the leading districts.

### 3.5. Type 5: Plan amendments for applicability and efficiency of a plan

The Type 5 includes the plan amendment proposals for applicability and efficiency of a plan. Almost 11% of all plan amendment proposals between 2014 and 2020 includes Type 5 and Fatih, Tuzla, and Kartal are the leading districts.

## 4. CONCLUSION

The main aim of this study was to contribute to the existing scare literature on the parcel based plan amendments, which include identification of the amendment types and analyze of the timing, location, and spatial distributions of these types. For this aim, parcel based plan amendments in Istanbul was examined as an explanatory case study. In the case study, more than 2.900 plan amendment proposals between the years 2014 and 2020 are analyzed. Based on this analyze, the main types of the parcel based plan amendments, and their classification are identified. The case study reveals the distribution of the types between 2014 and 2020, and Type 2 and Type 1.1 are the leading proposals which constitute nearly half of the parcel based plan amendments. In addition, Type 1.1 and Type 4 together constitute the 40% of all proposals. One reason of the high number of planning amendment proposals in these types can be the weak value capture tools. These types generally cause a value increase and in the time frame of the study, this increase was remaining to the landowners. However, with the recent change in the law, this type of plan amendments will be subject to development charge; therefore, a sharp decrease is expected in these types.

When the change trend of the parcel based plan amendment proposals is examined, a decrease in 2016 and 2017 (~30%) and an increase in 2018 (~30%) is observed. The reason of the change in the trend may be the elections that took place in March, 2019. In addition, in the Istanbul case, only 23% of all plan amendment proposals between 2014 and 2020 are rejected by the Municipal Council of Istanbul. Therefore, high number of planning amendments seem to reverse the hierarchy of a planning system and transfers the power to the last level of the planning scale.

## REFERENCES


Altın Y (2006). İstanbul metropoliten alanında imar planı değişiklikleri ile ilgili bir analiz. YL Tezi, İstanbul Teknik Üniversitesi, İstanbul.

Demir A M (2009). İmar planı değişikliklerinin değerlendirilmesi Zeytinburnu örneği. YL Tezi, İstanbul Teknik Üniversitesi, İstanbul.

Güler Z E & Ünverdi L (2009). Desantralizasyon, basitleştirme, deregülasyon ve yeniden-regülasyon politikaları kapsamında planlamanın araçsallaştırılması; Bursa'da riskli yapı tespitine dayalı parsel bazındaki plan değişikliklerinin kentsel mekana etkisi, Planlama, 29(3), 210–228.

Gülkan P (2001). Revision of the Turkish Development Law No. 3194 governing urban development and land use planning. NATO Science Series, Springer.

Gürsoy N & Edelman D J (2017). Regional development planning in Istanbul: recent issues and challenges. Current Urban Studies, (5), 146-163.

Healey P (1997). Collaborative planning, shaping places in fragmented societies, UBC Press.

Numan K & Türk Ş Ş (2018). İmar planı değişikliği talebi-arzı ve sosyo-ekonomik değişkenler arasındaki ilişki: İstanbul örneği, II. Kentsel Morfoloji Sempozyumu, İstanbul, Türkiye.

Özkan H & Türk Ş Ş (2016). Emergence, formation and outcomes of flexibility in Turkish planning practice. IDPR, (38), 25-54.

Tarakçı S & Türk Ş Ş (2018). Impact of planning on land value in urban renewal practice: the case of Istanbul Fikirtepe. FIG Congress 2018, Istanbul, Turkey.

UNECE (2008). Spatial planning: key instrument for development and effective governance, with special reference to countries in transition. UNECE.

UN-Habitat (2018) Planning law assessment framework, UN-Habitat.

Ünlü T (2006). Kentsel mekânda değişimin yönetilmesi. ODTÜ Mimarlık Fakültesi Dergisi, 23 (2), 63-92.

Yavuz U & Sertyeşilışık B (2019). Mekânsal alanlarda plan değişikliklerinin gayrimenkul üretim/ arz eğilimlerine etkileri. International Journal of Political Science and Urban Studies, 7(2), 543-567.

Intercontinental Geoinformation Days

http://igd.mersin.edu.tr/2020/

# Land readjustment method: Professional merit in determining implementation boundary

**Halil Burak Akdeniz*[1], Şaban İnam[1]**

[1]*Konya Technical University, Engineering and Natural Sciences Faculty, Geomatics Engineering Department, Konya, Turkey*

**Keywords**
Implementation boundary
Implementation area
Land readjustment
Merit

**ABSTRACT**

The development plan implementation in the land readjustment method made in accordance with the 18th article of the Land Development Act, No. 3194, consists of technical implementation stages that are related to each other. Determining implementation area and implementation boundary, constitute first and important stage of land readjustment method. The implementation boundary should determine to considering the implementation regulation, providing homogeneous distribution of government agency and public areas, protecting rights to use property and social justice, in other words, it should determine principle of professional merit consideringly. This case loom large in terms of the accuracy of the implementation in technical, economic, sociological dimensions. Although administration has legal authority on "where boundary will be determined in the implementation area", ithas responsibilities in terms of establishing the trust of the property owner in administration/state in an incorrect boundary detection. Therefore, technical personnel being in charge of on behalf of the administration and department making the approval of the boundary should act in professional/administration merit. In this study, will investigate to determining implementation boundaries studies in the development plan implementations are made by two different district municipality of Turkey's. Then, alternative suggestions will offer consideringly professional merit, ethical principles and the provisions of the legal legislation (Land Development Act No. 3194, Land Readjustment Regulation).

## 1. INTRODUCTION

The development plan are made in order to create a modern, aesthetic and livable city suitable for the science, health and environmental conditions of the settlements. With the implementation of development plans to field, possible ownership problems were solved and it is aimed to reveal the proper building parcels and public space with the construction conditions stipulated by the plan. 1/1000 scale implementary development plan are applied on any of in accordance with 'expropriation', 'applications on demand of owners' and 'land readjustment' method according to 03.05.1985 date, Land Development Act No. 3194 in Turkey. And this is done using a method "designated by the administration that will approve the implementation" (İnam et. al. 2015). However, "development plan implementation in the land readjustment method" is recommended method due to its advantages. Likewise, implementation in the land readjustment method; it is accepted as the most technically appropriate, economically most efficient, sociologically most equitable method. Both "opening planned use as a result of the ownership-development relationship with the existing public spaces and real estates which can't be built in their current form that are in the implementation area" and "after the implementation of the plan, changing ownership structure is accepted by the public and state" put forward this method (Çay and Özen 1998; Çelik 2006; Yıldız 2014). The purpose of the development plan implementation in this method create building parcels suitable according to the plan report, plan notes, Land Development Act and implementation regulations (Köktürk 1997; Köktürk and Köktürk 2007). When different applications around the world and the legislations in Turkey analyzed, it is seen that this method provides responsibilities and opportunities to the administrations which implement plan and real estate owners (Yıldız 1987; Bıyık and Uzun 1990; Atasoy et al. 2002). The plan implementation in the land readjustment method consists of many interrelated application stages. After determining implementation area by the administration responsible for the implementation, the process of 'determining

* **Corresponding Author**

*(hbakdeniz@ktun.edu.trl) ORCID ID 0000 – 0002 – 9504 – 051X
(sinam@ktun.edu.trl) ORCID ID 0000 – 0002 – 9101 – 6109

**Cite this study**

Akdeniz H B & İnam Ş (2020). Land readjustment method: Professional merit in determining implementation boundary. Intercontinental Geoinformation Days (IGD), 84-87, Mersin, Turkey

implementation boundary' constitutes the most important stage of implementation (Uzun 1992; Ülkü and Olgun 1993). As a matter of fact, when 'cancellation of development plan implementation' cases fiiled before in the administrative jurisdiction are examined, it has been determined that real estate owners generally object to 'inaccurate determining implementation boundary' and 'building parcel allocation' (Karavelioğlu 1999).

Land Readjustment (LR) made in accordance with Article 18 of the Land Development Act No. 3194 are the most important method for plan implementation (Yomralıoğlu 1992). However, technical and legal features of the real estate remaining within implementation boundary will undergo a change after the implementation and these changes will have to be equally allocated to each real estate. If this equality is not provided, specific problems will arise. One of these problems which is the subject of our study, is the incorrect and unsuitable problem of 'determining implementation boundary'. The implementation boundary are determined, according to 9th and 10th articles of the Land Readjustment Regulation 22 February 2020 date and number 31047;

-on the settlement area boundaries where settlement areas end,

-on the axis of the roads in the settlement areas,

- if implementation boundary divides a parcel into two or more parts, boundary includes those that do not enter another urban block outside the implementation area,

-anywhere appropriate on park, square and car parks (and similar areas) in accordance with the development readjustment share ratio (DOPO).

The implementation area should not be smaller than an urban block.

However, there are worthy of notice issue apart from these principles of implementation, they are a issue of professional ethics and merit. Also, the development readjustment share ratio values which determine the amount of land allocated to public use, which will be provided with without charge deductions to be made from the parcel in the area of implementation, should be as balanced as possible between implementation areas (İnam 1989). Therefore,

-implementation areas should not determine to cover a few urban blocks, they should be determined as sub-regions with common character (settlement area, trade area, industrial area) as much as possible. Thus computation of different amounts of DOPO in the implementation areas with similar features will be prevented.

- The amount of DOPO should determine, not to exceed upper limit of 45%, which is the upper limit of without charge deductions. Thus, an expropriation burden should not be created for the administration, except in compulsory situation.

In this study; the development plan implementation in the land readjustment carried out in the "settlement area" in Çayır, Fevzi Çakmak, Saraçoğlu and İstiklal neighborhoods of Karatay district, Konya province and in Çaylı neighborhoods of Dörtyol district, Hatay province will investigate. It will examine to what extent consider implementation legislation, principles of professional merit, public interest and social justice by local government that responsible determining implementation boundary. Information and documents regarding the application areas were obtained from the relevant administration. Alternative solutions will be suggested to taking into account principles of professional merit and public interest about subject.

## 2. METHOD

The sample implementation areas in this study are located within settlement area in the development plan. Determining implementation areas and implementation boundary were carried out by responsible municipal administrations. The implementation boundary has been approved by the municipal board and the implementations have been registered in the land registry. When sample implementation areas are examined; it can be said that boundaries are correctly in terms of "technical principles stipulated by land development implementation legislation", but wrongly in terms of "professional merit" and "ethical values in the protection of property rights".

The implementation legislation stipulates accurate calculation of the amount of deduction in other words "development readjustment share" rate (DOPO) to be made from the real estates included in the implementation. However, the implementation boundary was determined considering only technical principles in the sample implementations. Since the boundary is determined without paying attention to the homogeneous distribution of public space and government agency area included in the development plan, different DOPO rates has been calculated and hence it has been observed that causes unfairness in real terms in protecting property rights.

## 3. RESULTS

### 3.1. Evaluation of Implementation Areas in the Neighborhoods of Karatay District, Konya Province

Sample implementations areas are located in Fevzi Çakmak and İstiklal neighborhoods of Karatay district, Konya province. Implementation areas are adjacent to each other and they are separated by a 40.00-meter urban road. The site selection and determining boundary studies of the implementation areas in the settlement area were made by the responsible municipal administration and the implementation boundary was approved by the municipal board (Figure 1 and Table 1).

When the implementation areas which are similar land use decisions in the 1: 1000 scale development plan were examined, the boundaries were determined correctly in terms of technical principles, wrongly in terms of professional merit and ethical values by local government. When analyzed implementations, free DOP deduction of %35 was applied in one implementation area and %12 DOP deduction was applied in the other implementation area in Fevzi Çakmak neighborhood but the DOPO value of the neighborhood sub-region in the Fevzi Çakmak neighborhood was calculated as %14. In the other implementation areas in the İstiklal neighborhood, which is separated from the Fevzi Çakmak

neighborhood by a 40.00 meter road, %22 and %37 free DOP deduction were applied but the DOPO value of the neighborhood sub-region in the İstiklal neighborhood was calculated as %30. Although the implementation stages were considered "correct" in terms of implementation legislation, it was determined that they are "wrong" because "unjust / unbalanced free DOP deduction was made with different DOPO applications in the same region".

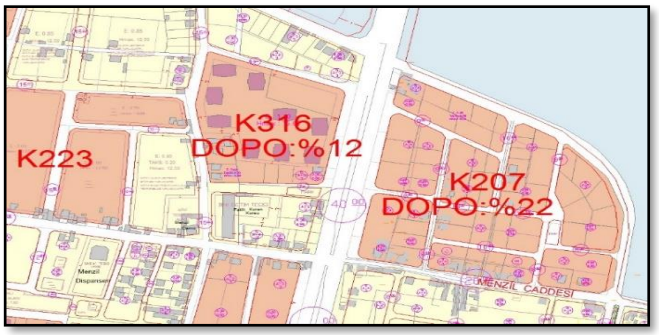


**Figure 1.** Implementation areas in the neighborhood of Karatay district, Konya province

**Table 1.** Implementation areas DOPO rate in the neighborhood of Karatay district, Konya Province

| Name of Implementation Areas | DOPO | Area ($m^2$) |
|---|---|---|
| Fevzi Çakmak Neighborhood | 35% | 368.038 |
| Fevzi Çakmak Neighborhood | 12% | 4.836.650 |
| Sub-Region DOPO Average | 14% | |
| İstiklal Neighborhood | 22% | 141.095 |
| İstiklal Neighborhood | 37% | 164.431 |
| Sub-Region DOPO Average | 30% | |

### 3.2. Evaluation of Implementation Areas in the Neighborhoods of Dörtyol District, Hatay Province

Sample implementations areas are located three separate stages in Çaylı neighborhood of Dörtyol district, Hatay province. Implementation areas are adjacent to each other. The site selection and determining boundary studies of the implementation areas in the settlement area were made by the responsible municipal administration and the implementation boundary was approved by the municipal board (Figure 2 and Table 2).

When the implementation areas which are similar land use decisions in the 1: 1000 scale development plan were examined, the boundaries were determined correctly in terms of technical principles, wrongly in terms of professional merit and ethical values by local government. When analyzed implementations, free DOP deduction of %27 was applied in the 1st implementation area, %19 DOP deduction was applied in the 2nd implementation area and %32 DOP deduction as applied in the 3rd implementation area but the DOPO value of the neighborhood sub region was calculated as %26. Although the implementation stages were considered "correct" in terms of implementation legislation, it was determined that they are "wrong" because "unjust / unbalanced free DOP deduction was made with different DOPO applications in the same region".


**Figure 2.** Implementation areas in the neighborhood of Dörtyol district, Hatay province

**Table 2.** Implementation areas DOPO rate in the neighborhood of Dörtyol district, Hatay province

| Name of Implementation Areas | DOPO |
|---|---|
| Çaylı Neighborhood (1st Stage) | 27% |
| Çaylı Neighborhood (2nd Stage) | 19% |
| Çaylı Neighborhood (3rd Stage) | 32% |
| Çaylı Neighborhood Average DOPO | 26% |

## 4. DISCUSSION AND CONCLUSION

It is not sufficient to consider only technical principles in determining the boundary that determining area of implementation. Balance of income and expenditures should preserve in the provision of free of up to 45% of government agency area and public spaces which have a significant contribution to the value of the region. The DOPO value should determine approximately equal or balanced to each other in the implementation areas and the implementation boundary should determine according to this approach.

Since 'site selection' and 'boundary determination' in the each implementation areas are rested with by responsible administration, DOPO values can be different from each other. Since stages on the implementation areas are accepted legally independent and different from each other, the judgments on the transaction files submitted to the court are also specific within implementation. For this reason, this kind of problem arising from determining implementation boundary but affecting the ownership should resolve on the basis of 'professional merit, equity and social justice' on the basis of 'institutional ethics and state guarantee'. Ownership of real estates owners must protected under all conditions. For this, the boundary of the implementation area should determine by making use of the developing information

technologies, in such a way that the government agency areas and public spaces corresponding to the implementation areas are balanced and the DOP rates are equal or close to each other; and then it is expected that the administrative management responsible for the implementation and the technical personnel will work within professional competence and ethical principles.

**REFERENCES**


Atasoy M, Demir O, Uzun B & Nişancı R (2002). İmar uygulamalarının iptal nedenleri ve öneriler. Selçuk Üniversitesi Jeodezi ve Fotogrametri Mühendisliği Öğretiminde 30. Yıl Sempozyumu, 184-192, Konya, Turkey.

Bıyık C & Uzun B (1990). Mevzuat ve uygulamaların ışığında arsa ve arazi düzenlemesinin proje çerçevesinde incelenmesi ve karşılaşılan problemler. 18. Madde Uygulamaları Semineri, 25-36, Ankara, Turkey.

Çay T & Özen H (1998). İmar uygulamalarında karşılaşılan problemler ve Konya örneği. Mülkiyet Dergisi, 28, 8-13.

Çelik K (2006). Planlama ve imar kanunu uygulaması, arazi ve arsa Düzenlemesi. Devran Matbaacılık, Ankara.

İnam Ş (1989). Arsa ve arazi düzenlemesi ve 3194 sayılı İmar Kanununun 18. maddesi uygulamaları. Phd Thesis, Selçuk University, Konya (in Turkish).

İnam Ş, Çay T & İşcan F (2015). Planlama ve İmar Kanunu tasarısının uygulanabilirliğinin araştırılması. S.Ü. Teknik Bilimler Meslek Yüksekokulu, Teknik-Online Dergisi, 14(1), 12-14.

Karavelioğlu C (1999). 3194 sayılı İmar Kanunu 18.madde uygulaması arazi ve arsa düzenlemesi – parselasyon. TOP-KAR Matbaacılık. Ankara.

Köktürk E (1997). İmar planı uygulamalarında karşılaşılan sorunlar ve kavramlaşma. TMMOB Harita ve Kadastro Mühendisleri Odası, Türkiye 6. Bilimsel ve Teknik Kurultayı, 15-22, Ankara, Turkey.

Köktürk E & Köktürk E (2007). Arsa düzenlemesinde eşdeğerlik ilkesinin modellenmesi. 11. Türkiye Harita Bilimsel ve Teknik Kurultayı, TMMOB Harita ve Kadastro Mühendisleri Odası, 1-8, Ankara, Turkey.

T.C. Resmi Gazete. 3194 sayılı İmar Kanunu, (18749), 03.05.1985.

T.C. Resmi Gazete. Arazi ve Arsa Düzenlemesi Hakkında Yönetmelik, (31047), 22.02.2020.

Uzun B (1992). Kentsel arsa düzenlemelerinde imar parseli üretme yöntemleri ve sonuçlarının irdelenmesi. PhD Thesis, KTÜ, Trabzon (in Turkish).

Ülkü H & Olgun Ö (1993). Arsa düzenleme sorunlar ve öneriler. TMMOB Harita ve Kadastro Mühendisleri Odası, Türkiye 4. Harita Bilimsel ve Teknik Kurultayı, Ankara, Turkey.

Yıldız F (2014). İmar bilgisi, planlama-uygulama-mevzuat. Nobel Yayınevi, ISBN: 978-605-5426-04-0

Yıldız N (1987). Arsa ve arazi düzenlemelerinde eşdeğerlik ve eşitlik ilkelerinin karşılaştırılması. Türkiye 1. Harita Bilimsel ve Teknik Kurultayı, 415-428, Ankara, Turkey.

Yomralıoğlu T (1992). Arsa ve arazi düzenlemesi için yeni bir uygulama şekli. HKMO Dergisi, 73, 30-43.

Intercontinental Geoinformation Days

http://igd.mersin.edu.tr/2020/

# GeoValueIndex Definition for Valuation of Public Property Assets

**Fatma Bunyan Unel*[1], Lutfiye Kusak[1], Murat Yakar[1]**

[1]*Mersin University, Engineering Faculty, Department of Geomatics Engineering, Mersin, Turkey*

**Keywords**
State Property Assets
Public Property Assets
Mass Real Estate Valuation
GeoValueIndex

**ABSTRACT**

The places under the jurisdiction and possession of the State, the places under the common use of the public and the places reserved for the public service and the immovable properties under the private ownership of the Treasury are the State Property Assets under the administration and management of the State. Of these, the places registered to the public legal entity and whose use is for the public benefit are Public Property Assets. Treasury Assets constitutes 37.6% of Turkey's surface and contributes significantly to the national economy.Most of the university immovable properties under the Council of Higher Education (YÖK) are public property allocated for education. Each university manages its real properties itself. The university properties are accounted; forms are filled and submitted to the General Directorate of National Real Estate for preparation of condensed statement. The aim of the study is to create a value-based GeoValueIndex depends on the features of Mersin University Çiftlikköy Campus properties. Analytic Hierarchy Process (AHP) was used as the analysis method. The GeoValueIndex obtained with AHP will both replace the trace value and provide a basis for mass real estate valuation and provide a practical solution for converting real estate to current market values.

## 1. INTRODUCTION

State property; refers to all property subject to public law or private law belonging to the state and public legal entities. State properties are divided into treasury and public property assets. Treasury properties are the private property of the Treasury, which is the owner of the state legal entity and registered in the name of the "Treasury" in the land registry. Public property assets; are properties allocated for the public interest, registered on behalf of public legal entities, subject to public law. In order for an immovable property to be considered a public property, it must be owned by a public legal entity and allocated to the public interest (Arslan, 2017; Gözler and Kaplan, 2018; Hazine, 2007; Yüksekkaya, 2018).

The General Directorate of National Real Estate (MEGM) is in charge of the administration of state property (MEGM, 1995). Sale, barter, construction in return for land or floor, lease, preliminary permit and establishment of easement rights on the immovable properties owned by the Treasury; It fulfills the procedures of renting the places under the jurisdiction and disposal of the state, granting preliminary permit and usage permission, and decriminalization and evacuation (Hazine, 2007). While MEGM was affiliated to the Ministry of Treasury and Finance, it has been taken under the Ministry of Environment and Urbanization (ÇŞBme, 2020).

Places under the jurisdiction and disposition of the state (forest, coastal, sea, lake, etc.), common property used by the public (pasture, threshing floor, road, bridge, etc.), assets in the service of public institutions (school, hospital, police station, place of worship, cemetery, etc.) and treasury property assets (immovable properties) vary in type. Showing them on cadastral maps and recording them in the land registry also differ (Kadastro, 1987).

Turkey area of 780 043 km$^2$ (HGM, 2020) is 37.6% of the assets that constitute the Treasury. There are three

* **Corresponding Author**

*(fatmabunel@mersin.edu.tr) ORCID ID 0000-0002-9949-640X
(lutfiyekusak@mersin.edu.tr) ORCID ID 0000-0002-7265-245X
(myakar@mersin.edu.tr) ORCID ID 0000-0002-2664-6251

**Cite this study**

Unel F B, Kusak L & Yakar M (2020). GeoValueIndex Definition for Valuation of Public Property Assets. Intercontinental Geoinformation Days (IGD), 88-91, Mersin, Turkey

types of treasury immovable properties portfolios: registered, under the jurisdiction and disposal of the State, and associated immovable properties. The registered areas are 267264.46 km$^2$, the places under the rule and disposition of the state are 19268.71 km$^2$ and the attached areas are 6391.98 km$^2$. Registered immovable properties privately owned by the Treasury; Forests, fields, lands, plots, vineyards, gardens, buildings, commons, water and aquaculture areas, mining and quarry areas, historical and cultural areas, coastal and embankment areas and other areas are classified according to their types and the number and surface area are given separately (MEGM, 2020).

Large campus areas are reserved for Council of Higher Education (Anayasa, 1982), which have public legal personality, far from city centers. The majority of the land used by the university campuses is allocated from the Treasury land and is public property. Provincial, district, neighborhood, area, type, value, etc. of immovable properties for public financial management and control. Forms containing the information are filled and submitted to MEGM. MEGM prepares condensed statement according to these forms (Kamu Kayıtları, 2006). Here, value is an important criterion and the accounting of immovable properties is kept. A study was carried out to facilitate the transactions in terms of value of the immovable properties located in the Mersin University Çiftlikköy Campus. The aim of the study is to create a value-based GeoValueIndex based on the geographic and attribute data of university immovable properties. Criteria are determined under five main headings consisting of title deed, parcel, land, location and usage information of the immovable properties. Data pertaining to each criterion were collected and edited. Analytic Hierarchy Process (AHP) method was used to create an index. The produced GeoValueIndex will both replace the trace value and provide a basis for mass real estate valuation and provide a practical solution for converting real estate to current market values.

## 2. MATERIAL AND METHOD

### 2.1. Study Area

İmmovable properties belonging to Mersin University (MEU) are located in Mersin city and district centers in parts. There are approximately 200 immovable properties within the boundaries of Çiftlikköy Campus, the largest part. The average altitude of the campus area from mean sea level is 133 meters and it is located at 36$^o$ 47 'Latitude and 34$^o$ 31' Longitude (Fig. 1).

Mersin University is responsible for the administration and management of the private properties it owns and the allocated immovable properties in their use. The management of the immovable properties located within the boundaries of Çiftlikköy Campus includes transactions such as expropriation of privately owned real estates, changes in their type and renting them out.

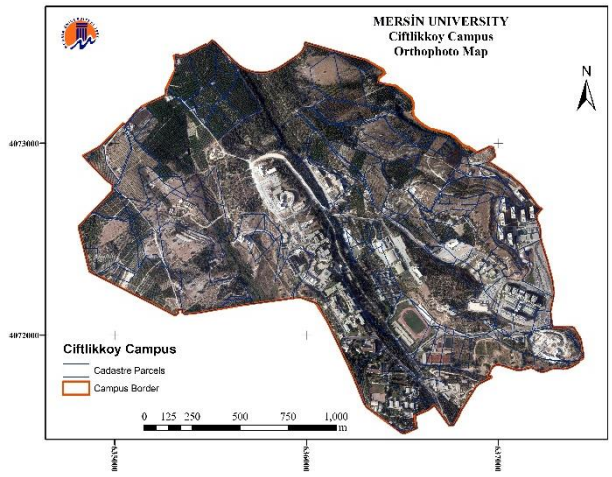


**Figure 1.** MEU, Ciftlikkoy Campus

### 2.2. Criteria of Mass Real Estate Valuation

Whether real estate is a state property or a private property, there are many criteria that affect its value. Topographic, hydrographic, geological and spatial features are among the criteria that do not change. Approximately 500 national and international literature reviews have been made, and 301 criteria for the land property type have been extracted Unel, (2017) and Unel & Yalpir, (2019). Legal, Physical, Spatial and Local are grouped under main headings and as a result of the criterion reduction, the criteria that affect the value the most have been found. Considering these criteria, the criteria for the valuation of public property assets have been investigated.

The criteria for the immovable properties within the boundaries of MEU Çiftlikköy Campus, which are among the public properties, have been determined based on the cadastral parcels. The immovable properties between the urban and rural areas, the agricultural areas are land; the places where the university buildings are located are in plot quality. Therefore, when determining the criteria, the features of the immovable properties and the trees, pools and buildings on them were taken into consideration (Table 1).

**Table 1.** Criteria of MEU properties

| A. REGİSTER FEATURES | B. PARCEL FEATURES | C. LAND FEATURES | |
|---|---|---|---|
| **1.** Type<br>**2.** Area<br>**3.** Owner<br>**4.** Ownership (Full-Shared) | **1.** Location on the Block (Corner-Inter.)<br>**2.** Geometric shape<br>**3.** Access to Road<br>**4.** The number of frontage<br>**5.** Length of the frontage<br>**6.** Technical Infrastructure | **Topography**<br>**1.** Elevation<br>**2.** Slope<br>**3.** Aspect<br>**Geology;**<br>**4.** Geology | **Hydrography**<br>**5.** Frontage Length of Water Line<br>**6.** Distance of Water Line<br>**7.** Length of Water Road |
| **D. LOCATİON FEATURES** | | **E. USAGE FEATURES** | |
| **1.** Distance to Main Road<br>**2.** Distance to City Centre<br>**3.** Distance to Mediterranean Sea | **4.** Distance to Shopping Centre<br>**5.** Distance to Green Area<br>**6.** Distance to Power Distribution Lines | **Building**<br>**1.** Total Building Area<br>**2.** Usage Type<br>**Vegetation**<br>**3.** Tree Type | **Water**<br>**4.** Pool Area<br>**5.** Pool Type |

In addition to these, there are the property number, province, district, neighborhood, block and parcel numbers in the General Directorate of Land Registry and Cadastre (TKGM in Turkish) system, which includes the address information of the property.

Criteria such as the number of floors of the building, building age, number of trees and tree age also affect the value significantly. However, as it requires time, cost and effort to access these data, they could not be included in the operations in this study.

### 2.3. Analytic Hierarchy Process

The Analytic Hierarchy Process (AHP) method, which is one of the Multi-Criteria Decision Analysis (MCDA), is very useful in making decisions about complex problems. "The most creative task in making a decision is to choose the criteria that are important for that decision. In AHP it is arranged these criteria, once selected, in a hierarchic structure descending from an overall goal to criteria, subcriteria and alternatives in successive levels." (Saaty, 1990).

To make a decision in an organized way it should be applied the decision into the following steps (Saaty, 2008);

**1.** Define the problem and determine knowledge kind.
**2.** Structure the decision hierarchy (goal and criteria).
**3.** Construct a set of pairwise comparison matrices.
**4.** Weigh criteria with calculations.

AHP method is used to solve complex problems in many different topics such as site selection (Jelokhani-Niaraki & Malczewski, 2015; Rahmat et al., 2016), city planning (Peng & Peng, 2018), landslide susceptibility mapping (Kayastha et al., 2013), sinkhole susceptibility mapping (Orhan et al., 2020), valuation criteria weighting (Bender et al., 2000; Kauko, 2003; Kryvobokov, 2005; Yılmaz, 2010; Unel, 2017), mortgage credit risk evaluating (Ferreira et al., 2014) etc. Moreover, An innovative structure of AHP has developed to capture the relationship between various levels of activities contributed by people to society (Saaty & Shang,, 2011).

## 3. RESULTS

The most complex part in mass real estate valuation is the criteria that make up the properties of real estates. These criteria that affect the immovable values are; it varies from country to country, from region to region, from person to person. At the same time, there are many criteria affecting the market value of the real estate. Especially citizens, appraisers, contractors, real estate agents, etc. can be given as an example (Ünel, 2017).

The hierarchical structure of the AHP method produces solutions by simplifying the complexity by listing the criteria from the main heading to the subtitles. It both weighs the criteria and provides the opportunity to rank in order of importance. Criteria for main titles and sub-headings can be compared with binary comparisons.

While creating the paired comparison matrix of the main topics (Table 2), the results of the previous surveys were used. By performing row and column operations of AHP method, weight calculation step (Saaty, 1987) was started.

**Table 2.** Pairwise comparison matrix of the main criteria

| | A. Register | B. Parcel | C. Land | D. Location | E. Usage |
|---|---|---|---|---|---|
| **A. Register** | 1 | 3 | 4 | 2 | 2 |
| **B. Parcel** | 1/3 | 1 | 2 | 1/3 | 1/3 |
| **C. Land** | 1/4 | 1/2 | 1 | 1/5 | 1/5 |
| **D. Location** | 1/2 | 3 | 5 | 1 | 1 |
| **E. Usage** | 1/2 | 3 | 5 | 1 | 1 |

The weights of the main headings of register, parcel, land, location and usage features, which form the first part of the hierarchy, have been calculated. The second part of the hierarchy is the sub-criteria, and after calculating their weights, they are multiplied with each other. The weights of the criteria are listed in descending order. The total weight should be 1 (1.0032). However, due to the rounding, numbers are seen in the 3rd and 4th digit of the decimal point.

As the public property owner (0.1727), MEU has been evaluated as Treasury, Forest and Private ownership and it is seen in the weights that it is of great importance in terms of value in parallel with the right to save as the university wants. Again, there are different structures for education, culture, sports, accommodation and food and beverage areas within the campus area. Construction costs vary depending on the variety of use. Based on this, Building Usage Type (0.1189) is the second important criterion. The ownership structure (0.0973), which indicates the full and shareholding status that affects the use of the real estate, is also of third importance. Contrary to these; frontage length and distance of water line, length of water road (0.0038); in parcel, the number of frontage and length of the frontage (0.0029) is seen to have the smallest weights.

## 4. CONCLUSION

It is of great importance to know the values of the state assets such as treasury, forest, pasture, coastal in a transparent and accountable way and to make optimum decisions within the borders of the country. Value consists of the combination of property properties. Collecting data on immovable properties, storing them by recording, organizing and preparing them for analysis in standard format requires serious labor.

GeoValueIndex was created by taking into account features of land, structure, trees and other facilities on Mersin University Çiftlikköy Campus. The index has brought an easier, faster and more practical solution to the accounting of university immovable properties as public assets. In continuation of the study, GeoValueIndex Map is going to be generated by visualizing the index.

**ACKNOWLEDGEMENT**

This study has supported by MEU, Scientific Research Projects with 2019-2-AP4-3511 cod and title of "Establishment of Valuation Substructure for Management of Real Properties of Mersin University".

**REFERENCES**

Anayasa, (1982). Türkiye Cumhuriyeti Anayasası, Kanun Numarası: 2709, Kabul Tarihi: 18/10/1982 Yayımlandığı Resmî Gazete Tarihi: 9/11/1982 Sayısı: 17863, (Mükerrer) Yayımlandığı Düstur: 5(22), 3.

Arslan, K.O. (2017). Determination of the Characteristics of Public Property and the Rules of Utilization of the Public Properties, TBB Dergisi, 131, 57-86.

Bender, A., Din, A., Hoesli, M. & Brocher, S. (2000). Environmental preferences of homeowners, further evidence using the AHP method, Journal of Property Investment & Finance, 18 (4), 445-455.

ÇŞBme, 2020, Çevre ve Şehircilik Bakanlığı Milli Emlak Personelinin Atama ve Yer Değiştirme Yönetmeliği Resmî Gazete Sayısı: 31128.

Ferreira, F.A.F., Santos, S.P. & Dias V.M.C. (2014). An AHP-based approach to credit risk evaluation of mortgage loans, International Journal of Strategic Property Management, 18(1), 38-55.

Gözler, K. & Kaplan, G. (2018). İdare Hukuku Dersleri, Bursa: Ekin Kitabevi Yayınları.

Hazine, (2007). Hazine Taşınmazlarının İdaresi Hakkında Yönetmelik, Resmî Gazete Tarihi: 19/06/2007 Resmî Gazete Sayısı: 26557

HGM, 2020, General Directorate of Mapping (Harita Genel Müdürlüğü-HGM), İl ve İlçe Yüzölçümleri, Ulusal Haritacılık Kurumu.

Jelokhani-Niaraki M. & Malczewski, J. (2015). A group multicriteria spatial decision support system for parking site selection problem: A case study, Land Use Policy, 42, 492–508.

Kadastro, (1987). Kadastro Kanunu Kanun Numarası: 3402 Kabul Tarihi: 21/6/1987 Yayımlandığı Resmi Gazete Tarihi: 9/7/1987 Sayısı: 19512, Yayımlandığı Düstur: 5(2)6, 229.

Kamu Kayıtları, (2006). Kamu İdarelerine Ait Taşınmazların Kaydına İlişkin Yönetmelik, Bakanlar Kurulu Kararının Tarihi: 13/9/2006 No: 2006/10970, KHK Yayımlandığı Resmi Gazetenin Tarihi: 2/10/2006 No: 26307 Yayımlandığı Düsturun Tertibi: 5(46).

Kauko, T. (2003). Residential Property Value and Locational Externalities on the complementarity and substitutability of approaches, Journal of Property Investment & Finance, 21(3), 250-270.

Kayastha, P., Dhital, M.R. & De Smedt, F. (2013). Application of the analytical hierarchy process (AHP) for landslide susceptibility mapping: A case study from the Tinau watershed, west Nepal, Computers & Geosciences, 52, 398–408.

Kryvobokov, M. (2005). Estimating the weights of location attributes with the Analytic Hierarchy Process in Donetsk, Ukraine, Nordic Journal of Surveying and Real Estate Research, 2(2), 5-29.

MEGM, (1995). Maliye Bakanlığı Millî Emlâk Genel Müdürlüğü Taşra Birimleri Kuruluş ve Görev Yönetmeliği, Resmî Gazete Tarihi: 24/08/1995 Sayısı: 22384

MEGM, (2020). Milli Emlak Genel Müdürlüğü, Faaliyet Raporu, Yayın No: 2020/2, Ankara.

Orhan, O., Yakar M. & Ekercin, S. (2020). An application on sinkhole susceptibility mapping by integrating remote sensing and geographic information system, Arabian Journal of Geosciences, 13, 886.

Peng, J. & Peng F.L. (2018). A GIS-based evaluation method of underground space resources for urban spatial planning: Part 1 methodology, Tunnelling and Underground Space Technology, 74, 82-95.

Rahmat, Z.G., Niri, M.V., Alavi, N., Goudarzi, G., Babaei, A.A., Baboli, Z. & Hosseinzadeh, M. (2016). Landfill site selection using GIS and AHP: a case study: Behbahan, Iran, KSCE Journal of Civil Engineering, 1-8.

Saaty, R.W. (1987). The Analytic Hierarchy Process-What It Is and How It Is Used, Mathl Modelling, 9(3-5), 161-176.

Saaty, T.L. (1990). How to make a decision: The Analytic Hierarchy Process, European Journal of Operational Research 48 (1990) 9-26 9 North-Holland.

Saaty, T.L. (2008). Decision making with the analytic hierarchy process, Int. J. Services Sciences, 1(1).

Saaty, T.L. & Shang, J.S. (2011). An innovative orders-of-magnitude approach to AHP-based mutli-criteria decision making: Prioritizing divergent intangible humane acts, European Journal of Operational Research, 214, 703-715.

Unel, F.B. (2017). Development of Geography Data Model For Criteria of Real Estate Valuation, Ph.D. Thesis, Selçuk University, Konya, Turkey.

Unel F.B. & Yalpir, Ş. (2019) Approach to Criteria Affecting Value of Real Properties in Turkey, Journal of Geomatics, 4(2), 112-133.

Yılmaz, A. (2010). Real estate valuation by using multicriteria decision support system (analytic hierarchy process) and ratio study, Master's Thesis, Yıldız Technical University, İstanbul.

Yüksekkaya, S.V. (2018). Kamu Taşınmazları Denetimi, Taşınmaz Semineri Ders Notları, Sayıştay Başdenetçisi.

Intercontinental Geoinformation Days

http://igd.mersin.edu.tr/2020/

# Agricultural land use and GHG emission in India and Turkey: A comparative trend analysis

**Mohd Kamil Vakil**

*Department of Civil Engineering, Indian Institute of Technology (IIT) Kanpur, Kanpur, India*

**Keywords**
Agriculture
Land use
GHG
Arable land

**ABSTRACT**

India and Turkey have a growing population to feed and supply as per the changing lifestyle. Land use efficiency is essential to minimize resource consumption and maximize production. The agriculture sector is one such domain where a high range of needs and wants of humans are met. Several agricultural reformations were adopted in India and Turkey between 1960-2017, which resulted in a rise in crop production and intensive consumption of agrochemicals and water. However, this came with the cost of the environment in elevated levels of greenhouse gas emissions. This study focuses on agricultural production and associated GHG emissions in two countries and comparative changes. The first part of the study found high variability in land use patterns in Turkey, while India gradually followed the demand-supply trend. In line with the gradual increment in land usage, the CO2 emissions from Indian agricultural production also observed a similar change pattern. Meanwhile, Turkey followed the reducing trend for two decades from 1990, then an increment was reported in 2013. It was also found that the process of enteric fermentation among animals is the single most contributor to agricultural emissions. Finally, a correlation study was carried out between arable land in Turkey and total agricultural GHG emission.

## 1. INTRODUCTION

India and Turkey have many similarities in terms of culture, heritage, economy, and geography. Speaking of geography, India has a coastline of around 7000 km while Turkey has 3% more than that. Coal and iron ore are selectively most common natural resources these two countries extract from their depths. Though India's climate varies from tropical monsoon to temperate, Turkey is mostly temperate, dry, and harsher in the interior. India (2.97 million sq km) acquires four times more than Turkey in terms of land area. The land dedicated to the agriculture sector in India is five times of Turkey. While the former has seven times more arable land area, the latter has two times greater arable land per capita. Other than similarities such as resources, the significant dissimilarity is agricultural products. While India produces rice, wheat, oilseed, cotton, etc., Turkey cultivates tobacco, cotton, grain, olives, etc. (Giray 2012). Turkey emits four times more overall $CO_2$ per 1000 based on global warming potential and two times more CO2 based on energy production per million (Garg et al. 2001; Evrendilek and Ertekin 2002). Turkey's ecological footprint is reported to be three times more than India (York et al. 2004; York et al. 2009).

## 2. METHOD

Generally, a comparative study is conducted to understand the causation processes involved in the conception by simplifying the variations in the explanatory variable(s) (Pickvance 2005). Conventionally, comparative analysis stressed the "description of differences and the clarification of similarities." There are numerous comparative analysis methods, and Tilly (1984) differentiates four main types: individualizing, universalizing, variation-finding, and encompassing. This study used the fourth type, i.e., encompassing, based on comparing different instances at various locations within the same system. The country-specific data on land use, emissions, and economic and political stability were taken from the open-sourced Food and Agricultural Organization (FAO) database engine (www.fao.org/faostat). MS Excel 365 was used to harmonize data and further analysis.

**Corresponding Author**

(kamilvakil@gmail.com) ORCID ID 0000-0001-6504-3296

**Cite this study**

Vakil, M. K. (2020). Agricultural land use and GHG emission in India and Turkey: A comparative trend analysis. Intercontinental Geoinformation Days (IGD), 92-95, Mersin, Turkey

## 3. RESULTS AND DISCUSSIONS

### 3.1. Land use

India and Turkey follow different land use patterns, and India leads in terms of total land under agriculture by 4.75 times. This factor in 1961 was 4.79, which is when the green revolution in India started. It ended in 1980, after which surplus production and export policy was empowered, which lasted till 2000. Between 1960 and 2018, India observed a change of 2.7% in the agricultural area while Turkey experienced more than 3.5% growth. Different agrarian reforms were observed in Turkey after 1980, 1990, and 2000. In the 1980s, reforms such as globalization of agriculture, privatization and farmer support were introduced, raising the land use area by 5.6% compared to 1961. Economic stabilization and structural adjustment program were introduced in the 1990s, which helped in a significant surge of 8.5%. In the 2000s, Turkey announced restructuring the agriculture and support policies, after which agricultural land use pattern increased by 10.9%, considering 1961 the base year. The highest increment of 12.9% was observed in 2002, which is influenced by 2000 reforms. The average yearly increment in India and Turkey's agricultural land areas is 2.7% and 6.2%, respectively.

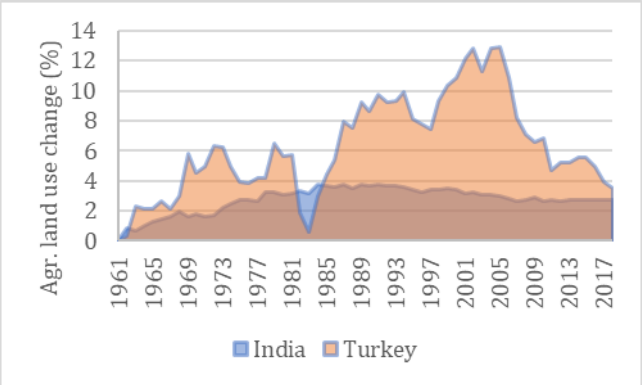


**Figure 1.** Agricultural land use change (%)

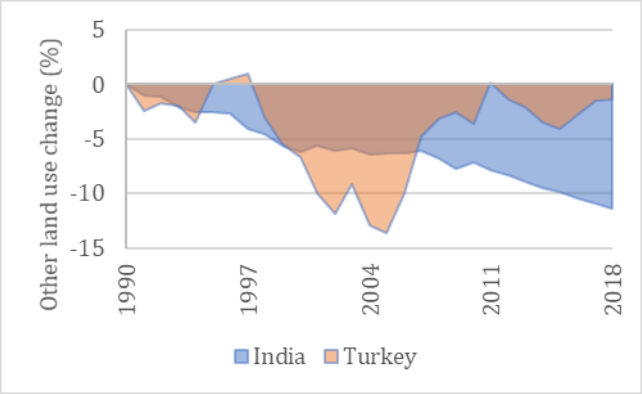


**Figure 2.** Other land use change (%)

On the other side, India's non-agricultural land use observed a gradual change between 1990 and 2018, with an average reduction of 6.2% per year. With an average growth of -4.3%, Turkey had seen mixed variation as the maximum rise (+1%) and dip (-13.6%) were detected during 1997 and 2005.

The agricultural land is further categorized into three types – (1) arable land; (2) land under permanent meadows and pastures; and (3) land under permanent crops. The most remarkable rise was observed under permanent crops with a percentage change of more than 150% and 60% for India and Turkey. On the opposing end, 26.5% of the pastures and meadows loss were observed in India and 14.3% arable land in Turkey. The average change in India's three types of agricultural land usage is estimated to be +2.9%, -15.8%, and +49.1%, respectively. Similarly, the three values for Turkey are +2.9%, +8.4%, and +30.4%.

### 3.2. Production

Cereals are one of the most important crops grown to fulfill the nutritional security of a country. Rice, wheat, and coarse grains such as maize, sorghum, and millets are vital for this class. While wheat is the top grown cereal in Turkey, India is known for producing wheat and rice. In 1961, India produced 87.4 Mt of grains, which was increased to 148 Mt in 1981 and 243 Mt in 2001. Between 1961 and 2018, cereal production has increased by 264% simultaneously with Turkey's 170%. Turkey produced 12.7 Mt in 1961, which was further raised by 100% in 1981 and 132% by 2001. Turkey observed a 15.5% reduction in terms of the cropped area, while India rose by 6.2%. This is reflected in yield values, which is increased by +220% for Turkey and +243% for India.

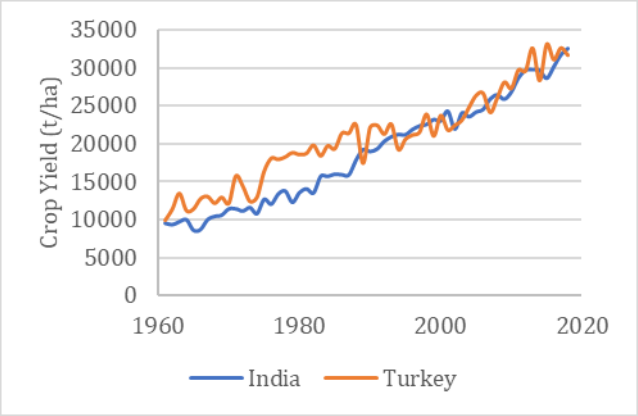


**Figure 3**. Crop yield plot between India and Turkey

The yield values for India and Turkey in 1961 were 9473 and 9894 t/ha, which were changed to 32479 and 31639 t/ha, respectively. After preceding behind for consecutive 26 years, it was 1989 when India passed Turkey's cereal yield potential by a margin of 1743 t/ha.

### 3.3. $CO_2$ emissions

The drivers, such as population trend and land use pattern, enabled the global economies to invest in the agriculture sector, which has observed crop intensification and rigorous irrigation and fertilizer consumption. Although agrochemicals such as chemical fertilizers, pesticides, insecticides, and herbicides helped grow crop productivity, it also affected the environment in the form of biodiversity loss, water and soil contamination, and greenhouse gas (GHG) emissions. GHG emissions are commonly caused by enteric

fermentation in livestock, farming, rice fields, and background sources such as the manufacturing of agrochemicals, etc.

Here, it is found that during 1990-2017, the agricultural GHG emissions were increased by up to 27.2% and 9.5% in India and Turkey, respectively. Former one had continuously experienced the increasing trend; however, Turkey followed the reducing sensation for the first 23 years; then, in 2013, a two percent increment was reported. The total CO2 emission from the Indian agricultural sector was said to be 502 thousand gigagrams (Gg) in 1990, which was changed to 639 thousand Gg in 2017. Similarly, Turkey emitted 42 and 46 thousand Gg of GHGs in 1990 and 2017, respectively.

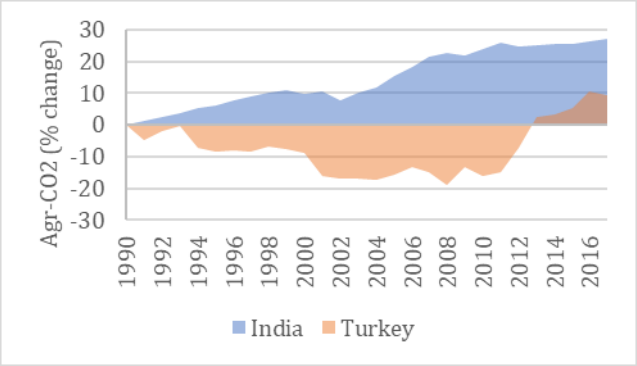


**Figure 4**. Change (%) in GHG emission

**Table 1.** Averaged CO2 emission from Agricultural sources

| Source | India (%) | Turkey (%) |
|---|---|---|
| Burning - Crop residues | 0.6 | 0.8 |
| Burning - Savanna | 0.1 | 0.2 |
| Crop Residues | 3.7 | 6.5 |
| Cultivation of Org. Soils | 0.1 | 0.0 |
| Enteric Fermentation | 46.8 | 35.7 |
| Manure applied to Soils | 2.4 | 1.1 |
| Manure left on Pasture | 10.5 | 30.2 |
| Manure Management | 4.7 | 1.8 |
| Rice Cultivation | 16.7 | 1.2 |
| Synthetic Fertilizers | 14.3 | 22.5 |

The highest contribution to GHG in both countries is enteric fermentation, a digestion process among animals. On the other hand, manure left on pasture is the second most contributor in Turkey, followed by synthetic fertilizers and crop residues. In India's case, rice cultivation emits the highest GHG in the domain of plant-based crop production. The other significant factors are the manufacturing and applying synthetic fertilizers, manure left on pasture and its on-field management, and crop residue.

### 3.4. Demographic representation in production and emission

The per capita food supply in Turkey observed variations between 2000 and 2017 multiple times. It started with 41 kcal/capita/day in 2000 and reached as high as 64 kcal in 2016 before settling at 63 kcal/capita in 2017. Meanwhile, Indian per capita food supply significantly reduced from 24 kcal to only 6 kcal per capita during 2000-2017. This country once recorded 63 kcal/capita in 2009 after scoring 50 kcal in 2008; however, it has subsequently degraded over the years. India's per capita food production, which reflects the economic and political stability, seems to be unchanged if we compare only two years – 2001 and 2015. The mean value is a little more than 5000 $/capita, and maxima and minima values of 7500 and 2000 $/capita were observed in 2003 and 2001, respectively. The last data reported during the study period is 2100 $/capita.

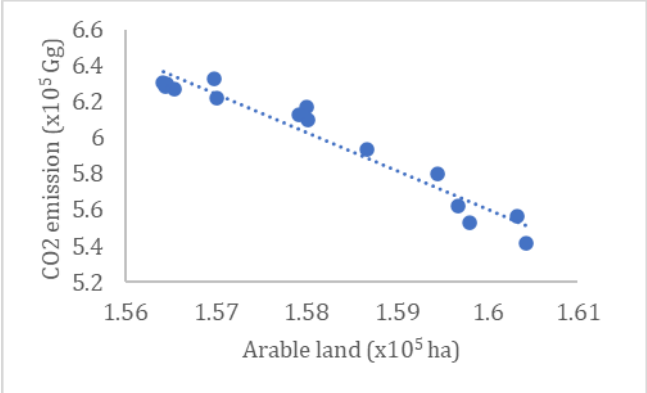


**Figure 5.** Scatter plot between GHG and Arable land, Turkey

The comparative study for Turkey revealed a significantly higher correlation coefficient of agricultural GHG emission with the area under arable land (0.9402) as compared to area under permanent crops (0.8992) and meadows and pastures (0.7912). This is also reflective of enteric fermentation as cattle used to gaze around involving respiration and excretion. On the other hand, Indian agricultural emission data is modeled and is in line with crop production and land utilization intensity. Therefore, such a correlation study was ignored to avoid a biased remark on crop production and associated emission.

## 4. CONCLUSION

India is a geographically blessed country due to its biodiversity and desirable meteorological as well as topological variables. Turkey, on the other hand, is known for terrestrial and coastline resources. Here, these two nations were used to understand their commonalities in agricultural production, including associated land and greenhouse gas footprints. This study also targeted political and economic stability factors such as per capita food production and supply to relate them with primary variables such as land use and related emissions. This study found high variability in Turkey's land-use patterns, while India gradually adapted the demand-supply trend. The crop productivity was almost similar in the later years; however, Turkey was leading until 1990. In line with the gradual increment in land usage, the CO2 emissions from Indian agricultural production also observed a similar change pattern.

On the other hand, Turkey followed the reducing trend for the first 23 years, then in 2013, an increment

was reported. Enteric fermentation is the single most contributor to agriculture sector led GHG emissions. Finally, a correlation study was carried out between arable land in Turkey and total agricultural GHG emission, which was significant ($R^2 = 0.9402$).

**REFERENCES**

Evrendilek, F., & Ertekin, C. (2002). Agricultural sustainability in Turkey: integrating food, environmental and energy securities. *Land Degradation & Development*, *13*(1), 61-67.

Garg, A., Bhattacharya, S., Shukla, P. R., & Dadhwal, V. K. (2001). Regional and sectoral assessment of greenhouse gas emissions in India. *Atmospheric Environment*, *35*(15), 2679-2695.

Giray, H. (2012). Turkish agriculture at a glance. *Journal of Food, Agriculture & Environment*, *10*(3&4), 292-295.

Pickvance, C. (2005). The four varieties of comparative analysis: the case of environmental regulation.

Tilly, C. (1984). *Big structures, large processes, huge comparisons*. Russell Sage Foundation.

York, R., Rosa, E. A., & Dietz, T. (2004). The ecological footprint intensity of national economies. *Journal of Industrial Ecology*, *8*(4), 139-154.

York, R., Rosa, E. A., & Dietz, T. (2009). A tale of contrasting trends: Three measures of the ecological footprint in China, India, Japan, and the United States, 1961-2003. *Journal of World-Systems Research*, 134-146.

Intercontinental Geoinformation Days

http://igd.mersin.edu.tr/2020/

# A House Valuation with Multiple Regression Analysis and Artificial Neural Networks

**Mehmet Emin Tabar*[1], Aslan Cihat Başara [1], Yasemin Şişman [2]**

[1]*Ondokuz Mayis University, Institute of Graduate Studies, Department of Geomatics Engineering, Samsun, Turkey*
[2]*Ondokuz Mayis University, Faculty of Engineering, Department of Geomatics Engineering, Samsun, Turkey*

**Keywords**
Real estate appraisal
Multiple regression analysis
Artificial neural network
Artificial intelligence
Matlab

**ABSTRACT**

Valuation, in its simplest form, is the determination of the amount that a property will be processed at a certain date. Valuation can be done for many purposes. These; can be listed as buying and selling, transfer, tax assessment, expropriation, inheritance distribution, investment, financing and credit. There are various methods of valuation. These methods are examined under 3 main groups as traditional, statistical and modern valuation methods. The aim of the article is to provide an overview of regression analysis, one of the statistical valuation methods, and artificial neural networks, one of the modern valuation methods, and to compare the accuracy values. Matlab software was used for artificial neural network modeling and Minitab software was used for regression analysis. The accuracies of the obtained values were determined by the average absolute percent error (MAPE) formula.

## 1. INTRODUCTION

Valuation of real estate and the reflection of these values to tax is one of the most important economic foundations of developed societies. With the development of real estate investment trusts, construction companies, education, technology and professionalism, the real estate market has gained a positive momentum. These developments have also brought professional real estate appraisals to the agenda in order to make the right investments (Atik, KÖSE, Yilmaz, & ERBAŞ, 2015).Real estate is independent and permanent rights registered on a separate page in the land register and independent parts of the property ownership register, which give the owner the right to use as she wishes, except for the restrictions developed for the benefit of the public (Açlar & Çağdaş, 2002). The concept of housing is the place where the consumer ultimately lives with his wife and children (Özdamar, 2004).

The concept of value is defined as the abstract measure used to determine the importance of something, the value of something, the value of something that can be measured with money, price (Yomralıoğlu, Nişancı, Çete, & Candaş, 2011). Real estate valuation is the provision for trading or corporate transactions that varies according to needs, wishes and financial capacity (Ring & Dasso, 1977).

According to another definition, it is the process of determining the provision of the seller according to the properties of the property for investment or long-term use (Brown, 1965). Real estate valuation is done in many different ways. However, for professional real estate valuation, a mathematical model should be mentioned rather than subjective value estimates. Statistical and modern methods involve less initiative as they depend on a mathematical model.

Traditional methods, on the other hand, are far from being objective compared to statistical and modern valuation methods since they do not depend on a mathematical model. Because in traditional valuation methods, valuation experts try to make value calculations by only estimating an exchange price. However, one of the most important issues in the valuation area is the need to ensure that the information provided to the customer is clear and clear. (Pagourtzi, Assimakopoulos, Hatzichristos, & French, 2003). When the methods used in the mathematical model are examined; Many methods such as fuzzy logic, artificial neural networks, spatial analysis, support vector machines, regression analysis are reached. Real estate valuation methods are shown in Table 1.

* **Corresponding Author**

*(mehmetemintabar@gmail.com) ORCID ID 0000 – 0002 – 3234 – 5340
(aslancihatbasara@gmail.com) ORCID ID 0000 – 0001 – 6644 – 6097
(ysisman@omu.edu.tr) ORCID ID 0000 – 0002 – 6600 – 0623

**Cite this study**

Tabar M E, Basara A C & Sisman Y (2020). A House Valuation with Multiple Regression Analysis and Artificial Neural Networks. Intercontinental Geoinformation Days (IGD), 96-99, Mersin, Turkey

**Table 1.** Real estate valuation methods

| Traditional methods | Statistical methods | Modern methods |
|---|---|---|
| Comparison method | Nominal method | Fuzzy logic |
| Income method | Multiple regression method | Artificial neural networks |
| Cost method | Hedonic pricing method | Support vector machine |

In this study, regression analysis, one of the statistical valuation methods, and artificial neural networks, one of the modern valuation methods, were used. Accuracy values obtained were calculated with the formula of average absolute percent error (MAPE).

$$MAPE = 100\frac{\sum_{i=1}^{n}\frac{|A_i - F_i|}{A_i}}{n}$$

The calculated accuracy values are compared and given in a table.

## 2. MATERIAL AND METHOD

Housing data were obtained from a residential sales site. While choosing the residences, care was taken to choose those with a facade to the tramway street. Housing values are valid from August to October 2020. Housing values were determined by modeling the obtained data with multiple regression analysis and artificial neural networks.

### 2.1. Multiple Regression Analysis

Regression analysis consists of dependent and independent variables. The number of dependent variables is single, but the number of arguments can be more than one. If there is only one independent variable, it is called simple linear regression, if there are two or more independent variables, it is called multiple linear regression. In regression analysis, it is aimed to explain the relationship between variables functionally and to define this relationship with a model (Chatterjee & Hadi, 2015).

It is based on the principle of examining how the other variable changes according to this level by keeping one of the variables or the category of the variable at predetermined levels. Regression is also interpreted as finding the unknown with the help of what is known in modern statistics (Akış, 2013). In the prediction, when the correlation between variables is zero, it is concluded that there is no relation about X, Y. However, if this correlation is not zero, the result will be less erroneous. If the correlation is ± 1.00, then the prediction probability is high and successful. When this correlation moves away from ± 1.00, the amount of error increases (Zeng & Zhou, 2001).

### 2.2. Artificial Neural Networks

Artificial neural networks emerged by artificially imitating the way the human brain works. It can be thought of as a complex system that occurs as a result of connecting many nerve cells in the brain with different levels of influence. In artificial neural networks, the system first performs the learning process by analyzing input data and output data (Öztürk & Şahin, 2018). It gives approximate outputs of new input data after learning process as a result of iterations. Artificial neural networks are especially used in engineering applications. Engineering problems that are difficult to solve with classical methods have gained a different dimension with artificial neural networks and have created an effective alternative (Yegnanarayana, 2009). Although the human brain is limited in mathematical operations such as division, multiplication, addition, subtraction, it is more successful than machines in many processes such as learning, remembering, and predicting. The main features of artificial neural networks are nonlinearity, learning, parallel working, generalization, working with missing data, using a large number of variables and parameters, applicability, fault tolerance and flexibility.

Artificial neural networks consist of 3 main components. These; architectural structure, learning algorithm and activation function. When we examine the architectural structure, the input layer consists of the hidden layer and the output layer. In the learning algorithm, the weights in the whole network should take optimal values. In fact, training the net is to find the best value of the weights (Graupe, 2013). The activation function provides the match between input and output layers.

Artificial neural networks learn by making mistakes. Basically, artificial neural networks learn in 3 stages. In the first step, outputs are calculated. In the second step, it compares the outputs with the target outputs and calculates the error. In the last stage, the process repeats by changing the weights (Livingstone, 2008). Artificial neural networks architecture is shown in Fig 1 as input layer, hidden layer and exit layer.

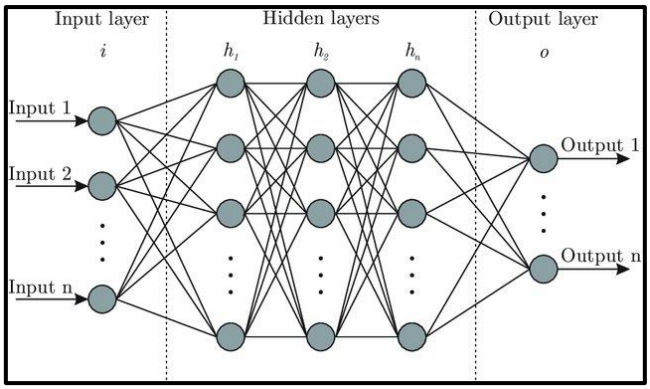


**Figure 1.** Artificial neural network architecture (Bre, Gimenez, & Fachinotti, 2018)

Artificial neural networks consist of multi-layer computational units. The data received from the external environment is applied to the input layer and processed at the entrance, the information is transmitted to the middle layer without any change in the flow direction. The information entering the process in these layers is transmitted forward to the output layer. Artificial neural networks based on the working principle of transmitting information in the forward direction from input to output are called forward feed artificial neural networks (Canan, 2006).

## 3. RESULTS

In Samsun, Atakum, Yenimahalle Quarter, 200 data were collected about the properties and values of the houses facing the tramway and these values were transformed into tables and normalized with maximum minimum normalization.

Normalized data were defined in Minitab program and analyzed by multiple regression. The result of the analysis was taken as a mathematical model and compared with the actual values of the test data.

For the other model, Matlab software was used. In the artificial neural network module in Matlab software, residential data are defined as input, output and test data. A feed forward network was created using this module. For the test data, the outputs of the Matlab software are taken and compared with the real residential values.

A comparison was made by calculating the accuracy values of the data obtained from both models. Real estate data are generally shown in Table 2.

**Table 2.** Real estate data

| Area | Number of rooms | Building age (Years) | Floor/Number of floors | Number of bathrooms | Balcony | Furnished | Value (TRY) |
|---|---|---|---|---|---|---|---|
| 45 | 1+1 | 0 | 0/4 | 1 | Yes | Yes | 205 000 |
| 125 | 3+1 | 21-25 | 0/4 | 2 | Yes | No | 300 000 |
| 160 | 4+1 | 11-15 | 8/8 | 2 | Yes | No | 375 000 |
| 85 | 2+1 | 0 | -1/4 | 1 | Yes | No | 260 000 |
| 130 | 3+1 | 5-10 | 5/8 | 2 | Yes | No | 435 000 |
| … | … | … | … | … | … | … | … |
| 130 | 3+1 | 4 | 1/5 | 1 | Yes | No | 349 000 |
| 145 | 3+1 | 0 | 1/6 | 2 | Yes | No | 475 000 |
| 135 | 3+1 | 0 | 1/6 | 2 | Yes | No | 495 000 |
| 145 | 3+1 | 16-20 | 6/6 | 1 | Yes | No | 290 000 |
| 95 | 2+1 | 11-15 | 0/7 | 2 | Yes | Yes | 260 000 |

### 3.1. Multiple Regression Analysis Application

Normalized real estate data were defined in Minitab software and regression equation was obtained. Housing values were calculated with the regression equation obtained.

*Regression Equation = (-0.612 + 0.405 area + 0.307 room + 0.4227 b.age + 0.1027 floor + 0.1712 bathroom + 0.2276 balcony - 0.0229 furnished)*

The calculated normalized value has been converted into the real house value with the maximum-minimum formula.

$$Normalized\ data = \frac{(x - \min)}{max - min}$$

Normal probability plot created according to the value of the house is shown in Fig 2.

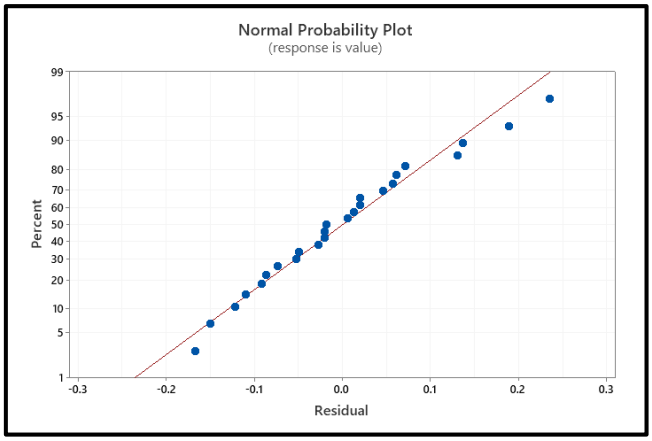


**Figure 2.** Normal probability plot

The values calculated by multiple regression analysis are shown in Table 3 together with the real house prices.

**Table 3.** Multiple regression analysis results

| MRA Value (TRY) | Resale Value (TRY) | Accuracy (%) |
|---|---|---|
| 219361,667 | 205000,000 | 92,994 |
| 294014,667 | 300000,000 | 98,004 |
| 410175,000 | 375000,000 | 90,620 |
| 286537,000 | 260000,000 | 89,793 |
| 380271,000 | 435000,000 | 87,418 |
| … | … | … |
| 331190,000 | 349000,000 | 94,896 |
| 437010,667 | 475000,000 | 92,002 |
| 426800,667 | 495000,000 | 86,222 |
| 295148,667 | 290000,000 | 98,224 |
| 267976,333 | 260000,000 | 96,932 |

### 3.2. Artificial Neural Networks Application

Normalized housing data are defined in Matlab software. The training of the network was carried out with 8 neurons using experimental data with the created feed forward artificial neural network.

The training process was repeated a few times to make the learning process more accurate. The maximum failure value was entered as 500, and the iteration amount was determined as 1000.

The accuracy and consistency values of the data were examined by looking at the regression chart after the training. The trained network is simulated with test data.

Housing values were determined by applying the maximum-minimum normalization reversed to the values obtained. Artificial neural network training regression is shown in Fig 3. The results are shown in Table 4.

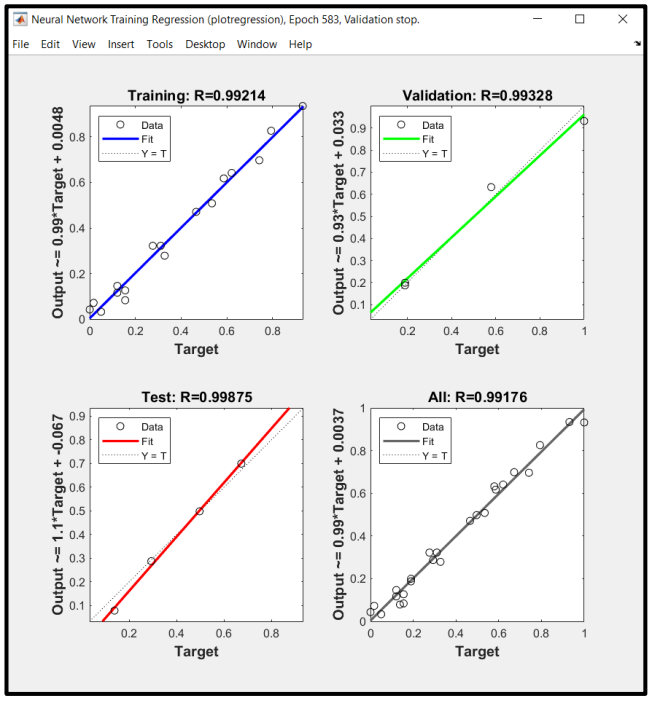


**Figure 3.** Artificial neural network training regression

**Table 4.** Artificial neural network results

| ANN Value (TRY) | Resale Value (TRY) | Accuracy (%) |
|---|---|---|
| 222862,080 | 205000,000 | 91,286 |
| 293771,863 | 300000,000 | 97,923 |
| 376021,579 | 375000,000 | 99,727 |
| 257108,193 | 260000,000 | 98,887 |
| 454902,955 | 435000,000 | 95,424 |
| … | … | … |
| 320026,201 | 349000,000 | 91,698 |
| 471619,035 | 475000,000 | 99,288 |
| 471124,399 | 495000,000 | 95,177 |
| 291098,107 | 290000,000 | 99,621 |
| 259925,188 | 260000,000 | 99,971 |

## 4. DISCUSSION

In the study, the values obtained in the house valuation model created using multiple regression analysis and artificial neural networks were compared with the real values of the houses and the accuracy values were determined. The houses used in the study were obtained from Samsun province Atakum district Yenimahalle neighborhood. In determining the residences, the ones facing the tramway street were chosen as the location.

The total accuracy value obtained in the multiple regression analysis was determined as 93.232%. The total accuracy value obtained in artificial neural networks was determined as 97.090%.

## 5. CONCLUSION

Considering the accuracy values obtained in the study, it is seen that the housing valuation model created with artificial neural networks gives a higher accuracy value. Multiple regression analysis is more suitable in terms of ease of application and understandability of the model. In artificial neural networks, there may be some results that vary with the change of the number of neurons and the selection of functions. The authors recommend the use of statistics and modern methods in frequent applications such as real estate appraisal.

## REFERENCES


Açlar, A., & Çağdaş, V. (2002). Taşınmaz (gayrimenkul) değerlemesi. *TMMOB Harita ve Kadastro Mühendisleri Odası, Ankara*.

Akış, B. (2013). *İstatistiki yöntemlerle değer belirleme ve değer haritası üretimi Selçuklu örneği.* Selçuk Üniversitesi Fen Bilimleri Enstitüsü.

Atik, M., KÖSE, Y., Yilmaz, B., & ERBAŞ, M. (2015). Şehirlerin İlerleme Yönlerinin Gayrimenkul Değerleri Üzerindeki Etkisinin Ölçülmesi. *Çankırı Karatekin Üniversitesi, 5*, 443-458.

Bre, F., Gimenez, J. M., & Fachinotti, V. D. (2018). Prediction of wind pressure coefficients on building surfaces using artificial neural networks. *Energy and Buildings, 158*, 1429-1441.

Brown, R. K. (1965). *Real estate economics: an introduction to urban land use*: Houghton Mifflin.

Canan, S. (2006). *Yapay sinir ağları ile GPS destekli navigasyon sistemi.* Selçuk Üniversitesi Fen Bilimleri Enstitüsü

Chatterjee, S., & Hadi, A. S. (2015). *Regression analysis by example*: John Wiley & Sons.

Graupe, D. (2013). *Principles of artificial neural networks* (Vol. 7): World Scientific.

Livingstone, D. J. (2008). *Artificial neural networks: methods and applications*: Springer.

Özdamar, N. (2004). 4822 Sayılı Yasa İle Değişik 4077 Sayılı Yasa'da Tanımlanan Konut Nedir. *Türkiye Barolar Birliği Dergisi, Yıl, 17*, 317-331.

Öztürk, K., & Şahin, M. E. (2018). Yapay Sinir Ağları ve Yapay Zekâ'ya Genel Bir Bakış. *Takvim-i Vekayî, 6*(2), 25-36.

Pagourtzi, E., Assimakopoulos, V., Hatzichristos, T., & French, N. (2003). Real estate appraisal: a review of valuation methods. *Journal of Property Investment & Finance*.

Ring, A. A., & Dasso, J. J. (1977). *Real estate principles and practices*: Prentice Hall.

Yegnanarayana, B. (2009). *Artificial neural networks*: PHI Learning Pvt. Ltd.

Yomralıoğlu, T., Nişancı, R., Çete, M., & Candaş, E. (2011). DÜNYA'DA VE TÜRKİYE'DE TAŞINMAZ DEĞERLEMESİ.

Zeng, T. Q., & Zhou, Q. (2001). Optimal spatial decision making using GIS: a prototype of a real estate geographical information system (REGIS). *International Journal of Geographical Information Science, 15*(4), 307-321.

Intercontinental Geoinformation Days

http://igd.mersin.edu.tr/2020/

# Four Dimensional Cadastre Design

**Tayfun Çay[1], Hasan Çevik[2]**

[1] *Konya Technical University, Faculty of Engineering and Natural Sciences, Geomatics Engineering Department, Konya, Turkey*
[2] *Burdur Mehmet Akif Ersoy University, Gölhisar Vocational School, Department of Architecture and Urban Planning, Burdur, Turkey*

**Keywords**
Cadastre
Time
Fourth Dimension
Rights
Restrictions

**ABSTRACT**

Due to the need to know the vertical positions of the objects such as electric cables, natural gas pipelines, rain water network, drinking water network, sewer line, energy transmission line under and above the real estate, three dimensional cadastral studies have come to the fore. In addition, since the cadastre has a dynamic structure and is a living phenomenon, changes in both geometric and legal terms can occur continuously on the property. For this reason, it will be important to be able to monitor the changes that occur at different times on the real estate instantly and continuously. In time, to be able to systematically record transactions such as development plan implementation, land consolidation, cadastral renewal work, expropriation, renunciation for road, subdivision, amalgamation, acquisition from road, land use conversion, distraint, mortgage, to be able to integration of the immovable into TAKBIS together with the objects under and above the property and in order to monitor all these processes in four dimensions, a fourth dimension, which we call time, is needed in the cadastre. Thus, changes occurring in the cadastre will can be monitored instantly in a four-dimensional environment.

## 1. INTRODUCTION

The relationship between human and soil has a very dynamic structure and human has a limited time to live. Besides the spatial aspect of the rights and restrictions of real estate, the fourth dimension, the temporal aspect, is an important aspect of cadastral registration. Rights, responsibilities and restrictions have a temporal element. One of the reasons for the need for four-dimensional cadastral information is that a date record is required for a particular property. Time always plays an important role in cadastral systems (Van Oosterom et al., 2006).

Temporal Land Registry and Cadastre data are heavily needed in our country. Land Registry and Cadastre data are constantly changing over time as a result of applications such as subdivision, development plan implementation, sales, donations, mortgages (Alkan & Cömert, 2005).

Temporal cadastral data is an important component for land management, public and private sectors and has a dynamic structure. Therefore, the land registry and cadastre system plays an important role together in a country (Alkan & Polat, 2017).

Land Registry and Cadastre Information System (TAKBİS) project, initiated by the General Directorate of Land Registry and Cadastre, constitutes one of the transaction steps of Cadastre-2014. In addition, since the cadastre is a living phenomenon, the importance of the time factor, which is the fourth dimension, increases (Çay et al., 2007).

Visualizing changes over time requires specific techniques in a geographic query tool (Van Oosterom, 1997). Advanced visualization techniques to show data based on space and time can apply as a time dimension in the future (Van Oosterom et al., 2002).

Geographical data are constantly changing over time. Therefore, the need to monitor, analyze and query the time-dependent changes of these data has brought the temporal geographical information system to the agenda (Alkan, 2005).

Four dimensional cadastral schema is given in Figure 1. The four-dimensional cadastre concept is formed by adding the time dimension to the third

* **Corresponding Author**
(tcay@ktun.edu.tr) ORCID ID 0000-0002-4661-5583
(hcevik@mehmetakif.edu.tr) ORCID ID 0000-0001-6359-3251

**Cite this study**
Çay T & Çevik H (2020). Four Dimensional Cadastre Design. Intercontinental Geoinformation Days (IGD), 100-103, Mersin, Turkey

dimension. In other words, there is no fourth dimension without a three-dimensional cadastre.

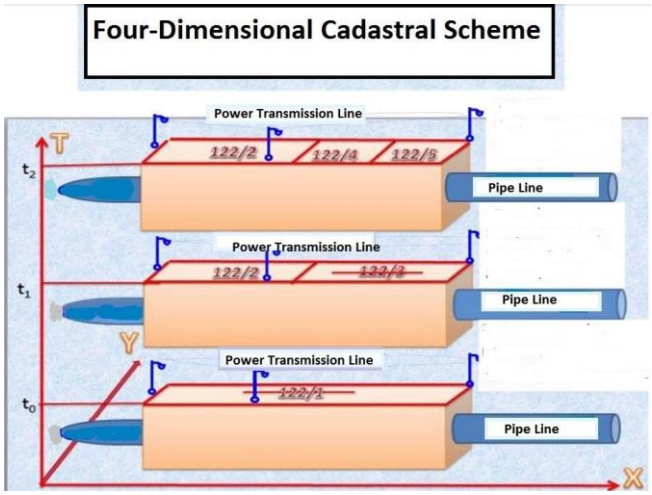


**Figure 1**. Four Dimensional Cadastre Schema

The importance and necessity of three- and four-dimensional cadastre in international platforms are carried out by FIG and emphasized in the 2014 and 2034 cadastral visions (Sürmeneli et al., 2018).

In the 3rd article of the Cadastre 2034 vision, the concept of "3D and 4D (3D + Time) Cadastre for land modeling, management, integration of property data and sustainability analysis" is discussed. In other words, the "Four Dimensional Cadastre" study takes its place among the targets of 2034.

In the 4th article of the Cadastre 2034 vision, the concept of "continuous updating of cadastral data and instant access to cadastral information" is also discussed. Here, the expression of instant updating of cadastral data means the fourth dimension of cadastre, the concept of time.

In our country, Land Registry and Cadastre Information System by the Land Registry and Cadastre General Directorate (TAKBIS), Land Registry Archive Information System (TARBİS), Spatial Property System (MEGSİS), Turkey's National Geographical Information System (TUCBS), Map Data Bank (HBB) and TUSAGA-ACTIVE Since the projects have been completed, an important step has been taken in reaching the 2034 vision of Cadastre (Döner & Bıyık, 2013).

TAKBİS 2020 vision studies are carried out in order to eliminate the deficiencies in TAKBİS. Thanks to this vision, data quality will be improved, temporal changes of spatial data will be monitored and a data infrastructure suitable for multidimensional cadastre will be established (Dursun et al., 2019).

In this study, four-dimensional cadastral design will be focused on as of today. Suggestions will be developed to eliminate the traditional problems of the cadastre and to enrich its content. In this study, with the vision of Cadastre 2014, the changes in the field of cadastre in the world and in our country will be examined, the missing situations will be determined and the necessary work to be done to reach the Cadastre 2034 vision will be discussed together with the four-dimensional cadastre.

The aim of this study is to create a system that will allow the changes in land registry and cadastre to be monitored instantly in four dimensions, together with the time dimension.

## 2. METHOD

In this study, the city map of the study area, parceling plan, science folders, land registers, implementary development plans, spatial data of illegal and licensed buildings, orthophoto map, drinking water, rain water, sewage and natural gas line network constitute the material part of the study.

The method used in this study; It is the four-dimensional modeling of the land by instantly and continuously entering the geometric and legal changes occurring in the study area into the database.

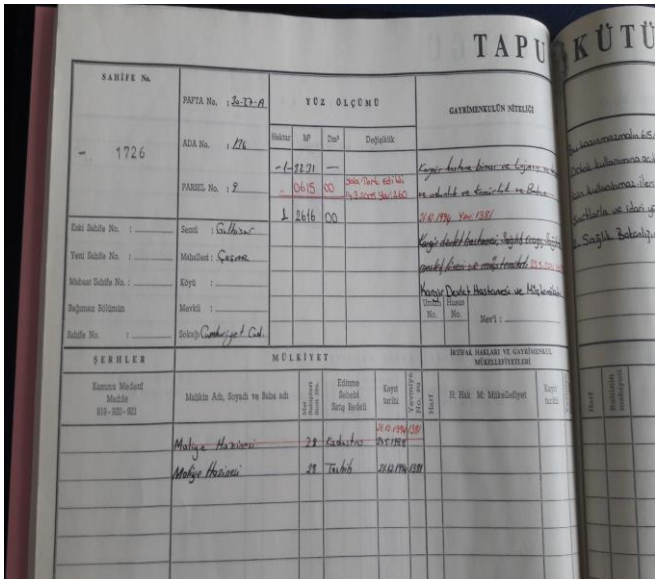


**Figure 2.** Land Registry of Immovables

An example of a land registry belonging to immovables show in Figure 2. In this study it is aimed to enter the information in the land registry records of the immovables that are within the scope of the study area, since the first facility cadastre, to the database and to monitor the changes that occur in the immovable properties instantly. Thus, the registration date and journal numbers of the changes occurring in the immovables, the rights and restrictions on the immovables will be monitored in four dimensions.

In Figure 3, the fourth dimension of the cadastre, the concept of time, is shown by entering the changes in the land registry chronologically into the database.

In Figure 4, the buildings forming the third dimension of the cadastre, objects such as natural gas, rain water, drinking water, sewage and energy transmission line located on or under the parcels will be combined with the time concept which is the fourth dimension of the cadastre. So a four dimensional cadastral design will be obtained.

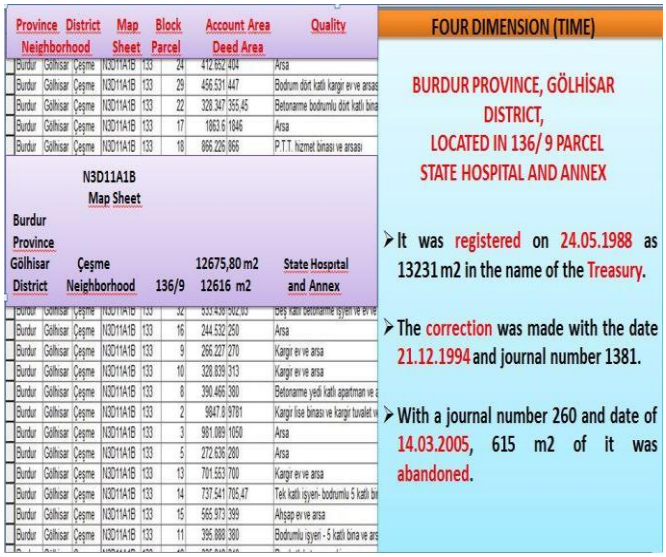


**Figure 3.** The concept of the fourth dimension

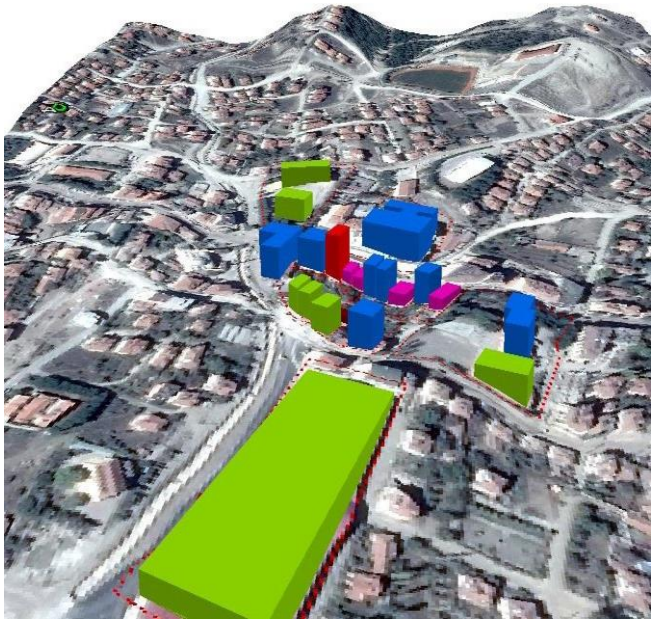

**Figure 4.** Three Dimensional View of Buildings

## 3. RESULTS

In Figure 4, the buildings are colored according to the number of floors. In addition to coloring according to the number of floors, it is possible to make classifications according to the license status, age and qualifications of the buildings. In this system, by adding new columns to the database, it can be shown what kind of changes the parcels in the study area are exposed to over time. By showing the processes such as development plan implementation, subdivision, amalgamation, renunciation for road, land use conversion, acqisition from road, expropriation, land consolidation in chronological order, the cadastre will gain a fourth dimension.

## 4. DISCUSSION

Public institutions and organizations that need to temporal data of immovable property in Turkey is shown in Figure 5. With the addition of the fourth dimension, the concept of time, to the cadastre, all documents related to the real estate will be recorded in four dimensions in digital environment, so document loss will be prevented to a great extent with duplicate processing. For example, in relation to a development plan implementation process made in the past, information such as when the implementation was registered, which municipal committee decisions were taken on which date, when the subdivision was arranged in which parcels, and which foot note were placed may be needed by public institutions and organizations. At the same time, the energy transmission lines on the parcel and the three-dimensional coordinates of the underground sewage, drinking water, rain water and natural gas networks may be needed.

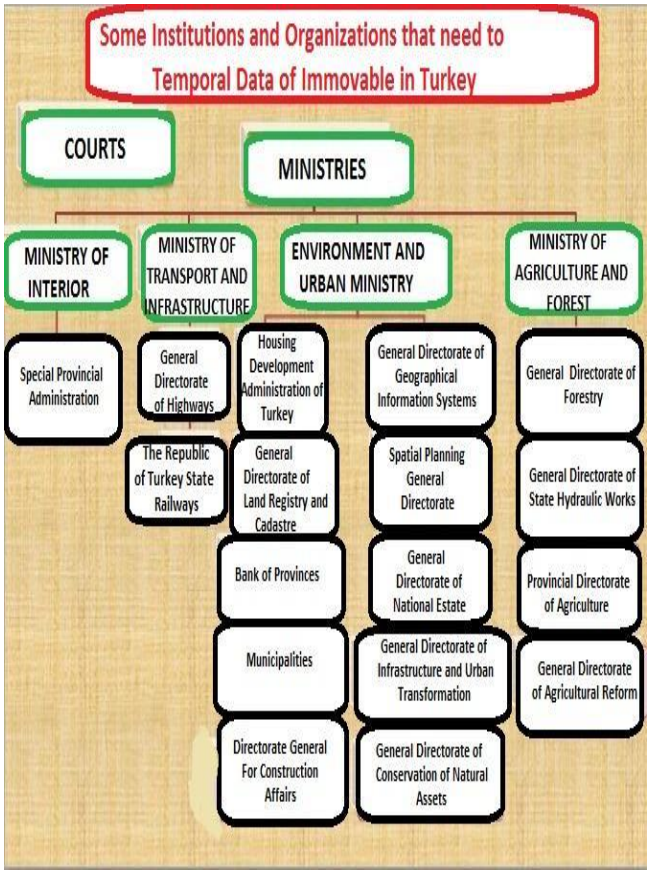


**Figure 5**. The institutions which need to temporal data in Turkey

## 5. CONCLUSION

After the parcels are processed on the three-dimensional digital land model, with the addition of buildings on it, all kinds of query and analysis operations will be made possible with the attribute information in the database.

Since time dimension will be used in four-dimensional cadastral studies, advanced technological devices will be needed. Three-dimensional photographs of the work area should be taken with high-resolution aerial cameras at certain periods and changes that occur over time should be easily monitored. Three-dimensional photographs taken with these high

resolution cameras should be analyzed with a quality software program designed for this purpose.

**ACKNOWLEDGEMENT**

I would like to thank Burdur LİHKAB director Murat MİNNETOĞLU and Gölhisar Land Registry Manager Yaşar POLAT for their assistance in collecting data in this study.

**REFERENCES**

Alkan, M. (2005). Temporal Geographic Information System Design for Land Registry and Cadastre Data. PhD Thesis, Karadeniz Technical University Institute of Science and Technology, Trabzon (in Turkish).

Alkan, M., & Cömert, Ç. (2005). The Need for Temporal Analysis of Land Registry and Cadastre Data. Paper presented at the Union of Chambers of Turkish Engineers and Architects Chamber of Survey and Cadastre Engineers 10. Turkey Scientific and Technical Conference, Ankara (in Türkish).

Alkan, M., & Polat, Z. A. (2017). Design and Determine the Spatio-Temporal Cadastral Data Infrastructure for LADM. Paper presented at the FIG Working Week 2017 Surveying the world of tomorrow - From digitalisation to augmented reality, Helsinki, Finland.

Çay, T., Erdi, A., Özkan, G., İnam, Ş., Durduran, S. S., Yalpır, Ş., & İşcan, F. (2007). An investigation on Integration of Turkish Cadastre to "Cadastre 2014 Vision". Chamber of Surveying and Cadastre Engineers Geodesy Geoinformation and Land Management Journal, 2(97), 40-46 (in Turkish).

Döner, F., & Bıyık, C. (2013). Conformity of LADM for modeling 3D-4D cadastre situations in Turkey. Paper presented at the 5th Land Administration Domain Model Workshop, Kuala Lumpur, Malaysia.

Dursun, İ., Aslan, M., & Sarıyüz, F. (2019). Land Registry and Cadastre Information System 2020 Project within the Scope of the Land Administration Domain Model. Paper presented at the Association of Turkish Engineers and Architects 6th Geographical Information Systems Congress, Ankara (in Turkish).

Sürmeneli, H. G., Polat, Z. A., & Alkan, M. (2018). How to be Created a New Terminology for 3- and 4-Dimensional Cadastre In Turkey. Paper presented at the FIG Congress 2018 Embracing our smart world where the continents connect: enhancing the geospatial maturity of societies Istanbul, Turkey.

Van Oosterom, P. (1997). Maintaining consistent topology including historical data in a large spatial database. Paper presented at the Auto-Carto, Apeldoorn, Netherlands.

Van Oosterom, P., Maessen, B., & Quak, W. (2002). Generic query tool for spatio-temporal data. International journal of geographical information science, 16(8), 713-748.

Van Oosterom, P., Ploeger, H., Stoter, J., Thompson, R., & Lemmen, C. (2006). Aspects of a 4D Cadastre: A First Exploration. Paper presented at the Shaping the Change XXIII FIG Congress Munich, Germany.

Intercontinental Geoinformation Days

http://igd.mersin.edu.tr/2020/

# Professional merit and ethics in choosing the development plan implementation method

**Şaban İnam*[1], Halil Burak Akdeniz[1]**

[1]*Konya Technical University, Engineering and Natural Sciences Faculty, Geomatics Engineering Department, Konya, Turkey*

**Keywords**
Professional merit
Method selection in development plan implementation
Overriding public interest
Development plan implementation

**ABSTRACT**

Development plan implementations in Turkey, can be made by three different methods according to the development regulation. The responsible administration for implementation has authority to subject of which method should be preferred/chosen under which conditions. In this sense, the administration should evaluate the content of the implementation from technical, legal, sociological and economic issues and should decide within the principles of professional merit and professional ethics. The implementation of development plans with public interest should also be in the public interest. In the present case, the decision to choose the most appropriate method within professional merit will also serve the overriding public interest. Therefore, the department that makes the decision on behalf of the responsible administration should conduct in professional and administrative merit. In this study, points to take into consideration that choice of method of the administration responsible for implementation of plan in Turkey will be investigated with a sample implementation. The subject of which method should choose under which conditions will be clarified by considering the legal regulations, professional merit and ethical principles.

## 1. INTRODUCTION

The development plans are prepared to protect and develop physical-natural-historical-cultural values in urban areas, to ensure the balance of protection and use, to support sustainable development at the country-region-city scale, and to create healthy and safe environments. Municipalities are obliged to implement development plan within boundaries of settlement and special provincial administrations are obliged to implement development plan outside boundaries of settlement. The implementation of the development plans is as important issue as the plan design. The aims of planning can only be achieved with an economic and social application (Yıldız 2020). Within this period, the relevant responsible administration decides which method should be applied under which conditions. The development plans can be applied in three different methods according to Turkish development regulations. İnam 1989; Uzun 1992; Akçeşme 2006; Çelik 2006; Yıldız 2020).

**a-)** The development plan implementation in the expropriation method: It is the process of "transferring to public ownership by purchasing real estates belonging to private ownership corresponding to technical infrastructure, public space and official institutions in the development plan for public interest". Technically, it does not reflect the plan integrity to the place, since only the place that will be needed by the public authorities are included in the plan implementation. While this method application often offends the property right of the real estate owner, it also creates an economic burden on the administration due to the payment of the price.

**b-)** The development plan implementation in the applications on demand of owners: This method is made upon the request of the property owner to the responsible administration. The plan is applied to ground piecewise, depending on the ownership-zoning relationship of the parcel. Since the plan is not implemented as a whole, public spaces cannot be consist of on time and in place. Increase in value and benefit-cost relationship that will occur with the implementation of the plan can't be allocated equally to the real estates in that area.

**c-)** The development plan implementation in the land readjustment method: This method is applied on area where implementation areas and boundaries are determined by the responsible administration for the implementation of the development plan. The

* **Corresponding Author**

*(sinam@ktun.edu.tr) ORCID ID 0000 – 0002 – 9101 – 6109
(hbakdeniz@ktun.edu.tr) ORCID ID 0000 – 0002 – 9504 – 051X

**Cite this study**

İnam S & Akdeniz H B (2020). Professional merit and ethics in choosing the development plan implementation method. Intercontinental Geoinformation Days (IGD), 104-107, Mersin, Turkey

implementation areas can't be smaller than one urban block. However, if urban lots are created on some part of the block, then the remaining part of the block can be subject to another land readjustment project as well. With this method, same amount of contribution ratio (up to 45%) is taken from all land owners in proportion to the size of their parcels for create public spaces and government agency areas in the implementation area. In this sense, while the development plan is applied to the ground as a whole, the places needed by the public are provided in the most economical way. Increase in value and benefit-cost relationship that will occur with the implementation of the plan can be allocated approximately equally ratio to the real estates in that area with implementation partnership share ratio (DOPO). In this sense, plan implementation in the land readjustment method is a technical, economic and fair a method. Land readjustment is the most effective and efficient plan implementation method, since the structures that shape the urban morphology and the public space correlated with it are handled with in a mechanical understanding.

In this sense, method selection in the development plan implementations is important and it should be evaluated in terms of overriding public interest and public finance within the principles of professional merit.

## 2. METHOD

In this study, development plan implementation in the expropriation method in Konya province, Karatay district, Hacıbali neighborhood will be evaluated within the professional merit and ethical principles. When a different development plan method is applied in the same implementation area, its effect on public interest and public finance will be discussed.

### 2.1. The Importance of Method Selection in Development Plan Implementations in terms of Public Interest and Public Finance

The municipalities should establish realistic and stable public policies regarding spatial planning and implementation of plans in urban areas. Municipalities have a duty to ensure sustainable urbanization and living standards, so they should create public spaces and stock of urban lot ready to be built, and also should provide management and organization functions within budget balances. The municipal administration is obliged to implement the development plans in order to ensure regular urbanization in the city and cater the housing-industry-trade area needs of the city. However, while the municipality is doing this implementation; it should choose a method that protects the property rights secured by article 35 of the Constitution of the Republic of Turkey, protects the public interest, is technically compatible with the development legislation and is economically and sociologically ergonomic. The development legislation in force has legally allowed these plans to be implemented in the "expropriation" method, the "applications on demand of owners" method and the "land readjustment" method. However, the legislation confer the responsibilities to the municipal administration for "which method should be used under which conditions". The municipal administration should choose the method within the ethics and merit of the institution and should consider the public interest and public finance under all conditions.

The municipal administration should carry out the evaluation in the principle of "public interest" and "wise use of public finance" when it make a choice in the implementation method of the development plan. Public interest is defined as, "the state or the services of public institutions representing the state and a criterion that is a public activity and shows the compliance of the transaction with public law". The wise use of public finance is defined as "the prediction of the most efficient and effective use of public funding". The concept of public interest ground on the wise use of public finance. When this approach is evaluated for the expropriation method which is the implementation alternative on the sample parcel; a part of the development plan (road and park area) which has decision of public interest has been think fitted to put into practice for purpose of "opening to public use" but "if the implementation was made in the method of land readjustment, these areas could have been created with free deductions at equal rates with the implementation partnership share (DOP) "and thus expropriation price payment would not be made from public finances by the administration. In this sense, the preference of "plan implementation in expropriation method" made by the municipal administration is not the right choice for the 'rationalistic and controlled' use of public finance. Because, unnecessary damage to public finance will be caused as much as the expropriation value.

### 2.2. Technical Evaluation of Method Selection in Development Plan Implementations

When the development plan implementation in the expropriation method are examined, it was seen that generally legal and social dimensions of expropriation are considered; the aim expected from the implementation of the plan was achieved in technical studies; however, as a result of the partial expropriation of the parcel, it has been observed that the remaining part can't be prevented from becoming inefficient in terms of shape, size and use of property. For this reason, it would be appropriate to consider the implementation of the development plan in the expropriation method 'as a method preferred by the municipality administration in special and necessary cases' rather than being an alternative method (Sadıç and Arabacı 2013; İnam et al. 2015; Danışman and İnam 2018).

The applications on demand of owners are a partial implementation made on the basis of parcel and the plan integrity will not reflect in the place. This will be against the essence of planning. Moreover, the municipal administration must not allow the implementation of the development plan in this method for the "cadastral parcel that has not been subject to a plan implementation before" according to Uniform Land Development Regulations in Planned Areas in force. However, this method will be used as a "secondary development

implementation" where the development plan has been renewed.

The plan implementation in the land readjustment method is made on the implementation area created at least the size of a urban block. In this method, the purpose of planning will be achieved, as public spaces and urban lots which suitable housing, are applied to on the ground. In addition, it is technically the most suitable method, as "equal rate of DOP" will be made from all parcels that are implemented to provide public spaces.

### 2.3. Sociological and Economic Evaluation of Method Selection in Development Plan Implementation

As a result of the development plan implementation in the expropriation method, while property use status of neighboring parcels and value of their real estates improve, persons whose real estate has been seized in accordance with the public interest generally express to be wronged after implementation. The same persons express that they are detached from the psychology of possession of their real estate and have a sociological adaptation problem in new addresses and they say that if there is a public interest in the implementation of the plan, benefit-loss balance between the parcel owners should preserve and allocate equally. These reactions have been main problem of the plan implementation in the expropriation method. For this reason, such economic and sociological problems that occur plan implementation in the expropriation method should be solved by the capable municipal administrators with "choosing the most appropriate method" or "public policies" (Danışman and İnam 2018).

The development plan implementation in the applications on demand of owners is the whole of 'leave some parts of the road - get some parts of areas from road' procedures made in order to "make suitable the parcel according to the development plan". In this process, the "implementation partnership area ratio and the use of their property" will be different specific to relationship of each parcel with the development plan. Therefore there is more individual benefit and the satisfaction of the owner than public interest in this method.

The plan implementation in the land readjustment method, if it is carried out by technical personnel who take into account merit and ethical principles, it will the most economical method in which social justice and equity are protected. Likewise, on the one hand, the plan will apply to the ground and will open to social use, on the other hand, existing property problems will resolve. If the parcel owners satisfy from the implementation outcomes, it will increase social peace and sense of trust in the state.

## 3. RESULTS

### 3.1. Evaluation of Method Selection in Development Plan Implementation: An Example of Implementation

When the sample parcel subject to implementation associate with the development plan, it is seen that the parcel coincides the 'road' and 'park' areas and cannot be used for 'construction purposes' in its existing state (Figure 1). However, when this situation for the sample parcel evaluate in the integrity of the development plan; it is not enough to open something up for discussion accuracy and objectivity of planning, appropriateness of public interest for plan. In this sense, the municipal administration;

- Since whole of the sample parcel coincides the public area which use for road and park purposes, the municipal administration may choose legally 'development plan implementation in the expropriation method' within the scope of the Expropriation Law No.2942 and the decision of the municipal board. However, it will be wronged to choose this method by the administration. Because both the parcel owner will be wronged and the public finance will be damaged due to the "payment of expropriation fee even though it is not compulsory / necessary" by the administration. In this case, the administration's choice to make "while there is an alternative to implementing in the land readjustment method, apply development plan implementation in the expropriation method", while it is considered legally "achievable" and technically "applicable", it will be "wrong choice" in terms of merit - public interest - public finance.

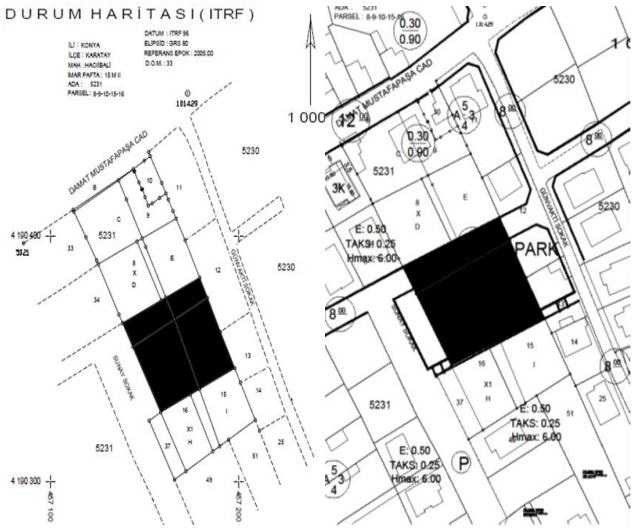


**Figure 1.** The relationship of the parcel with the development plan in the example implementation.

- Since the whole of the sample parcel coincides the public space, it will not be able to use the method of application on demand within the scope of Articles 15 and 16 of the Land Development Law No. 3194. Besides, if the sample parcel had coincided 'partly the urban block and partly the public space' in the development plan, the application on demand of owners method would not have used according to Uniform Land Development Regulations in Planned Areas (articles 5/12 and 7/1) in force due to a cadastral parcel which unperformed plan implementation.
- It will be best choice to decide on "development plan implementation in the land readjustment method" within the scope of the 18th article of the Land Development Law No. 3194 by determining implementation area where the sample parcel will also be located. Because in the this method implementation,

government agency areas and the public spaces will be occurred by free deductions up to %45 and in equal proportion from the parcels in the arrangement. Parcel owners will benefit from the increase in value arising from the implementation of the plan and the benefit-loss balance will be provided to occur with "distributing to all participating parcel in the implementation area".

## 4. DISCUSSION AND CONCLUSION

One of the most important of the ethical problems that arise due to the implementation of laws related to urban development and land use is "the neglect of the public interest at individual and institutional level". One of the fundamental responsibilities of the municipal administration is to know 'what should be done as well as what should not be done' (Kılınç et al. 2009). In terms of urban sustainability, social equality and environment / institution / individual ethics, there are inadequacies in both the development legislation and the supervision of implementation.

The method which prefer in the implementation of the development plan should not be determined according to the choice of the municipal administration. This case should determine according to the "most appropriate / rationalistic solution" that will arise as a result of the evaluation of multiple factors such as the property-zoning relationship of the parcel to be applied, development plan notes, expectations from the plan implementation, plan implementation principles, public interest public finance.

## REFERENCES

Akçeşme H (2006). The instruments used in implementation of ground plans and transfer of the urban annuity cost to the public – application of article 18. MSc Thesis, Gazi University, Ankara (in Turkish).

Çelik K (2006). Planlama ve İmar Kanunu uygulaması, arazi ve arsa düzenlemesi. Devran Matbaacılık, 9944-5113-0-7.

Danışman A İ & İnam Ş (2018). İmar planı uygulama yöntemlerinin teknik, ekonomik ve sosyolojik unsurlar içerisinde karşılaştırması. Phd Seminar, Selçuk University, Konya (in Turkish).

İnam Ş (1989). Arsa ve arazi düzenlemesi ve 3194 sayılı İmar Kanununun 18. maddesi uygulamaları. Phd Thesis, Selçuk University, Konya (in Turkish).

İnam Ş, Çay T & İşcan F (2015). Planlama ve İmar Kanunu tasarısının uygulanabilirliğinin araştırılması. S.Ü. Teknik Bilimler Meslek Yüksekokulu, Teknik-Online Dergisi, 14(1), 12-14.

Kılınç G, Özgür H & Genç F N (2009). Yerel yönetimlerde imar uygulamaları ve etik. Türkiye'de yolsuzluğun önlenmesi için etik projesi, TC Başbakanlık Kamu Görevlileri Etik Kurulu, Ankara.

Sadıç Ö & Arabacı C (2013). İmar planı uygulamalarında uygulama yöntemleri ve yaşanan sorunlar. 1. Uluslararası Kentsel Dönüşüm Sempozyumu, 1-24, Ankara, Turkey.

T.C. Resmi Gazete. 3194 sayılı İmar Kanunu, (18749), 03.05.1985.

T.C. Resmi Gazete. 5393 sayılı Belediye Kanunu, (25874), 13.07.2005.

T.C. Resmi Gazete. Planlı Alanlar İmar Yönetmeliği, (30113), 03.07.2017.

T.C. Resmi Gazete. Arazi ve Arsa Düzenlemesi Hakkında Yönetmelik, (31047), 22.02.2020.

Uzun B (1992). Kentsel arsa düzenlemelerinde imar parseli üretme yöntemleri ve sonuçlarının irdelenmesi. PhD Thesis, KTÜ, Trabzon (in Turkish).

Yıldız F (2020) İmar bilgisi, planlama – uygulama – mevzuat. Nobel Yayınevi, 978-605-5426-04-0.

## Photogrammetry and Remote Sensing – 2

**An investigation of supervised LCLU classification performance over UAV based orthophoto**

*Nizar Polat, Yunus Kaya**

**Data Fusion of Unmanned Aerial Vehicle (UAV)-Based Photogrammetry and Close-Range Photogrammetry in Historical Sites Monitoring**

*İrem Yakar*, Seda Nur Gamze Hamal, İldeniz Leyla Öztürk, Mehmet Özgür Çelik, Serdar Bilgi*

**Ecological Appraisal of Urban Heat Island in Zaria, Nigeria**

*Ebenezer Akomolafe*, Olalekan Isioye, Wilson Labija*

**Road Surface Extraction from MLS-Based Point Clouds**

*Mustafa Zeybek*, Serkan Biçici*

**Spatial Accuracy Analysis of Sentinel-1 SAR Satellite Images by Comparing Maps**

*Tevfik Fikret Horzum*, Nusret Demir, Ali Kılçık*

**Comparison of NDT and ICP Method's Point Cloud Registration Performance**

*Ramazan Alper Kuçak*, Mahmut Oğuz Selbesoğlu, Serdar Erol*

Intercontinental Geoinformation Days

http://igd.mersin.edu.tr/2020/

# An investigation of supervised LCLU classification performance over UAV based orthophoto

**Nizar Polat**[1], **Yunus Kaya***[1]

[1]*Harran University, Faculty of Engineering, Department of Geomatics Engineering, Sanliurfa, Turkey*

**Keywords**
Photogrammetry
Land cover land use
Supervised classification
Unmanned Aerial Vehicles

**ABSTRACT**

Nowadays, the development of digital image processing techniques has contributed to the determination of land cover land use (LCLU) through digital images. In this study, a supervised classification has been made over an orthophoto of an area in Harran University Osmanbey Campus. The purpose of the study is to examine the performance of the three popular supervised classification techniques that are Maximum Likelihood, Minimum Distance, and Mahalanobis Distance methods. In the study, a confusion matrix was produced, and overall accuracy and overall kappa were calculated with manually generated ground truth data. According to results, the highest overall accuracy was calculated for Maximum likelihood classification with a rate of 84.5 % and the Minimum Distance method has the lowest overall accuracy (43%). The research shows that due to the lack of spectral information the supervised classification methods shows omission and commission errors. This fact has a direct effect on overall accuracy calculation.

## 1. INTRODUCTION

Determination of LCLU, the spatial distribution of land, and their determination at the local and regional scales are important for monitoring changes (Gholami et al. 2010). Due to the easy data collection process with photogrammetry and remote sensing methods, images that covering large areas are obtained in a short time (El-Alahmadi and Hames 2009). Although remote sensing images provide information about very large areas, their spatial resolution is relatively low. Unmanned Aerial Vehicles (UAV), which have been used in many areas recently (Ulvi et al. 2020; Kaya and Polat 2019; Yiğit and Uysal 2019), can also be used to classify areas in the region. Compared to satellite images, UAVs that view smaller areas have a much higher spatial resolution. It is more advantageous to use UAV images especially in settlements where the spatial distribution changes frequently. Due to the small pixel dimensions, the UAV images better reflect the characteristics of the study area. Classification methods should be used to obtain meaningful results from these images. Supervised classification methods include Maximum Likelihood (Strahler 1980; Foody et al. 1992; Otukei and Blaschke 2010), Minimum Distance (Kranz 1993; Srivastava 2006), and Mahalanobis Distance (Moraes et al. 2002; Gemperline and Boyer 1995; Mei et al. 2016; Galeano et al. 2015) methods are frequently used in the literature. Kavzaoğlu and Colkesen (2010) used the maximum likelihood and decision trees method to classify the 2009 dated Landsat ETM+ image. Ahmed et al. (2015) revealed that the Maximum Likelihood method is better than the Mahalanobis Distance method for classifying tobacco areas in Pakistan. Yang and Everitt (2010), used supervised classification methods to map the broom gentian infestation. In this study, the success of three different classification methods proposed to distinguish the buildings in the campus area from each other was examined.

## 2. METHOD

### 2.1. Study Area

Harran University Osmanbey Campus has been chosen as the study area. The study area covers an area of approximately 650m x 450m (Fig. 1). The UAV flight plan and other parameters are not covered by this study, but It can be said that the orthophoto of the study area has only red green and blue bands and generated with a 25 cm spatial resolution.

* **Corresponding Author**

(nizarpolat@harran.edu.tr) ORCID ID 0000-0002-6061-7796
*(yunuskaya@harran.edu.tr) ORCID ID 0000-0003-2319-4998

**Cite this study**

Polat N & Kaya Y (2020). An investigation of supervised LCLU classification performance over UAV based orthophoto. Intercontinental Geoinformation Days (IGD), 108-111, Mersin, Turkey


**Figure 1.** Study area

### 2.2. Maximum Likelihood Classification

The Maximum Likelihood Classification technique is the most widely used technique in the literature (Paola 1994, Paola and Schowengerdt 1995; Erbek et al. 2003; Richards and Richards 1999). Suppose we have two different classes, 'i' and 'j'. If the probability of a pixel in 'X' position belonging to class i is higher than that of class j, the pixel is assigned to class i, vice versa (Ahmed et al., 2015). The input data is considered to have a normal distribution pattern and the discriminator for the MLC model is defined as:

$$g_i(x) = ln\ ln\ p(w_i) - \frac{1}{2} ln|C_i| - \frac{1}{2}(x - m_i)^t C_i^{-1}(x - m_i) \quad (1)$$

Where $g_i(x)$= *i*th class discriminant function
$p(w_i)$= Probability that class ωi has occurred
$|C_i|$= Determinant of class i's covariance matrix
x= A pixel's n-dimensional matrix of DN values (where n is the total number of bands)
$m_i$= Mean vector
t = transpose of the base matrix

### 2.3. Mahalanobis Distance Classification

The Mahalanobis Distance statistic is a measure of distance that takes into account correlation in the data using the precision matrix (Villaseñor 2019). The Mahalanobis distance is used for spectral matching, to detect outliers during calibration or prediction, or to detect extrapolation of the model during analyzes (Mark and Workman 2010). To be able to compute the MD, first, the variance-covariance matrix C is constructed:

$$C_x = \frac{1}{(n-1)}(X_c)^T(X_c) \quad (2)$$

where ***X*** is the data matrix containing n objects in the rows measured for p variables. X is the column-centered data matrix (Maesschalck et al. 2000). In the case of two variables, $x_1$ and $x_2$, the variance–covariance matrix. Mahalanobis Distance is defined as:

$$MD_i = \sqrt{(x_i - \underline{x})C_x^{-1}(x_i - \underline{x})^T} \quad (3)$$

### 2.4. Minimum Distance Classification

Minimum Distance Classification is a simple supervised classification method that uses the center point to represent a specific class in the training set. Euclidean distance between pixel values and the center of gravity is considered when determining the class. The pixel with the shortest distance from the class is assigned to that class (Sathya and Deepa 2017). Minimum Distance is defined as:

$$dist. = \sqrt{(Dv - Mt)^2} \quad (4)$$

where Dv is: Digital value of each pixel
mt is mean value of each class

## 3. APPLICATION and RESULTS

The orthophoto of the field was used as input data in the study. Supervised classification was made with all three classification methods over orthophoto. The orthophoto of the study area and the results of the classification methods are shown in Figure 2.

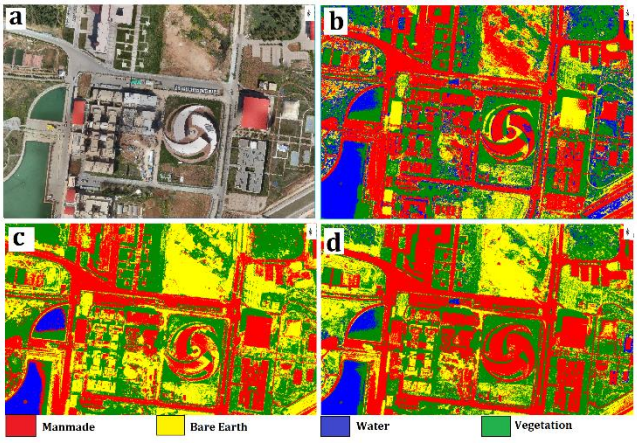


**Figure 2.** Orthophoto (a) and results of minimum distance classification (b), maximum likelihood classification (c), and mahalanobis distance classification (d).

Tables 1 summarize the accuracy assessment results for the three classification maps generated from orthophoto.

**Table 1.** Accuracy assessment results for the three classification methods

| | Classification Method | | | | | |
|---|---|---|---|---|---|---|
| | Minimum distance | | Maximum likelihood | | Mahalanobis distance | |
| | PA (%) | UA (%) | PA (%) | UA (%) | PA (%) | UA (%) |
| water | 1.14 | 6.40 | 8.66 | 100.00 | 0.28 | 10.81 |
| bare earth | 13.39 | 54.39 | 99.41 | 91.50 | 97.51 | 93.56 |
| vegetation | 86.97 | 33.69 | 98.09 | 45.51 | 88.30 | 34.16 |
| manmade | 78.70 | 44.76 | 81.93 | 92.95 | 86.09 | 99.92 |
| Overall Accuracy (%) | 43.0 | | 84.5 | | 83.72 | |
| Overall Kappa | 0.15 | | 0.76 | | 0.75 | |

PA = producer's accuracy; UA = user's accuracy

Table 1 shows that all three methods give unsuccessful results in detecting water areas. When the field research was done, it was understood that the reason for this was the pollution in the water. This pollution may affect the classification. Also, since the lakes are artificial, the shores are shallower. This can create different classification with deep water. While Maximum Likelihood and Mahalanobis Distance achieved high success in the detection of bare earth areas, the minimum distance method produced low accuracy. All three methods are successful in separating vegetation areas that are in the open areas. However, some shady regions are also classified as vegetation areas in three method.

## Conclusion

UAV systems quickly found a place in many areas of life thanks to the advantages they provide. In this study, the classification of the study area was made using the orthophoto produced from the aerial images obtained by the UAV. Three different classification methods, which are mostly used in the classification of satellite images, were applied in a supervised approach. Then the generated classified images were compared with manually obtained ground truth values. As a result, the highest overall accuracy calculated for the Maximum likelihood method with 84.5%. Since the data resolution is high, it is thought that the classification accuracy can be further increased by increasing the number of signatures and classes.

## REFERENCES


Ahmed A, Muaz M, Ali M, Yasir M, Ullah S & Khan S (2015). Mahalanobis distance and maximum likelihood-based classification for identifying tobacco in Pakistan. 7th International Conference on Recent Advances in Space Technologies (RAST), 255-260.

Al-Ahmadi F S & Hames A S (2009). Comparison of four classification methods to extract land use and land cover from raw satellite images for some remote arid areas, Kingdom of Saudi Arabia. Earth, 20(1), 167-191.

De Maesschalck R, Jouan-Rimbaud D & Massart D L (2000). The mahalanobis distance. Chemometrics and intelligent laboratory systems, 50(1), 1-18.

Erbek F S, Özkan C & Taberner M (2003). Comparison of maximum likelihood classification method with supervised artificial neural network algorithms for land use activities. International Journal of Remote Sensing, 25, 1733-1748.

Foody G M, Campbell N A, Trodd N M & Wood T F (1992). Derivation and applications of probabilistic measures of class membership from the maximum-likelihood classification. Photogrammetric engineering and remote sensing, 58(9), 1335-1341.

Galeano P, Joseph E & Lillo R E (2015). The Mahalanobis distance for functional data with applications to classification. Technometrics, 57(2), 281-291.

Gemperline P J & Boyer N R (1995). Classification of near-infrared spectra using wavelength distances: comparison to the Mahalanobis distance and residual variance methods. Analytical Chemistry, 67(1), 160-166.

Gholami A, Esfadiari M & Masihabadi M H (2010). The Survey and the Comparison of Maximum Likelihood, Mahalanobis Distance and Minimum Distance Methods in Preparing Landuse Map in the Western Part of Isfahan Province. International Journal of Geological and Environmental Engineering, 4(4), 118-121.

Kavzoğlu T & Çölkesen İ (2010). Karar Ağaçları ile Uydu Görüntülerinin Sınıflandırılması: Kocaeli Örneği Electronic Journal of Map Technologies, 2(1), 447-454.

Kaya Y & Polat N (2019). Buılding Modeling by UAV Images. 1. International Conference of Virtual Reality, 113-117, Şanlıurfa, Turkey.

Kranz H G (1993). Diagnosis of partial discharge signals using neural networks and minimum distance classification. IEEE transactions on electrical insulation, 28(6), 1016-1024.

Mark H & Workman J (2010). Chemometrics in spectroscopy. Elsevier.

Mei J, Liu M, Wang Y F & Gao H (2015). Learning a mahalanobis distance-based dynamic time warping measure for multivariate time series classification. IEEE transactions on Cybernetics, 46(6), 1363-1374.

Moraes J C T B, Seixas M O, Vilani F N & Costa E V (2002). A real time QRS complex classification method using Mahalanobis distance. In Computers in Cardiology, 201-204, Memphis, USA.

Otukei J R & Blaschke T (2010). Land cover change assessment using decision trees, support vector machines and maximum likelihood classification algorithms. International Journal of Applied Earth Observation and Geoinformation, 12, 27-31.

Paola J D & Schowengerdt R A (1995). A detailed comparison of backpropagation neural network and maximum-likelihood classifiers for urban land use classification. IEEE Transactions on Geoscience and remote sensing, 33(4), 981-996.

Paola J D (1994). Neural Network Classification of Multispectral Imagery, Master's Thesis, University of Arizona, USA.

Richards J A & Richards J A (1999). Remote sensing digital image analysis, 3, 10-38. Springer: Berlin.

Sathya P & Deepa V B (2017). Analysis of supervised image classification method for satellite images. International Journal of Computer Science Research (IJCSR), 5(2), 16-19.

Srivastava D (2006). Making or breaking the heart: from lineage determination to morphogenesis. Cell, 126(6), 1037-1048.

Strahler A H (1980). The use of prior probabilities in maximum likelihood classification of remotely sensed data. Remote sensing of Environment, 10(2), 135-163.

Ulvi A, Yakar M, Yiğit A Y & Kaya Y (2020). İHA ve Yersel Fotogrametrik Teknikler Kullanarak Aksaray Kızıl Kilise'nin 3 Boyutlu Nokta Bulutu ve Modelinin Üretilmesi. Geomatik Dergisi, 5(1), 22-30.

Villaseñor C (2019). Hyperellipsoidal Neural Network Trained With Extended Kalman Filter for Forecasting of Time Series. In Artificial Neural Networks for Engineering Applications, 9-19, Academic Press.

Yang C & Everitt J H (2010). Comparison of hyperspectral imagery with aerial photography and multispectral imagery for mapping broom snakeweed. International Journal of Remote Sensing, 31(20), 5423-5438.

Yiğit A Y & Uysal M (2019). Nesne Tabanlı Sınıflandırma Yaklaşımı Kullanılarak Yolların Tespiti. Türkiye Fotogrametri Dergisi, 1(1), 17-24.

Intercontinental Geoinformation Days

http://igd.mersin.edu.tr/2020/

# Data Fusion of Unmanned Aerial Vehicle (UAV)-Based Photogrammetry and Close-Range Photogrammetry in Historical Sites Monitoring

**İrem Yakar*[1], Seda Nur Gamze Hamal [2], İldeniz Leyla Öztürk [2], Mehmet Özgür Çelik [2], Serdar Bilgi [1]**

[1]*Istanbul Technical University, Faculty of Civil Engineering, Department of Geomatics Engineering, Istanbul, Turkey*
[2]*Mersin University, Faculty of Engineering, Department of Geomatics Engineering, Mersin, Turkey*

**Keywords**
Data Fusion
UAV
Photogrammetry
Documentation

**ABSTRACT**

There are various methods for monitoring historical sites ranging from classical drawing techniques to, classical surveying techniques etc. Along with developing technology, modern methods have become more preferable to classical methods. In this context, UAV-based photogrammetry and close-range photogrammetry appear as popular methods for historical sites monitoring and documentation studies. It can be said that each method has its own advantages and disadvantages. In this study, a historical monument was modeled by using UAV-based photogrammetry and close-range photogrammetry. Then, two models were integrated with each other in order to have a complete representation of the object to be modeled. The metric accuracy of the resulted model was also investigated.

## 1. INTRODUCTION

Photogrammetry is the process of determining shape and location of an object through image interpretations and measurements.

Usually, it is divided into two categories as close-range photogrammetry and aerial photogrammetry. In close-range photogrammetry, images are acquired from the locations near or on the surface of the earth. The close-range photogrammetric data provide detailed dimensional information of objects. In contrast, aerial photogrammetric data are collected via overhead shots from an aircraft and provides land use details (Jiang, Jáuregui, & White, 2008).

UAV photogrammetry introduces new application areas such as new real time applications to classical manned aerial photogrammetry with being able to combine both aerial and terrestrial photogrammetry.

Unmanned Aerial Vehicles (UAVs) have many different usage areas ranging from Computer Science to Robotics, Artificial Intelligence, Photogrammetry, and Remote Sensing. In addition, the terms such as Remotely Piloted Vehicle (RPV) or Unmanned Vehicle Systems (UVS) can be used in place of UAVs. RPV can be described as a robotic aircraft controlled by a human using a ground controller. The term UAV photogrammetry stands for a system that is remotely operated semi-autonomously or autonomously without having a human-being inside the vehicle. The systems also include a photogrammetric measurement platform which consists of video, thermal or infrared camera systems, airborne LIDAR or combination of both systems. Today, the registration and the determination of the position and orientation of the sensors carried by the UAV platforms are possible in a local or global reference system. Therefore, UAV photogrammetry can be accepted as a new photogrammetric measurement tool. There are various advantages of UAVs in comparison with classical aerial photogrammetry. The first advantage can be shown as the availability of operating in dangerous and inaccessible sites without endangering pilots. Such situations can be listed as, reaching the natural hazard zones such as floods, volcanic eruptions, earthquakes, etc. In this case, UAVs can be the only solution where reaching disaster sites is nearly impossible. This situation indicates the importance of UAVs in such cases. Besides, UAVs can fly and acquire data in low-altitudes which is not possible in classical manned photogrammetry. On the other hand, UAVs are both time and cost-efficient (Eisenbeiß, 2009). UAV technology is also a popular choice for historical sites monitoring and modeling studies due to being able to

* **Corresponding Author**

*(yakari@itu.edu.tr) ORCID ID 0000 – 0002 – 7823 – 9674
(sedanurgamzehamal@gmail.com) ORCID ID 0000 – 0002 – 1050 – 3088
(idenizleylaa@gmail.com) ORCID ID 0000– 0003 – 0598 – 9316
(mozgurcelik@mersin.edu.tr) ORCID ID 0000 – 0003 – 4569 – 888X
(bilgi@itu.edu.tr) ORCID ID 0000 – 0002 – 8396 – 3202

**Cite this study**

Yakar İ., Hamal S.N.G., Öztürk İ.L. Çelik M.Ö., Bilgi S., (2020). Data Fusion of Unmanned Aerial Vehicle (UAV)-Based Photogrammetry and Close-Range Photogrammetry in Historical Sites Monitoring. Intercontinental Geoinformation Days (IGD), 112-115, Mersin, Turkey.

produce high resolution and geo-tagged images (Themistocleous, Ioannides, Agapiou, & Hadjimitsis, 2015).

Close-range photogrammetry is a valuable tool for three-dimensional (3D) modelling with its long history. In recent years, there have been many important changes and growth in the close-range photogrammetric measurement area (Fraser & Hanley, 2004).

In this study, two point clouds were produced by using UAV and close-range photogrammetric images in Agisoft Photoscan software. Then, two point clouds were integrated in 3DF Zephyr software. The resulted point cloud was also examined.

## 2. METHOD

### 2.1. Close-Range Photogrammetry

Photogrammetry is basically a method which produces shape and location information of an object from photographs through measurement and image interpretation. In principle, it can be said that, photogrammetric techniques can be used in any situation where the photographs of the objects to be measured can be taken. The main objective of the photogrammetric process is to produce a 3D reconstruction of the object to be measured. Photographs or images which are the results of the photogrammetric process, supply information that can be used at any time (Luhmann, Robson, Kyle, & Harley, 2007).

The close-range photogrammetric survey is divided into two phases such as field work and office work. During the field work phase of the study, total of 106 photographs of Fountain of Ahmed III were captured, later 80 of them were used for 3D modeling process. The images were captured by using Nikon Coolpix A10 digital camera featured a 16.1 megapixel 1/2.3" CCD sensor. As the next step of field work, 4 Ground Control Points (GCPs) were established around the fountain. These GCPs were later used for bringing two models in a common reference system. The 3D coordinates of established GCPs were measured in Continuously Operating GNSS Kinematic Reference Stations System (CORS-TR) with Trimble R6 GNSS receiver in UTM projection, ITRF-96 datum (EPSG:5255), GRS80 ellipsoid, 2005.0 epoch and 3-degree zone 30. 81 detail points in total were determined on the facades of the fountain. 41 of the detail points were printed paper targets while remaining 40 points were selected from characteristic points of the fountain such as corners, eaves bottoms, etc. A tacheometric measurement was carried out by the use of Pentax R-1505N electronic tacheometer in order to determine the 3D coordinates of the detail points. The coordinates of detail points were calculated on Netcad software with respect to GCPs by using angle and distance measurements obtained from tacheometric measurements. In this way, both GCPs and each detail points were brought in a common reference system. 17 of detail points were used in geo-referencing of the close-range photogrammetric 3D model (Figure 1).


**Figure 1.** Detail points from one facade used for the geo-referencing in close-range photogrammetry

During the office work process of close-range photogrammetric survey, camera calibration parameters were determined at first by using Agisoft Lens software (Figure 2 & 3).

**Figure 2.** Agisoft Lens software calibration chessboard

| Parameter | Value | Std Error |
|---|---|---|
| Image width | 4608 | |
| Image height | 3456 | |
| Focal length (x) | 3547.47 | 1.50455 |
| Focal length (y) | 3547.61 | 1.46078 |
| Principal point (x) | 2353.24 | 0.743895 |
| Principal point (y) | 1775.38 | 0.604964 |
| Skew | 1.99832 | 0.11242 |
| Radial K1 | -0.0527827 | 0.00276451 |
| Radial K2 | 0.548142 | 0.0186619 |
| Radial K3 | -1.4373 | 0.0496565 |
| Radial K4 | 1.21602 | 0.00203453 |
| Tangential P1 | 0.00363844 | 5.37707e-05 |
| Tangential P2 | 0.00344985 | 6.89058e-05 |

**Figure 3.** Camera calibration in Agisoft Lens

Then, these parameters were imported into Agisoft Photoscan software. As the last step of the office work, the point cloud and textured model were produced by processing the photogrammetric data in Agisoft Photoscan software. The point cloud consists of approximately 12 million points and the textured model of the monument were obtained as a result of the close-range photogrammetric survey (Figure 4 & 5).

**Figure 4.** Point cloud produced after close-range photogrammetric survey

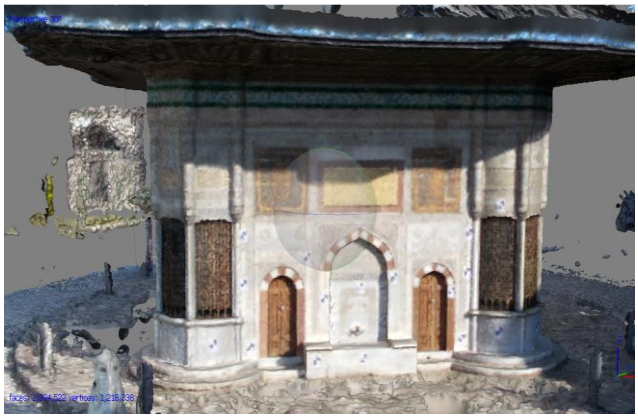

**Figure 5.** Textured model

### 2.2. UAV Photogrammetry

UAV-based photogrammetric survey is divided into two phases as well as the close-range photogrammetric survey such as field work and office work. During the field work process, a double grid mission flight plan for 100 m flight height was created in Pix4D Capture software and total of 48 photographs were captured by using Parrot Anafi UAV. The flight took approximately 10 minutes around the fountain. Due to obstacles around the artifact such as walls of Hagia Sophia Mosque and Topkapı Palace, acquiring data from facades of the object in double grid mission was not possible. Therefore, only roof of the fountain was documented by using UAV photogrammetry. In office work process, 48 images were processed in order to obtain point cloud in Agisoft Photoscan software. The 3D coordinates of the GCPs were used for geo-referencing the model. The resulted point cloud can be seen in figures 6 and 7.

**Figure 6.** Point cloud obtained from UAV imagery

**Figure 7.** Point cloud obtained from UAV imagery

### 2.3. Data Fusion

Data fusion (also known as data integration), is the process of combining data, acquired by using different sources or sensors. The fusion data coming from different sensors are generally acquired at different resolutions. On the other hand, the both data represent the same object for obtaining a complete and accurate representation of the object to be modeled. Data fusion can be classified as low, intermediate or high with respect to processing stage at which fusion takes place (Klein, 2004; Ramos & Remondino, 2015).

Since the two point clouds are in a common reference system, both of them were imported in 3DF Zephyr software and integrated with each other as shown in figure 8. Thus, a complete model of the monument was obtained.

**Figure 8.** The resulted point cloud after data fusion

### 2.4. Accuracy Assessment

In order to determine the accuracy of the resulted model; 15 distances in total were measured on the model between selected detail points. The distances were also calculated using 3D coordinates obtained by GNSS and electronic tacheometer measurements. The calculated distances were imported to Agisoft Photoscan software. The accuracy of the model is found ± 6.72 cm after creating scale bars between selected detail points.

## 3. RESULTS

In this study, a close-range photogrammetric and UAV-based photogrammetric surveys carried out respectively.

Fountain of Ahmed III was selected for the 3D reconstruction (Figure 9). The fountain was built in 1729 by the Sultan Ahmet III, upon the proposal of the grand vizier Nevşehirli Damat İbrahim Pasha. It is located in front of the Bab-ı Hümayun gate of Topkapı Palace in Fatih district of Istanbul.

**Figure 9.** Selected monument for the 3D reconstruction

Two separate models were generated in Agisoft Photoscan software by using UAV and close-range photogrammetric images. Acquiring images from the facades of the monument was not possible due to walls of Hagia Sophia Mosque and Topkapı Palace in double grid mission UAV survey. Therefore, the facades were acquired from the close-range photogrammetric survey. The two models were integrated for obtaining a complete 3D model of the monument. In order to integrate these models, each model should be in a common reference system. GNSS and tacheometric measurements were carried out in order to bring two models in the same reference system. Thus, the point clouds were integrated in 3DF Zephyr software. Then, accuracy of the resulted model was investigated by measuring the distances between selected detail points on the facades and comparing them with the ground truth data. The accuracy of the model is found ± 6.72 cm.

## 4. CONCLUSION

Documentation of cultural heritage elements is very important in terms of preserving and transferring them to future generations. In this context, many different methods have been used from past to present. Close-range photogrammetry and UAV photogrammetry can be shown as two of these methods.

It is seen that, the close-range photogrammetry is successful in documenting the facades of the monuments, while it cannot represent the roofs completely. In such cases, UAV photogrammetry can be a great solution since it can acquire data from the above. Hence, the both data can be integrated with each other in order to obtain a complete 3D model of the historical monuments.

Metric accuracy is one of the most important factors in the documentation of cultural heritage. The accuracy is extremely crucial in order to renew the building in accordance with its original situation and to create the models of the building properly and correctly. It has been observed that the 3D model obtained can be used as a base for the documentation and preservation of cultural heritage. These models play an important role in the restoration works as well as determining the deformations that will occur on the historical artifacts. In conclusion, it is thought that this study, which is examined for the purpose of documentation of cultural heritage, can contribute to studies in the field of preservation, photogrammetry and data fusion.

## REFERENCES

Eisenbeiß, H. (2009). UAV photogrammetry. ETH Zurich,

Fraser, C., & Hanley, H. (2004). Developments in close-range photogrammetry for 3D modelling: the iWitness example. Paper presented at the Presented paper, International Workshop: Processing and Visualization using High-Resolution Imagery, Pitsanulok.

Jiang, R., Jáuregui, D. V., & White, K. R. (2008). Close-range photogrammetry applications in bridge measurement: Literature review. Measurement, 41(8), 823-834.

Klein, L. A. (2004). Sensor and data fusion: a tool for information assessment and decision making (Vol. 138): SPIE Press, ISBN: 9780819481115.

Luhmann, T., Robson, S., Kyle, S., & Harley, I. (2007). Close range photogrammetry: Principles, Techniques and Applications, Wiley, 2007, ISBN 9780470106334.

Ramos, M. M., & Remondino, F. (2015). Data fusion in cultural heritage-A review. The International Archives of Photogrammetry, Remote Sensing and Spatial Information Sciences, 40(5), 359.

Themistocleous, K., Ioannides, M., Agapiou, A., & Hadjimitsis, D. G. (2015). The methodology of documenting cultural heritage sites using photogrammetry, UAV, and 3D printing techniques: the case study of Asinou Church in Cyprus. Third International Conference on Remote Sensing and Geoinformation of the Environment (RSCy2015).

Intercontinental Geoinformation Days

http://igd.mersin.edu.tr/2020/

# Ecological Appraisal of Urban Heat Island in Zaria, Nigeria

**Ebenezer Ayobami Akomolafe*[1], Olalekan Adekunle Isioye [1], Wilson Ojochonu Labija[1]**

[1]*Ahmadu Bello University, Faculty of Environmental Design, Department of Geomatics, Zaria, Nigeria*

**Keywords**
Urban Heat Island (UHI)
Land Surface Temperature (LST)
Urban Thermal Field Variance Index (UTFVI)
Landsat OLI/TIRS/ETM+
Normalized Difference Vegetation Index (NDVI)

**ABSTRACT**

With rapid population growth, urbanization, coupled with other anthropogenic activities, Zaria, Nigeria experiences, UHI, with a steady increase in surface and atmospheric temperatures over the years. This study evaluates the UHI in the study area and its effect on the ecology, using Landsat ETM+ and OLI/TIRS remotely-sensed data, between 2009 and 2019. The satellite data were used to derive NDVI and LST for 2009, 2015 and 2019 while the UHI effects on the quality of urban life was evaluated using UTFVI. Results indicate that there is an increase of 2.44°C in the mean surface temperature in Zaria between 2015 and 2019, with a slight overall decrease of 1.88°C between 2009 and 2019. The hot spot of UTFVI were found mainly in the bare, uncultivated lands, built-up areas, especially the commercial and industrial districts. These areas are the most vulnerable to UHI phenomenon and negatively affected in ecological quality. In general, a large portion of the city experiences ecologically worse UHI effects, indicating a need for continued UHI mitigation efforts.

## 1. INTRODUCTION

Urbanization influences local meteorological and climatic conditions. One of these environmental influences or impact is the formation of Urban Heat Islands (UHI) in affected areas (Khallef et al. 2020; Streutker 2002), which directly inspires environmental degradation. Moreover, rising temperatures due to global climate change is amplified by the effect of UHI (Della-Marta et al. 2017). UHI is the surplus temperature near the ground or urban areas, which is usually higher than those of nearby or surrounding areas (Voogt and Oke 2003). This phenomenon is widely analyzed and is one of the major themes of urban climatology, particularly its impact on human health (Huang and Lu 2018). UHI has been regarded as an example of anthropogenic climate modification within the field of urban climate (Arnfield 2003). Rapid urbanization is the greatest factor for the formation of UHI, which is a matter of global concern. This urbanization and the fact that temperatures are rising globally are motivating the urgency to study and understand urban areas and their climatic implications (Kaur and Pandey 2019).

While built-up areas and bare surfaces have been shown to accelerate the effect of UHI, green space and water bodies reduce the UHI intensity (Amiri et al. 2009). Land Surface Temperature (LST) is a parameter used to quantify UHI. It is the temperature of the land surface which can be measured when the surface is in contact with a measuring instrument.

Studying the thermal differences between urban and rural areas, retrieving LST and UHI have been made easier with the use of satellite remote sensing, aided by GIS. Several researches have been carried out to show some thermal comfort indices for measuring the effect of UHI intensity. These include: physiological equivalent temperature, temperature humidity index, wet-bulb globe temperature and urban thermal field variance index (UTFVI) (Guha et al. 2018; Kakon et al. 2010; Matzarakis et al. 1999; Willett and Sherwood 2012; Zhang 2006). However, UTFVI is the most commonly used index for the ecological evaluation of urban environment due to its relationship with surface temperature (Alfraihat et al. 2016; Isioye et al. 2020; Liu and Zhang 2011). It is therefore imperative to determine the thermal comfort level of every city in this regard.

The pattern, trend and characteristics of urbanization in Nigeria have been alarming. Town and cities have grown unbelievably with pace of urbanization in Nigeria showing high growth rates of 5% - 10% per annum (Egunjobi 1999). Over the years, Zaria has experienced a rapid population growth and urbanization, with the population growing from 698,000 in 2006 to over a 970,000 people in 2019 (Humanitarian Data Exchange 2020). With the accelerated rate of urbanization, UHI has developed more significant as it

* **Corresponding Author**

*(goldera2787@gmail.com) ORCID ID 0000-0001-6797-0114
(lekkyside4u@yahoo.com) ORCID ID 0000-0001-5734-5374
(wilsonlabija@gmail.com) ORCID ID 0000-0002-9592-1755

**Cite this study**

Akomolafe E A, Isioye O A & Labija W O (2020). Ecological appraisal of urban heat island in Zaria, Nigeria. Intercontinental Geoinformation Days (IGD), 116-120, Mersin, Turkey

has severe impact on urban development and human living environment (Chen et al. 2009). Meanwhile, increasing urban heat in Zaria and environs presents a significant health risk for the growing population and the related heat stress is likely to escalate with the increase in surface temperature.

This study seeks to utilize remotely sensed data and GIS to examine the distribution and changes in LST of the study area and analyze the impact of UHI phenomenon on the quality of urban life in the study area, using UTFVI. UHI phenomenon was investigated over the study area using Landsat 7 and 8 images covering the period 1999 through 2019 at 3 epochs. The relationship between LST and NDVI was also examined to investigate the effect of vegetation on dynamics of surface temperature. Satellite data with temporal, spatial and spectral characteristics makes it possible to study temperature changes spatio-temporally.

## 2. METHOD

### 2.1. Description of the Study Area

The study area is the city of Zaria in northern Nigeria which comprises of Zaria and Sabon Gari Local Government Areas in Kaduna state. It is located between latitudes 10° 57' and 11° 15' north of the equator and between longitudes 7° 35' and 7° 48' east of the Central Meridian. It occupies a total land area of approximately 545.77 km$^2$ at an average elevation of 644m above mean sea level. Zaria experiences a typical tropical climate and it records a mean daily maximum temperature of about 38$^o$C and a mean daily minimum of about 16$^o$C (Meteoblue 2020). Zaria has a population of 975,153, making it the second largest city in Kaduna state, Nigeria (Worldometer 2020). Due to urban sprawl and population growth being experienced in Zaria, there is a corresponding loss of vegetation which exerts a significant influence on the micro-climate of the area. A map of the study area is shown in Figure 1.

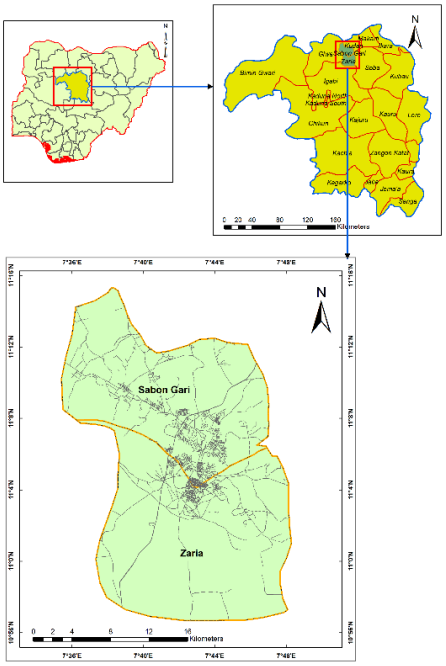


**Figure 1.** Map of the study area

### 2.2. Data Acquisition and Pre-processing

Cloud-free Landsat 7 ETM+ and Landsat 8 OLI/TIRS images were obtained from the earth explorer platform of the USGS website (earthexplorer.usgs.gov) for the years 2009, 2015 and 2019. The details of the Landsat images selected for this study are presented in Table 1.

**Table 1.** Details of the Landsat data used in this study

| Satellite/ sensor | Path/ Row | Acquisition date | Resolution (Spectral/TIRS) |
|---|---|---|---|
| Landsat 7(ETM+) | 189/52 | 04/03/2009 | 30m/60m |
| Landsat 8 (OLI/TIRS) | 189/52 | 29/03/2015<br>20/02/2019 | 30m/100m<br>30m/100m |

The Landsat images were all subjected to radiometric calibration to produce scaled and comparable data and to reduce scene-to-scene variability, while the Landsat 7 (ETM+) image was corrected for scan line error. The images were then subset for further analyses, using the administrative map of the study area.

### 2.3. Derivation of NDVI

The Normalized Difference Vegetation Index (NDVI) is calculated from the reflectance values of the visible red and near infrared bands. The NDVI can be calculated using equation (1).

$$NDVI = \frac{NIR - RED}{NIR + RED} \qquad (1)$$

NIR and RED in Landsat images are the reflectance in the near-infrared and visible red portion of Electromagnetic spectrum respectively.

### 2.4. Retrieval of LST

The following procedures were carried out to retrieve the LST of the study area. First, the digital numbers (DN) of the thermal bands were converted to at-satellite spectral radiance using the following equation.

$$L_\lambda = M_L \times QCal + A_L, \qquad (2)$$

Where $L_\lambda$ = at sensor spectral radiance in Watt/(m$^2$srμm); $M_L$ = the band-specific multiplicative rescaling factor from the metadata; QCal = the quantized and standard product pixel value (DN); and $A_L$ = the band-specific additive rescaling factor from the metadata

The spectral radiance converted from pixel DN values above was then used to compute Top of Atmosphere (TOA) brightness temperature ($T_B$) as follows.

$$T_B = \frac{K_2}{ln\, ln\left(\frac{K_1}{L_\lambda} + 1\right)} \qquad (3)$$

Where $T_B$ = the effective at-satellite temperature; K1 and K2 are two calibration constants, which are supplied by the metadata of Landsat images.

Subsequently, the emissivity-corrected LST (in Celsius) was computed as follows (Stathopoulou and Cartalis 2007).

$$LST(^oC) = \frac{T_B}{\left[1 + \left(\lambda \times \frac{T_B}{\rho}\right) ln\, ln\, (\varepsilon)\right]} - 273.15 \qquad (4)$$

Where λ = the wavelength of emitted radiance; ρ = h×(c/s) = 1.4388 × $10^{-2}$m K = 14388 μm K; h = the plank's constant (6.626 × $10^{-34}$Js); s = the Boltzmann constant (1.38 × $10^{-23}$J/K) ; c = velocity of light = 2.998 × $10^8 m/s$; ε = thermal emissivity.

In this study, the NDVI threshold method was used to obtain surface emissivity (ε) (Sobrino et al., 2004) while the proportion of vegetation (Pv) was computed from the NDVI according to (Carlson and Ripley 1997).

### 2.5. The Urban Thermal Field Variance Index (UTFVI)

The urban thermal field variance index (UTFVI) is commonly used to show the UHI effect or the thermal comfort level of an urban area. It can be estimated by equation (5) (Zhang et al. 2006).

$$UTFV = \frac{T_s - T_m}{T_s} \qquad (5)$$

Where $T_s$ is the LST and $T_m$ is the mean of the LST of the whole study area.

In order to examine the UHI effect, the UTFVI values are divided into six categories, each with the corresponding interpreted ecological evaluation index (Zhang et al. 2006), as shown in Table 2.

**Table 2.** Threshold values of urban thermal field variance index and ecological evaluation index

| UTFVI | UHI phenomenon | Ecological Evaluation Index |
|---|---|---|
| < 0 | None | Excellent |
| 0 - 0.005 | Weak | Good |
| 0.005 - 0.010 | Middle | Normal |
| 0.010 - 0.015 | Strong | Bad |
| 0.015 - 0.020 | Stronger | Worse |
| > 0.020 | Strongest | Worst |

## 3. RESULTS AND DISCUSSION

### 3.1. Spatial Pattern of LST

The spatial distribution of the LST of the study area derived from Landsat images are shown in Figure 2. Table 3 shows the statistical summary of LST distribution in Zaria in the study period.

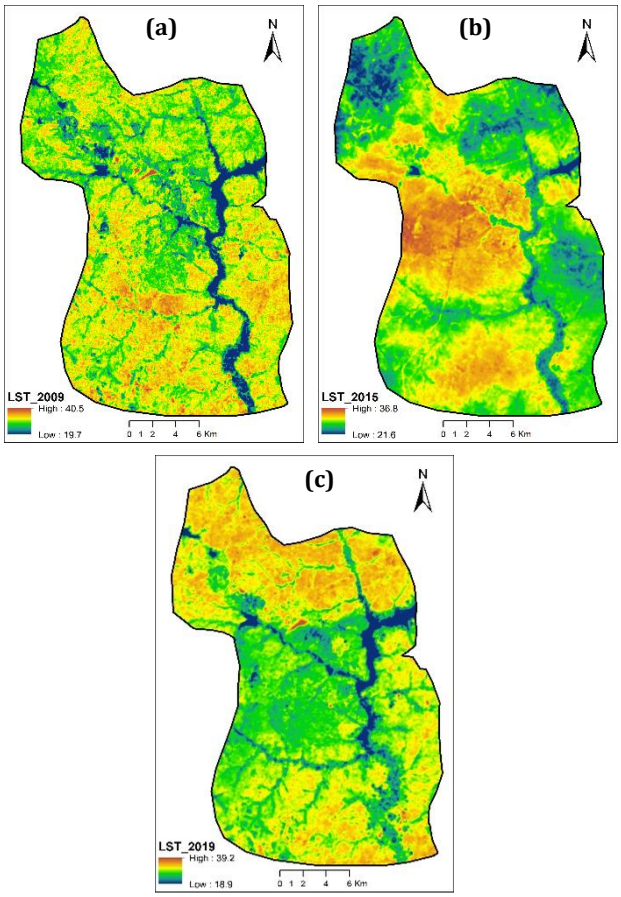


**Figure 2.** LST maps of Zaria in (a) 2009, (b) 2015, and (c) 2019

**Table 3.** Summary of LST distribution in Zaria between 2009 and 2019

| Year | Min. Temp. (°C) | Max. Temp. (°C) | Mean Temp. (°C) |
|---|---|---|---|
| 2009 | 19.74 | 40.48 | 33.87 |
| 2015 | 21.62 | 36.76 | 29.55 |
| 2019 | 18.95 | 39.16 | 31.99 |

From the results obtained, it was observed that overall, there was a 1.88°C decrease in mean surface temperature in the study area between 2009 and 2019, though the mean temperature increased by 2.44°C between 2015 and 2019. Generally, higher surface temperatures are found in the densely populated city center and bare lands, especially as seen in 2015, while the lower temperatures are along the water bodies, wetlands and the vegetated areas. The city center is the most populated area with a beehive of anthropogenic activities and release of greenhouse gases. These activities produce impervious surfaces, which in turn rise the surface temperature of this area compared to the surrounding localities. In 2019 though, the city centre is cooler with lower LST values while higher LST values are observed at bare surfaces and uncultivated farmlands in the northern and southern parts of the city.

### 3.2. Ecological Evaluation of Zaria using UTFVI

In this study, the ecological evaluation of the study area was carried out for the two extremes of the study period: 2009 and 2019, to investigate the change in thermal comfort level of the area. The UTFVI which measures urban ecological quality of life in terms of the degree of thermal comfort in relation to the existence of the UHI phenomenon was used for the evaluation. Figure 3 shows the ecological assessment of the effects of UHI in Zaria.

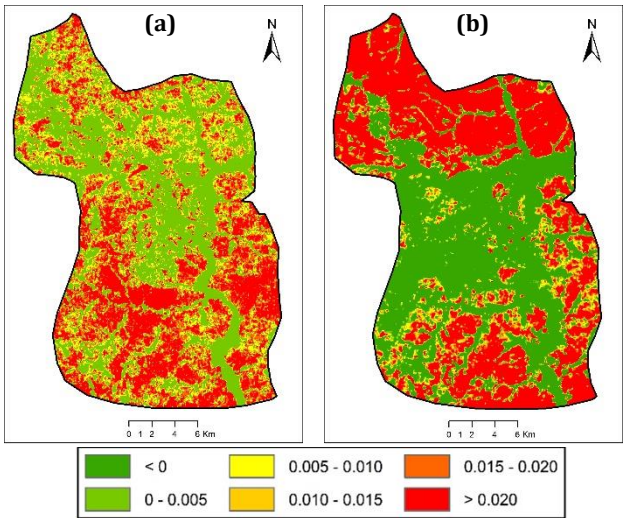


**Figure 3.** UTFVI maps of Zaria in (a) 2009 and (b) 2019

The effect of UHI were identified based on the degree of thermal comfort that is associated with the existence of UHI. From results obtained, it was found that the city experiences two extremes of thermal comfort: areas of thermal stress (UTFVI > 0.02) and areas of good micro climate (UTFVI < 0). Table 4 shows the quantitative distribution of the UTFVI threshold in the study area in 2009 and 2019.

**Table 4.** Ecological evaluation index of Zaria

| UTFVI | UHI phenomenon | Ecological Evaluation Index | Area occupied ($km^2$) | |
|---|---|---|---|---|
| | | | 2009 | 2019 |
| < 0 | None | Excellent | 0 | 231.66 |
| 0 - 0.005 | Weak | Good | 203.59 | 22.15 |
| 0.005 - 0.010 | Middle | Normal | 104.79 | 24.93 |
| 0.010 - 0.015 | Strong | Bad | 0 | 27.11 |
| 0.015 - 0.020 | Stronger | Worse | 100.71 | 27.91 |
| > 0.020 | Strongest | Worst | 136.65 | 211.98 |

Results show that areas that enjoy optimal thermal conditions (i.e. UTFVI < 0 ≤ 0.005) are areas with water bodies, vegetation and wetlands. In 2009, 203.59 $km^2$ of the total land mass has been weakly impacted by UHI, thus enjoying good thermal comfort level whereas 231 $km^2$ of the study area enjoyed excellent thermal comfort in 2019, with no impact of UHI. 136.65 $km^2$ and 211.98 $km^2$ are areas worst hit by UHI effect (UTFVI > 0.020) in 2009 and 2019 respectively. These areas are mostly bare lands and sparsely cultivated lands since the Landsat images were taken in the dry season.

Just as observed in the LST distribution, there is a significant improvement in areas experiencing excellent thermal comfort (UTFVI < 0) in 2019 as compared to 2009. This is evident in the decrease in surface temperature between 2009 and 2019. The largest portion of Zaria city experiences optimal thermal condition for habitation probably due to the presence of trees within residential areas in the city centre and its proximity to a dam and other wetlands. Higher UTFVI values occur in the extreme northern and southern regions of the study area. These areas are thermally stressed and consist of the bare lands and other impervious surfaces.

Generally, UHI phenomenon was more evidently seen in 2019, with large areas in the periphery of the city presenting extreme high UTFVI values (> 0.020). Accordingly, the ecological evaluation index also got worse in this year.

## 4. CONCLUSION

This study has demonstrated the capability of using remotely sensed dataset and Geographical Information System (GIS) to investigate and monitor the effect of UHI on a particular geographical location. It was also discovered that examining temperature dynamics can aid in analyzing the urban environment and consequently help in decision making processes for city development.

In this study, Landsat ETM+ and OLI/TIRS satellite data were processed to analyze the surface temperature dynamics in Zaria and subsequently study the thermal comfort level of the city using UTFVI. Results show a decrease in mean surface temperature in Zaria between 2009 and 2019 (from 33.87°C to 31.99°C). This may be as a result of the tree planting projects in the city in recent years, irrigation farming in the dry season, presence of wetland and the city's proximity to a dam. Though an increase in surface temperature was recorded in the city centre between 2009 and 2015 as a result of population increase and urban sprawl.

Two extremes of thermal comfort levels were observed from results of analyzing the city's UTFVI as the city experiences both good/excellent conditions of thermal comfort and worst conditions of thermal discomfort. The hot spot of UTFVI were found mainly in the city's commercial and industrial districts, bare surfaces and uncultivated farmlands at the periphery of the city. Other areas adversely affected by the UHI phenomenon include some residential areas around the city and other impervious surfaces such as pavements, asphalt roads etc. These are likely areas that are susceptible to UHI. It was observed in 2019 that a large portion of the city centre experiences excellent microclimate for living, which is encouraging.

However, there is a dire need to mitigate the effect of UHI in Zaria, Nigeria by increasing tree and vegetative cover, installing green roofs, and using cool pavements.

## REFERENCES

Alfraihat R, Mulugeta G & Gala T S (2016). Ecological evaluation of urban heat island in Chicago City, USA.

Journal of Atmospheric Pollution, 4(1), 23–29. https://doi.org/10.12691/jap-4-1-3.

Amiri R, Weng Q, Alimohammadi A & Alavipanah S K (2009). Spatial–temporal dynamics of land surface temperature in relation to fractional vegetation cover and land use/cover in the Tabriz urban area, Iran. Remote Sens. Environ., 113(12), 2606–2617. https://doi.org/10.1016/j.rse.2009.07.021.

Arnfield A J (2003). Two decades of urban climate research. a review of turbulence exchange of energy and water and the urban heat island. International Journal of Climatology, 23, 1-26. https://doi.org/10.1002/joc.859.

Carlson T N & Ripley D A (1997). On the relation between NDVI, fractional vegetation cover, and leaf area index. Remote Sensing of Environment, 62, 241–252. https://doi.org/10.1016/S0034-4257(97)00104-1.

Chen Q, Ren J, Li Z & Ni C (2009). Urban Heat Island Effect Research in Chengdu City Based on MODIS Data. International Conference on Bioinformatics and Biomedical Engineering (ICBBE 2009), 1 – 5, Beijing, China.

Della-Marta P M, Haylock M R, Luterbacher J & Wanner H D (2017). Doubled length of western European summer heat waves since 1880. Journal of Geophysical Research Atmosphere, 112(D15103), 1-11. https://doi.org/10.1029/2007JD008510.

Egunjobi L (1999). Our Gasping Cities, an inaugural lecture delivered at the University of Ibadan, Nigeria on Thursday, 21st October 1999.

Guha S, Govil H, Dey A & Gill N (2018). Analytical study of land surface temperature with NDVI and NDBI using Landsat 8 OLI and TIRS data in Florence and Naples city, Italy. European Journal of Remote Sensing, 51(1), 667-678. https://doi.org/10.1080/22797254.2018.147449.

Huang Q & Lu Y (2018). Urban heat island research from 1991 to 2015: a bibliometric analysis. Theor. Appl. Climatol., 131, 1055–1067. https://doi.org/10.1007/s00704-016-2025-1.

Humanitarian Data Exchange (HDX) (2020). Nigeria – Sub-national population statistics. Retrieved from https://data.humdata.org/dataset.

Isioye O A, Ikwueze H U & Akomolafe E A (2020). Urban Heat Island Effects and Thermal Comfort in Abuja Municipal Area Council of Nigeria. FUTY Journal of the Environment, 14(2), 19-34.

Kakon A N, Nobuo M, Kojima S & Yoko T (2010). Assessment of thermal comfort in respect to building height in a high-density city in the tropics. American Journal of Engineering and Applied Sciences, 3(3), 545–551. https://doi.org/10.3844/ajeassp.2010.545.551.

Kaur R & Pandey P (2019). Assessment of Urban Heat Island in India using Geospatial Technology - A Review. Environ. We Int. J. Sci. Tech., 14(2019), 89-109.

Khallef B, Biskri Y, Mouchara N & Brahamia K (2020). Analysis of Urban Heat Islands using Landsat 8 OLI/TIR Data: Case of the City of Guelma (Algeria). Asian Journal of Environment & Ecology, 12(4), 42-51. https://doi.org/10.9734/ajee/2020/v12i430167.

Liu L & Zhang Y (2011). Urban heat island analysis using the Landsat TM data and ASTER data: A case study in Hong Kong. Remote Sensing, 3, 1535–1552. https://doi.org/10.3390/rs3071535.

Matzarakis A, Mayer H & Iziomon, M G (1999). Applications of a universal thermal index: Physiological equivalent temperature. International Journal of Biometeorology, 43(2), 76–84. https://doi.org/10.1007/s004840050119.

Meteoblue (2020). Zaria climate. Retrieved from http://www.meteoblue.com/.

Sobrino J A, Munoz J C, & Paolini L (2004). Land surface temperature retrieval from Landsat TM5. Remote Sensing of the Environment, 9, 434–440. https://doi.org/10.1016/j.rse.2004.02.003.

Stathopoulou M & Cartalis C (2007). Daytime urban heat islands from Landsat ETM+ and Corine land cover data: an application to major cities in Greece. Solar Energy, 81(3), 358–368. https://doi.org/10.1016/j.solener.2006.06.014.

Streutker D R (2002). A remote sensing study of the urban heat island of Houston, Texas. International Journal Remote Sensing, 23(1), 2595–2608. https://doi.org/10.1080/01431160110115023.

Voogt J A & Oke T R (2003). Thermal remote sensing of urban climates. Remote Sensing of Environment, 86, 370-84. https://doi.org/10.1016/S0034-4257(03)00079-8.

Willett K M & Sherwood S (2012). Exceedance of heat index thresholds for 15 regions under a warming climate using the wet-bulb globe temperature. International Journal of Climatology, 32(2), 161–177. https://doi.org/10.1002/joc.2257.

Worldometer (2020). Nigeria population. Retrieved from https://www.worldometers.info/world-population/nigeria-population/.

Zhang Y, Yu T, Gu X, Zhang Y & Chen L (2006). Land surface temperature retrieval from CBERS-02 IRMSS thermal infrared data and its applications in quantitative analysis of urban heat island effect. J. Remote Sens. Beijing, 10(5), 789-797.

Intercontinental Geoinformation Days

http://igd.mersin.edu.tr/2020/

# Road Surface Extraction from MLS-Based Point Clouds

**Mustafa Zeybek*[1], Serkan Biçici [2]**

[1]Artvin Çoruh University, Engineering Faculty, Geomatics Engineering Department, Artvin, Turkey
[2]Artvin Çoruh University, Engineering Faculty, Civil Engineering Department, Artvin, Turkey

**Keywords**
Mobile LiDAR
Point cloud
Road surface
Pavement

**ABSTRACT**

Mobile mapping technology is one of the most commonly used technologies to collect three-dimensional spatial data. Geomatics engineering is the one discipline that used this technology the most. These systems are used extensively in which laser scanning systems are integrated, especially in corridor mapping purposes. In this study, it is proposed to extract the road surface automatically from Mobile LiDAR-based point clouds. The proposed methodology consists of three steps: (1)collecting MLS raw data; (2) producing three-dimensional dense point cloud; (3) classifying ground/non-ground point filtering and applying a piecewise linear regression model to extract the road surface. As a result, the proposed methodology successfully extracts the road surface from the MLS-based point cloud.

## 1. INTRODUCTION

Advanced Driver Assistance System and autonomous transmission technology are clearly among the hottest topics among existing transportation systems. Self-driving vehicles will become widespread in the near future, and millions of these vehicles will be on the road (Yao, Chen, Qin, Wu, & Zhang, 2018). High resolution three-dimensional (3D) maps will be primary sources to actively provide essential information to 3D dynamic self-driving vehicles, rather than just being static maps tracking a city's development. In addition, the signs on the road are essential for providing guidance and information to drivers and pedestrians (Soilan, Justo, Sanchez-Rodriguez, & Riveiro, 2020). This will also be important for high-resolution 3D transportation.

There are many measurement technologies available today to produce high-resolution 3D maps (Neupane & Gharaibeh, 2019). Laser scanning is one of the widely used technologies to produce high-resolution 3D maps. Every visible object can be digitized with high resolution in laser scanning.

Mobile LiDAR System (MLS) is a technology that collects 3D dense information around the road while platforms move at average speeds on the road (Yadav & Singh, 2018). Dense point cloud information is a widely used measurement technique with its high accuracy and reasonable price.

3D dense point cloud provides essential information in various research areas such as extracting the road surface, analyzing the road geometry, drive simulation, road maintenance studies, and self-driving autonomous vehicles (Wu, Xu, & Liu, 2019). However, MLS point clouds often contain irregular and noisy points. The 360-degree measurement of the MLS technology also makes it difficult to extract the road surface from the 3D dense point cloud. In addition, further difficulties are encountered in detecting the road surface from MLS point clouds. The irregular and noisy dense point cloud make data pre-processing difficult. Another difficulty is that the traffic flow might be intense and causes both interruptions on road surfaces and an increase of false point in point clouds. Therefore, the road surface extraction from MLS point clouds is an open research field for improvement.

In this study, an accurate and efficient method is presented to automatically extract the road surface from MLS point clouds. Our study's primary steps can be summarized into three steps: 1) collecting MLS data in normal traffic flow, 2) producing 3D dense point cloud in the pre-processing step, 3) introducing a new automated approach to extract road surface points from MLS point clouds.

* **Corresponding Author**

*(mzeybek@artvin.edu.trl) ORCID ID 0000-0001-8640-1443
(serkanbicici@artvin.edu.tr) ORCID ID 0000 – 0002 – 0621 - 9324

**Cite this study**

Zeybek M, Bicici S (2020). Road Surface Extraction from MLS-Based Point Clouds. Intercontinental Geoinformation Days (IGD), 121-124, Mersin, Turkey

The proposed pipeline starts with a pre-processing step to convert the raw data into a dense point cloud. With the help of the trajectory data, non-road scene points, such as buildings and fences, etc. are removed. That is, the number of points is decreased to improve the accuracy and reduce the processing time. Then, non-ground points are removed by applying the cloth simulation filtering (CSF) algorithm (Zhang et al., 2016). Finally, the points of the road surface are extracted using the piecewise linear regression model.

## 2. MATERIAL AND METHODS

Data was collected using the RIEGL VMX-450 system in Konya, Turkey. The MLS system is shown in Figure 1(a). The VMX-450 system includes tools such as two RIEGL VQ450 laser scanners, four optional RGB cameras, a GNSS antenna, an IMU system, and a distance measurement indicator. In the GNSS/IMU system-based measurements, a fixed RTK reference station, whose x, y, and z coordinates were known, was installed, and the GNSS system on the vehicle was made to receive corrections with this RTK reference station. An example of the scanned study area is shown in Figure 1(c). The proposed method has been conducted on an 80 m long study area. The flowchart of the proposed method is presented in Figure 2.

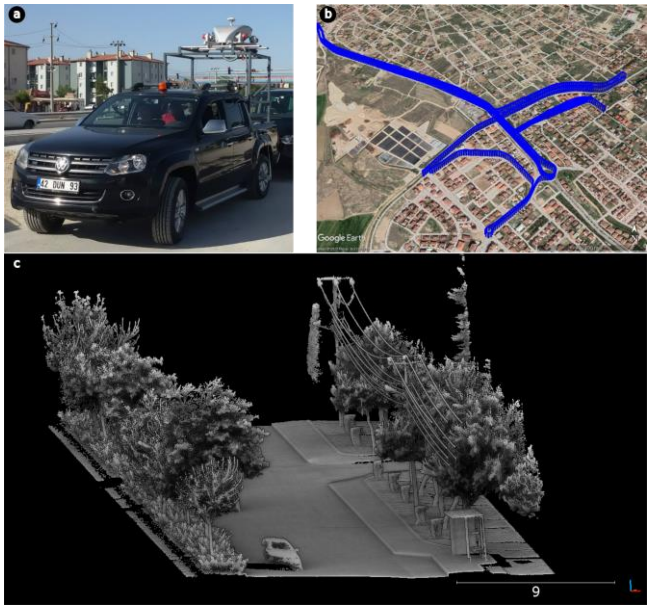


**Figure 1.** a) VMX-450 MLS system, b) trajectory, and c) acquired point cloud data.

### 2.1. Pre-Process

Applanix POSpac software was used to obtain 3D dense point cloud from collected MLS raw data. Processed point clouds were exported in las file format. In order to reduce the processing intensity and the processing time of the proposed method, a 20 m buffer zone covering the road and the road environment was created with the trajectory data provided by the point clouds VMX-450 system. The trajectory data of this study is presented in Figure 1(b). Then, the points that are outside the buffer zone are removed. The buffer threshold should be determined specifically for the road being measured. Wider roads might require larger buffer threshold values. After this pre-processing, both the number of points in the point clouds decreased, which leads to the short processing time for the proposed method.

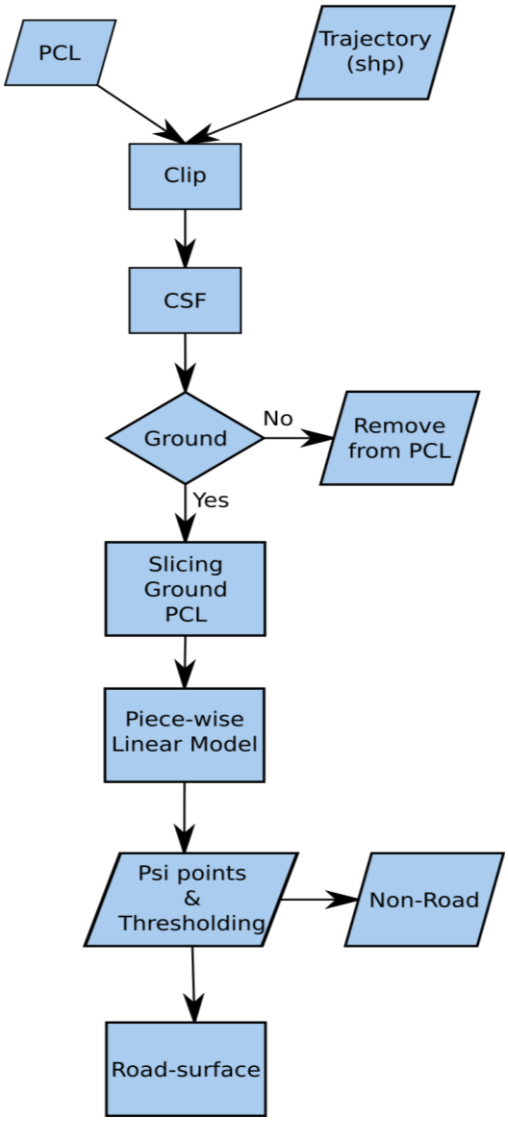


**Figure 2.** Flowchart of the proposed methodology.

### 2.2. Methods

In the proposed method, first point clouds are classified as ground and non-ground. The main reason for this step is that the road surface has to be on ground points. The cloth simulation filtering (CSF) algorithm was used for ground and non-ground classification (Zhang et al., 2016). This algorithm is based on the principle of reversing the point clouds concerning the *Z*-axis and covering with the cloth on it. In this way, points intersect with cloth grids are assigned as ground and non-intersecting points as non-ground. Figure 3 presents the ground and non-ground classification results. The point clouds are divided into cross-sections at 1 m intervals according to GNSS trajectory values. In this study, original coordinates are transformed using principal

component analysis (PCA) to prevent errors and provide straightforward interpretation in cross-sectional analysis.

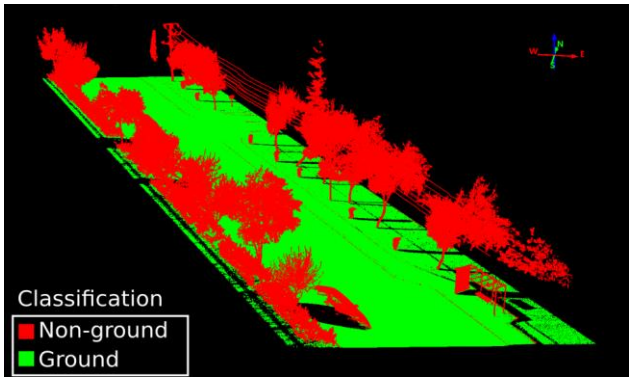


**Figure 3.** CSF-based point cloud classification.

PCA is one of the essential methods for multivariate data analysis (Bruce, Bruce, & Gedeck, 2020). PCA's primary purpose is a dimensional reduction and a commonly used method for calculating linear variables (components). In this study, PCA has been used to calculate a new coordinate system, which is orthogonal and uses only the most fundamental dimensions. Thanks to crucial components from PCA, distances between spatial variables are presented clearly. Figure 4(a) and (b) present the single cross-section with original coordinates and coordinates obtained from PCA, respectively. Finally, road points were extracted by applying piecewise regression over the cross-section points represented by PCA.

Piecewise linear model is a regression model where more than one straight line is fitted (Muggo 2003). These lines are connected to unknown values, which are usually called breakpoints. The piecewise linear relationship between response variable $Y$ and independent variable $X_i$ for observations $i$ = 1, 2, …., n can be defined as follows:

$$Y_i = \boldsymbol{\beta}_1 X_i + \boldsymbol{\beta}_2 (X_i - \boldsymbol{\psi}) \qquad [1]$$

where $\boldsymbol{\beta}_1$ is the left slope, $\boldsymbol{\beta}_2$ is the difference between slopes, and $\boldsymbol{\psi}$ is the breakpoint. $(X_i - \boldsymbol{\psi})$ is equal to $(X_i - \boldsymbol{\psi}) \times I(X_i > \boldsymbol{\psi})$ where I(.) is the indicator function equal to one when the statement is correct. Several software packages estimate the piecewise linear regression model given the data and the number of breakpoints (V. M. Muggeo, 2003). In this study, R software was used to estimate the parameters and breakpoints (Vito MR Muggeo, 2017; Team, 2019).

## 3. RESULTS

There were 5,434,846 points after converting MLS raw test data into a point cloud using Applanix POSpac software. The number of points decreased to 4,096,144 when removing non-essential points using GNSS Trajectory and 20 m buffer value. Then, the CSF algorithm was used to classify ground points, and 3,138,305 ground points were filtered. The point cloud was divided into cross-sections according to orthogonal to the GNSS/Trajectory data using the R software (in-house developed "slicer" package). 80 cross-sections of 1 m width were produced in this study. Figure 5 shows several cross-sections as an example. Finally, points representing the road surface were extracted using the piecewise linear model on these cross-sections.

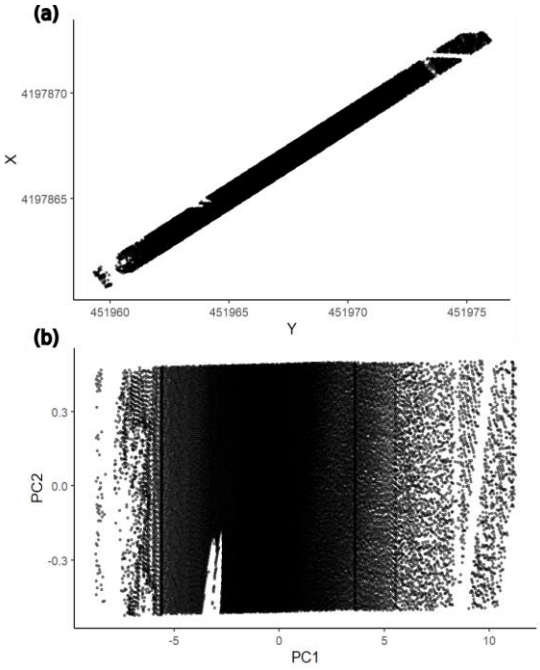


**Figure 4.** PCA employment on cross-sectioned data a) cross-section raw data, b) PCA transformed data.

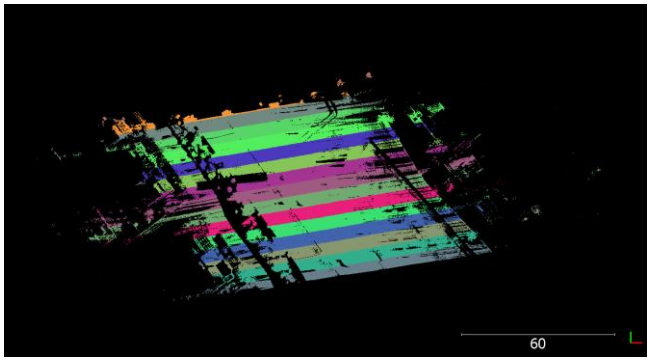


**Figure 5.** Cross-sections according to GNSS/Trajectory on Slicer R codes

The number of breakpoints (psi) to be predicted on the piecewise linear model is given as an input parameter. This value can be used to estimate the best fit in the cross-section data. In cases where psi value is not taken as input, the variable is assumed to be 1. Figure 6 shows the points, and the piecewise linear model results under different psi values. As the number of breaking points increases, the piecewise linear model fits better. Distance-threshold values are defined from these breaking points. Finally, points in between these distance-thresholds are extracted as the road surface—the extracted road surface points estimated as road surface 32,188 points from a single section (40,766).

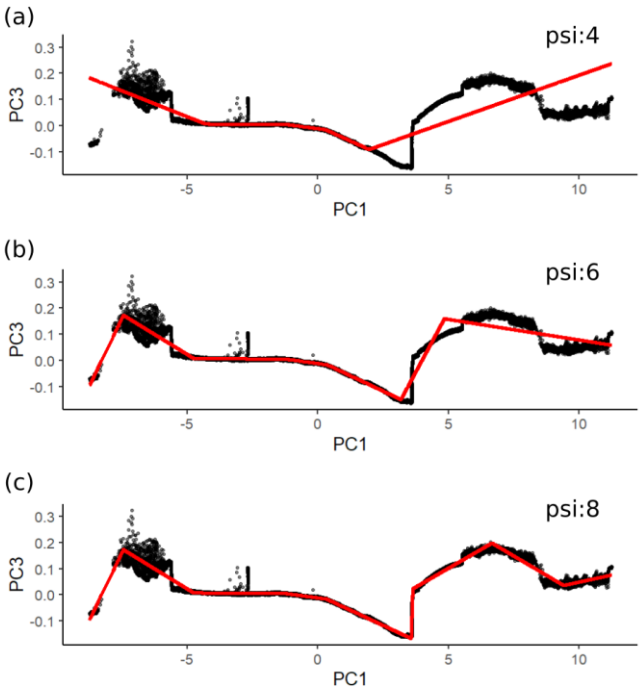


**Figure 6.** Piecewise based linear model on the cross-sectional model.

## 4. DISCUSSION

The orthogonal components of the cross-sections can be improved by using robust PCA methods. The main reason for this is that the PCA method is sensitive to outliers. Outliers are common in dense point cloud data obtained from Mobile LiDAR, and these values overestimate conventional measures of variance. The outlier's points will be in different directions than the directions since the PCA components follow their maximum variance direction. The piecewise linear method is proposed to extract the road surface with the number of breaking points as an input. Then, a distance-based threshold is defined from these breaking points. Under different road geometric conditions, the threshold values may need to be revised to accurately extract the road surface. Therefore, it is better to estimate psi breakpoints automatically in future studies. Besides, leverage points on the piecewise linear model are likely to occur regardless of psi breakpoints. In this case, it is necessary to determine and delete these outlier points from the point cloud with a distance-based threshold value or the clustering algorithms such as DBSCAN or connected component algorithms.

The proposed methodology has been developed for roads with raised curbs in urban areas. Its effectiveness has not been tested on rural roads or roads without a raised curb. Therefore, this method should be tested on different Mobile LiDAR data in a future study.

## 5. CONCLUSION

In this study, it is proposed to extract the road surface automatically from Mobile LiDAR-based point clouds and GNSS/Trajectory data. The Piecewise linear model algorithm was fitted using the points, and the road surface was extracted from the breakpoints in the road segment. The proposed methodology is an alternative and effective method for extracting the road surface using the mobile LiDAR data.

## ACKNOWLEDGEMENT

Acknowledgments of support for the Koyuncu LiDAR Harita Ltd, especially CEO Mustafa Koyuncu, provide Mobile LiDAR point cloud data.

## REFERENCES

Bruce, P., Bruce, A., & Gedeck, P. (2020). *Practical Statistics for Data Scientists: 50+ Essential Concepts Using R and Python*: O'Reilly Media.

Muggeo, V. M. (2003). Estimating regression models with unknown break-points. *Stat Med, 22*(19), 3055-3071. doi:10.1002/sim.1545

Muggeo, V. M. (2017). Interval estimation for the breakpoint in segmented regression: a smoothed score-based approach. *Australian & New Zealand Journal of Statistics, 59*(3), 311-322.

Neupane, S. R., & Gharaibeh, N. G. (2019). A heuristics-based method for obtaining road surface type information from mobile lidar for use in network-level infrastructure management. *Measurement, 131*, 664-670. doi:10.1016/j.measurement.2018.09.015

Soilan, M., Justo, A., Sanchez-Rodriguez, A., & Riveiro, B. (2020). 3D Point Cloud to BIM: Semi-Automated Framework to Define IFC Alignment Entities from MLS-Acquired LiDAR Data of Highway Roads. *Remote Sensing, 12*(14). doi:10.3390/rs12142301

Team, R. C. (2019). R: A Language and Environment for Statistical Computing In *R Foundation for Statistical Computing* (Vol. Vienna, Austria).

Wu, J. Q., Xu, H., & Liu, W. (2019). Points Registration for Roadside LiDAR Sensors. *Transportation Research Record, 2673*(9), 627-639. doi:10.1177/0361198119843855

Yadav, M., & Singh, A. K. (2018). Rural Road Surface Extraction Using Mobile LiDAR Point Cloud Data. *Journal of the Indian Society of Remote Sensing, 46*(4), 531-538. doi:10.1007/s12524-017-0732-4

Yao, L., Chen, Q., Qin, C., Wu, H., & Zhang, S. (2018). Automatic Extraction of Road Markings from Mobile Laser-Point Cloud Using Intensity Data. *ISPRS - International Archives of the Photogrammetry, Remote Sensing and Spatial Information Sciences, XLII-3*, 2113-2119. doi:10.5194/isprs-archives-XLII-3-2113-2018

Zhang, W. M., Qi, J. B., Wan, P., Wang, H. T., Xie, D. H., Wang, X. Y., & Yan, G. J. (2016). An Easy-to-Use Airborne LiDAR Data Filtering Method Based on Cloth Simulation. *Remote Sensing, 8*(6), 501. doi:10.3390/rs8060501

Intercontinental Geoinformation Days

http://igd.mersin.edu.tr/2020/

# Spatial accuracy analysis of Sentinel-1 SAR satellite images by comparing maps

**Tevfik Fikret Horzum*[1], Nusret Demir [2], Ali Kılçık [2]**

[1]*Akdeniz University, Vocational School of Technical Sciences, Dep. of Architecture and Urban Planning, Antalya, Turkey*
[2]*Akdeniz University, Faculty of Science, Department of Space Sciences and Technologies, Antalya, Turkey*

**Keywords**
Remote sensing
Sentinal-1(SAR)
Open Street Map(OSM)
Photogrammetric Digital Map (PDM)
Standard Deviation

**ABSTRACT**

Synthetic Aperture Radar (SAR) images are used in several different applications for Remote Sensing purposes. SAR is an imaging sensor that can detect high-resolution ground images under a wide variety of imaging conditions. As SAR is an active system, the data are already acquired with geo-position information. To investigate to verify the image spatial accuracy, a part of the Antalya region of Turkey was selected as test site. The Open Street Map (OSM) and Photogrammetric Digital Map (PDM) data of the area on the Antalya O25 map were used in comparison. First, characteristic common points were selected on the OSM data and the SAR satellite image both. The projected coordinates of these points were calculated with the QGIS software. Normal distribution of the coordinate differences in these data sets were plotted. It was confirmed that the data sets were in normal distribution and standard deviation and 2 * standard deviation values were calculated. The maximum and minimum confidence interval (95%) was determined according to the standard deviation limit values. X and Y coordinate differences were calculated for 49 selected points from both image pairs SAR&OSM and SAR&PDM. Finally, the maximum differences show that the SAR positional accuracy respect to OSM and PSM is below 1 pixel azimuthal resolution.

## 1. INTRODUCTION

Synthetic Aperture Radar (SAR) images are used in applications for Remote Sensing purposes. SAR data is an imaging sensor that can detect high-resolution ground images under a wide variety of imaging conditions (Demirci 2005). To investigate the accuracy of this receiver, the Antalya region test area was chosen.

The OpenStreetMap (OSM) and Photogrammetric Digital Map (PDM) data of the area on the Antalya map were used in comparison. It is also part of the open data movement.

OSM is used as a basic or data source in many websites and mobile applications (Ünen 2013). The attribute accuracy and positional accuracy (51.5%) of OSM data in the Wuhan region of China were determined (Wang 2015). In Turkey has made similar studies. For example (Çabuk 2015) 1: 50.000 scale OSM dataset is not enough to support the production process alone, when used with production. It has been observed that it will increase the quality.

Photogrammetric Digital Maps(PDM) are made for the use of public institutions and organizations and to provide data to the Geographical Information System (GIS). The accuracy analysis of Photogrammetric Digital Maps was carried out within the provincial borders of Erzincan (Kara 2019), the horizontal coordinate average was calculated as 6cm and the vertical coordinate average 10cm.

Synthetic Aperture Radar; S1A data products are already consistently providing highly accurate geolocation (Schubert 2015). Thus, we tried to expolore the spatial accuracy of Sentinel 1 SAR data in respect to the available existing sources OSM and PDM.

First of all, characteristic common points were determined on these data sets. 55 points were used in each data set. These points are building corners, road intersections, etc. Geographical coordinates system and perpendicular coordinates system of the selected points were calculated with the QGIS software. The QGIS Python software plug-in was used in the calculation process. This data was put into the process as raw data. The orthogonal coordinates of the raw data and the

* **Corresponding Author**

*(fhorzum@akdeniz.edu.tr) ORCID ID 0000-0003–4898–5999
(nusretdemir@akdeniz.edu.tr) ORCID ID 0000–0002–8756–7127
(alikilcik@akdeniz.edu.tr) ORCID ID 0000 –0002 –0094 –1762

**Cite this study**

Horzum T F, Demir N & Kılcık A (2020). Spatial accuracy analysis of Sentinel-1 SAR Satellite images by comparing maps. Intercontinental Geoinformation Days (IGD), 125-129, Mersin, Turkey

coordinate differences between the OSM and the SAR data and the PDM and the SAR data coordinate differences were found. It was decided that the data showed a normal distribution (Chart 1 & Chart 2).

Standard deviation and 2*Standard deviation values were calculated in the second step in order to remove the erroneous data points in these raw data. Maximum and minimum confidence intervals (95%) were determined according to the 2*Standard deviation limit values. Thus, erroneous data points were removed and 49 error-free data points were obtained in each data set. Coordinate differences (Ya-Yc) of 49 common points in OSM and SAR data set; Coordinate differences (Yd-Yc) of (Xa-Xc) and 49 common points in PDM and SAR data set; (Xd-Xc) were calculated separately. The standard deviations of these coordinate differences were 11.646m, 7.842m and 10.520m, and 8.438m, respectively.(Table1 & 2) Coordinate difference graphs and location graphs of these data sets were drawn. Finally, according to the comparison in these two data sets, it is understood that the SAR image data is have about 20m accuracy.

## 2. MATERIALS

In this study, Antalya is selected as a test site as shown in Figure 1. The used datasets are Sentinel 1 SAR image, OpenStreetMap(OSM) and photogrammetric digital map (PDM) which was provided by Municipality of Antalya.

Sentinel 1 has C band RADAR sensor, operated by European Space Agency, and the respective data can be provided from Copernicus data hub. The data have Range and Azimuth resolution 20x22 m respectively. They are provided with 10 m pixel spacing through Ground Range Detected (GRD) file format.

OSM is an online geodatabase with OpenData Commons license in the background (Çabuk 2015). OpenStreetMap is a dataset service, created by a OpenStreepMap Foundation that provide data about revery kind of features in the Earth. PDM dataset is created by Antalya Municipality with 1/5000 scale.

The accuracy of dataset is depending on the used data source (e.g. Satellite imagery, mainly optical) and the digitizer accuracy.

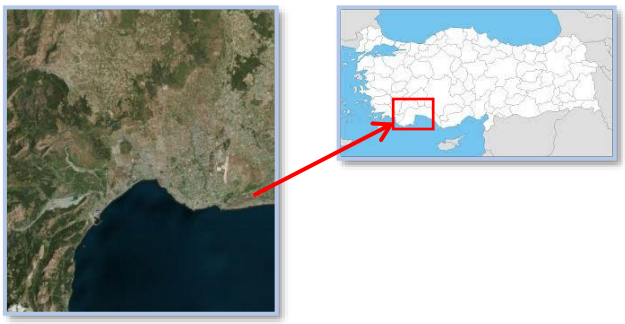

**Figure 1. Study Area**

## 3. METHOD

In this study, QGIS (3.12) and SNAP (7.0) software developed by ESA were used to evaluate the data in the study area. QGIS software is a multi-platform free and open source Geographic Information System (GIS) software that provides data viewing, editing, and analysis capabilities. SNAP software, on the other hand, is a common software called Sentinel Application Platform (SNAP) and is developed for fast viewing, layer management, geocoding and correction using ground control points.

The Subset calibration, Speckle filtering and Geometric correction procedures were applied to the SAR Sentinel-1 Satellite data in the SNAP program.

55 identical point data were selected from OSM (A) and SAR Sentinel-1 satellite data (C). OSM data (A) and SAR (C) data of the study area were registered using the QGIS program.

Orthogonal Coordinates were obtained with Python code software according to TUREF TM 30 reference information.

In the first step, the coordinate differences of these 55 data sets (Ya-Yc) and (Xa-Xc) were calculated and the histogram graphs of these coordinate differences were drawn. (Chart 1 & Chart 2)

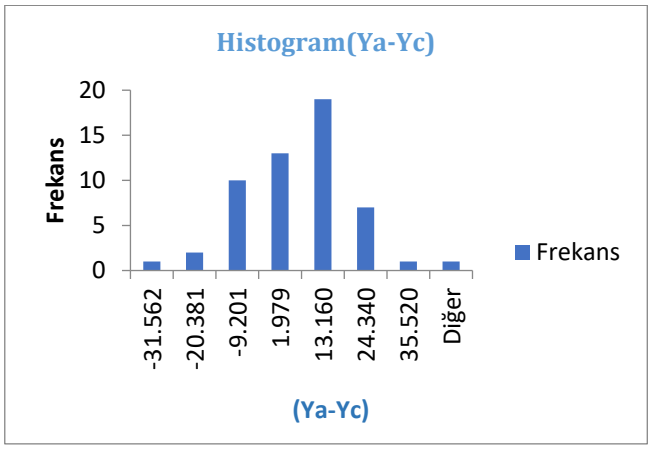


**Chart 1.** (Ya-Yc) Coordinate Differences Histogram

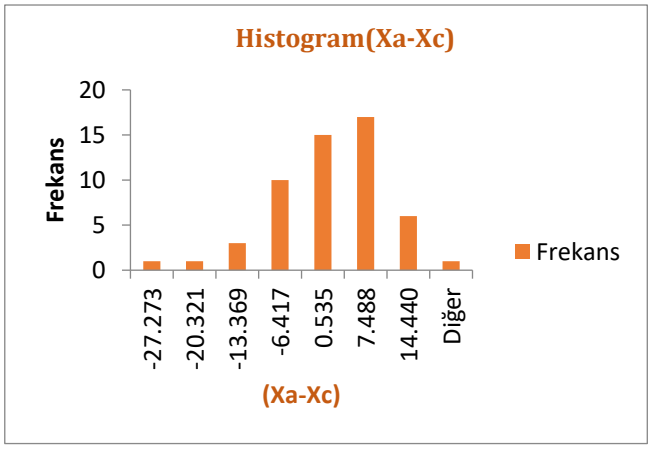


**Chart 2.** (Xa-Xc) Coordinate Differences Histogram

In the second step, 55 points were used in comparison of SAR (C) and PDM (D) data. These common points (Yd - Yc) and (Xd - Xc) coordinate differences were calculated and histogram graphics were drawn. (Chart 3 & Chart 4)

OSM (A), SAR (C) and PDM (D) data sets were determined to be in normal distribution.

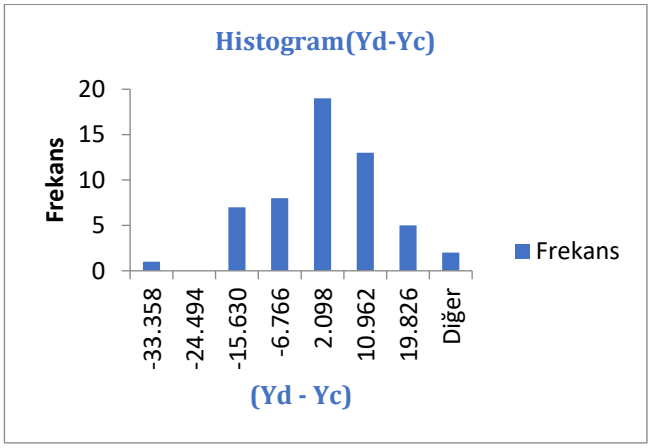


**Chart 3.** (Yd-Yc) Coordinate Differences Histogram

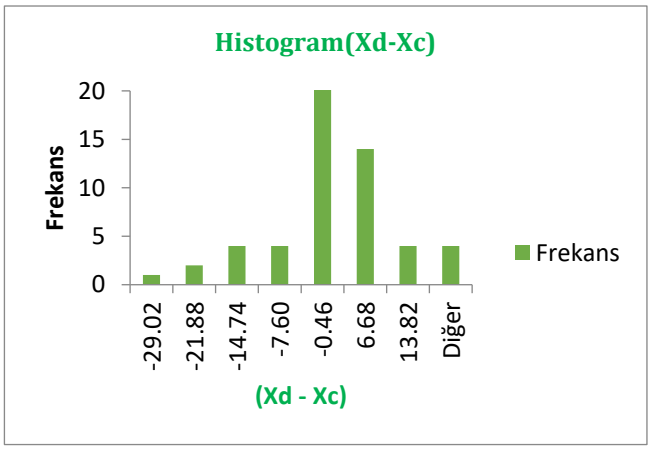


**Chart 4**. (Xd-Xc) Coordinate Differences Histogram

## 4. RESULTS

OSM data (A) and SAR (C) data set were determined to be normally distributed. The mean value of the (Ya - Yc) and (Xa - Xc) coordinate differences and standard deviation values were calculated. The standard deviation according to the 2 * standard deviation value (95%) is the minimum and maximum limit values have been determined and 49 error-free points were found to be compatible. (Table 1)

$$(\bar{X} - 2\sigma) \leq \mu \leq (\bar{X} + 2\sigma)$$

The standard deviation is 11.646m in the (Ya-Yc) differences and 7.842m in the (Xa-Xc) differences. In addition, according to the 2 * Standard Deviation limit values, in (Ya-Yc) differences; in the range of [-22.730m to 23.855m] and (Xa-Xc) differences; values have been reached in the range of [-17.216m to 14.152.86m]. (Table 1)

**Table 1.** Calculation Summary of 49 error-free point

| Calculation 1 | [Ya-Yc] m | [Xa-Xc] m |
|---|---|---|
| Ortalama | 0.563 | -1.532 |
| Std.Sapma | 11.646 | 7.842 |
| 2*Std.Sapma | 23.293 | 15.684 |
| Minimum | -22.730 | -17.216 |
| Maximum | 23.855 | 14.152 |

In this case, the percentage error rates [(Ya-Yc)/ Ya]*100 and [(Xa-Xc)/Xa]*100 of the difference values of the 49 points were calculated and found that it varies between [-0.004 to +0.004] and [-0.001 to +0.001], respectively.

The difference and position graphs of remaining 49 points were drawn. (Chart 5 & Chart 6)

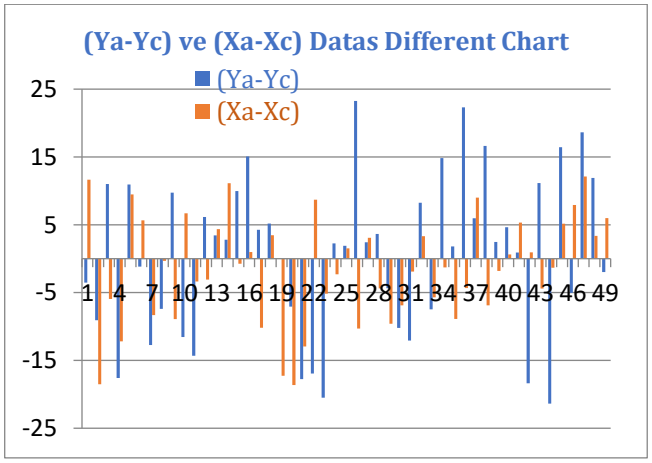


**Chart 5.** OSM and SAR data error free plot of coordinate differences of points.

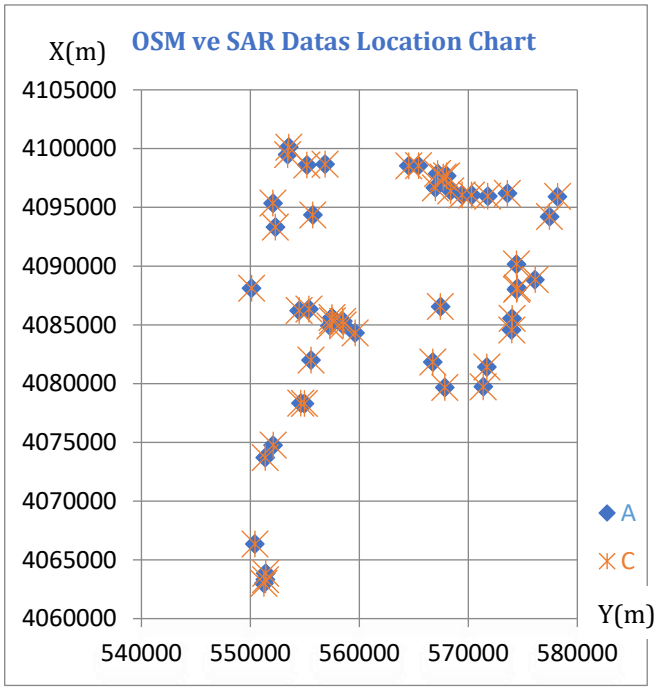


**Chart 6.** OSM and SAR data error free position graph of points.

It was decided that the PDM (D) and SAR (C) data set showed normal distribution. The average value of the (Yd - Yc) and (Xd - Xc) coordinate differences and standard deviation values were calculated. The standard deviation according to the 2 * standard deviation value (95%) is the minimum and maximum limit values have been determined and 49 error-free points were found to be compatible. (Tablo.2)

$$(\bar{X} - 2\sigma) \leq \mu \leq (\bar{X} + 2\sigma)$$

The standard deviation was 10.520m in the (Yd-Yc) differences and 8.438m in (Xd-Xc) differences. In

addition, according to the 2 * Standard Deviation limit values, in (Yd-Yc) differences; in the range of [-22.044m to 20.035m] and (Xd-Xc) differences; values in the range of [-18.298m to 15.452m] have been reached. (Table 2)

**Table 2.** Calculation Summary of 49 error-free point

| Calculation 2 | [Yd-Yc] m | [Xd-Xc] m |
|---|---|---|
| Ortalama | -1.004 | -1.423 |
| Std.Sapma | 10.520 | 8.438 |
| 2*Std.Sapma | 21.040 | 16.875 |
| Minimum | -22.044 | -18.298 |
| Maximum | 20.035 | 15.452 |

In this case, the percentage error rates of the difference values of 49 points were calculated using the formulas [(Ya-Yc) / Ya] * 100 and [(Xa-Xc) / Xa] * 100 and found that it varies between [-0.004 to +0.004] and [-0.001 to +0.001], respectively

The difference and position graphs of remaining 49 points were drawn. (Chart 7 & Chart 8)

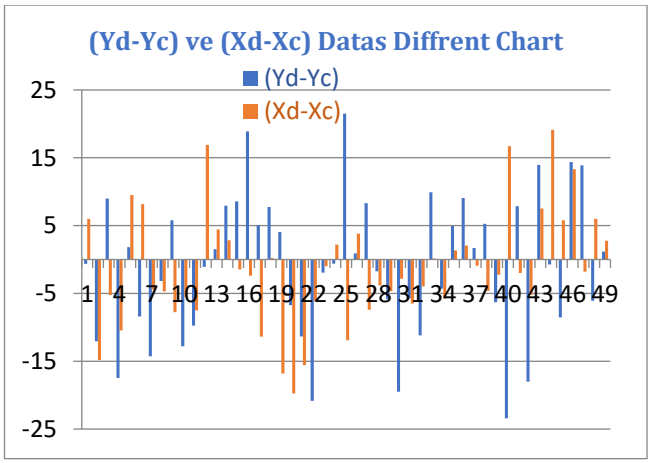


**Chart 7.** PDM and SAR data error free plot of coordinate differences of points.

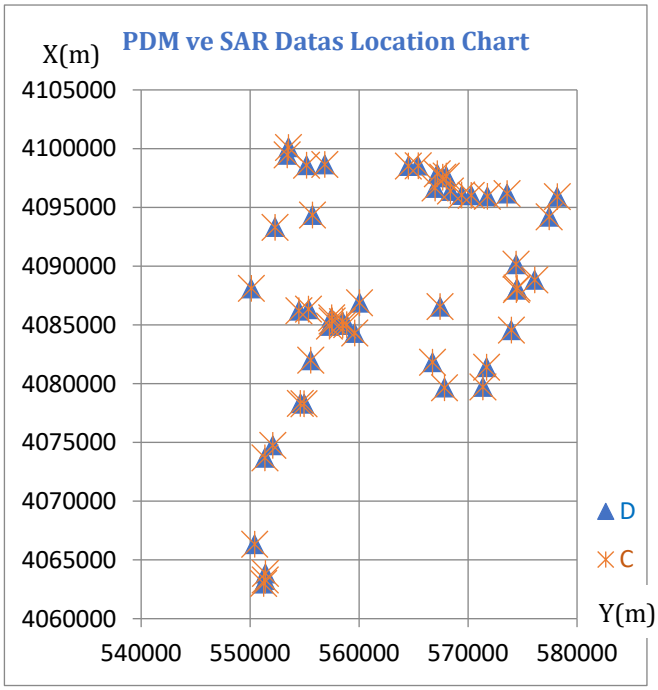


**Chart 8.** PDM and SAR data error free position graph of points.

Finally, a graph is drawn showing the coordinate difference values of both data sets. In both comparisons, it was observed that 95% of the coordinate differences were within the ± 25 m radius circle. The ratio of the (Yd-Yc) and (Xd-Xc) coordinate differences of the blue points within the ± 10m circle to all blue points is 53.1%, the coordinate differences (Ya-Yc) and (Xa-Xc) of the orange points within the ± 10m circle are its ratio compared to orange spots is 36.7%. (Chart 9)

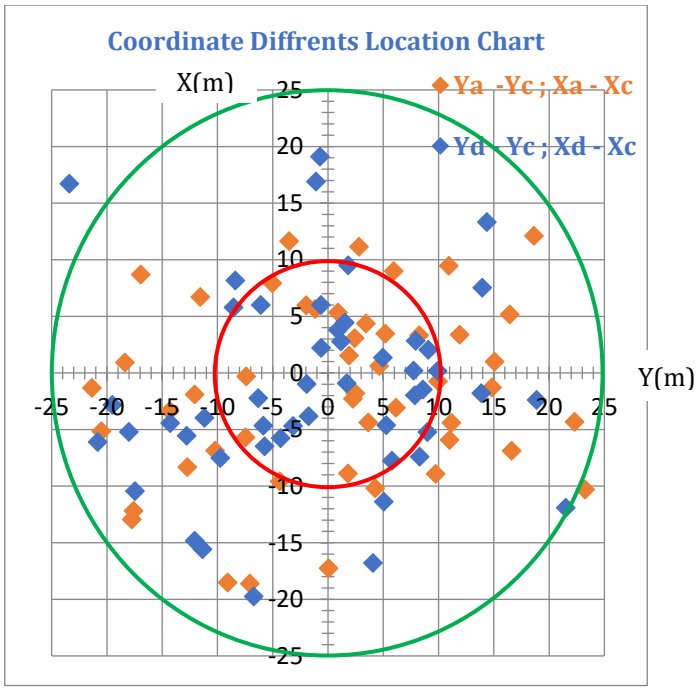


**Chart 9.** Location graph created according to OSM, PDM and SAR coordinate differences.

## 5. CONCLUSIONS

In the study of the spatial accuracy of Sentinel-1 SAR satellite images, Open Street Map (OSM) and Photogrammetric Digital Map (PDM) data were used for comparison. Open Street Map (OSM) and Photogrammetric Digital Map (PDM) data sets were used as precise data and SAR satellite data as experimental data set.

55 points were used to compare OSM (a), SAR (c) and PDM (d) data sets. 6 pieces of data were excluded from each data set because they were incompatible. Coordinate differences were calculated with 49 points in the comparison of the data sets without error on OSM (A), SAR (C) and PDM (d). Average and standard deviation values were found. The minimum and maximum values were determined according to the value of 2 * standard deviation (95%).

It was observed that the coordinate differences (Yd-Yc) and (Xd-Xc) were represented better than the coordinate differences (Ya-Yc) and (Xa-Xc) within the ± 10m radius circle.

As a result, it is concluded that SAR data with an maximum difference with 20m well fit with other data sources OSM and PDM.

**ACKNOWLEDGEMENT**

We, authors acknowledge Antalya Metropolitan Municipality for the Photogrammetric Digital Map data.

**REFERENCES**

Atak V.O (2019) Geospatial Accuracy of Google Earth Imagery Map Magazine, January 2019; 161: 11-25

Çabuk S, Erdoğan M & Önal E (2015) Researching of 1/50K Scaled Map Producibility Using Open Street Map Data. Map Magazine July 2015 Issue 154

Çabuk S, Erdoğan M, Eker O, Kaya M, Ardıç H&Önal E (2015) Use of OpenStreetMap Data In Topographic Data Production. TUFUAB VIII. Technical Symposium 21-23 May 2015 / Konya

Çakıcı M. (2000) Basic statistics 1. and 2. Hardback ISBN: -975-93705-0-6

Demirci Ş. (2005) Elimination of Unwanted Echoes in Sentinel Aperture Radar (SAR) Images Mersin University, Institute of Science. (in Turkish).

Demirel A. Ş (2002) Radarsat Images Spatial Investigation of Accuracies İTÜ Institute of Science. (inTurkish).

Kara G & Kemaldere H. (2019). Accuracy Analysis of Photogrammetric Digital Topographic Mapping, TMMOB Chamber of Survey and Cadastre Engineers, 17th Turkey Scientific and Technical Conference, 25-27 April 2019 in Ankara.

Schubert, A. Small, D. Miranda, N. Geudtner, D. & Meier, E. (2015). Sentinel-1A Product Geolocation Accuracy: Commissioning Phase Results. Remote Sensing. 7. 9431-9449. 10.3390/rs70709431.

Ünen HC, Yılmaz OM & Güngör O (2013) Free Map: OpenStreetMap. TMMOB Geographical Information System Congress_11-13 November 2013, Ankara

Üstüner M, Balık F.B, Abdikan S & Bilgin G(2017) Land Use and Cover Classification of Sentinel-1A SAR Imagery: A Case Study of Istanbul 978-1-5090-6494-6/17/ ©2017 IEEE

Wang M, Li Q, Hu Q & Zhou M. (2013) Qualıty Analysis of Open Street Map Data. International Archives of the Photogrammetry, Remote Sensing and Spatial Information Sciences, Volume XL-2/W1, 2013 8th International Symposium on Spatial Data Quality, 30 May - 1 June 2013, Hong Kong

Intercontinental Geoinformation Days

http://igd.mersin.edu.tr/2020/

# Comparison of NDT and ICP Method's point cloud registration performance

**Ramazan Alper Kuçak[1], Mahmut Oğuz Selbesoğlu[1], Serdar Erol[1]**

[1] *İstanbul Technical University, Faculty of Civil Engineering, Department of Geomatics Engineering, İstanbul, Turkey*

**Keywords**
Lidar
ICP
NDT
Point Cloud
Accuracy

**ABSTRACT**

The point cloud registration approaches are the key problem for three-dimensional reconstruction in reverse engineering, computer vision, cultural heritage and other fields. The Iterative Closest Point (ICP) is widely used in registering of point clouds in various fields of application. Furthermore, the performance of the Normal Distribution Transform (NDT) method directly depends on the selected cube cell size for the data. Choosing the optimum cell size is a challenging problem and there is no proved way for all cases. However, NDT has several advantages over ICP for data storage and speed. The main purpose of the study is to investigate the performance of NDT and ICP algorithms on point cloud registration. For this purpose, a sample dataset was used for comparative assessment. In the study, the fine registration analysis carried out for two different initial distances between point clouds as 10 cm and 5 cm. According to the results, NDT algorithm produced slightly lower root mean square error (RMSE) value for 10 cm initial alignment distances than ICP method while the ICP method produce lower RMSE value for 5 cm initial alignment distance. However, the calculated mean distances between the point clouds after registration demonstrate that the NDT method provides better results than the ICP method for this test data.

## 1. INTRODUCTION

Point clouds produced by Lidar (Light Detection and Ranging) or photogrammetric measurement methods are used in many 3D modeling studies. However, the point cloud registration approaches are essential steps in the integration of multi-platforms data (Cheng et al., 2018).

A registration process consists of two main steps: initial alignment (Initial registration) and fine registration (Yoshimura et al., 2016). Registration steps are for producing of 3D absolute modeling. So many scans of the object are required and these scans need to be registered for accurate modeling. However, fine registration starts after the coarse initial registration to achieve more accurate registration of the point clouds (Fangning and A. Habib, 2016). A fine registration procedure can be segmented into four sections and the most important part is a successfully performed initial registration (Fangning and A.Habib, 2016). Second step is the selecting of corresponding points, third is the estimation of transformation parameters between point clouds and last step is RMSE calculation according to threshold or given iteration number. The most widely used registration point cloud algorithm is the iterative closest point (ICP) that was first proposed by (Besl & McKay, 1992). It searches for the optimal matching of two point clouds by constantly searching for the optimal rigid body transformation matrix. However, if the initial position of point cloud data set varies greatly, ICP algorithm can fall into the local optimal solution. A new point cloud registration algorithm based on the NDT method can be used for special cases (Biber & Straßer, 2003; Magnusson, 2009).

In this study, ICP and NDT algorithms were analyzed in terms of RMSE and, the "cloud to cloud" mean distances after registration was compared. Also, Sample point cloud data in Matlab environment was used to compare the two fine registration algorithm.

## 2. METHOD

Iterative Closest Point (ICP) algorithms and its variants are often used for the fine registration (Besl & McKay, 1992). However, another preferred method for the registration problem is the 3D least squares surface matching (Gruen & Akca, 2005). The method depends on Least Squares 2D image matching. Magnusson et al. 2009

* **Corresponding Author**

*(kucak15@itu.edu.tr) ORCID ID 0000-0002-1128-1552
(selbesoglu@itu.edu.tr) ORCID ID 0000-0002-1132-3978
(erol@itu.edu.tr) ORCID ID 0000-0002-7100-8267

**Cite this study**

Kuçak R A, Selbesoğlu M O, Erol S (2020). Comparison of NDT and ICP Method's point cloud registration performance, 130-133, Mersin, Turkey

used NDT to register 3D point clouds. The advantage of this method is that it does not need to find the corresponding point, because it uses a set of Gaussian distribution to describe the point cloud.

### 2.1. ICP

ICP technique has many variations in point cloud studies. But, in the description of the main algorithm (Besl & McKay, 1992), a "data" shape P is registered to be in best alignment with a "model" shape X .(Besl & McKay, 1992)

The distance "E" between a single data point $\vec{p}$ and model point $\vec{x}$, belongs to point cloud model X, is shown as below (Equation 1) :

$$E(\vec{p}, X) = \min_{\vec{x} \in X} = \|\vec{x} - \vec{p}\| \quad (1)$$

The closest point in X that yields the minimum distance is represented. After calculating the closest point, the nearest points are calculated for each point in P according to the corresponding point Y. The least squares registration is computed with $Q$ operator as described below (Equation 2):

$$(\vec{q}, E) = Q(P, Y) \quad (2)$$

The positions of the aligned point set are updated by applying the registration vector to the point set P. The iteration is initialized by adjusting $P_0$ = P. The registration vectors are defined according to the initial points $P_0$ so that the final registration represents the 3D absolute transformation.(Besl & McKay, 1992)

The algorithm proceeds as follows:

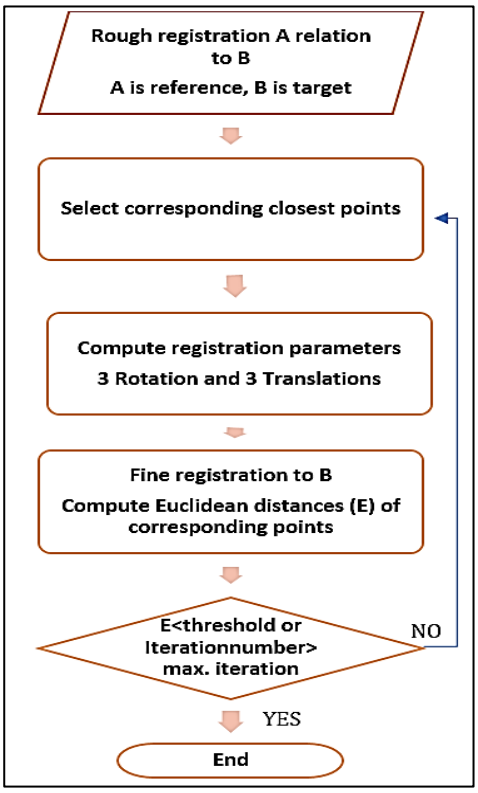


**Figure 1.** ICP algorithm process steps

When the RMSE change falls below a predetermined threshold ("t">0), it ends the iteration to indicate the desired sensitivity of the recording: $E_k$ — $E_{k+1}$ < "t". (Figure 1)(Besl & McKay, 1992)

### 2.2. NDT

The three-dimensional point cloud model is divided into cube cells with equal shape and size in NDT approach. Each cell contains at least six point cloud data and the distribution of point clouds for each cell estimated by normal distribution method by following equation (Magnusson, Nuchter, Lorken, Lilienthal, & Hertzberg, 2009).

$$P(x) = -\frac{1}{c}\exp\left[-\frac{(x-q)^T C^{-1}(x-q)}{2}\right] \quad (3)$$

Once the two point clouds to be matched are obtained, the first transformation matrix T is calculated using the odometer reading method, and then the data in the target point cloud can be converted into the reference point cloud by rotating the transformation matrix T (Equation 4). The probability distribution of each point to be matched is evaluated as the fraction value of each coordinate transformation parameter T by following formula.

$$s(p) = \sum_{i=1}^{n} \exp\left[-\frac{(x_i - q_i)^T C^{-1}(x_i - q_i)}{2}\right] \quad (4)$$

Where c is a constant and is determined by requiring that the probability mass of p equals one within the space spanned by a cell, x represents the point in the cube cell, q is the mean vector of points in the cube cell and C represents the covariance matrix of points (Equation 3&4).

## 3. RESULTS

In the case study, in order to evaluate the registration accuracy, two different initial alignment distances between point clouds as 10 cm and 5 cm were determined. The sample dataset in Matlab software was used in the study and the dataset was given in Figure 2. The performance of the algorithms was evaluated in terms of point to point cloud distances for two different initial distances. Moreover, the RMSE values of the registration process was also evaluated in order to determine the performance of both algorithms.

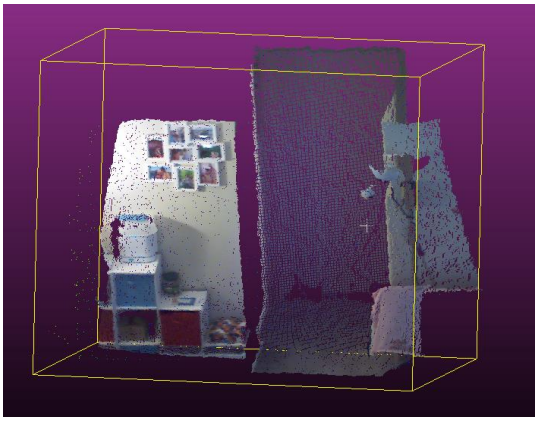

**Figure 2.** Living Room Point Cloud in Matlab

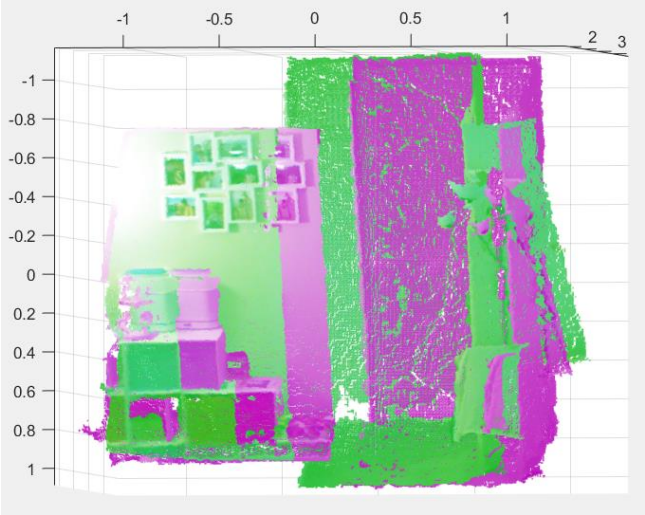


**Figure 3.** The point cloud of the living room1 and the living room 2 with 10 cm initial alignment in Matlab.

Figure 3 shows point cloud data aligned with 10 cm. The point clouds aligned with 5 cm are not much visually different in the Matlab environment, so the differences of only 10 cm are shown.

Two different initial alignment distances as about 10 cm and 5 cm were determined and they have been registered with the ICP and NDT methods. Two different comparisons were made in terms of RMSE values of fine registration and mean distance differences between two different surfaces as a result of registration. The mean distance differences between two different point clouds were made with the Cloud Compare Software (Figure 4 & 5). In the ICP method, while the RMSE is 0.0677 m and the mean distance is 0.0480 m for 10 cm alignment, the RMSE is 0.0519 m and the mean distance is 0.033 m for the 5 cm alignment (Figure 4, and Table 1).

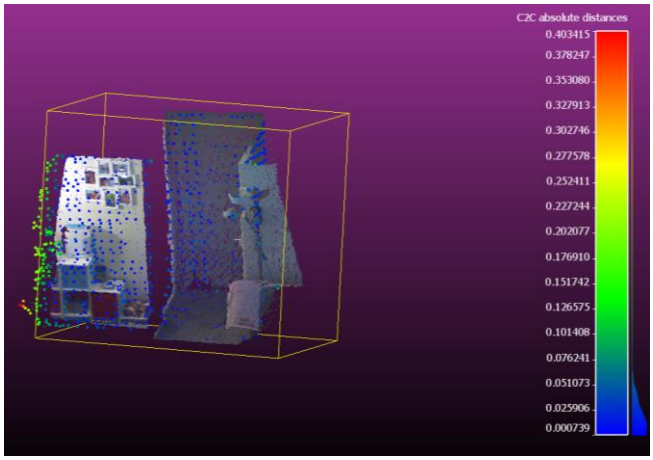


**Figure 4:** The mean surface differences after ICP registration

In the NDT method, while, the RMSE is 0.0625 m and the mean distance is 0.0365 m for 10 cm alignment, the RMSE is 0.0531 m and the mean distance is 0.0273 m for the 5 cm alignment (Figure 5 and Table 1).

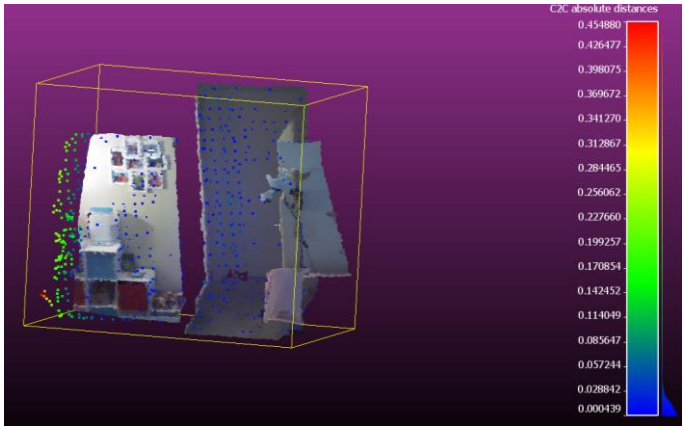


**Figure 5.** The mean surface differences after NDT registration

According to the results, NDT algorithm produced slightly lower root mean square errors for 10 cm initial alignment distances than ICP method while the ICP method produce lower RMSE values for 5 cm initial alignment distance. Briefly, if the initial alignment is given properly, ICP is better results as RMSE values. However, the mean distances between point clouds after registration was calculated by cloud to cloud compare demonstrate that the NDT method provides better results than ICP method for this data. But, the results are very close to the ICP.

**Table 1.** RMS values and C2C mean distance/standard deviation

| Statistics | ICP(10 cm) | ICP(5 cm) | NDT(10 cm) | NDT (5 cm) |
|---|---|---|---|---|
| RMS (m) | 0.0677 | 0.0519 | 0.0625 | 0.0531 |
| C2C (m) | 0.0480 | 0.0333 | 0.0365 | 0.0273 |

## 4. DISCUSSION

In this study, ICP and NDT registration algorithms were compared and sample point cloud data in Matlab environment was used to compare the two registration algorithm. The result shows that NDT and ICP make correct matches if the initial alignment is given properly. ICP differs from the NDT in terms of the approaches that use point to point transformation. Since NDT has advantages in terms of speed and data storage over ICP due to its algorithm that uses voxels, it can be used for cases such as robotic or autonomous driving applications that needs to be faster (Magnusson, M, 2009). In overall assessment, NDT produced slightly better results than ICP for the datasets which has initially aligned as 10 cm. For 5 cm initially aligned data, the ICP's RMSE value obtained lower than the NDT method. It can be gathered from the results that if the initial alignment is given correctly, ICP will give better results as RMSE values. According to the analysis based on cloud to cloud distances, NDT method provides better results for both initial distances than the ICP method. According to the results obtained from the study, both methods can be used for fine registration.

## 5. CONCLUSION

ICP can always reach the correct match, if the initial alignment is given properly. On the other hand, NDT has advantages over ICP in terms of data storage and speed. Therefore, it can be said that each of these methods has both advantages and disadvantages and one unique registration technique cannot recommendable. The success of the registration methods is differs according to the structure and density of the point cloud and especially depend on the initial alignment. So the methods that to be used should be determined by experience in this field.

In the future, these methods will be compared with larger and different data-sets and the accuracy of these methods will be evaluated.

## REFERENCES

Besl, P. J., & McKay, N. D. (1992). Method for registration of 3-D shapes. Paper presented at the Robotics-DL tentative.

Biber, P., & Straßer, W. (2003). The normal distributions transform: A new approach to laser scan matching. Paper presented at the Proceedings 2003 IEEE/RSJ International Conference on Intelligent Robots and Systems (IROS 2003)(Cat. No. 03CH37453).

Cheng, L., Chen, S., Liu, X., Xu, H., Wu, Y., Li, M., & Chen, Y. (2018). Registration of Laser Scanning Point Clouds: A Review. Sensors (Basel, Switzerland), 18(5), 1641. https://doi.org/10.3390/s18051641

Fangning, H., & Ayman, H. (2016). A closed-form solution for coarse registration of point clouds using linear features. Journal of Surveying Engineering, 142(3), 04016006.

Gruen, A., & Akca, D. (2005). Least squares 3D surface and curve matching. ISPRS Journal of Photogrammetry and Remote Sensing, 59(3), 151-174.

Magnusson, M. (2009). The three-dimensional normal-distributions transform: an efficient representation for registration, surface analysis, and loop detection. Örebro universitet.

Magnusson, M., Nuchter, A., Lorken, C., Lilienthal, A. J., & Hertzberg, J. (2009). Evaluation of 3D registration reliability and speed-A comparison of ICP and NDT. Paper presented at the 2009 IEEE International Conference on Robotics and Automation.

Yoshimura, R., Date, H., Kanai, S., Honma, R., Oda, K., & Ikeda, T. (2016). Automatic registration of MLS point clouds and SfM meshes of urban area. Geo-spatial Information Science, 1-11.

## Smart Cities

Intercontinental Geoinformation Days

http://igd.mersin.edu.tr/2020/

# Industry 4.0, Smart Cities, and Urban Transformation

**Yuksel Boz**[*1], **Tayfun Cay** [2]

[1]*Hacettepe University, Faculty of Engineering, Department of Geomatics Engineering, Ankara, Turkiye*
[2]*Konya Technical University, Faculty of Engineering and Nature Sciences, Department of Geomatics Engineering, Konya, Turkiye*

**Keywords**
Industry 4.0
Smart city
Urban transformation
Digital technology
ICT

**ABSTRACT**

We are experiencing the effects of the fourth industrial revolution (Industry 4.0) on our daily life to a greater extent everyday as getting involved in the digital technologies by using internet from different devices (e.g. smart phones, tablet PCs, smart watches). It is not only the people make use of these technologies, cities are also meeting with the advanced technologies and striving for providing better services to their habitants. Moreover, automation is getting widely used in technology-intense sectors as the digitization increases and the automation supersedes the labor force. This situation could destroy the economies of the countries, especially that are based on labor-intensive commodities and services. On the other hand, the adaptation and implementation of technological advancements is an important factor affecting the competitiveness of the cities. Smart city concept came in to the picture as a consequence of the fourth industrial revolution. The number of cities employing smart solutions has shown an increase in the past few years so that they can manage their resources more effectively and improve their service quality. It is inevitable now to imagine an urban transformation, no matter it is a renewal, redevelopment, etc., without making use of digital technologies.

## 1. INTRODUCTION

The fourth industrial revolution (Industry 4.0) is prone to generate essential changes in daily life of human beings, types of their works, and human interactions. Industry 4.0 gives rise to some technologies, which are getting popularity nowadays, such as artificial intelligence (AI), robotics, 3-D printing, autonomous vehicles, nano and bio technologies, materials science, energy storage and quantum computing etc. Deploying digital technologies for better waste recycling, less energy consumption, improving transportation will make the cities more habitable and enticing. (Schwab 2016).

The population living in the cities is steadily rising around the globe and as of 2010 more than 52% of the world population was living in urban areas (Mutunga et al. 2012). The increasing population poses new challenges to the cities and eventually to their governments since the resources need to be managed in a prudent way. At this point, the notion of smart city comes into play as a consequence of Industry 4.0. The number of cities, that have the intention to be smart, is increasing and it is estimated that the size of the smart city industry will be more than $1 trillion by 2025 (Anthopoulos 2017). While the term 'smart city' brings to mind the cities employing digital technologies, it also means better governance, providing better services, better public contribution to the municipal decisions, better resource usage etc.

By the accrued advances in information and communication technologies (ICTs), the governments have had the chance to utilize innovative solutions to different services. Haidine et al. (2016) give smart city application in different realms such as energy (e.g. smart metering, network monitoring and management) buildings (e.g. light and heating control, energy efficiency), transportation (e.g. monitoring and management of traffic, services for drivers and passengers depending on real/near real time information), water (e.g. smart metering, efficient usage, conservation), waste (e.g. management, treatment, tracking), safety/security (e.g. video surveillance, disaster monitoring), health care (e.g. smart hospitals, decent hygiene, controlling diseases), and education (e.g.

* **Corresponding Author**

*(yboz@hacettepe.edu.tr) ORCID ID 0000 – 0002 – 8135 – 8308
(tcay@ktun.edu.tr) ORCID ID 0000 – 0002 – 4661 – 5583

**Cite this study**

Boz Y & Cay T (2020). Industry 4.0, Smart Cities, and Urban Transformation. Intercontinental Geoinformation Days (IGD), 134-136, Mersin, Turkey

learning environments for adjustable and interactive learning, online courses).

Smart city is one of the concepts developed with the rise of Industry 4.0 and it is characterized as a city that contains six factors: smart economy, smart mobility, smart environment, smart living, smart people, and smart governance (Roblek et al. 2016).

Smart city is a new form of urban design that makes use of digital technologies in an efficient way and it is a shift from the conventional urbanization to technology-driven one. Urban transformation projects, which can be referred by different names such as renewal, regeneration, rejuvenation, redevelopment, revitalization, recovery etc., are important government decisions that shape the social, economic, and cultural lives, and physical structure. Urban transformation is now moving forward and taking a new form by means of digital technologies. Smart city applications are being embedded into the urban transformation projects in order to manage the limited resources, whereas the urban populations have a tendency to increase steadily.

## 2. SMART CITY GOVERNMENTS

Eden Strategy Institute and OXD consultancy firm published a joint report on smart cities in the world defining the basic characteristics of the cities to be considered as smart. In this report, ten factors were also introduced to rank the city governments (Eden Strategy Institute and OXD 2018). These factors are as follows:

- Vision
- Leadership
- Budget
- Financial incentives
- Support programs
- Talent-readiness
- People-centricity
- Innovation ecosystems
- Smart policies
- Track record

In this report, 50 cities were selected among 140 cities and they were rated on a scale of one to five for each of the ten factors, where five is the best score. Then, these cities were put in an order based on the total score they had from all ten factors. The resulting ranking for the top 10 cities is given in Table 1.

**Table 1.** Top 10 smart city governments

| Rank | City | Total Score |
|---|---|---|
| 1 | London | 33.5 |
| 2 | Singapore | 32.3 |
| 3 | Seoul | 31.4 |
| 4 | New York | 31.3 |
| 5 | Helsinki | 31.2 |
| 6 | Montreal | 30.1 |
| 7 | Boston | 29.6 |
| 8 | Melbourne | 29.5 |
| 9 | Barcelona | 29.4 |
| 10 | Shanghai | 29.2 |

Some of the conspicuous features of the smart city governments derived from the top 10 smart cities are:

- Making it possible for the city residents to access to the ICTs and providing them with the talents required to use these technologies,
- Appointing committees within the body of the governments to develop smart cities and direct the process,
- Promoting the small and medium-sized enterprises that are executing researches on smart cities and taking advantages of these studies,
- Enabling the citizens to contribute the on-going activities and taking the advantage of ICTs while doing this,
- Experience exchange with different smart city exemplars,
- Ensuring cooperation among the institutions and groups that can make contribution such as city administration, citizens, private sector, academia.

## 3. GOVERNMENT POLICIES REGARDING SMART CITIES IN TURKIYE

National Smart Cities Strategy and Action Plan was published by the Presidency on 24 December 2019 (Official Gazette 2019). Some of the prominent issues stated in this document are:

- Increasing the service quality in the cities,
- Developing human-centric solutions,
- Benefiting from the technology at best level,
- Boosting the welfare of the society,
- Improving the contribution of the citizens to the city governance,
- Using the resources efficiently,
- Increasing the gratification of the citizens concerning the provided services.

In addition, in the 11th Development Plan published by the Directorate of Strategy and Budget of the Republic of Turkiye, goals related to urban transformation and smart cities have been set. Some of these goals are as follows (Directorate of Strategy and Budget 2019):

- Making it possible for every citizen to utilize from urban services and doing this in a fair way,
- Establishing urban transportation system with high accessibility,
- Considering women, children, elderly people, and handicapped people during urban design,
- Performing needs analysis and improving the service quality for the vulnerable groups,
- Increasing the amount of green areas in the cities,
- Promoting local governments in preparation of smart city strategies and supporting domestic production about smart city applications,

- Adopting a participatory approach while performing urban transformation projects and conducting the process in cooperation,
- Designing the transportation systems as accessible, safe, time & cost-effective, and sustainable,
- Provoking bicycle use in cities and constructing bicycle routes.

## 4. DISCUSSION AND CONCLUSION

There are still many countries without access to the information and communication technologies (ICT) in the world, which hinders them from the benefits of the fourth industrial revolution. Therefore, governments should try to construct the basic infrastructure for the ICT in order to form cooperation with the rest of the world.

Many beneficial influences are expected from smart cities such as using resources more efficiently, increased productivity, better quality of life, lower crime rates, raise in mobility, decreased air and noise pollution, better access to education. In spite of many positive influences of smart cities, negative effects should be considered wisely. Some of these unfavorable effects are related to surveillance, privacy, risk of breakdown in case of failure in the energy system, threats of cyber-attacks, changes in social life (Schwab 2016). Furthermore, less-demanding jobs could be replaced by smart technologies (e.g. robotics, automation of production).

Turkiye has many regions being threatened by earthquakes and is expected to hit by earthquakes in near future, which has been occurred in Izmir recently. It is believed that a significant number of the existing buildings, especially those built before 2000, are not resistant enough to earthquakes or other natural hazards due to their construction conditions. Therefore, after 2010 Turkiye took initiative and expedited the urban transformation projects that are estimated to cost hundreds of billions USD. While performing these urban transformations projects, it is very important to benefit from smart technologies to use resources efficiently and build livable spaces. It is time to shift from the conventional urban transformation to the “smart” urban transformation.

## REFERENCES

Anthopoulos L. G (2017). Understanding Smart Cities: A Tool for Smart Government or an Industrial Trick?, Springer, ISBN: 978-3-319-57014-3.

Directorate of Strategy and Budget (2019). Eleventh Development Plan (2019-2023), Directorate of Strategy and Budget of the Republic of Turkiye.

Eden Strategy Institute and OXD (2018). Top 50 smart city governments.

Haidine A, El Hassani S, Aqqal A & El Hannani A, (2016). The role of communication technologies in building future smart cities, In: Smart Cities Technologies, Eds: Da Silva, I. N. ve Flauzino, R. A., IntechOpen, p. 55-76.

Mutunga C, Zulu E & De Souza R-M (2012). Population dynamics, climate change, and sustainable development in Africa, Population Action International (PAI) and African Institute for Development Policy (AFIDEP) Report.

Official Gazette 2019. Presidential Notice No. 2019/29 on National Smart Cities Strategy and Action Plan (original title: *Ulusal Akıllı Şehirler Stratejisi ve Eylem Planı ile İlgili 2019/29 Sayılı Cumhurbaşkanlığı Genelgesi*), Date: 24 December 2019, Number: 30988.

Roblek V, Meško M & Krapež A. (2016). A complex view of industry 4.0, Sage Open, 6 (2), 1-11.

Schwab K (2016). The Fourth Industrial Revolution, World Economic Forum. ISBN-13: 978-1-944835-01-9.

Intercontinental Geoinformation Days

http://igd.mersin.edu.tr/2020/

# Understanding Mobility as a Service: A Literature Review

**Ömer AKIN*[1], Hande DEMİREL [1]**

[1]*Istanbul Technical University, Civil Engineering Faculty, Geomatics Engineering Department, Istanbul, Turkey*

**Keywords**
Mobility as a Service
Smart mobility
Multi-modal transportation
Spatial
Network

**ABSTRACT**

Urbanization is a rapidly growing process for cities and it naturally increases the supply/demand ratio of citizens or businesses. Thus, managing the transportation component of urbanization becoming more complex and enhancing or shifting the current infrastructure does not contribute to the solution. With the development of new technologies and alteration of user behaviors, mobility solutions should also adapt to satisfy the needs. "Mobility as a Service (MaaS)" is an innovative accessibility-based concept that combines multi-modal transportation enabling the user to choose and manage their trips in a single mobile app or web interface. The concept is based on spatial analyses -mainly network analyses-, digitalization, and management of discrete mobility systems. It offers a manageable and sustainable mobility service by maximizing the benefits of the current infrastructure. MaaS ecosystem builds relations between users and different stakeholders such as public or private transport suppliers and municipal governments in a single platform and it offers personalization and customization for both sides. In this paper, MaaS is examined on the conceptual level based on the literature and existing implementations.

## 1. INTRODUCTION

The urban density of cities continues to increase and populous cities struggle to keep their transportation infrastructure active despite the increase. Strengthening existing infrastructure by adding new roads/connections or supporting different travel modes has contributed to the mobility of people and goods in the past. However, in today's conditions, such management of mobility is socially, environmentally, and economically insufficient. Reshaping the current roads or expanding the infrastructure is slow, costly, and non-ecologic way to solve the problem. Also, people no longer see the paradigm as a "more roads or more transit" choice, they tend to live in less vehicle-centric and sustainable cities (Goodall et al., 2017).

Technological advances enable different transportation modes (public transport, car-sharing, e-bikes, etc.) to be managed and used more efficiently. Nowadays, ICT solutions intertwined with mobile phones are widely used for different transportation modes such as cab services (Uber, Lyft, Bitaksi), car-sharing (Car2Go, DriveNow, blablacar), and micro-mobility devices (Isbike, Martı). These services eliminate intermediates by making the matchmaking between customers and entrepreneurs in a mobile app platform (Giesecke et al., 2016). Although these services have advantages on user-centric mobility individually, they are mostly service-based commercial apps and do not offer an all-in-one solution or a mobility management platform for users or authorities. In such approaches, different transportation modes and their payment systems are presented to the user as different services and travel modes such as public transportation are generally not evaluated. Thus, it does not solve the problem of the number of vehicles in traffic and this leads to an ownership-based transport system rather than an access-based one.

"Mobility as a Service (MaaS)" is described as a user-centric, personalized, door-to-door travel management platform that digitally unifies trip creation, payment, and delivery processes across all transportation modes (Ho et al., 2018). It is an emerging smart technology that combines multi-modal transportation while enabling the user to choose and manage their trips in a single mobile application. The increasing number of transportation modes emerging through technological developments could be examined, operated, and managed in an

* **Corresponding Author**

*(akinom@itu.edu.tr) ORCID ID 0000-0002-8109-0313
(hande.demirel@itu.edu.tr) ORCID ID 0000-0003-0338-791X

Akın O & Demirel H (2020). Understanding Mobility as a Service: A Literature Review. Intercontinental Geoinformation Days (IGD), 137-140, Mersin, Turkey

integrated system by using the concept of MaaS. Its ecosystem builds relations between users and different stakeholders such as public or private transport suppliers and municipal governments in a single platform and it offers personalization and customization for both sides. As a concept, MaaS redefines the interoperability of transportation modes by supplying point-based access (door-to-door) rather than any type of stop-based access.

## 2. BACKGROUND

Digitalization and technological developments change people's behavior in mobility as in every field. Rising energy and private auto ownership costs, increasing congestion and greenhouse gas emissions, and ease of technological developments lead to shared mobility services around the world (Shaheen and Cohen, 2013). Shared mobility services provide the user with short-term access to shared private vehicles according to the user's needs (Shaheen, Cohen and Zohdy, 2016). Carsharing is the mainstream shared mobility system, however, the concept has been expanded to different transport modes such as bike-sharing, moto-sharing, and scooter-sharing (Shaheen and Cohen, 2013; Aries-Molinares and García-Palomares, 2020). This mobility shift has encouraged new mobility business models that are managed and operated through mobile applications and are embedded with technology. However, from the user's perspective, it becomes difficult to navigate through all these applications, ticketing systems, and journey planning steps with the increasing mobility options (Matyas, 2020). Also, as these different transportation modes are operated individually under the respective commercial applications, it is difficult to plan trips from the exact starting point to the end point. The aforementioned challenges and the growing shared mobility economy have enabled the concept of MaaS, which was discussed to change the paradigm of mobility by integrating different mobility services into a single, user-friendly platform.

MaaS is a recent concept that has been studied for nearly 10 years. The idea is first mentioned and promoted as *transport as a service* in a paper called "The Transport Revolution" published by the Finnish Ministry of Transportation and Communication in 2011 (Hietanen, 2020). Then, Sweden has developed the first pilot MaaS application UbiGo in 2013, and Finland has developed "Helsinki Model" in 2014 (Karlsson et al., 2016; Heikkilä, 2014). Later in 2014, the project Whim app is started in Finland based on the visions of Helsinki Model (Polydoropoulou, 2020). In 2016, MaaS International Alliance, an international public-private partnership that creates foundations for a common MaaS approach, has been founded to facilitate a single, open market and full deployment of MaaS services (MaaS Alliance, 2020).

After successful pilot projects and the establishment of MaaS Alliance, the concept was recognized worldwide and the number of pilot projects increased. Kamargianni et al. (2016) has classified these pilot projects according to their integration level: partial, advanced, and advance with mobility packages.

Existing MaaS pilots according to the above classification are given in Table 1 (Kamargianni et al. 2016; Kriukelyte, 2018; Aries-Molinares and García-Palomares, 2020)

**Table 1.** Existing MaaS pilots

| Level of Integration | Explanation | MaaS Pilots |
|---|---|---|
| Basic | Partially possesses ticketing, payment, and ICT integration | Moovel, Switchh, Qixxit (Germany) and Cambio-STIB (Belgium) |
| Advanced | Fully possesses ticketing, payment, and ICT integration | Mobility Shop, Open Mobility (Germany), Smile (Austria), and Optymod (France) |
| Advanced with mobility packages | Offer monthly packages and pay-as-you-go options | UbiGo (Sweden), Whim app (Finland), Antwerp (Belgium), and West Midlands (UK) |

Although there are successful implementations, the dissemination and future of MaaS still depend on technological, social, and regulatory developments (Sarasini et al., 2018). Advanced applications of MaaS offer an integrated mobility service that consists of public transportation (bus, tram, ferry, etc.), car-sharing services, bike-sharing, and cab services while providing different monthly subscription services according to the demand and need of users (Giesecke et al., 2016). To achieve such a system with different stakeholders and options available, components of MaaS should be identified and examined in detail on the local scale.

## 3. COMPONENTS OF MaaS ECOSYSTEM and THE FUTURE OF MaaS

MaaS applications are mostly implemented in urban areas where required transportation infrastructure and necessary organizations already exist (Jittrapirom et al., 2018). The main aim is integrating these organizations and maximizing the infrastructure's performance to achieve a sustainable transportation management system. Since features of cities such as sociological texture, existing infrastructure, available transportation modes, or topography are different and unique, MaaS approaches should be examined on a local scale. Its success depends on the management of user behaviors, governmental/local policies, private sector contribution, deep research and modeling of systems, ICT infrastructure developments, and strong collaborations between these components. The major components and their relations within the MaaS ecosystem are shown in Fig. 1.

From the user's point of view, a MaaS operator must offer tailored and customized mobility packages according to the needs. Optimizing the interaction between user and MaaS is a challenging factor as many different personal attitudes such as health conditions, age, social behaviors, attitudes, and financial income are taken into account in mobility. MaaS operator should

provide a list of public and private travel options including traditional and new transport modes while considering the preferences and travel budgets of the user (Jittrapirom et al., 2017).

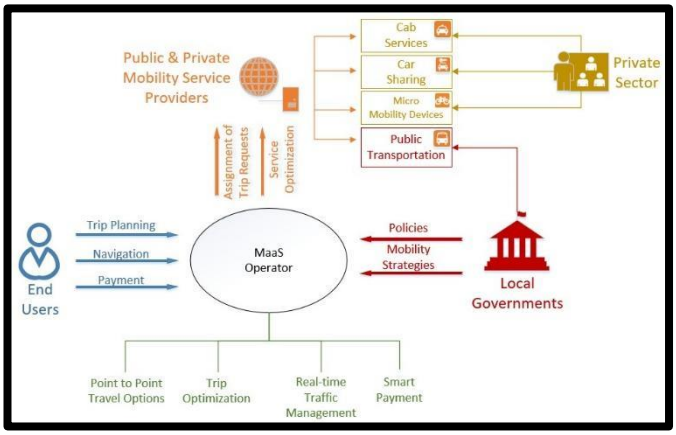


**Figure 1.** Components and their relations in the MaaS ecosystem

The strength and sustainability of the system depend on the provision of personalized real-time travel and activity planning alternatives within the MaaS operator. To optimize these needs, advanced technological techniques and methods should be used. For example, the Whim app of Helsinki, Finland has four different subscription methods consisting of different transportation modes and payment methods (monthly subscriptions & pay-as-you-go) according to the sociological pattern of citizens. Additionally, the sustainability of the system is supported by real-time user attitude data through these methods.

On the supply side, the MaaS operator must maintain the distribution and assignment of trip requests among mobility service providers. In that stage, strong collaboration between service providers (public or private) and the MaaS operator must be established through Application Programming Interfaces (APIs) to offer real-time mobility options to the users. In an advanced example of MaaS, even real-time traffic management could be performed with real-time data.

Transport authorities have vital importance to achieve a sustainable transportation system through MaaS. They play a key role by promoting collaboration between different stakeholders (Chang et al., 2019). They have a dominant impact on public transport operators that are the backbone of MaaS and the potential to enable MaaS through policies, regulations, and frameworks (Audouin, 2019). After enabling MaaS, a strong system fed with real-time data and user behaviors will help policymakers to get a clear vision about the current situation and to define mobility strategies to make future transport smarter, cleaner and equal (Pangbourne et al., 2018).

The effects and benefits of MaaS depend on the spatial scale of the city to be implemented. Therefore, before initiating the system at the conceptual level, existing examples, and unique spatial requirements & opportunities should be deeply researched. Integrated demand and supply mechanisms of MaaS should be investigated via advanced modeling, simulation, and optimization methods. Its ecosystem consists of many components in social, economic, spatial, and technological domains. Therefore, conventional modeling and simulation methods need to be enhanced to get clearer insights about the framework (Ho et al, 2018; Basu et al., 2018; Stiglic et al., 2018).

In the spatial domain, since there are many different types of user groups and available services in the ecosystem, the impacts of MaaS on transportation should be modeled and examined in detail in a Spatial Information environment. MaaS is an accessibility-based concept that includes multi-modal transportation, therefore these modes should be examined with different accessibility and network (transportation modes) parameters. Each mode of transport has different mobility characteristics such as being stop-based (bus, subway, etc.) or access-based (from A to B such as car-sharing or cab). Therefore, the integration of these unique features into a spatial application requires tailored network optimization techniques. Collecting valuable data as well as enhancing data through analysis and simulations is vital to ensure this integration. The ecosystem should be analyzed in detail through advanced network analysis to reveal impacts in terms of social, economic, and mobility convenience.

An advanced ecosystem should offer the integration of these services while helping to reduce carbon emissions. The term “sustainability” in the definition of MaaS also includes environmental sustainability. Therefore, besides the impacts on mobility, effects of MaaS on land use and environment should be modeled with advanced modeling techniques such as land-use interaction models or agent-based modeling to evaluate the different mobility scenarios. Additionally, the effects and contributions of the MaaS ecosystem to the sustainability and demography of the city should be evaluated with Artificial intelligence and machine learning techniques, as these tools can dynamically predict travel conditions and be used to automate processes.

## 4. CONCLUSION

MaaS is an emerging technology that is still being studied. It has several examples around the world, yet certain definitions, impacts, and benefits are uncertain. In this paper, existing implementations and the core elements of the architecture are examined and the future of MaaS is discussed. Although defining a precise roadmap is difficult, this paper is intended to be a basic reference and literature review for future studies.

## REFERENCES

Arias-Molinares D & García-Palomares J C (2020). The Ws of MaaS: Understanding mobility as a service from a literature review. IATSS Research.

Audouin, M U J (2019). Towards Mobility-as-a-Service: a cross-case analysis of public authorities' roles in the development of ICT-supported integrated mobility schemes (No. THESIS). EPFL.

Basu R, Araldo A, Akkinepally A P, Nahmias Biran B H, Basak K, Seshadri R, Deshmukh N, Kumar N,

Azevedo C L & Ben-Akiva M (2018). Automated mobility-on-demand vs. mass transit: a multi-modal activity-driven agent-based simulation approach. Transportation Research Record, 2672(8), 608-618.

Chang S J, Chen H Y & Chen H C (2019). Mobility as a service policy planning, deployments and trials in Taiwan. IATSS research, 43(4), 210-218.

Giesecke R, Surakka T & Hakonen M (2016). Conceptualising mobility as a service. Eleventh International Conference on Ecological Vehicles and Renewable Energies (EVER), 1-11

Goodall W, Dovey T, Bornstein J & Bonthron B (2017). The rise of mobility as a service, Deloitte Rev, 20, 112-129.

Heikkilä S (2014). Mobility as a Service-a proposal for action for the public administration case Helsinki, Aalto University.

Hietanen S (2020). A brief history of MaaS Global, the company behind the Whim app, Retrieved 19 October 2020, from https://whimapp.com/history-of-maas-global/

Ho C Q, Hensher D A, Mulley C & Wong Y Z (2018). Potential uptake and willingness-to-pay for Mobility as a Service (MaaS): A stated choice study. Transportation Research Part A: Policy and Practice, 117, 302-318.

Jittrapirom P, Caiati V, Feneri A M, Ebrahimigharehbaghi S, Alonso González M J & Narayan J (2017). Mobility as a service: A critical review of definitions, assessments of schemes, and key challenges, 2, 13-25

Jittrapirom P, Marchau V, van der Heijden R & Meurs H (2018). Dynamic adaptive policymaking for implementing Mobility-as-a Service (MaaS). Research in Transportation Business & Management, 27, 46-55.

Kamargianni M, Li W, Matyas M & Schäfer A (2016). A critical review of new mobility services for urban transport. Transportation Research Procedia, 14, 3294-3303.

Karlsson I M, Sochor J & Strömberg H (2016). Developing the 'Service' in Mobility as a Service: Experiences from a field trial of an innovative travel brokerage. Transportation Research Procedia, 14, 3265-3273.

Kriukelyte E (2018). New challenges for transport planning: The institutionalization of mobility as a service in the Stockholm region, Stockholm.

MaaS Alliance (2020). The Alliance, Retrieved 20 October 2020, from https://maas-alliance.eu/the-alliance/

Matyas M (2020). Opportunities and barriers to multimodal cities: lessons learned from in-depth interviews about attitudes towards mobility as a service. European Transport Research Review, 12(1), 7.

Pangbourne K, Stead D, Mladenović M & Milakis D (2018). The case of mobility as a service: A critical reflection on challenges for urban transport and mobility governance. Governance of the smart mobility transition, 33-48.

Polydoropoulou A, Pagoni I & Tsirimpa A (2018). Ready for Mobility as a Service? Insights from stakeholders and end-users. Travel Behaviour and Society, 21, 295-306.

Sarasini S & Linder M (2018). Integrating a business model perspective into transition theory: The example of new mobility services. Environmental innovation and societal transitions, 27, 16-31.

Shaheen S A & Cohen A P (2013). Carsharing and personal vehicle services: worldwide market developments and emerging trends. International journal of sustainable transportation, 7(1), 5-34.

Shaheen S, Cohen A & Zohdy I (2016). Shared mobility: current practices and guiding principles (No. FHWA-HOP-16-022). The United States. Federal Highway Administration.

Stiglic M, Agatz N, Savelsbergh M & Gradisar M (2018). Enhancing urban mobility: Integrating ride-sharing and public transit. Computers & Operations Research, 90, 12-21.

Intercontinental Geoinformation Days

http://igd.mersin.edu.tr/2020/

# Smart Mobility Recommendations in Multimodal Transport for Local Authorities

**Hatice Gül Önder**[*1], **Mustafa Ulukavak** [2]

[1]*Ankara Hacı Bayram Veli University, Academy of Land Registry and Cadastre, Department of Real Estate and Property Management, Ankara, Turkey*
[2]*Harran University, Engineering Faculty, Department of Geomatics Engineering, Şanlıurfa, Turkey*

**Keywords**
Local Governments
Smart City
Smart Mobility
Smart Transportation

**ABSTRACT**

Smart transportation systems are one of the most important components of the smart city, which was affected by the fourth industrial revolution. Smart transportation types, systems, and infrastructures, which are undergoing a rapid transformation in the information age with the effect of information-communication infrastructure and technological developments, have become one of the important issues that local governments should focus on. The rational use of smart transportation applications has great importance in terms of increasing the quality of urban life, preventing environmental pollution, and preventing many material and vital losses. Smart mobility defines a safe, clean, and effective smart transport framework in which different transport types and infrastructures are integrated with each other. Smart mobility elements that are successfully maintained in the world that should be adopted for Turkey's local government conditions for producing a successful transport policy. In this study, the legal-administrative structure in Turkey, the urban transport infrastructure, the extent of the permit application stage, and the type of transportation system that will help the local government recommendations are developed.

## 1. INTRODUCTION

Smart transportation, which is the most basic component of a smart city, that the whole of transportation types, systems, and infrastructures are supported by information and communication technology infrastructure, which is seen as an important building block of industry 4.0 (Kırmızı et al., 2012). A variety of smart transportation systems are implemented in the world and Turkey for transportation, traffic, and passenger management applications. These are traffic management system, electronic toll collection system, passenger information systems, smart public transportation systems, smart vehicle highway systems, smart stop, smart parking management and payment solutions, smart routing system, load-fleet management system, driver support and security systems, commercial vehicle management (Smart City Terminology, 2020; AUSDER, 2019).

On the other hand, smart mobility defines a safe, clean, and effective smart transportation framework in which different transportation types and infrastructures are integrated with each other. Four main components affect the working principle of smart mobility systems. These are traffic data collection, data transmission, traffic data analysis, and traveler information (Heremobility, 2020a). Smart mobility has many benefits for cities. The most important of these are; it reduces traffic congestion, prevents environmental pollution, reduces emission production, prevents traffic noise, is economical in terms of reducing costs, reduces traffic accidents (Heremobility, 2020b). Based on these benefits, green and smart mobility is always at the forefront. Green and smart mobility is mostly related to autonomous robots, the internet of things, cybersecurity, cloud software, artificial intelligence, machine learning, and big data.

The impact of the increasing world population on resource consumption raises the need for decision-making and rational solutions that will ensure the continuity of sustainability for local governments. Developing transportation approaches with rational approaches will have positive effects on quality of life (Mezei and Lazányi, 2018). For smart cities to have a smart mobility network, they must first adapt and

* **Corresponding Author**

*(gul.onder@hbv.edu.tr) ORCID ID 0000-0002-4794-6923
(mulukavak@harran.edu.tr) ORCID ID 0000-0003-2092-3075

**Cite this study**

Önder H.G. & Ulukavak M. (2020). Smart Mobility Recommendations in Multimodal Transport for Local Authorities. Intercontinental Geoinformation Days (IGD), 141-143, Mersin, Turkey

develop their existing infrastructure to smart mobility components. In this context, starting a new use of smart mobility elements in Turkey, the future uses of the considering potential of existing transport modes and systems with the urban transport infrastructure needs to be determined that could be used in how to be more efficient in terms of local governments.

## 2. METHOD

In this study, examples of smart mobility applications in countries such as the USA, France, the United Kingdom, South Korea, and especially in cities such as Los Angeles, Columbus, Singapore, Barcelona, Copenhagen, Amsterdam, Helsinki, Songdo, Dubai were analyzed from an analytical perspective. It also focuses on the development of multimodal and integrated smart mobility suggestions for local governments in Turkey.

## 3. RESULTS

### 3.1. Three Dimensions of Smart Mobility

The results obtained within the scope of this study show that the inferences obtained from the examples of the world make it necessary to consider smart mobility approaches with three dimensions of urban transportation. These will be in the fields of individual mobility, public transport, and urban freight transport. World examples of inferences derived from the smart mobility of local governments in Turkey are required to be presented as a set of suggestions. For this, firstly; it is beneficial to put forward the theoretical and applicability infrastructure as well as the legal-administrative framework for the use of type, system, and infrastructure information of smart mobility. In this context, evaluations will be presented under each heading.

#### 3.1.1. Individual mobility

Individual mobility is one of the most preferred modes of transport in Turkey. There are many types of transportation for individual mobility. Bicycles, motorcycles, private cars, and e-scooters, which are one of the micro-mobility types that have just been integrated into transportation systems can be given as examples. Individual mobility also has a shared mobility dimension. In this context, there are shared driving methods such as carsharing, ridesharing, carpooling, and vanpooling. Although few formal services offered by shared mobility company in Turkey, it can also be performed by friends and colleagues as informal surroundings. In this context, it is important for local governments to focus on individual mobility-based solutions in terms of responsibility, safety, and control.

#### 3.1.2. Public transport

With the effect of today's technology and smart city components, smart public transport approaches have great importance in increasing travel quality and travel satisfaction (Sutar et al., 2016). One of the most important focuses in smart public transport management is optimization in transportation. New self-driving autonomous vehicles will provide ease of use with higher efficiency and capacity due to flexibility in work and working hours (Durmuş, 2019). It has a smart public transport management system that can perform public transport, line, and route optimization shaped by the smart transportation network. The smart public transport management system provides real-time information flow to the users regarding the route information system, passenger density, headway frequency, vehicle attributes information, not only warns about accidents but also conveys the danger and current status information regarding the road (Akdemir and Önder, 2020).

Smart mobility systems have an important place in the provision of urban transportation services, especially in the field of public transport. In addition to rail systems and bus systems, there are paratransit modes such as minibus, taxi, and shuttle in public transport systems. Local governments can integrate private mobility and public transport systems using smart transportation system components. This situation allows the development of local governments' multimodal mobility infrastructure.

#### 3.1.3. Urban freight transport

It is important to evaluate autonomous systems, which are an important element of smart transportation systems, in the field of urban freight transportation, that is, urban logistics. Along with technological developments, the concept of logistics is developing in terms of resource planning, storage management, business management, smart transportation systems, and information security (Barreto et al., 2017). In the freight transport dimension of urban transport, a structure in which smart transport infrastructure is integrated with the logistics infrastructure is emphasized. Vehicles such as delivery vehicles, delivery drones, delivery robots are used in urban freight transportation. For the cargo and freight transportation area, which has become a large distribution market day by day with the concept of e-commerce, local governments have a significant role in preventing financial and vital losses caused by traffic congestion and traffic accidents, especially in urban transportation.

### 3.2. Recommendations for Local Authorities

When the evaluation of Smart Mobility's three dimensions, how smart mobility approach by local authorities in Turkey within the scope of this study can be applied with the suggestions to what extent and what steps are being developed. For local governments to achieve success in many issues such as increasing the quality of urban life, reducing emissions, preventing environmental pollution, minimizing noise, ensuring safety in public transportation, in the context of green and smart mobility; Transportation types, systems, and infrastructures should be integrated into smart transportation in three stages. These stages can be specified as (Heremobility, 2020c);

1. Information management and optimization,
2. Light infrastructure
3. Heavy infrastructure.

## 4. DISCUSSION

Although emerging technologies and smart mobility in the urban transport of the future will find great information-technology infrastructure in Turkey, though, it must be handled carefully with the applicability of context. There are difficulties that local governments will encounter in the field of smart mobility during the implementation phase. These can be specified as legal and administrative deficiencies, implementation problems, governance problems, maintenance problems, lack of qualified human resources, etc. However, Target 2023 Turkey Transport and Communication Strategy prepared by Republic of Turkey Maritime Transport and Communications Ministry in 2011; National Intelligent Transportation Systems Strategy Document and its Annex Action Plan which is prepared in 2014; Smart Transportation Systems Terms Dictionary prepared in 2017; 2019-2022 National Smart Cities Strategy and Action Plan and Smart Cities Whitepaper prepared by Republic of Turkey Ministry of Environment and Urbanization in 2019; The Eleventh Development Plan 2019-2023, prepared by Republic of Turkey Presidency of Strategy and Budget in 2019 can be useful for the legal administrative framework for smart cities and smart mobility in Turkey while offering ideas about responsibilities and priorities.

## 5. CONCLUSION

The results obtained from this study show that there are many issues that need to be focused on sensitively to ensure smart mobility by local governments by improving transportation in the focus of green and smart mobility. To list a few of them;

- Transportation types should minimize the use of fossil fuels and prefer alternative energy types.
- Individual mobility and public transport systems need to be integrated with each other.
- Transport infrastructure needs to be updated to include smart transport components.
- Most importantly, it needs to be reconsidered in the context of the sustainability of Turkey's legislation in the field of transportation.

## REFERENCES


Akdemir, F. & Önder, H. G. (2020). Endüstri 4.0'dan Toplum 5.0'a Güncel Yaklaşımlar içinde *Endüstri 4.0'ın Etkisindeki Akıllı Kentin Arazi Kullanım ve Ulaşım Paradigmaları* (Ed. S. Çiğdem ve A. Boztaş). Nobel Yayınevi.

AUSDER-Akıllı Ulaşım Sistemleri Derneği, http://www.ausder.org.tr/, Date of Access: 05/10/2020.

Barreto, L., Amaral, A., & Pereira, T. (2017). Industry 4.0 implications in logistics: an overview. Procedia Manufacturing, 13, 1245-1252.

Durmuş, A. (2019). Endüstri 4.0 Eğitim 4.0 Liderlik 4.0 Toplum 5.0, İstanbul: Efe Akademi Yayınları.

Heremobility, (2020a). Smart Transport Systems: An Intro, https://mobility.here.com/learn/smart-transportation/smart-transport-systems-intro, Date of Access: 13/10/2020.

Heremobility, (2020b). **S**mart Mobility in Tomorrow's Smart Cities https://mobility.here.com/learn/smart-mobility/smart-mobility-tomorrows-smart-cities, Date of Access: 13/10/2020.

Heremobility, (2020c). How to Build a Smart City Transport System in Three Phases https://mobility.here.com/learn/smart-city-mobility/how-build-smart-city-transport-system-3-phases, Date of Access: 13/10/2020.

Kırmızı Z., Kolağasıoğlu M.Ş. & Çalışkan F.T., (2012). Kentiçi Ulaşım Terimleri Sözlüğü, İstanbul: Cinius Yayınları.

Mezei, J. I. & Lazányi, K. (2018). Are We Ready for Smart Transport? Analysis of Attitude Towards Public Transport in Budapest. Interdisciplinary Description of Complex Systems: INDECS, 16(3-A), 369-375.

Sutar, S. H., Koul, R., & Suryavanshi, R. (2016). Integration of Smart Phone and IOT for development of smart public transportation system. In 2016 International Conference on Internet of Things and Applications (IOTA) (pp. 73-78). IEEE.

T.C. Çevre ve Şehircilik Bakanlığı (2019). 2019-2022 Ulusal Akıllı Kentler Stratejisi ve Eylem Planı

T. C. Çevre ve Şehircilik Bakanlığı (2019). Akıllı Kentler Beyaz Bülten, 2019-2022 Ulusal Akıllı Kentler Stratejisi ve Eylem Planı Yönetici Özeti

T.C. Çevre ve Şehircilik Bakanlığı, (2020). 2020 Akıllı Şehir Terminolojisi, 2020-2023 Ulusal Akıllı Şehirler Stratejisi ve Eylem Planı.

T.C. Ulaştırma Denizcilik ve Haberleşme Bakanlığı. Ulusal Akıllı Ulaşım Sistemleri Strateji Belgesi ve Eki Eylem Planı, Ankara, Türkiye, 2014.

T.C. Ulaştırma Denizcilik ve Haberleşme Bakanlığı. Hedef 2023 Türkiye Ulaşım ve İletişim Stratejisi 2011. Ankara, Türkiye, 2011.

T.C. Ulaştırma, Denizcilik ve Haberleşme Bakanlığı, (2017). Akıllı Ulaşım Sistemleri Terimleri Sözlüğü, Ankara: Özel Matbaası.

T.C. Cumhurbaşkanlığı Strateji ve Bütçe Başkanlığı, On Birinci Kalkınma Planı 2019-2023. Ankara, Türkiye, 2019.

## Photogrammetry and Remote Sensing – 3

**Training data development strategy for applying deep learning in remote sensing applications**

*Vaibhav Katiyar*, Masahiko Nagai*

**Spatiotemporal analysis of land-use changes in a metropolitan city in Malaysia using geospatial techniques**

*Abdulwaheed Tella*, Abdul-lateef Balogun, Asmau Balogun*

**Remote Sensing Image Fusion Using Transform Domain Based on Optimization Algorithms**

*Asan Ihsan Abas*, Nurdan Akhan Baykan*

**Land Use and Shoreline Dynamics in Lagos State, Nigeria**

*Swafiyudeen Bawa*, Adamu Bala, Abubakar Sadiq Sani*

**Indoor navigation application using augmented reality technology**

*Salih Hamdi Çalık*, Fatih Gülgen*

**An investigation of Triangular Greenness Index performance in vegetation detection**

*Nizar Polat*

Intercontinental Geoinformation Days

http://igd.mersin.edu.tr/2020/

# Training data development strategy for applying deep learning in remote sensing applications

**Vaibhav Katiyar*[1], Masahiko Nagai [1,2]**

[1]*Yamaguchi University, Environmental Engineering, Graduate School of Sciences and Technology for Innovations, Ube, Yamaguchi Japan*
[2] *Yamaguchi University, Center for Research and Application of Satellite Remote Sensing, Ube, Yamaguchi Japan*

**Keywords**
DCNNs
Training Data preparation
Remote sensing
U-Net
SegNet

**ABSTRACT**

Deep Convolution Neural Networks (DCNNs) are playing a very important role in remote sensing applications. However, one of the major challenges in utilizing DCNNs is, of access to the training data. Firstly, there are very few training data available in various fields such as in natural disaster area, secondly, even if it's available it may not be suited to the area we are planning to implement. In such a case creating training data by oneself becomes very important. However, we need to understand that there is a big difference between computer vision dataset and remote sensing dataset. As in the latter case, one scene may cover thousands of Kilometers and the total number of scenes are limited. This is why there is a concept of 'chips' used in remote sensing domain which means a subset of the satellite scene to be used as an 'image' in computer vision sense. This study is comparing the various possible strategies to make the chips from the ALOS-2 scenes and recommending the best after utilizing these chips with popular segmentation network U-Net and SegNet.

## 1. INTRODUCTION

In recent time, we have seen lots of applications of deep learning in the remote sensing domain. DCNNs have achieved significantly higher accuracy in comparison to other image processing methods especially in cases like road segmentation (Li, Comer and Zerubia 2019), building detection (Li et al. 2019), land cover classification (Zhang et al. 2019) etc. However, we need to understand that these higher accuracies were achieved due to well established public datasets, provided through SpaceNet challenges (Etten et al. 2018), ISPRS labelling contest (Gerke et al, 2014), DeepGlobe challenge (Demir et al. 2018) etc. These kinds of public datasets are not available in many other areas such as in more dynamic cases of natural disasters. Moreover, most of the datasets are available for optical high-resolution images. Synthetic Aperture Radar (SAR) dataset are very scarce, which created the need to develop our own datasets. This study has used ALOS-2 level 2.1 image scenes of HH polarization.

As satellite scenes are too big that is why we need to create image-chips out of it (Han et al. 2017), which can be feed to DCNNs that can run efficiently on the GPUs memory. As per Ning et al. (2020), training a network with a higher number of image chips normally leads to greater accuracy. Also, data augmentation has proved a successful mechanism to increase the variability from limited data and in-turn improves the performance of the networks.

Our main objectives in this study were, studying different strategies to make image-chips for training and then cross-comparing them on two very popular segmentation network, U-Net (Ronneberger et al. 2015) and SegNet (Badrinarayanan et al. 2017).

## 2. METHOD

For simplicity, this study has selected binary class situation i.e. images with the flooded area and non-flooded area.

Three different satellite scenes subsets have been used to create the training data and the fourth scene subset has been used for testing. U-Net and SegNet have been used as the network for the segmentation.

In the paper, Methodology follows two steps that are creating data and training & testing.

* **Corresponding Author**

*(i502wd@yamaguchi-u.ac.jp) ORCID ID 0000-0003-3453-3158
(nagaim@yamaguchi-u.ac.jp) ORCID ID 0000-0002-0625-762X

**Cite this study**

Katiyar V & Nagai M (2020). Training data development strategy for applying deep learning in remote sensing applications. Intercontinental Geoinformation Days (IGD), 144-147, Mersin, Turkey

### 2.1. Training Data Preparation

The chip size for the training data has been selected as 512x512 pixels. This size has been chosen with keeping in mind that flood is the phenomenon which affects a larger area, so to better capture the context the bigger chips size has been chosen. However, we also need to take care of the GPU memory as bigger chips mean smaller batch size and larger training time. Another point to consider is that flooded region is much smaller in comparison to the non-flooded region, this creates an imbalance in the dataset. To reduce this imbalance, the study has selected only those image-chips which has at least 10% of total pixels belonging to a flooded area, called in this paper as valid chips. 10% pixels from ALOS-2 image with 3m spatial resolution means approx. 8-hectare area, over which very few surface water bodies occur in that area. This helps to remove the noise from a smaller lake/ponds. Following methods have been used to extract image chips- 1) Sliding Window 2) Randomized sampling.

#### 2.1.1. Sliding window method

Under this method, a sliding window has been used to slide over the scene and create the chips with the different overlap of successive steps. Four sets of overlap have been used, no overlap, 30% of overlap, 50% overlap and 70% overlap as shown in Fig.1.

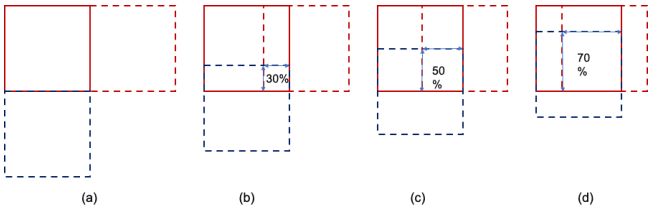


**Figure 1.** Overlap in successive steps in the case of a sliding window. (a), (b), (c) and (d) are showing the different scenario- 0%, 30%, 50% and 70% overlap for the chips.

As different overlap will result in a different number of the chips, and a greater number of chips may give a better result (Ning et al. 2020). So, in this study, we have decided to select an equal number of chips for each scenario. To decide that how many chips should be selected, we have used 70% overlap, as in this scenario the maximum number of chips will be created to cover the whole scene (Fig. 2), the total valid image-chips have been found around 200 (this number depends upon the size of the image as well as the abundance of foreground pixels). For this reason, in all scenario we have created 200 image-chips, if the total number of valid chips is less than this limit such as in no-overlap scenario, then we just duplicated the valid chips to satisfy the condition.

#### 2.1.2. Randomized sampling method

In this method, the 200 random patches have been selected using a 'sampling' method. The validity of these patches was calculated and recursively sampling has been done till the time the total number of valid image-chips reach to 200 or more (shown by Red square in Fig. 2). In the end, only 200 of valid-chips has been saved for the training step (Yellow square in Fig. 2).

This way we have created the training set of total 600 image chips from three different satellite scenes for each method and scenario.

### 2.2. Training and Testing

The training datasets have been used, to train U-Net and SegNet for each method and scenario. Each of these networks has five encoder and five decoder blocks with one bottleneck block, each block having two convolutions. Each kernel of an encoder is of 3x3 size with 'same' padding while decoder kernel size has been chosen as 2x2. The network has been trained for 50 epochs with the batch size of 10 and validation split of 20%, along with the binary-cross-entropy as loss function and the optimizer Adam.

All the trained models have been tested on the same test set and the result has been compared based on F1-Score, Accuracy and Jaccard Score.

$$F1\ Score = \frac{2 * Precision * Recall}{(Precision + Recall)}$$

$$Accuracy = \frac{Correctly\ identified\ pixels}{Total\ Pixels\ in\ the\ Image}$$

$$Jaccard\ Score = \frac{GroundTruth\ \cap Predicted}{GroundTruth\ \cup Predicted}$$

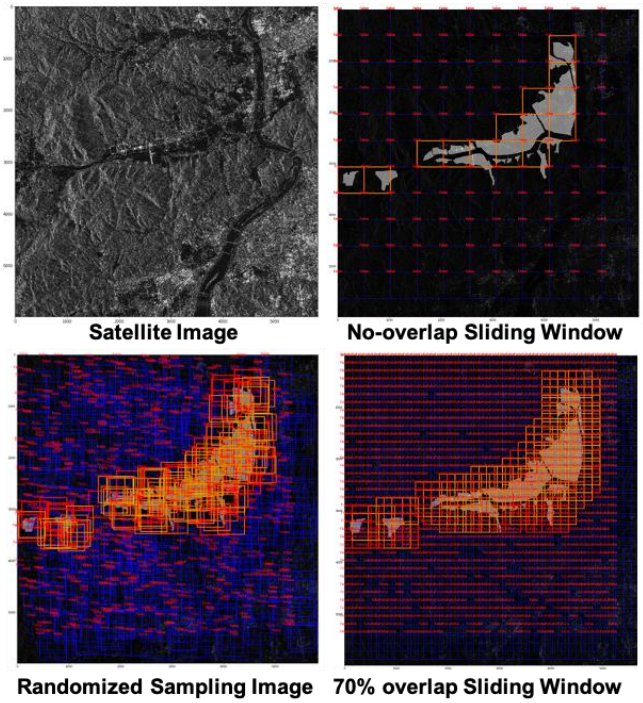


**Figure 2.** Training data creation. Image-chips were created concerning the flood mask as can be seen in all the images above leaving satellite image aside. Blue colour bounding boxes (BBs) in the images are invalid due to not meeting the condition of 10% water pixels and Red colour BBs are valid while yellow BBs are the selected chips from total valid ones.

## 3. RESULTS

In the step of the creation of the training data, maximum time was spent in randomized sampling method and in case of sliding window method, time is decreasing with decreasing overlap. So, the fastest method for image-chip creation was sliding window with no overlap.

After training data preparation, U-Net and SegNet were trained on each training set i.e. five different training sets. Each training took between 15-20 mins for finishing 50 epochs. Here it needs to be focused that, hyper tuning of the network has not been done and rather than saving the best model, the model has been saved after 50 epochs. As the main aim was to do the cross-method comparison for different methods of training data preparation.

Training accuracy and binary cross-entropy loss during the training have also been plotted (Fig. 3). As per the plot, the no-overlap scenario was converging fastest, while randomized sampling one was more versatile and showing less sudden peaks with increasing epochs.

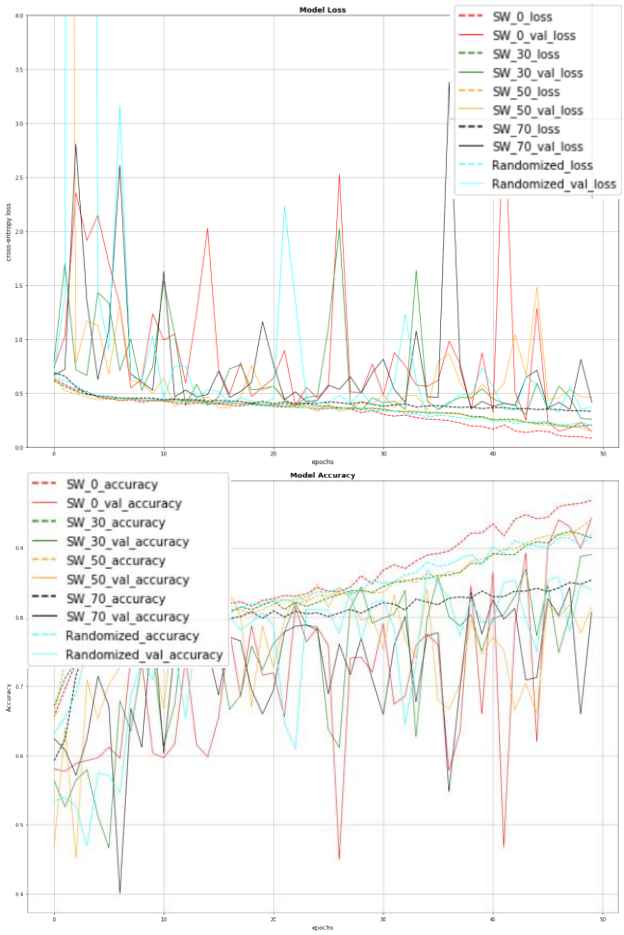


**Figure 3.** Cross-entropy loss and accuracy plot during the SegNet training.

The accuracy of the trained model has been measured on the testing scene which is a completely different flood event happened at a different place. The comparison based on Accuracy, Jaccard Score and F1 Score have been charted as shown in Fig. 4.

## 4. DISCUSSION

As we can see by our result that the F1 score and Jaccard score is very low throughout the different networks as well as different method or scenarios. This is the case because we have selected one of the most difficult problems, first SAR images segmentation already a difficult problem and on top of that flooded area segmentation which has included urban flood, mountainous region, paddy field area etc. making this a very difficult case. However, we need to focus on our main objective and that is the cross-method comparison for the training data development.

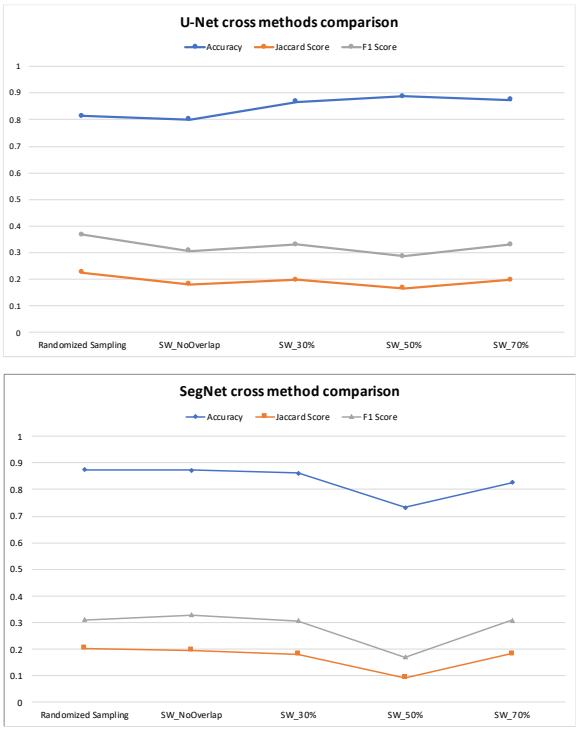


**Figure 4.** Image-chips creation. SW here represents a sliding-window method and different % in number shows the overlap per cent of consecutive windows.

The study has found that 50% overlap has poorest scores throughout, one of the possible reasons can be that it has learned more on the negative samples, this can be seen in Fig. 4, U-Net cross method comparison. In the figure, 50% overlap scenario is showing the highest accuracy which is just a measure of total correct pixels predicted and as non-flooded pixels are much higher in the scene, so predicting most of the pixels as non-flooded area leads to increase the accuracy. However, F1 Score and Jaccard score are lowest showing the failure of predicting the right class for foreground i.e. flooded area.

Overall Randomized sampling shows best or approx. equal score around all the parameters. This seems logical too as all the methods in the study can also be seen as image-chips creation along with data augmentation in the manner of 'translation' (moving image to X and Y direction). Randomized sampling can be seen as translation of the image with an arbitrary factor within (0,512), whereas other method and scenarios have a fixed-step translation.

As per the time concerned for image-chips creation, it was the fastest in the case of the sliding window with no overlap. It was the case due to a smaller number of chips possible with this condition and then for making the desired number of chips, we have just duplicated the valid chips. This duplication is the reason why Fig. 3 shows sharp convergence of SW_O (in Red colour) but with multiple bigger peaks at each interval. This behaviour may be better monitored when training for a greater number of epochs.

Although we have found that randomized sampling is best suited in this case, still it needs a greater number of test cases, for checking that either this observation holds in other cases or not. Moreover, we need to emphasize here that these strategies are not an alternative to more data. As in this case, data information remains the same and the only augmentation happens but augmentation has its limit.

## 5. CONCLUSION

Training data is a very important first step in implementing the DCNNs in the remote sensing areas. We have presented the different strategies to create the training data especially when we have limited satellite scenes. These training datasets has been tested on two very popular segmentation network U-Net and SegNet. Overall both networks show better learning capability with the randomized sampling method. This is justifiable when we compare randomized sampling as a variant of translation of the image chips with an arbitrary data augmentation factor. However, randomized sampling may not give a better result when total selected image-chips are few, as random image chips possibly not be distributed in the whole image but this problem reduces with the increasing number of tiles chosen.

## ACKNOWLEDGEMENT

Authors are thankful to JAXA (Japan Aerospace Exploration Agency) for giving access to the ALOS-2 images as well as to the GSI (Geospatial Information Authority of Japan) for proving the flood mask.

## REFERENCES

Badrinarayanan, V., Kendall, A., & Cipolla, R. (2017). SegNet: A Deep Convolutional Encoder-Decoder Architecture for Image Segmentation. IEEE Transactions on Pattern Analysis and Machine Intelligence, 39, 2481-2495.

Demir, I., Koperski, K., Lindenbaum, D., Pang, G., Huang, J., Basu, S., Hughes, F., Tuia, D., & Raskar, R. (2018). DeepGlobe 2018: A Challenge to Parse the Earth through Satellite Images. 2018 IEEE/CVF Conference on Computer Vision and Pattern Recognition Workshops (CVPRW), 172-17209.

Etten, A.V., Lindenbaum, D., & Bacastow, T.M. (2018). SpaceNet: A Remote Sensing Dataset and Challenge Series. ArXiv, abs/1807.01232.

Gerke, M., Rottensteiner, F., D Wegner, J., Sohn, G.: Isprs semantic labeling contest (09 2014)

Han, S., Fafard, A., Kerekes, J., Gartley, M.G., Ientilucci, E., Savakis, A., Law, C., Parhan, J., Turek, M., Fieldhouse, K., & Rovito, T. (2017). Efficient generation of image chips for training deep learning algorithms. Defense + Security.

Li, T., Comer, M., & Zerubia, J. (2019). Feature Extraction and Tracking of CNN Segmentations for Improved Road Detection from Satellite Imagery. 2019 IEEE International Conference on Image Processing (ICIP), 2641-2645.

Li, W., He, C., Fang, J., Zheng, J., Fu, H., & Yu, L. (2019). Semantic Segmentation-Based Building Footprint Extraction Using Very High-Resolution Satellite Images and Multi-Source GIS Data. Remote. Sens., 11, 403.

Ning, H., Li, Z., Wang, C., & Yang, L. (2020). Choosing an appropriate training set size when using existing data to train neural networks for land cover segmentation. Annals of Gis: Geographic Information Sciences, 1-14.

Ronneberger, O., Fischer, P., & Brox, T. (2015). U-Net: Convolutional Networks for Biomedical Image Segmentation. In International Conference on Medical Image Computing and Computer-Assisted Intervention , 234–241, Munich Germany.

Zhang, C., Wei, S., Ji, S., & Lu, M. (2019). Detecting Large-Scale Urban Land Cover Changes from Very High-Resolution Remote Sensing Images Using CNN-Based Classification. ISPRS Int. J. Geo Inf., 8, 189.

Intercontinental Geoinformation Days

http://igd.mersin.edu.tr/2020/

# Spatiotemporal analysis of land-use changes in a metropolitan city in Malaysia

**Abdulwaheed Tella*[1], Abdul-Lateef Balogun [1], Asmau Balogun[2]**

[1]*Geospatial Analysis and Modelling (GAM) Research Laboratory, Department of Civil and Environmental Engineering, Universiti Teknologi PETRONAS (UTP), 32610 Seri Iskandar, Perak, Malaysia*
[2]*Department of Petroleum Geoscience, Universiti Teknologi PETRONAS (UTP), 32610 Seri Iskandar, Perak, Malaysia*

**Keywords**
Urban sustainability
Land-use
Malaysia
Error matrix
ArcGIS

**ABSTRACT**

Land-use/cover change is an essential element for global environmental development. Rapid changes in the types of land cover can impact the ecosystem and urban sustainability. Thus, this study investigated the land-use changes in a Kuala Lumpur, the most urbanised and populated city in Malaysia. Landsat 8 OLI imageries were used to examine the five (5) years transformation in the land use/cover from 2015 to 2020. The classification of the land use was done in ArcGIS environment, while the error matrix approach was used to validate the classification. From the result, there was an observable built-up expansion from 2015 to 2020 with an estimated 2% increase since 2015. In the land use/cover area mass, there were 0.26% and 4.3% decrease in the water bodies and thick vegetation respectively recorded in 2020. These findings may be attributed to the transformation of the lands for building and construction purposes. Also, the 2.26% increase in the light vegetation in 2020 may be due to the growth of green foliage for enhancing good air quality and breeze. Due to the expected expansion and an increase in urban development, strategical urban planning is necessary to sustain the environment and reduce the impacts of hazards.

## 1. INTRODUCTION

Rapid urbanisation, coupled with some anthropogenic activities, has led to some changes in the land use and cover. Due to some development and growth, land use has influenced the landscape patterns in many cities (Dadashpoor, Azizi, & Moghadasi, 2019). The changes which do not only impact the green ınfrastructure but social, economic and technological forces (Hersperger et al., 2018). Thus, the study of land-use change is critically essential in global environmental change (Lawler et al., 2014; Verburg et al., 2015). Moreover, land-use change is a critical factor for understanding and forecasting climate change and natural hazards (Ning et al., 2018; Tella & Balogun, 2020). Therefore, it becomes essential to understand the series of changes that has transcended to predict some future events and ensures urban sustainability.

Considering the expected increase in urban sizes by 2050 (United UN, 2014), the effects on land use patterns are inevitable. The impact of changes in the land such as deforestation which is common in Southeast Asia (Guo, Lenoir, & Bonebrake, 2018) due to necessity or expansion of conurbations has led to the adverse effect of climate change (Guo et al., 2018; Halim et al., 2020). The changes in the green vegetation, water bodies, and bare surface to build-up due to urban expansion have led to the declination and degradation of the land surface (Halim et al., 2020; Xu et al., 2016). This study, therefore, aims to study the land change pattern in Kuala Lumpur, a megacity in Malaysia. Kuala Lumpur is a metropolitan city, which is the federal capital of Malaysia with an approximate land area of 243 sq. km (Althuwaynee, Balogun, & Al Madhoun, 2020). Due to rapid urban expansion, industrialisation, and commercialisation in this region, it has led to the transformation of landscapes and contamination of the surrounding (Sanusi et al., 2017).

In order to understand the land-use changes and patterns in this city, it is necessary to investigate and examine the alteration in the land use/cover over the previous years. The outcome of this study will assist urban planners and stakeholders in spatial planning on land-use change for urban and environmental

* **Corresponding Author**

*(Tellaabdulwaheed01@gmail.com) ORCID ID 0000 – 0002 – 4380 – 3343
(geospatial63@gmail.com) ORCID ID 0000 – 0002 – 0418 – 3487
(asmaumusa060@gmail.com) ORCID ID 0000 – 0003 – 2306 – 2039

**Cite this study**

Tella A, Balogun A & Balogun A (2020). Spatiotemporal analysis of land-use changes in a metropolitan city in Malaysia. Intercontinental Geoinformation Days (IGD), 148-151, Mersin, Turkey

sustainability. For this purpose, remote sensing and geographical information system (GIS) is used to examine the land-use and cover change. Thus, this research investigates the changes in land use and cover in the last five years in Kuala Lumpur.

## 2. METHOD

Kuala Lumpur is a metropolitan city in Malaysia, with an estimated land area of 243 km$^2$ (Althuwaynee & Pradhan, 2017). It has a relatively flat terrain with an elevation range of 0 to 420m above the sea level (Althuwaynee et al., 2020). The study area is also referred to as Kuala Lumpur Extended Mega Urban Region being the centroid for socio-economic development, coupled with being a national capital of Malaysia (Halim et al., 2020). Over 33% of the total population in Malaysia are residing in Kuala Lumpur, with an expectance of increase in the population density in the future (Abdul Samad & Shaharudin, 2017). Fig.1 shows the location of the study area.

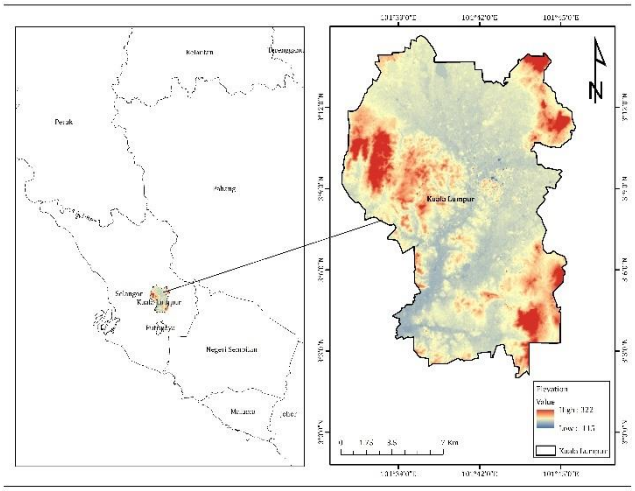


**Figure 1.** Study area

The land use and land cover (LULC) map of the study area was generated from the Landsat 8 OLI (Table 1).

**Table 1.** Landsat 8 OLI data source

| Satellite | Format | Grid Cell | Year | Source |
|---|---|---|---|---|
| Landsat OLI/TIRS | Raster | 30m | 2015 | USGS: https://espa.cr.usgs.gov/ |
| Landsat OLI/TIRS | Raster | 30m | 2020 | USGS: https://espa.cr.usgs.gov/ |

The five years transformation in the land-use and cover of the study area was investigated from the Landsat imageries of the years 2015 and 2020. Supervised classification (Maximum likelihood), one of the most frequently adopted methods used for quantitative analysis of remote sensing data (Rwanga & Ndambuki, 2017) was used in this study while detecting the significant changes. Finally, the error matrix was used to assess the accuracy of the classification.

Fig. 1 shows the flow chart of the methodology employed in this study.

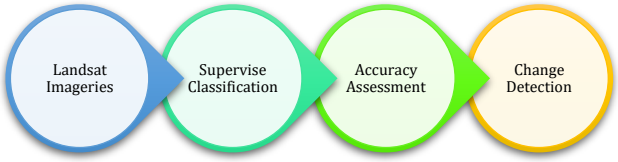


**Figure 1.** Methodology flowchart

## 3. RESULTS

The Supervised classification map for this study was carried out in ArcGIS 10.5 software. There are four land cover classes in the maps produced. The classes include water bodies, thick vegetation, light vegetation, and built up. The description of the land use and cover adopted from (Rwanga & Ndambuki, 2017) was shown in Table 2.

**Table 2.** Land use and land cover structure

| Land use/cover | Description |
|---|---|
| Water bodies | Streams, rivers, lakes, swamps, and reservoirs |
| Thick vegetation | Evergreen and deciduous forest land, |
| Light vegetation | Crop fields, shrubs, and less than 15% vegetated cover |
| Built-up | Residential area, buildings, commercial hub, industrial area, urban area and structures |

The four classes of the land use/cover maps are shown in Fig. 3 and 4. The land use/cover classification was validated using the error matrix approach in order to assess the confidence level of the selected pixel (Bai, Feng, Jiang, Wang, & Liu, 2015). In order to evaluate the accuracy, the pixel of the classified LULC was compared with the actual value pixel of the high-resolution World Imagery in the ArcGIS environment. The overall accuracy of the LULC classification was gotten using equation (1) below. The overall accuracies for classified LULC maps for 2015 and 2020 are 95% and 92.5% respectively.

$$\text{Overall accuracy (\%)} = \frac{\text{total true point}}{\text{total sample point}} \times 100\% \qquad (1)$$

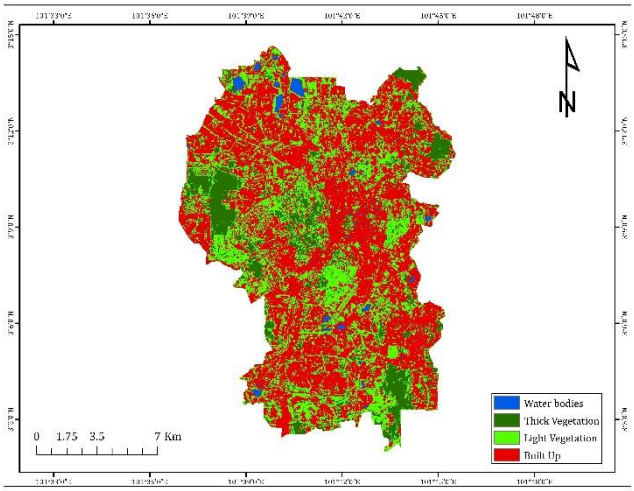


**Figure 3.** Land use and land cover map for the year 2015

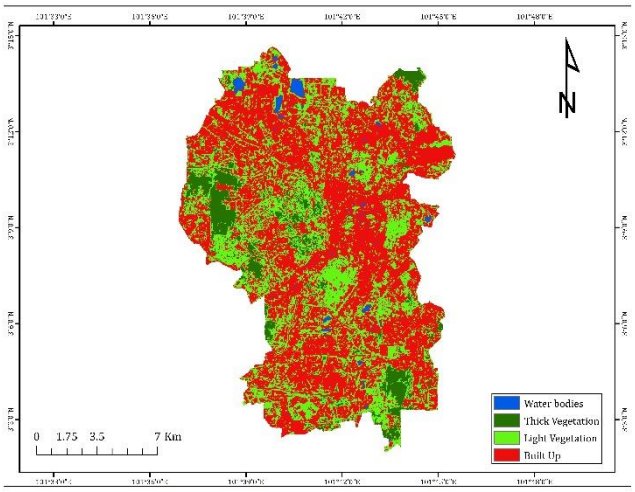


**Figure 4.** Land use and land cover map for the year 2020

The area covered of each class was calculated in square kilometre (km²) and percentage area (%) covered. Table 3 represents the area cover of the LULC. It was observed that there is a 0.26% reduction in the water bodies within the five years interval. This may be due to the transformation of water bodies into built-up or the erection of buildings above the water bodies.

**Table 3.** Area of the land use and land cover map

| | 2015 | | 2020 | |
|---|---|---|---|---|
| | km² | % | km² | % |
| **Water bodies** | 3.17 | 1.31 | 2.54 | 1.05 |
| **Thick vegetation** | 27.81 | 11.5 | 17.43 | 7.2 |
| **Light vegetation** | 74.1 | 30.63 | 79.57 | 32.89 |
| **Built-up** | 136.84 | 56.56 | 142.4 | 58.86 |

Also, clearing of the thick vegetation such as forest might have led to 10.38 km² decrease within the five years interval. Contrarily, light vegetation. Shows a considerable 2.26%. The increase in light vegetation might be due to the planting of some green vegetation in the country to balance the atmospheric elements and sustain the environment.

As hypothesised, the area covered by the built-up increase by approximately 2% affirming the hypothesis that urbanisation influence the changes in land use and cover. According to Halim et al. (2020), rapid urbanisation could affect the land-use patterns resulting in the transformation of an area to another. For instance, the transformation of the vegetated regions to built-up areas. Therefore, it is evident that there is an increasing trend in land-use change. Also, there is an expected increase in alteration of landscape forms in the future (Dadashpoor et al., 2019).

## 4. DISCUSSION

The changes in land use and land cover (LULC) have significant impacts on the sustainability of an environment. Over time, urbanisation and population density have been regarded as the two common factors that influence the changes in the LULC. This study examines the spatiotemporal variations in the LULC by considering two Landsat 8 imageries with a difference of five (5) years. Therefore, this paper reveals the transformation and changes in the LULC in Kuala Lumpur, Malaysia, using geospatial techniques. In order to validate the classification of LULC for accuracy assessment, error matrix method was used. The classification outcome exhibit acceptable accuracy. The government can leverage on the outcome of this study in controlling, monitoring and managing the urban settlement and population growth.

In the last five years, there has been some reduction in some land cover such as the water bodies, and thick vegetation. This might be due to the necessity to expand and transform some landscape for anthropogenic activities. This study aligned with the findings of Shahbaz, Loganathan, Muzaffar, Ahmed, and Ali Jabran (2016), which claimed that surge in the urbanisation and population has led to the transformation of agricultural land to industrial areas in Malaysia.

Increase in urban population demands for more housings, infrastructures and amenities leading to rise in the built-ups. According to Hussain and Byrd (2016), urban population influences the changes in the land cover due to the high demands of housings, and technology to sustain the inhabitants. An over 2% increase of the built-ups is therefore expected given the inevitable need of it.

Although further studies are required to investigate and understand the nexus between urbanisation and LULC, however, this study has shown the behavioural trend of LULC. This proofs that LULC is an important factor to be considered while studying environmental disasters such as flooding, landslide, air pollution, and drought. Also to facilitate sustainable development in the environment, LULC is an essential factor.

## 5. CONCLUSION

This paper examined the land-use changes in Kuala Lumpur, an industrialised and highly populated city in Malaysia. The study used satellite remote sensing imageries of two years 2015 and 2020. The study reveals the five years of transformation in land use. Thus, this research analysed the patterns and changes in the land use for five years interval. Compared to the year 2015, there has been a reduction in water bodies and thick vegetation in the year 2020. However, a significant increase in the built-up and light vegetation was observed in the year 2020. These findings expostulates an urban expansion and the planting of light vegetation around the vicinity for a balanced atmosphere. Considering the dynamic behaviour of the land use/cover, policies and regulations should be enforced to sustain the urban population and environment.

## ACKNOWLEDGEMENT

The authors gratefully acknowledge the United States Geological Survey (USGS) for making the data available for use, and the reviewers for their keen discerning comments to improve this paper.

**REFERENCES**


Abdul Samad, H., & Shaharudin, I. (2017). The Emerging Kuala Lumpur Extended Mega Urban Region (KLEMUR): Implications on Urban Prosperity in Malaysia. *Int. J. Malay World Civilis, 5*, 67-74.

Althuwaynee, O. F., Balogun, A. L., & Al Madhoun, W. (2020). Air pollution hazard assessment using decision tree algorithms and bivariate probability cluster polar function: evaluating inter-correlation clusters of PM10 and other air pollutants. *GIScience & Remote Sensing, 57*(2), 207-226.

Althuwaynee, O. F., & Pradhan, B. (2017). Semi-quantitative landslide risk assessment using GIS-based exposure analysis in Kuala Lumpur City. *Geomatics, Natural Hazards and Risk, 8*(2), 706-732.

Bai, Y., Feng, M., Jiang, H., Wang, J., & Liu, Y. (2015). Validation of land cover maps in China using a sampling-based labeling approach. *Remote Sensing, 7*(8), 10589-10606.

Dadashpoor, H., Azizi, P., & Moghadasi, M. (2019). Land use change, urbanization, and change in landscape pattern in a metropolitan area. *Science of The Total Environment, 655*, 707-719. doi:https://doi.org/10.1016/j.scitotenv.2018.11.267

Guo, F., Lenoir, J., & Bonebrake, T. C. (2018). Land-use change interacts with climate to determine elevational species redistribution. *Nature Communications, 9*(1), 1315. doi:10.1038/s41467-018-03786-9

Halim, N. D. A., Latif, M. T., Mohamed, A. F., Maulud, K. N. A., Idrus, S., Azhari, A., . . . Sofwan, N. M. (2020). Spatial assessment of land use impact on air quality in mega urban regions, Malaysia. *Sustainable Cities and Society, 63*, 102436. doi:https://doi.org/10.1016/j.scs.2020.102436

Hersperger, A. M., Oliveira, E., Pagliarin, S., Palka, G., Verburg, P., Bolliger, J., & Grădinaru, S. (2018). Urban land-use change: The role of strategic spatial planning. *Global Environmental Change, 51*, 32-42. doi:https://doi.org/10.1016/j.gloenvcha.2018.05.001

Hussain, N. H. M., & Byrd, H. (2016). Balik Kampong': Is Malaysia Facing the Trends of De-Urbanization. *International Journal of the Malay World and Civilisation (Iman), 4*(2016), 35-43.

Lawler, J. J., Lewis, D. J., Nelson, E., Plantinga, A. J., Polasky, S., Withey, J. C., . . . Radeloff, V. C. (2014). Projected land-use change impacts on ecosystem services in the United States. *Proceedings of the National Academy of Sciences, 111*(20), 7492-7497.

Ning, J., Liu, J., Kuang, W., Xu, X., Zhang, S., Yan, C., . . . Du, G. (2018). Spatiotemporal patterns and characteristics of land-use change in China during 2010–2015. *Journal of Geographical Sciences, 28*(5), 547-562.

Rwanga, S. S., & Ndambuki, J. M. (2017). Accuracy assessment of land use/land cover classification using remote sensing and GIS. *International Journal of Geosciences, 8*(04), 611.

Sanusi, M., Ramli, A., Hassan, W., Lee, M., Izham, A., Said, M., . . . Heryanshah, A. (2017). Assessment of impact of urbanisation on background radiation exposure and human health risk estimation in Kuala Lumpur, Malaysia. *Environment international, 104*, 91-101.

Shahbaz, M., Loganathan, N., Muzaffar, A. T., Ahmed, K., & Ali Jabran, M. (2016). How urbanization affects CO2 emissions in Malaysia? The application of STIRPAT model. *Renewable and Sustainable Energy Reviews, 57*, 83-93. doi:https://doi.org/10.1016/j.rser.2015.12.096

Tella, A., & Balogun, A.-L. (2020). Ensemble fuzzy MCDM for spatial assessment of flood susceptibility in Ibadan, Nigeria. *Natural Hazards, 104*(3), 2277-2306. doi:10.1007/s11069-020-04272-6

UN. (2014). World urbanization prospects: The 2014 revision, highlights. department of economic and social affairs. *Population Division, United Nations, 32*.

Verburg, P. H., Crossman, N., Ellis, E. C., Heinimann, A., Hostert, P., Mertz, O., . . . Golubiewski, N. (2015). Land system science and sustainable development of the earth system: A global land project perspective. *Anthropocene, 12*, 29-41.

Xu, G., Jiao, L., Zhao, S., Yuan, M., Li, X., Han, Y., . . . Dong, T. (2016). Examining the impacts of land use on air quality from a spatio-temporal perspective in Wuhan, China. *Atmosphere, 7*(5), 62.

Intercontinental Geoinformation Days

http://igd.mersin.edu.tr/2020/

# Remote sensing image fusion using transform domain based on optimization algorithms

**Asan Ihsan Abas*[1], Nurdan Akhan Baykan[1]**

[1]*Konya Technical University, Department of Computer Engineering, Konya, Turkey*

**Keywords**
Remote sensing
Image fusion
Optimization algorithms
Laplacian transform
Pan-sharpening

**ABSTRACT**

With the rapid development of technology today in different fields like military, medicine, robotics, remote sensing, finding underground sources, target tracking, target identification, microscopic imaging, and security applications are need clearer and more meaningful images. Sometimes images from a single sensor are not enough for analysis. For this reason, images taken by different sensors and different features are used together. For this purpose, image fusion (Pan-sharpening) has got great importance. The image obtained by fusion methods contains more meaningful and clear information. In this study, metaheuristic algorithms are used to sharpen the Multispectral (MS) image with a Panchromatic (Pan) image in remote sensing. In this study, the coefficients obtained from Curvelet and Laplacian Pyramid transformations are using with weights that are generated by Particle Swarm Optimization (PSO) and Bat Algorithm (BAT) in the fusion process. A fused image has been successfully achieved by preserving the spatial information of the high-resolution Pan image and the color information of the low-resolution MS image. The obtained results have had a clearer, brighter, and richer edge information. Visual and quantitative comparison of the obtained results were also evaluated.

## 1. INTRODUCTION

Image Fusion process aims to combine images from more than one sensor at the same time and belong to the same region, thereby improving the image quality. Image fusion is used in many applications. With the emergence of new sensors and the advancement and development of technology and hardware, it is possible to analyze and process real-time data in image fusion. Many different methods, especially Artificial Intelligence (AI) algorithms, are used to increase the image quality of fusion applications. Today, with developing technologies and decreasing costs, satellite images are used in many areas. However, nowadays, data can be received from sensors on satellites at certain frequency ranges and certain resolutions. For this reason, the fusion process is used to obtain more robust and more informational satellite images. In remote sensing, the Image fusion is the process of combining high spatial resolution panchromatic (Pan) image with low-resolution Multispectral (MS) image, which are recorded simultaneously from different satellites (Abas et al. 2015). It is aimed to obtain a single image containing complementary information by detecting the features from two different images and this process is called pan-sharpening. In this study, Particle Swarm Optimization (PSO) and Bat Algorithm (BAT) were used to determine the weights in the fusion process with the coefficients obtained from Curvelet and Laplacian Pyramid transformations. In the study, the proposed method was evaluated by using Landsat-7ETM + satellite images. The proposed technique was compared visually and quantitatively.

## 2. MATERIAL AND METHOD

### 2.1. Laplacian Pyramid (LP)

Laplacian Pyramid (LP) provides low pass filtering and subsampling images in the image analysis. LP is an extension of the Gaussian Pyramid (GP). Different frequency bands are used in LP instead of a single low pass filter. Each level of LP is obtained by calculating the difference between the signal at the top level of GP and each lower resolution level of GP. LP Transformation is obtained by applying Filter to the previous level of the GP, then taking the difference between this level and the signal "Eq. 1" (Burt and Adelson 1983; Colores-Vargas et al. 2013; Gupta 1999; Wang and Chang 2011).

* **Corresponding Author**

*(e138129002004@ktun.edu.tr) ORCID ID 0000-0002-9977-6663
(nbaykan@ktun.edu.tr) ORCID ID 0000 – 0002- 4289 - 8889

**Cite this study**

Abas A I & Baykan N A (2020). Remote sensing image fusion using transform domain based on optimization algorithms. Intercontinental Geoinformation Days (IGD), 152-157, Mersin, Turkey

$$G_l(i,j) = \sum_{x=-2}^{2}\sum_{y=-2}^{2} w(x,y)G_{l-1}(2i+x, 2j+y) \quad l \in [1,N), i \in [0,X_l), j \in [0,Y_l) \tag{1}$$

Here, $G_l$ is Gaussian pyramid, $w(x,y)$ is the Gaussian weighting function at low pass filters. The source image in the initial layer is the $G_0$ and $N$ is the number of the Gaussian layers; $X_l$ and $Y_l$ represented the number of columns and rows in the $i^{th}$ layers of the pyramid.

The second stage Laplacian Pyramid decomposition can be calculated as given in "Eq. 2".

$$LP_L = f(x) = \begin{cases} G_l - G^*_{l+1}, & L \in [0,L) \\ G_l, & l = L \end{cases} \tag{2}$$

Where $G^*_{l+1}$ is Gaussian expanded of $G_l$. $LP_L$ is the Laplacian pyramid and *l* is the *l*-th level decomposed; *L* is the number of LP levels.

## 2.2. Curvelet Transform (CVT)

The Curvelet transformation was first described by Candès and Donoho (Candes and Donoho 2000). To solve the problem limitation of Gabor and Wavelet transform. It's suitable for mapping edges in image processing problems. Mathematically, it is used for the analysis of big data set and remove the noise. In this work we used a 2-D discrete CVT version implemented fast Fourier Transform and proposed by Candès et al. in 2006 (Candes et al. 2006) "Eq. 3".

$$C(j,l,k) = \frac{1}{(2\pi)^2}\int \hat{f}(\omega)\,\bar{\varphi}_{i,j,k}d(x) = \frac{1}{(2\pi)^2}\int \hat{f}(\omega)\,U_j\left(R_{\theta_i}\omega\right)exp\left[i < x_k^{(i,j)}, >\right]d\omega \tag{3}$$

Where $\hat{f}(\omega)$, is the Fourier coefficients and *i, j* is the index of the pixel image; θ is orientation in the range and $\hat{U}$ is a parabolic window, $\varphi$ scale of coefficient, $C(j,l,k)$ is the CVT coefficient (Starck et al. 2001).

## 2.3. Fusion With Metaheuristic Algorithms

### 2.3.1. Parameter selection with PSO

The Particle Swarm Optimization (PSO) algorithm was purposed by Kennedy and Eberhart (Kennedy and Eberhart 1995) in 1995 to solve a complex nonlinear problem. PSO is started with a group of random solutions (particles) and populations, each particle updates to find an optimal solution. At each iteration, each particle is updated according to the two "best" values. The first of these is the best fitness value a particle has ever found. Also, this value is kept in memory for use later and is named as "pbest", the other best value is obtained so far by any particle in the population, and it is the solution with the best fitness value in the group. This value is the global best particle and is called "gbest". Every particle in the PSO Each particle in the PSO looks for the best solution. The position and velocity are determined by "Eq. 4" and "Eq. 5" (Lin et al. 2015)

$$V_l^{k+1} = \omega \times V_l^k \times C1 \times rand \times \left(Pbest_l^k - X_l^k\right) + C2 \times rand \times \left(Gbest^k - X_l^k\right) \tag{4}$$

$$X_l^{k+1} = X_l^k + V_l^{k+1} \quad , l = 1,2,\ldots.Q \tag{5}$$

Where $V_l^{k+1}$ is velocity and $X_l^{k+1}$ is a position of $l^{th}$ particle in iteration *k+1*. *Pbest* is the best value of fitness function achieved by $i^{th}$ particle before iteration $k$ and *Gbest* is the best fitness function value achieved so far by any particle. *c1* and *c2* acceleration coefficients, *rand* is a random variable between [0, 1], and $\omega$ is represented the inertia weight factor used to provide well balanced mechanism between global and local exploration abilities.

### 2.3.2. Parameter selection with BAT

Bat algorithms is a swarm intelligence based algorithm. It is echolocation behavior inspired to locate their food and prey, it is an algorithm proposed by Mirjalili et al. in 2010 and it is a metaheuristic algorithm used to solve many different problems (Mirjalili et al. 2014; Yang 2010a, 2010b; Yildizdan and Baykan 2020). Every bat in the population uses a form of radar called "echolocation" to locate and communicate with their prey. Bat echolocation is a perceptual system. It is a perceptual system in which a series of loud ultrasonic waves are released to create an echo. These waves return with various sound levels that enable bats to find specific prey. Velocity and position and they are updated using "Eq. 6-8".

$$f_i = f_{min} + (f_{max} - f_{min})\beta \tag{6}$$

$$v_i^t = v_i^{t-1} + (x_i^{t-1} - x_*)f_i \tag{7}$$

$$x_i^t = x_i^{t-1} + v_i^t \tag{8}$$

Where $\beta$ is a random vector, the frequency *f* is in a range $[f_{min}, f_{max}]$ and it is velocity increment. And $v_i$ is the velocity at position $x_i$ with time iteration *t*.

The parameters of the PSO and BAT are given in "Table 1", below.

**Table 1**. Parameters of PSO and BAT for fusion

| | PSO | BAT |
|---|---|---|
| Population size (s) | 40 | 40 |
| Inertia weight (w) | 0.1 | X |
| Max. Iteration (iter) | 40 | 40 |
| Learning constants | Constants c1=c2=2 | X |
| Parameter value Frequency | X | Frequencies $f_{min}$=0 and $f_{max}$=2 |
| Initial Pulse rate (r) | X | 0.5 |
| Initial Loudness (A) | X | 0.25 |

X: Not parameter value

## 2.4. Image Fusion

In image fusion, first, the source images are decompositions into low and high-frequency sub-image components by one of the transformation methods such as LP or CVT.

High-frequency subband images reflect detailed components and contain edge detail information from

different directions and scales of the source image. On the other hand, low-frequency subband images indicate the component representing the main information of the source image. After decomposed; the fusion rule in the high-frequency domain is the absolute maximum rule "Eq. 9", and the average or weighted average rule is commonly used in the low-frequency domain "Eq. 10".

$$CF_{ij}^{H} = \begin{cases} CA_{ij}^{H}, & CA_{ij}^{H} > CB_{ij}^{H} \\ CB_{ij}^{H}, & CA_{ij}^{H} < CB_{ij}^{H} \end{cases} \quad (9)$$

$$CF_{ij}^{L} = \frac{1}{2}\left(CA_{ij}^{L} + CB_{ij}^{L}\right) \quad (10)$$

In "Eq. 9", where $CF_{ij}^{H}$ is high-frequency fusion image coefficient, $CA_{ij}^{H}$ and $CB_{ij}^{H}$ are high-frequency source images coefficients. In "Eq. 10", where $CF_{ij}^{L}$ is a low-frequency fusion image coefficient, $CA_{ij}^{L}$ and $CB_{ij}^{L}$ are low-frequency source images coefficients.

The fusion rules are very important to fusion quality because they control the contrast and intensity of a fused image. Therefore, a new fusion rule for the low-frequency band has been proposed in this study to obtain better image fusion.

Instead of taking the average of the coefficients of the source images in the low-frequency band, image-based adaptive-weighted coefficients are produced using metaheuristic algorithms, and fusion was performed "Eq. 11".

$$CF_{ij}^{L} = \frac{\left(\omega 1 \times CA_{ij}^{L} + \omega 2 \times CB_{ij}^{L}\right)}{\omega 1 + \omega 2}, \omega \in (0,1) \quad (11)$$

The optimization algorithm, it is aimed to obtain $\omega 1$ and $\omega 2$ coefficients that minimize the mean square error (RMSE) "Eq. 14" while maximizing the entropy (EN) "Eq. 12" and correlation coefficient (CC) "Eq. 13".

$$Entropy = -\sum_{i=0}^{255} p(i) \times \log_2(p(i)) \quad (12)$$

In "Eq. 12", p(i) is the probability value of the brightness of the fused image.

$$CC = {}^{1}/_{2}\left(\frac{\sum_{i=1}^{M}\sum_{j=1}^{N}(I_1(i,j)-\bar{I}_1)(F(i,j)-\bar{F})}{\sqrt{\sum_{i=1}^{M}\sum_{j=1}^{N}(I_1(i,j)-\bar{I}_1)^2}\sqrt{\sum_{i=1}^{N}\sum_{j=1}^{M}(F(i,j)-\bar{F})^2}} + \frac{\sum_{i=1}^{M}\sum_{j=1}^{N}(I_2(i,j)-\bar{I}_2)(F(i,j)-\bar{F})}{\sqrt{\sum_{i=1}^{M}\sum_{j=1}^{N}(I_2(i,j)-\bar{I}_2)^2}\sqrt{\sum_{i=1}^{N}\sum_{j=1}^{M}(F(i,j)-\bar{F})^2}}\right) \quad (13)$$

$$RMSE = {}^{1}/_{2}\left(\sqrt{\frac{1}{M\times N}\sum_{i=1}^{M}\sum_{j=1}^{N}\left(\left(I_1(i,j)\right)-F(i,j)\right)^2} + \sqrt{\frac{1}{M\times N}\sum_{i=1}^{M}\sum_{j=1}^{N}\left(\left(I_2(i,j)\right)-F(i,j)\right)^2}\right) \quad (14)$$

In "Eq. 13" and "Eq. 14" the I1 and I2 are input images and Fi is the fusion image. M, N are the image dimensions.

Accordingly, the linear combination given in "Eq. 15" was used for the multi-objective function (Rao 2009)

$$f(x) = (\alpha_1 * CC) + (\alpha_2 * Entropi) + (\alpha_3 * 1/RMSE) \quad (15)$$

The objective function is given in "Eq. 15", as well as α1,α2, and α3, are tested for different values and the best results are taken as α1=α2=0.25 and α3=0.5. With the proposed methods the meaningful information was transferred from the source images to the fusion image, and better results were obtained. In this study, the parameters of the objective function ("Eq. 15") were optimized with PSO/BAT. The flow diagram of the proposed method is given in "Fig. 1". The steps of the proposed method can be summarized as follows:

**Step1:** Read the remote sensing image1 (MS) and image2 (Pan).

**Step2:** Source images (MS, PAN) are converted to LP/ CVT space to obtain the Low and High-frequency bands for each image, respectively.

**Step3:** Apply the fusion rule in "Eq. 11" with the coefficients and weights (w1, w2) generated by the PSO/ BAT for each region in the low-frequency bands of LP/ CVT.

**Step4:** Fused high-frequency coefficients using maximum selection fusion rule defined in "Eq. 9".

**Step5:** Using the last obtained coefficients to get a fused image by applying the inverse LP / CVT transformation.

## 3. EXPERIMENTAL RESULTS

Remote sensing data sets used in fusion study are Landsat-7ETM + MS and Landsat-7ETM + PAN satellite images. Detailed information about the features of these images is given in "Table 2" (Saeedi and Faez 2011).

**Table 2.** Landsat-7ETM+ satellite images features

| Sensor | Spectral Band (Spectral resolution) (μm) | | Spatial resolution (m) | Radiometric Resolution (m) | Image Size |
|---|---|---|---|---|---|
| Landsat -7ETM+ (MS) | 1 | 450–515 (Blue) | 28.5 | 2 | 7348 x 6208 |
| | 2 | 525–605 (Green) | 28.5 | 2 | |
| | 3 | 630–690 (Red) | 28.5 | 2 | |
| | 4 | 760–900 (NIR) | 28.5 | 2 | |
| | 5 | 1550–1750(MID-IR1) | 28.5 | 2 | |
| | 6 | 2080–2350(MID-IR2) | 28.5 | 2 | |
| Landsat -7ETM+ (Pan) | 1 | 520–920nm (Pan) | 28.5 | 2 | 14696 x 12416 |

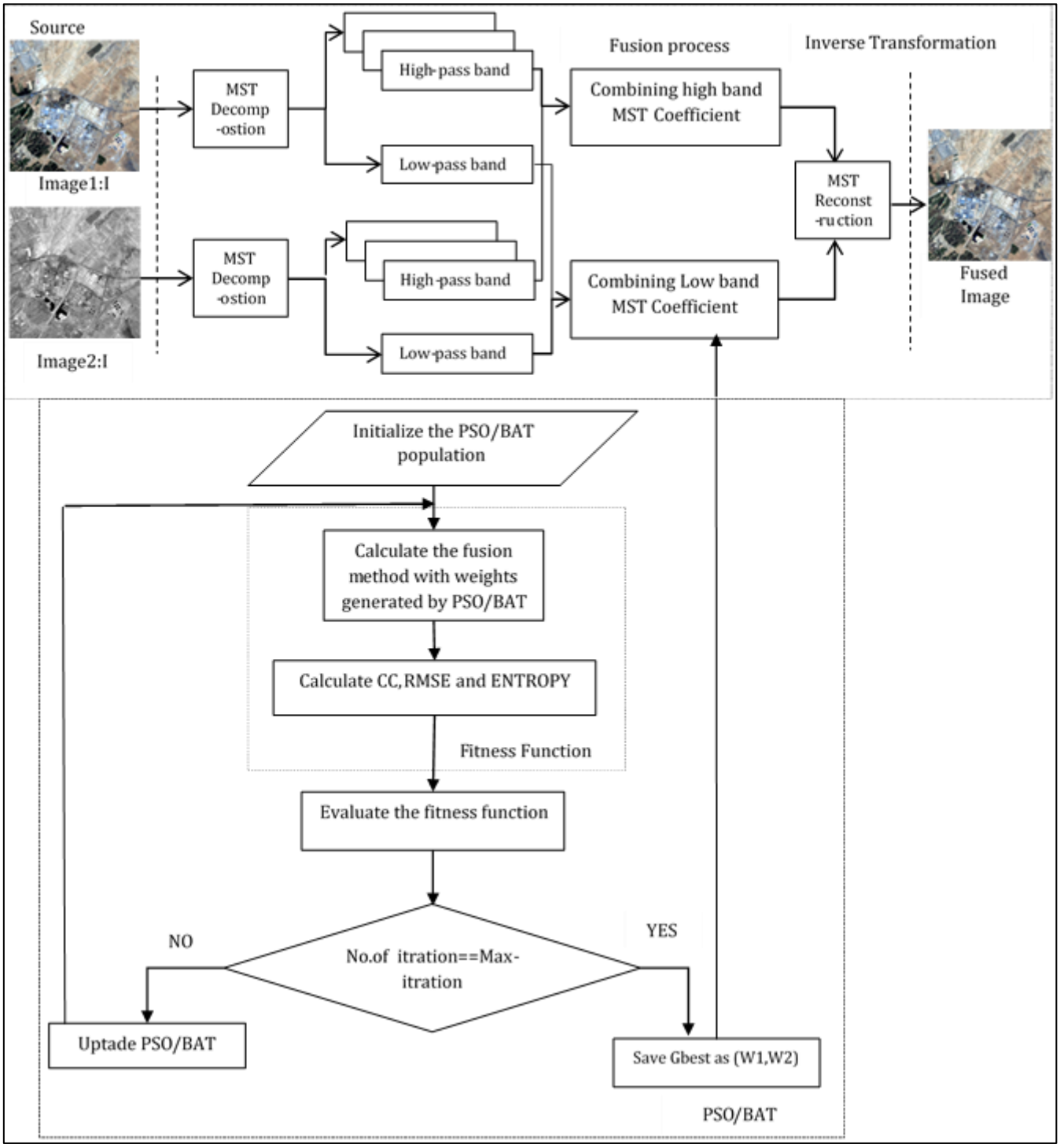


**Figure 1.** The image fusion process step with PSO and BAT algorithms

In measuring the success of the fusion image obtained from the fusion processes, while the resulting images are expected to preserve spectral values, on the other hand, quality analyzes need to be made quantitatively to increase the spatial resolution. To compare the results of experiments, three quality metrics ERGAS (Relative Dimensionless Global Error in Synthesis) (Wald 2000), RASE (Relative average spectral error) (Ranchin and Wald 2000) and CC (CC-Correlation Coefficient) (Zhou et al. 1998) were used. The results obtained are given in "Table 1" and the result of the satellite images is given in "Fig. 2".

**Table 3.** Fusion Test Results

| Fusion Methods | ERGAS | RASE | CC | Weights |
|---|---|---|---|---|
| CVT | 3.4110 | 13.5698 | 0.9293 | $w_1 = 0.5$<br>$w_2 = 0.5$ |
| CVT + PSO | 2.6735 | 11.9325 | 0.9501 | $w_1 = 0.59$<br>$w_2 = 0.41$ |
| CVT + BAT | 2.5726 | 10.2362 | 0.9637 | $w_1 = 0.62$<br>$w_2 = 0.38$ |
| | | | | |
| LP | 2.4232 | 10.9564 | 0.9590 | $w_1 = 0.5$<br>$w_2 = 0.5$ |
| LP + PSO | 2.1927 | 10.0702 | 0.9663 | $w_1 = 0.51$<br>$w_2 = 0.49$ |
| LP + BAT | **1.9978** | **9.3303** | **0.9718** | $w_1 = 0.324$<br>$w_2 = 0.676$ |

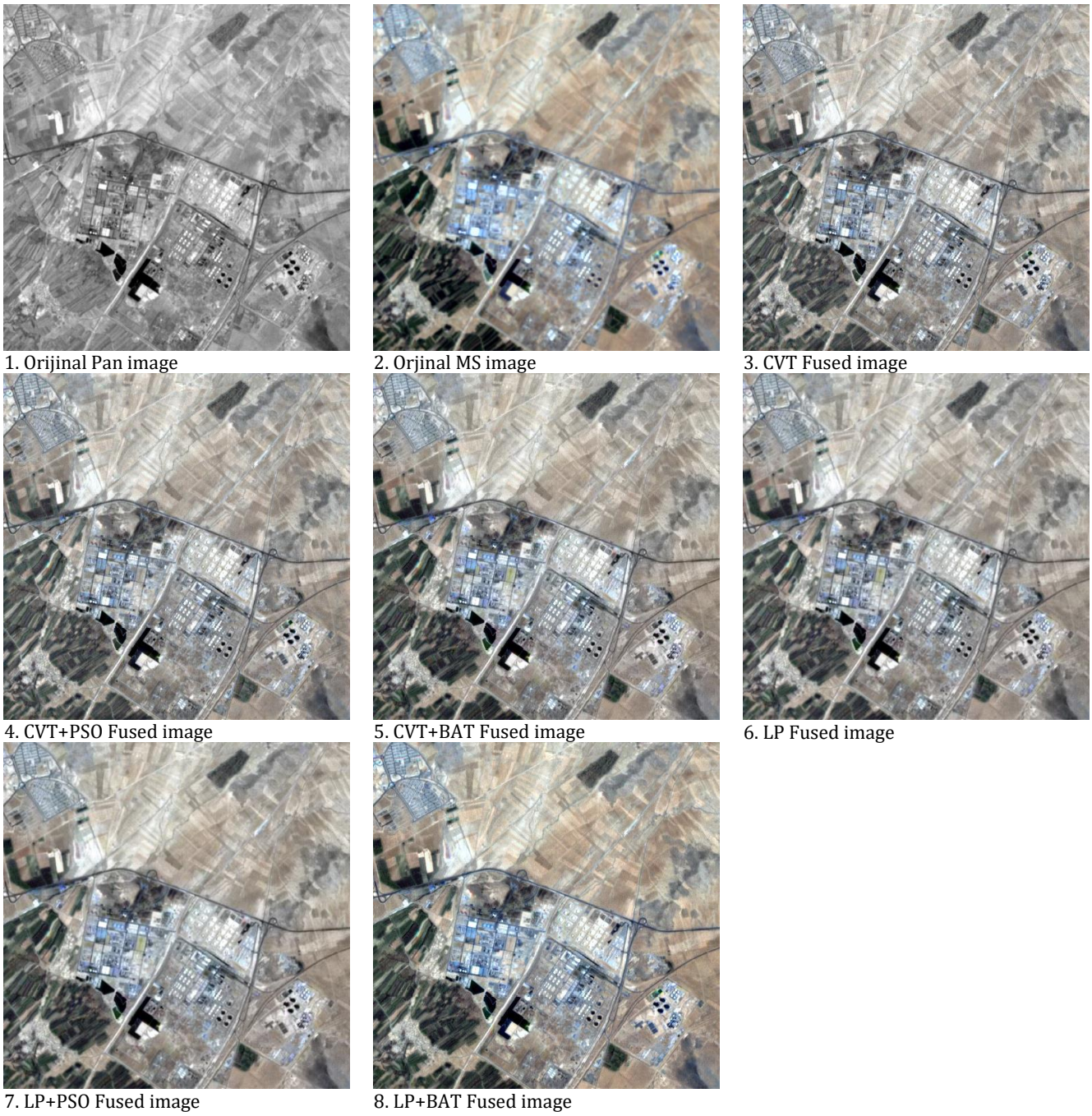

1. Orijinal Pan image
2. Orjinal MS image
3. CVT Fused image
4. CVT+PSO Fused image
5. CVT+BAT Fused image
6. LP Fused image
7. LP+PSO Fused image
8. LP+BAT Fused image

**Figure 2.** The results of satellite images

## 4. CONCLUSION

In this study, for combining Landsat-7ETM + MS and Landsat-7ETM + PAN satellite images a fusion method LP and CVT transformations, based on PSO and BAT algorithms are proposed. In the literature, generally, most of the standard fusion methods (weights are taking equal values) usually leading to loss of contrast in the fused image. However, this problem has been solved by the weights are optimized in the best way in the proposed method. In the study, the proposed method was evaluated using Landsat-7ETM + satellite images. In general evaluation, the best result was obtained using the LP + BAT fusion method.

## REFERENCES

Abas A, Yakar M and Baykan N (2015) Image Fusion in Remote Sensing Sistems. TUFUAB VIII. Technical Symposium, (s. 183-189), Konya.

Burt P & Adelson E (1983). The Laplacian pyramid as a compact image code. IEEE Transactions on communications, 31(4), 532-540.

Candes E, Demanet L, Donoho D & Ying L (2006). Fast discrete curvelet transforms. Multiscale Modeling & Simulation, 5(3), 861-899.

Candes E J & Donoho D L (2000). Curvelets: A surprisingly effective nonadaptive representation for objects with edges. Retrieved from

Colores Vargas J M, García Vázquez, M, Ramírez Acosta A, Pérez-Meana H & Nakano-Miyatake M. (2013). Video images fusion to improve iris recognition

accuracy in unconstrained environments. Paper presented at the Mexican Conference on Pattern Recognition.

Gupta M M (1999). Soft computing and intelligent systems: theory and applications: Elsevier.

Kennedy J & Eberhart, R (1995). Particle swarm optimization. Paper presented at the Proceedings of ICNN'95-International Conference on Neural Networks.

Lin J, Chen C L, Tsai S F, & Yuan C Q. (2015). New intelligent particle swarm optimization algorithm for solving economic dispatch with valve-point effects. Journal of Marine Science and Technology, 23(1), 44-53.

Mirjalili S, Mirjalili S M & Yang X S (2014). Binary bat algorithm. Neural Computing and Applications, 25(3-4), 663-681.

Ranchin T & Wald L (2000). Fusion of high spatial and spectral resolution images: The ARSIS concept and its implementation.

Rao S S (2009). Engineering Optimization: Theory and Practice, Copyright© 2009 by John Wiley & Sons. In: Inc.

Saeedi J & Faez K (2011). A new pan-sharpening method using multiobjective particle swarm optimization and the shiftable contourlet transform. Isprs Journal of Photogrammetry and Remote Sensing, 66(3), 365-381.

Starck J L, Donoho D L & Candes E J (2001). Very high quality image restoration by combining wavelets and curvelets. Paper presented at the Wavelets: Applications in Signal and Image Processing IX.

Wald L (2000). Quality of high resolution synthesised images: Is there a simple criterion.

Wang W & Chang F (2011). A Multi-focus Image Fusion Method Based on Laplacian Pyramid. JCP, 6(12), 2559-2566.

Yang X S (2010a). Nature-inspired metaheuristic algorithms: Luniver press.

Yang X S (2010b). A new metaheuristic bat-inspired algorithm. In Nature inspired cooperative strategies for optimization (NICSO 2010) (pp. 65-74): Springer.

Yildizdan G & Baykan Ö K (2020). A novel modified bat algorithm hybridizing by differential evolution algorithm. Expert Systems with Applications, 141, 112949.

Zhou J, Civco D & Silander J (1998). A wavelet transform method to merge Landsat TM and SPOT panchromatic data. International Journal of Remote Sensing, 19(4), 743-757.

Zhou Y, Xie J, Li L & Ma M (2014). Cloud model bat algorithm. The Scientific World Journal, 2014.

Intercontinental Geoinformation Days

http://igd.mersin.edu.tr/2020/

# Land Use and Shoreline Dynamics in Lagos State, Nigeria

**Swafiyudeen Bawa** *[1], **Adamu Bala**[1], **Abubakar Sadiq Sani** [2]

[1]*Department of Geomatics, Faculty of Environmental Design, Ahmadu Bello University, Zaria, Nigeria*
[2]*Department of Geography Federal College of Education, Zaria, Nigeria*

**Keywords**
Land Use
Shoreline
Lagos State
Nigeria
DSAS

**ABSTRACT**

The city of Lagos, Nigeria has experienced remarkable changes in terms of land use and land cover (LULC) and shoreline changes as a result of increase in population, industrialization and urbanization. These have led to coastal erosion, depletion, loss of settlement and other socio-economic problems. This contribution uses remote sensing technique to delineate coastal changes from 1999-2019 as well as LULC with a view to determine the shoreline dynamics during the study period. Landsat 7 ETM+ and Landsat 8 OLI were acquired and subjected to image pre-processing and processing techniques. The digital shoreline analysis system (DSAS) was employed to delineate the shoreline change parameters, viz: Net Shoreline Movement (NSM), End Point Rate (EPR) and Linear Regression Rate (LRR) of the shoreline for the years 1999, 2009 and 2019 respectively. The LULC result indicate that, bare-land decreases from 0.96-0.45%, vegetation decreases from 53.11-45.25% and water body decreases from 25.58-22.99%, while built-up-area increase from 20.35-31.16%. NSM values for erosion rate ranges from -36.61 to -857.46m/period, while accretion ranges from 72.72 to 260.85m/year. EPR for erosion rate ranges from -1.84 to -2.48m/year, while accretion ranges from 4.64 to 13.04m/year. LRR for erosion rate ranges from -1.83 to -2.47m/year, while accretion ranges from 3.54 to 13.04m/year. The findings revealed shoreline movement toward the sea (accretion) or movement of the shoreline inland (erosion).

## 1. INTRODUCTION

Change detection alludes to the identification of differences in the condition of land features by observing them at different temporal scale. This process can be achieved manually or with the guide of remote sensing techniques. (Karl and Axel, 2013). It is a process that measures how attributes of a particular location in question have changed between two or more epoch (Anusha and Bharathi, 2019).

An idealized definition of shoreline is seen as the intersection of the physical interface of land and water (Boak and Turner, 2005). On the other hand, coastal areas are locations where water is the dominant factor that encompasses or bounds it. Coastal changes caused by natural and human activities have important consequences for coastal ecosystem and coastal communities. Coastlines are natural boarders which separate water and land. Changes of coastline are of great importance, therefore, it is needed to detect these changes for economic and social purposes (Temiz and Savaş Durduran, 2016).

Coastal region of Lagos state, Nigeria is affected by considerable amount of coastal deformation caused by both natural and human activities. This study tends to examine the Land use changes and shoreline dynamics in Lagos state, Nigeria. This is with a view to detect and analyse the dynamics of the Lagos coastline over time. This study therefore, considers both the coastal and lagoon region of Lagos, as against Akinluyi et al. (2018) who only considered the coastal zone.

### 1.1 Study Area

Lagos state (Fig. 1) located in South-Western Nigeria. It is bounded to the North-east by Ogun state and to the West by the republic of Benin. Atlantic Ocean provides a coastline to the South. It covers an approximate area of 3907.968m$^2$ (Akinluyi et al., 2018).

## 2. DATA SOURCES AND METHOD

For the purpose of this study, satellite datasets from several sensors: Operational Land Imager (OLI), Landsat 7 Enhanced Thematic Mapper plus (ETM+) for the year 1999, 2009 and 2019 were downloaded from United States Geological Survey (USGS) through its website (http://earthexplorer.usgs.gov/) along with the

* **Corresponding Author**

*(bswafiyudeen@gmail.com) ORCID ID 0000-0002-2384-9432
(adamubala09@gmail.com) ORCID ID 0000-0002-9666-5722
(abusadiqsan@gmail.com) ORCID ID 0000-0003-4835-2710

**Cite this study**

Bawa S, Bala A & Sani A S (2020). Land Use and Shoreline Dynamics in Lagos State Nigeria. Intercontinental Geoinformation Days (IGD), 158-161, Mersin, Turkey

administrative map of Nigeria (shape file format) downloaded from (diva-gis.org/datadown).

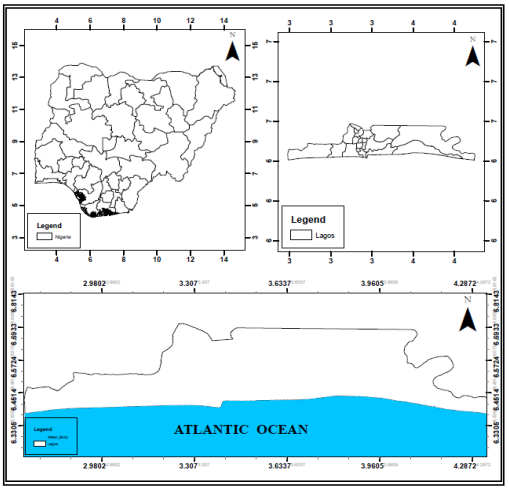


**Figure 1.** Map of Nigeria (top left); Lagos (top right); Lagos and South part of Atlantic Ocean (bottom)

ERDAS Imagine 9.2 was used for the pre-processing and processing of the Landsat data. While digital shoreline analysis system (DSAS)(Himmelstoss et al. 2018) was used for shoreline delineation and analysis. Fig. 2 is the summary of the workflow diagram adopted for the study. NMS, EPR and NSM are the embedded DSAS statistics used. The NSM is the distance between oldest and the youngest shorelines for each transect; EPR is the ratio of NSM by the time elapsed between the oldest and the most recent shoreline; a least-squares regression line is fitted to all shoreline points for a transect to compute the LRR.

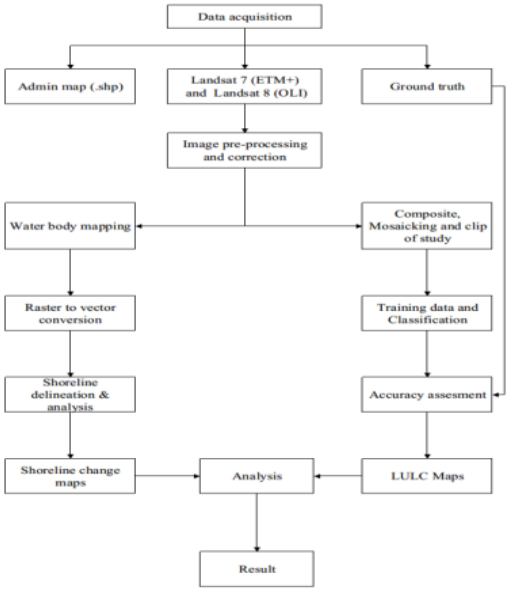


**Figure 2**. Workflow diagram adopted for the study

## 3. RESULTS

### 3.1. Land Use Land Cover (LULC) Distribution

The bar chat in Fig. 3 and Table 1 show the overall Land Use Land Cover change (LULC) for the duration of twenty (20) years from 1999-2019 of Lagos state. Fig. 4, 5 and 6 depict the derived LULC map of the study area for the year 1999, 2009 and 2019 respectively. However, calculated values from the classified multi-temporal satellite imageries show a remarkable change in terms of the classified classes namely: bare-land, built-up-area, vegetation and water body respectively. Base on the trend analysis, results show that bare-land; vegetation and water body experience a noticeable decrease which is as a result of urbanization. In Table 1, it is presented that, bare-land decrease from 0.96 to 0.41%. Similarly, vegetation decreases from 53.11 to 45.25% and the area covered by water body is 25.58%, 22.98% and 22.99% for years 1999, 2009 and 2019 respectively. On the other hand, built-up-area experiences a remarkable increase. The areas covered are 20.35%, 23.77% and 31.16% for the years 1999, 2009 and 2019 respectively.

Accuracy assessment was then performed by a collection of 100 random points from ancillary data and the overall accuracy, producer and user accuracy as well as the Kappa coefficient is reported in Table 2.

**Table 1**. Land use classes from 1999-2019

| Classes | 1999 | | 2009 | | 2019 | |
|---|---|---|---|---|---|---|
| | Area (Ha) | Area (%) | Area (ha) | Area (%) | Area (Ha) | Area (%) |
| Bare-land | 3643.6 | 0.96 | 1692.56 | 0.45 | 1558.34 | 0.41 |
| Built-up-Area | 76968.7 | 20.35 | 89881.98 | 23.77 | 118752.8 | 31.35 |
| Vegetation | 200844.9 | 53.11 | 199688.4 | 52.8 | 171433.4 | 45.25 |
| Water Body | 96741.58 | 25.58 | 86935.92 | 22.98 | 87106.25 | 22.99 |
| **TOTAL** | **378198.8** | **100** | **378198.8** | **100** | **378850.8** | **100** |

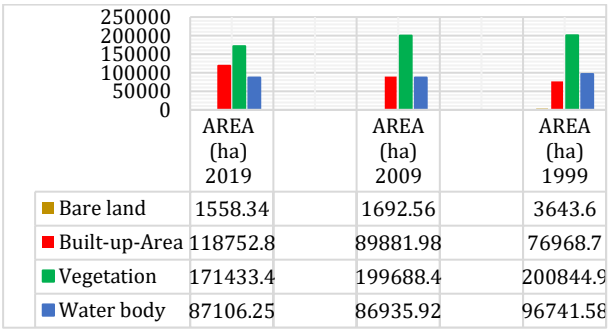


**Figure 3.** Land Use Land Cover (LULC) trend of Lagos from 1999-2019

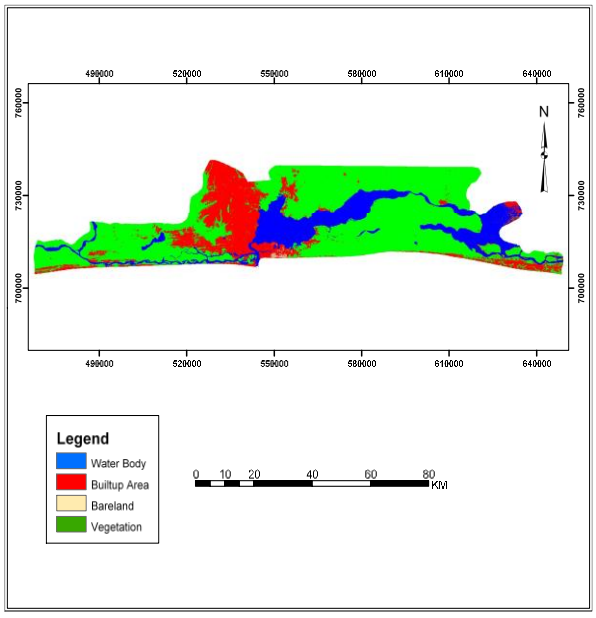


**Figure 4.** Derived LULC map of Lagos, Nigeria 1999

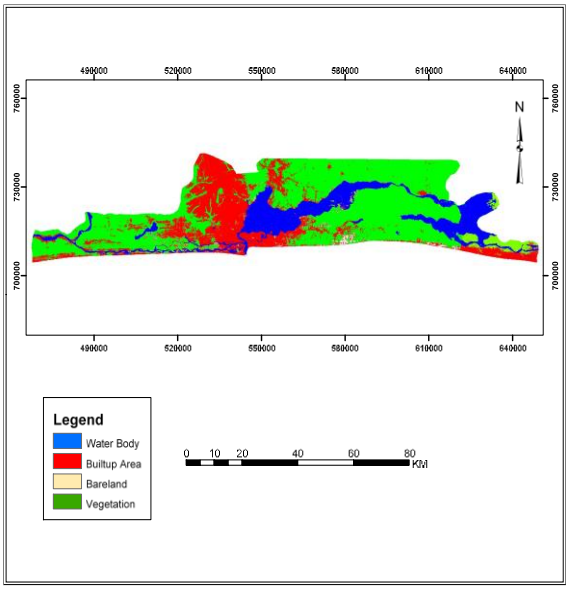


**Figure 5.** Derived LULC map of Lagos, Nigeria 2009.

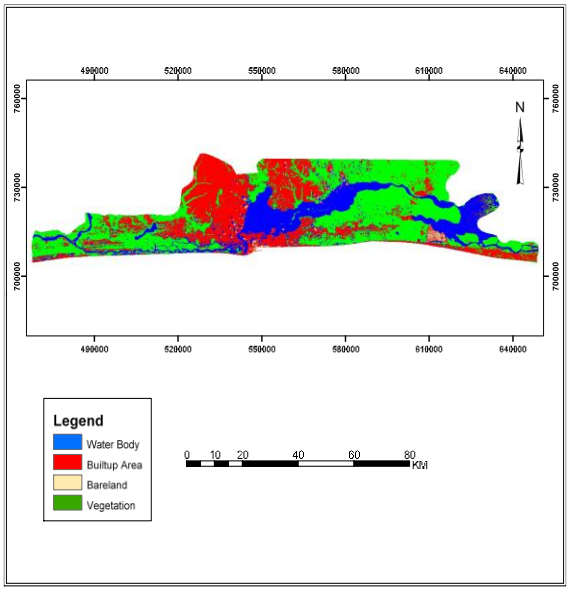


**Figure 6.** Derived LULC map of Lagos, Nigeria 2019.

**Table 2.** Accuracy result of the classified images

| Classes | 1999 | | 2009 | | 2019 | |
|---|---|---|---|---|---|---|
| | Producer accuracy (%) | User accuracy (%) | Producer accuracy (%) | User accuracy (%) | Producer accuracy (%) | User accuracy (%) |
| Bare-land | 95.83 | 92 | 100 | 92 | 98 | 96 |
| Built-up-Area | 100 | 96 | 96.15 | 100 | 100 | 97.83 |
| Vegetation | 96.15 | 100 | 96.15 | 100 | 100 | 98.24 |
| Water Body | 92.31 | 96 | 98 | 96 | 92.59 | 100 |
| Kappa statistics | 0.95 | | 0.96 | | 0.97 | |
| Overall accuracy | 96.00 | | 97.00 | | 97.00 | |

### 3.2. Shoreline Change Rate from 1999-2019

The total length of the extracted shoreline was computed using South Atlantic Ocean part of Lagos and lagoon as reference. The extracted shoreline length for Landsat 7 ETM+ image of the year 1999 is 186.51km, for 2009 is 187.04km, and that of the Landsat 8 OLI of the year 2019 is 188.84km respectively with reference to the open sea (South Atlantic Ocean). On the other hand, when Lagoon is considered, the extracted shoreline length for the year 1999 is 549.00km, 551.87km for 2009, and 579.02km for the year 2019 respectively. From 2009 to 2019, results show the movement of the shoreline towards the sea (accretion rate) to a distance of approximately 2 kilometres as result of the construction of Eko Atlantic city along the coast in the southern axis.

Over time, the extracted shorelines reveal that there is a remarkable change in the shoreline width (see Fig. 7 and 8). A total of over 2000 number of transects were generated with 200m spacing and averaged change rate of the shoreline was calculated from 1999-2019. Tables 3 and 4 show the result of the shoreline change statistics, positive estimations of the change insights speak to a shoreline development towards the ocean (accretion) rate and negative values speaks to a shoreline development inland (erosion) rate.

**Table 3.** Lagos Shoreline change rate from 1999-2019

| Shoreline change statistics | Erosion | Accretion |
|---|---|---|
| NSM (m/period) | -36.61 | 260.85 |
| EPR (m/year) | -1.84 | 13.04 |
| LRR (m/year) | -1.83 | 13.04 |

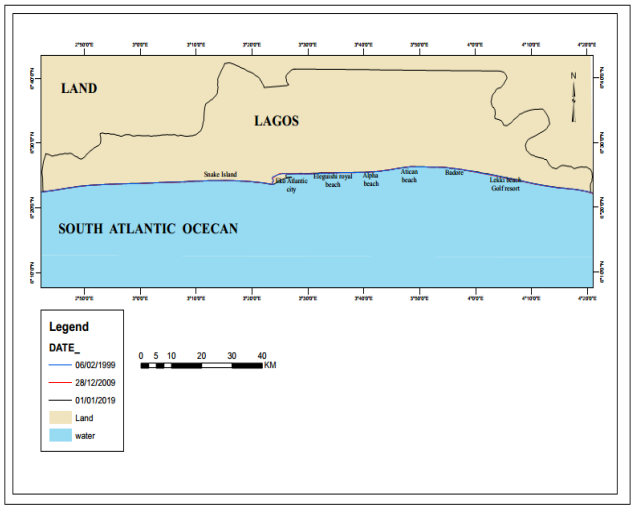


**Figure 7.** Shoreline change map of Lagos coastline 1999-2019

**Table 4.** Lagos and Lagoon Shoreline change rate from 1999-2019

| Shoreline change statistics | Erosion | Accretion |
|---|---|---|
| NSM (m/period) | -857.46 | 72.72 |
| EPR(m/year) | -2.48 | 4.64 |
| LRR (m/year) | -2.47 | 3.54 |

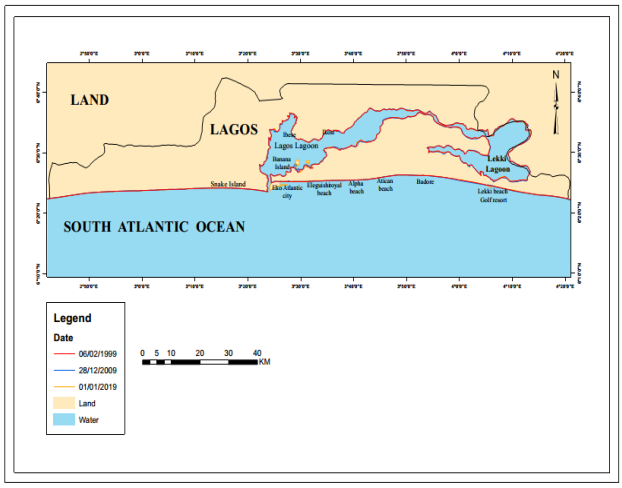


**Figure 8.** Shoreline change map of Lagos coastline and the lagoon 1999-2019

## 4. DISCUSSION

The study presents remarkable land use and shoreline changes in Lagos state Nigeria by taking advantage of multi-temporal satellite mission and state of the art geospatial software.

The dominant land use class for the study period (1999, 2009 and 2019) increasing at a very fast rate is the built-up areas (see Table 1 and Fig. 3). This is consistent with the study of (Akinluyi et al., 2018). The water body decreased by about 3.6% from 1999-2019. This might be attributed to land reclamation activities by the Lagos state government.

When only the coast line is considered, the NSM reveal that about 78.05% of the transects had negative distances while 21.95% had positive values. These values are the same for the percentage of EPR that have erosional and accretional values respectively. For the LRR, 78.02% of the transects are erosional while 21.98% are accretional. When only the coast line and Lagoon are considered, the NSM reveal that about 35.14% of the transects had negative distances while 64.86% had positive values. These values are the same for the percentage of EPR that have erosional and accretional values respectively. For the LRR, 35.16% of the transects are erosional while 64.84% are accretional.

For the first case, possible reason for high erosional rate in the coastline is a result of destruction of vegetation for residential purposes (see Figs. 4, 5 and 6). While for the second case, the effort to the authorities concerned to reclaim land might have resulted to the high percentage of accretion.

## 5. CONCLUSION

The contribution has illustrated the use of remote sensing technique in monitoring coastal changes in terms of Land Use Land Cover (LULC) and long term coastline geometry change study with reasonable accuracy.

The LULC classes (bare land, vegetation and water body) are migrating to build up area class. It was also observed that the coastline of the city of Lagos, Nigeria has experience a change in both position and geometry.

Based on the findings it was observed that significant changes occurred in the coastal region as a result of both natural and anthropogenic activities.

The calculated shoreline change results indicate the shoreline movement toward the sea (accretion) or movement of the shoreline inland (erosion). Therefore, the use of remote sensing and GIS technique prove to be useful in monitoring changes in the coastal region for decision making.

## ACKNOWLEDGEMENT

We acknowledge United States Geological Survey (USGS) for providing Landsat imageries free of charge.

## REFERENCES

Akinluyi, F. O., Adebola, A. O., & Adeseko, A. A. (2018). Assessment of Shoreline and Associated Landuse/Land cover Changes along Part of Lagos Coastline, Nigeria. Contemporary Trends in Geoscience, *7*, 59–70. doi: 10.2478/ctg-2018-0004

Anusha, N., & Bharathi, B. (2019). An overview on Change Detection and a Case Study Using Multi-temporal Satellite Imagery. *2019* International Conference on Computational Intelligence in Data Science (ICCIDS), 1–6. doi: 10.1109/ICCIDS.2019.8862160

Boak, E. H., & Turner, I. L. (2005). Shoreline Definition and Detection: A Review. Journal of Coastal Research, *21*(4 (214)), 688–703. doi: 10.2112/03-0071.1

Himmelstoss, E. A., Henderson, R. E., Kratzmann, M. G., & Farris, A. S. (2018). Digital Shoreline Analysis System (DSAS) version 5.0 user guide. In Digital Shoreline Analysis System (DSAS) version 5.0 user guide (USGS Numbered Series No. 2018–1179). Reston, VA: U.S. Geological Survey. doi: 10.3133/ofr20181179

Karl, J., & Axel, A. (2013). Change Detection. Retrieved October 11, 2020, from https://wiki.landscapetoolbox.org/doku.php/remote_sensing_methods:change_detection

Temiz, F., & Savaş Durduran, S. (2016). Monitoring Coastline Change Using Remote Sensing and GIS Technology: A case study of Acıgöl Lake, Turkey. *44*, 042033. Doi: 10.1088/1755-1315/44/4/042033

Intercontinental Geoinformation Days

http://igd.mersin.edu.tr/2020/

# Indoor navigation application using augmented reality technology

**Salih Hamdi Çalık*[1], Fatih Gülgen [1]**

[1]*Yildiz Technical University, Faculty of Civil Engineering, Department of Geomatics Engineering, Istanbul, Turkey*

**Keywords**
Navigation
Augmented reality
GNSS
Tracking
Indoor areas

**ABSTRACT**

Modelling indoor and outdoor areas and designing navigation applications based on the created models has been one of the most preferred working areas of geomatics engineers in the last 20 years. Navigation applications that answer the question of how to get there have now become an indispensable part of human life. While the Global Navigation Satellite System (GNSS) provides sufficient solutions for tracking the location of users in outdoor navigation applications, it is not a suitable solution due to signal interruptions in indoor areas. For this reason, researchers have developed different alternative methods to obtain and track the location information of users indoors. However, these methods have limitations such as the need for additional hardware and high cost. This study aims to develop an indoor navigation application for Android-based smartphones using Augmented Reality technology without the need for any additional equipment for user location tracking.

## 1. INTRODUCTION

In recent years, people spend most of their time in indoor areas such as university buildings, shopping malls and hospitals. The complexity of these areas causes people who have to reach their destination to prefer using navigation tools (Wang 2009). Maps and map-based navigation applications that can be understood by most people regardless of language and culture are tools that help navigate users in an unfamiliar area (Mistry 2008). Most navigation applications use the global navigation satellite system (GNSS) to determine both user and target locations. While GNSS can provide a good solution in outdoor areas, it is not suitable for indoor positioning and navigation applications due to the weakening of GNSS signals in indoor areas and no signal in some areas (Farid 2013; Kim 2004; Rehman 2016; Dardari 2015). Many indoor applications to obtain device positions utilize wi-fi fingerprinting, wireless local area network (WLAN), bluetooth low energy (BLE), radio frequency identification (RFID), ultra-wideband (UWB), inertial sensors, computer vision, hybrid technologies and techniques (Dardari 2015; DiVerdi 2008; Liu 2007; Werner 2001; Chen 2017).

Also, navigation applications use a background map to guide users. This background provides users to match real-world objects with the map symbols. The matching process sometimes can be a challenging task for the map users. Today augmented reality (AR) technology is used to overcome this challenge and increase the interaction between the user and the map interface (Tatzgern 2011). AR systems expand users' visual and auditory perceptions of their environment by enriching the real environment with information generated in the computer environment (Patron 2005; Huey 2011). The users do not need to establish a connection between maps and the real environment as in conventional navigation applications, and thus they can use navigation more interactively and immersively (Vogl 2009; Guzmán 2014). This study focuses on the use of AR technology in indoor navigation. In this context, an indoor navigation application using AR technology was developed with a mobile device with basic equipment suitable for today's technology and accuracy analysis was performed for location tracking accuracy.

## 2. METHOD

### 2.1. Study Area

This study was developed for the entrance floor of the Faculty of Architecture located in the South Campus

* **Corresponding Author**

*(salihcalik95@gmail.com) ORCID ID 0000 – 0002 – 6451 – 1147
(fgulgen@yildiz.edu.tr) ORCID ID 0000 – 0002 – 8754 - 9017

**Cite this study**

Çalık S H, & Gülgen F (2020). Indoor navigation application using augmented reality technology. Intercontinental Geoinformation Days (IGD), 162-165, Mersin, Turkey

of the Karlsruhe Institute of Technology. The floor plan of the study area is shown in Fig 1.

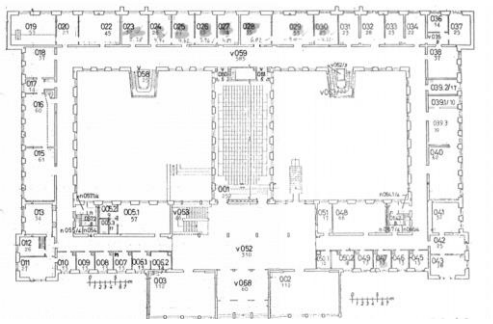

**Figure 1.** The study area

### 2.1. Hardware

In this study, the Samsung Galaxy Note 9 device with Google ARCore support was used as a test device and the technical features of the device were given in Table 1.

**Table 1.** Technical features of the Samsung Galaxy Note 9

| | |
|---|---|
| Processor | Samsung Exynos 9810 |
| Memory | 6 GB RAM |
| Camera | 12 MP, f/1.5-2.4, 26mm |
| Sensors | Accelerometer, Gyro, Compass, Barometer |
| Screen Size and Resolution | 6.4 inches – 1440x2960 |
| Operating System | Android 8.1 |

The technical features of the device such as processor, RAM, camera, sensors, and version of the operating system are convenient and efficient both in tracking user's positions and directions, as well as the processing and viewing auxiliary guidance arrows. The most important hardware of a mobile device is the processor that provides the connection between other hardware. A mobile phone camera is used to detect the real environment. A user's location and orientation can be tracked by combining visual information detected from the real environment and sensor data. The screens allow the user to communicate with the application. The device must be running Android 7.0 or newer for using Google ARCore.

### 2.1. Software

The mobile application, which uses augmented reality technology to help users navigate indoors, was developed on the Unity 3D platform, using the ARCore software development tool and the C# programming language. Google's ARCore is a software development tool that use to track the location of the mobile device. It detects visually different perceptible points called point of interest in the environment with the camera image of the mobile device, and can combine this visual information with the data from the mobile device's sensors to track users. With the mobile device's camera and sensors, ARCore uses a hybrid-based tracking technique, using a combination of computer vision and sensor-based tracking systems.

The interface design of the application was carried out using the Unity 3D development engine and the C# programming language supported by this platform. Unity 3D development engine has wide ease of use and provides library support and a hybrid-based development platform to programmers. The user interface of the application developed is shown in Fig. 2.

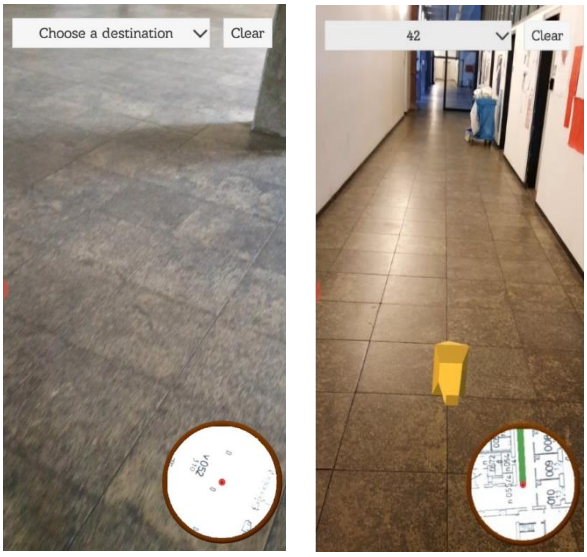


**Figure 2.** Left: The user interface. Right: Display of the auxiliary arrow used in guiding the user in real environment

While designing the interface, it has been prioritized that the users can use it in the most comfortable and easy way. Therefore, there are only 2 buttons in the application where users can select the location they want to go and delete this selection. In addition to these 2 buttons, there is a mini map where the users can follow their position on the floor plan. As seen in the image on the right of Figure 1, after the user determines the target point, the shortest path is calculated and the path the user will go on the floor plan is shown. In addition to this display, guiding arrows created as the main element in directing the users are displayed on the camera images of the users by using AR technology. Thus, the user does not have to establish a connection between the real world and the application as in classical navigation applications.

## 3. RESULTS

In order to evaluate the developed system, five test routes with different navigation distances starting from a certain fixed point and ending with the return to that fixed point were determined and a total of six separate walks were performed in these test routes and local position information was recorded on the mobile device. Then, at the end of the walks, the position of the starting point calculated by the application and the actual position value was compared, and the position accuracy was calculated. The position accuracy of the system for different navigation distances are shown in Table 2.

**Table 2.** Relationship between distance and position accuracy

| Navigation Distance (m) | Position Accuracy (m) |
|---|---|
| 34 | 0.1092 |
| 36 | 0.0397 |
| 66 | 0.5459 |
| 80 | 0.7307 |
| 220 | 4.3877 |
| 220 | 3.4066 |

According to Table 2, the application has sufficient accuracy at short navigation distances without the need for additional equipment. However, as a result of the 220-meter navigation distance, it was observed that an average error of 3.86 m occurred. The tracking accuracy curve created using the navigation distance and position accuracy shown in Table 2 is shown in Fig. 3.

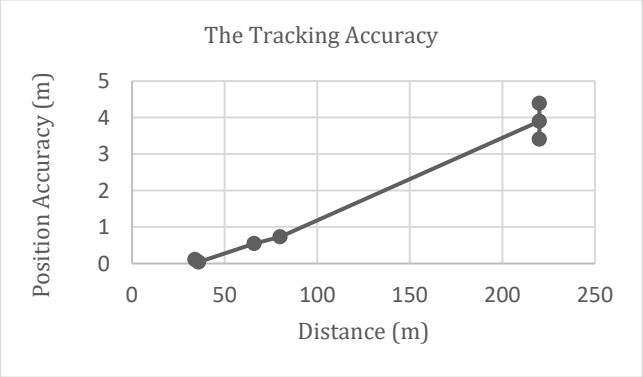


**Figure 3.** The tracking accuracy

The graph shows that the location accuracy of the system is within one meter until the navigation distance is approximately 100 m.

## 4. DISCUSSION

In this study, a hybrid-based tracking method using phone sensors and computer vision-based tracking methods together was used. With this system, low-cost user tracking was performed without the need for additional equipment. Accuracy analysis of the system was made according to different walking distances, and as a result of this analysis, it was seen that the system did not give good results after 100 meters and gave good results up to 100 meters. It can be said that one reason for this result is that in some parts of the corridors inside the building, the patterns on the floor continue the same and there are long white walls. Because it has been observed that the location tracking was stopping from time to time since sufficient points of interest for location calculation could not be detected in these areas. Another reason can be said to be the drift effects that may occur in the long-distance tracking of the phone sensors.

In order to improve system performance, location can be updated using a marker at 100m, where position accuracy is rapidly increasing. In addition, more realistic results should be obtained by using more data sets to determine the location accuracy.

## 5. CONCLUSION

In this study, we examined the effectiveness of indoor navigation application with AR technology. In order to determine the accuracy of the system, the position accuracy resulting from different navigation distances was calculated. According to the position accuracy, it was concluded that users can be tracked without the need for additional equipment. However, it is possible for the accuracy analysis results to change with the change of the test area and the change in the perceptible point of interest in the environment. Therefore, in our future research, it is planned to evaluate the performance of the system by using more data sets and for a different Indoor area. Besides the accuracy analysis of the system, the contribution of augmented reality technology to navigation applications will be researched further, considering the evaluation of user-application performance measurements, including navigation time, ease of use, and user satisfaction.

## ACKNOWLEDGEMENT

We gratefully thank Dr.-Ing. Sven Wursthorn for sharing his experiences and data of this study area with us.

## REFERENCES

Chen A T Y, Fan J, Biglari-Abhari M, Kevin I, & Wang K (2017). A computationally efficient pipeline for camera-based indoor person tracking. International Conference on Image and Vision Computing New Zealand (IVCNZ), 1-6, Christchurch, New Zealand.

Dardari D, Closas P, & Djurić P M (2015). Indoor tracking: Theory, methods, and technologies. IEEE Transactions on Vehicular Technology, 64(4), 1263-1278.

DiVerdi S, & Höllerer T (2008). Heads up and camera down: A vision-based tracking modality for mobile mixed reality. IEEE Transactions on visualization and computer graphics, 14(3), 500-512.

Farid Z, Nordin R, & Ismail M (2013). Recent advances in wireless indoor localization techniques and system Journal of Computer Networks and Communications, 1-12, https://doi.org/10.1155/2013/185138.

Guzmán Guzmán, J D (2014) Augmented Reality user interface analysis in mobile devices. MS Thesis, Polytechnic University of Catalonia, Barcelona.

Huey L C, Sebasian P, & Drieberg M (2011). Augmented Reality based indoor positioning navigation tool. In IEEE Conference on Open Systems, 256-260, Langkawi, Malaysia.

Kim J W, Jang H J, Hwang D H, & Park C (2004). A step, stride and heading determination for the pedestrian navigation system. Journal of Global Positioning Systems, 3(1-2), 273-279.

Liu H, Darabi H, Banerjee P, & Liu J (2007). Survey of wireless indoor positioning techniques and systems. IEEE Transactions on Systems, Man, and Cybernetics, Part C (Applications and Reviews), 37(6), 1067-1080.

Mistry P, Kuroki T, & Chang C (2008). TaPuMa: tangible public map for information acquirement through the things we carry. In Proceedings of the 1st

international conference on Ambient media and systems,1-5, Brussels, Belgium.

Patron C (2005) The concept for the use of augmented reality in assembly planning. PhD Thesis, Technical University of Munich, Munich (in German).

Rehman U, & Cao S (2016). Augmented-reality-based indoor navigation: A comparative analysis of handheld devices versus google glass. IEEE Transactions on Human-Machine Systems, 47(1), 140-151.

Tatzgern M, Kalkofen D, Grasset R, & Schmalstieg D (2011). Embedded virtual views for augmented reality navigation. In Proc. Int. Symp. Mixed Augmented Reality-Workshop Vis. Mixed Reality Environ., 115-123, Basel, Switzerland.

Vogl W (2009) Eine interaktive räumliche Benutzerschnittstelle für die Programmierung Von Industrierobotern. Herbert Utz Verlag. ISBN:3-83160-869-5

Wang P P, Wang T, Ding D, Zhang Y, Bi W, & Bao Y (2009). Mirror world navigation for mobile users based on augmented reality. In Proceedings of the 17th ACM international conference on Multimedia,1025-1026, Beijing, China.

Werner M, Kessel M, & Marouane C (2011). Indoor positioning using smartphone camera. International Conference on Indoor Positioning and Indoor Navigation, 1-6, Guimarães, Portugal.

Intercontinental Geoinformation Days

http://igd.mersin.edu.tr/2020/

# An investigation of Triangular Greenness Index performance in vegetation detection

**Nizar Polat**[*1]

[1]*Harran University, Faculty of Engineering, Department of Geomatics Engineering, Sanliurfa, Turkey*

**Keywords**
Photogrammetry
Triangular Greenness Index
Color Slices
Unmanned Aerial Vehicles

**ABSTRACT**

Vegetation is one of the most important elements of environment. With the use of satellite systems and especially multispectral images including NIR wavelength, vegetation-oriented studies have increased intensely. With today's advancing technology, besides satellite systems, the unmanned aerial vehicles (UAV) systems are also used to generate similar spectral information being as a platform. However, there are mostly RGB sensors rather than NIR band sensors. More intensive use of RGB sensors has led to the need to use these data in vegetation research. The visible region vegetation index called Triangular Greenness Index (TGI) in the literature is one of the indexes arising from this need. In this study, aerial photographs of an orchard were obtained by the UAV and an orthophoto was produced. Then, the trees detection performance of the TGI in the orchard was compared with the reference data. As a result, the TGI approach can be able to obtain trees with a 95% rate of producer accuracy. This index provides significant support for plant detection studies in the absence of NIR data.

## 1. INTRODUCTION

With the recent use of unmanned aerial vehicles (UAV) in civilian areas, new opportunities have emerged in many disciplines. Today UAVs are used in many areas such as agriculture, firefighting, transportation, natural life surveillance, aerial shooting, post-earthquake damage and radiation detection. The use of UAVs in agriculture are generally passive applications for disease and pest detection, water stress detection, yield and maturity estimation, weed flora detection, water resources control and monitoring of workers based on remote sensing and plant monitoring techniques that will constitute the infrastructure of data to be used in precision agriculture. The use of unmanned aerial vehicles for agricultural purposes is extremely important, especially in terms of sustainable and sensitive agricultural practices. In terms of agriculture, UAVs can be used in many different areas such as control of water resources, product observation, equipment and building observation, mapping, yield control, soil erosion, water stress, disease, pest and weed detection and control (Türkseven 2016; Özgüven 2018 ; Şin and Kadıoğlu 2019). For this, different featured cameras are used, and it becomes possible to fight these weeds (Bannari et al. 1995). The data to be obtained from the UAVs mounted cameras can be passed through different processes and the existing flora can be mapped (Özgüven 2018), and the product losses that may occur are calculated. Due to the sensitivity of green plants to infrared wavelengths, NDVI and similar studies are carried out (Türkseven et al. 2018). However, visible region indexes are also available in the scientific literature. In this study, an orchard was observed by producing the Triangular Greenness Index (TGI) from UAV based RGB orthophoto.

## 2. METHOD

### 2.1. Study Area and Equipment

The study was held in orchards located in the northern part of the Harran University Osmanbey Campus (Figure 1). A 22 minutes flight was carried out with TurkUAV Octo V3 automatically depending on the flight plan. The flight plan was prepared as 6 columns from 60 m height. The Sony RX100 camera (20.2 Megapixel CMOS sensor) was mounted to UAV and 223 geotagged images were taken.

* **Corresponding Author**

*(nizarpolat@harran.edu.tr) ORCID ID 0000-0002-6061-7796

**Cite this study**

Polat N (2020). An investigation of Triangular Greenness Index performance in vegetation detection. Intercontinental Geoinformation Days (IGD), 166-168, Mersin, Turkey

**Figure 1.** Study area in Harran University Osmanbey Campus (Rectangle site)

### 2.2. Triangular Greenness Index (TGI)

Today, spectral information is very important for agriculture in both separating vegetation and deeper examination of vegetation. Generally, these studies are based on spectral indices which are generated either calculating band ratios or normalizing band differences (Jackson and Huete 1991). Most of this index uses NIR wavelengths which is sensitive to both chlorophyll content and leaf area index (LAI). Haboudane et al. (2008) suggested the triangular chlorophyll index based on green, red and red-edge bands to detect leaf nitrogen amount. Later, red-edge bands are used on many satellite sensors (Eitel et al. 2007; Herrmann et al. 2011; Ramoelo et al. 2012) and this increase the sensitivity to chlorophyll detection (Gitelson 2012). However, NIR or red-edge bands are generally not available on low-cost multispectral sensors, which have only at visible wavelengths bands; therefore, a visible-band index called the triangular greenness index (TGI) was developed (Hunt et al. 2011). The proposed method is depending on the chlorophyll content.

**TGI:** $0.5(120(Red - Green) - 200(Red - Blue)$ **(1)**

Within the scope of the study, TGI image was divided into two classes as the vegetation and the other. For this, the color slicing method was applied. Color Slicing process assigns the same colors to the pixels with similar values in a user decided values range (Harris Geospatial 2016). This tool, which is available in many commercial and open source software, provides ease of visual perception of data and the possibility to obtain the desired color class in vector format. This step is applied for to calculate accuracy of detection rate of trees. Green vegetation such as grass in the study area were visually monitored by orthophoto overlay analysis. However, a metric accuracy analysis was also made with reference data of the trees in the region.

$$\textbf{Producer Accuracy (PA):} \frac{TP}{TP+FN} \quad (2)$$

$$\textbf{User Accuracy (UA):} \frac{TP}{TP+FP} \quad (3)$$

$$\textbf{Quality (Q):} \frac{TP}{TP+FN+FP} \quad (4)$$

Where TP is true positive, FP is false positive, and FN is false negative values of detected trees with respect to reference data.

## 3. RESULTS

Within the scope of the study, an UAV flight was performed. The flight is planned as 70% overlap from 60 m height. A total of 223 suitable geotagged images were selected and processed. The GSD value calculated for the study is 1.28 cm/pix and 2 521 581 features are matched and 162 085 970 3D points belonging to the study area were obtained. The camera locations, image overlaps and generated orthophoto can be seen in Figure 2.

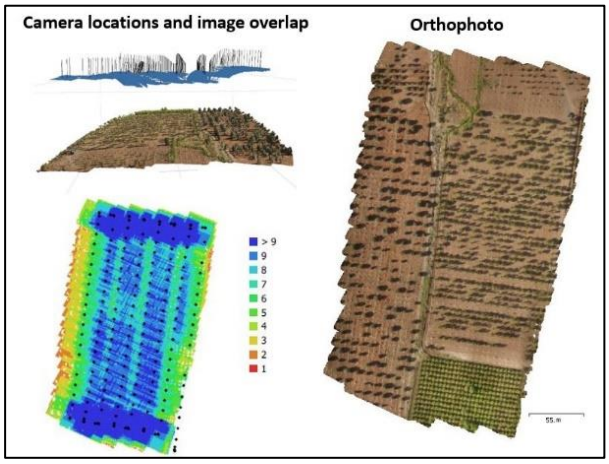


**Figure 2.** Camera locations, Image overlaps and Orthophoto

In the next part of the study is the TGI generation. This step is performed with band math tool in Envi software in accordance with the given equation 1. Then the color slice is applied to generated TGI image. TGI, color slice and color slice overlaid orthophoto can be seen in Figure 3.

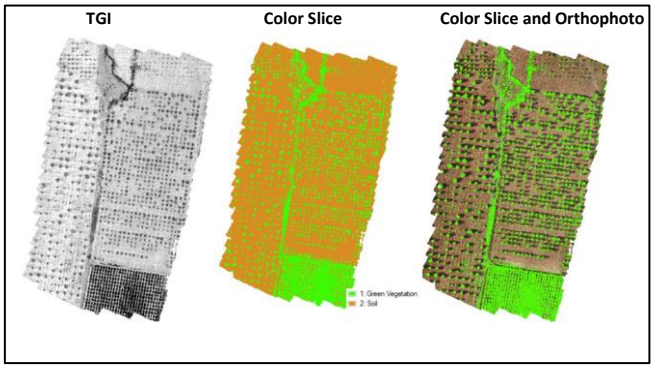


**Figure 3.** TGI, color slice and color slice overlaid Orthophoto

As seen in Figure 3, the TGI result has an obvious match over vegetation area. The trees and grassland are successfully detected. To get a metric comparison about TGI performance, an accuracy assessment is performed according to equations 2, 3, and 4. A reference shape file of trees is used to make the calculations (Figure4).

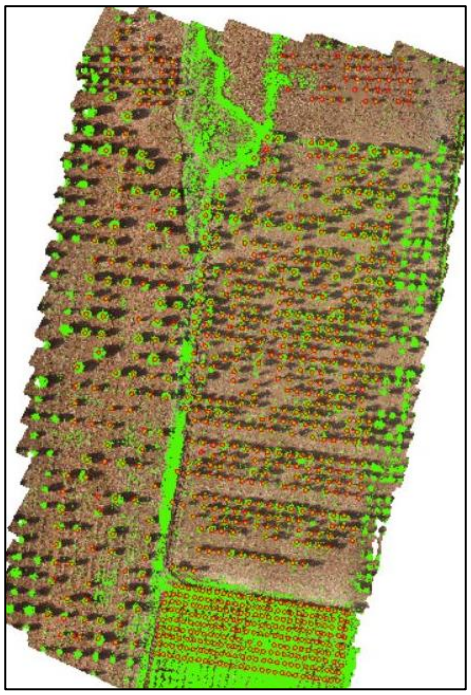

**Figure 4.** TGI vegetation class and reference tree overlaid to Orthophoto

As seen in figure 4, the vegetation areas have good match with reference trees (red circles). The calculations are performed manually counting but grassland was ignored in this calculation. The calculating results can be seen in Table 1.

**Table1.** Accuracy analysis

| | |
|---|---|
| Producer Accuracy (%) | 95 |
| User Accuracy (%) | 98 |
| Quality (%) | 94 |

The high User Accuracy means that the areas classified as green vegetation are indeed green vegetation. The lower Quality value is that some saplings that appear as trees in the reference data could not be detected. Since TGI is sensitive to green color / chlorophyll, these saplings without green leaves have not been detected yet and the accuracy has been reduced.

## CONCLUSION

Vegetation indexes are digital images that are being used in many applications. These indexes, which are mostly obtained by using the NIR and Red bands of the satellite images, provide information about the vegetation existence with high accuracy. However, it is possible to obtain vegetation index with standard digital cameras without NIR data. In this study, TGI was produced and its performance in detecting green vegetation areas was evaluated. The TGI produced over the orthophoto generated from the aerial photographs taken with the UAV and the result of the TGI was compared with the reference data by considering only the trees. As a result, green vegetation areas were obtained with 94% of quality value.

## REFERENCES


Bannari A, Morin D, Bonn F, and Huete A R (1995). A Review of Vegetation Indices. Remote Sensing Reviews, 13: 1, 95- 120

Eitel J U H, Long D S, Gessler P E, Smith A M S, (2007). Using in situ measurements to evaluate the new RapidEyeTM satellite series for prediction of wheat nitrogen status. International Journal of Remote Sensing 28, 4183–4190.

Gitelson A A (2012). Nondestructive estimation of foliar pigment (chlorophylls, carotenoids, and anthocyanins) contents: evaluating a semianalytical three band model. In: Thenkabail P S, Lyon J G, Huete A (Eds.). Hyperspectral Remote Sensing of Vegetation. CRC Press, Boca Raton, FL, pp. 141–165.

Haboudane D, Tremblay N, Miller J R, Vigneault P (2008). Remote estimation of crop chlorophyll content using spectral indices derived from hyperspectral data. IEEE Transactions of Geoscience and Remote Sensing 46, 423–437.

Harris Geospatial. (2016). Raster Color Slices. https://www.harrisgeospatial.com/docs/ColorSlices.html. Accessed 24 September 2020

Herrmann I, Pimstein A, Karnieli A, Cohen Y, Alchanatis V, Bonfil D J (2011). LAI assessment of wheat and potato crops by VENS and Sentinel-2 bands. Remote Sensing of Environment 115, 2141–2151

Hunt E R, Daughtry C S T, Eitel J U H, Long D S, (2011). Remote sensing leaf chlorophyll content using a visible band index. Agronomy Journal 103, 1090–1099

Jackson R D, Huete A R (1991). Interpreting vegetation indices. Preventive Veterinary Medicine 11, 185–200.

Ramoelo A, Skidmore A K, Cho M A, Schlerf M, Mathieu R, Heitkönig I M A, (2012). Regional estimation of savanna grass nitrogen using the red-edge band of the spaceborne RapidEye sensor. International Journal of Applied Earth Observation and Geoinformation 19, 151–162.

Şin B, Kadıoğlu İ (2019) İnsansız Hava Aracı (İHA) ve görüntü işleme teknikleri kullanılarak yabancı ot tespitinin yapılması. Turkish Journal of Weed Science 20(2):211-217

Türkseven S, Kızmaz M Z, Tekin A B, Urkan E, Serim A T (2016). Tarımda dijital dönüşüm, insansız hava araçlarının kullanılması. Tarım makinaları bilim dergisi, 12 (4), 267-271.

Türkseven S, Tekin B, Kızmaz M Z, Urkan E., Serim A T (2018). İnsansız hava araçları ile pamukta yabancı ot florasının tespit edilme olanakları. Türkiye VII. Bitki Koruma Kongresi (Uluslararası Katılımlı), 14-17 Kasım 2018, Muğla Türkiye

Özgüven M M (2018). Hassas Tarım. Akfon kitap kırtasiye, 334s. Ankara. ISBN: 978-605-68762-4-0

## Surveying and Geodesy – 2

**GPS-IR for accurate tide gauge measurement at South Beach, Oregon, United States**

*Kutubuddin Ansari*, Tae-Suk Bae*

**Comparison of Static PPP Performance of CSRS-PPP Float and Trimble RTX-PP Services**

*Bilal Mutlu*, Serdar Erol, Reha Metin Alkan*

**Long Short Term Memory (LSTM) Network Models for Ionospheric Anomalies Detection: A Case Study for Mw=7.7 Awaran, Pakistan Earthquake**

*Mohd Saqib*, Sanjeev Anand Sahu, Erman Şentürk*

**Precipitable Water Vapour Retrieval and Analysis over Nigeria from Ground and Spaced-based GNSS Observations**

*Olalekan Isioye*, Mefe Moses, Usman Ibrahim Sai, Ebenezer Ayobami Akomolafe*

**Detecting Outliers With The Least Trimmed Squares**

*Hasan Dilmaç*, Yasemin Şişman*

**Analysis of the contribution of the multi-GNSS to long-distance RTK**

*Ceren Konukseven*, Omer Faruk Atiz, Salih Alcay, Sermet Ogutcu*

Intercontinental Geoinformation Days

http://igd.mersin.edu.tr/2020/

# GPS-IR for accurate tide gauge measurement at South Beach, Oregon, United States

**Kutubuddin Ansari**[*1], **Tae-Suk Bae** [1]

[1]*Department of Geoinformation Engineering, Sejong University, Seoul 05006, Korea*

**Keywords**
Tide Gauge
Global Positioning System
Singular Spectrum Analysis
ARMA

**ABSTRACT**

Global positioning system-Interferometric Reflectometry (GPS-IR) method is applied to measure the sea level measurement by utilizing the geodetic quality of GPS receiver for detecting the adjacent ecosystem, including the advantages of climate related or non-related sea level information. The comparative analysis of tide gauge (TG) measurement interpretations collaborates with an essential role for nowcasting and forecasting variability within the selected region. In recent years, Auto-Regressive Moving Average (ARMA) and Singular Spectrum Analysis (SSA) have been showed to be the strong techniques providing a comparatively perfect estimation in time-series evaluation comparable to the fashionable methods. In the current study, GPS derived TG (GPS-TG) records from the station named SEPT (44.63 $^0$N, 124.05 $^0$W) located at South Beach, Oregon, USA are predicted with the ARMA (ARMA-TG) and SSA (SSA-TG) methods. The analysis demonstrates that the GPS-TG is correlated with SSA-TG about 99.8% and has a correlation of about 98.1% with ARMA-TG predicted values. We believe the methodology applied in the current study will contribute to the numerical modeling of TG records as well as other studies related to the reflectometry techniques.

## 1. INTRODUCTION

Global positioning system (GPS) is the modern systems in the field of geodesy frequently used for multiple purposes such as crustal deformation, coordinate transformation, ionosphere, troposphere, positioning, surveying etc (Ansari 2014; Akala et al 2015; Alshawaf et al 2016; Mukul et al 2014; 2018; Ansari et al 2018). The Global Positioning System-Interferometric Reflectometry (GPS-IR) technique has been established and proved for measuring sea-level measurements, storm signature tide records, inland water, flooding inundation, tsunamis, surface soil moisture, snow depth, and vegetation water content (Vey et al 2016; Tabibi et al 2020). Several studies have been agreed that a single geodetic receiver is capable to deliver comparable accuracy of such type measurement, which includes traditional tide gauges (TG) (Larson et al 2013; Ansari et al 2020). The design of GPS antenna is arranged in such a way that the receiver can receives both direct signal (Right-Handed Circularly Polarized or RHCP), and the reflected signal (Left-Handed Circularly Polarized or LHCP) as shown in Fig. 1. The strength of GPS signal which includes phase and code observations is measured as signal-to-noise ratio (SNR) from the RINEX observable data. The unit of SNR measurement is measured in decibel (dB) or decibel-Hertz (dB-Hz) implies the power ratio to the measured noise of the GPS signals. In the current study we used seasonal SNR measurements of GPS station located at South Beach, Oregon, United States and analyzed the tide gauge analysis by taking advantages of global forecasting Auto-Regressive Moving Average (ARMA) and Singular Spectrum Analysis (SSA) models. The summary of mathematical equations can be found in Section 2, data description in Section 3, result and discussion in Section 4 and finally conclusion in Section 5.

## 2. METHOD

The studies related to GPS-IR usually based on the multipath mitigation, or obstruction of direct and reflected signals from surface object. The oscillation waves of reflected signal directly influence the signal strength (SNR measurement). The mathematical formulation such wave signal is given by most equations as follows (Roesler and Larson 2018; Peng et al 2019):

$$SNR = A\cos\left(\frac{4\pi}{\lambda} H_0 \sin\theta + \phi\right) \quad (1)$$

* **Corresponding Author**

*(kdansarix@gmail.com) ORCID ID 0000-0002-6151-6241
(baezae@sejong.ac.kr) ORCID ID 0000-0002-7537-8732

**Cite this study**

Ansari K & Bae TS (2020). GPS-IR for accurate tide gauge measurement at South Beach, Oregon, United States. Intercontinental Geoinformation Days (IGD), 169-172, Mersin, Turkey

where A denotes the amplitude for the function deviation from zero (in meter), $\phi$ is called the phase (in radians). $H_0$ is reflector height (meter), $\lambda$ is wavelength (meter) and $\theta$ is elevation angle (degree). Axelrad et al. (2005) approved that if we take $f_M$ as a spatial frequency multipath measurement that cycles per full satellite arc from 0 to 90° then it can be easily estimated by using following formula:

$$f_M = \frac{2H_0}{\lambda} \quad (2)$$

The SNR attained values from Eq (1) is utilized to calculate the $f_M$ by applying Lomb-Scargle periodogram (LSP) (Press et al 1996), which is called the dominant frequency ($f_{m,t}$). Then the simple planar reflector distance can be transferred like to an effective reflector height ($H_{eff}$) following the Eq. (2) (Larson et al 2013).

$$f_{m,t} = \frac{2H_{eff}}{\lambda} \quad or \; H_{eff} = \frac{1}{2} f_{m,t}\lambda \quad (3)$$

Here the unit dominant frequency ($f_{m,t}$) is dimensionless, later the wavelength (meter) multiplication to the reflector height ($H_{eff}$), it will transform in meter (meter).

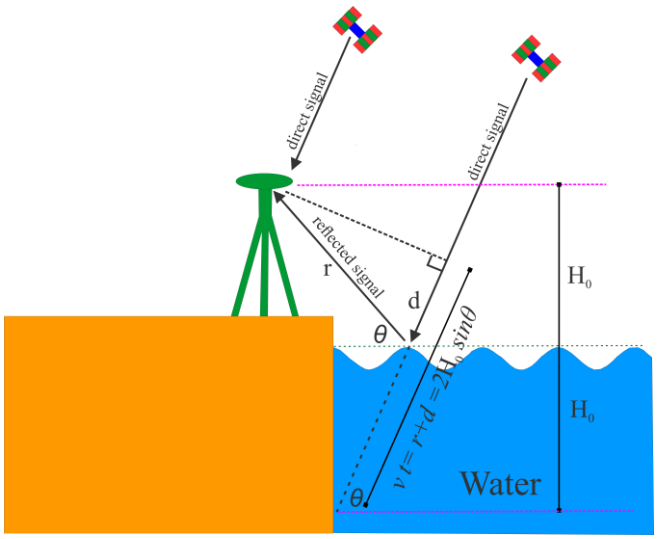


**Figure 1.** GPS-IR technique where the GPS antenna is arranged in such a way that the receiver can receives both direct signal (Right-Handed Circularly Polarized or RHCP), and the reflected signal (Left-Handed Circularly Polarized or LHCP)

## 3. DATA

The study investigates TG record estimation (GPS-TG) by exploiting the SNR data measurement from GPS station located at South Beach, Oregon, United States with the geographical coordinates of (44.63$^0$N, 124.05$^0$W). Global forecasting models such as Auto-regressive Moving Average (ARMA) and Singular Spectrum Analysis (SSA) are used for the current study. The GPS antenna elevation height is measured -16.5564 m in ITRF14 reference frame. The GPS station consists of choke-ring zenith pointing antenna TRM29659.00 have standard geodetic quality. A dual frequency of receiver with carrier-phase named ASTERX-U with 1 Hz frequency was applied during the data collection. The marker name of GPS site was named SEPT (Fig. 2). There were very high strength GPS signals available in USA, hence in the current study only GPS satellites L-Band dual frequency signals with wavelength of 19.05 cm (for L1 signal) and 24.45 cm (for L2 signal). Later we compared the results of GPS-TG records with the nearest National Water Level Observation Network (NWLON) sentinel station (Station ID: 9435380) for the purpose of validation.

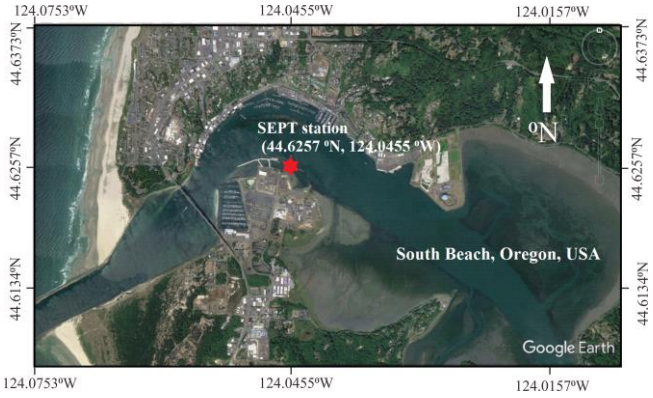


**Figure 2.** GPS station location geographical coordinate of 44.6257 $^0$N, 124.0455 $^0$W (with red star and marker name SEPT) at South Beach, Oregon, USA. The station consists of choke-ring zenith pointing antenna TRM29659.00 (Trimble Inc.) and dual-frequency carrier-phase GNSS ASTERX-U receiver.

## 4. RESULT AND DISCUSSION

The data was collected by considering of seasonal variation for the year and found the best recorded dates like this: for spring season on 04 April 2017, for summer season on 10 August 2017, for autumn season on 10 October 2017 and for winter season on 01 January 2018. Each epoch satellites data (both L1 and L2 signals) are processed and compared the NWLON secondly data to handle the estimated errors. In this way, it was very easy to exclude the records which have high difference from each other. Relative difference between GPS-TG and corresponding NWLON-TG is visible in Fig. 3. There were few circles (GPS-TG) well matched with dash lines (NWLON-TG) and few of them are overestimating and underestimating. Only the point which have positive values are selected because the model does not consider negative value, then correlation coefficient (CC) and root mean square (RMS) between GPS-TG and NWLON-TG are estimated as shown in Table 1. Results shows that GPS-TG and NWLON-TG are correlated with the CC of 0.942 and RMS of 12.90 cm. These GPS-TG records forecasted with ARMA model and obtained results also have been shown in Table 1. Now if we look at the table the GPS-TG and ARMA-TG records are correlated with CC of 0.981 and RMS of 4.80 cm. This correlation and RMS are better than NWLON-TG, hence we can conclude that ARMA model results perfectly estimated measured GPS-TG and indicates the applicability in the field of reflectometry.

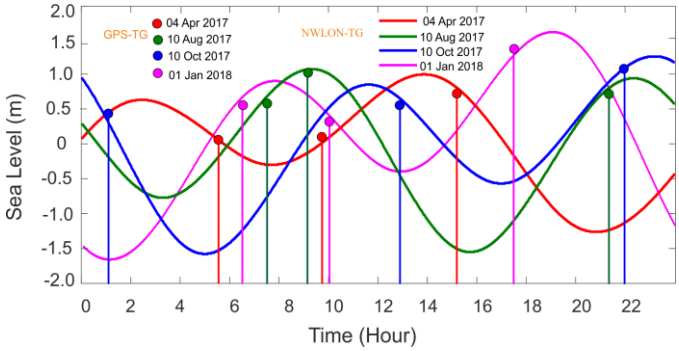


**Figure 3.** Three points per day GPS-TG records in seasonal dates with dotted points and vertical lines. NWLON-TG data is represented by horizontal lines. Best recoded GPS-TG dates are distributed like this: for spring season on 04 April 2017, for summer season on 10 August 2017, for autumn season on 10 October 2017 and for winter season on 01 January 2018.

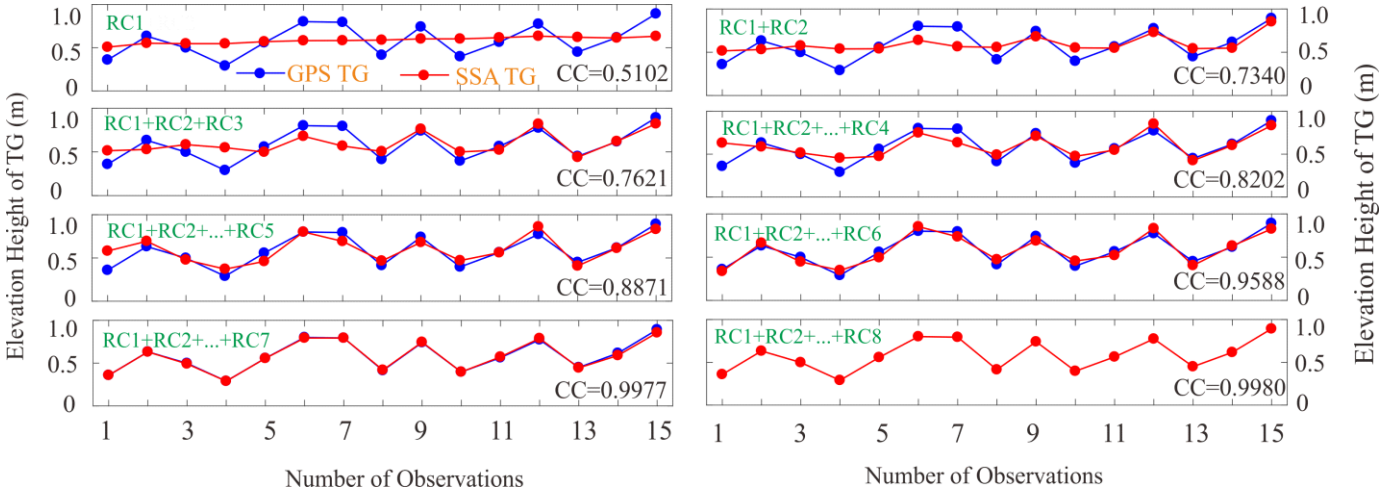


**Figure 4.** GPS tide gauge (GPS-TG) plot on selected seasonal days with Singular Spectrum Analysis reconstruction of tide gauge (SSA-TG) time-series. The correlation coefficient (CC) of each set have been given in respctive column.

**Table 1**. Tide gauge (TG) observation comparisons

| Predicted vs Observed TG | (CC) | RMS (cm) |
|---|---|---|
| NWLON-TG vs GPS-TG | 0.942 | 12.90 |
| ARMA-TG vs GPS-TG | 0.981 | 4.80 |
| SSA-TG vs GPS-TG | 0.998 | 0.88 |

In the paragraph above we discussed the comparative analysis of NWLON-TG vs GPS-TG and ARMA-TG vs GPS-TG and found that ARMA model better estimates TG records. Now we forecasted GPS-TG with SSA-TG by taking window length of eight and examined the CC of reconstructed components (RC) from beginning to the end. The CC between RC (SSA-TG) and GPS-TG has been shown in Fig. 4. As we can see from figure that first RC showed that the observed GPS-TG and first RC (RC1) are correlated with the CC of 0.5102, which means they have 51.02% relationship with each other. Now the second RC (RC2) is added in RC1 and the CC of each other (GPS-TG vs RC2-TG) again checked, that has been found to be equal to 0.7340. This indicates that RC1+RC2 estimated TG and GPS-TG have 73.40% relationship. Similarly, third and fourth RCs are added and then the CC between RCs-TG and GPS-TG are checked. It has been noticed that CC of RC1+RC2+RC3 and RC1+RC2+ RC3+RC4 improved till 76.21% and 82.02% respectively. This means that RC3 and RC4 support improving correlation of 2.81% and 5.81% respectively. Finally, all RCs (RC1+RC2+…+RC8) are added and it has been noticed that CC increase continuously and reached up to approximately 0.998, means SSA-TG and GPS-TG have almost one to one relationship. The scientific explanation of each RC components can be found in our journal paper (see Ansari et al 2020). If we look at the Table 1, the results showed that GPS-TG and SSA-TG are correlated with the CC of 0.998 and RMS of 0.88 cm. This correlation and RMS are better than both NWLON-TG and ARMA-TG. Hence in support to the SSA we can conclude that SSA is best forecasting tool and successfully able to forecast the TG records.

## 5. CONCLUSION

The study investigates SNR observation from GPS station located at (44.6257 $^{0}$N, 124.0455 $^{0}$W) South Beach, Oregon, USA by collected seasonal data. GPS-TG were estimated during the study and the results are compared with NWLON sentinel station with ID: number of 9435380 for the purpose of validation. Results showed that GPS-TG and NWLON-TG are correlated with correlation coefficient (CC) of 0.942 and root mean square (RMS) of approximately 12.90 cm. Later these GPS-TG data is predicted the global model know as Auto-regressive Moving Average (ARMA) and Singular Spectrum Analysis (SSA) methods. Results showed that GPS-TG and ARMA-TG are correlated with the CC of 0.981 and RMS of approximately 4.80 cm while GPS-TG and SSA-TG are correlated with CC of 0.998 and RMS of approximately 0.88 cm. Hence, we can conclude that SSA is the best forecasting tool and successfully able to forecast the TG records.

**REFERENCES**


Akala AO, Somoye EO, Adewale AO, Ojutalayo EW, Karia SP, Idolor RO, Okoh D and Doherty PH (2015) Comparison of GPSTEC observations over Addis Ababa with IRI-2012 model predictions during 2010–2013. Adv. Space Res. 56(8), 1686–1698 https://doi.org/10.1016/j.asr.2015.07.017

Alshawaf F, Dick G, Heise S, Simeonov T, Vey S, Schmidt T and Wickert J (2016) Decadal variations in atmospheric water vapor time series estimated using ground-based GNSS

Ansari K (2014) Quantification of slip along deformation using Finite Element Method. Journal of research in environmental and earth sciences, 1(1), pp.25-28.

Ansari K, Corumluoglu O and Verma P (2018) The triangulated affine transformation parameters and barycentric coordinates of Turkish permanent GPS network. Survey Review, 50(362), pp.412-415.; https://doi:10.1080/00396265.2017.1297016

Ansari K, Bae TS and Inyurt S (2020) Global positioning system interferometric reflectometry for accurate tide gauge measurement: Insights from South Beach, Oregon, United States. Acta Astronautica; https://doi.org/10.1016/j.actaastro.2020.04.060

Axelrad P, Larson KM, Jones B (2005), Use of the correct satellite repeat period to characterize and reduce site-specific multipath errors. In Proceedings of the ION GNSS, 2638-2648

Larson KM, Löfgren JS, Haas S (2013) Coastal sea level measurements using a single geodetic GPS receiver. Advances in Space Research, 51, 1301-1310, http://dx.doi.org/10.1016/j.asr.2012.04.017

Mukul M, Jade S, Ansari K and Matin A (2014) Seismotectonic implications of strike–slip earthquakes in the Darjiling–Sikkim Himalaya. Current Science, 106(2), pp.198-210.

Mukul M, Jade S, Ansari K, Matin A and Joshi V (2018) Structural insights from geodetic Global Positioning System measurements in the Darjiling-Sikkim Himalaya. Journal of Structural Geology, 114, pp.346-356; https://doi.org/10.1016/j.jsg.2018.03.007

Peng D, Hill EM, Li L, Switzer AD, Larson KM (2019) Application of GNSS interferometric reflectometry for detecting storm surges. GPS Solutions, 23, 47, https://doi.org/10.1007/s10291-019-0838-y

Press F, Teukolsky S, Vetterling W (1996) Numerical Recipes in Fortran 90: The art of parallel scientific computing, second ed. Cambridge University Press

Roesler C and Larson KM (2018) Software tools for GNSS interferometric reflectometry (GNSS-IR). GPS Solutions, 22, 80; https://doi.org/10.1007/s10291-018-0744-8

Tabibi S, Geremia-Nievinskib F, Francisa O, van Dama T (2020) Tidal analysis of GNSS reflectometry applied for coastal sea level sensing in Antarctica and Greenland, Remote Sensing of Environment 248 (2020), https://doi.org/10.1016/j.rse.2020.111959

Vey S, Güntner A, Wickert J, Blume T, Ramatschi M (2016) Long-term soil moisture dynamics derived from GNSS interferometric reflectometry: A case study for Sutherland, South Africa. GPS solutions, 20, 641-654, https://doi.org/10.1007/s10291-015-0474-0

Intercontinental Geoinformation Days

http://igd.mersin.edu.tr/2020/

# Comparison of Static PPP Performance of CSRS-PPP Float and Trimble RTX-PP Services

**Bilal Mutlu*[1], Serdar Erol [1], Reha Metin Alkan [1]**

[1]*Istanbul Technical University, Civil Engineering Faculty, Geomatics Engineering Department, Istanbul, Turkey*

**Keywords**
PPP
GNSS
Online GNSS Processing Services
CSRS-PPP
Trimble RTX-PP

**ABSTRACT**

Although various positioning methods are used in many engineering projects, Precise Point Positioning (PPP) technique, which enables more economical and accurate positioning, stands out among these positioning methods. The most important criteria affecting the positioning accuracy during the solution of the PPP are the quality of the precise satellite products, as well as the resolution of the phase ambiguity as fixed or float. The aim of the study is to test the static PPP performances of the online services under different satellite constellations as a function of occupation time. Within the scope of this study, PPP solutions were carried out with Canadian Spatial Reference System Precise-Point Positioning (CSRS-PPP) and Trimble CenterPoint Real Time eXtended Post-Processing (Trimble RTX-PP) web-based online GNSS processing services. The daily observations of the International GNSS Service (IGS) stations ANKR, ISTA, IZMI, MERS and KRS1, which are in Turkey, dated January 1, 2020 were used. The daily observations were divided into 1, 2, 4, 8, and 12 hour sub-sessions, and each observation session was processed with the aforementioned services using GPS-only and combination of GPS and GLONASS satellites data. As a result of the solutions, it has been shown that although CSRS-PPP provides PPP float solution, it offers a better solution than the Trimble RTX-PP, but still these two online tools were suitable for applications that require centimeter accuracy. Regarding the occupation time, the study revealed that at least 2 hours of observation period was necessary to determine the horizontal position and height with a few cm accuracies. Besides GPS and GLONASS combined PPP solutions provided more accurate results than GPS-only solutions.

## 1. INTRODUCTION

Precision Point Positioning (PPP) is a technique that makes it possible to determine centimeter-level accuracy with only single GNSS receiver without the need for any reference station data. In this method, GNSS observations with only single receiver are processed with the precise satellite orbits and clocks data produced by global or regional analysis centers to determine high accurate static or kinematic positioning. Although PPP was introduced by J. Anderle in the 1970s, developments in positioning systems such as web-based online data processing services, multi-GNSS and precise clock and orbit data, made it possible to produce high accurate positional information with economical and easier way. PPP is widely used in many applications including surveying, mapping, landslide monitoring, crustal movements monitoring, establishing early warning systems, glacial movements monitoring, agriculture, structural deformation monitoring, marine survey, photogrammetric studies and UAV measurements and so on.

There are various type of PPP processing software and web-based online services are available, but in this study, Canadian Spatial Reference System Precise-Point Positioning (CSRS-PPP) and Trimble CenterPoint Real Time eXtended Post-Processing (Trimble RTX-PP) services were used. In order to understand the effect of multi-GNSS and occupation time on static PPP performance, GPS-only and GPS&GLONASS combination, with different observation time, were processed in the study.

## 2. WEB-BASED PPP SERVICES

PPP's current form was defined by Zumberge et al. in 1997, although it was first put forward by Anderle (1976). Since then, the PPP technique has been used successfully in many different scientific and practical

* **Corresponding Author**

*(mutlubil@itu.edu.tr) ORCID ID 0000-0002-9763-0345
(erol@itu.edu.tr) ORCID ID 0000-0002-7100-8267
(alkanr@itu.edu.tr) ORCID ID 0000-0002-1981-9783

**Cite this study**

Mutlu B., Erol S. & Alkan R. M. (2020). Comparison of Static PPP Performance of CSRS-PPP Float and Trimble RTX-PP Services. Intercontinental Geoinformation Days (IGD), 173-176, Mersin, Turkey

applications all over the world. (Zumberge et al. 1997; Héroux and Kouba 2001; Choy, et al. 2017; Kiliszek et al. 2018; DeSanto et al. 2019; Katsigianni et al. 2019; Dawidowicz 2020; Facio and Berber 2020).

Nowadays, there are various web-based GNSS processing services operated by different organizations, institutes and research centers. The main advantages of web-based GNSS services are that they are free, accurate and easy to use. It does not require any additional software or specific features on the computer. Besides the PPP services work without the need for data from any reference station (Bahadur and Üstün 2014). Many scientific articles have revealed that the web-based online services provided cm to dm level of accuracy mainly depend on the type of used data, precise products, occupation time and observation conditions (Alkan et al. 2020; İnyurt and Ulukavak 2020). In this study, the PPP solutions were performed by using the CSRS-PPP and Trimble RTX-PP services, which use different precise products and ambiguity solution types.

### 2.1. Canadian Spatial Reference System-Precise Point Positioning (CSRS-PPP)

The CSRS-PPP service operated by Natural Resources Canada (NRCan) has been providing static and kinematic multi-GNSS PPP solutions to all users around the world since 2003. It is a web-based online service that allows the user to easily make a PPP solution even without a GNSS data processing background (Klatt and Johnson 2017). The service process the single/dual-frequency GPS or GPS&GLONASS data using the best available precise satellite orbit and clock products (ultra-rapid, rapid or final) produced by IGS or NRCan and calculates PPP coordinates as static or kinematic. CSRS-PPP service has provided solutions based on ambiguity-float until October 20, 2020. After this date, started to offer ambiguity-fixed solutions. In this study, the solutions were obtained as ambiguity-float because it was processed before October 2020.

### 2.2. Trimble CenterPoint RTX Post-Processing Service (Trimble RTX-PP)

The Trimble RTX-PP service that was operated by Trimble Inc., enables free processing of the multi-GNSS data collected in only static mode. RTX-PP service calculates the PPP coordinates of the points with the ambiguity-fixed solution. This situation significantly shortens the convergence time. The service uses its own precise products (Doucet et al. 2012).

## 3. CASE STUDY

In this study, ANKR, ISTA, IZMI, KRS1 and MERS stations, which included in IGS Network were used. All stations are located within the borders of Turkey (Fig. 1). Observation files were obtained from EUREF Permanent GNSS Network website.

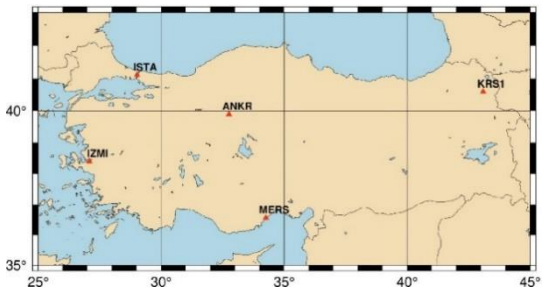


**Figure 1.** Distribution of used stations on the map. (Wessel et al. 2019)

The daily observation data at 1st day of 2020 (GPS Day 1) for all IGS stations in Turkey were split into different shorter sessions as 1, 2, 4, 8 and 12 hours with respect to satellite systems as GPS-only and GPS&GLONASS (Fig. 2). For this purpose, the GFZRNX software was used (Nischan 2016).

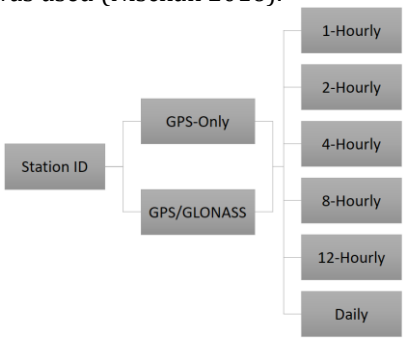


**Figure 2.** File hierarchy of the used data sessions

All the 24 hourly and 1, 2, 4, 8 and 12-hour sub-session RINEX data files were uploaded to the online services. After a short time, the PPP-derived coordinates were retrieved via e-mail. In the results, there were no solutions for some epochs of ANKR station, because the number of tracked GPS satellites from the station was limited for each epoch. So that, ANKR station was not taken into consideration in this study. Statistics for the number of satellites and mean PDOP values were emphasized in Table 1.

**Table 1.** The number of used satellites and DOP values.

| Station ID | GPS-Only | | | | GPS&GLONASS | | | |
|---|---|---|---|---|---|---|---|---|
| | Min. | Mean | Max. | PDOP | Min. | Mean | Max. | PDOP |
| ANKR | 5 | 6 | 8 | 8.4 | 9 | 13 | 17 | 2.1 |
| ISTA | 10 | 12 | 14 | 1.8 | 18 | 21 | 25 | 1.3 |
| IZMI | 10 | 12 | 14 | 1.8 | 17 | 19 | 22 | 1.4 |
| KRS1 | 10 | 12 | 14 | 1.7 | 16 | 20 | 23 | 1.3 |
| MERS | 10 | 12 | 15 | 1.8 | 19 | 22 | 26 | 1.3 |

### 3.1. GPS-Only Results

The static PPP-derived coordinates obtained from CSRS-PPP and Trimble RTX-PP services were compared with the reference (known) coordinates of the IGS station. Calculated horizontal (2D) and height difference values are given in Fig. 3 and Fig. 4 for each station, considering the observation time and the used service.


**Figure 3.** 2D positional differences between known-coordinates and online services for GPS only constellation (*left*; CSRS-PPP, *right*: Trimble RTX-PP).


**Figure 5.** 2D positional differences between known-coordinates and online services for GPS&GLONASS combination (*left*; CSRS-PPP, *right*: Trimble RTX-PP).


**Figure 4.** Height differences between known-coordinates and online services for GPS only constellation (*left*; CSRS-PPP, *right*: Trimble RTX-PP).


**Figure 6.** Height differences between known-coordinates and online services for GPS&GLONASS combination (*left*; CSRS-PPP, *right*: Trimble RTX-PP).

### 3.2. GPS&GLONASS Combined Results

The PPP-derived coordinates by processing of the GPS&GLONASS GNSS data were compare to the known values and the differences were plotted. The calculated horizontal (2D) and height differences are given in Fig. 5 and Fig. 6 for each station considering the observation time and the used service.

## 4. DISCUSSION

In this study, GPS-only and GPS&GLONASS combined observations with different observation time interval were evaluated by using CSRS-PPP and Trimble RTX-PP online services. The differences between the obtained coordinates and reference coordinates are given in the Fig. 3-6.

It has been observed that the number of GPS&GLONASS satellites is higher than GPS-only and accordingly DOP values have improved. Consequently, significant improvements have been achieved in the solutions of GPS&GLONASS data groups in both 2D position and height components when compared to GPS-only solutions. With the observation time of 1 hour, it is possible to obtain differences below the decimeter. In the 2-hour GPS-only data groups, with some exceptions, the differences were below 4 cm in both 2D and height components for both services. Besides, in 2-hour GPS&GLONASS data groups, the differences were below 2.5 cm for both two components and two services, with some exceptions. According to using GPS-only and GPS&GLONASS constellations with both services, the differences in horizontal position and height were decreased from 2 cm to 1-2 mm in the 4, 8, 12 and 24-hour data groups, respectively. Although CSRS-PPP performs an ambiguity-float solution, its accuracy was found higher than Trimble RTX-PP. The reason for this is considered to be that CSRS-PPP uses IGS final precise products, while the Trimble RTX-PP uses its own precise products.

## 5. CONCLUSION

This study has investigated the performance of static Precise Point Positioning (PPP) using different GNSS constellations with different online processing services. As a result of the processing results, the CSRS-PPP service was provided better performance than the Trimble RTX-PP service, although the differences between the services were not significant. Within the scope of any project where accuracy under decimeter is sought, the 1-hour observation time obtained from the combination of GPS&GLONASS is sufficient for both CSRS-PPP and Trimble RTX-PP web-based services. In cases where an accuracy of a few centimeters is required, observation should be made for at least 2 hours or more.

As a conclusion, it is emphasized that any projects requiring centimeter-level accuracy can be conducted by using PPP technique very easy and economically.

## ACKNOWLEDGEMENT

The authors thank CSRS-PPP and Trimble RTX-PP web-based online GNSS PPP services.

## REFERENCES

Alkan R M, Erol S, Ozulu I M & Ilci V (2020). Accuracy Comparison of Post-processed PPP and Real-time Absolute Positioning Techniques. Geomatics, Natural Hazards and Risk, 11(1), 178-190. https://doi.org/10.1080/19475705.2020.1714752

Anderle R J (1976). Satellite Doppler Positioning. Proceedings of the International Geodetic Symposium, Las Cruces, New Mexico, 12-14 October 1976, 47-75.

Bahadur B & Üstün A (2014). İnternet Tabanlı GNSS Veri Değerlendirme Servisleri. Harita Dergisi, 152, 40-50.

Choy S, Bisnath S & Rizos C (2017). Uncovering Common Misconceptions in GNSS Precise Point Positioning and Its Future Prospect. GPS Solutions, 21(1), 13-22. https://doi.org/10.1007/s10291-016-0545-x.

Dawidowicz K (2020). Sub-hourly Precise Point Positioning Accuracy Analysis-Case Study for Selected ASG-EUPOS Stations. Survey Review, 52(373), 341-351. https://doi.org/10.1080/00396265.2019.1579988.

DeSanto J B, Chadwell C D & Sandwell D T (2019). Kinematic Post-processing of Ship Navigation Data Using Precise Point Positioning. Journal of Navigation, 72(3), 795-804. https://doi.org/10.1017/S0373463318000887.

Doucet K, Herwig M, Kipka A, Kreikenbohm P, Landau H, Leandro R, Moessmer M & Pagels C (2012). Introducing Ambiguity Resolution in Web-hosted Global Multi-GNSS Precise Point Positioning with Trimble RTX-PP. Proceedings of the 25th International Technical Meeting of the Satellite Division of the Institute of Navigation, 1115-1125. Nashville, TN, USA

Facio Y & Berber M (2020). Subsidence is Determined in the Heart of the Central Valley Using Post Processed Static and Precise Point Positioning Techniques. Journal of Applied Geodesy. 14(1). https://doi.org/10.1515/jag-2019-0043.

Héroux P & Kouba J (2001). GPS Precise Point Positioning Using IGS Orbit Products. Physics and Chemistry of the Earth, Part A: Solid Earth and Geodesy, 26(6-8), 573-578. https://doi.org/10.1016/S1464-1895(01)00103-X

İnyurt S & Ulukavak M (2020). Web tabanlı GNSS Yazılımlarının (CSRS-PPP, Trimble-RTX) Performansının Araştırılması. Geomatik, 5(2), 120-126. https://doi.org/10.29128/geomatik.586990.

Katsigianni G, Loyer S & Perosanz F (2019). PPP and PPP-AR Kinematic Post-processed Performance of GPS-only, Galileo-only and Multi-GNSS. Remote Sensing, 11(21). https://doi.org/10.3390/rs11212477.

Kiliszek D, Szołucha M & Kroszczyński K (2018). Accuracy of Precise Point Positioning (PPP) with the Use of Different International GNSS Service (IGS) Products and Stochastic Modelling. Geodesy and Cartography, 67(2), 207-238. https://doi.org/10.24425/gac.2018.125472.

Klatt C & Johnson P (2017). Estimating Benefits to Canada and The World: Canadian Spatial Reference System Precise Point Positioning Service. Geomatica. 71(1), 37-44. https://doi.org/10.5623/cig2017-104

Nischan T (2016). GFZRNX - RINEX GNSS Data Conversion and Manipulation Toolbox. V. 1.13. GFZ Data Services. https://doi.org/10.5880/GFZ.1.1.2016.002

Wessel P, Luis J F, Uieda L, Scharroo R, Wobbe F, Smith W H F & Tian D (2019). The Generic Mapping Tools version 6. Geochemistry, Geophysics, Geosystems, 20, 5556–5564. https://doi.org/10.1029/2019GC008515

Zumberge J F, Heflin M B, Jefferson D C, Watkins M M & Webb F H (1997). Precise Point Positioning for the Efficient and Robust Analysis of GPS Data from Large Networks. Journal of Geophysical Research: Solid Earth, 102(B3), 5005-5017. https://doi.org/10.1029/96JB03860

Intercontinental Geoinformation Days

http://igd.mersin.edu.tr/2020/

# Long Short Term Memory (LSTM) Network Models for Ionospheric Anomalies Detection: A Case Study for Mw=7.7 Awaran, Pakistan Earthquake

**Mohd Saqib**[*1], **Sanjeev Anand Sahu** [1], **Erman Şentürk** [2]

[1]*Mathematics and Computing Department, Indian Institute of Technology (Indian School of Mines), Dhanbad, Jharkhand, India*
[2]*Department of Surveying Engineering, University of Kocaeli, Kocaeli, Turkey*

**Keywords**
Anomaly Detection
EQ Forecast
Long Short Term Memory
Time Series Analysis
Total Electron Content

**ABSTRACT**

Since ionospheric variability changes dramatically before the major earthquakes (EQs), the detection of ionospheric anomalies to EQ forecasts has become a new trend in the current era. Therefore, there is a call to identify highly accurate, advance, and intelligent models to identify these anomalies. In this study, we have proposed a deep learning-based method, long short-term memory (LSTM) network, to detect ionospheric anomalies using the Total Electron Content (TEC) time series of Awaran, Pakistan (Mw=7.7) EQ on September 24, 2013. We have taken 45 days of TEC data with a 2-h temporal resolution and train the models with an accuracy of 0.07 TECU. After fitted models with optimal hyperparameters, we have applied both to forecast TEC values for one week before the EQ. The anomalies, high differences (crossing the threshold value) between forecasted and observed TEC, are an indication of abnormal activities, e.g. earthquake, space weather, etc. In this study, we detected anomalies for the Awaran EQ. We conclude our results with the identification of ionospheric anomalies that occurred before the EQ results showed that strong positive anomalies are recorded 3 days before (on Sep 21) the EQ. These anomalies are thought to be related to Awaran EQ due to the quiet space weather conditions on the anomalies days. This study brings new insights into the AI techniques in seismoionospheric EQ forecasting.

## 1. INTRODUCTION

Earthquakes are the most destructive natural hazards, which may claim a huge number of human lives along with huge economic losses for any country (Athukorala and Resosudarmo, 2005). If we become able to found any single clue or prior knowledge about the upcoming EQ, then we will be able to save many lives and escape from capital losses by using precautions. Researchers are working hard to find any prior signal of major EQs and forecasting EQs have become a hot topic among geologists, astronomers, geophysicists, etc. Many studies have been already conducting to show a correlation among anomalies occur in the ionosphere just a few days before EQs (Hattori et al., 2014). However, all of them are based on some statistical analysis or just a complex mathematical model. Artificial Intelligence (AI) can bring revolutionary changes in this field of forecasting EQs based on ionospheric anomalies.

Nowadays, earthquake warning has taken a new turn of prediction when some anomalies are detected in the ionosphere ahead of the major EQ (Hattori et al., 2014). Many researchers have elaborated on different theories and proofs to get the reason behind this correlation. For example, Klimenko et al. 2011, has introduced a mechanism behind the effectuation of ionospheric perturbation due to the electric field that originates from high internal gravity waves. Rozhnoi et al. 2007, has study the lithosphere-ionosphere high coupling by the gravity waves and presented case studies of three major EQs (M>7) which happened in November, 2004 in Japan. Pulinets 2009, has acknowledged another reason for ground and atmosphere coupling is a potential difference between them. However, any physical reason behind this coupling did not approve yet. So, we have only way to understand such theory is that conduct statistical analysis of TEC values before major EQs and that is why much statistical analysis have previously been proposed for different EQs e.g. in Guo et al. 2015, investigates TEC anomalies respond to the EQ (M=8.2) of 1 April, 2014 in Chile. Ouzounov et al. 2011, analyzed the ionospheric perturbation that occurred before the Tohoku EQ (M=9)

* **Corresponding Author**

*(msaqib.cs@gmail.com) ORCID ID 0000-0003-2125-2162
(sanjeev@iitism.ac.in) ORCID ID 0000-0002-3514-6400
(erman.senturk@kocaeli.edu.tr) ORCID ID 0000-0002-0833-7113

**Cite this study**

M. Saqib, S. A. Sahu & E. Şentürk (2020). Long Short Term Memory (LSTM) Network Models for Ionospheric Anomalies Detection: A Case Study for Mw=7.7 Awaran, Pakistan Earthquake. Intercontinental Geoinformation Days (IGD), 177-180, Mersin, Turkey

happened on 11 March, 2011 in Japan, and Akhoondzadeh et al. 2010, investigate four EQs (M>6) using GPS data and found positive results of coupling. Liu et al. 2013 have successfully concluded about the lithosphere-ionosphere coupling from all these investigations and it has also revealed that major anomalies detected 1-4 days before major EQs. Now, when it is so clear that TEC perturbations reveal several days before any EQ, it can play an important role as a significant feature in EQs forecasting.

Past decades were emerging for AI, machine learning, sensing techniques, Internet of Things (IoT) and have been applied for multiple fields of seismology e.g. EQ magnitude prediction (Adeli and Panakkat, 2009), seismic signal acceleration classification (Andreadis et al., 2007), EQ detection (Beyreuther and Wassermann, 2008), seismic arrival prediction (Beyreuther and Wassermann, 2008). Furthermore, Li et al, 2018 have been shown that the EQ data can be to distinguish EQ and non-EQ based on P-wave and S-wave arrival times using ML. Another study has presented a generative adversarial network (GAN) an automatic feature extractor and trained a Random Forest classifier with about 700,000 EQ and noise waveforms which can recognize 99.2% of the EQ P waves and 98.4% of the noise signals (Li et al. 2018). That is why taking TEC values as an important feature for a strong forecast about an EQ becomes crucial and many more already started like in a study (Akhoondzadeh, 2013) used Genetic Algorithm (GA) to predict TEC values before the Solomon EQ (M=8) and investigated that if the difference between forecasted and observed value, exceeds the pre-defined threshold value, then it could be EQ anomaly. In the same way, we also processed our research but using a different approach. In our study, we have taken LSTM, a Recurrent Neural Network (RNN), deep learning method to time series analysis of TEC values so that we can get an idea about TEC values in normal days. After forecasting TEC, we used these values as an estimator for anomalies detector.

## 2. MODELING AND EVALUATION

### 2.1. Data Description and Preprocessing

We have selected the strong (Mw=7.7) Awaran EQ for the analysis and examine the proposed model. The EQ occurred on Sep 24, 2013, 11:29:47 (UTC) and the epicenter was 61 km north-north-east (NNE) of Awaran, Pakistan (26.951°N 65.501°E). The detail of EQ recorded from the National Centers for Environmental Information (https://www.ngdc.noaa.gov/hazard/). After, finalizing EQ, we fetch the TEC value from the same coordinates and time as well. The unit of TEC is TECU where 1 TECU is equal to $10^{16}$ el/m$^2$. The ionospheric TEC data are provided by the Crustal Dynamics Data Information System (CDDIS). CDDIS is one of the Earth Observing System Data and Information System (EOSDIS) Distributed Active Archive Centers (DAACs), part of the NASA Earth Science Data and Information System (ESDIS) project. Datasets and related data products and services are provided by CDDIS, managed by the NASA ESDIS project. The parent directory is available on CDDIS NASA (ftp://cddis.nasa.gov/gnss/products/ionex/).

We have split the data into three parts: 1) the data from Aug 1, 2013, to Sep 14, 2013, has chosen for the training of the model, 2) data from Sep 14, 2013, to Sep 19, 2013, has selected for evaluating the accuracy of the model, and 3) from Sep 19, 2013, to Sep 26, 2013, are the actual data for which has chosen for forecast TEC, take the difference and detecting the anomalies.

The magnetic activity indices Kp, disturbance storm-time (Dst), and solar activity indices solar radio flux (F10.7), and solar wind speed ($V_{SW}$), which are freely available on the OMNI website (https://omniweb.gsfc.nasa.gov/form/dx1.html) were also analyzed to reveal the space weather effect on ionospheric anomalies.

### 2.2. Space-weather conditions before the EQ

We used the Dst, $V_{SW}$, Kp, and F10.7 space weather indices to show the effect of space weather on the TEC time series from Sep 19 to Sep 24, 2013. Fig. 1a and 1c demonstrate the variations of Dst and Kp magnetic activity indices. These indices indicate the quiet magnetic activity before the EQ where Dst values range between ±20 nT. Kp values are less than 4 except for Sep 19 and 24. Figures 1b and 1d present the variations of $V_{SW}$ and F10.7 solar activity indices. The $V_{SW}$ values indicate a solar wind on Sep 19 and 20, the index values vary between 500-600 km/s. F10.7 values are between 105-115 sfu before the EQ, which indicates low solar activity.

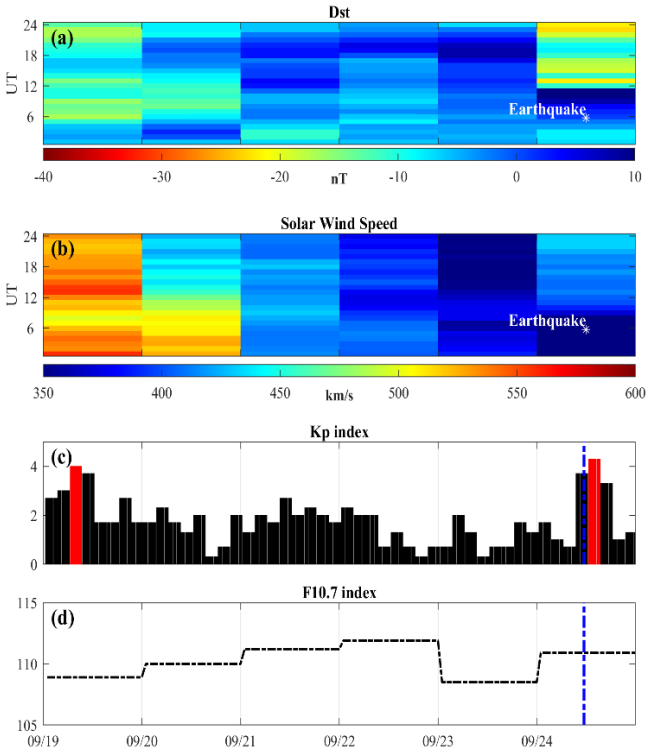


**Figure 1.** Space weather indices from Sep 19-24, 2013. (a) Dst, (b) solar wind speed, (c) Kp index, (d) F10.7 index values. The vertical blue dash-dotted lines in graphs indicate EQ time.

### 2.3. Model Formulation

The proposed model, LSTM, is an extension of RNN which overcome the problem of vanishing gradient. The special architectures of the LSTM-RNN network (**Error! Reference source not found.**) made it possible to keep those learning within the network which is far away from the forecast point and predict based on these learning. LSTM has various components which can forget or store the information using the following formulations:

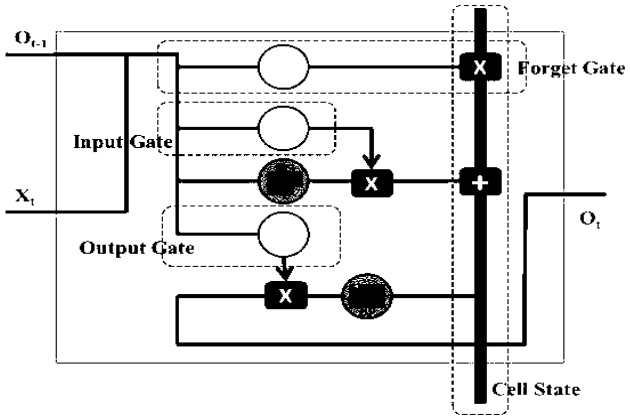


**Figure 2.** Node architecture for LSTM

$$f_t = \sigma(w_f[O_{t-1}, X_t] + b_f) \quad (1)$$

$$i_t = \sigma(w_i[O_{t-1}, X_t] + b_i) \quad (2)$$

$$C_t^{\sim} = tanh(w_c[O_{t-1}, X_t] + b_c) \quad (3)$$

$$C_t = f_t * C_{t-1} + i_t * C_t^{\sim} \quad (4)$$

$$h_t = \sigma(w_o[O_{t-1}, X_t] + b_o) \quad (5)$$

$$O_t = h_t * \tanh(C_t) \quad (6)$$

Where, $X_t$ is the input vector, $W_t = \begin{bmatrix} w_f \\ w_i \\ w_c \\ w_o \end{bmatrix}$ weight vector, bias $b_t = \begin{bmatrix} b_f \\ b_i \\ b_c \\ b_o \end{bmatrix}$, and output $O_t$ at time t.

### 2.4. Evaluation Criteria

Various metrics employed to evaluate the performance of the purposed model; Mean Square Error (MSE), Root Mean Square Error (RMSE), Normalized Mean Square Error (NMSE), Normalized Root Mean Square Error (NRMSE), and Standard Deviation (SD). The calculation methods for each are the following:

$$\text{MSE} = \frac{1}{n}\sum_{i=1}^{n}(\text{TEC}_{\text{Predicted}} - \text{TEC}_{\text{Actual}})^2 \quad (7)$$

$$\text{RMSE} = \sqrt{\frac{1}{n}\sum_{i=1}^{n}(\text{TEC}_{\text{Predicted}} - \text{TEC}_{\text{Actual}})^2} \quad (8)$$

$$\text{NMSE} = MSE/[\max(\text{TEC}_{\text{Actual}}) - \min(\text{TEC}_{\text{Actual}})] \quad (9)$$

$$\text{NRMSE} = RMSE/[\max(\text{TEC}_{\text{Actual}}) - \min(\text{TEC}_{\text{Actual}})] \quad (10)$$

$$\text{SD} = \sqrt{\frac{1}{n-1}\sum_{i=1}^{n}(\text{TEC}_{\text{Actual}} - \overline{\text{TEC}_{\text{Actual}}})^2} \quad (11)$$

Where, n is the number of observation involves in evaluating the model and $\overline{\text{TEC}_{\text{Actual}}}$ is the value of mean for actual TEC observations employed for evaluation.

## 3. IMPLEMENTATION

To implement the proposed model, code written in Python.3 using Keras library, debugged on Jupyter Notebook which can be download from the link: https://jupyter.org/. Jupyter Notebook is a nonprofit organization created to "develop open-source software, open-standards, and services for interactive computing across dozens of programming languages". We have used two hidden layers with 48-48 nodes in each with a 20% dropout in LSTM. Also, we take batch size 12 observations (number of the data point in a day) and 30% data for validation. We have also used Adam Optimizer to update the hyperparameters of LSTM and MSE for improving accuracy.

## 4. RESULTS AND DISCUSSIONS

We implemented the model and evaluate using evaluation data. We used different matrices for evaluating the model which has present in Table 1. The RMSE is 3.51 and NRMSE is 0.07 which is good accuracy. We forecasted TEC values for one week before the EQ which is represented in Figure 3. After forecasting TEC for a normal situation, differences between observed and forecast TEC calculated, and the error crossing a threshold is called anomalies (see Figure 4). In Figure 4, the red colour circle shows a strong positive anomaly on Sep 21, 2013, which is three days before the EQ.

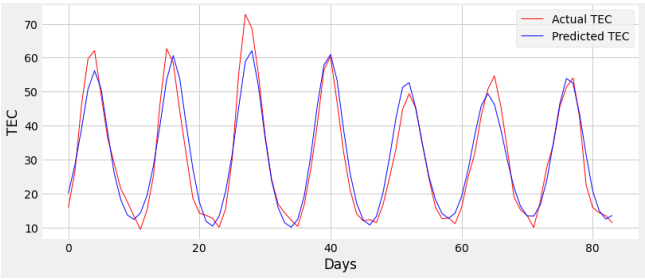


**Figure 3.** Forecast and observed TEC values

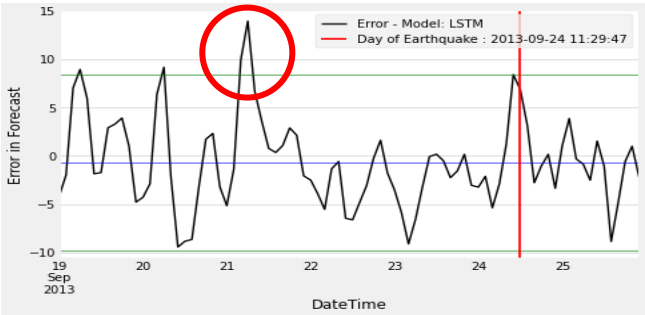


**Figure 4.** Error calculated

**Table 1** Matrices of the proposed model

| Matrices | MSE | RMSE | NMSE | NRMSE | SD |
|---|---|---|---|---|---|
| Values | 12.34 | 3.51 | 0.25 | 0.07 | 3.24 |

## 5. CONCLUSION

We have implemented an AI-based technique, LSTM to forecast ionospheric TEC values. The forecasting values gives a deep insight into the future estimated TEC values (what it should be during a normal day). And, when we become able to forecast TEC, we can estimate the significant differences between forecasted and observed TEC and abnormalities of the data which have been observed because of a sudden change in the ionosphere. In our case, we detected anomalies three days before the Awaran EQ. Such a proposed model can be a new method to make an earthquake warning system.

## ACKNOWLEDGEMENT

The authors are thankful to the IGS network for providing the Global Ionosphere Maps, the United States Geological Survey (USGS) for providing information about the EQ, and NASA OMNIWeb for providing the space weather indices.

## REFERENCES

Adeli, H., & Panakkat, A. (2009). A probabilistic neural network for earthquake magnitude prediction. Neural networks, 22(7), 1018-1024.

Akhoondzadeh, M. (2013). Genetic algorithm for TEC seismo-ionospheric anomalies detection around the time of the Solomon (Mw= 8.0) earthquake of 06 February 2013. Advances in Space Research, 52(4), 581-590.

Akhoondzadeh, M., Parrot, M., & Saradjian, M. R. (2010). Electron and ion density variations before strong earthquakes (M> 6.0) using DEMETER and GPS data. *Natural Hazards and Earth System Sciences*, *10*(1), 7–18.

Andreadis, I., Tsiftzis, I., & Elenas, A. (2007). Intelligent seismic acceleration signal processing for damage classification in buildings. IEEE Transactions on Instrumentation and Measurement, 56(5), 1555-1564.

Athukorala, P. C., & Resosudarmo, B. P. (2005). The Indian Ocean tsunami: Economic impact, disaster management, and lessons. Asian economic papers, 4(1), 1-39.

Beyreuther, M., & Wassermann, J. (2008). Continuous earthquake detection and classification using discrete Hidden Markov Models. Geophysical Journal International, 175(3), 1055-1066.

Guo, J., Li, W., Yu, H., Liu, Z., Zhao, C., & Kong, Q. (2015). Impending ionospheric anomaly preceding the Iquique Mw8.2 earthquake in Chile on 2014 April 1. *Geophysical Journal International*, *203*(3), 1461–1470.

Hattori, K., Hirooka, S., Kunimitsu, M., Ichikawa, T., & Han, P. (2014, August). Ionospheric anomaly as an earthquake precursor: Case and statistical studies during 1998–2012 around Japan. In 2014 XXXIth URSI General Assembly and Scientific Symposium (URSI GASS) (pp. 1-1). IEEE.

Klimenko, M. V., Klimenko, V. V., Karpov, I. V., & Zakharenkova, I. E. (2011). Simulation of seismo-ionospheric effects initiated by internal gravity waves. Russian Journal of Physical Chemistry B, 5(3), 393-401.

Li, W., Narvekar, N., Nakshatra, N., Raut, N., Sirkeci, B., & Gao, J. (2018, March). Seismic data classification using machine learning. In 2018 IEEE Fourth International Conference on Big Data Computing Service and Applications (BigDataService) (pp. 56-63). IEEE.

Li, Z., Meier, M. A., Hauksson, E., Zhan, Z., & Andrews, J. (2018). Machine learning seismic wave discrimination: Application to earthquake early warning. Geophysical Research Letters, 45(10), 4773-4779.

Liu, J. Y., Yang, W. H., Lin, C. H., Chen, Y. I., & Lee, I. T. (2013). A statistical study on the characteristics of ionospheric storms in the equatorial ionization anomaly region: GPS-TEC observed over Taiwan. Journal of Geophysical Research: Space Physics, 118(6), 3856-3865.

Ouzounov, D., Pulinets, S., Romanov, A., Romanov, A., Tsybulya, K., Davidenko, D., ... & Taylor, P. (2011). Atmosphere-ionosphere response to the M9 Tohoku earthquake revealed by multi-instrument space-borne and ground observations: Preliminary results. Earthquake Science, 24(6), 557-564.

Pulinets, S. A. (2009). Physical mechanism of the vertical electric field generation over active tectonic faults. Advances in Space Research, 44(6), 767-773.

Rozhnoi, A., Solovieva, M., Molchanov, O., Biagi, P. F., & Hayakawa, M. (2007). Observation evidences of atmospheric Gravity Waves induced by seismic activity from analysis of subionospheric LF signal spectra. *Natural Hazards and Earth System Sciences*, *7*, 625–628.

Intercontinental Geoinformation Days

http://igd.mersin.edu.tr/2020/

# Precipitable water vapour retrieval and analysis over Nigeria from ground and spaced-based GNSS observations

**Olalekan Adekunle Isioye*[1], Mefe Moses [1], Ibrahim Usman Sai [1], Ebenezer Ayobami Akomolafe [1]**

[1]*Ahmadu Bello University, Faculty of Environmental Design, Department of Geomatics, Zaria, Nigeria*

**Keywords**
GNSS Meteorology
Precipitable water vapour
Radio Occultation
Climate Monitoring
Weather Forecasting

**ABSTRACT**

The recent development of the Global Navigation Satellite Systems (GNSS) radio occultation (RO) technique has overcome many observational limitations inherent in conventional atmospheric sounding instruments and offers an exciting potential for meteorological and climatic researches. This study examines the practicability of GNSS RO technique in observing the atmosphere over Nigeria. A prominent climate change indicator (precipitable water vapour (PWV)) dominant in the upper-tropospheric and lower-stratospheric region were derived from COSMIC profiles (2013-2016) over Nigeria, the results revealed very prominent seasonal patterns in the GNSS RO derived PWV which precisely describes the atmosphere and seasons of the Nigerian region. The PWV agree with ground-based GNSS measurements in the range of -0.40 to 5.58 mm. With the expected improvements and follow on missions for the GNSS RO missions, the quantity and quality of occultation events will improve and lengthen in the Nigerian region thereby making the GNSS RO technique an indispensable tool for future operational atmospheric and climate research in Nigeria and the sub-Sahara Africa region at large.

## 1. INTRODUCTION

Climate monitoring, prediction and research have become an indispensable pillar of the global effort in climate change mitigation and adaptation. Enhanced correctness about the rapidity of climate change and improved definition of uncertainty levels can inform policy decisions and may accelerate a global consensus on climate change. The need for observation systems with highly accurate estimates of climate variables at global or at least regional coverage is thus paramount to accelerate the global accord on climate change mitigation and adaptation.

Recently, ground and space-based global navigation satellite system (GNSS) atmospheric sounding techniques have evolved as important technologies for observing the troposphere and stratosphere. They both offer excellent capabilities for meteorological and climate change researches (see, Kuleshov et al. 2016). The ground-based technique can automatically monitor the water vapour content in the atmosphere over networks of GNSS stations across the globe (i.e., Jones 2016; Liang et al. 2015; Rozsa et al. 2014). In Nigeria, GNSS observations from ground-based GNSS reference networks have been employed to generate useful atmospheric water vapour information (see, Isioye et al. 2017a and references therein). The GNSS space-based technique or GNSS radio occultation (RO) technique probes the Earth's atmosphere and ionosphere using GNSS receivers onboard Low Earth Orbit (LEO) satellites (see, Anthes et al. 2000; Kursinski et al. 1995). This GNSS technique offers an innovative approach for monitoring global temperatures, pressures, and moisture distributions with a high spatial resolution. The GNSS RO technique provides global coverage, all-weather capability, long-term measurement stability, high vertical resolution and high-accuracy measurements in the middle to upper troposphere, stratosphere and ionosphere. High accuracy of the GNSS RO approach is of specific significance for dependable estimates of the atmospheric peculiarities over regions where conventional upper air sounding observations from radiosondes are sparse or non-existing, i.e., in Africa, the network of radiosonde stations are very sparse and where available are most often than not in a deplorable state (see Isioye et al. 2016).

This paper attempts to appraise the potentials of GNSS RO technique to monitor the weather and climate over Nigeria. To achieve this goal the paper, firstly, gives an overview of GNSS RO missions. Secondly, the paper presents the results of the analysis of atmospheric vapour in the Nigerian region using space-based RO techniques substantiated with in-situ ground-based GNSS measurement. Lastly, the paper gives insight into the planned future expansion of GNSS RO infrastructures. With an expected increase and modernizations in GNSS RO infrastructure, it is expected that GNSS space-based RO techniques would be able to deliver a larger amount of data, which in turn could suggestively advance

* **Corresponding Author**

*(olalekanisioye@gmail.com) ORCID ID 0000 – 0001 – 5734 – 5374
(mefemoses@gmail.com) ORCID ID 0000 – 0003 – 4029 – 3736
(saeeusmansai@gmail.com) ORCID ID 0000 – 0001 – 9810 – 9554
(goldera2787@gmail.com) ORCID ID 0000 – 0001 – 6797 – 0114

**Cite this study**

Isioye O.A, Moses, M., Ibrahim, S.U. & Akomolafe E.A (2020). Precipitable water vapour retrieval and analysis over Nigeria from ground and spaced-based GNSS observations. Intercontinental Geoinformation Days (IGD), 181-185, Mersin, Turkey

weather forecasting services and climate monitoring, prediction and research in Nigeria or Africa at large.

## 2. METHOD

### 2.1. Datasets from Spaced and Ground based GNSS Observations

Post-processed data from the Taiwan/U.S. Formosat-3/COSMIC (Formosa Satellite Mission 3/Constellation Observing System for Meteorology, Ionosphere, and Climate) (Anthes et al. 2008), are used for all discussions in this paper. The post-processed data product from COSMIC is comprised of the raw GPS data, orbit determination, atmospheric profiles, total electron content and ionospheric profiles, scintillations, and tiny ionospheric photometer. We use the level 2 product "wetPrf". The "wetPrf" atmospheric profiles offer water vapour pressure, temperature, refractivity and water vapour information with a vertical resolution of 0.1 km and altitude range of 0 to 39.9 km.

Ground based GNSS derived precipitable water vapour (PWV) estimates were used to evaluate the COSMIC derived PWV. Ground-based GNSS meteorology has long offered the prospect of complementing other meteorological observations by providing an integrated vertical column of PWV content over respective GNSS sites. Dataset from the from the new Nigerian GNSS network (NIGNET) in Nigeria were utilized in this study (Jatau et al. 2010; Naibbi and Ibrahim 2014). These stations are primarily for surveying and positioning applications in Nigeria.

To investigate seasonal variations in the PWV, the estimated PWVs were grouped into four seasonal groups that typically represents the seasons in Nigeria, i.e., December-January-February (DJF), March-April-May (MAM), June-July-August (JJA), and September-October-November (SON).

### 2.2. PWV Retrieval from Spaced based GNSS Observations

To analyse the state of atmospheric water content from GNSS RO in the Nigerian region, we used GNSS RO data from COSMIC for the period of 2013-2016. We adopted an innovative approach to the estimation of PWV from GNSS RO profile data, first the zenith tropospheric delay (ZTD) was estimated from the numerical integration of a profile refractivity using the following relations;

$$ZTD = \int_{l}^{r} (n-1)ds = 10^{6} \int_{l}^{r} N ds \qquad (1)$$

In the discrete form, the equation (1) can be written as;

$$ZTD \approx \sum_{p}^{r} \left( \frac{N_{i+1} + N_i}{2} \right) \cdot \Delta s_i \qquad (2)$$

In equation (2), $\Delta s_i$ is absolute difference between successive heights of an individual occultation profile, $N_i$ and $N_{i+1}$ are successive refractivity values at respective heights, $i$ is the index denoting discrete heights/refractivity pairs and $k$ is the number of discrete linear segments between the occultation satellite $(r)$ and the lowest (or ground) point of the occulting event. A total of 1902 daily occultation profiles were processed for the period of 2013 to 2016 for the Nigerian region. The resulting ZTD was grouped into seasonal averages.

In furtherance of discussions to explore the potential of the occultation technique in estimating atmospheric water content over Nigeria, we estimated the Precipitable water vapour (PWV) from the ZTD values for each of the 1902 wet profiles from COSMIC observations. To achieve this, we choose an approach to separate the ZTD into the dry (ZHD) and wet (ZWD) components. The ZHD was estimated using the relation of Saastamoinen (1972) as presented in equation (3),

$$ZHD = 0.002277 \times \left[ \frac{P}{1 - 0.00266\cos(2\phi) - 0.28 \times 10^{-6} \times h} \right] \qquad (3)$$

where the pressure $(P)$ in mbar is the pressure at the ground point of the occultation profile, the ground latitude $\phi$ of the occultation event is in radians and the height $(h)$ is the corresponding height of the occultation event at ground point (in m). The resultant ZHD was subtracted from the ZTD to get the ZWD, we then adopted the formula of Isioye et al. (2017a) as presented in equation (4) to estimate the PWV for each occulting event. Equation (4) is suggested to users as a handy formula to estimate PWV (in mm) in Nigeria using $T_s(K)$ and ZWD (mm) as inputs. Again, PWV estimates were grouped into seasonal means.

$$PWV = ZWD \times \left[ 9.80392 - \frac{16917.64}{0.053499 T_s + 1739.07624} \right]. \qquad (4)$$

### 2.3. PWV Retrieval from Ground-based GNSS Observations

Daily GNSS observation data files in RINEX format with a 30-seconds sampling rate were collected from seven stations representing the different climatic zones in Nigeria for the period 2013-2016 via file transfer protocol (ftp) from the NIGNET server (http://server.nignet.net/). The GNSS stations were carefully selected based on their proximity to automatic (synoptic) weather observing stations (AWOS). Data from the AWOS were obtained from the Nigerian Meteorological Agency (NIMET). The GAMIT/GLOBK software (Herring et al. 2006) was used to estimate the ZTD. It employs a forced batch least squares inversion process. The GAMIT/GLOBK software parameterises the ZTD as a stochastic deviation of the uncomplicated representation of the Saastamoinen hydrostatic delay model (see Saastamoinen 1972) with a Gauss–Markov power density of $2cm/hour^{1/2}$.

The ZTD at each GNSS station was estimated daily within a 24-hour window session. The International GNSS Service (IGS) final orbits (SP3) and IGS final Earth rotation parameter (ERP) products were used. Satellite elevation cut-off was set to $10^{\circ}$ during the data

processing. Station coordinates were heavily constrained to their ITRF 2008 values (Altamimi et al. 2011). Solid earth tide based on the IERS03 and FES2004 models were used for solid earth tide and ocean tide loading corrections, respectively. The constraint used for zenith delay was 0.2m, as it is recommended to set it loosely enough to encompass any error in wet delay (Herring et al. 2006). Satellite antenna phase centre offset and phase centre variation is based on AZEL for IGS absolute ANTEX files (Gendt and Schmid, 2005). The a priori tropospheric model used is the Saastamoinen model (1972) based on meteorological sources from the Global Pressure and Temperature (GPT) model. The Vienna Mapping Function (Boehm et al. 2006) was used to calculate the zenith delay. To retrieve PWV estimates from GNSS-derived ZTDs, station temperature and pressure values are fundamental to separate the ZTD into its wet and dry components. Thus, surface temperature and pressure data from nearby AWOS were transferred to the GNSS sites employing the technique demonstrated by Musa et al. (2011). The resultant ZWD component was transformed to PWV using the formulation of Isioye et al. (2017b) presented herein as Equation (4):

## 3. RESULTS AND DISCUSSİON

The ZTD estimates as presented in the Figure 1 show clear evidence of seasonal variations which are in good agreement with the result of Isioye et al. (2017b) from ground-based GNSS stations across Nigeria. Nigeria's climate is characterized by strong a latitudinal dependence and becomes increasingly drier as one moves northwards from the coast of the Atlantic Ocean. Rainfall is the main climate indicator and there is a discernible difference between the wet and dry seasons across Nigeria. By April or May of every year, the rainy season is underway in most parts of the south of the Niger and river Benue valleys. Farther north the rains do not begin until the months of June or July. From the months of December through February northeast trade winds, called the Harmattan, sweeps through the country. In addition, these winds are often loaded with dust particles from the Sahara Desert giving rise to characteristic Harmattan haze which reduces visibility.

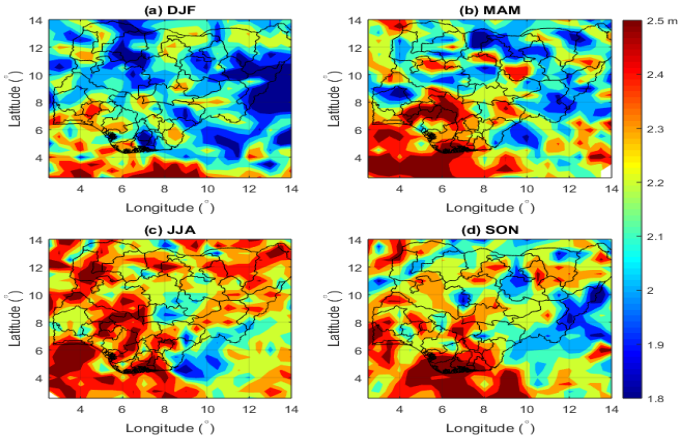


**Figure 1.** *Seasonal mean ZTD, a) DJF, b) MAM, c) JJA, c) SON derived from COSMIC for the period of 2013-2016 over the Nigerian region*

The Figure 2 shows the PWV from COSMIC observations for the four the different seasons. Expectedly, it can be seen that the PWV also follow similar pattern with the ZTD. The maximum or very high amount of PWV was recorded in the moths of June, July and August which often symbolises the peak of the wet season in Nigeria.

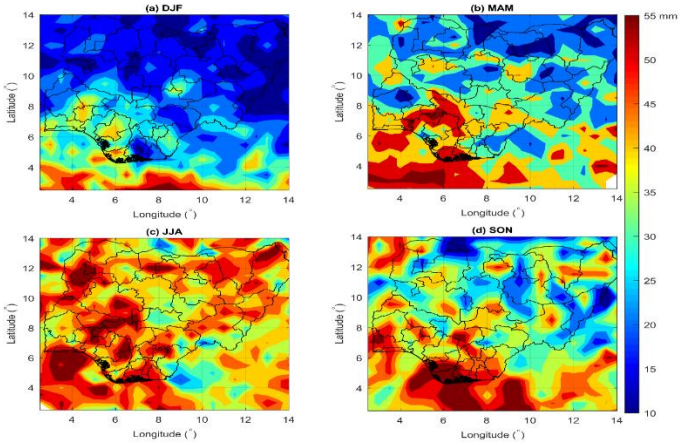


**Figure 2.** Seasonal mean PWV, a) DJF, b) MAM, c) JJA, c) SON derived from COSMIC for the period of 2013-2016 over the Nigerian region

Figure 3 presents the PWV values for the four seasons. According to Figure 3, the seasonal PWV confirms an apparent agreement with those in figure 2 for the GNSS RO. Both Figures 2 and 3 exhibits lower values in the dry season (DJF and MAM) and higher values in the wet season (JJA, SON), which reflects that in the wet (rainy) season, because of the strong moisture field (high water vapour pressure) the PWV magnitude is higher. PWV values at all the GNSS stations and GNSS RO events exhibit a recognised seasonal signal, which can be explained by a cosine function, as the increase to the maximum in the JJA season, which is the peak of the rainy season in both the north and south of Nigeria, and a decrease to the minimum in the months of DJF, the dry season in the south and the Harmattan in the north of Nigeria. There is little rain in the months of MAM and SON in the north and the temperature is high, while the south is not as dry as the north, thus the climate in the south is very humid and tends to keep the PWV values very high.

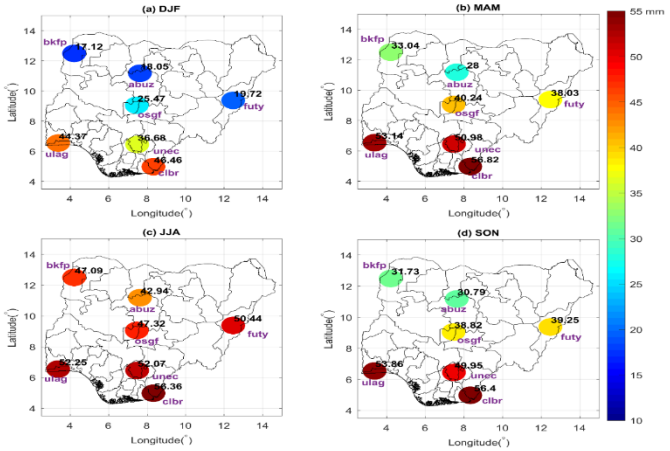


***Figure 3.*** Seasonal mean PWV, a) DJF, b) MAM, c) JJA, c) SON derived from NIGNET for the period of 2013-2016 over the Nigerian region

From the Figures 2 and 3, the amount of PWV is greatly varied at the coastal regions of Nigeria. For instance, the magnitude of PWV is greater at all seasons along the shorefront of the Atlantic Ocean at the ground GNSS stations (CLBR and ULAG) and the occultation points. The seasonal range (i.e. difference between maximum and minimum seasonal values) of PWV at the different GNSS stations as seen in Figure 3 is 24.88 mm, 10.36 mm, 30.72 mm, 9.49 mm, 15.39 mm, 21.85 mm and 29.97 mm for ABUZ, CLBR, FUTY, ULAG, UNEC, OSGF, and BKFP, respectively. It is obvious that the range in PWV at the stations increases with latitude (i.e., movement from south to north), this pattern is also evident in PWV from GNSS RO observations. A sharp increase in the range values is seen at the location of GNSS stations (ABUZ, FUTY, OSGF, and BKFP) and occultation points in the northern part of Nigeria. This is expected because of the extreme cold and hot weather during the dry season in the northern part of Nigeria, which often results in great variations in surface temperature. These results show that variability in PWV estimates as observed by both GNSS techniques is closely related to rainfall and confirms the efficiency of the GNSS techniques in storm prediction and possibly in improving future forecasting models in Nigeria.

To further, ascertain, the agreement between ground-based GNSS derived PWV and that from GNSS RO, we found and calculated the mean absolute difference between the duo techniques for occultation events at a maximum distance of 100km from the individual GNSS station. The summary of the result is presented in Table 1 for the four seasons, in some of the seasons; there were no occultation events within the 100km buffer zone from the GNSS station(s).

**Table 1.** Mean absolute difference of precipitable water vapour (PWV) estimates from GNSS RO and ground-based GNSS over Nigeria

| Ground GNSS Station | Mean Difference (COSMIC – Ground GNSS Station) (mm) | | | |
|---|---|---|---|---|
| | DJF | MAM | JJA | SON |
| abuz | 1.323 | 4.425 | 4.655 | - |
| bkfp | 2.235 | 0.400 | 5.576 | 2.459 |
| clbr | - | 3.94 | 0.577 | 0.580 |
| futy | 2.283 | 0.895 | 2.668 | 1.245 |
| osgf | 0.800 | 2.355 | 1.052 | - |
| unec | 6.47 | 0.995 | 0.623 | 0.403 |
| ulag | 4.973 | 1.687 | 0.700 | 2.425 |

From the Table 1, it is evident that the GNSS RO can estimate PWV to accuracy limit of less than about 5mm as compared to the ground-based GNSS technique. These results are very attractive for weather forecast, climate and atmospheric research since PWV is a very important climate pointer.

## 4. CONCLUSION

The paper has demonstrated the capability of the GNSS RO technique for the monitoring the Nigerian weather and climate. This emerging technique uses radio signals between the Low Earth Orbit (LEO) and GNSS satellites, probes the Earth's atmosphere and ionosphere from space. The quality of GNSS RO derived atmospheric profiles was assessed with other observing systems in this study, the outcome shows good agreement with the Ground-based GNSS stations and have been considered as a good data source for atmospheric and climate related researches. The GNSS RO technique has a strong potential to provide useful information for assimilation as a new data source into the Nigerian weather forecasting framework. The recent improvements in the COSMIC (COSMIC-2), GRACE (GRACE-FO), and proposed improvement in MetOp missions (MetOp-SG) are expected to increase the number of RO events globally and will further enhance the capacity of the technique. Such a large volume of stream-in new high resolution atmospheric profiles will no doubt have great impacts on future meteorological studies and applications.

## ACKNOWLEDGEMENT

The authors acknowledge the office of the Surveyors General of the Federation (OSGOF) and CDAAC for the ground and spaced based GNSS data respectively. We remain thankful to all reviewers as well.

## REFERENCES

Altamimi Z, Collilieux X & M´etivier L (2011). ITRF2008: An improved solution of the international terrestrial reference frame, *Journal of Geodesy*, 85(8):457–473.

Anthes R A, Bernhardt P A, Chen Y, Cucurull L, Dymond K F, Ector D, Healy S B, Ho S P, Hunt D C, Kuo Y H, Liu H, Manning K, McCormick C, Meehan T K, Randel W J, Rocken C, Schreiner, W S, Sokolovskiy S V, Syndergaard S, Thompson D C, Trenberth K E, Wee T K, Yen, N L & Zeng Z (2008). The COSMIC/FORMOSAT-3 mission: Early results, *Bull. Am. Meteorol. Soc*., 89, 313–333, doi:10.1175/BAMS-89- 3-313.

Anthes R A, Rocken C & Kuo Y H (2000). Applications of COSMIC to Meteorology and Climate, Terrestrial, Atmospheric and Oceanic Sciences, Special issue on COSMIC, 39, 2000.

Boehm J, Werl B & Schuh H (2006). Troposphere mapping functions for GPS and very long baseline interferometry from European centre for medium-range weather forecasts operational analysis data. *Journal of Geophysical Research B: Solid Earth*, 11(2), Article ID B02406.

Gendt G & Schmid R (2005). Planned Changes to IGS Antenna Calibrations. *IGSMAIL-5189, IGS Central Bureau*. Available online at http://igscb.jpl.nasa.gov/mail/igs.

Herring T A, King R W & McClusky, S C (2006). *Reference Manual for the GAMIT/GLOBK GPS software, release, 10.3.* Department of Earth, Atmospheric, and Planetary Sciences, Massachusetts Institute of Technology, Boston, USA.

Isioye O A, Combrinck L & Botai J O (2016). Modelling Weighted Mean Temperature in the West African Region: Implications for GNSS Meteorology, *Meteorological Applications*, 23(4):614-632, http://dx.doi.org/10.1002/met.1584

Isioye, O A, Combrinck L & Botai O J (2017a). Retrieval and analysis of precipitable water vapour based on GNSS, AIRS, and reanalysis models over Nigeria. *International Journal of Remote Sensing,* 38(20):5710-5735, https://doi.org~/10.1080/01431161.2017.1346401

Isioye, O A, Combrinck L & Botai O J (2017b). Evaluation of Spatial and Temporal Characteristics of GNSS-derived ZTD Estimates in Nigeria, *Theoretical and applied climatology*, 2017, 1-18, doi: 10.1007/s00704-017-2124-7

Jatau B, Rui M, Adeyemi A & Nuno G (2010). NIGNET: The New Permanent GNSS Network of Nigeria. *FIG Congress 2010: Facing the Challenges – Building the Capacity,* Sydney: Australia. [Online], Available: http://fig.net/pub/fig2010/papers/fs02h%5Cfs02h_~ jatau_fernandes_et_al_4549.pdf

Jones J (2016). *The current status and future of GNSS-Meteorology in Europe.* A presentation at the 2016 UNAVCO Science Workshop, Broomfield, Colorado, USA, March 29-31. Available at https://www.unavco.org/community/meetings-events/2016/sciworkshop16/presentations/presentations.html

Kuleshov Y, Choy S, Fu E F, Chane-Ming F, Liou Y A & Pavelyev A G (2016). Analysis of Meteorological Variables in the Australasian Region using Ground and Space Based GPS Techniques. *Atmospheric Research,* 176-177(2016):276-289, http://dx.doi.org/10.1016/j.atmosres.2016.02.021

Kursinski E R, Hajj G A, Hardy K R, Romans L J & Schofield J (1995). Observing tropospheric water vapor by radio occultation using the Global Positioning System, *Geophysical Research Letters*, 22(1995):2365-2368.

Liang, H., Cao, Y., Wan, X., Xu, Z., Wang, H., Hu, H., 2015. Meteorological Applications of Precipitable Water Vapour Measurements Retrieved by the National GNSS Network of China. *Geodesy and geodynamics,* http://dx.doi.org/10.1016/j.geog.2015.03.001

Musa T A, Amir S, Othman R, Ses S, Omar K, Abdullah K, Samsung L & Rizos C (2011). GPS meteorology in a low latitude region: Remote sensing of atmospheric water vapour over Malaysian Peninsula, *Journal of Atmospheric and Solar Terrestrial Physics*, 73:2410-2422. doi: 10.1016/j.jastp.2011.08.014

Naibbi A I & Ibrahim S S (2014). An Assessment of the Existing Continuously Operating Reference Stations (CORS) in Nigeria: An Exploration using Geographical Information System (GIS). *American Journal of Geographic Information Systems*, 3(4):147–157, doi:10.5923//j.ajgis.20140304.01

Rozsa S, Kenyeres A, Weidinger T Z & Gyöngyösi A (2014). Near Real Time Estimation of Integrated Water Vapour from GNSS Observations in Hungary. *International Association of Geodesy Symposia.* 139:31-39. doi:10.1007/978-3-642-37222-3_5

Saastamoinen J (1972). Atmospheric correction for troposphere and stratosphere in radio ranging of satellites. In Henriksen, S.W., Mancini, A., Chovitz, B. H., (Eds.). *The Use of Artificial Satellites for Geodesy*, of *Geophysics Monograph Series*, 15:247–252. Washington, DC: American Geophysical Union (AGU), AIAA, NOAA, U.S.ATC.

Intercontinental Geoinformation Days

http://igd.mersin.edu.tr/2020/

# Detecting Outliers With The Least Trimmed Squares

**Hasan Dilmaç*[1], Yasemin Şişman[2]**

[1]*Ondokuz Mayis University, Faculty of Engineering, Department of Geomatics Engineering, Samsun, Turkey*

**Keywords**
The Least Squares
Outliers
Robust Estimation
The least trimmed squares

**ABSTRACT**

Classical outlier tests made classically based on the least-squares (LS) have significant disadvantages in some situations. The results of adjustment computation and classical outlier tests performed with classical methods are deteriorated when observations are not distributed independently and this distribution is not normal. To detect outliers that do not have a normal distribution, the robust techniques that are not sensitive to outliers have been developed. The least trimmed squares (LTS) known as having a high-breakdown point have been dealt with in this study. Adjustment computation has been carried out based on the least-squares (LS) and the least trimmed squares (LTS). A certain polynomial with arbitrary values has been used. In this way, the performances of these techniques have been investigated.

## 1. INTRODUCTION

Various observations are done in geodesy. Physical and geometric quantities, such as angles, distances, heights, and gravity are measured and processed. In this case, a great number of data appears (Fan 1977). Since the accuracy of data is always questioned, it is preferred that the number of observations is bigger than the number of unknowns. A quantity is always measured differently from each other even though it is measured many times under the same conditions (Ingram 1911). It is clear that observations are never exact, and they always contain error, however careful they are performed. Thus, an adjustment computation is applied to get unique solutions from these redundant measurements (Ghilani 2017; Mikhail and Ackermann 1982).

There are a lot of adjustment methods. The least-squares (LS) is a frequently used method. LS is a sort of regression that examines and models the relationship between data (usually obtained from observations). It is one of the most adopted methods because of its tradition and ease of computation (Cizek and Visek 2005; Rousseeuw and Leroy 1987). But, it has turned out with time that outliers (observations with different distribution compared to the distribution of majority) affect the LS method negatively.

Outliers in observations are encountered very often in applications (Rousseeuw and Leroy 1987). The results of adjustment with classical methods such as LS, which should meet some conditions like normal distribution are deteriorated. So, these outliers must be detected and eliminated from observations. There are outliers tests based on classical methods, especially LS. These outliers tests can be contaminated. Therefore, new statistical methods have been sought instead of LS sensitive to outliers. (Yetkin and Berber 2013).

The robust statistics deals with developing estimators insensitive to discrepancies from basic assumptions in classical models (Fabozzi et al. 2014). To overcome effects of outliers, robust methods aim to find results that are closest to adjustment results that would be found without outliers. Then, outliers can be detected through their residuals. (Rousseeuw and Hubert 2018). Many robust techniques have been developed. These techniques can be divided into classes with some concepts like a high-breakdown point, influence function, etc. The least trimmed squares (LTS) is a high-breakdown point estimator.

In this study, adjustment computations and outlier analysis have been performed according to LS and LTS method in different scenarios. Then, the results of LS and LTS have been compared with each other.

* **Corresponding Author**

*(hasan.dilmac@omu.edu.tr) ORCID ID 0000-0001-6877-8730
(ysisman@omu.edu.tr) ORCID ID 0000-0002-6600-0623

**Cite this study**

Dilmac H & Sisman Y (2020). Detecting Outliers with The Least Trimmed Squares. Intercontinental Geoinformation Days (IGD), 186-189, Mersin, Turkey

## 2. METHOD

### 2.1. Adjustment Computation

When there is the redundant observation in a problem, adjustment computation is performed to get unique values for the unknowns (Ogundare 2018). Adjustment is only meaningful when observations are more than the unknown number (Mikhail and Ackermann 1976). In this case, the problem is solved according to an objective function. For the solution of the problem, a mathematical model (model briefly) that represents the mathematical relationship of observations and unknowns is established (Schaffrin 2019). The mathematical model accounts for an essential part of adjustment computation, and it is usually composed of two parts: a functional model and a stochastic model. When observations are made, a functional model is typically chosen to represent the physical situation. The stochastic model determines variances and covariances of observations (Ghilani 2017; Mikhail and Ackermann 1976; Ogundare 2018). In the classical Gauss-Markov model, the functional and stochastic model can be expressed as below:

$$v = Ax - l$$
$$P = Q_{ll}^{-1} = \sigma_0^2 C_{ll}^{-1}$$

where v, A, x, l, P, $\sigma_0^2$ and $C_{ll}$ are the residual or correction vector, the coefficient matrix, unknown vector, the observation vector, the weight matrix, a priori variance, and the covariance matrix, respectively.

In this case, both the functional model and the stochastic model must be correct if adjustment computation is to give real results (Ghilani 2017). After a mathematical model is formed, an optimization is made according to chosen objective function. Optimization means minimization or maximization of function (Grafarend and Sanso 2012).

### 2.2. The Least Squares

The Least Squares (LS) is a method used in adjustment computation by minimizing the sum of the squared weighted differences to get unique values with redundant measurements (Amiri-Simkooei 2003; Mikhail and Ackermann 1982; Wells and Krakiwsky 1971). The objective function of LS can be given the following:

$$v^T P v = \sum_{i=1}^{n} p_i v_i^2 \rightarrow min$$

The main problem of LS is that even one outlier might severely affect the LS method (Muhlbauer et al. 2009). LS can propagate errors in one observation to another observation. Therefore, masking and swamping effects occur. A bad observation could seem like a good one because of the propagation of errors; this is called a masking effect. On the contrary, the good observation could seem bad; this is called the swamping effect (Hekimoglu 2005). As a result, test for outliers like Baarda test (Data-snooping, W-test) and Pope test (Tau test) based on LS also can be affected negatively.

### 2.3. Robust Estimation and Determination of Outliers

Real data sets frequently contain outliers (Rousseeuw 1990). Therefore, methods that cannot be affected easily by outliers should be developed. These are the methods named as robust methods. Robustness usually means insensitivity to outliers (Huber 1981).

There are many robust methods. $L_1$-norm is the oldest method of these robust methods. Then, M-estimators, R-Estimators, and L-Estimators appeared. To compare the robustness of these methods, the 'breakdown point' has been used. The breakdown point means the smallest number of outliers, which may affect an estimator negatively (Hofmann et al. 2010). These methods above have a low-breakdown point (Rousseeuw and Leroy 1987). Because of this, generalised M-Estimators was developed. Then, Repeated Median, The Least Median Squared (LMS) (1984), S-Estimators, MM-Estimators, and The Least Trimmed Squares (LTS) were developed respectively (Hubert et al. 2008; Staudte and Sheather 2011; Toka and Cetin 2011).

### 2.4. The Least Trimmed Squares

The least trimmed squares (LTS) was developed by Rousseeuw. This method is quite similar to LS except that the largest squared residuals are removed from the data (Knight and Wang 2009). The objective function of LTS can be given the following:

$$Min \sum_{i=1}^{h} P v_i^2$$

where, h is the number of residuals (or corrections) after data removing

There are different criteria to determine the number of residuals in LTS that will be included in the sum. The h= n/2 (n, number of observations) should be taken for maximum robustness since LTS can give satisfactory results until %50 contamination (Cizek 2005). LTS problem requires dealing with finding the minimum one from $\binom{n}{h}$ LS solutions (Hofmann et al. 2010).

## 3. RESULTS

In numerical applications, a linear regression model such as $y=a_1x+a_2$ was used. Regression coefficients were taken as 2 and 0.5, respectively. y values were calculated according to x values that were chosen arbitrarily for 10 observations. In the first application, both LS and LTS methods were performed using x values and y values with random errors. In LTS, h was taken as 8 and $\binom{10}{8}$ solutions were made. Then, for the second application, gross errors were added to

some y values, and LS and LTS methods were performed again. Regression results are shown in Table 1 and Table 2. Distribution of x and y values and regression lines in Application 2 are shown in Figure 1. It was expected that LTS could detect precisely y values with gross errors.

The results of Application 1 have shown that the observations (measurements) are typically distributed, and they have only random errors. Thus, the results of LS and LTS are close to each other (Table 1). But, it is shown that the results of LTS are closer to real values than LS. In Application 2, it is clear that the products of LS are quite contaminated, and the sum of residuals squared has increased very much (Table 2). The coefficient $a_2$ of LS in Application 2 is quite different from expected. Compared to LS in Application 2, the results of LTS in Application 2 are more correct, and the sum of residuals squared is relatively much smaller.

**Table 1.** The regression results of Application 1

| Methods | $a_1$ | $a_2$ | [VV] |
|---|---|---|---|
| LS | 2.03 | 0.37 | 1.24 |
| LTS | 2.01 | 0.38 | 0.15 |

**Table 2.** The regression results of Application 2

| Methods | $a_1$ | $a_2$ | [VV] |
|---|---|---|---|
| LS | 2.14 | 1.76 | 208.38 |
| LTS | 2.07 | 0.09 | 0.96 |

It can be seen that the outliers have affected the results of LS regression in Application 2. Point 6 and, which is designed as outliers have drawn LS regression line towards themselves. However, LTS regression has not been affected by outliers (Figure 1).

The residuals of LS regression in Application 1 are small as expected (Figure 2a). The effects of outliers on the residuals for LS in Application 2 can be seen in Figure 2b. Also, it is seen that the gross errors added to Point 6 and 7 have been distributed to the other points in the LS method (Figure 2b).

LTS regression in Application 2 could determine outliers precisely and remove outliers (6 and 7. Points) from the observations. Also, LTS regression has not distributed outliers effects to the other points (Figure 3).

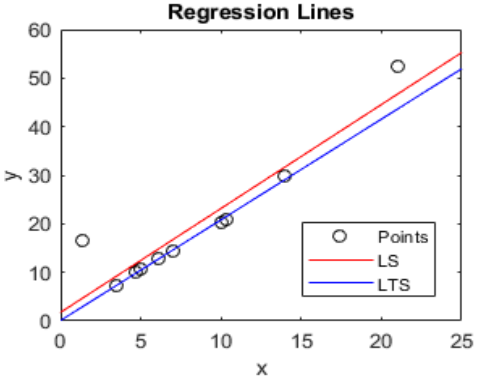


**Figure 1.** The regression lines of LS and LTS in Application 2

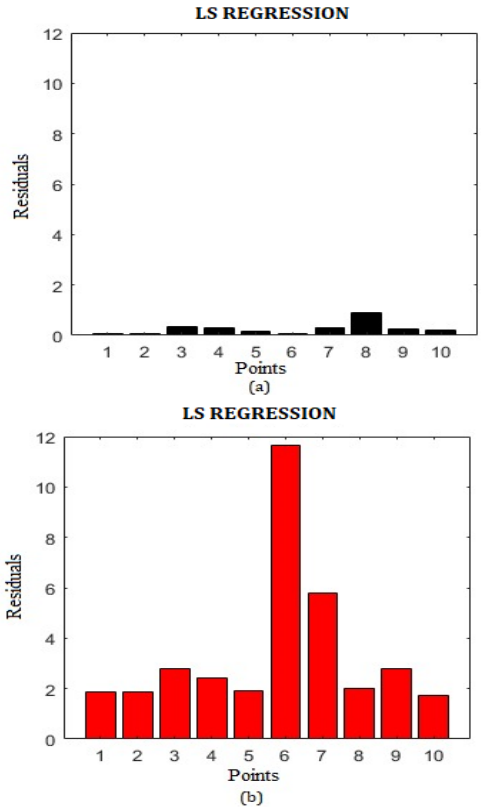


**Figure 2.** The residuals of LS regression in Application 1 (a). The residuals of LS regression in Application 2 (b)

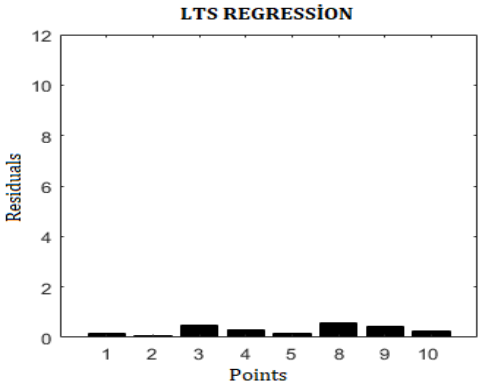


**Figure 3.** The residuals of LTS regression in Application 2

## 4. DISCUSSION AND CONCLUSION

A linear regression model was used in this study. The analysis were performed according to LS and LTS method using different scenarios. In the first application, points with only random errors were used. The LS and LTS methods gave good results. But, LTS had a little better results. In the second application where contaminated points were used, although LS results were affected badly from outliers, LTS results gave results close to ones in Application 1.

As a result, LTS results are as good as LS results when observations are normally distributed. On the other hand, LTS can give much better results than LS when observations have outliers. Also, the LS method can distribute the outlier effect to the other points.

**REFERENCES**


Amiri-Simkooei A (2003). Formulation of L1 Norm Minimization in Gauss-Markov Models. *Journal of Surveying Engineering*, 129:1, 37:43. doi: 10.1061/(ASCE)0733-9453(2003)129:1(37)

Čížek P & Víšek J Á (2005). Least Trimmed Squares. *XploRe®—Application Guide*,49-63. Springer, Berlin, Heidelberg.doi: 10.1007/978-3-642-57292-0_2

Cizek P (2005). Least trimmed squares in nonlinear regression under dependence. *Journal of Statistical Planning,* 136, 3967-3988, doi: 10.1016/j.jspi.2005.05.004

Fabozzi F J, Focardi S M, Rachev S T & Arshanapalli B G (2014). *The Basics of Financial Econometric: Tools, Concepts and Asset Management Applications*. John Wiley ve Sons, Inc.

Fan H (1993). *Theory of errors and least squares adjusment*. Royal Institute of Technology, 72, 100-44, Stockholm, Sweden.

Ghilani C D (2017). *Adjustment computations: Spatial data analysis* (Sixth edition). John Wiley ve Sons, Inc., Hoboken, New Jersey.

Grafarend E W & Sansò F (Editors) (2012). *Optimization* and *design of geodetic networks*. Springer Science & Business Media, Heidelberg, Berlin.

Hekimoglu S (2005). Do Robust Methods Identify Outliniers More Reliably Than Conventional Tests for Outliniers? *Zeitschrift für Vermessungwesen, 3, 174-180.*

Hofmann M, Gatu C & Kontoghiorghes E J (2010). An Exact Least Trimmed Squares Algorithm for a Range of Coverage Values*, Journal of Computational and Graphical Statistics,* 19:1, 191-204, doi: 10.1198/jcgs.2009.07091

Huber P J (1981). *Robust Statistics*. John Wiley and Sons, Inc.

Hubert M, Rousseeuw P J & Van Aelst S (2008). High-breakdown robust multivariate methods. *Statistical science*, 23:1, 92-119. doi: 10.1214/088342307000000087

Ingram E L (1911). *Geodetic surveying and the adjustment of observations* (methods of least squares). McGraw-Hill Book Company, Inc. 370 Seventh Avenue, New York.

Knight N L & Wang J (2009). A comparison of outlier detection procedures and robust estimation methods in GPS positioning. *The Journal of Navigation,* 62:4, 699-709 doi: 10.1017/S0373463309990142

Mikhail E M & Ackermann F E (1976). *Observations and least squares*. Thomas Y. Crowell Company, Inc. 666 Fifth Avenue, New York.

Montgomery D C, Peck E A & Vining G G (2012). *Introduction to linear regression analysis* (Fifth edition). John Wiley & Sons, Inc, 821, Hoboken, New Jersey.

Muhlbauer A, Spichtinger P & Lohmann U (2009). Application and comparison of robust linear regression methods for trend estimation. *Journal of Applied Meteorology and Climatology,* 48:9, 1961-1970 doi: 10.1175/2009JAMC1851.1

Ogundare J O (2018). *Understanding Least Squares Estimation and Geomatics Data Analysis*. John Wiley ve Sons, Inc, 111 River Street, Hoboken, NJ 07030, USA

Rousseeuw J R & Leroy A M (1987). *Robust Regression and Outlier Detection.* John Wiley ve Sons, Inc.

Rousseeuw J R (1990). Robust estimation and identifying outliers. *Handbook of statistical methods for engineers and scientists*, 16-1.

Rousseeuw P J & Huber M (2018). Anomaly detection by robust statistics. *Wiley Interdisciplinary Reviews: Data Mining and Knowledge Discovery,* 8:2, e1236. doi: 10.1002/widm.1236

Schaffrin B (2019). Notes On Adjustment Computations Part I.

Staudte R G & Sheather S J (2011). *Robust estimation and testing*. John Wiley ve Sons, Inc, 918.

Toka O & Cetin M (2011). The comparing of S-estimator and M-estimators in linear regression. *Gazi University Journal of Science,* 24:4, 747-752

Wells D & Krakiwsky E (1971). The Method of least squares. University of New Brunswick: Canada

Yetkin M & Berber M (2013). Application of the sign-constrained robust least-squares method to surveying networks. *Journal of Surveying Engineering,* 139:1, 59-65. doi: 10.1061/(ASCE)SU.1943-5428.0000088

Intercontinental Geoinformation Days

http://igd.mersin.edu.tr/2020/

# Analysis of the contribution of the multi-GNSS to long-distance RTK

**Ceren Konukseven*[1], Omer Faruk Atiz[1], Salih Alcay[1], Sermet Ogutcu[1]**

[1]*Necmettin Erbakan University, Faculty of Engineering and Architecture, Department of Surveying Engineering, Konya, Turkey*

**Keywords**
GALILEO
BEIDOU
RTK
Network RTK

**ABSTRACT**

Global Navigation Satellite System (GNSS) can provide users a fast, cost-effective, and reliable positioning service. With Real-Time Kinematic (RTK) method, it has become a practical tool for real-time positioning in many engineering applications. However, the accuracy of RTK method depends on the base distance between the reference station and the rover due to the orbital error and atmospheric errors. In classical RTK, while a reliable accuracy can obtain for short baseline length, the accuracy decreases for long baseline lengths. The effect of baseline length can be mitigated by using the Network RTK technique. Nevertheless, the accuracy highly depends on the nearest reference station. With the new emerging satellite systems such as GALILEO and BEIDOU, it has been possible to perform multi-GNSS RTK surveying. In this study, the contribution of multi-GNSS to long-distance RTK is examined. For this purpose, a field test is conducted on an approximately 80 km baseline using different satellite combinations. The results are examined regarding the accuracy.

## 1. INTRODUCTION

In the last decade, the Global Navigation Satellite System (GNSS) is widely used for positioning in real-time or post-process. With the developments related to GNSS, the Real-Time Kinematic (RTK) and Network-RTK methods emerged (Inal et al. 2014). The real-Time Kinematic method is a relative positioning method that allows users to estimate rover's coordinates based on a reference station. Today, these methods have an essential role in the surveying community. The accuracy of the method depends on ionospheric-tropospheric errors, signal obstructions, multipath, the geometric configuration of satellites and other errors (Baybura et al. 2019). As the atmospheric conditions are changed between the reference and rover's location, the accuracy depends on the baseline length. In general, baseline length is limited to 15-20 km when correction information is provided by radio connection. The network-RTK method can mitigate the baseline limit of traditional RTK since the correction is calculated from the network and sent via the Internet. However, in Network-RTK the accuracy highly depends on the nearest reference station.

In recent years, new satellite systems are developed such as GALILEO and BEIDOU. With the new emerging GNSSs, it has been possible to perform multi-GNSS RTK. Several studies have been conducted for multi-GNSS RTK. Odolinski et al. in 2015 presented a new approach to single-frequency multi-GNSS RTK. Accordingly, multi-GNSS was improved the integer phase ambiguity resolution (Odolinski et al. 2015). The combination of GPS+GALILEO for RTK was showed better accuracy at the high cut off angles than only-GPS (Castro-Arvizu et al. 2020). He and Chen in 2020 proposed a network RTK algorithm that can process observations of five GNSS systems (BDS-2/BDS-3, GPS, GLONASS, GALILEO and QZSS) (He and Chen 2020). According to this, including multi-GNSS observations to the Network-RTK model gives better results compared with the classical Network RTK. Wang et al. in 2020 compared the traditional single baseline RTK and their newly developed multi-baseline RTK methods. They concluded that GPS/BDS combination gives better results compared with the only-GPS for the kinematic experiment (Wang et al. 2020). Xi et al. in 2020 investigated bridge monitoring with multi-GNSS RTK (Xi et al. 2020). They demonstrated that even for high cut-

* **Corresponding Author**

*(ceren.konukseven@ogr.erbakan.edu.tr) ORCID ID 0000-0001-6598-9479
(oatiz@erbakan.edu.tr) ORCID ID 0000 – 0001 – 6180 – 7121
(salcay@erbakan.edu.tr) ORCID ID 0000 – 0001 – 5669 – 7247
(sermetogutcu@erbakan.edu.tr) ORCID ID 0000-0002-2680-1856

**Cite this study**

Konukseven C, Atiz O F, Alcay S & Ogutcu S (2020). Analysis of the contribution of the multi-GNSS to long-distance RTK. Intercontinental Geoinformation Days (IGD), 190-193, Mersin, Turkey

off angles, 2 mm and 7 mm precisions can be obtained for horizontal and vertical components, respectively.

In addition to multi-GNSS RTK, some studies have been conducted for long distance RTK. Baybura et al. in 2019 compared Network-RTK and long distance RTK methods using GPS/GLONASS satellite combination (Baybura et al. 2019). They concluded that the two methods showed similar results. Zhang et al. in 2020 investigated the contribution of QZSS to GPS+GLONASS+GALILEO RTK using a new triple frequency observation model (Zhang et al. 2020). The results showed that for longer baselines, QZSS improved the accuracy and ambiguity fixing rate. Bramanto et al. 2019 examined long distance RTK for cadastral surveying with a new algorithm (Bramanto et al. 2019). They demonstrated that long distance RTK -up to 90 km- can be used for cadastral measurements.

Despite many studies have been conducted for multi-GNSS or long distance RTK, it is worth to examine comprehensively the contribution of multi-GNSS to long distance RTK. In this study, the positioning performance of GPS, GPS+GLONASS and GPS+GLONASS+GALILEO+BEIDOU satellite combinations for long distance RTK is investigated. For this purpose, a field test is conducted. The results are analyzed in terms of accuracy.

This paper is organized as follows. In Section 2 the functional model of RTK is briefly described. Section 3 explains the field test. In section 4 the results and discussions are given. In Section 5 the work is concluded.

## 2. FUNCTIONAL MODEL OF RTK

RTK mathematical model is based on the double difference (DD) of carrier phase observations (Figure 1). DD technique eliminates the satellite/receiver clock offsets, most of the ionospheric error and many other error sources.

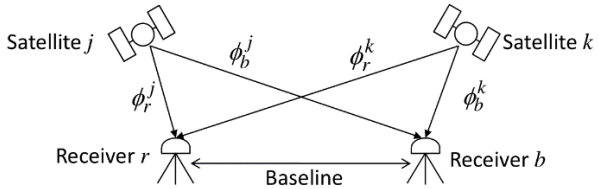


**Figure 1.** Double differences (Takasu 2013)

Although there are some small differences in the algorithms according to the device and software used, the fundamental steps are similar. Accordingly, first single differences (SD) then DD are composed. After obtaining the float solution, ambiguity resolution is performed. When the integer ambiguity is solved, fixed solution is obtained. Also, the ambiguity resolution part includes searching and validating steps (Aydin et al. 2004). For a satellite-receiver pair, the carrier phase observation can be written as follows:

$$\emptyset = \rho - I + Tr + c(b_{Rx} - b_{Sat}) + N\lambda + \varepsilon_{\emptyset} \quad (1)$$

where $\rho$ indicates the geometric range between the receiver and satellite; $I$ is the ionospheric delay; $Tr$ is the tropospheric delay; $b_{Rx}$ and $b_{Sat}$ are receiver and satellite clock offsets, respectively; $\lambda$ is the wavelength of carrier phase; $N$ is the integer ambiguity term and $\varepsilon_{\emptyset}$ is the measurement noise. The geometric range can be extracted using ECEF coordinates of receiver and satellite as given in Equation 2.

$$\rho = \sqrt{(X_{Sat} - X_{Rx})^2 + (Y_{Sat} - Y_{Rx})^2 + (Z_{Sat} - Z_{Rx})^2} \quad (2)$$

For two satellite-receiver pair as shown in Figure 1, the DD equation can be written as follows:

$$\emptyset_b^{jk} - \emptyset_r^{jk} = \rho_b^{jk} - \rho_r^{jk} - I_b^{jk} + I_r^{jk} + Tr_b^{jk} - Tr_r^{jk} + \lambda(N_{b,r}^{jk}) + \varepsilon_b^{jk} - \varepsilon_r^{jk} \quad (3)$$

where superscript $j$ and $k$ denote the satellites and subscript $r$ and $b$ indicates the rover and base stations, respectively. The clock offsets are directly removed by DD. The tropospheric and ionospheric errors are can be neglected relatively. When $N_{b,r}^{jk}$ term is solved as an integer value in some way, RTK positioning is obtained in cm level and so-called "fixed" solution. If the ambiguity term could not solve as an integer, the solution is called "float". Usually, the accuracy of the float solution is at a few meters level. For RTK, the integer ambiguity is solved by on-the-fly (OTF) ambiguity resolution techniques (Wang 1999).

## 3. FIELD TEST

For examining the contribution of multi-GNSS combinations to the long distance RTK, a field test is performed on an approximately 80 km baseline, in Konya closed basin area. The location of the field test is given in Figure 2.

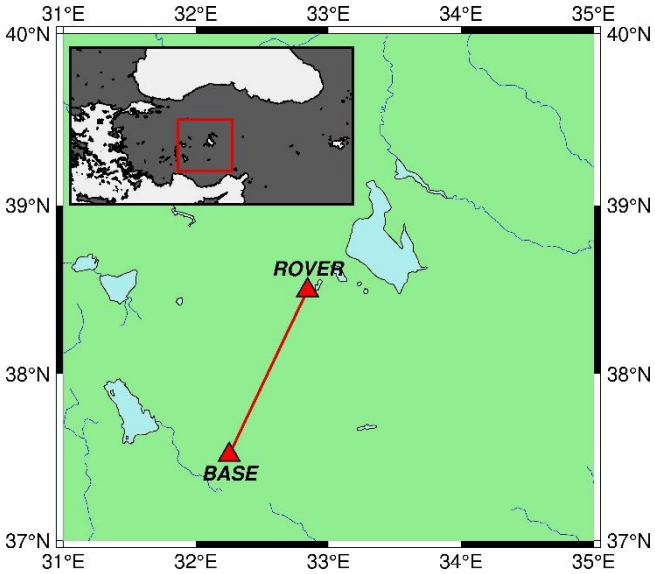


**Figure 2.** The location of the field test

The field test is conducted considering three different satellite options: GPS, GPS+GLONASS, GPS+GLONASS+GALILEO+BEIDOU. For the sake of clarity, hereafter these options are called G, GR and GREC. In order to make equivalent and simultaneous observation using three receivers, an apparatus was used which allows placing receivers on the same stand. Further, a power supply was provided to each receiver for the probability of battery out. As the rover, the CHCNav i50 GNSS receiver was used which takes

advantage of GPS, GLONASS, GALILEO, and BEIDOU signals with embedded 624-channel GNSS technology. The status of rovers during the measurements is shown in Figure 3.

**Figure 3.** The rovers during the test

The permanent GNSS receiver established at the rooftop of the Engineering and Architecture Faculty of Necmettin Erbakan University, in Konya, was used as the reference station. This station is composed of a CHC N72 reference receiver connected by a TNC type connector to the CHC C220GR choke ring antenna. The reference receiver is a multi-frequency GNSS receiver and capable of monitoring all GPS (L1/L2/L5), GLONASS (L1/L2), BEIDOU (B1/B2) and GALILEO (E1/E5A/E5B) signals. The communication between the reference station and rovers is provided by the Internet (GSM), using NTRIP (Networked Transport of RTCM via Internet Protocol).

The satellite elevation cut-off angle is taken as 10° since the location of the field test has an open sky. With these configurations, 1-hour RTK surveying with 1-second epoch interval was performed. Besides, to determine the reference coordinates 5-hour static surveying was performed.

## 4. RESULTS AND DISCUSSION

For analyzing the results, first, reference coordinates were obtained by the post-process relative positioning method. The static data of the reference station and the data of rovers from 5-hour static surveying were used. The processes were applied using GAMIT which is a well-known and powerful GNSS data processing software (Herring et al. 2010). Only GPS data was used for estimating reference coordinate values. The coordinates of both reference and RTK generated in ITRF 2014 reference coordinate system. After obtaining reference coordinates of rovers, the cartesian coordinates were transformed to topocentric coordinate system, which can be expressed as north (n), east (e) and up (u) components. Also, topocentric coordinates can be used for accuracy representation.

For a proper analysis, an alignment was performed between the results of G, GR and GREC configurations considering time. However, only fixed results were taken into consideration. The topocentric coordinate components for each satellite configuration (G, GR and GREC) are provided in Figure 4-6, for north, east and up, respectively.

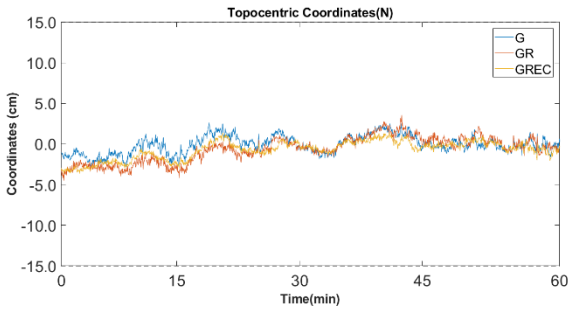


**Figure 4.** Coordinates for north component

In Figure 4 coordinates of G, GR and GREC satellite for north component are given. According to this, ± 4 cm accuracy is achieved for G, GR and GREC. In the first 30 minutes, G shows better accuracy of ± 2 cm compared with the GR and GREC combinations.

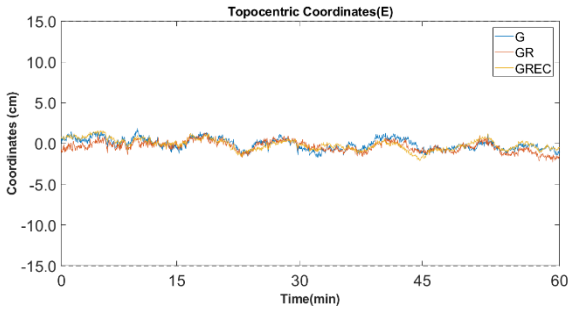


**Figure 5.** Coordinates for east component

In figure 5 coordinates for east component are given. It is seen that the accuracy of ± 2 cm is achieved for all options. Besides, it is not clear to recognize one of the G, GR, and GREC configurations have a superiority.

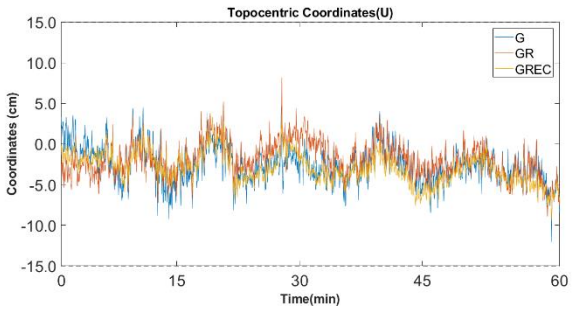


**Figure 6.** Coordinates for up component

In figure 6 coordinates for up component are given. Accordingly, the accuracy of ± 9 cm is achieved for all options. In the first 10 minutes, GREC shows better accuracy of ± 2 cm compared with the G and GR. However, after the first 10 minutes, all options showed almost similar results.

Furthermore, absolute maximum, absolute minimum, mean and root mean square error (RMSe) values were calculated. The statistical values for each satellite configuration are given in Table 1.

**Table 1.** The statistical values for G, GR and GREC

| | | n (cm) | e (cm) | u (cm) |
|---|---|---|---|---|
| G | Maximum (abs) | 2.93 | 1.87 | 12.09 |
| | Minimum (abs) | 0.00 | 0.00 | 0.01 |
| | Mean | -0.08 | -0.07 | -2.63 |
| | RMSe | 1.10 | 0.69 | 3.43 |
| GR | Maximum (abs) | 4.49 | 2.30 | 9.32 |
| | Minimum (abs) | 0.00 | 0.00 | 0.00 |
| | Mean | -0.65 | -0.37 | -1.93 |
| | RMSe | 1.66 | 0.74 | 2.89 |
| GREC | Maximum (abs) | 3.65 | 2.10 | 9.47 |
| | Minimum (abs) | 0.00 | 0.00 | 0.01 |
| | Mean | -0.73 | -0.12 | -2.96 |
| | RMSe | 1.63 | 0.78 | 3.51 |

As can be seen from Table 1, for absolute maximum GR and GREC combinations give better results in up component. When mean values are analyzed, it is seen that similar results are obtained. Furthermore, the RMSe values are less than 1.7 cm and 0.8 cm for north and east components, respectively. In the up component, RMSe values are bigger than horizontal components and similar for three configurations.

## 5. CONCLUSION

In this study, the contribution of multi-GNSS combinations to long distance RTK is investigated. For this purpose, a field test was conducted. In the field test, 1-hour RTK measurement was conducted with three satellite combinations, namely G, GR, and GREC. The results demonstrated that the accuracy of ± 5 cm and ± 10 cm were obtained in long distance RTK for horizontal and vertical components, respectively. In addition, the results are investigated using basic statistical parameters and RMS errors. According to this, G, GR and GREC configurations have similar results and there are no significant differences. In the open sky conditions, when the number of visible satellites is sufficient and have a good geometry, different GNSS configurations give almost equal results.

## ACKNOWLEDGEMENT

This study was supported by Necmettin Erbakan University Scientific Research Projects (BAP), Turkey. The project id is 201319004. We appreciated the technical team of CHC Turkey and Ufuk R. Ozbey for their support during this study.

## REFERENCES

Aydin Ö, Ata E & Pirti A (2004). RTK GPS Sisteminin Poligon Ölçmelerinde Kullanımı. Sigma Mühendislik ve Fen Bilimleri Dergisi.

Baybura T, Tiryakioglu I, Ugur M A, Solak H I & Safak S (2019). Examining the accuracy of network RTK and long base RTK methods with repetitive measurements. Journal of Sensors, 2019. https://doi.org/10.1155/2019/3572605

Bramanto B, Gumilar I, Taufik M & Hermawan I M D (2019). Long-range Single Baseline RTK GNSS Positioning for Land Cadastral Survey Mapping. In E3S Web of Conferences (Vol. 94, p. 01022). EDP Sciences.

Castro-Arvizu J M, Medina D & Ziebold R (2020). Impact of Satellite Elevation Mask in GPS+ Galileo RTK Positioning. In Institute of Navigation International Technical Meeting 2020, ITM 2020 (pp. 487-498). Institute of Navigation.

He X & Chen J (2020, May). First Implementation and Evaluation of Five Systems Network RTK. In China Satellite Navigation Conference (pp. 265-278). Springer, Singapore.

Herring T A, King R W & McClusky S C (2010). Introduction to GAMIT/GLOBK. Massachusetts Institute of Technology, Cambridge, Massachusetts.

Inal C, Gunduz A M & Bulbul S (2014). Klasik RTK ve AĞ-RTK yöntemlerinin karşılaştırılması.

Odolinski R, Teunissen P J & Odijk D (2015). Combined BDS, GALILEO, QZSS and GPS single-frequency RTK. GPS solutions, 19(1), 151-163. https://doi.org/10.1007/s10291-014-0376-6

Takasu T (2013). RTKLIB ver. 2.4.2 Manual. RTKLIB: An Open Source Program Package for GNSS Positioning, 29-49.

Wang J (1999). Stochastic Modeling for Real-Time Kinematic GPS/GLONASS Positioning. Navigation, 46(4), 297-305. https://doi.org/10.1002/j.2161-4296.1999.tb02416.x

Wang J, Xu T, Nie W & Xu G (2020). GPS/BDS RTK Positioning Based on Equivalence Principle Using Multiple Reference Stations. Remote Sensing, 12(19), 3178. https://doi.org/10.3390/rs12193178

Xi R, He Q & Meng X (2020) Bridge monitoring using multi-GNSS observations with high cutoff elevations: A case study. Measurement, 168, 108303. https://doi.org/10.1016/j.measurement.2020.108303

Zhang Y, Kubo N, Chen J, Chu F Y, Wang H & Wang J (2020). Contribution of QZSS with four satellites to multi-GNSS long baseline RTK. Journal of Spatial Science, 65(1), 41-60. https://doi.org/10.1080/14498596.2019.1646676

## Geographic Information Systems and Cartography – 2

**Using a 3D city model for monitoring flash flood risks in Salalah (Oman)**

*Khalid Al Kalbani*, Alias Abdul Rahman*

**Cloud Based Disaster Management and Monitoring Information System**

*Mohd Mustaqeem*, Sani Hasan, Mohd Saqib, Abdullah Talib*

**The Application of GIS in the Selection of Suitable Areas for Afforestation of Konya**

*Ceren Yağcı*, Fatih İşcan*

**Identifying equality and accessibility to health centers via Spatial Information Science**

*Ömer Akın*, Hande Demirel*

**Investigation of Pedestrian Accessibility to Schools: A case study of Rize**

*Sabire Edanur Mamat*, Aziz Şişman*

**Creation of Wind Speed Maps of Kirklareli City**

*Celal Bıçakcı*, Kamil Karataş, Selim Serhan Yıldız*

**Developing an Algorithm on the Reporting Of Outages in the Electricity Distribution System with GIS Integration**

*Ahmet Ünverdi*, Aziz Şişman*

**GIS-Based Landslide Susceptibility Mapping Using Frequency Ratio and AHP Methods**

Aslan Cihat Başara*, Mehmet Emin Tabar , Yasemin Şişman

Intercontinental Geoinformation Days

http://igd.mersin.edu.tr/2020/

# Using a 3D city model for monitoring flash flood risks in Salalah (Oman)

**Khalid Al Kalbani*, Alias Abdul Rahman**

*Universiti Teknologi Malaysia, 3D GIS Research Lab, Faculty of Built Environment and Surveying, Johor Bahru, Malaysia*

**Keywords**
Flood risk management
3D city model
CityGML

**ABSTRACT**

The paper investigates the issues and challenges to use a 3D city model for monitoring flash flood risks in Salalah (Oman) by using the Geography Markup Language (CityGML) standards version 2.0. In fact, 2D and 2.5D GIS solutions cannot analyse flood complex problems inside the urban area. Hence, the study seeks to reduce time and effort for the decision-makers by proposing a 3D city model for flood risk management. The study has used geospatial tools and databases such as ArcGIS, Watershed Modeling System (WMS), FME, PostgreSQL-PostGIS, and 3D City Database (3DCityDB) to generate the 3D model and to test the capability of establishing unified geospatial data structure including 3D city objects, hydrology data, and geological data. The findings show the importance of addressing flood risks data and arranging it in the 3D geodatabase. The findings also show that establishing a 3D city model based on CityGML standard requires homogenized definitions and standards for city objects (surface and subsurface) and hydrology data. Besides, it needs to address the issues and challenges in the level of the data structure. Based on the results, the researchers will further study the solutions to integrate the 3D city model and natural hazards management applications in Oman.

## 1. INTRODUCTION

Oman has coasts that have a length of 3165 kilometers located towards the Indian Ocean where tropical storms occur. Therefore, it experiences frequent climatic events such as tropical depression and cyclone (Al-Kalbani, 2011; Dube et al., 2020). In addition to that, the low parts of the coastal areas can be exposed to coastal floods caused due to high waves that come along with the climactic event. Moreover, these climatic events affect humans' lives and cause damage to city infrastructure, which costs millions of dollars. Salalah is one of the south Omani cities that has faced several climatic events such as cyclone Mekunu in 2018 and tropical depression from 27 May to 1 June 2020, as shown in Fig. 1.

The impact of these events has led to the importance of evaluating Salalah city infrastructure by using the 3D geospatial data approach to test the extent to which the Salalah city infrastructure matches with the hydrological system in that area. This study, thus, investigates the issues and challenges of implementing a 3D city model to monitor, evaluate and manage these dangers based on developing a small-scale 3D city model using CityGML standard version 2.0.

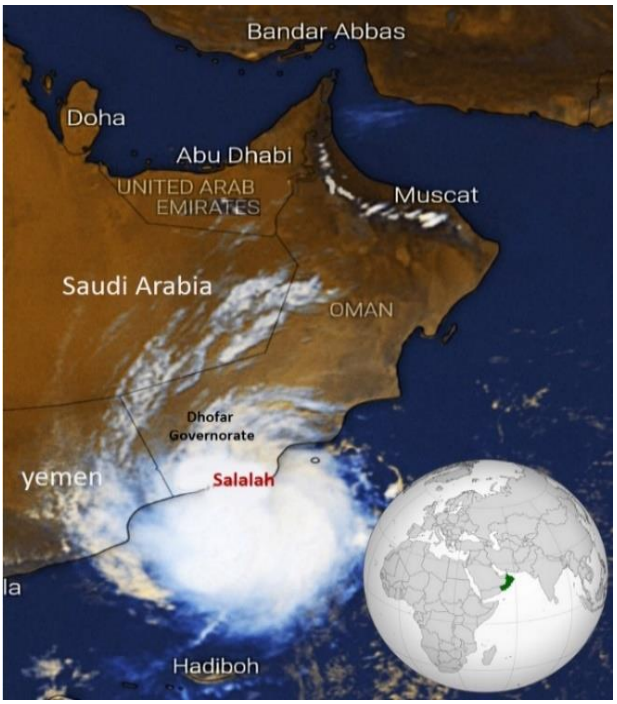


**Figure 1.** The tropical depression, 30 May 2020

* **Corresponding Author**

*( asakkhalid2@graduate.utm.my) ORCID ID 0000-0002-3268-6831
(alias@utm.my) ORCID ID 0000-0001-5263-8266

**Cite this study**

Al Kalbani K & Rahman A A (2020). Using 3D city model for monitoring flash flood risks in Salalah (Oman). Intercontinental Geoinformation Days (IGD), 194-199, Mersin, Turkey

Monitoring and assessing flash floods and managing mitigation measures is a complex project that requires great effort and a relatively long period of time. The study seeks to reduce time and effort by employing a 3D city model, which mainly depends on the design of the 3D city model databases to manage the influence of flood risk on the city infrastructure (surface and sub-surfaces spatial objects). Bee et al., (2008), Ruíz (2015) and Tymkow et al., (2016) show that a mechanism could be established to deal with flood risk data by linking geospatial data and identifying effective models, analyzing appropriate simulation, estimation techniques, and designing a flood intensity scale. On the other hand, The Bureau for Crisis Prevention and Recovery (BCPR) in its 2004 international report indicated that more efforts should be made to collect disaster-related data, as well as pointing out, in its recommendations, to the need to support the national risk instrument to fund the production of information needed for decision-making at a national level (UNDP, 2004).

Nowadays, the infrastructure, such as multi-floor buildings and underground utilities, indoor and outdoor spatial objects in the urban areas is complicated as it requires using 3D geodata sets and 3D geospatial platforms with high performance. Additionally, employing the current geospatial solutions may not be useful to analyze and visualize complex problems, so there is an urgent need to develop 3D city model based on interoperability solutions (Biljecki et al., 2015b; Stoter et al., 2014, 2010). 3D geospatial platforms, 3D database and their related applications are considered as good initiatives for representing the 3D spatial objects and entire cities. The capability of these geospatial technologies has some solution to analyse complex data structure issues (Abdul Rahman et al., 2019; Siew and Kumar, 2019; Yao et al., 2018). Hence, efforts to make the 3D city model successful for flood risk management requires a homogenous and stable environment for all the models and standards such as hydrology, meteorology, geomorphology, geology, hydrogeology, CityGML, BIM /IFC and Shapefile.

A number of countries around the world have applied the GIS for flood risk management, while other countries are working toward 3D GIS by using their standard, data format and database (Al-Kalbani, 2011; Ruíz, 2015). At this point, the 3D geospatial institutions and researchers have made an effort to develop a framework for flood modeling based on using the OGC CityGML standard, CityJSON and others. Nevertheless, the pre-implementation has exposed several issues and challenges that need to be addressed in the level of data processing, data integration, data modeling, data converting, and data visualizing (Al Kalbani and Abdul Rahman, 2019; Kumar et al., 2018; Zlatanova et al., 2014). Part of the challenges is related to DEM sources' efficiency in 3D flood modeling and complex hydraulic simulation. In this context, Bakuła et al., (2016) and Li and Wong (2010) investigated how hydraulic modeling and application can be influenced by the source of different elevation data. While, Muhadi et al., ( 2020) discussed the use of Digital Elevation Model (DEM) that extruded from LiDAR for flood applications.

Establishing a flood risk database within the 3D city model is a complex task at the national level. On the one hand, dealing with 3D city model requires new solutions for integrating the data structure for both the surface and subsurface spatial objects (Al Kalbani and Abdul Rahman, 2019), where, most of the 3D geospatial initiatives focus on surface spatial objects data structure with less interest to model subsurface spatial objects. On the other hand, there is a need to find an approach that bridges between different available 3D geospatial standards in terms of geometric and semantics information to supports the interoperability between DBMSs, services, and stakeholders (Stoter et al., 2010).

This paper is arranged in eight Sections, where the Second section discusses the study area. Then, Section three reviews the CityGML standard. While Section four reviews the current state of Oman geospatial data and SDI, the methodology is explained in Section five. The sixth Section includes the discussion and outcomes of the study. The benefit of implementing 3D city model for flood risk management is summarized in Section seventh and the eighth Section ends with the conclusion.

## 2. STUDY AREA

Salalah is one of the main cities in the Dhofar Governorate (southwest of the Sultanate of Oman) (Zerboni et al., 2020). The population of the governorate is more than 450,000, distributed between the coastal plain and mountainous and desert areas (NCSI, 2020). The urban area in Salalah is spread on a narrow coastal plain where it is located between mountains, that are more than 1700 meters high (see Fig. 2), and coastal line and passing throughout it are a number of wadis and alluvial fans.

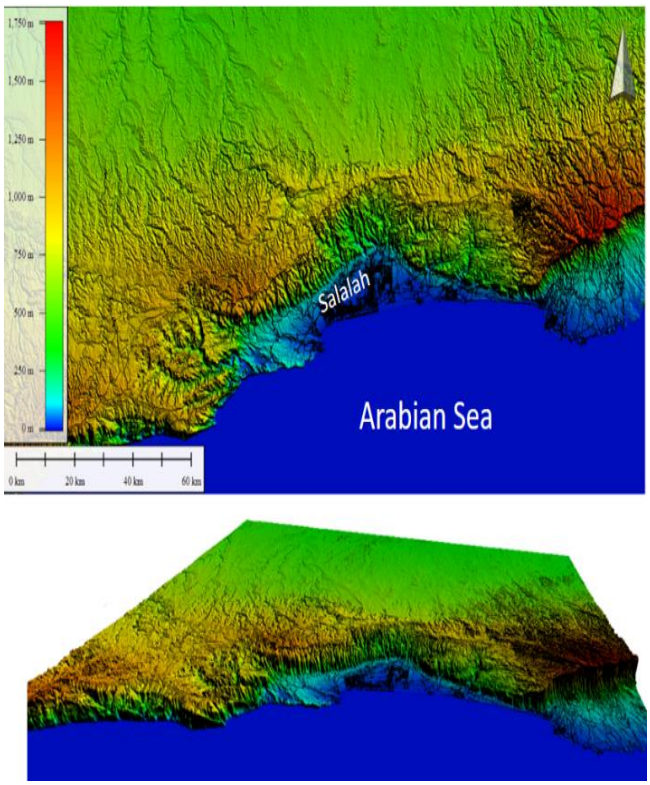


**Figure 2.** Salalah Digital Elevation Model (DEM)

The coastal plain can reach 13 km in its maximum width. The Dhofar mountain range was formed by the tectonic fault and uplift movement. Most of the rocky structure scattered in this region is dominated by solid limestone.

Moreover, Dhofar is considered a semi-arid area with approximately 100 – 400 mm of rainfall per year (Zerboni et al., 2020). Also, this area has a monsoon from July to August, in which the weather becomes cloudy with little rain. This area can also be affected by cyclones and tropical depressions. One of the clime events Dhofar had experienced is the tropical depression (27 May to 1 June 2020) which caused heavy rains so much so that some of the Dhofar districts received more than 1000 mm in 5 days. Salalah (study area) received 531 mm, causing flash floods and destroying some city infrastructure (Mrmwroman, 2020).

Rapid development in Salalah played a role in natural phenomena such as floods becoming as challenges. Moreover, the accelerated pressure on urban spatial holdings contributed to the exploitation of flood-prone areas, and in most of this exploitation was not accompanied by providing the infrastructure of water drainage (Al-Kalbani, 2011). The Crisis and Recovery Office has indicated in its global report to UNDP 2004 that "it does not necessarily mean that the urban transformation increases flood risk and can actually reduce it if it is well managed" (UNDP, 2004). However, the damage caused by floods cannot always be the main natural factor for exacerbating events. Instead, it is often the human factor that provides the right environment for these risks to develop into disasters.

Moreover, the high cost for constructing and maintaining the flood protection infrastructure was constrained integration of flood risk measures into urban planning efforts effectively. In fact, establishing flood risk infrastructure at the government level can be affected by two elements, which are the economic feasibility and practical feasibility, and often the economic factor is the dominant factor in addition to the amount of available budget (Al-Kalbani, 2011). In all scenarios, when planning deviates from the inclusion of flood risk as a priority, this uncontrolled planning may cause challenges in normal rainfall and make matters worse in the case of heavy rains.

## 3. CityGML STANDARD

CityGML is an open XML file format for exchanging, storing, and representing 3D objects. Moreover, the CityGML initiatives have been developed by the Special Interest Group3D (3D SIG), and it is organized now by Open Geospatial Consortium (OGC). CityGML standard has been adopted as an international standard for exchanging the format of 3D geospatial objects and the 3D city model based on the XML file format and the GML 3xx. Besides, CityGML (version 2.0) includes 13 models to store the spatial objects and five levels of detail (LoD) (Biljecki, 2017; Biljecki et al., 2015b; Stouffs et al., 2018).

CityGML presents the most common natural and human spatial features that can be found in the cities and their surroundings by determining their geometric and semantic information (Arroyo Ohori et al., 2018; Biljecki, 2017; Biljecki et al., 2017, 2015a, 2015b; Kensek, 2014; Stoter et al., 2016). Furthermore, the structure of CityGML file format is developed based on a hierarchy structure both for geometric and semantic information. Now, there are various spatial applications for CityGML standard such as solar potential estimation, flood risk assessment and noise monitoring. (Biljecki, 2017; Biljecki et al., 2015b; Preka and Doulamis, 2016; Soon et al., 2016; Yao et al., 2018).

## 4. THE CURRENT STATE OF OMAN GEOSPATIAL DATA AND SDI

Oman government established its national SDI in 2014 to standardize the geospatial activities and business at the national level. Since then, the geospatial workflow of Oman NSDI and its partners (Oman GIS stakeholders) are limited to the 2D and 2.5D geospatial data (Al Kalbani et al., 2018; Das et al., 2017; NCSI, 2017a, 2017b). In fact, Oman is one of the developed countries which has a complex city infrastructure. As a result, using 2D and 2.5D geospatial data may not be efficient in analysing flood risk inside the big cities and complex structures. Hence, the decision-makers in Omani municipalities need GIS solutions based on utilizing a 3D city model.

## 5. METHODOLOGY

The study created a small-scale 3D city model for Salalah district by using CityGML version 2.0 and spatial data collected from the related geospatial agencies in Oman (2D, 2.5D geospatial data). Geospatial tools such as FME engine was used to generate 3D spatial objects for surface and subsurface spatial objects based on using CityGML standard version 2.0 and also for exchanging the file format from one model to the others. Besides, databases PostgreSQL-PostGIS and 3DCityDB were used to register and store the 3D models for surface and subsurface objects in a relational database.

The study created a building model at CityGML LoD1 by extruding the building footprint using the high value from the file attributes. Also, LoD1 was used to create the terrain model. Since the CityGML 2.0 does not fully support the subsurface spatial objects and models, the study used the CityGML generic module to develop some of these subsurface models such as geological model and pipeline networks.

The study used ArcGIS (hydrology tools), the Watershed Modeling System (WMS) to extract wadi (stream) networks and watershed using ASTER DEM with a resolution of 30 meters. Besides, WMS applications were used to produce flood spread layers based on digital terrain data and floodwater estimative elevation values between 1 – 3 meters.

On the one hand, the study has carried some experiments to investigate further the issues and challenges for constructing a unified 3D data structure based on the use of CityGML standard version 2.0 for surface and subsurface spatial objects. On the other hand, the study has explored the integration challenges

between geological models, hydrological models and 3D city models.

The study has investigated how to integrate the benefits of satellite images and 3D city models for flood risk management. Satellite images (Sentinel-2) with a resolution of 10 meters for the tropical depression from 1-3 June 2020 were obtained from https://eos.com/landviewer, and analysed using change detection methods. The role of satellite images in this study is to draw a map of the flood spread in the study area by overlapping the 3D models (road and building) in the 3D city model with 2D satellite images that are classified using change detection. In addition, this step contributed to tracking and highlighting some of the flooding problems related to the failure of drainage networks along highways and inside cities.

Since there is no professional 3D viewer to visualize both surface and subsurface spatial objects, the study has used several visualizing tools such as FME Data Inspector, Google Earth, FZK viewer and Cesium.

## 6. DISCUSSION AND RESULTS

The study has created a small-scale 3D city model for most surface city spatial objects in LoD 1 (see Fig. 3), but it faced a challenge to go higher to LoD 3 and LoD 4 due to missing rich data such as BIM/IFC. Also, the study has been able to generate wadi (stream) networks and watershed using Salalah digital terrain data.

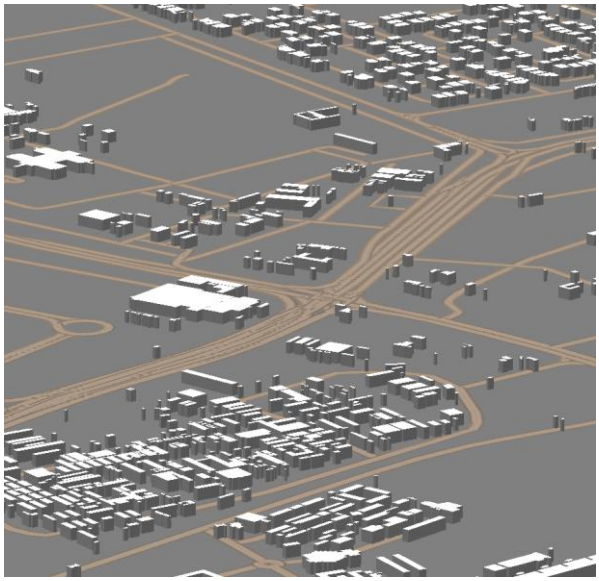

**Figure 3.** Small-scale 3D city model for Salalah

The real challenge in developing the 3D city model was how to create subsurface spatial objects, in which CityGML version 2.0 does not provide a definition to support subsurface objects except for the CityGML Application Domain Extension (ADE) for utility network. Thus, the study created some of the subsurface spatial objects in LoD1 using the CityGML generic module. However, there are some challenges related to semantic, geomatic and topology that need to be addressed to enhance 3D subsurface models. Other challenges are related to 3D spatial analysis and the process of creating a unified relational database for surface and subsurface spatial objects.

Since the CityGML version 2.0 does not include hydrological models and flooding simulation, the study used several applications separately and outcomes were linked to one 3D city model. During this stage, the experiments showed that the 3D city model is able to determine the areas that might be subject to water flooding by linking the 3D city model, terrain and flood layer exported from WMS, as shown in Fig. 4.

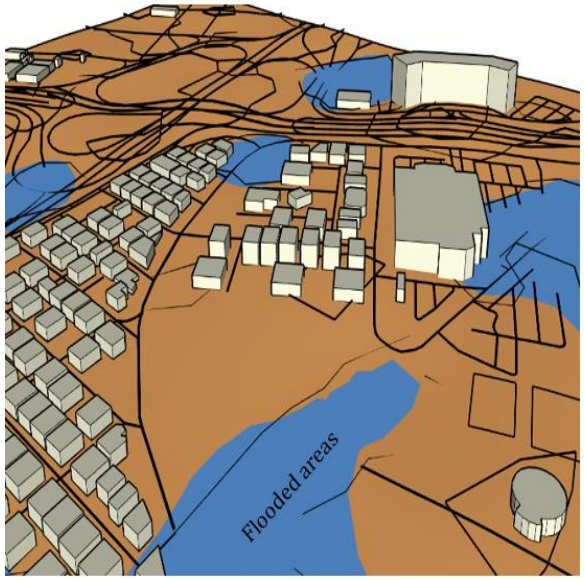


**Figure 4.** Areas subject to flooding

Another advantage of managing flood data in 3D city model is providing the capability to determine the level to which floodwater can reach in each of the city buildings. Nevertheless, there is still a challenge in registering the value to which floodwater can reach automatically in the database for each of the building faces and edges due to the complexity of CityGML data structure in terms of systematic and geometric information.

Moreover, the experiments demonstrated that there is a possibility to integrate the analysis of satellite images using change detection methods and 3D city models to map the distribution of internal floods in residential areas and to highlight some issues in the city infrastructure. Based on this approach, the results revealed that floodwater collects on the sides of highways and some modern bridges. Also, it revealed that floodwater was collecting in residential areas. This is due to many reasons, and the most important ones are lack of water drainage networks, failure of drainage channels, due to the accumulation of impurities coming from the watershed, the incompatibility of the engineering design of the drainage channels and the volume of water flow. There are other challenges due to low level of the ground surface in some residential areas and weak water infiltration into the ground.

Research is still ongoing to address the issues listed below:

- Defining the water stream paths inside the city in the absence of Light Detection and Ranging (LiDAR) data, which is a restricted data in Oman and needs several official permissions.

- Integrating CityGML and the current mathematic hydrological models in a unified ADE, data structure and 3D geodatabase.
- Designing equations that are suitable for estimating the peak of the floods considering Salalah environment, climate, the nature of urban patterns and characteristics of dams and their ability to drain water. Therefore, creating hydrodynamic modeling of flood flows using CityGML standard needs to determine the relation with other factors such as the surface of the wadi, slope, velocity, leakage rate to the underground, evaporation, and 3D objects resistance.
- Upgrading 3DCityDB data structure to import subsurface spatial objects.
- Developing homogenized definitions within CityGML standard to manage relationships between different subsurface spatial objects, geological models and hydrological models.
- Developing a new logarithm of hydrodynamic modeling of flood flows based on CityGML standard and 3D raster map (voxel).
- Calculating the water drainage that comes from the city's infrastructure, where the roofs of buildings and paved areas contribute to the gathering of rainwater in residential areas and low areas.
- Designing a mechanism to predict urban infrastructure behavior during the flooding, where the failure of bridges, roads and drainage channels can shut down the natural paths of valleys and change the direction of their flow, causing internal flooding in residential areas.
- Integrating indoor and outdoor navigation and flood risk management.
- Updating the hydrology simulation results automatically into the databases at the level of CityGML schema(s) and LoD(s).
- Examining the performance of the JavaScript Object Notation (JSON) and CityJSON datasets as alternative solutions to create a flood spatial data structure in the 3D city model.

Other challenges are related to CRS/SRID, quality of data structures, geomatics representation, the problem of semantic cording, creating the data structure in terms of schema(s) and LoD(s), integration with the DEM, the topology issues, data retrieval, data size, data index, 3D spatial analysis, spatial operations and rendering over Cesium.

## 7. THE BENEFIT OF IMPLEMENTING 3D CITY MODEL FOR FLOOD RISK MANAGEMENT

The expected benefits of using 3D city model for flood risk management study are summarized below:

- A suitable environment for the modeling of floods and their impact on the urban areas in 3D
- The ability to test infrastructure projects before implementation on the ground
- A suitable environment for flood risk management and rescue operations

## 8. CONCLUSION

This paper attempts to investigate the challenges of using a 3D city model for monitoring flood risks in Salalah. The outcomes of the study show that a 3D city model based on CityGML still needs to address some issues and challenges related to the efficiency of this standard for hydrological analysis and for managing surface and subsurface spatial objects in the unified data structure.

The study results also demonstrated that 3D geospatial data is more efficient in solving planning problems and defining the issues that may increase flood risks. This, in turn, it helps to understand and assess the nature of risks and design clear vision to manage rescue efforts. This research is still a work-in-progress and the authors believe that the initial outcomes of this paper can highlight the importance of including 3D geospatial solutions for flood risk management in Oman.

## ACKNOWLEDGEMENT

The authors would like to acknowledge the Ministry of Higher Education, Research, and Innovation (MoHERI) of the Sultanate of Oman for supporting this project. The research leading to these results has received funding from MoHERI under the GRG program. Funding Agreement No: MoHERI/GRG/INT.S/09/2020.

## REFERENCES

Abdul Rahman, A., Rashidan, H., Musliman, I.A., Buyuksalih, G., Bayburt, S., Baskaraca, P., 2019. 3D Geospatial Database Schema for Istanbul 3D City Model. ISPRS - Int. Arch. Photogramm. Remote Sens. Spat. Inf. Sci. XLII-4/W16, 11–16. https://doi.org/10.5194/isprs-archives-XLII-4-W16-11-2019

Al-Kalbani, K., 2011. Monitoring and Assessing Flood Risks & Maintaining the Procedures to Limit their Danger using Geographical Information Systems, Remote Sensing and Hydrological Modeling (Case Study :Al-Seeb Willayat) ". Sultan Qaboos University.

Al Kalbani, K., Abdul Rahman, A., 2019. Integration Between Surface and Subsurface Spatial Objects for Developing Oman 3D SDI Based on the CityGML Standard. Int. Arch. Photogramm. Remote Sens. Spat. Inf. Sci. XLII-4/W16, 79–84. https://doi.org/10.5194/isprs-archives-XLII-4-W16-79-2019

Al Kalbani, K., Abdul Rahman, A., Al Awadhi, T., Alshannaq, F., 2018. Development Of A Framework for Implementing 3D Spatial Data Infrastructure In Oman – Issues And Challenges. ISPRS - Int. Arch. Photogramm. Remote Sens. Spat. Inf. Sci. XLII-4/W9, 243–246. https://doi.org/10.5194/isprs-archives-XLII-4-W9-243-2018

Arroyo Ohori, K., Biljecki, F., Kumar, K., Ledoux, H., Stoter, J., 2018. Modeling Cities and Landscapes in 3D with CityGML, in: Building Information Modeling. Springer International Publishing, Cham, pp. 199–215. https://doi.org/10.1007/978-3-319-92862-3_11

Bakuła, K., StĘpnik, M., Kurczyński, Z., 2016. Influence of

Elevation Data Source on 2D Hydraulic Modelling. Acta Geophys. 64, 1176–1192. https://doi.org/10.1515/acgeo-2016-0030

Bee, M., Benedetti, R., Espa, G., 2008. Spatial Models for Flood Risk Assessment. Environmetrics 19, 725–741. https://doi.org/10.1002/env.932

Biljecki, F., Ledoux, H., Stoter, J., 2017. Generating 3D City Models Without Elevation Data. Comput. Environ. Urban Syst. 64, 1–18. https://doi.org/10.1016/j.compenvurbsys.2017.01.001

Biljecki, F., Ledoux, H., Stoter, J., 2015a. Improving the Consistency of Multi-LoD CityGML Datasets by Removing Redundancy. pp. 1–17. https://doi.org/10.1007/978-3-319-12181-9_1

Biljecki, F., Stoter, J., Ledoux, H., Zlatanova, S., Çöltekin, A., 2015b. Applications of 3D City Models: State of the Art Review. ISPRS Int. J. Geo-Information 4, 2842–2889. https://doi.org/10.3390/ijgi4042842

Biljecki, F., 2017. Level of Details in 3D City Models,Published PhD Thesis. Delft University of Technology. https://doi.org/10.4233/uuid:f12931b7-5113-47ef-bfd4-688aae3be248

Das, A., Chandel, K., Narain, A., 2017. Value of Geospatial Technology in Boosting Omans Economy, in: Oman Geospatial Forum 2017. Oman National Survey Authority, Muscat, pp. 1–74.

Dube, A., Ashrit, R., Kumar, S., Mamgain, A., 2020. Improvements in Tropical Cyclone Forecasting through Ensemble Prediction System at NCMRWF in India. Trop. Cyclone Res. Rev. https://doi.org/10.1016/j.tcrr.2020.04.003

Kensek, K.M., 2014. Building Information Modeling. Build. Inf. Model. 1–285. https://doi.org/10.4324/9781315797076

Kumar, K., Ledoux, H., Stoter, J., 2018. Dynamic 3D Visualization of Floods: Case of the Netherlands. ISPRS - Int. Arch. Photogramm. Remote Sens. Spat. Inf. Sci. XLII-4/W10, 83–87. https://doi.org/10.5194/isprs-archives-XLII-4-W10-83-2018

Li, J., Wong, D.W.S., 2010. Effects of DEM Sources on Hydrologic Applications. Comput. Environ. Urban Syst. 34, 251–261. https://doi.org/10.1016/j.compenvurbsys.2009.11.002

Mrmwroman, 2020. Precipitation Report from 27 May to 1 June, Mrmwroman Report.

NCSI, 2020. Monthly Statistical Bulletin,June 2020, Monthly Statistical Bulletin. https://doi.org/10.36548/jsws.2020.2

NCSI, 2017a. Oman National Spatial Data Infrastructure Strategy V5.0. National Center for Statistics and Information, Oman.

NCSI, 2017b. Oman National Spatial Data Infrastructure, 1st ed. National Center for Statistics and Information, Oman.

Muhadi, N.A., Abdullah, A.F., Bejo, S.K., Mahadi, M.R., Mijic, A., 2020. The Use of LiDAR-Derived DEM in Flood Applications: A Review. Remote Sens. 12, 2308. https://doi.org/10.3390/rs12142308

Preka, D., Doulamis, A., 2016. 3D Building Modeling in LoD2 Using the CityGML Standard. ISPRS - Int. Arch. Photogramm. Remote Sens. Spat. Inf. Sci. XLII-2/W2, 11–16. https://doi.org/10.5194/isprs-archives-XLII-2-W2-11-2016

Ruíz, A.A.B., 2015. An Urban Flooding Simulation Technique by Using 3D City Information Model 3, 54–67.

Siew, C., Kumar, P., 2019. CitySAC: A Query-Able CityGML Compression System. Smart Cities 2, 106–117. https://doi.org/10.3390/smartcities2010008

Soon, K.H., Tan, D., Khoo, V., Soon, K.H., Tan, D., Khoo, V., 2016. Initial Design to Develop a Cadastral System that Supports Digital Cadastre, 3D and Provenance for Singapore, in: 5th International Workshop on 3D Cadastres. pp. 419–432.

Stoter, J., Brink, L. Van Den, Vosselman, G., Goos, J., Verbree, E., Klooster, R., Berlo, L. Van, Vestjens, G., Reuvers, M., Thorn, S., 2010. A Generic Approach for 3D SDI in the Netherlands. Lect. Notes Comput. Sci. 1–22.

Stoter, J., Ploeger, H., Roes, R., Riet, E. Van Der, Biljecki, F., Stoter, J., Ploeger, H., Roes, R., Riet, E. Van Der, Biljecki, F., 2016. First 3D Cadastral Registration of Multi-level Ownerships Rights in the Netherlands, in: 5th International Workshop on 3D Cadastres. pp. 491–504.

Stoter, J., Vosselman, G., Dahmen, C., Oude Elberink, S., Ledoux, H., 2014. CityGML Implementation Specifications for a Countrywide 3D Data Set. Photogramm. Eng. Remote Sens. 80, 1069–1077. https://doi.org/10.14358/pers.80.11.1069

Stouffs, R., Tauscher, H., Biljecki, F., 2018. Achieving Complete and Near-Lossless Conversion from IFC to CityGML. ISPRS Int. J. Geo-Information 7, 355. https://doi.org/10.3390/ijgi7090355

Tymkow, P., Karpina, M., Borkowski, A., 2016. 3D GIS for Flood Modelling in River Valleys. ISPRS - Int. Arch. Photogramm. Remote Sens. Spat. Inf. Sci. XLI-B8, 175–178. https://doi.org/10.5194/isprsarchives-XLI-B8-175-2016

UNDP, 2004. Bureau for Crisis Prevention and Recovery ( Bcpr ) 2004 Report : Thematic Trust Fund for Crisis Prevention and Recovery United Nations Development Programme. Bur. Cris. Prev. Recover.

Yao, Z., Nagel, C., Kunde, F., Hudra, G., Willkomm, P., Donaubauer, A., Adolphi, T., Kolbe, T.H., 2018. 3DCityDB - a 3D Geodatabase Solution for the Management, Analysis, and Visualization of Semantic 3D City Models Based on CityGML. Open Geospatial Data, Softw. Stand. 3. https://doi.org/10.1186/s40965-018-0046-7

Zerboni, A., Perego, A., Mariani, G.S., Brandolini, F., Al Kindi, M., Regattieri, E., Zanchetta, G., Borgi, F., Charpentier, V., Cremaschi, M., 2020. Geomorphology of the Gebel Qara and Coastal Plain of Salalah (Dhofar, Southern Sultanate of Oman). J. Maps 16, 187–198. https://doi.org/10.1080/17445647.2019.1708488

Zlatanova, S., Ghawana, T., Kaur, A., Neuvel, J.M.M., 2014. Integrated Flood Disaster Management and Spatial Information: Case Studies of Netherlands and India. ISPRS - Int. Arch. Photogramm. Remote Sens. Spat. Inf. Sci. XL–8, 147–154. https://doi.org/10.5194/isprsarchives-XL-8-147-2014

Intercontinental Geoinformation Days

http://igd.mersin.edu.tr/2020/

# Cloud Based Disaster Management and Monitoring Information System

**Mohd Mustaqeem** *[1], **Sani Hasan** [1], **Mohd Saqib** [2] **Abdullah Talib** [3]

[1] *Department of Computer Science, Institute of Technology and Management, Aligarh, UP, India*
[2] *Mathematics and Computing Department, Indian Institute of Technology (ISM), Dhanbad, Jharkhand, India*
[3] *Department of Civil Engineering, Indian Institute of Science, Bangalore (IISC), India*

**Keywords**
Cloud Computing
Disaster
Remote Sensing
IoT
ICT

**ABSTRACT**

Natural disasters are by far destructive acts of nature for living beings. No one can stop natural disaster but the level of distraction can be reduced by using some precautionary measures. Here, in this paper, we are focusing mainly upon the after-effects management of any natural calamities by proposing cloud-based disaster management and information system. The primary goal of this application is to help to find lost people in disasters; cloud-based monitoring, real-time evaluation so that the help will reach at right time to the right person, statistical analysis in low cost and minimum time, emergency request receiver, and financial support to affected people and rehabilitation to needy people. Data uploaded regarding affected family members by the management team so that the organizations working for the rescue operation, police helpers etc. will help after seeing on information system.

## 1. INTRODUCTION

There are mainly two types of disasters one is man-made (technological, terrorism, violence and complex humanitarian emergencies. other is natural floods, earthquake, hurricanes, tornadoes, volcanic eruptions, tsunamis. (Mahar et al., n.d.). But our main focused is Natural disasters; the Natural calamities are the natural processes of the earth resulting in a hazard for the creature. it causes distractions of many ways like livelihood, economy, social, ecological, political, legal and outbreak of serious diseases plague. (Pile, 2001). There are lots of challenges people faces during the disaster, one of them is the food security challenge. (Ainehvand et al., 2019). Hospitals face safety, security and malfunctioning problem during natural disaster etc. In 26th January 200, The Gujarat Earthquake which was one of the most shocking events in India it drastically affects the economy and life. A post-earthquake scenario of Gujarat-Earthquake was rescued on the bases of relief and rehabilitation. (Shaw & Sinha, 2003).

Landslides are one of the main geological vulnerability in the Himalaya, in the northern part of the Indian subcontinent. On 23 September 2003, India was affected by Varunavat hill landslides, in Uttarkashi town, Garhwal Himalaya. (Sarkar et al., 2011). Floods are natural events that may catastrophic impacts on human's life. In 2019 August, Assam hit a flood, it misbalanced sustainability of agriculture, destroying standing crops, creating waterlogging, soil erosion and affecting large crop areas which ultimately affected human life. (Weekly, 2005). The studies show that the people live near gulf coast has high exposure to hurricane, Katrina and Rita, controlling for historically based hurricane risk and county population density, demographics, individual hurricane experience, and dispositional optimism. Data were collected in January 2006 through a mail survey sent to 1,375 households in 41 counties on the coast ($n$ = 824, 60% response). (Trumbo et al., 2011). In April, and May 2011 Tornado hit the USA during spring and it was the historic hit, a series of major outbreaks of tornadoes affected hundreds of fatalities and thousands of millions of $US in damage. (Iii et al., 2011).

Predicting accurately the natural events like landslides, earthquake and volcanic eruptions is one of the most difficult tasks for scientists and researchers, it is a conflicting and confusing event. Volcanoes have created a spatial relationship with the human population in the global distribution

According to Christopher and Terry study that the almost 9%(455 x $10^6$ people) of the world's 1990 population lived within 100km of a historically active volcano and 12 % within 100km of a volcano believed to have been active during the last 10,000 years. (Small & Naumann, 2001). On 11 March 2011, Japan was affected

* **Corresponding Author**

*(mohdmustaqeem34@gmail.com) ORCID ID 0000 – 0001 – 5055 – 5969
(sanihasan513@gmail.com) ORCID ID 0000– 0002 – 2725 – 3054
(msaqib.cs@gmail.com) ORCID ID 0000 – 0003 – 2125 – 2162
(abdullahtalib106@gmail.com) ORCID ID 0000 – 0002 – 2733 – 935X

**Cite this study**

Mustaqeem M, Hasan S, Saqib M & Talib A (2020). Cloud based disaster management and monitoring information system. Intercontinental Geoinformation Days (IGD), 200-203, Mersin, Turkey

by two big natural disasters earthquake and tsunami, which further transform into a new disastrous one, because its impact was on the Fukushima Daiichi nuclear power plant and the nuclear radiation start emitting from the plant which was too dangerous. It results in the economic crisis in Japan, financial markets, interest rates and the yen-dollar exchange rate but a slighter effect on the world trade and financial markets. It was also affected the U.S citizens and American co. working in Japan. (Nanto, 2011). Due to the above mentioned natural disasters and its dangerous effect we have to take precautions first if a natural disaster happened then the post measure should be taken that we are proposing a system.

The document is ordered as follows. "Overall Demonstration of the Model" explains working proposed model for the community. "Cloud-based disaster management and information system" describes the software description for developing prototypical cloud-based disaster management and information system. In "Proposed System Output Parameters" the procedural feature of the developed system is outlined along with the problems that may happen in the application execution. Three case studies are presented in "Case Studies" followed by the conclusion in "Conclusion".

## 2. OVERALL DEMONSTRATİON OF THE MODEL

This proposed Cloud-based disaster management and information system explain the major cloud-based model.

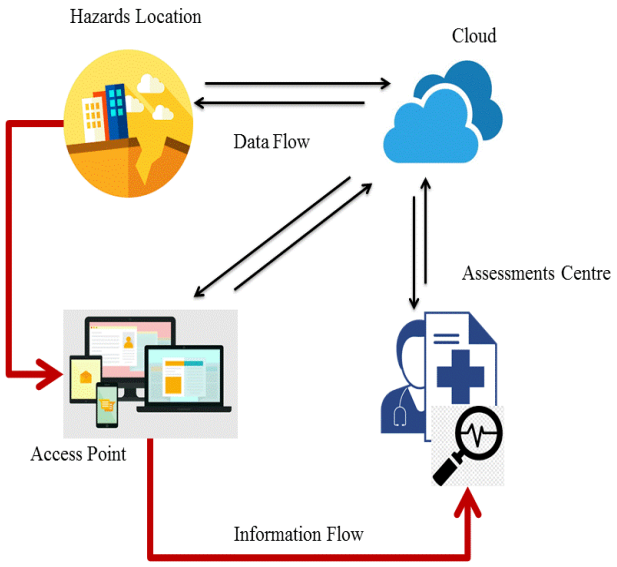


**Figure 1**. Overall Demonstration

Its main focus is to develop an effective and smart cloud-based disaster management and information system for affected people in the given area. Software is developed using Asp.net technology to have better graphic user visualization for frontend and for backend functions we have used C# language.

For the management of data and its manipulation, we have used MSSQL 2008, for computational and analytical work such as login (authentication), searching, and evaluation of data in regards of disaster information at multiple locations. The proposed system will tell about the people affected by natural hazards to the rescue team and other organizations so that they can detect them and provide necessary help; the proposed system will give real-time data. Apart with this, it will also help for direct financial access to the hazard-prone persons it will help to reduce the corruptions and other types of theft done by involved personalities. As shown in Fig.1.

In the given figure the dark black arrows show the cloud communication and the red arrows shows the information flow among multiple sources.

The system will manage their user through application performing a task such as manipulation of people data, places where the given hazard may affect in near future, financial help information provided by persons.

## 3. SOFTWARE DESCRİPTİON OF THE PROPOSED SYSTEM

Given section presents the detailed software explanation of the prototype system using multiple models for representing communication among entities, the diagram description, the organization and data flow among the involved actors etc.

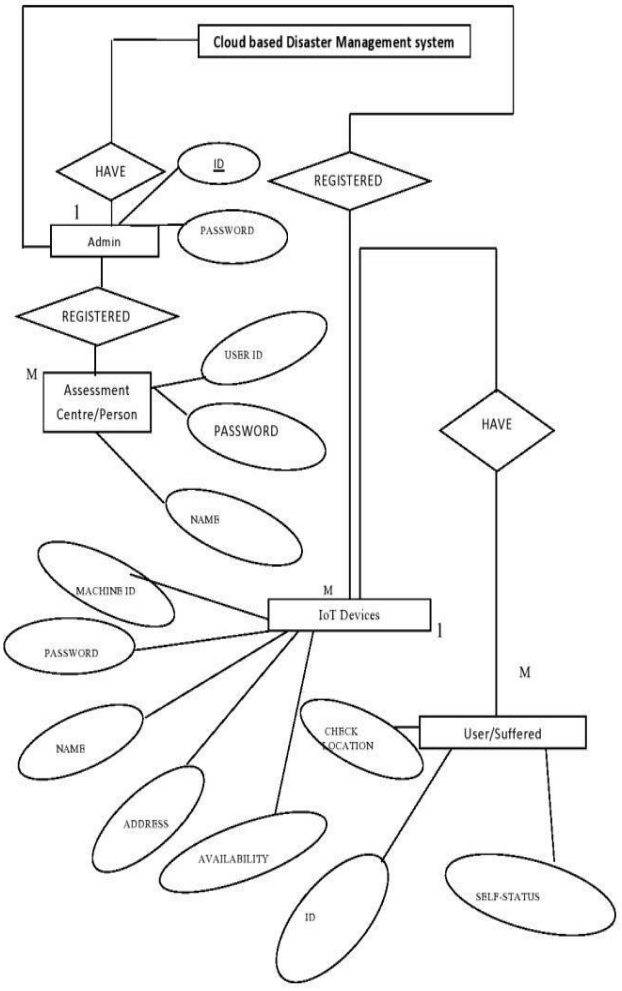


**Figure 2.** ER-Diagram

### 3.1. Entity-Relationship (ER) Diagram

In our ER-diagram representation relationships is given among multiple entities sets stored in the database. In the given information system three entities are involved:-

**Admin**: The "Admin" role will perform by any centralized user or higher authority to control the available as well as new information. This is managed by an authorized user or organization. The system user will provide the necessary information along with pictures and admin will verify and update the system accordingly. The "Admin" may have two major features "Admin Id" and "password" to login into the cloud-based system and performed all necessary works.

**Assessment centre/person:** The Assessment centre or person is registered by admin or higher authority with a unique USER_ID and an assigned a password which can be changed by Assessment centre or person. Moreover, attributes of Assessment centre or person are USER_ID, PASSWORD and NAME.

**IoT device manager:** The IoT device manager is registered by admin with a unique MACHINE_ID and assigned a password which can be modified by IoT device manager. Furthermore, IoT devices are MACHINE_ID, PASSWORD and NAME, ADDRESS and AVAILABILITY.

**User/victim:** A user or victim can add themselves in information system and it will have CHECK_LOCATION and SELF_STATUS attributes.

In the given Fig.2. The rectangle represents the entities Natural Disaster Management System, Admin, IoT devices and User/Suffered. Oval shaped represents the attributes possess by entities and diamonds represent the relationship among the entities.

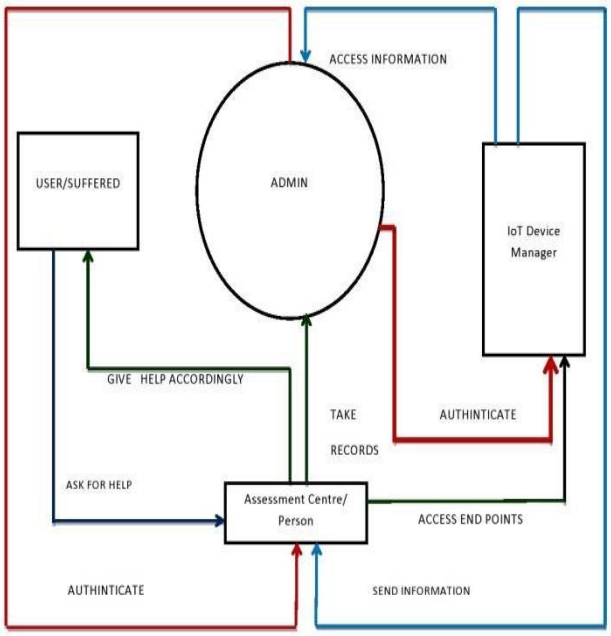


**Figure 3.** DFD of the Proposed Model

### 3.2. Data Flow Diagram

In our system, data will flow among multiple entities of the software. Organization of software modelling, a DFD can tell the data flow steps. In the cloud-based application, the Admin will authenticate the assessment centre or person if any suffered person or victim need any kind of help he/she may directly contact to the information system and assessment team will help them and the data will be updated into the system by admin. In the next phase If any IoT devices want to connect with the information system, it will first request from admin, Admin will give permission accordingly and the device can assess the granted information from the system meanwhile device can also send information to the assessment centre and the assessment centre finds the access endpoints and will keep the record of the IoT devices and send data to admin for evaluation.

In the given Fig.3. the circle shows the ADMIN, the square represents USER/SUFFERED, rectangle shows Assessment centre/person and IoT devices, the dark red lines represents authentication of assessment centre or person and IoT devices from the admin. Blue and black line shows the necessary help, data access and send.

## 4. SIGNIFICANCE AND RESULTS

The process of rescuing Natural disaster via traditional and conventional is time-consuming, robust, biased and less effective with high cost**.** Therefore, the demand of today is a cloud-based effective and efficient management system which can be developed by trending technologies e.g. Cloud computing, IoT, ICT (information and communication technology). In the proposed model we have developed a cloud-based disaster management system to rescue the suffered people from the natural system, the advantages of this model are as follows:-

- When the disaster occurs, many times it happens that the help is not reached to people on correct time due to which they highly suffered but now our proposed system will provide help on time.
- If the system is present they are not easy to access and use we have developed such kind of system which is easy to use and maintain for a layman also.
- We can easily see that the given systems are too costly to use but we have designed a cost-effective system.
- We have seen many times in the world that if there is any kind of financial help is provided to victims, it does not reach to them properly. Our proposed system will provide such kind of platform that it will remove corrupted middle persons so the financial help will directly reach to the needy person.

## 5. CONCLUSION

Wearable devices, cloud computing, ICT, many other trending technologies have made disaster

management very convenient, efficient and cost-effective. In the proposed model

We have demonstrated disaster management and monitoring system cloud computing which provide a more effective way to tackle natural disasters compare to the conventional and traditional methods. We have explained the overall idea of the system in the form of ER-diagram and DFD. As we know in, ICT is growing very rapidly and empowering many fields there is a huge opportunity that we can apply trending technologies to tackle such destructive circumstances e.g. Artificial Intelligence can enhance capabilities of such information system and convert in an expert system.

**REFERENCES**


Ainehvand, S., Raeissi, P., Ravaghi, H., & Maleki, M. (2019). Natural disasters and challenges toward achieving food security response in Iran. *Journal of Education and Health Promotion*, *8*, 51. https://doi.org/10.4103/jehp.jehp_256_18

Iii, C. A. D., Carbin, G. W., & Brooks, H. E. (2011). *The tornadoes of spring 2011 in the USA : an historical perspective*. *2010*(April 1974), 88–94.

Mahar, P., Lynch, J. A., Wathen, J., Tham, E., Berman, S., Doraiswamy, S., & Maina, A. G. K. (n.d.). *Disasters and their Effects on the Population : Key Concepts*.

Nanto, D. K. (2011). *Japan?`s 2011 Earthquake and Tsunami: Economic Effects and Implications for the United States*. DIANE Publishing Company. https://books.google.co.in/books?id=Ih7Hip-RcgAC

Pile, K. W. (2001). Disaster planning and management. *Pulp and Paper*, *75*(11), 20.

Sarkar, S., Kanungo, D. P., & Chauhan, P. K. S. (2011). Varunavat landslide disaster in Uttarkashi, Garhwal Himalaya, India. *Quarterly Journal of Engineering Geology and Hydrogeology*, *44*(1), 17–22. https://doi.org/10.1144/1470-9236/09-029

Shaw, R., & Sinha, R. (2003). Towards Sustainable Recovery: Future Challenges After the Gujarat Earthquake, India. *Risk Management*, *5*(3), 35–51. https://doi.org/10.1057/palgrave.rm.8240155

Small, C., & Naumann, T. (2001). The global distribution of human population and recent volcanism. *Global Environmental Change Part B: Environmental Hazards*, *3*(3), 93–109. https://doi.org/10.3763/ehaz.2001.0309

Trumbo, C., Lueck, M., Marlatt, H., & Peek, L. (2011). *The Effect of Proximity to Hurricanes Katrina and Rita on Subsequent Hurricane Outlook and Optimistic Bias*. *31*(12). https://doi.org/10.1111/j.1539-6924.2011.01633.x

Weekly, P. (2005). *Flood Damages and Sustainability of Agriculture in Assam*. *40*(26), 2723–2729.

Intercontinental Geoinformation Days

http://igd.mersin.edu.tr/2020/

# The application of GIS in the selection of suitable areas for afforestation of Konya

**Ceren Yağcı*[1], Fatih İşcan [2]**

[1]*Konya Technical University, Faculty of Engineering and Natural Sciences Geomatics Engineering, Konya, Turkey*

**Keywords**
GIS
AHP
Afforested

**ABSTRACT**

In order for the land management to be applied correctly and effectively, importance should be given to the location selection studies. Determining the most suitable area according to the purpose and initiating studies will provide social and economic gain for our country. As forest areas occupy large lands, it is actually a necessity to determine the areas to be afforested by site selection. In the study, Konya province, which has an arid and semi-arid climate, afforestation area selection was made using Geographical Information Systems (GIS) and Analytic Hierarchy Process (AHP) method. Six different criteria were determined as precipitation, land use capability (LUC), large soil groups (LSG), rainfall, slope, aspect, and erosion. It has been determined that 15% of the study area is the most suitable for the afforestation area, 25.52% is suitable, 28.95% is medium, 12.76% is low and 17.77% is very low. The fields obtained were presented to the public with the help of the website created. The spatial appearance of these areas, which are deemed suitable for tree planting, is expected to increase tree planting activities.

## 1. INTRODUCTION

With the beginning of the 2000s, technology has made a rapid entry into our lives and the existing industrialization has increased. With these developments, technology and industrialization have increased the comfort it provides to human beings while increasing the damage to nature and the environment. Problems such as global warming, depletion of the ozone layer, increase in environmental and air pollution, noise pollution, climate change, and the increase of greenhouse gases in the atmosphere have started to threaten nature. These problems are solved directly or indirectly with the help of afforestation studies. Therefore, some researches have been carried out under the name of afforestation studies (Hossain and Lin, 2003; Gilliams et al 2005; Eslami et al.; 2010, Kantarcı et al 2011; Çelik, et al, 2016; Tonguç et al, 2017; Muğla and Türk, 2020). In these studies, it was emphasized that many current problems can be solved by increasing afforestation studies. The primary goal of afforestation studies is to maintain sustainability. To ensure sustainability, the site selection of the area to be planted is very important. Therefore, in this study, afforestation area selection was made using Geographical Information Systems (GIS) and Analytic Hierarchy Process (AHP) method in Konya. Within the scope of the study, six different criteria were determined as precipitation, land use capability (LUC), large soil groups (LSG), rainfall, slope, aspect, and erosion. As a result, suitable areas for afforestation map for Konya province was obtained. Next 10 sample areas were selected from among the most suitable areas to be afforested spatially, attribute information was integrated into these areas and a questionable platform was created on the web.

## 2. MATERIALS and METHODS

### 2.1 Study Area

Konya is the biggest city of Turkey with respect to the surface area which covers 5% of the total surface area of Turkey. Konya is geographically situated between 36.51 and 39.51 north latitudes and 31.51 and 34.51east longitudes. Since it has an agricultural area of approximately 3.5 million ha and the annual average rainfall is around 300-350 mm (Yılmaz, 2017).

* **Corresponding Author**

*(cyagci@ktun.edu.tr) ORCID ID 0000–0002–4429-7809
(fiscan@ktun.edu.tr) ORCID ID 0000-0002-0669-5830

**Cite this study**

Yağcı C. & İscan F.(2020). The Application of GIS in the Selection of Suitable Areas for Afforestation of Konya. Intercontinental Geoinformation Days (IGD), 204-207, Mersin, Turkey

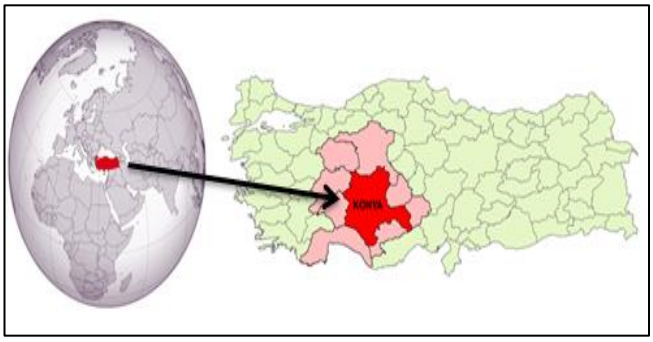


**Figure 1.** Study Area

### 2.2 Spatial Database

**Land Use Capability (LUC)**

Lands are divided into 8 classes according to their ability to use. It is classified between the 1st and the 8th grades according to the decrease of their suitability for agricultural production starting from the 1st grade to the 8th grade. 1st class, 2nd class, 3rd class and 4th class areas are considered suitable for agriculture and these areas are not used legally for afforestation studies.

**Large Soil Groups (LSG)**

In Konya, there are five types of soil in density: alluvial soil, brown soil, brown forest soil, lime-free brown forest soil, chestnut colored soil .An evaluation has been made among these soil groups**.**

**Rainfall**

If there is no rain and irrigation activities do not take place, the yield and growth of plants and trees will decrease. Since Konya is a region with low precipitation, the regions with 430-530 mm of precipitation where precipitation is ideal have been taken as the most suitable areas for afforestation works.

**Aspect**

In terms of geography, aspect is generally defined as the part of a slope, a surface facing the sun or the direction of receiving sunlight in mountainous areas. The sun rays in Baku were taken as the northeastern, north and northwestern ones that are the most suitable for afforestation or among others**.**

**Slope**

Slope is very important in terms of agricultural and afforestation works. In places where the slope is very low, it can have a negative effect in terms of drainage. According to the researches, slope intervals between 4% - 9% slope values have been determined as suitable for afforestation studies. It is not desired that there is no slope and the slope value is more than 30%.

**Erosion**

Two types of erosion have been investigated, namely water erosion and soil erosion. Separate classification has been made for erosion degrees and wind erosion.

### 2.3 Determination of the most suitable areas to be afforested using AHP method.

The AHP (Saaty, 1980) has found its way into various decision areas. It compares alternatives pair-wise, finds a complete ranking of the alternatives, and provides an overview of the complex relationships between decision elements (i.e., criteria and alternatives) by structuring them into hierarchies. An important step in this method is the construction of an evaluation matrix for each criterion, within which the values of the attributes of the different alternatives are compared amongst each other in pair-wise fashion. Each comparison is based on a verbal or numerical (ranging from 1 to 9) scale.

**Table 1.** Comparison matrix and weights of layers

| LAYERS | 1 | 2 | 3 | 4 | 5 | 6 | Ağırlıklar |
|---|---|---|---|---|---|---|---|
| LUC | 1 | | | | | | 0.36 |
| (LSG) | 1 | 1 | | | | | 0.36 |
| Rainfall | 1/5 | 1/5 | 1 | | | | 0.14 |
| Aspect | 1/7 | 1/7 | 1/5 | 1 | | | 0.05 |
| Slope | 1/9 | 1/9 | 1/7 | 1/3 | 1 | | 0.03 |
| Erosion | 1/7 | 1/7 | 1/3 | 3 | 5 | 1 | 0.08 |
| (CR) | | | | 0.08459 | | | |

The weights of each criterion (Table 1) were calculated using the paired comparison matrices created. The consistency rates of paired comparison matrices were found below 0.10. The map of the study area was produced by collecting all layers by using the weighted sum overlay method in ArcGIS software with the obtained weights (Figure 2).

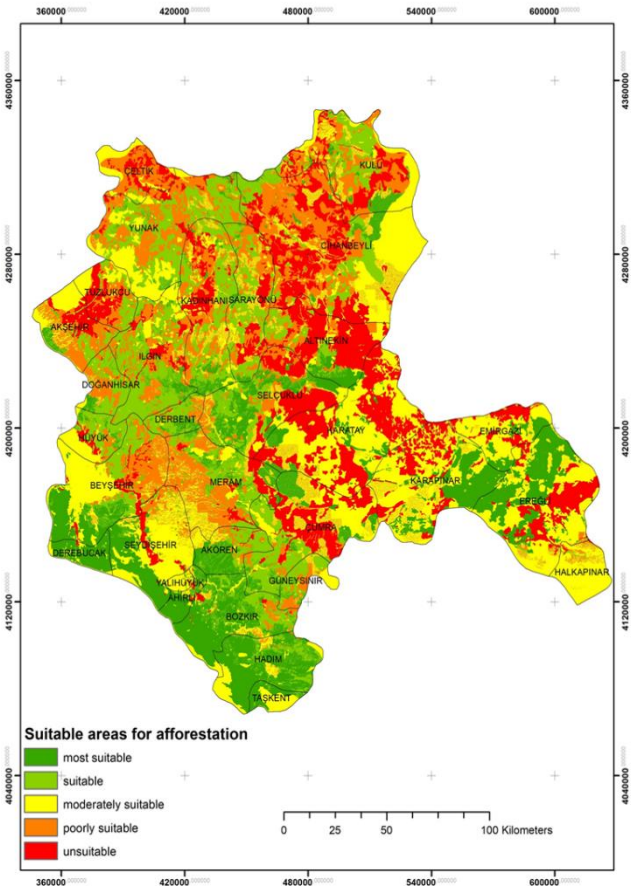


**Figure 2:** Suitability map of the area to be planted with trees produced using AHP

### 2.4 Website design

After the determination of the areas to be afforested in Konya the information on the suitable areas for afforestation obtained as a result of the study was displayed on the website with the "html code" created using the blogger website. The location of the suitable areas, the capacity of the fields, which type of saplings are suitable for planting, and when the planting begins, is made available to everyone at https://konyagac.blogspot.com/.In addition, information about the transition to the websites of the General Directorate of Forestry and TEMA (The Turkish foundation for combating erosion reforestation and the protection of natural habitats) and the sapling planting stages were shared with the public in order to get information on the site (Figure 3).

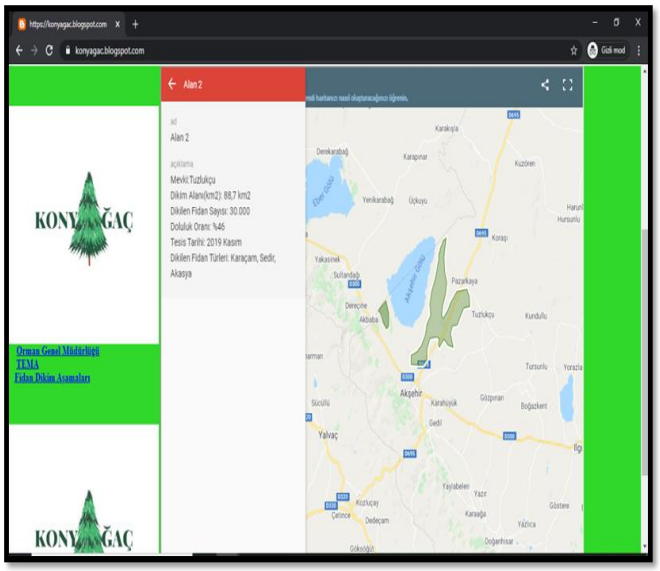


**Figure 3:** Sample view from the website

### 3.RESULTS and DISCUSSION

Afforestation studies have gained importance in recent years in order to reduce the negative effects of industrialization and urbanization on the environment in cities. While developing technology causes the relationship with the environment to shake, on the other hand, it helps to eliminate this negativity. One of these Technologies is GIS it is a powerful tool for environmental data analysis and planning. In this study, the suitable location selection of the areas that can be afforested in Konya is determined by GIS and presented on the web. In the evaluations made in the areas that can be afforested according to the AHP method for Konya province, it has been determined that 15% of the study area is the most suitable for the afforestation area, 25.52% is suitable, 28.95% is medium, 12.76% is low and 17.77% is very low. The map showing these determined areas and the boundaries of Konya district were overlapped (Figure 2) and the distributions of the areas that can be afforested in the districts of Konya were determined. Derebucak, Ahırlı, Bozkır, Hadim, Akören, Derbent districts, south of Seydişehir, south of Seydişehir, south-east of Karapınar and north-facing areas of Ereğli were found to be suitable for afforestation. In the central districts, it was observed that the west of the Selçuklu district, the north and north east of the Meram district were suitable for afforestation, and the Karatay district was moderately suitable and unsuitable for afforestation. By determining the areas to be afforested, and combining the information of the sample areas among the areas deemed appropriate positionally, a platform open to everyone was created on the web. With this platform, which is broadcast on the internet, it has been ensured that different users can access other services and other platforms simultaneously. A web map is more than just any map because it makes GIS more accessible, more affordable and more common.

### 4.CONCLUSION

In this study, the map of the areas to be afforested in Konya province was produced by using AHP method and GIS. This map was created from, land use capability (LUC), large soil groups (LSG), rainfall, erosion, aspect and slope map using 6 factors. The map produced was classified in 5 categories as "most suitable, suitable, moderately suitable, poorly suitable and unsuitable areas. As a result of the study, it was observed that the south and south west of Konya are more suitable for afforestation. In the second stage of the study, 10 different areas determined from these maps were presented to those who wanted to plant trees on the internet. It is thought that this pilot application theme can be further developed with the participation of the Ministry of Forestry and local people in such studies.

### REFERENCES

Çelik, N., Çömez,A., Güner, Ş., Karataş, R., Özkan &, K.( 2016). Modelling the productivity of Anatolian black pine plantations in Turkey. Journal of the Faculty of Forestry Istanbul University.66(1), 159-172.

Eslami A.,Roshani M. &,Hassani M.(2010).The application of GIS in selection of suitable species for afforestation in southern forest of Caspian Sea.Journal of Environmental Sciences 4(3),223-226.

Gilliams S., Raymaekers D., Muys B. & VanOrshoven J.(2005). Comparing multiple criteria decision methods to extend a geographical information system on afforestation. Computers and Electronics in Agriculture) 142-158.

Hossain MD. S. & Lin C. K. (2003). Remote Sensing and GIS Applications for Suitable Mangrove Afforestation Area Selection in the Coastal Zone of Bangladesh. Geocarto International, 18 (1),61-65.

Kantarcı M. D., Özel H.B., Ertekin M. & Kırdar E. (2011). An assessment on the adaptatıon of 6 tree specıes to steppe habıtat durıng Konya-Karapınar sand-dune afforestatıons. Journal of Bartın Faculty of Forestry, 13 ( 19),107-127.

Muğla M.K. & Türk T. (2020). Detection of potential afforestation fields by analytical hierarchy process and geographical information systems. Journal of geodesy and geoinformation, 2,103-120.

Saaty T.L. (1980). The Analytical Hierarchy Process. McGraw-Hill, New York .

Tonguç F., Kadıoğulları A.İ. & Gürkaynak M. (2017). Kahta Devlet Orman İşletme Şefliği Potansiyel Ağaçlandırma Sahalarının Önceliklerinin Coğrafi Bilgi Sistemleri İle Belirlenmesi, Journal of Bartin Faculty of Forestry, 19(1), 229-239.

Intercontinental Geoinformation Days

http://igd.mersin.edu.tr/2020/

# Identifying equality and accessibility to health centers via Spatial Information Science

**Ömer Akın*[1], Hande Demirel [1]**

[1]*Istanbul Technical University, Civil Engineering Faculty, Geomatics Engineering Department, Istanbul, Turkey*

**Keywords**
Accessibility
Geographical Information System (GIS)
Health accessibility
Access equality
Decision making

**ABSTRACT**

Citizens living in mega cities need easy and fast access to health services and hospitals. In situations such as natural disasters or pandemics, it is critical to reaching such services rapidly to prevent losses and reduce health damages. Furthermore, ensuring equality in accessibility for such services is a vital responsibility for the governments. Quantifying accessibility and serving equality among the population is a significant challenge, where Geographical Information Systems (GIS) environment could provide solutions. In this paper, adequacy of the existing health services for the European side of Istanbul is analyzed spatially and quantitatively via open data sources. Then, the proportion of both rural and urban population that has access to the health services within walking distance is determined. Within this context, Urban and Rural Health Accessibility Indexes are proposed to generalize developed concepts. According to the achieved results, ~93% of the total population has access to a health service. Furthermore, the achieved results also represent the spatial distribution of the citizens having access to health services which is not previously provided via former studies in the region. The proposed concept is applicable for every city either in Turkey or in the world to help decision-makers prioritizing of their actions.

## 1. INTRODUCTION

Easy access to health centers and/or hospitals is a vital indicator for the public since every person has the right to get health care. Health investments should be prioritized and monitored by using quantified indicators to assure this condition. Relevant data, analysis and visualizations aid decision-makers and the public to understand the infrastructure performance against health cases (Krizek, 2010). Within the current pandemic conditions, accessibility to health services in equality is one of the top priorities of policy makers. Hence, informed decisions are highly appreciated.

This highly important aspect is monitored via local/national/international organizations, where quantitative Key Performance Indicators (KPI) for each spatial granularity are required. Accessibility to health services and access equality are also indicated in the United Nations' (UN) Sustainable Development Goals (SDG) that are international indicators described as the blueprint for peace and prosperity for people and the environment (SDKP, 2015). Goal nine of SDG is about the industry, innovation and infrastructure and several indicators/measures are presented within this goal to ensure the access equality.

In this study, two new indicators named Urban and Rural Health Accessibility Index are proposed that are applicable at the local level to identify the accessibility ratio and the spatial distribution of population towards health services. Quantifying accessibility is a spatial information science problem therefore it should be evaluated in a Geographical Information Systems (GIS) environment. Developed indicators are aimed to be useful for decision-makers and researchers to analyze the problem spatially to find quantitative and spatial insights about the situation. All data used are obtained from the open database, thus the methodology is applicable for all, where data is available.

Further sections are organized as follows: Study area, data and methodology are described in the following section. In section 3, results in both quantitative and spatial ways are presented and findings are interpreted. Finally, the subject is concluded in the last section.

* **Corresponding Author**

*(akinom@itu.edu.tr) ORCID ID 0000-0002-8109-0313
(hande.demirel@itu.edu.tr) ORCID ID 0000-0003-0338-791X

**Cite this study**

Akın O & Demirel H (2020). Identifying equality and accessibility to health centers via Spatial Information Science. Intercontinental Geoinformation Days (IGD), 208-211, Mersin, Turkey

## 2. METHOD

### 2.1. Study Area and Data

Istanbul is Turkey's most crowded metropolitan city and its urban pattern is continuously changing due to the rapid population growth. The distribution, service capacities and accessibility conditions of the health services are vital. The challenge is significant in the case of natural/human-made disasters and/or pandemics. In this study, the European side of Istanbul where the population concentration is high and dense was examined in a GIS environment to analyze the access equality towards these health services.

To perform the analyses, location of current health services, road network and population information of Istanbul are needed. In the study, all data used for the analyses were obtained from open data portals and databases. Aforementioned required data were obtained from Istanbul Metropolitan Municipality (IBB) Open data portal, OpenStreetMap (OSM) and Turkish Statistical Institute (TUIK) respectively. For this high-resolution spatial analyses, the spatial resolution of the TUIK population data that is at district-scale should be increased. To solve the problem, 1km*1km grid-based population data was created from district-scaled data. For this preprocessing step, land cover/use information of Istanbul was used to distribute the population information into 1km*1km grids more precisely. The necessary land cover use data was obtained from the EU Copernicus Land Monitoring Service's open-source Corine Land Cover (CLC) database for the year 2018. The spatial resolution of land cover/use data is 100m * 100m. Urban class of land cover/use was used to identify the concentration of population; thus, the distribution was done in parallel with this information. All input data then were stored in a spatial database to later connect it to GIS environment. Turkish National Reference Frame (TUREF) TM 30 projected coordinate system was selected to represent the European side of Istanbul on the spatial database. Study area and data are shown in Fig. 1.

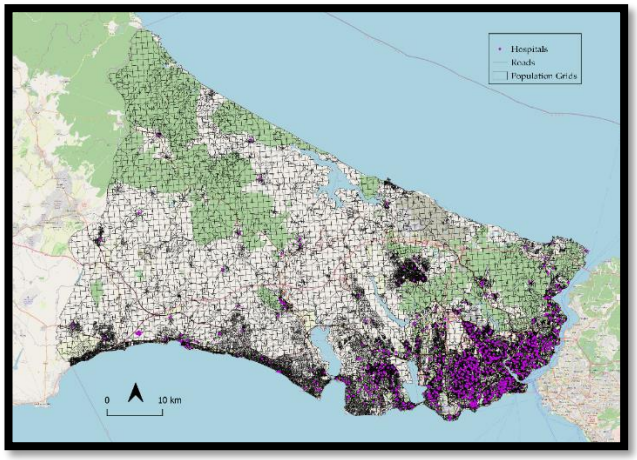


**Figure 1.** Study area and used data

### 2.2. Methodology

Within the scope of the study, the urban and rural population were evaluated separately to analyze access equality among citizens towards health services. So before starting the analysis, a consistent and reliable urban/rural definition is needed to separate the population characteristics. To ensure this, European Commission's urban-rural typology definition: "Rural areas are all areas outside urban clusters which are clusters of grid cells of 1km by 1km with a density of at least 300 inhabitants per $km^2$" was used (Eurostat, 2016).

According to the definition above, urban and rural grids were separated. 1km*1km grids having population value over 300 were selected as urban grids and rest as rural grids. Also, grids having population value under 20 were extracted from the rural grids since those grids represent water areas and barren lands. Resulted grids are shown in Fig. 2.

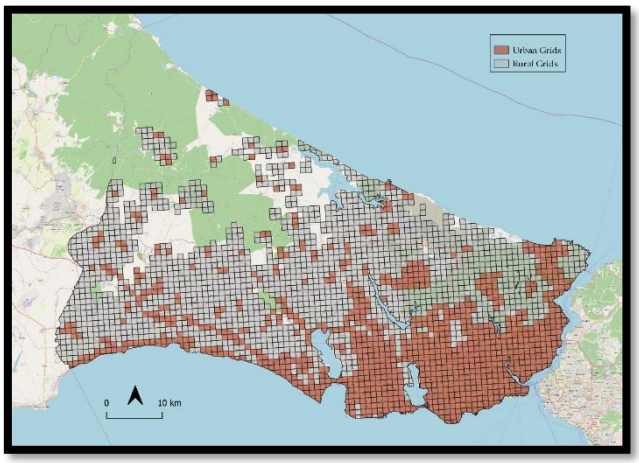


**Figure 2.** Urban and rural grids

To analyze the transport equality among different groups of citizens, walking distance accessibility condition for critical services was used as approximately 2 kilometers according to the definition of the United Nation's Sustainable Development Goals definitions (UN, 2018). To achieve this, hospitals' service area over the network was found by using the locations of the hospitals and the road network of Istanbul. Hospital locations were used to generate accessibility polygons toward them having 2 km radius over the network.

After this step, rural grids and urban grids were overlayered with resulted polygons to find the total population having access to hospitals in 2km walking distance. In this context, Urban and Rural Health Accessibility Indexes were proposed within this study. Equation of the proposed indexes is the following:

$$UHAI\ (RHAI) = \frac{Urban\ (Rural)\ Population\ Having\ Access\ to\ Hospitals}{Total\ Urban\ (Rural)\ Population}$$

Limitations within the study are listed as; (a) As health services, only IBB's open data was used. Services such as public hospitals, city hospitals, medical centers, family health centers, polyclinics and diagnosis centers exist in the data. (b) Road network quality depends on the OSM database that is a collaborative mapping project that provides a free and editable map of the world (Corcoran et al., 2013). It is one of the greatest resources for acquiring spatial data and its data quality is generally quite high (Haklay, 2010).

## 3. RESULTS & DISCUSSION

Resulted accessibility polygons in the 2km service area of the hospitals are shown in Fig. 3. Accessibility polygons then were intersected with urban and rural grids separately to show the distribution of relevant population having access to health services. Resulted maps are shown in Fig. 4 and Fig. 5.

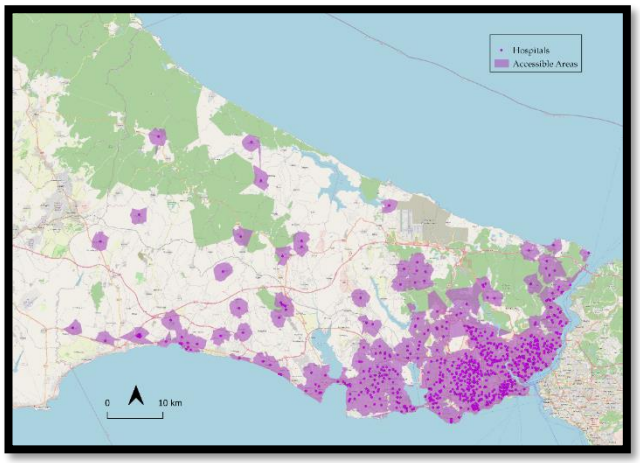


**Figure 3.** Areas accessible to hospitals in 2km walking distance

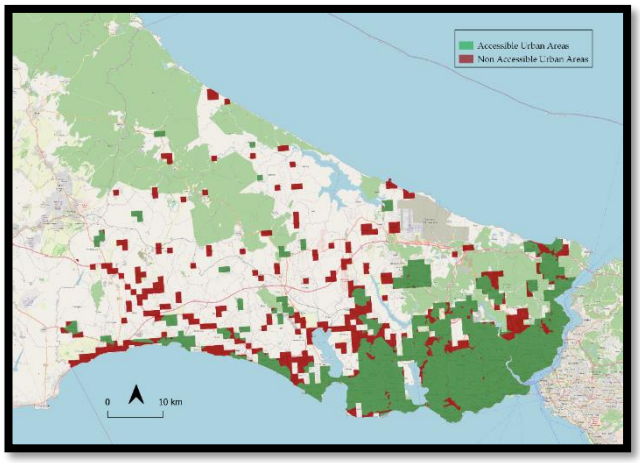


**Figure 4.** Urban areas accessible to hospitals

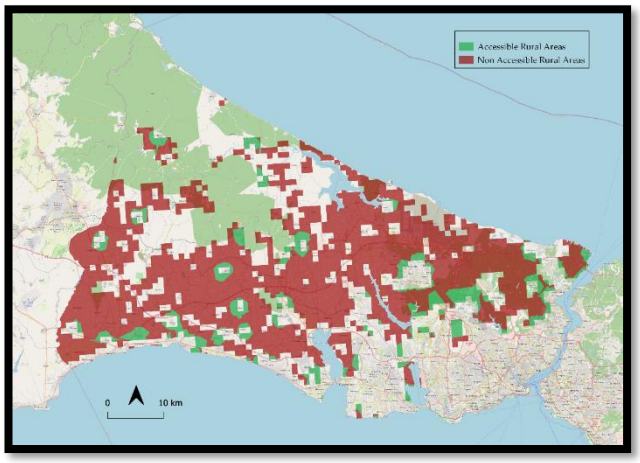


**Figure 5.** Rural areas accessible to hospitals

When accessibility maps are examined, it could be seen that most of the urban areas have access to hospitals spatially. However, the same could not be said for the rural areas. After interpreting the maps, the proportions of the population were quantified to get the quantitative results. Results of the proposed indexes are given in Table 1.

**Table 1.** Urban and Rural Health Accessibility Indexes (UHAI/RHAI)

| **Population** | Urban Population | Rural Population | UHAI | RHAI |
|---|---|---|---|---|
| Having Access | 8.430.474 | 40.814 | 93,5% | 29,7% |
| Total | 9.016.550 | 137.408 | | |

92.5% of the total population have access to health services. While the urban population constitutes 99% of the total population of the European side of Istanbul, the rural population constitutes 1%. Results showed ~94% of the urban population has a health service where is accessible in 2km walking distance. However, in rural areas, this ratio is decreased to ~30%.

For the urban population, it is seen that current road structures are sufficient but it is hard to say the same thing for rural areas. It is an interesting finding for the health sector and also for governments to inspect the infrastructures or investments' impact on public accessibility. However, as mentioned in the assumptions section, used data quality depends solely on the open-source database. By using more detailed data, these concepts could be improved to get more realistic outputs. For example, bed capacities, intensive care capacities or unit-specific weights can be given as attributes to the hospital data to improve the methodology.

## 4. CONCLUSION

Health accessibility indicators are important to control the public's health accessibility conditions and to analyze the performance of health services. Also, urban and rural separation is a critical indicator for ensuring access equality among citizens. In this paper, open-source data and environments are used for each step of implementation of the proposed indicators. The methodology is applicable for every city either in Turkey or in the world to help decision-makers prioritize their actions. With simulated data, the methodology can be applied for future years to analyze the effects of taken decisions. Furthermore, support of decision-makers on open spatial thinking and adaptation of distribution policies are utmost importance, since without such data it would be very difficult or impossible to perform such analyses.

## REFERENCES

Krizek K (2010). Measuring Accessibility: Prescriptions for Performance Measures of the Creative and Sustainable City. International Journal of Sustainable Design, 13, 149-160.

Sustainable Development Knowledge Platform. (2015). The 2030 Agenda for Sustainable Development. Available: http://sustainabledevelopment.un.org/post2015/transformingourworld, Accessed: 14.10.2020.

United Nations. (2018), Metadata for Indicator 9.1.1. Available: https://unstats.un.org/sdgs/metadata/files/Metadata-09-01-01.pdf, Accessed: 14.06.2020.

Corcoran P, Mooney P & Bertolotto M (2013). Analyzing the growth of OpenStreetMap networks. Spatial Statistics, 3:21 – 32.

Haklay M (2010). How good is volunteered geographical information? A comparative study of OpenStreetMap and Ordnance Survey datasets. Environment and Planning B: Planning and Design, 37(4), 682–703.

Eurostat (2016). Urban-Rural Typology, Available: https://ec.europa.eu/eurostat/web/rural-development/methodology, Accessed: 14.06.2020.

Intercontinental Geoinformation Days

http://igd.mersin.edu.tr/2020/

# Investigation of Pedestrian Accessibility to Schools; A case study of Rize

**Sabire Edanur Mamat*[1], Aziz Şişman[2]**

[1]Ondokuz Mayıs University, Graduate Education Institute, Department of Geomatics Engineering, Samsun, Turkey
[2]Ondokuz Mayıs University, Faculty of Engineering, Geomatics Engineering, Samsun, Turkey

**Keywords**
Accessibility
School
Network Analysis

**ABSTRACT**

Geographic Information Systems (GIS) which we frequently use in many areas today, with the capabilities of spatial analysis and query we can access information that will enable us to make the right decision in a shorter time. The rapid population growth experienced with the rapid development of cities brought many problems with it. Nowadays GIS is used the solutions of spatial problems such as transportation and infrastructure services. In this study, pedestrian access of the schools was examined in the Merkez districts of Rize. The accessibility of primary schools, secondary schools and high schools within the study area was examined and access maps were created in 5 min and 10 min time zones depending on the average pedestrian speed. In the Merkez district, schools were seen to be more density in neighbourhoods close to the coastal area. It was observed that, pedestrian access was sufficient in these parts, but it has been observed that the access was not sufficient because of the decrease in the number of schools towards the inner parts. In addition, the access problem in high schools is more than secondary and primary schools. Public transport or shuttle service is used where pedestrian access is not sufficient.

## 1. INTRODUCTION

The city can be defined as the place where people who have a common cultural and economic cooperation gather (Göney 2017).

Migration from rural to urban has accelerated with the industry developing in the city and its surroundings. The number of people working in the industrial sector has increased rapidly with the development of the industry in many settlements that previously had a high population of trade (Sezer et al. 2018). Population growth has led to the emergence of more diverse functions in cities. While previously only the industry was the majority, the service sector has started to develop in later (Çelikyay 2013).

With the rapid increase population of the citiessmart applications have been tried using developing technology in order to find solutions to problems such as transportation, health, safety and environment (Örselli et al 2019). Smart cities where a constant flow of data is provided about the physiological and sociological status of that place, and by combining and synthesizing these interconnected data for a common purpose, they are cities where the quality of life is increased(Batty et al. 2019).Smart cities have become more popular over the past 20 years. Most of the methods of being smart cannot be obtained in a short time, they can be implemented with longer time and stability (Örselli et al 2019). In order to call a settlement a city, attention should be paid to its urban functions (Tümertekin 1973). Functions are used to determine the boundaries of the city as well as to show urban characters. The development of educational activities and functions is one of the most important features of that city (Çetin 2007). The content and accessibility of education should be given to all people on equal terms. Governments are trying to develop various methods in order to provide equal opportunity to their citizens (Sezer et al. 2018).

Geographic Information Systems (GIS) can be used in many areas which related to the spatial data, such as settlement, health, transport, education etc. The studies of GIS in the field of education are supported with examples such as locations, accessibility and distribution of schools.

*Corresponding Author

*(edanur.mamat.em@gmail.com) ORCID ID 0000 – 0003 – 4809 – 6673
(asisman@omu.edu.tr) ORCID ID 0000 – 0001 – 6936 – 5209

Cite this study

MamatS.E. &Sisman A. (2020). Investigation of Pedestrian Accessibility to Schools; A case study of Rize. Intercontinental Geoinformation Days (IGD), 212-215, Mersin, Turkey

In the current study, the accessibility of the children to the schools in the Central District of Rize. It was conducted with the network analysis in the neighborhoods of the Central district of Rize province. The study is also aimed to be a guide in determining suitable and unsuitable places in terms of access to schools.

## 2. METHOD

This study carried an analysis of the children access to primary, secondary and high schools on foot is put forward, in Rize Central district

Study based on network analysis and ArcGIS software was used. Road network data and neighbourhood maps were obtained from Rize Municipality. Population data were obtained from Turkish Statistical Institute and location data of schools were obtained with the help of Google earth.

The road network data set was created in the analysis. On this dataset, the average pedestrian speed of children is 1.1 m/s, and the adult pedestrian speed is 1.4 m/s (TSE ts12174 standards). In the light of these data, it was analysed how much areas the schools could reach in 5 minutes and 10 minutes.

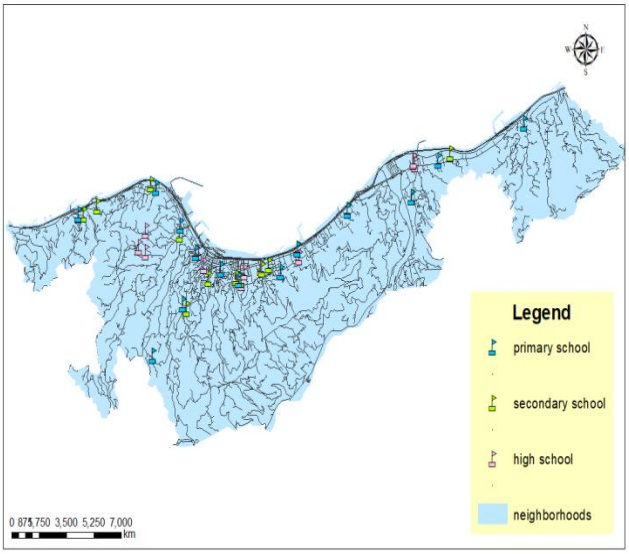


**Figure 1.** The road network of the study area and the location of the schools

### 2.1. Location and Features of the Research Area

Rize province is located in the Eastern Black Sea and is adjacent to the provinces of Trabzon, Artvin, Bayburt, Erzurum and has a coast to the Black Sea.

The total area of the city is approximately 3921 km$^2$, which is 5% of Turkey's territory. It is the smallest province in the eastern Black Sea provinces after Bayburt and ranked 72nd in terms of acreage in all of Turkey (Turkish Statistical Institute 2013).

The research area includes the neighbourhoods of Central district of Rize. The population of the province is 343,212 according to 2019 Turkish Statistical Institute data and the population of the Central District is 147,411 according to 2019 Turkish Statistical Institute data.

Besides tea production in Rize province, where 98.7% of the agricultural land consists of tea gardens, kiwi and hazelnut are among the other agricultural products (Rize Food Agriculture and Livestock Provincial Directorate Data, 2014).

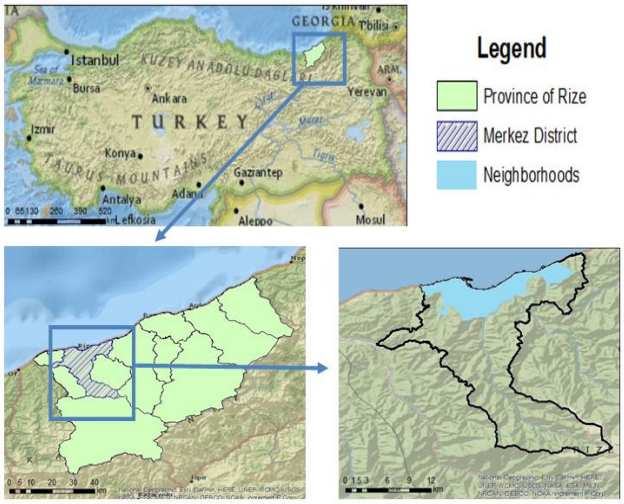


**Figure 2.** Location map of the study area

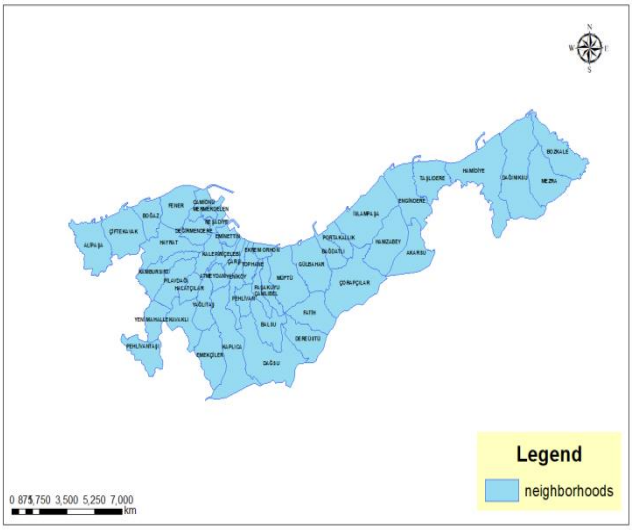


**Figure 3.** Central district's neighbourhoods

## 3. RESULTS

In the analysis, it was tried to reveal how sufficient the pedestrian access of primary, secondary and high schools is. It has been determined that the total number of primary schools is 14, the number of secondary schools is 19 and the number of high schools is 17 in the neighbourhoods in the Central district.

According to the population density map (Figure 4) of the central neighbourhoods, it was seen that the density is high towards the middle of the study area and in the neighbourhoods close to the sea. And also, it was seen that more schools were located in areas where the population density was high. It can be concluded that the population density and the distribution of schools increase and decrease in direct proportion to each other.

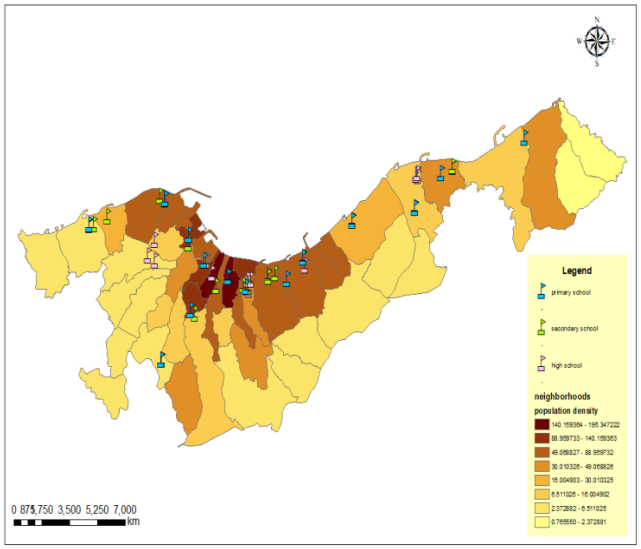


**Figure 4.**Population density of neighbourhoods and distribution map of schools

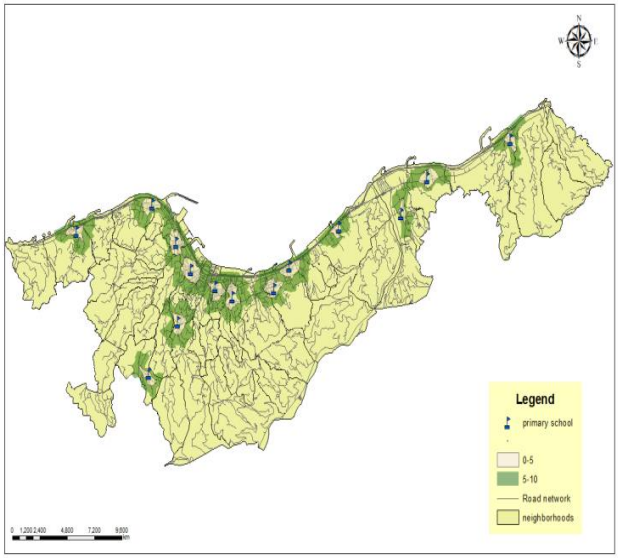


**Figure 5.**Accessibility to primary schools for children

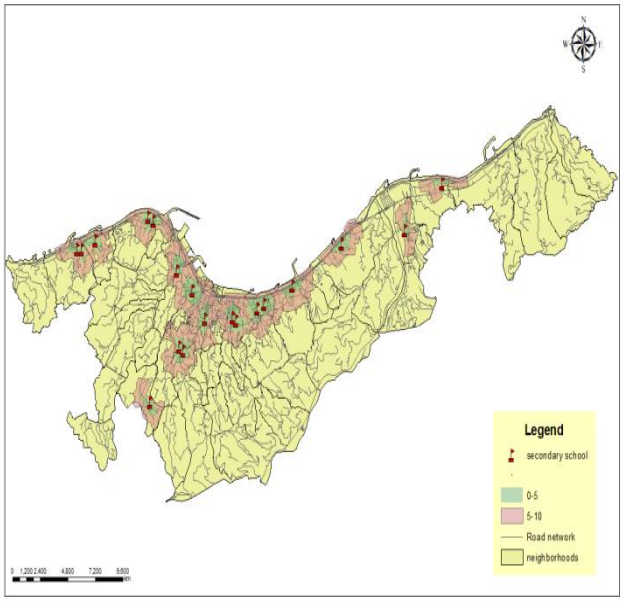


**Figure 6.**Accessibility to secondary schools for children

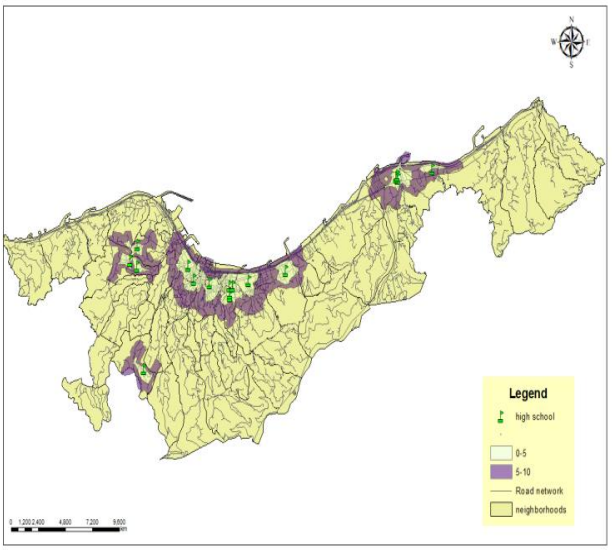


**Figure 7.**Accessibility to high schools for young

In the study area, the accessibility analysis of children in primary and secondary schools based on 5 min and 10 min time with a speed of 1.1 m/s showed that access to primary schools was 19.8% (Figure 5) of the total neighbourhood face measurement and access to secondary schools was 27.2% (Figure 6) of the total neighbourhood face measurement. In the same way, the accessibility analysis of adults based on 5 min and 10 min time at 1.4 m/s in high schools concluded that the reach of high schools was 38.2%(Figure 7) of the total neighbourhood facial measurement.

## 4. DISCUSSION

In the current study according to the access maps, it was seen that accessibility was sufficient in the districts of Çarşı, Yeniköy, Tophane, Atmeydanı, Piriçelebi and Mermerdelen neighbourhoods to primary schools, secondary schools and high schools. At the same time, it was seen that the neighbourhoods with high density are parallel to the coastline, and the density decreases as one goes further inland. The mountainous and rugged terrain of Rize province can be said as a reason for this. Due to the lack of schools in some of the neighbourhoods with medium and low populations, children and adults have never been included in pedestrian access distances. There were problems in access to schools in these neighbourhoods.

## 5. CONCLUSION

The decrease in the number of schools in the neighbourhoods away from the coast has required the use of public transport or shuttle transport.

According to the results of the analysis, it can be said that the numbers of primary and high schools in Central district neighbourhoods were insufficient since they have less access than secondary schools. The fact that there were no schools in the southern neighbourhoods and that they were not within the calculated access areas show that the service transportation is more common in these neighbourhoods.

It can be said that shuttle transportation can be more dangerous in the city where transportation is difficult due to the land structure. Increased travel distance can increase the risk of accidents. Based on the principle of equal opportunity in education, not everyone can go to schools under equal conditions creates an important problem.

In the analysis, we also saw the effect of the education function on the population density of the city. Increasing the number of schools and the diversity of locations may be effective in a more balanced distribution of the population.

As a result, the Central district neighbourhoods seem quite trouble in terms of access to schools, except for some well-located neighbourhoods. As a solution; It may be considered to increase the number of schools in the southern part of the region within 5 and 10 minutes walking distance.

**REFERENCES**

Batty, M.;Axhausen, K. W.; Giannotti, F.; Pozdnoukhov, A.; Bazzani, A.; Wachowicz, M.; Ouzounis, G. &Portugali, Y. (2012). Smart cities of thefuture. TheEuropeanPhysicalJournal Special Topics, 214(1), 481- 518.

Çelikyay, H. H. (2013). TeknolojiGirdabındanAkıllıŞehreDönüşüm: İstanbul Örneği. Bursa: II. TürkiyeLisanüstüÇalışmalarıKongresi - BildirilerKitabı V 6-8 Mayıs 2013, Bursa

Çetin, B. (2007). Burdur Kent Coğrafyası. YayınlanmamışDoktoraTezi, Atatürk Üniversitesi, SosyalBilimlerEnstitüsü, Uşak.

Göney, S. (2017). Şehircoğrafyası, yerleşmecoğrafyası, Cilt:1, İstanbul: İstanbul ÜniversitesiEdebiyatFakültesi Yay. No:3537, CoğrafyaEnstitüsü. Yay. No:91.

ÖRSELLİ, Erhanve AKBAY, Can(2019).-Teknolojive Kent YaşamındaDönüşüm: AkıllıKentler. UluslararasıYönetimAkademisiDergisiYıl: 2019, Cilt: 2, Sayı: 1, ss.228-241

Sezer, A., Deniz, M., &Topuz, M. (2018). UşakŞehrindeOkullaraErişebilirliğinCoğrafiBilgiSistemleri (CBS) İle Analizi. Journal of HistoryCultureand Art Research, 7(5), 470-494. doi:http://dx.doi.org/10.7596/taksad.v7i5.1802

Tümertekin, E. (1973). Türkiye'deŞehirleşmeveŞehirselFonksiyonlar. İstanbul: İstanbul Üniversitesi Yay. No:1840, CoğrafyaEnstitüsü Yay. No: 72.

Intercontinental Geoinformation Days

http://igd.mersin.edu.tr/2020/

# Creation of wind speed maps of Kirklareli City

**Celal BIÇAKCI*[1], Kamil KARATAŞ [2], Selim Serhan YILDIZ [3]**

[1]*Osmaniye Korkut Ata University, Osmaniye Vocational High School , Architecture and Urban Planning Department, Osmaniye, Turkey*
[2]*Aksaray University, Engineering Faculty, Geomatics Engineering Department, Aksaray, Turkey*
[3]*Osmaniye Korkut Ata University, Faculty, Engineering Faculty, Geomatics Engineering Department, Osmaniye, Turkey*

**Keywords**
Wind Speed
GIS
Energy

**ABSTRACT**

Wind energy has been an important element in our country's energy policy. According to the report of Turkish Wind Energy Association (TUREB), while the share of wind power plants in electricity production in Turkey in 2018 is 6.78%, with newly established wind power plants, it was 7.42% in 2019. The most important problem for the newly established wind power plants is that the wind energy estimation of the place where the plant will be established is unknown. In this study, a study was carried out to create wind maps of Kırklareli province. Wind maps of Kırklareli province were created for estimation of new plant locations. The average wind speed data obtained from the 10 meter height wind stations were obtained from the General Directorate of Meteorology and then the wind speed data were moved to 80 and 100 meters height, and wind speed maps were created at 80 and 100 meters height.

## 1. INTRODUCTION

One of basic needs in the development of countries is energy production but systems used for energy production cause soil, air and water pollution. The most important means of reducing this pollution are renewable and sustainable energy systems (Dünvar et al. 2002). While developed countries come ahead in the development of renewable energy sources , in developing countries with limited reserves of fossil fuels such as Turkey is seen that investment in renewable energy sources(Şenol 2017). Wind energy is a low cost, commercially viable and clean energy source that can be found all over the world (Köse et al. 2004). Therefore, there is growing interest in wind energy in Turkey and in the world. (Bayraç 2004). In order to benefit from the wind efficiently and economically ,the location of wind power plant facilities is very important. The most important problem for newly established wind power plants is that the wind energy estimation of the place where the plant will be established is not known (Şimşek and Doğru 2019). For the power plant, the energy potential of the area where the plant will be installed is an important parameter. Different meteorological parameters are measured at the observation stations which are belong to the General Directorate of Meteorology (MGM).

Wind speed is one of these parameters. Wind speed maps are created with the appropriate interpolation method using Geographical Information Systems (GIS) from MGM data. The maps created are used as a base for location selection. While creating the wind speed map, the data is the number of stations used and the parameter is the wind speed. The aim of this study is to produce a highly accurate wind velocity map that will be used as a base for the location selection of wind power plants.

### 1.1. Study Area and Data

Kırklareli province was chosen as the study area. The study area in the Marmara region is between 41 - 42 north latitude and 26 - 28 degrees east longitude. Its surface area is 6650 km$^2$ and the city center is 203 meters above sea level. In this study, 12 sensors belonging to the General Directorate of Meteorology in Kırklareli province and daily average speed data of these sensors between 2014 and 2019 were used. The height of sensors are 10m and their geographical location is shown in Figure 1.

* **Corresponding Author**

*(celalbicakci@osmaniye.edu.tr) ORCID ID 0000-0002-4743-2391
(kkaratas@aksaray.edu.tr) ORCID ID 0000-0001-5174-7153
(serhan@osmaniye.edu.tr) ORCID ID 0000-0001-6221-7035

**Cite this study**

Bıçakcı C, Karataş K & Serhan S S (2020). Creation Of Wind Speed Maps Of Kirklareli City. Intercontinental Geoinformation Days (IGD), 216-218, Mersin, Turkey

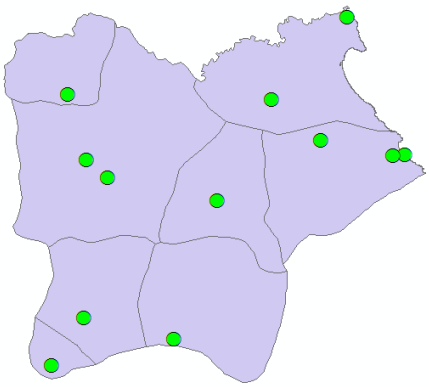

**Figure 1.** Locations of MGM stations used in the study

In order to find the friction coefficients of the stations used in the study, the CORINE land cover map and Copernicus Services inventory was used. For the purpose of the study, Hellmann equation was used to obtain wind speed at 80 and 100 meters height. In the Hellmann equation, calculations are made depending on the surface roughness of the area where the stations are located and the height to which the speed will be carried (Tar 2008).

### 1.2. Application

The locations of the stations were obtained from the MGM web page. Table 1 shows the station points and their locations used in the application.

**Table 1.** Location of station points

| Station No | Station | Lat. | Long. |
|---|---|---|---|
| 18407 | Pehlivanköy | 41,3556 | 26,9394 |
| 17631 | Lüleburgaz TIGEM | 41,3513 | 27,3108 |
| 18405 | Babaeski | 41,4433 | 27,0622 |
| 17052 | Kırklareli | 41,7382 | 27,2178 |
| 18406 | Kofçaz | 41,9411 | 27,1539 |
| 18398 | Pınarhisar | 41,6311 | 27,5236 |
| 18408 | Vize Yumurtatepe | 41,7084 | 27,8655 |
| 19900 | Kırklareli Üniversitesi | 41,7884 | 27,1683 |
| 17447 | Midye Kıyıköy Batı Mendire Fener (Ana) | 41,6317 | 28,1019 |
| 18102 | Demirköy | 41,8228 | 27,7489 |
| 18103 | Vize Kıyıköy | 41,6378 | 28,0661 |
| 18795 | Demirköy Beğendik Köyü | 41,9639 | 28,0233 |

Average daily wind speed between 2014-2019 of 12 meteorology stations in the study area were taken from MGM. Wind speeds at the stations are measured by sensors located on poles 10 meters high. With the Hellmann equation given in Equation 1, The wind speed at 80m height and 100 m height was estimated by using data of wind speed at 10m height.

$$\frac{V}{V_0} = \left(\frac{H}{H_0}\right)^{\alpha} \qquad (1)$$

In Equation 1, $V_0$ is the wind speed at a height of 10 m, H is the wind height to be carried, α is the friction coefficient and V is the wind speed at the height to be carried. In this study, $H_0$ was taken as 10 m. The CORINE land cover map Copernicus Services inventory (EEA 2019) was used to determine the friction coefficient. Table 2 shows the land type classes and the corresponding friction coefficients (Masters 2004).

**Table 2**. Friction coefficients according to land characteristics (Masters, 2004)

| Terrain Characteristics | Friction coefficient (α) |
|---|---|
| Smooth hard ground, still water | 0.10 |
| Tall grass at ground level | 0.15 |
| High crop and shrubs | 0.20 |
| Rural forest area, many trees | 0.25 |
| Small town with trees and bushes | 0.30 |
| Cities with tall buildings | 0.40 |

For each station point, the land class of the area where the station is located was determined with the help of the CORINE land cover map and satellite images, and the friction coefficient corresponding to the terrain characteristics was determined accordingly. The wind speed of 12 stations at 80 and 100 meters height were calculated using Equation 1. Data for maps to be created using Geographic Information Systems software has been converted into an appropriate format. Since the interpolation method to be used will affect the accuracy of the result, the appropriate interpolation method has been determined. Wind speed maps were created by inverse distance weighting (IDW), krigging and natural neighbor interpolation methods. When the real MGM wind speed data and interpolation methods were compared, it was determined that the most suitable method was IDW. The distribution of the sampled points in the work area greatly affects the result. Both 80m and 100 m height wind speed maps were created in grids of 200 x 200 m as raster.

## 2. RESULTS AND CONCLUSION

The 80m high wind speed map created for Kırklareli province is shown in Figure 2. When wind speeds are examined for a height of 80 meters in the study area, it is seen that the speed varies between 2.79 m / s and 7.12 m / s.

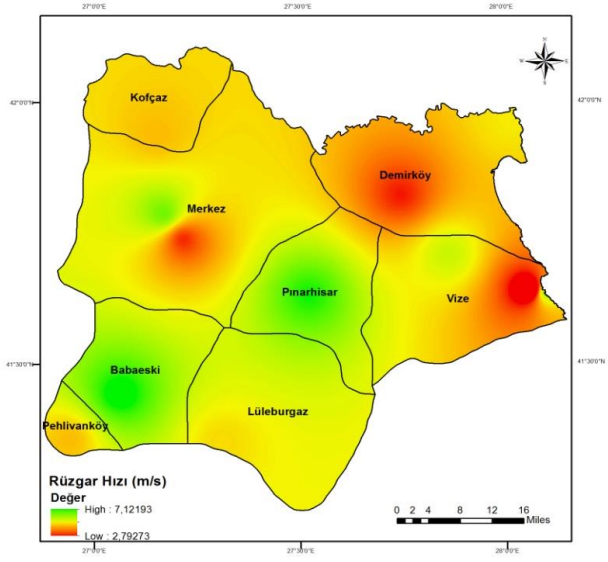


**Figure 2.** Wind Speed Map of Kırklareli Province (at 80 m height)

The wind speed map created for a height of 100 m is shown in Figure 3. When the wind speeds are examined for height of 100 meters in the study area, it is seen that the speed varies between 2.95 m / s and 7.79 m / s.

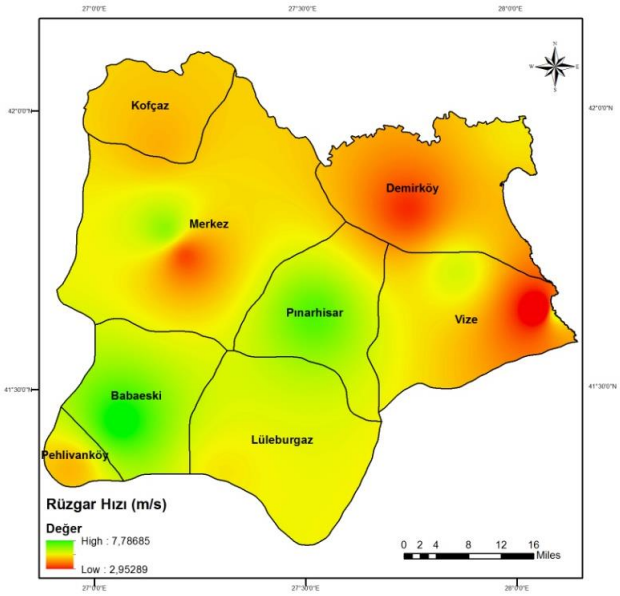


**Figure 3.** Wind Speed Map of Kırklareli Province (at 100 m height)

When the speed distributions are evaluated positionally, the wind speed around Demirköy and Vize is low ; In Pınarhisar, Lüleburgaz and Babaeski regions, wind speed is higher at both 80 and 100 meters height.

When creating wind maps, the distribution of reference points is of great importance so that the result is the closest to the expected accurate. When creating wind maps, the distribution of reference points is of great importance so that the result is the closest to the expected precision. In order to reach the most accurate result, the appropriate interpolation method should be determined and maps should be created using this interpolation method. In this study, when the maps created with the inverse distance weight (IDW) interpolation method were examined, it was determined that the wind speed was higher in the south of Kırklareli compared to other regions and it was more suitable for wind power plant location selection.

## REFERENCES

Bayraç H N (2004). Küresel Rüzgâr Enerjisi Politikaları ve Uygulamaları, Uludağ Üniversitesi İktisadi ve İdari Bilimler Fakültesi Dergisi, Cilt: XXX, Sayı: 1, 37-57.

Dündar C, Canbaz M, Akgün N & Ural G (2002). Türkiye rüzgar atlası, DMİ ve EİE ortak yayını,Ankara.

Köse R,Özgür M, Arif E O & Tugcu A (2004.) The analysis of wind data and wind energy potential in Kutahya,Turkey, Renewable and Sustainable Energy Reviews Volume: 8, pp.: 277–288

Masters, G M (2004). Renewable and Efficient Electric Power Systems, New Jersey, John Wiley and Sons Publication, USA.

Şenol Ü (2017). Rüzgar enerjisi ve rüzgar enerjisi potansiyelinin yapay sinir ağları yöntemiyle tahmini, Yüksek Lisans Tezi, Bozok Üniversitesi, Fen Bilimleri Enstitüsü, Yozgat.

Şimşek G & Doğru A Ö (2019). Rüzgar haritası üretimine yönelik uygun ara değer hesap yöntemi seçimi, 17. Türkiye Harita Bilimsel ve Teknik Kurultayı, Ankara

Tar K (2008). Some statistical characteristics of monthly average wind speed at various heights. Renewable and Sustainable Energy Reviews, 12 (6), 1712-1724.

Intercontinental Geoinformation Days

http://igd.mersin.edu.tr/2020/

# Developing an Algorithm on the Reporting Of Outages in the Electricity Distribution System with GIS Integration

**Ahmet Bahadır ÜNVERDİ[1], Aziz ŞİŞMAN [2]**

[1]Ondokuz Mayıs University, Graduate Education Institute, Department of Geomatics Engineering, Samsun, Turkey
[2]Ondokuz Mayıs University, Faculty of Engineering, Geomatics Engineering, Samsun, Turkey

**Keywords**
GIS
OMS
DMS
Integration
Outage
Distribution
Algorithm

**ABSTRACT**

Modern Electricity Distribution Systems can use many auxiliary management and analysis systems actively and effectively, as well as communicating these systems with each other and obtain more specific and quality results. It is of great importance that systems such as OMS or DMS, which are used in this context, that have tasks such as management and analysis of outages in the Electricity Distribution System, are integrated with GIS, which contains spatial and non-spatial data in relation, and allows many spatial analyzes on these data. Especially the creation of a geometric network by obtaining the topologies of spatial data by GIS creates a connection model for the analysis of data with network characteristics and allows many analyzes to be performed. In this study, the algorithm for analyzing and reporting an outage in Electricity Distribution Systems with GIS integration is discussed. Considering that the Water and Gas distribution systems have similar characteristics with the Electricity Distribution Systems, what is stated in the study is also valid for these sectors.

## 1. INTRODUCTION

Electricity Distribution Systems assume the distribution role of a region's electrical energy need. The scope in this role is to transfer the electrical energy from the transformer centers to the demanders by adding the energy produced in the production facilities with medium and low voltage network elements to the distribution system under control. Many different information processing systems are used to fulfill requirements of Electricity Distribution Systems.

Considering that all elements in a dense and complex network such as Electricity Distribution Systems have spatial characteristics; It is understood that using GIS is a necessity for analysis, data management, graphic viewing and querying processes.

The Energy Market Regulatory Authority (EPDK) requests some tables from the relevant institutions regarding the Service Quality Regulation (2012) (URL3) on Electricity Distribution and Retail Sales. With the reporting created using these tables, controls are made regarding the practices, supply continuity, and the rules to be followed on the basis of commercial and technical quality.

In Electricity Distribution Systems, there are indices such as System Average Outage Frequency Index (SAIFI) and System Average Interruption Duration Index (SAIDI) that show the quality and reliability of the system and reports containing these indices. These reports are produced over the interruptions in the system and are regularly monitored in accordance with the applicable legislation.

Systems such as SCADA, OSOS, which are established to monitor and control the electricity network remotely, give warning signals for the de-energized region. The interruptions of these warning signals are processed in the database of the same system. Subsequently, reports are produced with the relevant data and the status of exceeding the limits determined for the relevant parties is analyzed both in this state and through other reports derived as a result of integration between other systems.

GIS, in which the topology of spatial data can be created and analyzes can be run by transforming it into a geometric network structure, constitutes the main data part of many reports to be obtained. The data generated in systems such as OSOS and SCADA at the moment of the interruption comes from the cabinets, transformers and feeders where these systems receive signals. The network elements in question are given unique codes

* **Corresponding Author**

*(ahmetbahadirunverdi@gmail.com) ORCID ID 0000-0002-7175-2029
(asisman@omu.edu.tr) ORCID ID 0000-0001-6936-5209

**Cite this study**

Unverdi A & Sisman A (2020). Developing an Algorithm on the Reporting Of Outages in the Electricity Distribution System with GIS Integration. Intercontinental Geoinformation Days (IGD), 219-222, Mersin, Turkey

defined both in the field and in the GIS data, and GIS integration is provided with this setup.

In case of any interruption, customers affected by the said integration can be identified and notified (Emiroğlu et al., 2007). Here, determination of customers affected in case of outage is possible with the network connection model created and stored in GIS. In addition, systems such as SCADA, DMS, OMS can produce many results, such as the state of energy flow on the network, the summary of the network elements affected by the outage, the grouping of the affected customers and the approach to find the real fault point using the grid connection model (Yıldırım, 2020).

## 2. SYSTEMS AND INTEGRATIONS

Many advanced information systems are used to manage and analyze processes in Electricity Distribution Systems, and to report analysis results.

Geographical Information Systems (GIS), which presents spatial and verbal data in a related way, serves many spatial analysis. It is able to create and analyze a very valuable connection model for infrastructure systems, thanks to its ability to store the topology of spatial data inside and transform it into a geometric network structure.

Modeling of the infrastructure and superstructure network networks in our world is possible with geometric networks. Electricity distribution networks are one of the flows that can be modeled by creating a geometric network (Anonymous, 2020b).

Supervisory Control and Data Acquisition (SCADA) is an information system tool used for remote monitoring, control and protection of the network in distribution systems processes (Taylor & Kazemzadeh, 2009). As a result of the integration of this system with GIS, a change to be made in the SCADA system that will affect the switch positions will be sent to the GIS side and change the flow direction of the geometric network. This is an important condition for accurate and precise reporting on the GIS data and using the geometric network.

Outage Management Systems (OMS) is an information processing tool that can perform operations on many processes, such as combining failure notifications delivered by customers, enabling analysis and estimation of interruptions, managing fault teams accurately and effectively, and determining reliability criteria (Taylor & Kazemzadeh, 2009). Nowadays, OMS and GIS integration has become a project that must be implemented for the development of Electricity Distribution Systems processes. Realization of this project provides positive feedback to the relevant institution in terms of customer satisfaction, practical and effective process management.

Distribution Management System (DMS) is used for the management of interruptions in distribution systems and also for reporting as a result of the management and analysis of planned or routine network operations. The need to transfer the energy obtained from production facilities such as renewable energy to the distribution systems and to carry out the demand-forecasting processes, which have increased in intensity with this development, increases the importance of DMS (Taylor & Kazemzadeh, 2009). GIS, in which data is obtained and managed with high accuracy and precision, is of great importance for DMS to provide maximum benefit (Chakravarty & Wickramasekara, 2014). With the integration of DMS and GIS, it will be possible to identify the regions and subscribers affected by the processes to be carried out or the connections to the distribution system. In addition, the connection model will be updated over the new network structure and power analysis can be performed.

As stated above, the capabilities of these systems will provide more benefits as a result of the integration they will create with other systems (Sekhar et al., 2008). This situation will return to the institutions as the optimum management of the processes and reaching the maximum level of earnings. Integration method should be selected by evaluating many criteria such as applications, systems and corporate policies that are or will be used by the relevant parties. As each integration method has advantages and disadvantages, these features are a reason for preference for the institution (Zhang et al., 2019).

Corporate Application Integration will provide added value by associating the applications in the organization and the databases that these applications process. At the end of the said process, there will not be duplicate data in the systems except for the integration areas, so the updating and maintenance needs of the data will be reduced and costs will be minimized (Singh & Caceres, 2004).

Each investment is carried out in order to provide profit for institutions. However, the success of the investment and therefore the gain to be made depends on a comprehensive and careful process analysis strategy. Defining the processes completely and placing the processes considering their relations with each other should definitely be done before deciding on the integration method (Dönmez, 2013). With the integrations to be made through these processes, business processes will be optimized and the efficiency and dominance of the working personnel will increase significantly.

The Common Information Model (CIM) method used by electrical distribution systems includes the relationships, classes and attributes of objects (Singh & Caceres, 2004). The first method that comes to mind as integration using CIM standards is to perform point-to-point integration by using relational connections between databases designed in accordance with the standard. The point-to-point integration method to be built between databases generally has a good connection performance and is implemented quickly. This method is found to be insufficient in terms of performance and maintenance when improvements need to be made on the database and new systems need to be included in the integration. The method should be implemented among limited systems or used temporarily until a more suitable method is adopted (Dönmez, 2013). Even if this integration method is not used completely, it will be beneficial to design the database structures of the

systems that will require integration in accordance with the CIM standard design.

In summary, the Enterprise Information Architecture (EIA) method is one of the architectures that allow multiple data sharing support, and stands out with its flexibility and speed. Systems are communicated with each other by using a third software in architecture. Corporate information systems structure generally consists of commercially diverse applications and systems. Considering this difference, realizing the integration between systems with a third software is the first challenge to be encountered in the process.

Enterprise Service Bus (ESB) is a software architecture that controls and directs system data to communicate with systems. There is no need for a code writing such as EIA architecture and a third software for this communication. Communication between systems is carried out by the transmission of messages or data in a structure similar to a physical computer bus. Messages and data must be transmitted in a format that each system can understand. A common planning should be made for all systems within the institution before moving to the ESB architecture. One of the main disadvantages for this architecture is the difficulty of finding comprehensive ESB developers.

It offers a Service-Oriented Architecture (SOA) method for the integration of separate types of systems in distributed environments (Dönmez, 2013). The most prominent features of SOA; Independence from systems and platforms can be defined as usability, reliability, flexibility and ease of maintenance provided that the services created meet the conditions specified in the required applications. In this architecture, unlike EIA, there is no need for a third software and transactional communication and data transfer methods are preferred instead of collective communication and data transfer principles. Of course, these features brought by SOA bring some needs with them. Its features such as security principles and being independent from systems extend the response times of services and require high performance hardware. Although this situation requires an important upfront investment, it creates extra costs. In addition, many transactional services to be created in each system in accordance with the needs may cause the service management to become complex.

## 3. ALGORITHM

The required information per deduction can be obtained by many methods derived from verbal tables prepared specifically for the subject or from a geometric network created using GIS data or from the cooperation of these two methods. The methods in question and the way these methods work manually or automatically can be determined after evaluating the relevant institutions and the systems and data they have. When all the related processes of Electricity Distribution Systems are examined, it is seen that the most appropriate method is to create a service that operates at specified periods or instantaneously using geometric network data. With this method, no extra intensity will occur in the processes, and the desired information can be obtained with high precision as a result of interruption.

The positions of the switching elements in the inventories of the Electricity Distribution Systems (open / closed) can be changed as a result of maintenance, repair, malfunction and investment works. Since this situation will also change the flow direction of the geometric network consisting of network data, instant operation of the analysis service is important for producing sensitive and highly reliable results (Yıldırım, 2020).

An outage in the network is detected by systems such as OMS or DMS and recorded in databases. There is a unique value in the outage data structure that will allow integration with GIS. This value will be processed or transmitted to the outage analysis service created by the GIS and the analyzes will start. The information or data required as a result of the analysis will be transmitted to the desired environment in the specified format.

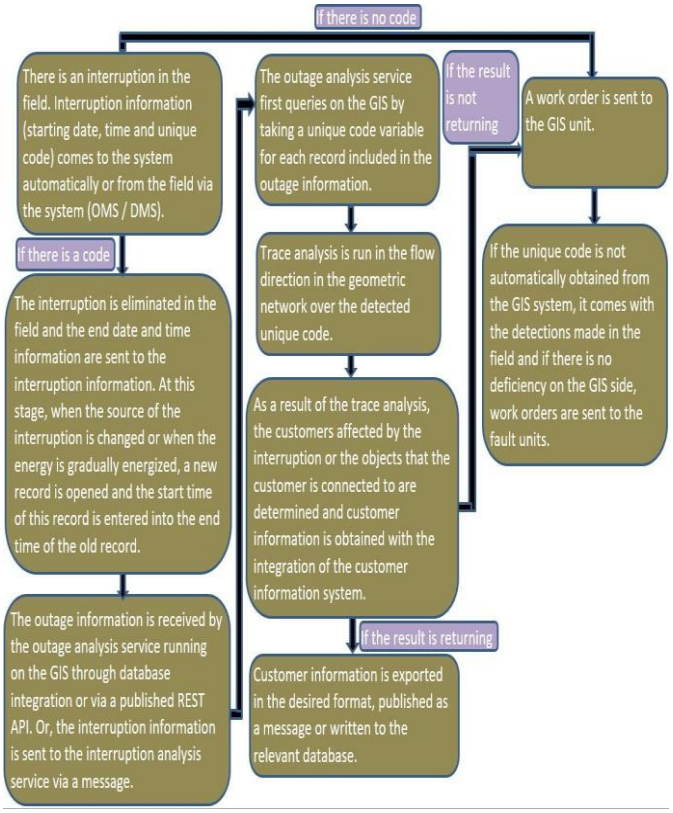


**Figure 1.** Algorithm

Figure 1. The deduction information specified in can be obtained with database integration. In addition, as soon as the interruption information is created in the relevant systems, the analysis can be run and the results can be obtained by sending the integration area to the web service where the interruption analysis is located.

A geometric network is required for flow direction analysis in the analysis section. The said geometric network is produced in GIS and many processes such as trace analysis can be performed in the flow direction or reverse.

The information or data produced as a result of the analysis can be sent to the relevant fields of the database from which the interruption information is received, as well as to a separate format or structure. In addition,

analysis result information can be published as a message and can be used by many clients in accordance with their systems.

## 4. CONCLUSION

Many data processing systems are used to perform, manage and analyze and report processes in Electricity Distribution Systems. As these systems serve their own purposes, they can produce much more beneficial results and processes by communicating with other systems through integration. The integrations to be realized must be in accordance with the needs and current situation of the relevant institution.

Monitoring and reporting of an outage in Electricity Distribution Systems through systems such as OMS / DMS is carried out in today's technology. It is of great importance to report the number of subscribers affected per outage according to the quality and reliability criteria carefully followed by the relevant institutions and higher institutions. For this reason, it is necessary to integrate GIS and outage or distribution management systems, which can create, protect and analyze the connection model.

In this study, an algorithm is presented on how GIS and OMS / DMS systems can be operatively integrated to obtain the number of subscribers per outage.

With the integration solution produced by realizing the said algorithm, the subscriber and network elements that will be affected by any interruption can be detected instantly and reliably in accordance with the processes. Reports expected for the outage will be produced and actions can be taken to provide corporate-customer benefits.

## REFERENCES

Anonymous, 2020b. What are geometric networks?, https://desktop.arcgis.com/en/arcmap/10.3/manage-data/geometric-networks/what-are-geometric-networks-.htm (Access date: 21.03.2020)

Chakravarty, P., & Wickramasekara, M. G. (2014, March). A better GIS leads to a better DMS. In 2014 Clemson University Power Systems Conference (pp. 1-5). IEEE.

Dönmez, I. M. (2013). Smart Grids and Integration. http://www.emo.org.tr/ekler/07d7d1f0a2dc3ff_ek.pdf (Access date: 15.03.2020)

Emiroğlu C., Tanrıöven K., & Akbulut F. (2007). GIS Applications in Electricity Distribution Companies. National Geographic Information Systems Congress, 30 October –02 November, KTÜ, Trabzon.

Sekhar, A. N., Rajan, K. S., & Jain, A. (2008, November). Spatial informatics and geographical information systems: Tools to transform electric power and energy systems. In TENCON 2008-2008 IEEE Region 10 Conference (pp. 1-5). IEEE.

Service Quality Regulation on Electricity Distribution and Retail Sales (2012, December 21). Official Gazette (Number: 28504). Access address is https://www.mevzuat.gov.tr/Metin.Aspx?MevzuatKod=7.5.16869&MevzuatIliski=0&sourceXmlSearch%20%20=Elektrik%20Da%C4%9F%C4%B1t%C4%B1m

Singh, U., & Caceres, D. (2004, November). An integrated approach for implementing a distribution automation system. In 2004 IEEE / PES Transmision and Distribution Conference and Exposition: Latin America (IEEE Cat. No. 04EX956) (pp. 332-337). IEEE.

Taylor, T., & Kazemzadeh, H. (2009). Integrated SCADA / DMS / OMS: Increasing distribution operations efficiency. Electric Energy T&D Magazine, 1 (1), 31-34.

Yıldırım E. (2020). Creating Electricity Distribution Network Connection Model with Geographical Information System. http://www.emo.org.tr/ekler/51f168282907ed8_ek.pdf (Access date: 15.03.2020)

Zhang K., Zhang S., Huang B.and Ma X. (2019). Research on Integration Technology Between Distribution Automation System and Geographical Information System. In 2009 Asia-Pacific Power and Energy Engineering Conference (pp. 1-4). IEEE.

Intercontinental Geoinformation Days

http://igd.mersin.edu.tr/2020/

# GIS-Based Landslide Susceptibility Mapping Using Frequency Ratio and AHP Methods

**Aslan Cihat Başara*[1], Mehmet Emin Tabar [1], Yasemin Şişman [2]**

[1]*Ondokuz Mayis University, Institute of Graduate Studies, Department of Geomatics Engineering, Samsun, Turkey*
[2]*Ondokuz Mayis University, Faculty of Engineering, Department of Geomatics Engineering, Samsun, Turkey*

**Keywords**
Landslide
Susceptibility mapping
Frequency Ratio
Analytical Hierarchy Process

**ABSTRACT**

In this study, the Landslide Susceptibility Map of Samsun province was produced. Slope classes, altitude classes, land use classes, soil classes, proximity to river networks classes and proximity to fault lines classes were used during the study. The Frequency Ratio method was applied to determine the relationship between the attribute classes of the parameters and the landslide events. Paired comparison matrices were created to determine the weights of the parameters and the Analytical Hierarchy method was applied. Weighted Overlay operation was applied to the classified and weighted map data using ArcMap 10.7 program. As a result of the process, the data were divided into 5 classes and the Landslide Susceptibility Map was produced.

## 1. INTRODUCTION

Disasters are events that can destroy the ability of the society to use its own resources, humanitarian effects, financial and economic problems, or have negative consequences and effects in the context of the environment in which they occur (Reduction, 2009).

The damage caused by disasters is analyzed in Turkey, landslides are seem to be the disasters because of loss of life and property (Ildır, 1995).

Landslides are formed as a result of the downward movement or sliding of parts such as soil and rocks, under the influence of gravity or external factors such as earthquakes and continuous rains (Afet & Başkanlığı, 2014).

The accurate and up-to-date production of landslide susceptibility maps is extremely important to prevent material and moral losses. The production process of these maps requires the evaluation and analysis of all influencing factors together (Kavas, 2009).

In this study, the Landslide Susceptibility Map of Samsun, which is located in the coordinates 41 ° 17 ′ 25 ″ N - 36 ° 20 ′01 E, was produced. Given in Fig 1.


**Figure 1.** Location Map

## 2. MATERIAL AND METHOD

In the literature, it is stated that there is no consensus among researchers about the methods and parameters used during the preparation of landslide susceptibility maps. Many parameters and methods are used because each researcher takes into account the parameters of the field she is working on (Gökçeoğlu & Ercanoğlu, 2001).

### 2.1. Material

The slope, elevation, land use status, soil condition, river networks and fault lines were selected as parameters for the study. The data of the material to be used in the study were mapped using ArcMap program.

Slope, elevation, land-use, river networks, soil, fault lines maps are given in Fig 2-7.

* **Corresponding Author**

*(aslancihatbasara@gmail.com) ORCID ID 0000 – 0001 – 6644 - 6097
(mehmetemintabar@gmail.com) ORCID ID 0000 – 0002 – 3234 - 5340
(ysisman@omu.edu.tr) ORCID ID 0000 – 0002 – 6600 - 0623

**Cite this study**

Basara A.C, Tabar M.E & Sisman Y (2020). GIS-Based Landslide Susceptibility Mapping Using Frequency Ratio and AHP Methods in Samsun Province. Intercontinental Geoinformation Days (IGD), 223-226, Mersin, Turkey

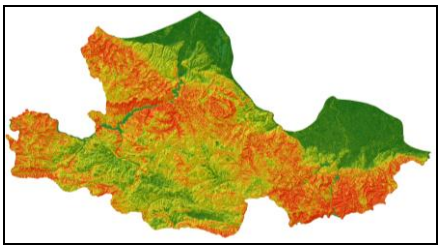

**Figure 2.** Slope Map

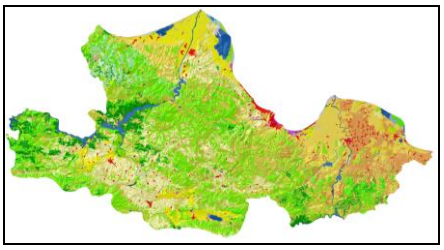

**Figure 4.** Land Use Map

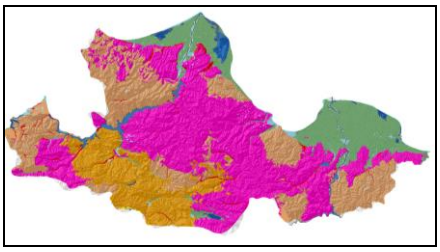

**Figure 6.** Soil Map

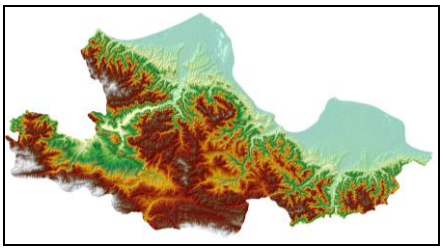

**Figure 3.** Elevation Map

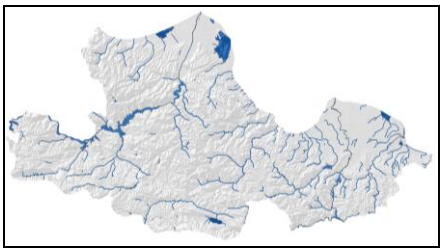

**Figure 5.** River Networks Map

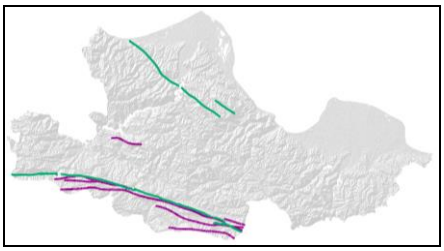

**Figure 7.** Fault Lines Map

### 2.2. Method

In the creation of the landslide susceptibility map, the values of the parameter classes were calculated with the Frequency Ratio Method (FR) by using given in Fig. 2-7 to determine the importance of the parameters and the intervals in which they affect the analysis.

A binary comparison matrix was created using the Analytical Hierarchy Method (AHP). The comparison values used in the method were determined by considering the landslide susceptibility studies and the region characteristics. Landslide Inventory Map is given in Fig 8.

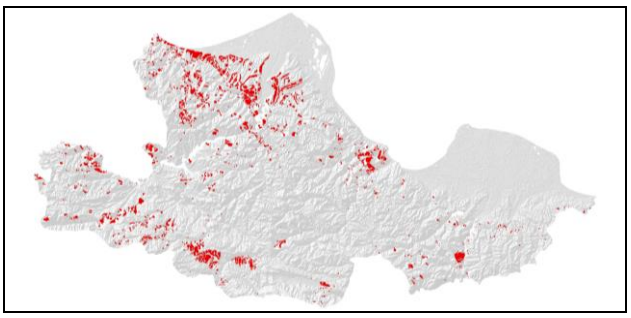

**Figure 8.** Landslide Inventory Map

#### 2.2.1. Frequency Ratio Method

The Frequency Ratio (FR) method is based on density analysis. The basic principle is based on transferring all parameters to the GIS and making density analysis with the landslide inventory map (Lee & Talib, 2005).

Frequency ratio is defined as (b) / (a), where (a) corresponds to the ratio of the number of pixels with landslides in the parameter subgroup to the total number of pixels with landslides, and (b) corresponds to the ratio of the number of pixels of the parameter subgroup in the area considered, to the total number of pixels in the area under consideration (Lee & Talib, 2005).

Slope, elevation, land use, proximity to the stream, soil, proximity to fault lines classes are given in Table 1-6.

**Table 1.** Slope Classes

| Attribute | Landslide area (% b) | Total area (% a) | Frequency ratio (b/a) |
|---|---|---|---|
| 0 – 10 | 22,66 | 33,73 | 0,67 |
| 10 – 20 | 36,08 | 21,21 | 1,68 |
| 20 – 30 | 20,49 | 17,86 | 1,15 |
| 30 – 40 | 12,10 | 13,13 | 0,92 |
| 40+ | 8,66 | 13,71 | 0,63 |

**Table 2.** Elevation Classes

| Attribute | Landslide area (% b) | Total area (% a) | Frequency ratio (b/a) |
|---|---|---|---|
| -27 – 100 | 13,26 | 21,18 | 0,63 |
| 100 – 400 | 33,26 | 17,83 | 1,86 |
| 400 – 700 | 21,65 | 23,65 | 0,92 |
| 700 – 1000 | 24,41 | 27,40 | 0,89 |
| 1000+ | 7,51 | 10,11 | 0,74 |

**Table 3.** Land Use Classes

| Attribute | Landslide area (% b) | Total area (% a) | Frequency ratio (b/a) |
|---|---|---|---|
| Artificial areas | 1,63 | 2,00 | 0,82 |
| Agricultural areas | 67,96 | 52,36 | 1,30 |
| Forest areas | 30,03 | 42,64 | 0,70 |
| Swampy areas | 0,00 | 1,02 | 0,00 |
| Water areas | 0,46 | 2,17 | 0,21 |

**Table 4.** Proximity to River Networks Classes

| Attribute | Landslide area (% b) | Total area (% a) | Frequency ratio (b/a) |
|---|---|---|---|
| 0 – 500 | 3,29 | 6,86 | 0,48 |
| 500 – 1000 | 3,98 | 4,62 | 0,86 |
| 1000 – 2000 | 10,98 | 10,44 | 1,05 |
| 2000 – 3000 | 13,52 | 10,96 | 1,23 |
| 3000+ | 68,31 | 67,31 | 1,01 |

**Table 5.** Soil Classes

| Attribute | Landslide area (% b) | Total area (% a) | Frequency ratio (b/a) |
|---|---|---|---|
| Class A | 1,64 | 2,31 | 0,71 |
| Class B | 22,57 | 23,88 | 0,94 |
| Class C | 18,30 | 13,75 | 1,33 |
| Class D | 1,25 | 1,40 | 0,89 |
| Class E | 0,00 | 0,09 | 0,00 |
| Class F | 0,00 | 0,94 | 0,00 |
| Class G | 0,83 | 14,18 | 0,06 |
| Class H | 0,03 | 0,06 | 0,44 |
| Class I | 55,19 | 41,39 | 1,33 |

**Table 6.** Proximity to Fault Lines Classes

| Attribute | Landslide area (% b) | Total area (% a) | Frequency ratio (b/a) |
|---|---|---|---|
| 0 – 1000 | 16,38 | 7,02 | 2,40 |
| 1000 – 2500 | 13,97 | 6,87 | 2,03 |
| 2500 – 5000 | 14,27 | 8,62 | 1,66 |
| 5000 – 10000 | 19,14 | 17,57 | 1,09 |
| 10000+ | 35,67 | 60,12 | 0,59 |

### 2.2.2. Analytical Hierarchy Process

The Analytical Hierarchy Method (AHP) was developed by L. Saaty in 1977 as a model that will enable the solution of multi-parameter decision making problems (Kavzoğlu, Şahin, & Çölkesen, 2012).

Priority and weight vectors are calculated by normalizing the pairwise comparison matrix. Therefore, the elements in the columns of the matrix are divided by the sum of each column to form a normalized pairwise comparison matrix. The row elements in the new matrix are summed and the value obtained as a result of the sum is divided by the number of elements in the row. In this way, a weight vector or priority vector is created (Kavas, 2009; Tombuş, 2005).

Weights take a value between 0 and 1 and their sum equals 1 (Malczewski, 1999; Öztürk & Batuk, 2010). The weights of this study are given in Table 7.

**Table 7.** Map Weights

| | a | b | c | d | e | f | Weights |
|---|---|---|---|---|---|---|---|
| a | 1 | | | | | | % 17,20 |
| b | 1,00 | 1 | | | | | % 16,60 |
| c | 0,50 | 0,33 | 1 | | | | % 9,10 |
| d | 2,00 | 2,00 | 2,00 | 1 | | | % 22,40 |
| e | 0,50 | 0,50 | 1,00 | 0,50 | 1 | | % 9,50 |
| f | 1,00 | 2,00 | 2,00 | 2,00 | 2,00 | 1 | % 25,20 |

a. slope, b. height, c. land use status, d. soil, e. proximity to river networks, f. proximity to fault lines

The weight of the parameters was calculated after the comparison matrix. The consistency ratio was found as CR = 0.039. Since the ratio we obtained was below 0.10, which is the highest value determined for the correct execution of the study, there was no need to repeat the pairwise comparison method (Wind & Saaty, 1980).

## 3. RESULTS

The parameters to be used in the field of study were determined. The data of the parameters were mapped with the help of Geographical Information Systems.

The maps were weighted by using the Frequency Ratio Method (FR) by calculating the areal rates associated with the landslide inventory map. The data pixels have been reclassified according to their weight.

The weights of the parameters relative to each other were determined using the AHP.

A susceptibility map was produced by applying the weighted registration process. The map produced was reclassified 5 as very low, low, medium, high and very high. Landslide susceptibility map is given in Fig 8.

## 4. DISCUSSION

It was realizen an investigation in the produced landslide susceptibility map with map classes.

Although it was seen that landslides could occur in every class, the highest risk interval was determined as the range of 10-20 degrees with 19.54% in Slope Classes.

When the altitude classes are examined, it was seen that landslide events are less in the range of 0-100 meters. The highest risk interval was determined as the range of 700-1000 meters with 18.56%.

While it was observed that landslide events were less in artificial areas, swampy areas and water areas in the land use classes, the highest risk areas were determined as agricultural areas with a rate of 36.80 %.

In the soil classes, it was observed that landslide events were less in colluvial soil, red yellow podzolic soil, hydromorphic soil, alluvial soil and brown soil classes. The highest risk soils were determined to be brown forest soils with a rate of 32.39 %.

When the proximity to river networks classes are examined it was found that the rate of landslides in each class, although the parameter is not distinctive for the study area.

For the proximity to fault lines classes, it was observed that landslide events are less in areas more than 10 kilometers away. The highest risk range has been determined as the 5-10-kilometer range with 13.85 %.

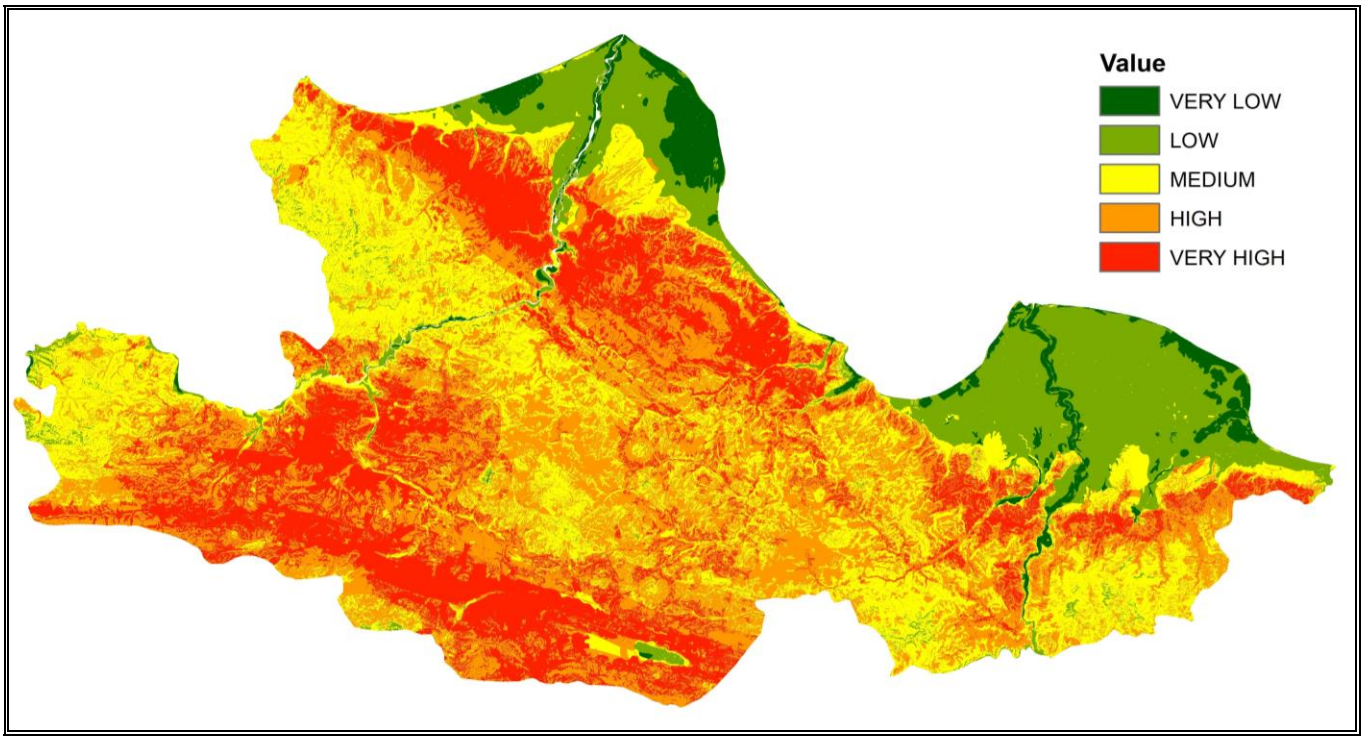


**Figure 8.** Landslide Susceptibility Map

## 5. CONCLUSION

The areas and rates of the landslide susceptibility classes are given in Table 8.

**Table 8.** Landslide Susceptibility Classes

| Attribute | Landslide area ($km^2$) | Total area ($km^2$) | Landslide incident (%) | Total area (%) |
|---|---|---|---|---|
| Very Low | 0,04 | 332,59 | 0,01 | 3,50 |
| Low | 3,57 | 1280,23 | 0,95 | 13,47 |
| Medium | 64,25 | 2364,19 | 17,01 | 24,88 |
| High | 114,29 | 3381,41 | 30,27 | 35,58 |
| Very High | 195,46 | 2144,45 | 51,76 | 22,57 |

When susceptibility classes are examined it was seen that 82.03% of the old landslide events occurred in high and very high class, 17.01% occurred in middle class and 0.96% occurred in low and very low class.

In the spatially analysis of landslide events, it was seen that the sensitivity classes are examined spatially, high-risk areas constitute 58.15% of all areas, medium-risk areas constitute 24.88% of all areas and low-risk areas constitute 16.97% of all areas.

Landslide susceptibility maps are of great importance in predicting future landslides and ensuring land use planning.

As a result, it is possible to say the following. Risk analysis methods should definitely be used in order to prevent future financial and moral losses caused by landslides that occur in different spatial structures.

## REFERENCES

Afet, T. B., & Başkanlığı, A. D. Y. (2014). Açıklamalı Afet Yönetimi Terimleri Sözlüğü. *TC Başbakanlık Afet ve Acil Durum Yönetimi Başkanlığı Deprem Dairesi Başkanlığı, Ankara*.

Gökçeoğlu, C., & Ercanoğlu, M. (2001). Heyelan duyarlılık haritalarının hazırlanmasında kullanılan parametrelere ilişkin belirsizlikler. *Yerbilimleri Dergisi, 22*(23), 189-206.

Ildır, B. (1995). Türkiye'de Heyelanların Dağılımı ve Afetler Yasası İle İlgili Uygulamalar. *Ulusal Heyelan Sempozyumu Bildiriler Kitabı, Sakarya*, 1-9.

Kavas, E. (2009). Analitik hiyerarşik süreç yöntemiyle İzmir ilinde heyelan duyarlılığının coğrafi bilgi sistemleri tabanlı incelenmesi. *TMMOB Coğrafi Bilgi Sistemleri Kongresi. İzmir*.

Kavzoğlu, T., Şahin, E. K., & Çölkesen, İ. (2012). Heyelan Duyarlılığının İncelenmesinde Regresyon Ağaçlarının Kullanımı: Trabzon Örneği. *Harita Dergisi, 147*(3), 21-33.

Lee, S., & Talib, J. A. (2005). Probabilistic landslide susceptibility and factor effect analysis. *Environmental Geology, 47*(7), 982-990.

Malczewski, J. (1999). *GIS and multicriteria decision analysis*: John Wiley & Sons.

Öztürk, D., & Batuk, F. (2010). Konumsal karar problemlerinde analitik hiyerarşi yönteminin kullanılması. *Yıldız Teknik Üniversitesi Sigma Mühendislik ve Fen Bilimleri Dergisi, 28*, 124-137.

Reduction, D. R. (2009). UNISDR terminology on disaster risk reduction: Bangkok.

Tombuş, F. E. (2005). *Uzaktan algılama ve coğrafi bilgi sistemleri kullanılarak erozyon risk belirlemesine yeni bir yaklaşım, Çorum ili örneği.* Anadolu Üniversitesi.

Wind, Y., & Saaty, T. L. (1980). Marketing applications of the analytic hierarchy process. *Management science, 26*(7), 641-658.

## Surveying and Geodesy – 3

**Tropopause Height Variabilities Derived from COSMIC GNSS Radio Occultation Observations over Nigeria**

*Olalekan Isioye*, Mefe Moses, Usman Ibrahim Sai, Ebenezer Ayobami Akomolafe*

**A Study on Comparison of Observed and Derived Gravity Data**

*Serkan Doğanalp*

**The Accuracy Assessment of Terrestrial and Mobile Lidar Systems for 3D Modeling**

*Ramazan Alper Kuçak*, Serdar Erol, Mehmet İşiler*

**Identifying the best fitting 3D deformation model using information criteria**

*Alaz Andaç Ortaköy*, Cüneyt Aydın*

**An experimental study on the effect of antenna orientation on GNSS-IR**

Cemali Altuntaş*, Nursu Tunalıoğlu

Intercontinental Geoinformation Days

http://igd.mersin.edu.tr/2020/

# Tropopause Height Variabilities Derived from COSMIC GNSS Radio Occultation Observations over Nigeria

**Olalekan Adekunle Isioye*[1], Mefe Moses [1], Ibrahim Usman Sai [1], Ebenezer Ayobami Akomolafe [1]**

[1]*Ahmadu Bello University, Faculty of Environmental Design, Department of Geomatics, Zaria, Nigeria*

**Keywords**
GNSS Radio Occultation
Tropopause Height
Radiosonde
Climate change

**ABSTRACT**

This paper investigates the use of GNSS radio Occultation (RO) technique for tropopause height estimation over Nigeria. The changes or variations in the tropopause height is/are key indicators to anthropogenic climate change in the different region of the world. In this study, RO data from the Formosat-3/COSMIC (Formosa Satellite Mission 3/Constellation Observing System for Meteorology, Ionosphere, and Climate) mission for the period of 2012-2016 were used to probe the tropopause height over Nigeria. Firstly, the atmospheric profiles from the COSMIC mission were checked with ground in-situ observations (radiosonde) at two different epochs and good agreement was established between the two observing systems. The COSMIC mission is able to map the variations in solar illumination as represented in the tropopause height variation over the Nigerian region. The tropopause height varies between 15 and 18km across the different seasons and a typical range of difference between -0.235 to 3.125km was recorded between the COSMIC RO and radiosonde observations. In view of the great potential that the COMIC RO has demonstrated, the study recommends for further exploration of the troposphere utilizing datasets from recent and expected follow-on missions for the different RO missions.

## 1. INTRODUCTION

The Global Navigation Satellite System (GNSS) Radio Occultation (RO) technique is an innovative approach for probing the Earth's atmosphere and ionosphere using GNSS receivers on-board Low Earth Orbit (LEO) satellites (see, Kursinski et al. 1995).

The GNSS RO technique provides global coverage, all-weather capability, long-term measurement stability, high vertical resolution and high-accuracy measurements in the middle to upper troposphere, stratosphere and ionosphere for monitoring global temperatures, pressures, and moisture distributions.

The GNSS RO has been invaluable for many aspects of atmospheric and climate-related studies that rely on high-resolution atmospheric observations (see, Kuleshov et al. 2016). Studies have demonstrated the potential of GNSS RO profiles for characterizing troposphere structures and changes (Liu et al. 2014). For other examples, the global gravity wave signatures in the upper troposphere and stratosphere can be obtained from GNSS RO profiles (Alexander et al., 2008; Torre et al. 2009). Studies of atmospheric waves, turbulences and tides have been carried out using GNSS RO data (Zeng et al., 2008; Cornman et al. 2009).

One atmospheric parameter that is important to monitor with GNSS RO is the height of tropopause. The tropopause is the region between troposphere and stratosphere. The troposphere is the layer of the atmosphere closest to the earth´s surface, which extends to about 18 km above sea level. Between the troposphere and the stratosphere, there is a middle layer called the tropopause. The tropopause plays a key role in the upper troposphere and lower stratosphere (UTLS) by affecting chemical tracers exchange. Changes in height of the global or regional tropopause can be an indicator of anthropogenic climate change (Santer et al. 2003).

Conventionally, radiosonde observations are used for atmospheric profiling in many parts of the world, the accuracy measurement from radiosonde observations as an in-situ observation system is well documented and often used to validate other systems (see, i.e., Soden and Lanzante, 1996; Soden et al. 2004). However, the spatial and temporal distribution of radiosonde observations is a disturbing issue in Nigeria and many other African countries alike. Thus, there is the need to explore potentials of other observing systems with better spatial resolution of which the GNSS RO technique is a topmost contender in this regard.

In this study we present preliminary discussions on the structure of the tropopause over Nigeria as derived from GNSS RO observations from the Taiwan/U.S. Formosat- 3/COSMIC (Formosa Satellite Mission 3/Constellation Observing System for Meteorology, Ionosphere, and Climate) (Anthes et al., 2008), which was launched in 2006.

* **Corresponding Author**

*(olalekanisioye@gmail.com) ORCID ID 0000 – 0001 – 5734 – 5374
(mefemoses@gmail.com) ORCID ID 0000 – 0003 – 4029 – 3736
(saeeusmansai@gmail.com) ORCID ID 0000 – 0001 – 9810 – 9554
(goldera2787@gmail.com) ORCID ID 0000 – 0001 – 6797 – 0114

**Cite this study**

Isioye O.A, Moses, M., Ibrahim, S.U. & Akomolafe E.A (2020). Tropopause Height Variabilities Derived from COSMIC GNSS Radio Occultation Observations over Nigeria. Intercontinental Geoinformation Days (IGD), 227-231, Mersin, Turkey

## 2. METHOD

To discuss the structure of the tropopause over Nigeria from COSMIC GNSS RO observation, we first validated the quality of atmospheric profiles from the COSMIC mission using available Radiosonde data. Thereafter the estimated tropopause height was also validated with the same radiosonde data.

Records from the Integrated Global Radiosonde Archive (IGRA, www.ncdc.noaa.gov ) show very low data record for the region of Nigeria. Fig. 1 shows the record of radiosonde stations around Nigeria. The IGRA is the most comprehensive record of radiosonde data in the world; they provide sounding-derived parameters at fixed observing stations. The IGRA record indicates that most of the radiosonde stations in Nigeria are not functional as only one station (WMO no: 65125) has few data records in recent times, other stations do not have data record is at least the last 25 years.

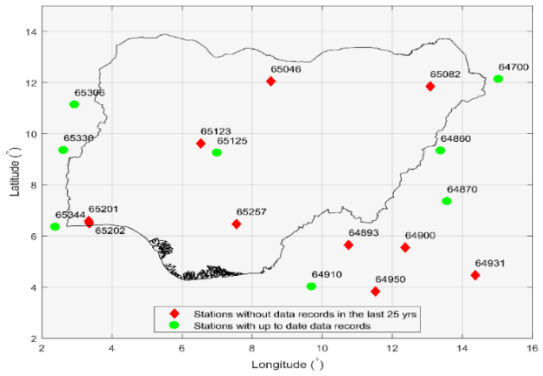


**Figure 1**. Distribution of Radiosonde Stations (with WMO Id) around the Nigerian Region based on Records from the IGRA, stations with up-to-date data records are marked in green diamond symbol

### 2.1. Evaluating Atmospheric Profiles from COSMIC GNSS RO

The GNSS RO data are accessible as single profiles comprising of bending angle, refractivity, temperature, pressure, and geopotential height in the altitude range up to 40 km for all RO missions processed at the COSMIC data analysis and archive centre (CDAAC, https://cdaac-www.cosmic.ucar.edu/cdaac/products.html). The horizontal resolution of is around 200 km with a less than 100 km horizontal drift at the height of its tangent point for each profile. The vertical resolution of each profile is ~100 m to 200 m in the lower troposphere and ~1400 m in the stratosphere. The temporal resolution is about +/- 4hrs for each profile and randomly distributed in space.

To verify the effectiveness of the profiles of temperature, pressure, refractivity, and water vapour pressure in the atmosphere over the Nigerian region from COSMIC. We collected COSMIC RO data at two epochs in 2012 and 2016, each of the epoch consists of five (5) RO events occurring during that year at distances not greater than 200 km from the radiosonde launch at Ndamena (WMO No: 64700). These COSMIC RO events are presented in Table 1. The ten (10) GNSS RO events were collected as wetPrf files in Network Common Data Form (NetCDF) format, the quality flag in all the ten (10) events indicated "bad=0" implying that all passed the quality control successfully.

**Table 1.** *COSMIC RO event near radiosonde launch site (WMO No: 64700)*

| Date | Long (°) | Lat (°) | COSMIC RO Events |
|---|---|---|---|
| **Epoch 1** | | | |
| **11 Jan 2012** | 14.015 | 12.978 | C001.2012.011.14.13.G10 |
| **15 Feb 2012** | 14.665 | 13.061 | C006.2012.046.14.44.G01 |
| **28 Jun 2012** | 14.115 | 12.059 | C002.2012.180.02.39.G08 |
| **4 Jul 2012** | 14.619 | 13.787 | C002.2012.186.12.24.G14 |
| **03 Oct 2012** | 14.720 | 12.549 | C002.2012.277.08.55.G15 |
| **Epoch 2** | | | |
| **10 May 2016** | 15.946 | 12.077 | C001.2016.131.07.58.G15 |
| **30 Jun 2016** | 15.168 | 13.836 | C002.2016.182.19.45.G09 |
| **9 Jul 2016** | 15.068 | 13.943 | C001.2016.191.11.00.G15 |
| **11 Jul 2016** | 14.889 | 11.830 | C001.2016.193.19.08.G28 |
| **26 Jul 2016** | 15.249 | 12.997 | C001.2016.208.18.50.G32 |

The COSMIC atmospheric profiles were at different vertical resolutions with the radiosonde. So, MATLAB interpolation code utilizing the '*interp1*' function was used to interpolate the height of profiles of temperature, pressure, refractivity and water vapour pressure from COSMIC GNSS RO to the same height as those of the radiosonde to enhance the comparison of the two. The height of the radiosonde profile typically ranges from 0.295km to about 30km. To avoid extrapolation errors, profiles from COSMIC that are less than the original height from the COSMIC file are excluded from the results of the interpolation.

### 2.2. The Estimation of Tropopause Height from COSMIC GNSS RO Observations

The World Meteorological Organisation (WMO) (1957) has defined the tropopause as "the lowest level at which the lapse rate decreases to $2K/km$ or less, provided that the average lapse rate between this level and all higher levels within 2 km does not exceed $2K/km$", which is also known as thermal tropopause. The lapse rate is calculated using the following relation;

$$\delta T_i = (T_{i+1} - T_i)/(H_{i+1} - H_i) \qquad (1)$$

In the equation (1), $T$ and $H$ represents the temperature and altitude respectively of individual RO profile at specific pressure level. Starting from lower to higher altitude levels at the first point where $dT/dH > -2K/km$ and the average lapse rate between this level and all higher levels within 2 km does not fall below $-2K/km$ is the tropopause height.

The thermal definition of the tropopause was adopted to determine the tropopause height using COSMIC observations. To avoid unrealistically high or low tropopause heights and to increase computational speed, the search range for the algorithm is limited to between 550 hPa and 75 hPa (approx. 5–18 km). If the calculated tropopause exceeds one of these limits, the result is rejected. Based on this condition, a total of 1223 profiles of occultation events from the COSMIC mission for the period of 2012-2016 were processed. To investigate seasonal variations in tropopause height, the

RO events were grouped into four seasonal groups that typically represents the seasons in Nigeria, i.e., December-January-February (DJF), March-April-May (MAM), June-July-August (JJA), and September-October-November (SON).

To ascertain the efficacy of the results from the RO technique, we computed the tropopause height utilising datasets (temperature and geopotential height) from a numerical weather model (ERA-Interim) of the European Centre for Medium weather forecast(ECMWF) (see De et al., 2011). The monthly temperature and geopotential height from the ERA-Interim was obtained from http://apps.ecmwf.int /dataset/data/interim-full-monthly/ and the tropopause height was computed using the thermal definition as presented herein.

To further ascertain the agreement between GNSS RO derived tropopause height and that from radiosonde, we found and calculated the difference between the duo techniques for occultation events at a maximum distance of 200km from the radiosonde site (WMO no: 64777). It would have been ideal to consider more radiosonde sites to gain a more comprehensive insight into the variation and trend of the tropopause as observed by the duo, we are constrained by availability of sounding observations from radiosondes in the region.

## 3. RESULTS AND DISCUSSION

### 3.1. Accuracy of Atmospheric Profiles from COSMIC

The Figs. 2 and 3 depict the difference between profiles of temperature, pressure, refractivity, and water vapour pressure at the respective common heights of the profiles for the two epochs (2012 and 2016).

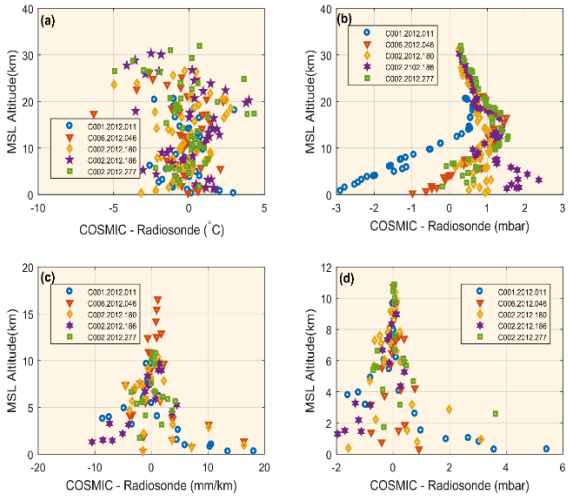


**Figure 2**. Shows the differences between a) temperature, b) pressure, c) refractivity, and d) water vapour pressure from FORMOSAT-3/COSMIC RO and radiosonde against the altitudes in 2012

From Figs. 2 and 3, it is evident that the differences in temperature profile between COSMIC and radiosonde are larger than that of the other profiles (pressure, refractivity, and vapour pressure). There was no clear pattern as to the difference between the COSMIC and radiosonde data; the differences range from -5.79 to +5.76 Celsius. There were more negative differences, which indicated that radiosonde reports hotter temperature over the region. A look at the pressure profiles gives a result quite different from that of the temperature profile. From Figs. 7 and 8, the differences between the pressure estimates along the profile seem to converge toward zero with an increase in altitude. Thus, larger pressure differences between the two datasets in the troposphere are found when compared with those in the stratosphere. The differences in pressure estimates along the profile range from -2.89 to +2.98 mbar. The results of the refractivity and water vapour pressure are quite promising and have a very clear pattern; it can be seen from the Figs. 2&3 that the agreement between COSMIC and radiosonde refractivity and water vapour pressure profiles is stronger at an altitude greater than 7km. A more general look at all the profiles can further reveal that COSMIC profiles don't agree with radiosonde profiles at a very low altitude of less than 7-10 km, this observation corroborates the fact GNSS RO profiles are not suitable low troposphere studies. The results from the various comparisons are evident in the quality of observations from the GNSS RO technique. However, a more comprehensive comparison test may be required which is out the scope of the current paper.

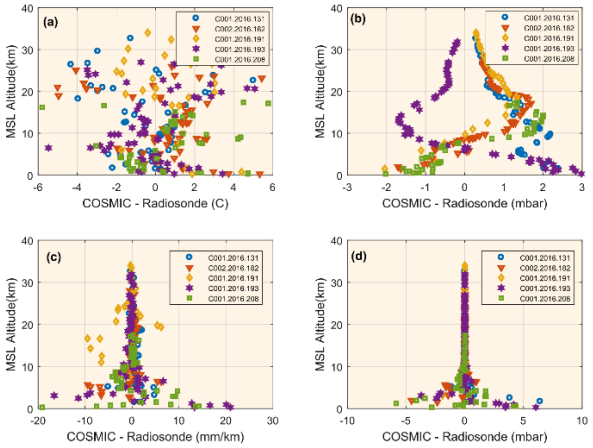


**Figure 3**. Shows the differences between a) temperature, b) pressure, c) refractivity, and d) water vapour pressure from FORMOSAT-3/COSMIC RO and radiosonde against the altitudes in 2016

The Fig. 4 depicts the distribution of the combined differences between the two epochs of 2012 and 2016 for the COSMIC and radiosondes observations. The absolute mean value for the temperature difference was estimated at $1.42\,^{\circ}C$ with a standard deviation of $1.21\,^{\circ}C$. The pressure profiles showed a better agreement between the observing systems than that of the temperature profiles. The absolute mean value and standard deviation of the residuals stood at 0.97 and 0.58 mbar, respectively. Fig.4 is also able to reveal that pressure value is higher from COSMIC for most of the height profiles. It can be seen in Fig.4 that the refractivity and water vapour pressure profiles agreed well with each from the COSMIC and radiosondes observations, the frequency of near zero differences or residual were very high and thus clearly demonstrates the efficacy of the observing systems.

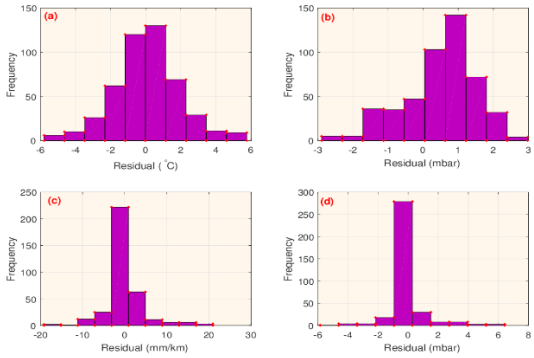


**Figure 4.** Frequency plot of residuals of between COSMIC and radiosonde atmospheric Profiles, a) is the temperature, b) pressure, c) refractivity , and d) water vapour profiles

### 3.2. Results of Tropopause Height from COSMIC and ERA-Interim

The Fig. (5) shows a clear seasonal variation in tropopause height within 10-18km with highest values during MAM. The months of March, April and May (MAM) are the hottest in the north, with few records of rain in the southern part of Nigeria. The average tropospheric temperature controls the tropopause height. This accounts for the high tropopause heights in the summer (MAM). The lowest tropopause height values were recorded in DJF, during this season, the northern part of Nigeria is dry with very low temperature because of the Harmattan, while the south is also dry and humid. Also from the Fig. (5), high tropopause values were reported in JJA, though much lower than MAM and higher than in SON. The peak of the wet season in all parts of Nigeria is in the months of June, July and August (JJA). The months of September, October and November (SON) signify the end of the wet season in the north, while in the south, it is a period often characterised by scanty rains and severe thunderstorms. From the foregoing, it is evident that there is a high variation in solar illumination through the year over Nigerian region and the GNSS RO technique is able to map the variations in solar illumination as represented in the tropopause height variation over the region.

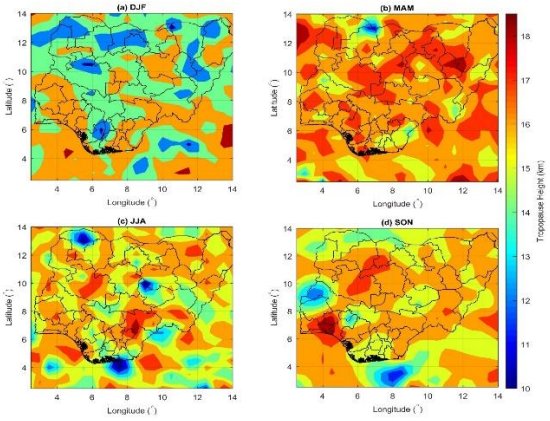


**Figure 5.** Seasonal mean tropopause height, a) DJF, b) MAM, c) JJA, c) SON derived from COSMIC for the period of 2012-2016 over the Nigerian region

The Fig.6 presents the seasonal estimates of the tropopause height over the Nigerian region from ERA-Interim dataset for the period of 2012-2016.

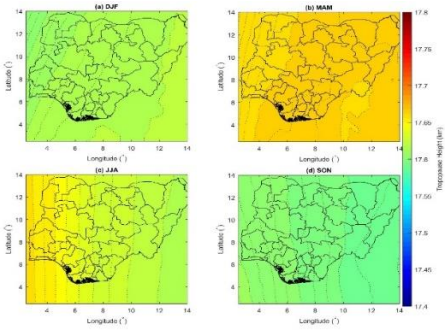


**Figure 6.** Seasonal mean tropopause height, a) DJF, b) MAM, c) JJA, d) SON derived from ECMWF for the period of 2012-2016 over the Nigerian region

A comparison of the seasonal pattern of GNSS RO and Era-Interim from Figs. ((5) and (6)) reveals a similar cyclic behaviour across the different seasons, however, it can be seen that in terms of the averaged seasonal variations, the Era-Interim tropopause height doesn't show any significant variation over Nigeria. The estimated tropopause from the Era-Interim is typically about 17km. The difference in the tropopause height between ERA-Interim and GNSS RO can sometimes times be larger than 5km and this layer difference may arise due to the low change in vertical temperature gradient. This low variability in temperature gradient leads to the higher/lower tropopause heights than actual tropopause height. Overall, GNSS RO captures the variability in the vertical temperature gradient better.

### 3.3. Accuracy of Tropopause Height from COSMIC

The summary of the result is presented in Table 2 for the four seasons, in some of the seasons there were no occultation events within the 100km buffer zone from the GNSS station(s).

**Table 2.** Difference in estimated tropopause height from COSMIC and radiosonde observations

| COSMIC RO Events & ( Date) | Tropopause height (km) | | |
|---|---|---|---|
| | COSMIC | Radiosonde | Difference |
| EPOCH 1 | | | |
| C001.2012.011.14.13.G10 (11 January 2012) | 17.550 | 14.425 | 3.125 |
| C006.2012.046.14.44.G01 (15 February 2012) | 16.894 | 15.405 | 1.489 |
| C002.2012.180.02.39.G08 (28 June 2012) | 15.650 | 16.165 | -0.515 |
| C002.2012.186.12.24.G14 (4 July 2012) | 15.850 | 16.085 | -0.235 |
| C002.2012.277.08.55.G15 (03 October 2012) | 17.050 | 15.745 | 1.305 |
| EPOCH 2 | | | |
| C001.2016.131.07.58.G15 (10 May 2016) | 14.850 | 16.825 | -1.975 |
| C002.2016.182.19.45.G09 (30 June 2016) | 17.050 | 10.485 | 6.565 |
| C001.2016.191.11.00.G15 (9 July 2016) | 16.750 | 16.585 | 0.165 |
| C001.2016.193.19.08.G28 (11 July 2016) | 15.150 | 14.885 | 0.265 |
| C001.2016.208.18.50.G32 (26 July 2016) | 15.550 | 16.385 | -0.835 |

As a final point, though the foregoing discussions were based on a single GNSS RO mission. The determined tropopause heights from COSMIC data and its agreement with in-situ observations from radiosonde over the Nigeria region clearly demonstrate the significance and the great potential of the GNSS RO technique. These results indicate that the GNSS RO derived tropopause height is a strong climate fingerprint and can be used for the observation of different trace constituents within the troposphere and give a better understanding of the transition region between the troposphere and stratosphere over the Nigerian region.

## 4. CONCLUSION

The paper presents the results of preliminary probes into the quality of atmospheric profiles from COSMIC GNSS RO and their consequential impact on the understanding of the tropopause height variability in the Nigerian region. Atmospheric profiles (temperature, refractivity, pressure, water vapour pressure) from COSMIC GNSS RO provided very high quality results from comparison with radiosonde observations. The GNSS RO technique is in no doubt capable of providing superior (vertical, horizontal and temporal) resolutions for atmospheric observations as compared to the radiosonde. The GNSS RO technique is able to map the variations in solar illumination as represented in the tropopause height variation over the Nigerian region. The tropopause height had some evidence of seasonal variability with value ranges of 15 to 17km. Even though, the Space-based instruments offer even broader (hypothetically global) coverage than national or regional ground-based networks now, it is likely to become more useful for climate monitoring as the time series lengthens. Certainly, climatology will benefit significantly from the high accuracy, high-resolution and consistent information to be obtained from future missions as the number of RO events will increase over Nigeria. The importance of applying the GNSS RO meteorological technique in Nigeria will be never underestimated since Nigeria has large landmass (with limited weather observation stations), and large areas surrounded by ocean.

## ACKNOWLEDGEMENT

The authors acknowledge the ECMWF, IGRA and CDAAC for the ERA-Interim, Radiosonde, and COSMIC GNSS RO data respectively. We remain thankful to all reviewers as well.

## REFERENCES

Alexander, P, de la Torre, A & Llamedo, P (2008). Interpretation of gravity wave signatures in GPS radio occultation, *Journal of Geophysical Research*, 113, doi:10.1029/2007jd009390.

Anthes, R A, Bernhardt, P A, Chen, Y, Cucurull, L, Dymond, K F, Ector, D, Healy, S B, Ho, S P, Hunt, D C, Kuo, Y H, Liu, H, Manning, K, McCormick, C, Meehan, T K, Randel, W J, Rocken, C, Schreiner, W S, Sokolovskiy, S V, Syndergaard, S, Thompson, D C, Trenberth, K E, Wee, T K, Yen, N L & Zeng, Z (2008). The COSMIC/FORMOSAT-3 mission: Early results, *Bull. Am. Meteorol. Soc*., 89, 313–333, doi:10.1175/BAMS-89- 3-313.

Cornman, L B, Weekley, A, Goodrich, R K & Frehlich, R (2009). Using airborne GNSS receivers to detect atmospheric turbulence. In Steiner, A, Pirscher, B, Foelsche, U, and Kirchengast, G (Eds.), *New Horizons in Occultation Research Studies in Atmosphere and Climate,* Springer, pp.315.

Kuleshov Y, Choy S, Fu E F, Chane-Ming F, Liou Y A & Pavelyev A G (2016). Analysis of Meteorological Variables in the Australasian Region using Ground and Space Based GPS Techniques. *Atmospheric Research,* 176-177(2016):276-289, http://dx.doi.~org/10.1016/j.atmosres.2016.02.021

Kursinski E R, Hajj G A, Hardy K R, Romans L J & Schofield J T (1995). Observing tropospheric water vapour by radio occultation using the Global Positioning System, *Geophysical Research Letters*, 22(1995): 2365-2368.

Liu Y, Xu T & Liu J (2014). Characteristics of the seasonal variation of the global tropopause revealed by COSMIC/GPS data. *Advances in space research,* 54:2274-2285. http://dx.doi.org/10.1016/j.asr~.2014. 08.020 .

Santer B D, Sausen R, Wigley T M L, Boyle J S, AchutaRao K, Doutriaux C, Hansen J E, Meehl G A, Roeckner E, Ruedy R, Schmidt G & Taylor K E (2003). Behaviour of tropopause height and atmospheric temperature in models, reanalyses, and observations: Decadal changes, Journal of Geophysical Research, vol. 108, no. D1, p. 22.

Soden B J, Turner D D, Lesht B M & Miloshevich L M (2004). An analysis of satellite, radiosonde, and lidar observations of upper tropospheric water vapour from the Atmospheric Radiation Measurement program. *J. Geophys. Res.*, 109(D04105), doi:10.1029/2003JD003828.

Soden B M & Lanzante J R (1996). An assessment of satellite and radiosonde climatologies of upper-tropospheric water vapour. *J. Climate*, 9:1235-1250.

Son S W, Tandon N F & Polvani L M (2011). The fine-scale structure of the global tropopause derived from COSMIC GPS radio occultation measurements. *J. Geophys. Res.* 116(D20113), http://dx.doi.org/10.1029/2011JD016030 .

Torre, A D L, Alexander, P, Llamedo, P, Schmidt, T & Wickert, J (2009). Recent advances in gravity wave analysis from long term Global GPS radio occultation observations. In Steiner, A., Pirscher, B., Foelsche, U., Kirchengast (Eds.), *New Horizons in Occultation Research Studies in Atmosphere and Climate*, G., Springer, pp.315.

Zeng, Z, Randel, W J, Sokolovskiy, S V, Deser, C, Kuo, Y H, Hagan, M, Du, J & Ward, W (2008). Detection of migrating diurnal tide in the tropical upper troposphere and lower stratosphere using the Challenging Minisatellite Payload radio occultation data, *Journal of Geophysical Research,* 113:12.

Intercontinental Geoinformation Days

http://igd.mersin.edu.tr/2020/

# A Study on Comparison of Observed and Derived Gravity Data

**Serkan Doğanalp**[*1]

[1]*Konya Technical University, Faculty of Engineering and Natural Sciences, Department of Geomatic Engineering, Konya, TURKEY*

**Keywords**
Global Geopotential Models
Gravity
EGM2008
GOCE
GRACE

**ABSTRACT**

In studies in earth sciences such as geodesy and geophysics, it is important to determine the gravity field as precisely as possible. In the determination of this field, it is quite common to use data sets obtained from satellites as well as terrestrial measurements. Especially, thanks to Low Earth Orbits (LEO), research conducted to determine the gravity field of the earth has gained speed in recent years. CHAMP (CHAllenging Minisatellite Payload-2000), GRACE (Gravity Recovery And Climate Experiment-2002) and GOCE (Gravity field and steady-state Ocean Circulation Explorer-2009) satellites are at the top of these satellites, respectively. The data collected from these satellites has contributed and continues to contribute to the production of many Global Geopotential Models (GGMs). This study aimed to demonstrate the performance of the eight Global Geopotential Models published by ICGEM (International Centre for Global Earth Models). In this context, the results were evaluated by making a numerical comparison between the gravity values obtained from the GGMs and the observed gravity data.

## 1. INTRODUCTION

The definition of height can be defined, in the most general sense, as the distance between a point on the ground and the starting surface. Heights may have definitions that are physical and geometric. In general, in engineering applications, it is more fitting to use heights related to gravity, i.e. physical heights. Determining the performance of GGMs produced by many scientists using different data sets is still one of the issues that are being studied. In addition, many scientists conduct regional and global tests in different geographies of the world in order to reveal the performances of GGMs and share the results with the scientific world. Various methods and approaches have been suggested by scientists while conducting these tests. For example, one of the most common methods used to determine the best GGM for a region's gravity field is to compare GGMs using independent data sets. These independent datasets are GNSS/leveling, gravity, etc. (Doğanalp 2016).

As gravity force, the sum of centrifugal and gravity forces on an object is described. Determining the gravitational field of the earth is the same as determining its potential. Since this potential is harmonic from earth-forming masses, spherical harmonic series are typically used to determine the field of gravity (Kaula 1966; Heiskanen and Moritz 1984; Rummel et al. 2002; Seeber 2003; Hofmann-Wellenhof and Moritz 2005; Doğanalp 2016). In this study, gravity values will be calculated with Global Geopotential Models (GGMs) and information about their sensitivity will be given by comparing with observed gravity values.

## 2. METHOD

GGMs are generally split into three basic classes. These are models, satellite-only models, combined models and tailored models. In the first models, the coefficients of these GGMs are derived from orbit deviation analyses of artificial earth satellites. The second model is generated by combining satellite altimeter data in marine areas, terrestrial gravity observations, gravity data derived from satellite data, and airborne gravimetry. The last models are produced as a result of improving harmonic coefficients of GGMs using special mathematical techniques within the first and second models (Vaníček and Featherstone 1998; Featherstone 2002; Doğanalp 2016). GGMs are described in various wavelengths as spherical harmonic coefficients representing the gravity field of the earth. From satellite orbit deviation analyses, satellite altimeter data, gravity gradiometer data, and gravimeter data,

* **Corresponding Author**

*(sdoganalp@ktun.edu.tr) ORCID ID 0000 – 0001 – 7229 – 6355

**Cite this study**

Doğanalp S (2020). A Study on Comparison of Observed and Derived Gravity Data. Intercontinental Geoinformation Days (IGD), 232-235, Mersin, Turkey

these coefficients are obtained. The gravity value is obtained by Eq (1). This equation is calculated from spherical harmonics.

$$g=\sqrt{\left[W_{ar}+\Phi_r\right]^2+\left[\frac{1}{r\cos\phi}\left(W_{a\lambda}+\Phi_\lambda\right)\right]^2+\left[\frac{1}{r}\left(W_{a\phi}+\Phi_\phi\right)\right]^2}$$

$$W_{ar}=-\frac{GM}{r^2}\sum_{n=0}^{n_{max}}\left(\frac{R}{r}\right)^n(n+1)\sum_{m=0}^{n}P_{nm}(\sin\phi)(C_{nm}\cos m\lambda+S_{nm}\sin m\lambda)$$

$$W_{a\lambda}=\frac{GM}{r}\sum_{n=0}^{n_{max}}\left(\frac{R}{r}\right)^n\sum_{m=0}^{n}m\,P_{nm}(\sin\phi)(S_{nm}\cos m\lambda-C_{nm}\sin m\lambda)$$

$$W_{a\phi}=\frac{GM}{r}\sum_{n=0}^{n_{max}}\left(\frac{R}{r}\right)^n\sum_{m=0}^{n}\frac{\partial P_{nm}(\sin\phi)}{\partial\phi}(C_{nm}\cos m\lambda+S_{nm}\sin m\lambda)$$

$$\Phi_r=\omega^2 r\left(\cos\phi\right)^2$$
$$\Phi_\lambda=0 \qquad (1)$$
$$\Phi_\phi=-\omega^2 r^2\cos\phi\,\sin\phi$$

where $r$, $\phi$, $\lambda$ are the spherical geocentric coordinates of the computation point: radial distance, co-latitude and longitude, respectively, $GM$ is the gravitational constant $(G)$ times mass $(M)$ of the earth, $R$ is the mean earth's equatorial radius, $C_{nm}, S_{nm}$ are fully normalized geopotential coefficients with degree $n$ and order $m$, $P_{nm}$ fully normalized associated Legendre functions, and $n_{max}$ is the maximum degree of the GGM (Barthelmes 2013; Turgut 2016).

## 3. RESULTS

In this study, 2918 data points of gravity used as of March 21, 2016, in the Milford, Utah FORGE project were used. This data set compared the performance of the GGMs produced in recent years with some of the models produced in previous years. For detailed information about the data set, please see the reference given in the references section. The data set consists of latitude and longitude (decimal degrees), ellipsoidal height (m), gravity observed (mGal), terrain correction of the inner zone (mGal), terrain correction of the outer zone (mGal), values of the free air anomaly (mGal) and values of the complete Bouguer gravity anomaly (mGal).

**Table 1.** Characteristics of GGMs

| Model Name | Year | $n_{max}$ | Data | References |
|---|---|---|---|---|
| AIUB-CHAMP01S | 2007 | 70 | S(Champ) | Prange et al. 2009 |
| EGM2008 | 2008 | 2190 | A,G, S(Grace) | Pavlis et al. 2008 |
| ITU_GGC16 | 2016 | 280 | S(Goce) S(Grace) | Akyilmaz et al. 2016 |
| GOCO06s | 2019 | 300 | S | Kvas et al. 2019 |
| EIGEN-GRGS. RL04.MEAN-FIELD | 2019 | 300 | S | Lemoine et al. 2019 |
| ITSG-Grace2018s | 2019 | 200 | S(Grace) | Mayer-Gürr et al. 2018 |
| GO_CONS_GCF_ 2_TIM_R6e | 2019 | 300 | G(Polar) S(Goce) | Zingerle et al. 2019 |
| XGM2019e _2159 | 2019 | 2190 | A,G,T S(GOCO06s) | Zingerle et al. 2019 |

S: satellite tracking data, G: gravity (ground) data,
A: satellite altimetry data, T: topography

The gravity values of the 2918 points used in the study were obtained separately for the GGMs given in Table 1 with the help of the calculation service on the International Centre for Global Earth Models (ICGEM) website (http://icgem.gfz-potsdam.de/ICGEM). The gravity differences obtained from the GGMs are shown in Figure 1. For a better understanding of the difference values, the difference values were transferred to histogram graphics and reinforced with statistical information (Figure 2). The statistical information obtained as a result of the evaluation of the GGMs is presented in Table 2.

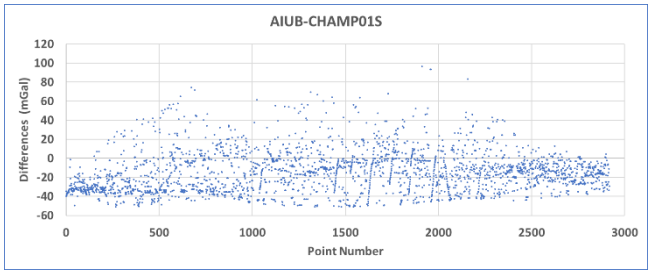


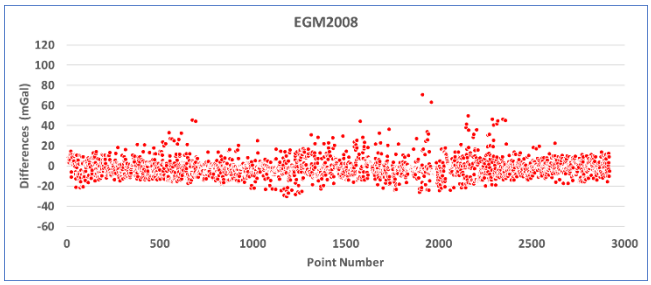


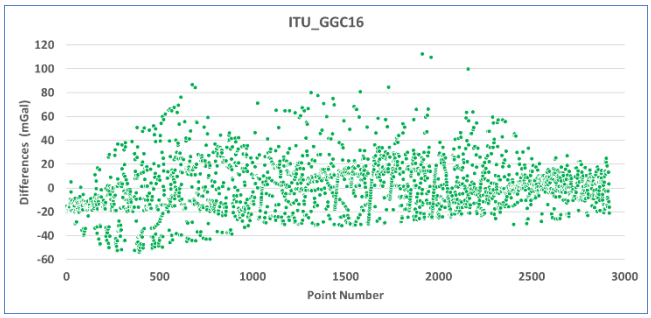


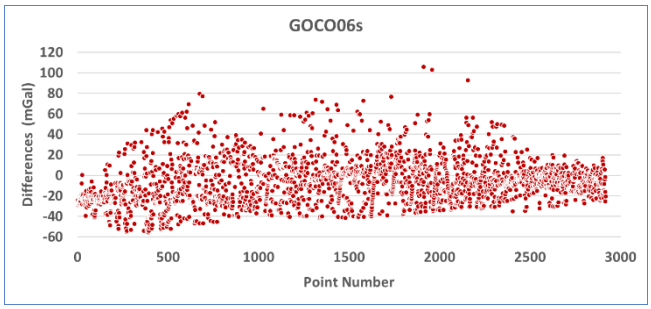


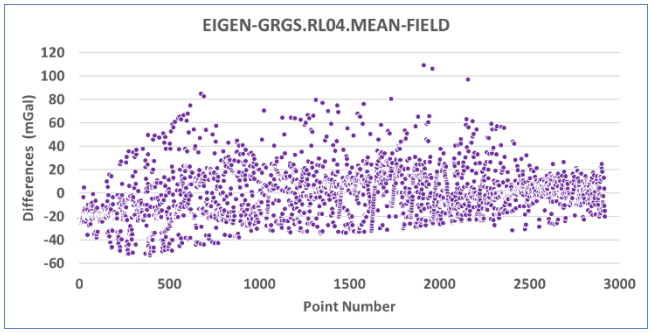

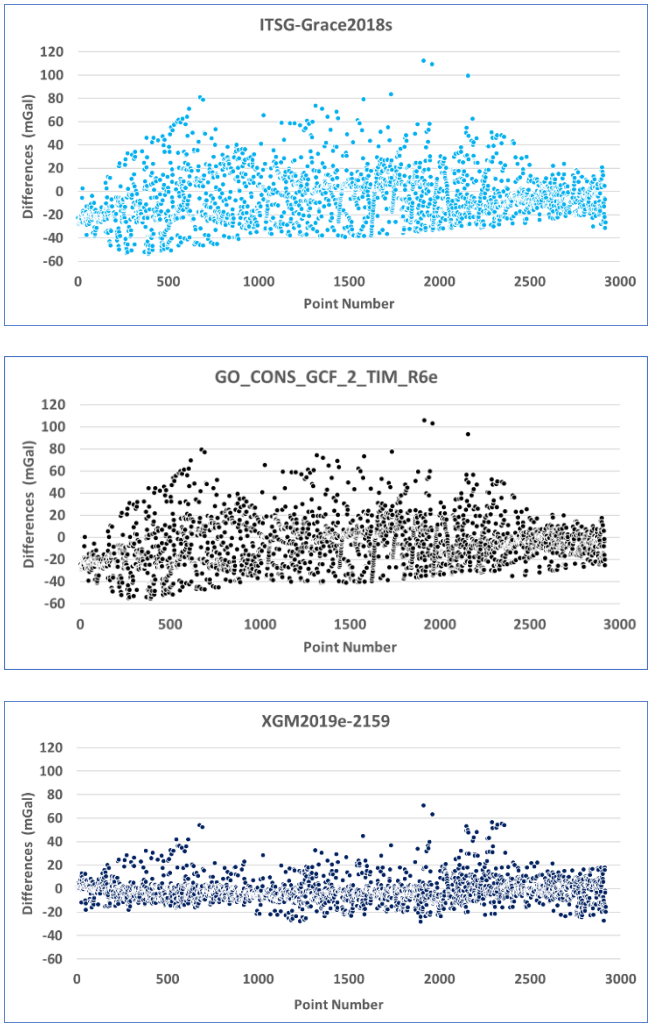


**Figure 1.** The gravity differences (unit: mGal)

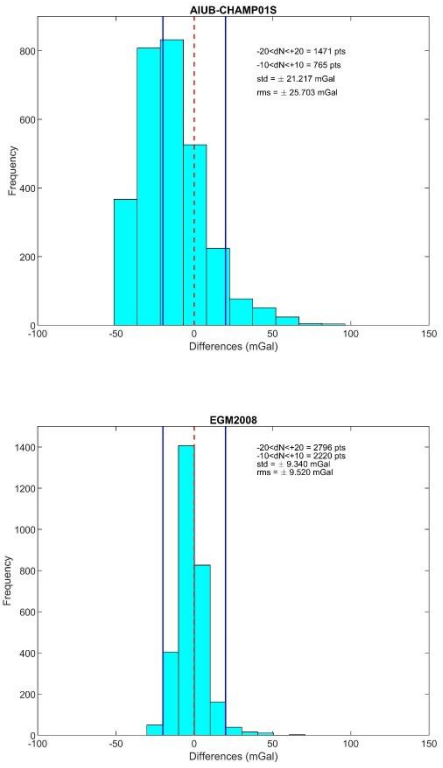


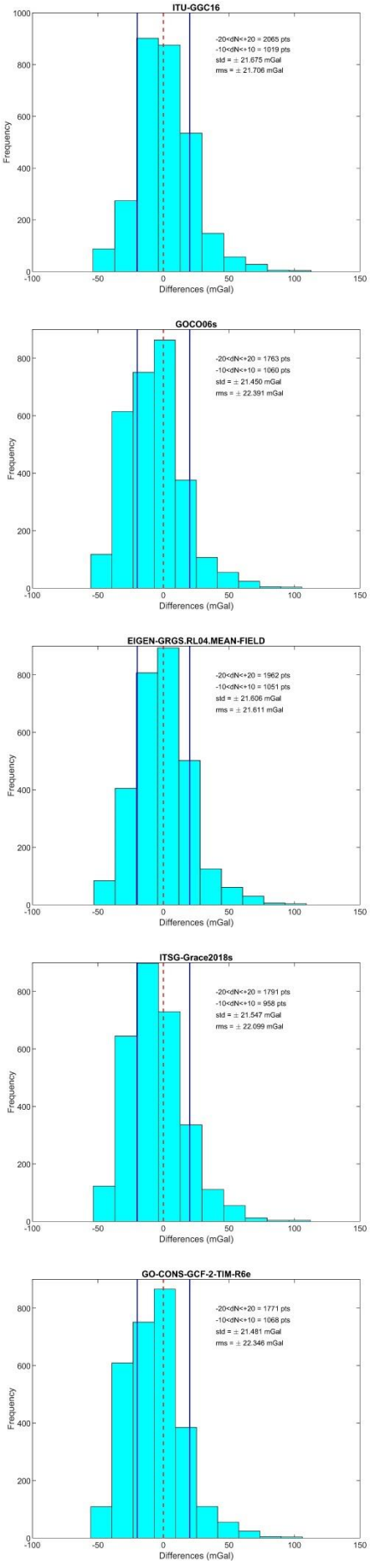

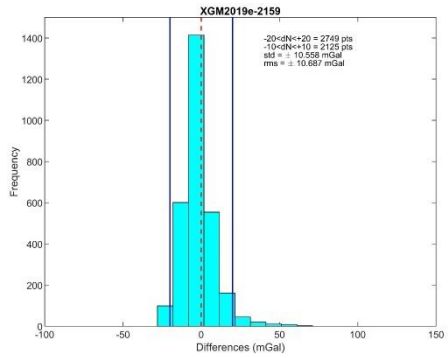


**Figure 2.** The gravity difference values as a histogram (unit: mGal)

**Table 2.** Statistics of gravity differences (mGal)

| Model Name | min | max | mean | std |
|---|---|---|---|---|
| AIUB-CHAMP01S | -51.189 | 96.365 | -14.513 | 21.217 |
| EGM2008 | -30.248 | 70.852 | -1.853 | 9.340 |
| ITU_GGC16 | -53.765 | 112.650 | 1.231 | 21.675 |
| GOCO06s | -55.345 | 105.621 | -6.436 | 21.450 |
| EIGEN-GRGS... | -53.042 | 109.037 | -0.622 | 21.606 |
| ITSG-Grace2018s | -53.532 | 112.304 | -4.923 | 21.547 |
| GO_CONS...R6e | -55.461 | 105.983 | -6.167 | 21.481 |
| XGM2019e_2159 | -27.940 | 71.009 | -1.667 | 10.558 |

## 4. CONCLUSION

As a result of the calculations, it was seen that the best GGMs for this test area were EGM2008 and XGM2019e_2159. The standard deviation values were obtained 9.340 mGal from the EGM2008 model and 10.558 mGal from the XGM2019e_2159 model. In other GGMs, very close standard deviation values have been calculated. For this study, it can be said that one of the most important reasons affecting accuracy is the variety of data used (altimetry, gravity, and satellites) and a high degree ($n_{max}$) model.

## REFERENCES

Akyilmaz O, Ustun A, Aydin C, Arslan N, Doganalp S, Guney C, Mercan H, Uygur S.O, Uz M & Yagci O, (2016). ITU_GGC16 The combined global gravity field model including GRACE & GOCE data up to degree and order 280. GFZ Data Services. https://doi.org/10.5880/icgem.2016.005

Barthelmes F, (2013). Definition of functionals of the geopotential and their calculation from spherical harmonic models, Theory and formulas used by the calculation service of the International Centre for Global Earth Models (ICGEM). Scientific Technical Report (Revised Edition), STR09/02.

Doganalp S, (2016). An evaluation of recent global geopotential models for strip area project in Turkey, Earth sciences research journal 20 (3), C1-C10. http://dx.doi.org/10.15446/esrj.v20n3.55440

Energy and Geoscience Institute at the University of Utah. (2016). Utah FORGE: Milford Gravity Data Shapefile [data set]. Retrieved from https://dx.doi.org/10.15121/1405037.

Featherstone WE, (2002). Expected Contributions of Dedicated Satellite Gravity Field Missions to Regional Geoid Determination with Some Examples from Australia. Journal of Geospatial Engineering, 4(1): 1-19

Heiskanen WA & Moritz H, (1984). Physical Geodesy, Institute of Physical Geodesy, Technical University Graz, Austria

Hofmann-Wellenhof B & Moritz H, (2005). Physical Geodesy. ISBN-13978-3-211-23584-3. Springer-Verlag Wien.

Kaula W, (1966). Theory of Satellite Geodesy-Applications of Satellites to Geodesy. Dover Publications, Inc., Mineola, New York.

Kvas A, Mayer-Gürr T, Krauss S, Brockmann JM, Schubert T, Schuh WD, Pail R, Gruber T, Jäggi A & Meyer U, (2019). The satellite-only gravity field model GOCO06s. GFZ Data Services. https://doi.org/10.5880/ICGEM.2019.002

Lemoine JM, Biancale R, Reinquin F, Bourgogne S & Gégout P, (2019). CNES/GRGS RL04 Earth gravity field models, from GRACE and SLR data. GFZ Data Services. https://doi.org/10.5880/ICGEM.2019.010

Mayer-Gürr T, Behzadpur S, Ellmer M, Kvas A, Klinger B, Strasser S & Zehentner N, (2018). ITSG-Grace2018 - Monthly, Daily and Static Gravity Field Solutions from GRACE. GFZ Data Services. https://doi.org/10.5880/ICGEM.2018.003

Pavlis NK, Holmes SA, Kenyon SC & Factor JK, (2008). An Earth Gravitational Model to Degree 2160: EGM2008; Vienna, Austria.

Prange L, Jäggi A, Beutler G, Dach R, Mervart L & Sideris M, (2009). Gravity Field Determination at the AIUB – The Celestial Mechanics Approach; Springer, Vol 133, p. 353-362. https://doi.org/10.1007/978-3-540-85426-5_42

Rummel R, Balmino G, Johannessen J, Visser P & Woodworth P, (2002). Dedicated gravity field missions-principles and aims. Journal of Geodynamics, 33:3–20.

Seeber G, (2003). Satellite Geodesy. 2nd edition Walter de Gruyter, Berlin

Turgut B, (2016). The Estimation of Gravity Values by the Back Propagation Artificial Neural Networks. AKU J. Sci. Eng. 16 (2016) 035503 (660-664). doi: 10.5578/fmbd.37325.

Vaníček P & Featherstone WE, (1998). Performance of three types of Stokes's kernel in the combined solution for the geoid. Journal of Geodesy , 72, 12, pp. 684-697.

Zingerle P, Pail R, Gruber T & Oikonomidou X, (2019). The experimental gravity field model XGM2019e. GFZ Data Services. https://doi.org/10.5880/ICGEM.2019.007

Zingerle P, Brockmann JM, Pail R, Gruber T & Willberg M, (2019). The polar extended gravity field model TIM_R6e. GFZ Data Services. https://doi.org/10.5880/ICGEM.2019.005

Intercontinental Geoinformation Days

http://igd.mersin.edu.tr/2020/

# The Accuracy Assessment of Terrestrial and Mobile Lidar Systems for 3D Modelling

**Ramazan Alper KUÇAK*[1], Serdar EROL[1], Mehmet İŞİLER[1]**

[1]Istanbul Technical University, Faculty of Civil Engineering, Department of Geomatics Engineering, İstanbul, Turkey

**Keywords**
Lidar
MLS
TLS
Point Cloud
Accuracy

**ABSTRACT**

The use of high-precision and sufficiently collected point clouds for 3D data modeling is very important for geomatics and other branches of engineering (such as mechanical and construction), and architectural applications. For this reason, various filtering and interpolation methods are improved for 3D modeling. However, if the point cloud is collected inaccurate or missing, the 3D data modeling is always an issue. Therefore, before the 3D modeling process, the point positioning accuracy and resolution of the point cloud should be investigated. The accuracy assessment can be performed by comparing data obtained from a measurement system that is considered to be more accurate. These analyses are used the accuracy assessment of the maps produced by different Lidar (Light Detection and Ranging) point clouds. In this study, the accuracy of the point clouds obtained using Terrestrial Lidar Systems (TLS) and Mobile Lidar Systems (MLS) was determined by using the Euclidean distances between the surface points measured by total station. The results showed that the accuracy of the TLS system was better than the MLS system. In addition, while TLS should be preferred in studies requiring high accuracy such as 3D cultural heritage documentation, MLS should be preferred in applications such as various topographic maps and 3D city models.

## 1. INTRODUCTION

Studying with highly accurate and enough point cloud data in 3D modeling is very important. If the point clouds' accuracy and resolution are sufficient for the desired purposes, the steps of the point clouds' registration or modeling can be realized. However, if the accuracy and the resolution of the existing point cloud are not sufficient, it must be georeferenced with a more accurate point cloud.

LIDAR (Light Detection and Ranging) is a measurement technique that allows the collection of large amounts of 3D data in a short time, from airborne or terrestrial. LIDAR creates a point cloud with density values in the local coordinate system and also RGB values of the point cloud are usually provided by internal or external digital cameras of the system (Kuçak, Kiliç, & Kisa, 2016; Kuçak, Özdemir, & Erol, 2017)

Mobile LIDAR systems (MLS) is a widely used method to get rapid and detailed point cloud acquisition in various applications such as cultural heritage, GIS (Geography Information System), geodetic applications, and spatial decision support systems (Rusu, Marton, Blodow, Dolha, & Beetz, 2008) or 3D city modeling (Chen, Weng, Hay, & He, 2018) and also rail and road deformation analysis systems (Wang et al., 2019).

Mobile LIDAR systems consist of laser scanners, cameras, as well as IMU (Inertial Measurement Unit) and GNSS (Global Navigation Satellite System) systems. All of these systems work together to generate the point cloud in a three-dimensional (3D) coordinate system (Kuçak, Özdemir & Erol, 2017). The LIDAR systems having multiple laser scanners may suffer from noise and other error sources such as inertial drift, rigid platform calibration, GNSS errors, etc. The measurements with multiple scanners in Mobile Mapping Systems (MMS) require calibration in order to overcome the disadvantages by high noise rates and errors as well as the overlapping problem in strips. After the calibration steps, CCD Cameras and Laser scanners can become ready to use. However, the calibration may not be sufficient to eliminate all errors and provides inappropriate point clouds for 3D modeling. In such situations, the adjustment (coarse and fine registration) of the multiple scans to minimize the discrepancies in LIDAR point clouds are necessary (Rieger, Studnicka, Pfennigbauer, & Zach, 2010). In well GNSS measurement conditions, the accuracy of the MLS trajectory could be

* **Corresponding Author**

*(kucak15@itu.edu.tr) ORCID ID 0000-0002-1128-1552
(erol@itu.edu.tr) ORCID ID 0000-0002-7100-8267
(isiler@itu.edu.tr) ORCID ID 0000-0003-0543-0029

**Cite this study**

Kucak R A, Erol S & İşiler M (2020). The Accuracy Assessment of Terrestrial and Mobile Lidar Systems for 3D Modelling. Intercontinental Geoinformation Days (IGD), 236-239, Mersin, Turkey

realized in cm-level. On the contrary, in difficult conditions, the error increases to decimeters-level (Haala, Peter, Kremer, & Hunter, 2008a). In such situations, the accuracy of the point cloud can be increased with georeferencing or registration during the post-processing stage.

In this study, the accuracy of the point clouds, which were obtained by using the TLS and MLS systems were investigated. However, since the error sources mentioned above are common problems in mobile LIDAR systems, the accuracy comparison of the LIDAR systems carried out relatively using the distance differences of some points taken from each point cloud data to eliminate the error sources in the comparison. In this study, ITU (Istanbul Technical University) Yılmaz Akdoruk Student Dormitory was selected as a test area. The dormitory is located in Ayazaga Campus of ITU in Turkey (Figure 1).


**Figure 1.** Yılmaz Akdoruk Student Dormitory

## 2. DATA and METHOD

The study area scanned with Leica C10 TLS, which can get 50,000 points per second with 6 mm accuracy until 50 m and uses impulse method for distance measurement. 3D point cloud of the building processed with Cyclone Software by Leica Geosystems (Figure 2).

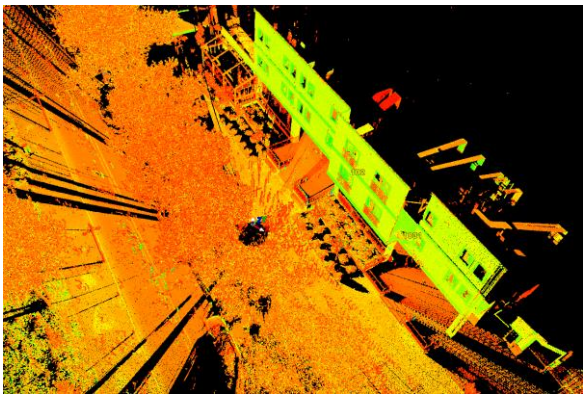

**Figure 2.** Point Cloud with Leica C10 Scanning

Mobile Mapping data was obtained by using the Riegl VMX 450 LIDAR System, which can get 1,000,000 points per second with 8 mm accuracy and use impulse method for distance measurement (Figure 3).

**Figure 3.** ITU Ayazaga Campus Scanning by Riegl VMX 450 MLS

### 2.1. Error Propagation

The error propagation was applied for some test points from the surface to determine the point positioning accuracy of instruments. The test points of the surface also positioned with the "Pentax W1503" total station for the accuracy assessment of the TLS and MLS point clouds. The reflectorless distance measurement accuracy of the total station is "3 mm + 2 ppm" and the angle measurement accuracy is 3″. The Leica C10 TLS distance measurement accuracy is 4 mm, angle measurement accuracy is 12″ and the positional accuracy is 6 mm. The Riegl VMX 450 MMS system (Figure 4) includes VQ-450 laser sensors (2-laser scanners) and the laser sensors' positional accuracy is 8 mm. Table 1 also gives the technical specifications of the sensor' in VMX 450 (Toschi et al., 2015).


**Figure 4.** Riegl VMX-450 MMS System

**Table 1.** Technical characteristics of the RIEGL VMX-450 MMS (Toschi et al., 2015).

| **Sensor** | **VQ-450** |
|---|---|
| Measuring principle | Time of Flight |
| Laser wavelength | Near infrared |
| Laser measurement rate | 300 – 1100 kHz |
| Maximum range | 140 – 800 m |
| Minimum range | 1.5 m |
| Accuracy | 8 mm, 1$\sigma$ |
| Precision | 5 mm, 1$\sigma$ |
| **Sensor** | **IMU/GNSS** |
| Absolute position | 0.020 – 0.050 m |
| Roll and pitch | 0.005 ° |
| True heading | 0.015 ° |
| **Sensor** | **VMX-450-CS6** |
| Resolution | 5 Mpx |
| Sensor size | 2452 x 2056 px |
| Pixel size | 3.45 µm |
| Nominal focal length | 5 mm |

According to given measurement accuracies, the error propagation was applied to the following equations.

$$X_B = X_A + (S_{Slope} * CosZ_a * Cost_a) \quad (1)$$

$$Y_B = Y_A + (S_{Slope} * CosZ_a * Sint_a) \quad (2)$$

$$Z_B = Z_A + (S_{Slope} * SinZ_a) + i_a \quad (3)$$

In Equations 1-3, $X_A$ is the x coordinate component of the local coordinate system at the standing point, $X_B$ is the x coordinate component of the measured point, "$t_a$" is the horizontal angle, "$Z_a$" is the vertical angle (slope angle) "$i_a$" is instrument height, "S" is distance. The accuracy $(m_{X_B}, m_{Y_B}, m_{Z_B})$ of the measured point coordinate components (x, y, z) could be calculated as;

$$m_{X_B}^2 = m_{X_A}^2 + (Cost_a^2.CosZ_a^2)m_s^2 + (S^2.CosZ_a^2.Sint_a^2 * ) \frac{m_t^2}{\rho^2} + (S^2.Cost_a^2.SinZ_a^2 *) \frac{m_Z^2}{\rho^2} \quad (4)$$

$$m_{Y_B}^2 = m_{Y_A}^2 + (CosZ_a^2.Sint_a^2)m_s^2 + (S^2.Cost_a^2.CosZ_a^2) \frac{m_t^2}{\rho^2} + (S^2.Sint_a^2.SinZ_a^2) \frac{m_Z^2}{\rho^2} \quad (5)$$

$$m_{Z_B}^2 = m_{Z_A}^2 + (SinZ_a^2)m_s^2 + (S^2.CosZ_a^2) \frac{m_Z^2}{\rho^2} \quad (6)$$

In Equations 4-6, $m_t$ is the angle measurement accuracy and $m_s$ is the distance measurement accuracy of the instrument ( $\rho = 200/\pi$).

According to error–propagation, the calculated position accuracy was between 4.02 – 4.21 mm for the total-station, and was between 5.56-5.67 mm for the TLS in the test points.

## 3. RESULTS

In the building facade, the most prominent and corner points were selected as test points. The coordinates of the test points obtained from the Total station measurements are accepted as reference coordinates and the Euclidean distance between the surface test points was calculated. Then, the distances between the test points derived from TLS and MLS point clouds compared with the reference distance calculated from the total-station. The position of the selected test points is given in Figure 5.

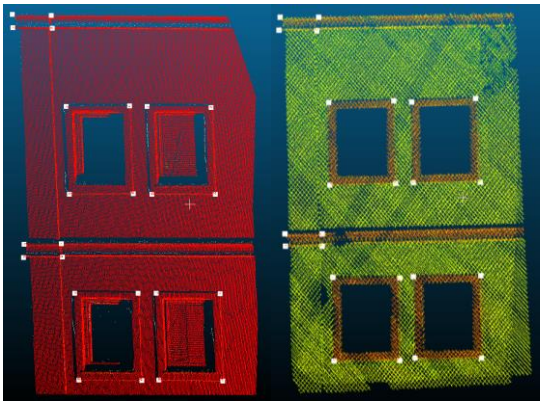

**Figure 5.** Key points TLS (Left), MLS (Right)

The distance differences and its statistics between the TLS and MLS key points distances with total station distances are given in Table 2 and in Figures 6a and 6b.

According to the results, the standard deviation of the TLS was obtained 1.5 cm. On the other hand, the standard deviation of the MLS was 2.8 cm. (Haala et al., 2008a) mentioned that with the obtained cm-level positional accuracy, MMS could be used for some applications include mapping purposes.

**Table 2.** The distance differences between TLS, MLS key points' distances and Total Station corner' distances

| TLS_Total | 0 | 1 | 2 | 3 | 7 | 8 | 10 | 11 | 16 | 18 |
|---|---|---|---|---|---|---|---|---|---|---|
| 0 | - | | | | | | | | | |
| 1 | -0.021 | - | | | | | | | | |
| 2 | -0.009 | 0.011 | - | | | | | | | |
| 3 | -0.020 | 0.000 | -0.016 | - | | | | | | |
| 7 | -0.023 | -0.004 | 0.020 | -0.010 | - | | | | | |
| 8 | -0.042 | -0.020 | 0.039 | 0.017 | -0.003 | - | | | | |
| 10 | -0.027 | -0.005 | 0.041 | 0.010 | -0.020 | 0.013 | - | | | |
| 11 | -0.023 | -0.001 | 0.040 | 0.006 | -0.011 | 0.018 | -0.003 | - | | |
| 16 | -0.019 | 0.002 | 0.023 | 0.011 | -0.015 | 0.020 | 0.007 | -0.002 | - | |
| 18 | -0.018 | 0.004 | 0.030 | 0.005 | -0.003 | 0.024 | 0.006 | 0.007 | -0.010 | - |
| **MLS_Total** | **0** | **1** | **2** | **3** | **7** | **8** | **10** | **11** | **16** | **18** |
| 0 | - | | | | | | | | | |
| 1 | 0.008 | - | | | | | | | | |
| 2 | 0.086 | 0.080 | - | | | | | | | |
| 3 | 0.049 | 0.042 | -0.042 | - | | | | | | |
| 7 | 0.038 | 0.064 | 0.064 | 0.002 | - | | | | | |
| 8 | 0.010 | 0.021 | 0.069 | 0.019 | 0.032 | - | | | | |
| 10 | 0.048 | 0.051 | 0.040 | -0.020 | 0.025 | 0.033 | - | | | |
| 11 | 0.027 | 0.044 | 0.078 | 0.020 | -0.028 | 0.025 | 0.037 | - | | |
| 16 | 0.083 | 0.083 | 0.029 | 0.019 | 0.035 | 0.062 | 0.030 | 0.057 | - | |
| 18 | 0.088 | 0.097 | 0.044 | 0.008 | 0.047 | 0.077 | 0.046 | 0.075 | -0.002 | - |

In Figures 6a and 6b, the distributions of 45 Euclidean distances differences were shown for MLS and TLS after removing the blunders from the data groups. While MLS-Total differences show the normal distribution, TLS-Total differences show a close curve to the normal distribution. According to the differences between Total-station and TLS, the mean value was -1 mm, and the maximum difference was 3 cm. On the other hand; MLS had a 3.3 cm mean, and the maximum difference was 8.6 cm. (Haala, Peter, Kremer, & Hunter, 2008b) investigated the quality of building facades of an existing 3D city model of the city of Stuttgart. They proved that an accuracy better than 3 cm (standard deviation of the differences between measured and reference data) can be achieved by the system in robust GNSS conditions. Similar results are seen in the literature. A similar result was also obtained in this study.

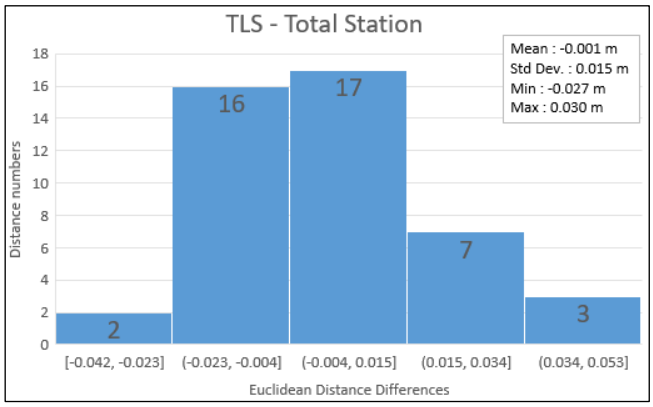


**Figure 6a.** The distribution of distance differences between TLS and Total station.

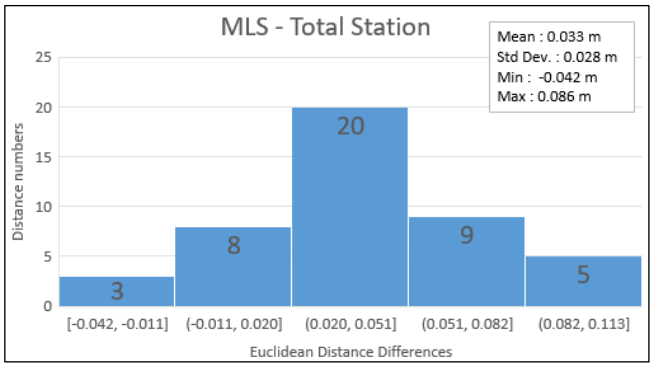


**Figure 6b.** The distribution of distance differences between MLS and Total station.

In this study, Total station data is accepted as the most accurate measurement system and the Euclidean distances between the surface points were calculated. The accuracy $(m_{X_B}, m_{Y_B}, m_{Z_B})$ of the measured points was calculated to determine the point position accuracy with free from point cloud resolution errors. The primary reason for using the Euclidean distance between surface points is to compare the accuracy of the two systems, neglecting GNSS and calibration errors. The results show that the accuracy of the TLS system is much better than the MLS system as expected.

## 4. DISCUSSION

The distance differences of surface points between reference distances calculated by Total Station and the distances calculated from the TLS and MLS point clouds were obtained and the blunders were removed from both data groups, and then the statistics calculated. According to the calculated standard deviations of the distance differences, the accuracy of the point clouds was obtained as 1.5 cm for TLS and 2.8 cm for MLS. These histograms show that the accuracy of TLS and Total station are close to each other. However, the accuracy of MLS is low due to un-eliminated errors in the system.

This study shows that each of these systems has both advantages and disadvantages. MLS (Mobile LiDAR System) is a product of the latest technology towards the fast acquisition of 3D spatial data. However, the lack of calibration in these systems leads to undesirable results. These misalignments frequently appear in MLS (Rieger, Studnicka, Pfennigbauer, & Zach, 2010). The errors mentioned above text are common problems in Mobile LIDAR Systems. Because of that, the point cloud coordinates are not compared directly in this study.

The results show that TLS can be preferred for studies that require high accuracy such as cultural heritage, Building Information Management (BIM). However, MLS should be preferred in applications such as various topographic maps and 3D city models rather than 3D cultural heritage documentation.

## 5. CONCLUSION

TLS and MLS Technology is a rapidly developing technology today. The experiments performed in this study show that each of these methods has both advantages and disadvantages. The ease of use in the field and the ability to measure millions of points in a very short time provide great convenience to the user. The advantages of the LIDAR systems are seen when compared with other 3D documentation methods in terms of time. Under proper GNSS conditions and with good calibration values, 3D models and topographic maps can be produced by MLS in a very short time and with the desired accuracy. The results obtained in this study show that LIDAR systems comply with the regulation (Regulation on Production of Large Scale Maps and Map Information, 2018) for 3D topographic map production.

## ACKNOWLEDGEMENT

"*Koyuncu Lidar Harita ve Mühendislik*" Company is acknowledged for providing the mobile mapping systems for this study.

## REFERENCES

Chen, G., Weng, Q., Hay, G. J., & He, Y. (2018). Geographic object-based image analysis (GEOBIA): emerging trends and future opportunities. *GIScience & Remote Sensing, 55*(2), 159-182.

Haala, N., Peter, M., Kremer, J., & Hunter, G. (2008a). Mobile LiDAR mapping for 3D point cloud collection in urban areas—A performance test. *Int. Arch. Photogramm. Remote Sens. Spat. Inf. Sci, 37*, 1119-1127.

Haala, N., Peter, M., Kremer, J., & Hunter, G. (2008b). Mobile LiDAR mapping for 3D point cloud collection in urban areas—A performance test. *The international archives of the photogrammetry, remote sensing and spatial information sciences, 37*(Part B5).

Kuçak, R., Kiliç, F. & Kisa, A. (2016). Analysis of terrestrial laser scanning and photogrammetry data for documentation of historical artifacts. *The International Archives of Photogrammetry, Remote Sensing and Spatial Information Sciences, 42*, 155.

Kuçak, R., Özdemir, E. & Erol, S. (2017). The segmentation of point clouds with k-means and ANN (artifical neural network). *The International Archives of Photogrammetry, Remote Sensing and Spatial Information Sciences, 42*, 595.

Rieger, P., Studnicka, N., Pfennigbauer, M., & Zach, G. (2010). Boresight alignment method for mobile laser scanning systems. *Journal of Applied Geodesy, 4*(1), 13-21.

Rusu, R. B., Marton, Z. C., Blodow, N., Dolha, M., & Beetz, M. (2008). Towards 3D point cloud based object maps for household environments. *Robotics and Autonomous Systems, 56*(11), 927-941.

Toschi, I., Rodríguez-Gonzálvez, P., Remondino, F., Minto, S., Orlandini, S., & Fuller, A. (2015). Accuracy evaluation of a mobile mapping system with advanced statistical methods. *The International Archives of Photogrammetry, Remote Sensing and Spatial Information Sciences*, *40*(5), 245.

Wang, Y., Chen, Q., Zhu, Q., Liu, L., Li, C., & Zheng, D. (2019). A survey of mobile laser scanning applications and key techniques over urban areas. *Remote Sensing, 11*(13), 1540.

Intercontinental Geoinformation Days

http://igd.mersin.edu.tr/2020/

# Identifying the best fitting 3D deformation model using information criteria

**Alaz Andaç Ortaköy**[*1], **Cüneyt Aydın** [2]

[1]*Yıldız Technical University, Civil Engineering Faculty, Dept. of Geomatics Engineering, Istanbul, Turkey*

**Keywords**
Deformation Analysis
Total Least-Squares
3D Cartesian Coordinates
Coordinate Transformation

**ABSTRACT**

3D deformation studies are usually based on 12-parameter affine transformation model. Deformation part of this model is expressed with three scale factors and three skew parameters along x, y, z axes. However, actual deformation of the monitored object may have a different structure than the one prescribed by this model. For instance, there may exist skewness along only xy plane, or one dilation along only z-axis. In this sense, we encounter with possible fifteen different deformation models such as 7-parameter (similarity), 8-parameter affine, 10-parameter affine, etc. The question arising is which one fits best to the coordinates. For this aim, we use Akaike Information Criterion (AIC) and Bayesian Information Criterion (BIC). The efficiencies of these criteria are studied within many deformation examples using Monte-Carlo simulations. According to the numerical examples, both criteria can detect the true model successfully with a success rate ranging from 53 to 97% if the deformation parameter is three times bigger than its standard error.

## 1. INTRODUCTION

Terrestrial, aerial and space methods today yield continuous and (near) real-time 3D spatial data with unprecedented precision and resolution thanks to the advanced measuring sensors. This high-quality data allows us to monitor the earthbound bodies (the Earth crust or engineering structures) and analyze their deformations continuously (or discretely) in 3D space.

The temporal (Cartesian) coordinate changes of the points characterizing the monitored body consist of relative and non-relative parts. The relative part deals with translation and rotation of the body whereas the non-relative part corresponds to the shape and size change (deformation) of the body in time (Aydin 2017). To discriminate two parts against each other, the following 3D strain model is applied to the coordinate differences (**d**) monitored between two epochs of time:

$$\mathbf{d}=\mathbf{y}-\mathbf{x}=\mathbf{t}+\mathbf{E}\mathbf{x}$$

where **x** and **y** denote the coordinate vectors in the initial and present epochs, respectively; **t** denotes the translation, and **E** is the anti-symmetric strain tensor including nine different elements. With these strain elements, can define the dilation, shear, differential rotation etc. We may also consider 12-parameter affine transformation between **x** and **y** coordinates (Amiri-Simkooei 2018):

$$\mathbf{y}=\mathbf{t}+\mathbf{R}\mathbf{L}\mathbf{M}\mathbf{x}$$

where **R** is the skew-symmetric differential rotation matrix; **L** is the diagonal scale factor matrix, and **M** is the matrix of skew parameters. If we subtract the initial coordinates "**x**" from both sides of this affine model, we obtain "**E=RLM-I**", where **I** denotes the identity matrix. Therefore, 3D strain model is a 12-parameter affine transformation model applied between initial and present epoch coordinates.

In deformation analysis, we deal with the scale matrix **L** and the skew matrix **M**. In the above-given affine model, they represent three scale factors along x, y, z axes and three skew parameters along each pair of axes, namely between x-y, x-z and y-z axes (Note that scale factors correspond the dilations while skew parameters correspond to the shears in continuum mechanics). However, actual deformation model may be different from the one in the prescribed model. For instance, no skewness may exist in the xz plane while only x axis has a significant scale change. In such a combinatorial way, we may consider fifteen different deformation models,

* **Corresponding Author**

*(alzandac@gmail.com) ORCID ID 0000-0002-2122-931X
(caydin@yildiz.edu.tr) ORCID ID 0000 – 0003 – 0888 – 0316

**Cite this study**

Ortaköy A A & Aydın C (2020). Identifying the best fitting 3D deformation model using information criteria. Intercontinental Geoinformation Days (IGD), 240-243, Mersin, Turkey

which are summarized in Table 1. Each of them includes common translations and rotations but has different scale factors and skew parameters.

**Table 1.** Models and their number of parameters (u) (Note: Shaded elements exist in the model; S=Similarity, A=Affine; […]=groups)

| Model (u) | Scale | | | Skew | | |
|---|---|---|---|---|---|---|
| | x | y | z | x-y | x-z | y-z |
| **1**-S (7) | Common | | | | | |
| **2**-A (7) | ■ | | | | | |
| **3**-A (7) [i] | | ■ | | | | |
| **4**-A (7) | | | ■ | | | |
| **5**-A (8) | | ■ | ■ | | | |
| **6**-A (8) [ii] | ■ | | ■ | | | |
| **7**-A (8) | ■ | ■ | | | | |
| **8**-A (9) | ■ | ■ | ■ | | | |
| **9**-A (10) | ■ | ■ | ■ | | | ■ |
| **10**-A (10) [iii] | ■ | ■ | ■ | | ■ | |
| **11**-A (10) | ■ | ■ | ■ | ■ | | |
| **12**-A (11) | ■ | ■ | ■ | | ■ | ■ |
| **13**-A (11) [iv] | ■ | ■ | ■ | ■ | | ■ |
| **14**-A (11) | ■ | ■ | ■ | ■ | ■ | |
| **15**-A (12) | ■ | ■ | ■ | ■ | ■ | ■ |

The question we mainly pose here is how to identify the best fitting model. Conventional model tests with Fisher-distribution (Demirel 2005) may not be useful to obtain the best model among the other possible models since this test compares only two models at a time. We, therefore, consider information criteria, which are easily adapted to our potential models as shown in (Lehmann 2014) and (Even-Tzur 2020) for coordinate transformations. Two criteria, called Akaike Information Criterion (AIC) and Bayesian Information Criterion (BIC), are considered to find out the best 3D deformation model. The "Method Section" briefly expresses these criteria. To investigate how they can identify the "true" model successfully, we use many deformation examples generated by a Monte-Carlo simulation strategy. The success rates are given in the "Results Section". In the last two sections, we discuss the results and concludes our study.

## 2. METHOD

### 2.1. AIC and BIC for the 3D Deformation Models

The previously given 12-parameter affine model deals with one object point. Using the same notation "**y**" and "**x**" for the coordinate vectors of all points in the deformation study, we give the linearized observation equations as follows:

$$\mathbf{y}-\mathbf{x}-(\mathbf{e}_y-\mathbf{e}_x)=\mathbf{A}\mathbf{c}$$

where **e** denotes the error vector of the coordinates; **A** is the design matrix and **c** are the vector of unknown u=12 parameters (translations, differential rotations, scale factor changes and skew parameters). Note that the least-squares method applied to this mathematical model yields the equivalent results with those from total-least squares solution (e.g. Uygur et al. 2020) since the **RLM** in the second equation goes to identity matrix in deformation studies, and the noises in the coordinates are relatively too low. Expressing the error differences with "$\mathbf{e}=(\mathbf{e}_y-\mathbf{e}_x)$", we obtain the quadratic form of the 12-parameter affine model as "$\Omega=\mathbf{e}^T\mathbf{P}\mathbf{e}$", where **P** is the weight matrix set based on the known cofactor matrix of the coordinate difference "**y–x**". The AIC and BIC associated with the model then can be obtained by (Even-Tzur 2020):

$$AIC=3p\times\ln(\Omega)+2u\times 3p/(3p-u-1)$$
$$BIC=3p\times\ln(\Omega/3p)+u\times\ln(3p)$$

where p is the number of points.

The AIC and BIC of each potential model in Table 1 can be obtained with the same methodology but using the corresponding design matrix **A** and the number of parameters u associated with the model (Note: For saving space, we do not give the design matrices of the models explicitly here. The readers can derive this matrix from (Amiri-Simkooei 2018) easily or can contact the corresponding author of our study). Finally, the model which gives the minimum AIC (or BIC) is accepted as the best model describing the deformation structure of the investigated body.

### 2.2. Generating Deformed Bodies

In order to investigate how AIC (or BIC) is successful in identifying the best fitting model, we need different examples in which we know which model is the true one. A "true" model can be known beforehand if and only if we generate these examples ourselves by a Monte-Carlo simulation strategy. For this aim, we follow the strategy given in (Uygur et al. 2020). Our random simulation consists of the following steps:

- The x, y and z coordinates of the object points, of which numbers were selected randomly between 7 and 15, were generated between $10^3$ and $10^5$ m locating the points into the proper grids. With these grids, a proper constellation without any bad condition is guaranteed.
- The coordinates generated now correspond to the "errorless" coordinates in the initial epoch. Later on, the fully populated and positive definite covariance matrices of the initial and present epochs were produced. The standard errors of the parameters were obtained having applied an approximate transformation using the epoch covariance matrices.
- Zero-translations and rotations were assumed. The scale factors and skew parameters were generated randomly by

  Scale Factor=1+τ×(its standard error)
  Skew Parameter=τ×(its standard error)

  where τ is a random number ranging from 2 to 6. The sign of the amplitude τ was also randomly selected.
- The present epoch "errorless" coordinates were evaluated using the "true" model based on the above-given scales and skewness. In such a way, the

deformation is being incorporated into the coordinates. Afterward, the random errors, normally distributed according to the previously mentioned covariance matrices, were added to the initial and present epoch "errorless" coordinates to get the vectors **x** and **y**. This set of pairs represent one random sample.

### 2.3. Mean Success Rate (MSR)

For each "true" model, we produced m=1000 random samples. Each random sample was solved by each model in Table 1. The number of samples (k) in which the corresponding model was identified as the best fitting model based on the AIC (or BIC) was counted to get the following MSR (Hekimoglu and Koch 1999):

$$MSR=(k/m)\times 100$$

## 3. RESULTS

Totally 15 MSRs were evaluated for each "true" model. It is expected that the MSR associated with the "true model" goes to 100%. However, statistically speaking, it is not possible to have this probability. The MSRs for different cases are given in this section.

Successfully identification of the true model relies on the magnitude of the scale change and skew parameters. Firstly, the amplitude τ was selected between 2 and 3 such that the deformation parameters lie in the range of 2σ-3σ (σ=stands for the standard error of the corresponding parameter). The obtained MSRs for this range are shown as a color matrix in Figure 1.

The diagonal elements of this matrix in Figure 1 refer to the successfully identifying the true model while the off-diagonals refer to the wrongly identification (the percentage values over the off-diagonals denote the minimum and maximum MSRs of the incorrect results). In both information criteria, the most successful results are obtained for the models in group-i (Affine-7) whereas the least successful results are obtained for the Affine-9 model (MSR is 25%). The BIC is more successful (MSR=57%) than the AIC (MSR=34%) if the true model is the Affine-12 model. However, in general, there is no other significant difference between AIC and BIC since the range of 2σ-3σ is too low as is known from deformation and outlier detection studies. We, therefore, increase the range to 3σ-6σ, and repeat the above-expressed procedure. The evaluated MSRs are shown in Figure 2. We discuss these results in the next section.

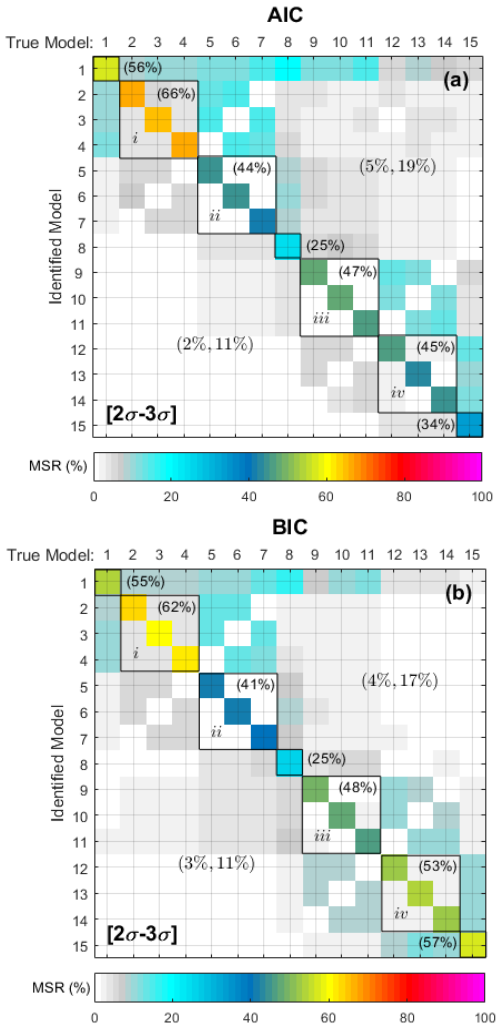


**Figure 1.** MSRs for fifteen models by using a) AIC and b) BIC while the deformation range is 2σ-3σ

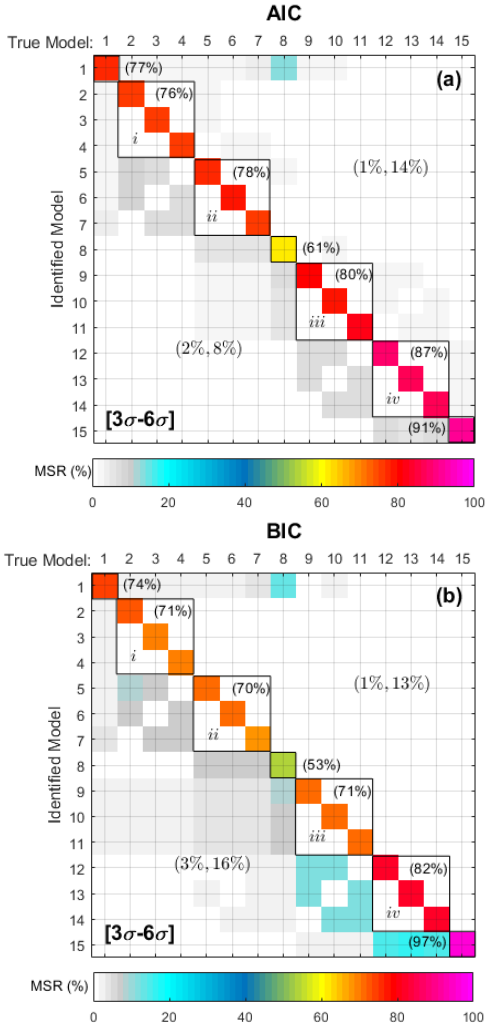


**Figure 2.** MSRs for fifteen models by using a) AIC and b) BIC while the deformation range is 3σ-6σ

## 4. DISCUSSION

According to the results in Figure 2, we see that the AIC provides more successful identification of the true model except for the Affine-12 deformation model. The BIC can identify the Affine-12 model with the success rate of 97%. The MSRs range from 61% to 91% (79% on average) and 53% to 97% (74% on average) using AIC and BIC, respectively. Both criteria fail for the Affine-9 model, which actually correspond to the rigid body volume change. This is because the Affine-9 model is usually wrongly identified as the Similarity-7 model. Hence, it may not be easy to discriminate the Affine-9 model against the Similarity-7 model.

Furthermore, we repeat our analysis using geodetic coordinates. Similar results are also valid for these geodetic constellations. Due to lack of space, however, we left these analyses to our next studies.

Correspondingly, although there are some minor differences between the AIC and BIC in different deformation models, we can interpret that one may identify the true deformation model with a success rate of about 75% using both criteria if the deformation parameters are 3 times bigger than their standard errors. This result is important for practical studies seeking for the best fitting deformation model among many different models.

## 5. CONCLUSION

We study the AIC and BIC in identifying the best fitting 3D deformation model. For this aim, fifteen different deformation models are considered.

In order to investigate how these criteria are successful in identifying the true deformation model among the potential fifteen models, we adapt the MSR concept. For this aim, we use the simulated random samples by considering a Monte-Carlo simulation strategy.

According to the numerical results, both criteria may fail in identifying the true model if the deformation parameters lie between 2σ and 3σ. They can identify the true model with a reasonable probability if the range is between 3σ and 6σ. This is not a surprising result because the "3σ" magnitude refers also to the minimum detectable outlier and deformation with 80% test power as is known from geodetic studies. For this range, we see that the AIC and BIC can identify the true model with the success rates of about 79% and 74%, respectively. The type of the actual deformation model affects these statistics. For instance, the worst results belong to the Affine-9 deformation model which generally is confused with the Similarity-7 model by the criteria. However, it is worth mentioning that these bad results may come from the random samples since we do not take into account how much dilation differences between x, y and z axes should be involved in the simulation strategy. This issue is dealing with deriving the minimum identifiable (detectable) deformation parameter by using the information criteria, which needs a more detailed statistical investigation.

## REFERENCES

Amiri-Simkooei A R (2018) Parameter estimation in 3D affine and similarity: implementation of variance component estimation. Journal of Geodesy, 92, 1285-1297.

Aydın C (2017) Effects of displaced reference points on deformation analysis. Journal of Surveying Engineering, 143(3). 1285-1297.

Demirel H (2005) Adjustment computation. Yıldız Technical University Press, Istanbul. ISBN: 975-461-375-3.

Even-Tzur G (2020) Coordinate transformation with variable number of parameters. Survey Review, 52(370), 62–68.

Hekimoglu S & Koch K R (1999) How can reliability of robust methods be measured?" Third Turkish-German Joint Geodetic Days, M. O. Altan, and L. Gründig, eds., Vol. 1, 179–196, Istanbul, Turkey. https://doi.org/10.1061/(ASCE)SU.1943-5428 https://doi.org/10.1080/14498596.2020.1776170

Lehmann R (2014). Transformation model selection by multiple hypotheses testing. Journal of Geodesy, 88 (12), 1117–1130.

Uygur S Ö, Aydın C & Akyılmaz O (2020) Retrieval of Euler rotation angles from 3D similarity transformation based on quaternions. Journal of Spatial Science.

Intercontinental Geoinformation Days

http://igd.mersin.edu.tr/2020/

# An experimental study on the effect of antenna orientation on GNSS-IR

**Cemali Altuntaş*[1], Nursu Tunalıoğlu [1]**

[1]*Yildiz Technical University, Faculty of Civil Engineering, Department of Geomatic Engineering, Istanbul, Turkey.*

**Keywords**
Multipath
Signal to noise ratio (SNR)
Median absolute deviation (MAD)
GNSS-IR
Horizon-looking antenna

**ABSTRACT**

Signal to noise ratio (SNR) data provided by the Global Navigation Satellite Systems (GNSS) receiver indicates the power of the received signal. Estimation of the quantities related to the reflection surface by analysis of the SNR data is called GNSS Interferometric Reflectometry (GNSS-IR). When a geodetic receiver is oriented to a direction, it receives stronger signals from the direction it is looking. In this study, two-day observations for a total of four days with zenith-looking (ZL) and horizon-looking (HL) receivers were performed. The data were analyzed comparatively in terms of amplitude and reflector height estimations. According to the reflector height estimations, it was seen that it is more appropriate to use HL receiver for elevation angles greater than 20°, while there is no significant difference from low elevation angles. Furthermore, since HL receivers receive reflected signals stronger than ZL receivers, the amplitudes of fluctuations in SNR data are found to be higher for HL receivers. Therefore, it can be said that it may be more appropriate to use HL receiver in GNSS-IR studies to determine quantities such as soil moisture to which SNR amplitude is sensitive.

## 1. INTRODUCTION

Multipath is the interference between direct signals from the satellites and those reflected before received by the antenna especially at low satellite elevation angles. Although as originally, GNSS was developed for accurate positioning facilities for various purposes while depending on eliminating this effect, recently several studies for novel applications using multipath have been introduced. Global Navigation Satellite System Interferometric Reflectometry (GNSS-IR) using the advantages of the reflected signals has been implemented in various applications such as soil moisture estimation (Han et al. 2020; Larson et al. 2010; Roussel et al. 2016; Zhang et al. 2017), snow depth retrieval (Gutmann et al. 2012; Larson et al. 2009; Ozeki and Heki 2011; Tunalioglu et al. 2019), sea-level changes (Anderson 2000; Xi et al. 2018) to extract features where the signals were reflected since it has been first proposed in 1993 by Martin-Neira (1993). The method can be classified as non-geometrical and geometrical in which amplitude or the power of signal, and range difference of the direct and reflected signals are considered, respectively (Yang et al. 2019) depending on the application characteristic.

The aim of this article is to apply GNSS-IR technique to two types of oriented GNSS receivers that have the same antenna gain pattern, which are established as zenith-looking (ZL) and horizon-looking (HL) and to investigate whether the orientation affects the gain of the signals or not in terms of amplitude, phase, and reflector height changes.

## 2. METHOD

The signals transmitted by GNSS satellites can be reflected from one or more surfaces before arriving at the GNSS receiver. Receivers record direct and reflected signals simultaneously. These signals interfere at the antenna phase center of the receiver. The power of the composite signal resulting from the interference can be obtained by the $C/N_0$ data provided by the receiver.

$C/N_0$ data were considered approximately equal to the SNR, which can be expressed by the following equation,

$$SNR^2 = {A_d}^2 + {A_m}^2 + 2A_d A_m \cos\Delta\varphi \quad (1)$$

where $A_d$ is the amplitude of the direct signal, $A_m$ is the amplitude of the reflected signal, $\Delta\varphi$ is the phase of

* **Corresponding Author**

*(cemali@yildiz.edu.tr) ORCID ID 0000-0002-9660-6124
(ntunali@yildiz.edu.tr) ORCID ID 0000-0001-9345-5220

**Cite this study**

Altuntaş C & Tunalıoğlu N (2020). An experimental study on the effect of antenna orientation on GNSS-IR. Intercontinental Geoinformation Days (IGD), 244-247, Mersin, Turkey

the composite signal. The changes in the received angle of the GNSS signal due to the movement of the satellite alter the reflection geometry that result in oscillations in the power of the composite signal, i.e. SNR data. To find the contribution of the reflected signals to the SNR data, i.e. to eliminate the contribution of the direct signals, it is appropriate to fit a quadratic polynomial to the SNR data. By removing the trend from the data, detrended SNR (dSNR) is obtained. dSNR can be expressed by the following equation,

$$dSNR = A_m cos(2\pi f \sin\varepsilon + \Delta\varphi) \quad (2)$$

where $f$ is the frequency of the multipath signal, $\varepsilon$ is the satellite elevation angle. Since dSNR data is a function of the sine of the satellite elevation angle, it is sampled irregularly. In this study, Lomb Scargle Periodogram (LSP), which is the commonly used method to determine the frequency of irregularly sampled data, was used to compute the dominant frequency.

There is a relationship between the reflector height and the frequency of the multipath signal as follows,

$$h = f\lambda/2 \quad (3)$$

where $h$ is the reflector height, $\lambda$ is the wavelength of the GNSS signal.

### 2.1. Study Area and Experimental Setup

The study area is a stadium located in Yildiz Technical University Davutpaşa Campus with a wide flat surface and open sky view. The experiment was carried out on 4 days with the CHC i50 geodetic GNSS receiver. The receiver was established on DoY (Day of Year) 267 and 268 by being oriented towards the zenith (ZL). The antenna was oriented towards the horizon (HL) on the DoY 275 and 276 (Figure 1).


**Figure 1.** Study area and experimental setup

In-situ measurements of reflector heights are 2.127 m for ZL receiver and 2.025 m for HL receiver.

### 2.2. Data and Analysis

The duration of daily observations was set to 5 hours. The data-sampling interval is set to 1 second. SNR signals at L1 frequency (S1C, S1X, S1I) transmitted from all satellite systems (GPS, GLONASS, Galileo, BeiDou) were evaluated. The range of 0°-20° where the number of multipath signals increases was selected as the satellite elevation angle range. Data with a range of at least 10° elevation angles were evaluated, other than these, were excluded. The SNR trend has been removed using a 2nd order polynomial. The dominant frequency and amplitude of the dSNR were estimated by LSP. The reflector height was obtained by using Eq. (3).

Four different ways have been used to remove the defective ones from the estimated reflector heights. In the first three of these, the MAD (Median Absolute Deviation) value and its different coefficients were used. In the last one, the estimations that the maximum amplitude of the dSNR is not greater than 4 times of the background noise were accepted as an outlier. Besides, the results in which all measurements were evaluated, were also shared. The analyses were carried out in two different ways in plane: for data from all directions (0°-360°), and only for the direction range where the horizon line is open (200°-300°).

## 3. RESULTS

The usual setup of geodetic GNSS receivers is such that the maximum gain of the antenna is oriented to the zenith. When the receiver is set up in this way, the antenna has the maximum gain for signals from the 90°, while the minimum gain for the signals coming from the 0° or below satellite elevation angles. Depending on the antenna gain pattern of the receiver, the power of the received signal changes depending on the satellite elevation angle.

When the receivers are oriented in a direction parallel to the surface, the angle at which the strongest signal received changes by the same amount. In this study, on DoY 275 and 276, the receiver was setup oriented to 250° in azimuth. When the receiver is setup in this way, the antenna has the maximum gain for signals from the 0°, while the minimum gain for the signals from the 90° satellite elevation angle. Since the multipath effect is more intense at low elevation angles, when the antenna is oriented in this way, it receives the reflected signals with high gain like direct signals. This means that this antenna orientation can be used in GNSS-IR studies.

Figure 2 shows the satellite elevation angles and logarithmic display of the SNR data from the G04 satellite on DoY 268 and 276. On DoY 268, at low elevation angles where multipath is intense, the mean SNR starts from ~35 dB and increases with the elevation angle. On DoY 276, the mean SNR starts from ~50 dB at low elevation angles and decreases as the elevation angle increases.

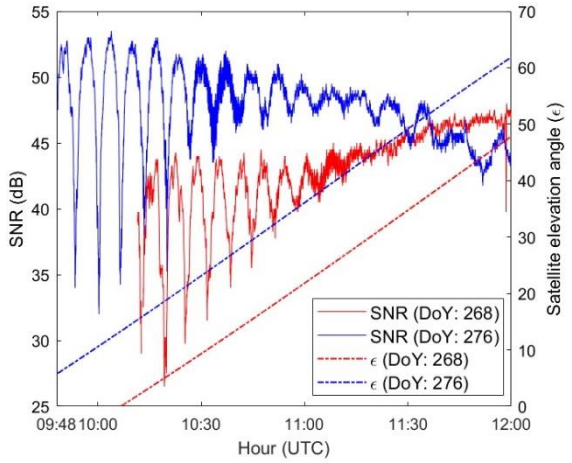


**Figure 2.** SNR plots and elevation angles of G04 satellite on DoY 268 and 276

In Figure 3, the dSNR data of the G04 satellite for all observation days are shown. The amplitude of the dSNR data on the days when the receiver is HL is ~4 times greater than the days when the receiver is ZL. However, in the 30°-60° satellite elevation angle range, it is seen that there is no significant sinusoidal signal in the dSNR data of the ZL receiver, while there are oscillations in the data of the HL receiver due to reflected signals. LSP analyses of these dSNR data are given in Figure 4. Accordingly, it can be said that the background noise increases with the amplitudes in the HL receiver and there is no improvement in determining the dominant frequency compared to the ZL receiver.

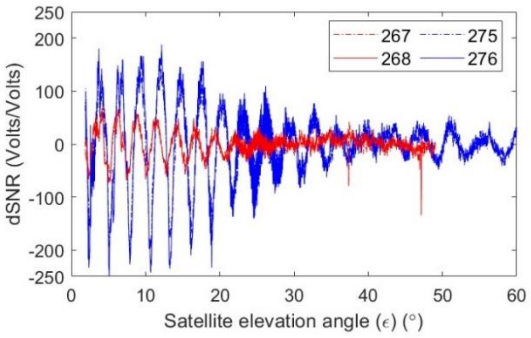


**Figure 3.** dSNR plots for the 0°-60° satellite elevation angle range of G04 satellite for all observation days

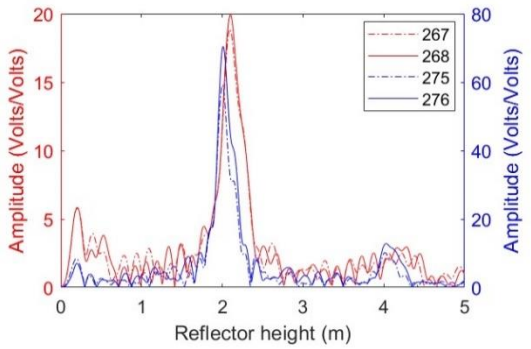


**Figure 4.** LSP of dSNR data for the 0°-60° satellite elevation angle range of G04 for all observation days

In Figure 5, the mean amplitudes of dSNR data obtained from satellites with sufficient number of common observations in four days in the 0°-20° elevation angle range are given. It is seen that installing the antenna horizon-oriented increases the mean dSNR amplitude for all satellites.

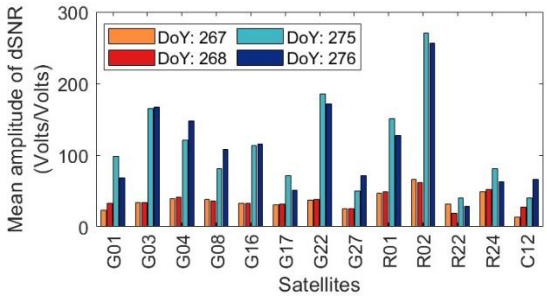


**Figure 5.** Mean amplitudes of dSNRs obtained from the data of common satellites for all observation days

The data were evaluated in two different ways, for the azimuth range of 0°-360° and 200°-300°. In Table 1, the analysis results of the signals coming from the 0°-360° azimuth range (i.e. from all directions) are given. The results obtained for different coefficients of MAD are given in the table. 4BG indicates that estimations where the maximum amplitude is less than four times the background noise are removed. RMSE1 means the standard deviations of the estimates from the in-situ reflector heights (i.e. accuracy), and RMSE2 means the standard deviations from the means of the estimates (i.e. precision).

**Table 1.** Results of 0°-360° azimuth angle range

| | DoY: | 267 | 268 | 275 | 276 |
|---|---|---|---|---|---|
| Num. of Est. | NONE | 41 | 44 | 33 | 33 |
| | 1MAD | 23 | 26 | 19 | 23 |
| | 2MAD | 34 | 37 | 24 | 29 |
| | 3MAD | 36 | 40 | 27 | 31 |
| | 4BG | 26 | 29 | 28 | 26 |
| RH Est. (m) | NONE | 2.097 | 2.080 | 2.032 | 2.033 |
| | 1MAD | 2.135 | 2.125 | 2.057 | 2.055 |
| | 2MAD | 2.127 | 2.130 | 2.062 | 2.053 |
| | 3MAD | 2.123 | 2.123 | 2.053 | 2.044 |
| | 4BG | 2.121 | 2.127 | 2.042 | 2.056 |
| RMSE1 (cm) | NONE | 8.7 | 18.2 | 5.6 | 6.5 |
| | 1MAD | 1.5 | 1.7 | 3.4 | 3.9 |
| | 2MAD | 3.3 | 2.9 | 4.3 | 4.7 |
| | 3MAD | 3.7 | 3.8 | 4.3 | 5.3 |
| | 4BG | 3.3 | 2.6 | 5.4 | 5.8 |
| RMSE2 (cm) | NONE | 8.3 | 17.8 | 5.6 | 6.6 |
| | 1MAD | 1.3 | 1.6 | 1.2 | 2.5 |
| | 2MAD | 3.3 | 2.9 | 2.1 | 3.8 |
| | 3MAD | 3.7 | 3.8 | 3.2 | 5.0 |
| | 4BG | 3.3 | 2.6 | 5.1 | 4.6 |

According to the results in Table 1, using 1MAD to remove bad estimates decreases the number of estimates, but increases accuracy and precision. In Table 2, the analysis results of the signals coming from the 200°-300° azimuth range where the horizon direction is open are given.

**Table 2.** Results of 200°-300° azimuth angle range

| | DoY: | 267 | 268 | 275 | 276 |
|---|---|---|---|---|---|
| Num. of Est. | NONE | 12 | 17 | 15 | 14 |
| | 1MAD | 10 | 10 | 9 | 11 |
| | 2MAD | 11 | 14 | 11 | 14 |
| | 3MAD | 12 | 16 | 14 | 14 |
| | 4BG | 11 | 17 | 15 | 14 |
| RH Est. (m) | NONE | 2.132 | 2.130 | 2.055 | 2.057 |
| | 1MAD | 2.131 | 2.130 | 2.060 | 2.055 |
| | 2MAD | 2.130 | 2.127 | 2.063 | 2.057 |
| | 3MAD | 2.132 | 2.127 | 2.061 | 2.057 |
| | 4BG | 2.132 | 2.130 | 2.055 | 2.057 |
| RMSE1 (cm) | NONE | 1.4 | 2.0 | 4.0 | 3.8 |
| | 1MAD | 1.0 | 0.7 | 3.6 | 3.4 |
| | 2MAD | 1.0 | 1.1 | 3.9 | 3.8 |
| | 3MAD | 1.4 | 1.6 | 3.9 | 3.8 |
| | 4BG | 1.4 | 2.0 | 4.0 | 3.8 |
| RMSE2 (cm) | NONE | 1.3 | 2.1 | 2.7 | 2.1 |
| | 1MAD | 0.9 | 0.7 | 0.5 | 1.7 |
| | 2MAD | 1.0 | 1.2 | 0.8 | 2.1 |
| | 3MAD | 1.3 | 1.7 | 1.6 | 2.1 |
| | 4BG | 1.4 | 2.1 | 2.7 | 2.1 |

According to Table 2, more accurate and precise estimates were made by using 1MAD.

## 4. DISCUSSION

In Tables 1 and 2, it is seen that the accuracy and precision values are very close to each other for the estimates of DoY 267 and 268, while there are differences in the estimates of DoY 275 and 276. Additionally, considering the final reflector height estimates, it is seen that the estimates of DoY 267 and 268 (2.131 m and 2.130 m) are close to the in-situ height (2.127 m), while there is a difference of approximately 3 cm between the in-situ height (2.025 m) and estimates of DoY 275 and 276 (2.060 m and 2.055 m). These results show that the in-situ measurement for the HL receiver may have an offset. However, to strengthen this inference, more daily observations should be performed. In this initial study, we will be content with stating that there is a high probability of such an offset for CHC i50, and we will leave it to further studies to verify this with longer experiments.

## 5. CONCLUSION

According to the precision values, it can be concluded that establishing the receiver ZL or HL does not make a significant difference in the precision of reflector height estimation for low elevation angles (0°-20°). However, we can infer from the dSNR plot shown in Figure 3 it is appropriate to use a HL receiver for higher elevation angles (e.g. 30°-60°). Besides, as seen in Figure 5, it can be said that setting the receiver HL collects the reflected signals stronger and is particularly suitable for use in GNSS-IR studies to determine the quantities related to dSNR amplitude (e.g. soil moisture).

In future studies, a better modeling of the dSNR signal of the HL receiver can be developed. In addition, the observations of a nadir-looking receiver can be examined similarly.

## REFERENCES


Anderson K D (2000). Determination of water level and tides using interferometric observations of GPS signals. Journal of Atmospheric and Oceanic Technology. 17(8), 1118-1127, doi:10.1175/1520-0426(2000)017<1118:DOWLAT>2.0.CO;2.

Gutmann E D, Larson K M, Williams M W, Nievinski F G & Zavorotny V (2012). Snow measurement by GPS interferometric reflectometry: an evaluation at Niwot Ridge, Colorado. Hydrological Processes, 26(19), 2951-2961, doi:10.1002/hyp.8329.

Han M, Zhu Y, Yang D, Chang Q, Hong X & Song S (2020). Soil moisture monitoring using GNSS interference signal: proposing a signal reconstruction method. Remote Sensing Letters, 11(4), 373-382. DOI: 10.1080/2150704X.2020.1718235.

Larson K M, Gutmann E D, Zavorotny V U, Braun J J, Williams M W & Nievinski F G (2009). Can we measure snow depth with GPS receivers?. Geophysical Research Letters, 36(17), doi:10.1029/2009GL039430.

Larson K M, Braun J J, Small E E, Zavorotny V U, Gutmann E D & Bilich A L (2010). GPS Multipath and Its Relation to Near-Surface Soil Moisture Content. IEEE Journal of Selected Topics in Applied Earth Observations and Remote Sensing, 3(1), 91-99. doi: 10.1109/JSTARS.2009.2033612.

Martin-Neira M (1993). A passive reflectometry and interferometry system (PARIS): Application to ocean altimetry. ESA Journal, 17(4), 331-355.

Ozeki M & Heki K (2012). GPS snow depth meter with geometry-free linear combinations of carrier phases. Journal of Geodesy, 86(3), 209-219, doi:10.1007/s00190-011-0511-x.

Roussel N, Frappart F, Ramillien G, Darrozes J, Baup F, Lestarquit L & Ha M C (2016). Detection of Soil Moisture Variations Using GPS and GLONASS SNR Data for Elevation Angles Ranging From 2° to 70°. IEEE Journal of Selected Topics In Applied Earth Observations And Remote Sensing, 9(10), 4781.

Tunalioglu N, Dogan A H, Durdag U M (2019). GPS sinyal gürültü oranı verileri ile kar kalınlığının belirlenmesi. HKMOJJD, 6(1), 1-9. Doi: 10.9733/JGG.2019R0060 1001.T.

Xi R, Zhou X, Jiang W & Chen Q (2018). Simultaneous estimation of dam displacements and reservoir level variation from GPS measurements. Measurement, 122, 247-256. doi:10.1016/j.measurement.2018.03.036.

Yang Y, Zheng Y, Yu W, Chen W & Weng D (2019). Deformation monitoring using GNSS-R technology. Advances in Space Research. 63, 3303–3314.

Zhang S, Roussel N, Boniface K, Ha M C, Frappart F, Darrozes J, Baup F & Calvet J C (2017). Use of reflected GNSS SNR data to retrieve either soil moisture or vegetation height from a wheat crop. Hydrol. Earth Syst. Sci., 21, 4767–4784, https://doi.org/10.5194/hess-21-4767-2017.

## Photogrammetry and Remote Sensing – 4

**UAVs and Photogrammetry**

*Imole Favour Okediji*

**UAV Based 3D Modeling of Ancient Quarry Nearby the Göbeklitepe**

*Nizar Polat, Mustafa Ulukavak, Abdulkadir Memduhoğlu, Halil İbrahim Şenol*, Yunus Kaya*

***UAV Based Crop Monitoring***

*Mustafa Özkan*, Nizar Polat*

***Using of Hybrid Data Acquisition Techniques for Cultural Heritage a Case Study of Pompeiopolis***

*Seda Nur Gamze Hamal*, Binnaz Sarı, Ali Ulvi*

**Modeling of Adamkayalar Reliefs with Current Techniques**

*İldeniz Leyla Öztürk*, Mehmet Özgür Çelik, Erkan Baygül*

**Documentation of complex structure using unmanned aerial vehicle (UAV) photogrammetry method and terrestrial laser scanner (TLS)**

Binnaz Sarı*, Seda Nur Gamze Hamal, Ali Ulvi

Intercontinental Geoinformation Days

http://igd.mersin.edu.tr/2020/

# UAVs and Photogrammetry

**Imole Favour Okediji**[1]

[1]Universityof Lagos, Faculty of Engineering, Department of Surveying and Geoinformatics, Lagos, Nigeria

**Keywords**
UAV
Photogrammetry
Mapping
Geomatics

**ABSTRACT**

The Unmanned Aerial Vehicle (UAV) is a remote-controlled aircraft. It can be operated remotely in real-time or pre-programmed to fly autonomously on the pre-defined routes. Popularly known as a drone, the use of this type of aircraft is increasing in all sectors. Within the last few years, UAVs have opened a new realm of opportunities for Surveying and Mapping, introduced better, faster, and cost-effective methods for the practice of Photogrammetry. In this paper, we discuss the evolution of Photogrammetry, the evolution of UAV, UAV in Geomatics, the impact of UAV in Photogrammetry, the current trend, and future implications.

## 1. INTRODUCTION

Photogrammetry is the art and science of determining the position and shape of objects from photographs (Kraus 1994). It has been in existence for quite a while now, and back in 1480, Leonardo da Vinci wrote the following: "Perspective is nothing else than the seeing of an object behind a sheet of glass, smooth and quite transparent, on the surface of which all the things may be marked that are behind this glass. All things transmit their images to the eye by pyramidal lines, and these pyramids are cut by the said glass. The nearer to the eye these are intersected, the smaller the image of their cause will appear." The principles of perspective and projective geometry form the basis from which photogrammetric theory is developed. However in the 19th century, precisely in 1849, Aime Laussedat, known as the father of Photogrammetry, was the first to use terrestrial photographs for topographic map compilation. He was also the first person to experiment with aerial photography using kites and balloons. It must be noted as well that Photogrammetry in America started with the military and world war. It is generally believed that there are two types of Photogrammetry namely Terrestrial and Aerial Photogrammetry. However, the development cycles are more than two. The developments in photogrammetry, from around 1850, have followed four development cycles (Konecny 1985). Each of these periods extended about fifty years. These cycles include: Plane table, Analog, Analytical and Digital Photogrammetry. The fourth cycle is still prevalent, and the use of UAVs is associated with it.

There is already an extensive scope for geomatics applications of Unmanned Aerial Vehicle (UAV) imagery. Some of the applications put into operation include archaeology, architecture, cultural heritage, large scale mapping, 3D city modeling, change detection in urban and suburban areas, cadastral mapping, agriculture and forestry, natural and man-made hazards, environmental and construction monitoring (Gruen 2012). This study aims to investigate the evolution of UAV and how it has impacted Photogrammetry.

## 2. METHOD

This study is based on literature review. Accessible journals, papers, and books on UAV and UAV photogrammetry have been examined. Relevant information, results and conclusions made have been included in the results section.

### 2.1. Evolution of Photogrammetry

Photogrammetry has witnessed massive evolution from the early 1900s till date.

In the early 1900s, before 1930, people had to walk the land and early map production was by foot (ASPRS 2009). In the 1930s, the Zeiss multiplex stereoplotter was created. In the 1940s, Bausch and Comb Multiplex stereoplotter and 5 lens camera system were produced. In the 1950s, Fairchild single lens camera and Kelsh stereoplotter were created. In the 1960s, Wild and Zeiss Cameras were created, as well as mechanical projection plotters. In the 1970s, Digital output on stereoplotter was created, low distortion lenses were made and LANDSAT came into being. In the 1980s, analytical stereoplotter, CADD based digital mapping and image

*Corresponding Author

*(e-mail) ORCID ID xxxx – xxxx – xxxx – xxxx

Cite this study

Okediji I F (2020). UAVs and Photogrammetry. Intercontinental Geoinformation Days (IGD), 248-251, Mersin, Turkey

motion compensation cameras were created. In the 1990s, softcopy photogrammetry, digital orthophotography, and digital cameras were all created. It was from this period that GIS got integrated in mapping and digital photogrammetry really took off.

Photogrammetry as we know, reached its apex of evolution because of the ability to digitize directly. Now anyone can access a map on their computers or mobile devices, the field has become ubiquitous (ASPRS 2009). In recent times, UAVs have taken the place of manned aircraft and are now used as platforms for sensors through which aerial photographs are captured.

### 2.2. Evolution of UAV

UAVs were first created and used in military applications where flight recognition in enemy areas, unmanned inspection, surveillance, reconnaissance and mapping of enemy areas without any risk for human pilots were the primary military aims (Nex and Remondino 2014). The earliest recorded use of a UAV dates back to 1849 when the Austrians attacked the Italian city of Venice using unmanned balloons that were loaded with explosives. Although balloons would not be considered a UAV today, this was a technology the Austrians had been developing for months before, which led to further advancements. In 1915, British military used aerial photography to their advantage in the Battle of Neuve Chapelle. They were able to capture more than 1,500 sky view maps of the German trench fortifications in the region.

The United States began developing UAV technology during the First World War in 1916 and created the first pilotless aircraft. Shortly after, the U.S Army built the Kettering Bug. While continuing to develop UAV technology, in 1930 the U.S Navy began experimenting with radio-controlled aircraft resulting in the creation of the Curtiss N2C-2 drone in 1937. During WWII, Reginald Denny created the first remote-controlled aircraft called the Radioplane OQ-2. This was the first massed produced UAV product in the U.S and was a breakthrough in manufacturing and supply drones for the military.

Drones were previously known to be an unreliable and an expensive toy, but in the 1980s this attitude began to change. The Israeli Air Force's victory over the Syrian Air Force in 1982 contributed to this change. Israel used both UAVs and manned aircraft to destroy a dozen of Syrian aircraft with minimal losses. Further, in the 1980s, The U.S created the Pioneer UAV Program to fulfill the need for inexpensive and unmanned aircraft for fleet operations. In 1986 a new drone was created from a joint project between the U.S and Israel. The drone was known as RQ2 Pioneer, which was a medium sized reconnaissance aircraft. More recently, in 1990 miniature and micro UAVs were introduced and in 2000 the U.S deployed the Predator drone in Afghanistan while searching for Osama Bin Laden. Although many of the most notable drone flights have been for military purposes, technology is continuing to advance and receive more attention. The term UAV is used commonly in the geomatics community, but also terms like Remotely Piloted Vehicle (RPV), Remotely Operated Aircraft (ROA), Remote Controlled (RC) Helicopter, Unmanned Vehicle Systems (UVS) and Model Helicopter are often used (Remondino et al. 2011). In terms of nomenclature, UAVs have had different names over the years, the most popular being drone.

Nowadays, UAVs are increasingly being used in civil and scientific research activities in different fields of application (Koeva et al. 2018). For example, for agriculture (Grenzdörffer and Niemeyer 2011), mapping (Nex and Remondino 2014), surveying and cadastral applications (Cunningham et al. 2011; Manyoky et al. 2011; Cramer et al. 2013; Barnes et al. 2014), archaeology and architecture (Chiabrando et al. 2011), geology (Eisenbeiss 2009), coastal management (Delacourt et al. 2009), disaster management (Choi and Lee 2011; Molina et al. 2012), damage mapping (Vertivel et al. 2015) and cultural heritage (Remondino et al. 2011; Rinaudo et al. 2012).

#### 2.2.1. Uav and photogrammetry

The signs clearly point in the direction that the use of UAVs has been established, generally accepted, and vigorously growing (Lemmens 2015). Moreover, a group of experts on Global Geospatial Information Management has identified the increased demand for applying high-resolution imagery and the increase use of UAVs as a tool for rapid geospatial data collection as key emerging trends for the next ten years (UN-GGIM 2013).

The impact UAV has had on Photogrammetry is tremendous. This is evidenced by the number of papers that have been written within the past few years, and also by how much attention discussions around UAV receive in conferences. In 2004, the ISPRS congress in Istanbul hosted three UAS-related papers but did not feature any session specifically devoted to un-manned platforms (Colomina and Molina 2014). The trend changed in 2008, in Beijing, where 21 papers related to the use of UAS for Photogrammetry and Remote Sensing (PaRS) and mapping purposes were presented in three different sessions. At the ISPRS congress in Melbourne in 2012, nine sessions related to UAS were held, featuring around 50 UAS-related papers. The international photogrammetric community has set up a dedicated biennial conference that began in 2011: the UAV-g (UAV-g 2011 in Zürich, Switzerland, UAV-g 2013 in Rostock, Germany and UAV-g 2015 in Toronto, Canada). The increase in UAS related publications at these conferences is clear, yet not exclusive (Colomina and Molina 2014)

The IEEE Geoscience and Remote Sensing Society (IGARSS) has featured UAS-related papers at its annual symposiums since 2005. UAS-related papers have also been presented at the American Society for Photogrammetry and Remote Sensing (ASPRS) congresses, from 2005 in Baltimore up to present editions. Furthermore, the Multidisciplinary Digital Publishing Institute (MDPI) Open Access Journal of Remote Sensing published a special issue called ''Unmanned Aerial Vehicles (UAVs) based Remote Sensing,'' closed in June 2012, with around 12 peer-reviewed papers (Colomina and Molina 2014). Since

then, more papers have been written, and a lot more research has been carried out. The trend in drone research and applications is a continuing one which will still be effective many years from now.

## 3. RESULTS

In the last years, more and more applications of UAVs in the geomatics field became common (Remondino et al. 2011). UAV photogrammetry indeed opens various, new applications in the close-range aerial domain and introduces also a low-cost alternatives to the classical manned aerial photogrammetry (Colomina et al. 2008; Eisenbeiss 2009).

With photogrammetry it is possible to determine size, shape and location of depicted objects by measuring in images (Cramer 2001), this without a need of physical contact to the object (Linder 2009). Measurements can be performed using a single image, a stereo pair or in a block of two or more images (Cramer 2001). Measurements done in one image can only give 2D coordinates, while 3D coordinates can be obtained using two or more images of the same object, captured from different positions (Gustafsson and Zuna 2017). Different types of sensors including Light Imaging Detection and Ranging (LiDAR) and Radio Detection and Ranging (RADAR) can be mounted on UAVs and be used to capture geographic data which can be processed to form Orthophoto, Digital Terrain Model (DTM), Digital Surface Model (DSM), Digital Elevation Model (DEM), 3D model amongst others. The products that can be derived from aerial photographs captured through UAVs are applicable in diverse fields and not limited to photogrammetry alone. With the kind of software we have now, such as Agisoft photoscan and Pix4DMapper, processing aerial imagery can be done in a short time with the production of accurate models. This is faster and easier than using Analytical photogrammetry methods which included the rigorous least squares mathematical process and the use of stereoplotters. Some UAVs now come with inbuilt software that aid the processing of images captured.

## 4. DISCUSSION

Technically, UAVs can fly almost everywhere. Their flexibility is high and this fact allows them easily to change the observed location and viewing angle in a short time (Koeva et al. 2018). For that reason, it is important to pay attention to the safety of the users of aerial spaces, including manned or other unmanned aircraft, to the people and property on the ground, as well as their impact on the environment (Watts et al. 2012). This emerges from a concern regarding how this flying system, which does not have pilots on board, can be safely deployed in public space. With the ability to carry cameras, infrared sensors and facial recognition technology, they can present a serious threat to privacy. However, in daily practice, one obstacle is a missing or unfavourable regulatory framework. This is being controlled in many countries where UAVs are allowed to fly, for instance, China, Japan, U.S.A, and Sweden among other countries have strict regulations on where and how UAVs can fly, at what altitude and how long.

Although the battery life of UAVs is considered to be a drawback, provisions have been made to extend how long they remain in the air. Based on size, weight, endurance, range and flying altitude, UVS International defines three main categories of UAVs (Remondino et al. 2011), they are: (i) tactical UAVs which include micro, mini, close-, short-, medium-range, medium-range endurance, low altitude deep penetration, low altitude long endurance, medium altitude long endurance systems. The mass ranges from few kilograms up to 1,000 kg, the range from few kilometers up to 500 km, the flight altitude from few hundred meters to 5 km, and the endurance from some minutes to 2-3 days; (ii) strategical UAVs, including high altitude long endurance, stratospheric and exo-stratospheric systems which fly higher than 20,000 m altitude and have an endurance of 2-4 days; and (iii) special tasks UAVs like unmanned combat autonomous vehicles, lethal and decoys systems (Remondino et al. 2011). The primary airframe types are fixed and rotary wings while the most common launch/take-off methods are, beside the autonomous mode, air-, hand-, car/track-, canister-, bungee cord launched (Remondino et al. 2011). In any case, it is clear now that some types of UAVs can cover large areas since they can last more than two days. This shows that improvements have been made with specific UAVs which remove the drawback of them only being able to cover small areas because they do not last long in the air.

## 5. CONCLUSION

As opposed to the early 20th century when manned aircraft was the way aerial photographs were obtained, we now use UAVs/drones to capture images. The benefits that come with the use of UAVs are quite immense, for one; a reduced number of people are required during any flight operation thus making the process labour intensive. It is also a lot cheaper than the use of manned aircraft. These days, most drones come with inbuilt cameras and sensors which usually have high resolutions. In the event that other sensors are required, they can just be added to the drone as part of the payload. Not only do UAVs save money and reduce labour, they also consume less time. An operation that will take a week with the use of manned aircraft may take three days with UAVs. This is because flight planning can be done before reaching the site, also because drones can be set to fly autonomously.

UAVs will continue to thrive and grow in Photogrammetry not only because they offer cheaper and better options, but also because they are versatile and flexible. Producers of UAVs will continue to find ways around their limitations and therefore make them indispensable to Surveyors, Geomaticians and all other professions that currently use UAVs. İn a few years from now, manned aircrafts will not even be used anymore as platforms for capturing aerial photographs. UAVs are here to stay and they will continue to remain relevant in the field of Photogrammetry.

**ACKNOWLEDGEMENT**

First of all, I would like to thank Mr. Goke Daramola and Mr. Chukwuma Okolie for their encouragement and support. I would also like to thank Akinnusi Samuel, Ajayi-Abu Feyisayo, Adebayo Joel, Olanrewaju Hamed, Abioye Hannah, Alpha Adebayo, Dominion Eromosele and all members of DELITe for their help throughout the period of writing this paper. I am also very grateful to Dr. Lola Olayinka, NIFES, and my parents.

Finally, all thanks and glory to God Almighty.

**REFERENCES**

Al-Tahir R (2014). Training and research for developing applications using UAV Imagery. Presented in National Surveyors Conference 2014, St Andrews, Canada.

Barnes G et al. (2014). Drones for peace: Part 1 of 2 design and testing of a UAV-based cadastral surveying and mapping methodology in Albania. In: World bank conference on land and poverty, Washington DC, USA, 24–27 March 2014.

Chiabrando F et al. (2011). UAV and RPV systems for photogrammetric surveys in archaeological areas: two tests in the piedmont region (Italy). Journal of Archaeological Science, 38 (3), 697–710.

Choi K & Lee I (2011). AUAV based close-range rapid aerial monitoring system for emergency responses. ISPRS – International Archives of the Photogrammetry, Remote Sensing and Spatial Information Sciences, XXXVIII-1/C22, 247–252.

Colomina I and Molina P (2014). Unmanned aerial systems for photogrammetry and remote sensing: A review. ISPRS Journal of Photogrammetry and Remote Sensing, 92: pp79–97,

Colomina I, Blázquez M, Molina P, Parés M E & Wis M (2008), Towards a new paradigm for high-resolution low-cost photogrammetry and remote sensing. IAPRS&SIS, Vol. 37(B1), Beijing, China, pp. 1201-1206

Cramer M (2001). On the use of direct georeferencing in airborne photogrammetry. Institut f˙ur Photogrammetrie

Cramer M et al. (2013). On the use of RPAS in national mapping—The EUROSDR point of view. ISPRS – International archives of the photogrammetry, remote sensing and spatial information sciences, XL-1/W2, 93–99.

Cunningham K et al. (2011). Cadastral audit and assessments using unmanned aerial systems.' In: UAV-g: conference on unmanned aerial vehicle in geomatics. Zurich, Switzerland, 14–16 September 2011.

Delacourt C et al (2009). DRELIO: an unmanned helicopter for imaging coastal areas. Journal of Coastal Research, 56 (SI), 1489–1493. doi: 10.1016/j.isprsjprs.2014.02.013.

Eisenbeiss H (2009). UAV photogrammetry. Diss. ETH No. 18515, Institute of Geodesy and Photogrammetry, ETH Zurich, Switzerland, Mitteilungen Nr.105, p. 235.

Eisenbeiss H (2009). UAV photogrammetry. Ph.D. Thesis, Institut für Geodesie und Photogrammetrie, ETH-Zürich. Zürich, Switzerland.

Grenzdörffer G J & Niemeyer F (2011). UAV based BRDF-measurements of agricultural surfaces with pfiffikus. International Archives of the Photogrammetry, Remote Sensing and Spatial Information Sciences, 38 (1/C22), 229–234

Gruen A (2012). Unmanned Aerial Vehicles - From Toys to Tools. GEOInformatics, 15(1), 14-16.

Gustafsson H & Zuna L (2017). Unmanned Aerial Vehicles for Geographic Data Capture: A review. Bachelor's thesis, Royal institute of Technology, Stockholm, Sweden

Koeva M, Muneza M, Gevaert C, Gerke M & Nex F (2018) Using UAVs for map creation and updating. A case study in Rwanda, Survey Review, 50:361, 312-325, DOI: 10.1080/00396265.2016.1268756

Konecny G (1985). "The International Society for Photogrammetry and Remote Sensing - 75 Years Old, or 75 Years Young", Keynote Address, Photogrammetric Engineering and Remote Sensing, 51(7), 919-933.

Kraus K (1994) Photogrammetry, Verd. Duemmler, Bonn

Lemmens M (2015). Confusion. GIM International. Volume 29, Issue 5, page 13.

Linder W (2009). Digital Photogrammetry. Springer Berlin Heidelberg

Manyoky M et al. (2011). Unmanned aerial vehicle in cadastral applications. In: UAV-g: conference on unmanned aerial vehicle in geomatics. Zurich, Switzerland, 14–16 September 2011.

Molina P et al (2012). Drones to the rescue! unmanned aerial search missions based on thermal imaging and reliable navigation. Inside GNSS, 7, 36 –47.

Nex F & Remondino F (2014). UAV for 3D mapping applications: a review. Applied Geomatics, 6(1), 1–15

Remondino F, Barazzetti L, Nex F, Scaioni M , Sarazzi D (2011) UAV Photogrammetry for mapping and 3D Modeling –Current Status and Future Perspectives, IAPRS & SIS, Volume XXXVIII-1/C22, pp 25-31

Rinaudo F et al (2012). Archaeological site monitoring: UAV photogrammetry can be an answer. ISPRS – International Archives of the Photogrammetry, Remote Sensing and Spatial Information Sciences, XXXIX-B5, 583–588.

UN-GGIM (2013). Future Trends in Geospatial Information Management: the five to ten year vision. United Nations initiative on Global Geospatial information Management. (15 Aug. 2015).

Vetrivel A et al (2015). Identification of damage in buildings based on gaps in 3D point clouds from very high resolution oblique airborne images. ISPRS journal of photogrammetry and remote sensing, 105, 61–78.

Intercontinental Geoinformation Days

http://igd.mersin.edu.tr/2020/

# UAV Based 3D Modeling of Ancient Quarry Nearby the Göbeklitepe

**Nizar Polat[1], Mustafa Ulukavak [1], Abdulkadir Memduhoğlu [1] Halil İbrahim Şenol [*1] Yunus Kaya [1]**

[1]*Harran University, Faculty of Engineering, Department of Geomatics Engineering, Sanliurfa, Turkey*

**Keywords**
Göbeklitepe
Ancient Quarry
UAV
3D Modelling

**ABSTRACT**

Documentation of historical artifacts and archaeological sites is a very important process in terms of preserving cultural heritage. Because such cultural heritages that should be passed on to future generations are destroyed or even disappeared over time. The documentation process is a versatile multi-disciplinary process. Today, methods in the documentation process started to change with the developing technologies. In recent years, image-based 3-dimensional (3D) modeling by using Unmanned Aerial Vehicles (UAV) has also been widely used. In this study, UAV based 3D modeling of an ancient quarry located on another hill relatively close to Göbeklitepe and the produced topographic products such as digital elevation model and orthophoto are presented.

## 1. INTRODUCTION

The Unmanned Aerial Vehicle (UAV) platforms are very important data source that enables inspection, surveillance and analysis for different disciplines and different application areas in photogrammetric data production. These systems, which have been used since the 1960s, are getting more and more attention from scientists and researchers. The main reason for the increasing popularity of UAV systems is that thanks to the developing photogrammetric sensor, platform, and remote sensing technologies, they provide higher spatial and temporal resolution compared to classical aerial photogrammetry (Kaya et al., 2019; Ulvi, 2018; Uslu et al., 2016). Also, this method has significant speed and low-cost advantages in photogrammetric data production. Provided by the UAV systems, it has many civil and commercial applications due to the advantage of fast and economical access to up-to-date data (Yakar et al., 2016; Kaya et al., 2019; Remondino, 2011). Today, it is used in different disciplines such as agriculture, archaeology, forestry, wildlife research, geomatic engineering, habitat studies, landscape planning, mining, environmental surveillance, natural disasters, traffic management, transportation, energy, geology (Vacca, Onishi, 2017; Näsi et al., 2018; Calleja et al., 2018; Bagaram, 2018; Onitsuka et al., 2018; Azhari et al., 2017; Tziavou et al., 2018; Toprak et al., 2019, Ulukavak et al., 2019).

There are many studies on the use of UAVs in photogrammetric modeling and mapping. These studies mostly involve the production of orthophotos, point clouds and DEMs (Uysal et al., 2015; Polat, Uysal, 2018). Some studies also have rock relief modeling (Toprak et al., 2019). Similar applications are also made in open minefields. Especially at actively used mines, UAV systems are used in operations such as determination of production and stripping amount, stock and dump area cubage calculations, rock detection, geological mapping (Muammer et al., 2017). UAVs, also have been used widely in the documentation of historical artifacts and archaeological sites in recent years. In this study, an UAV based modeling of an ancient quarry located on a hill which is very close to the Göbeklitepe archaeological site is presented.

## 2. METHOD

In the study, TurkUAV Octo V3 UAV was used to produce an orthophoto of the archaeological site. The images obtained with the UAV were processed with Agisoft Photoscan, a very popular, photogrammetry software.

* **Corresponding Author**

(nizarpolat@harran.edu.tr) ORCID ID 0000-0002- 6061- 7796
ORCID ID 0000-0003-2092- 3075
ORCID ID 0000-0002 -9072- 869X
*(hsenol@harran.edu.tr) ORCID ID 0000-0003-0235-5764
ORCID ID 0000-0003-2319- 4998

**Cite this study**

Polat N, Ulukavak M, Memduhoğlu A, Şenol H İ & Kaya Y (2020). UAV Based 3D Modeling of Ancient Quarry Nearby the Göbeklitepe. Intercontinental Geoinformation Days (IGD), 252-255, Mersin, Turkey

### 2.1. Study Area

The study area is on another hill about 3km away from the Göbeklitepe archaeological site. Although the ancient quarry is mostly covered with soil, the linear rock cuts and room like parts are obvious. The location of the study area with the Göbeklitepe is given in Figure 1.


**Figure 1.** An aerial image that shows the Ancient quarry and Göbeklitepe locations

### 2.2. Equipment

The study was performed with TurkUAV Octo V3 UAV as a photogrammetric platform. The weight of the UAV is approximately 8kg and the payload is a maximum of 3 kg. Flying time depends on both battery and payload weight. A lot of features of this model are available such as Altitude Hold, GPS Hold, CareFree, Coming Home, Fail-Safe, Low Battery Protection, Auto Take-Off and Landing, Waypoint Flight. Mikrocopter (MK Tools) software lets us view the navigation and flight status information in real-time. It is possible to perform an autonomous flight plan over the online basemaps. Moreover, some details such as horizontal and vertical speed, altitude, direction, waiting time at willing points, coordinate information, and camera angle are also can be specified. Waypoint Flight electronic is capable of autonomous flight in a 1000m radius area and 250m fly height for a standard route. The digital camera was a Sony RX100 MII. It has been featured with a 20.2 Megapixel and 13,2x8,8mm CMOS image sensor. Single, continuous, and self-timer drive abilities are among the digital camera features. The Bodyweight of the device is 281g. An image of the unmanned aircraft and the camera are shown in Figure 2.

Multiple parameters should be taken into consideration when working with UAVs. First, the flight plan should be done well and the scenarios of any errors that may arise should be reviewed carefully. The weather conditions (temperature, pressure, humidity) at the time of flight of the region should be checked. To identify the obstacles that may be encountered in the area where the flight will take place, it is necessary to check the dangerous high objects on the land by going to the area before the flight. A flat surface should be chosen as far as possible for the UAV to be able to take off smoothly. Before starting the flight, pre-flight preparations should be checked step by step and then the flight should be started.


**Figure 2.** The UAV system and Digital camera

### 3. RESULTS and DISCUSSION

Since the working area is wide, two different flights were carried out. As a result of these flights planned from an average height of 60 m, a total of 917 photographs were obtained. The ground sampling interval of the photographs was calculated as 1.33 cm. The total area covered by the photographs is approximately 0.169 km$^2$. Photogrammetric flights made with 80% transverse and longitudinal overlap. Camera locations and image overlap is given in Figure 3.

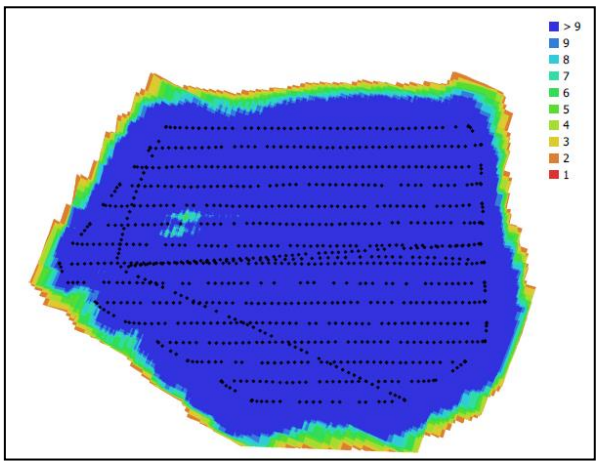


**Figure 3.** Camera locations and image overlap

The obtained geotagged photos were processed with Agisoft software. Aproxiamtely 62 million points were obtained from the photographs. These points were used in the production of a high-resolution digital elevation model and orthophoto of the land surface. The produced model and orthophoto are shown in Figure 4.

When the study area is examined in more detail, it is seen that the stones in the region are linearly cut (Figure 5). The proximity of Göbeklitepe reminds us that stones were removed from here during the construction of the area.

It is also observed that irregular new excavations were made in the area. Since the area is known to be close to a site like Göbeklitepe and does not have an

active quarry, it is thought that randomly irregular excavations were carried out in this area to search for treasure. Images of the excavated areas can be seen in Figure 6.

At the end of the study, a 3D model covered with a true color texture of the entire region was produced. This model can be used in different environments such as virtual reality or GIS with different export options. A few examples of the model are given in the view Figure 7.

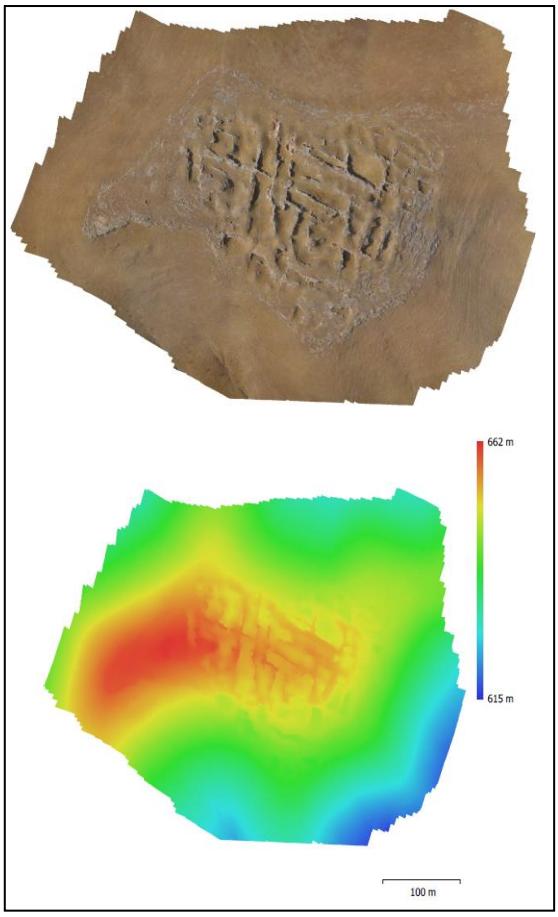


**Figure 4.** Reconstructed digital elevation model and orthophoto

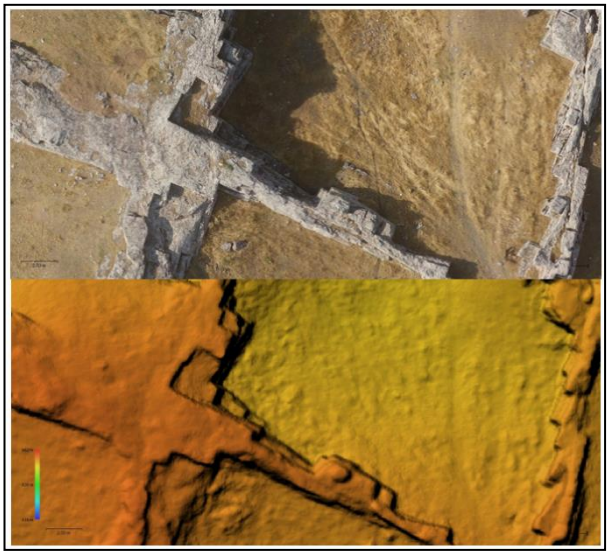

**Figure 5.** Linearly cut stones

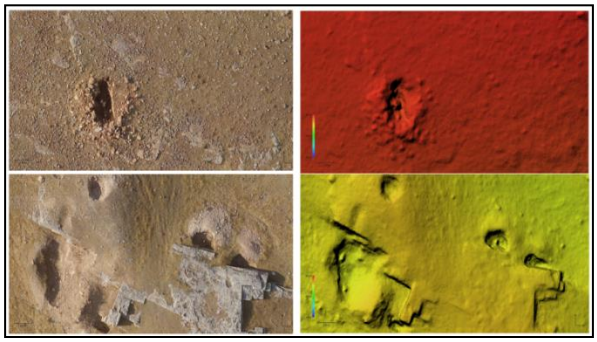

**Figure 6.** Excavated areas for treasure search

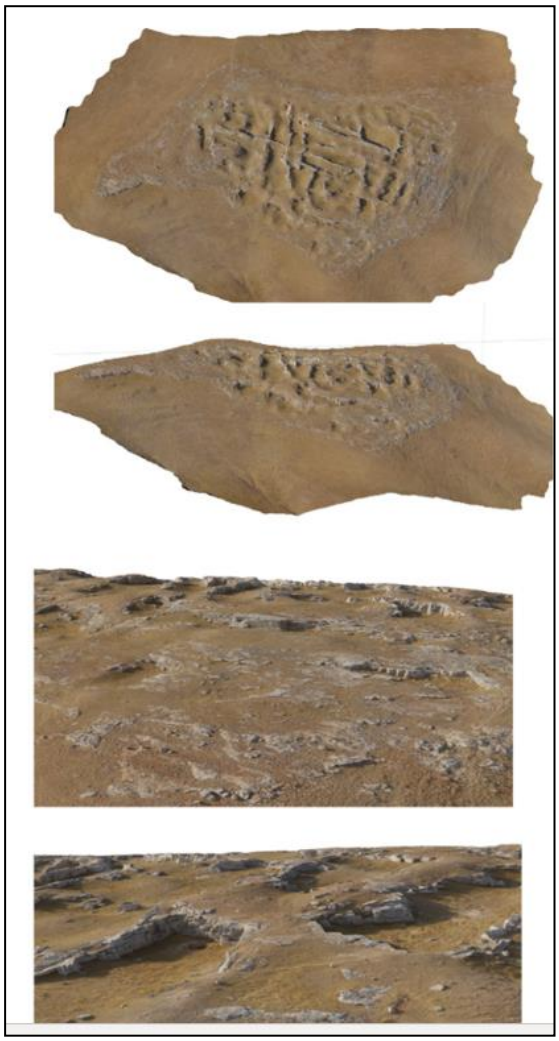

**Figure 7.** Scenes from the generated 3D model of the ancient quarry

## 4. CONCLUSION

UAVs are very important platforms because they are portable, useful, and cheap. Tenders used in many application areas today can also be used in 3D modeling of open minefields. Within the scope of the study, a historical stone quarry was modeled using an UAV flight. It is also important that the region is close to Göbeklitepe. Because when the model produced with high resolution was examined, it was seen that new excavations were made in the region, which was thought to be for treasure purposes. In this context, changes occurring in such regions can be observed regularly with tenders.

**REFERENCES**


Azhari F, Kiely S, Sennersten C, Lindley C, Matuszak M & Hogwood S, (2017). A comparison of sensors for underground void mapping by unmanned aerial vehicles. Underground Mining Technology, Australian Centre for Geomechanics, 419-430, Perth.

Bagaram M B, Giuliarelli D, Chirici G, Giannetti F & Barbati A (2018). UAV remote sensing for biodiversity monitoring: Are forest canopy gaps good covariates?. Remote Sensing, 10(9), 1397.

Calleja J F, Pagés O R, Díaz-Álvarez N, Peón J, Gutiérrez N, Martín-Hernández E, Relea A C, Melendi D R & Álvarez P F (2018). Detection of buried archaeological remains with the combined use of satellite multispectral data and UAV data. International journal of applied earth observation and geoinformation, 73, 555-573.

Kaya Y, Şenol H İ, Memduhoğlu A, Akça Ş, Ulukavak M & Polat N (2019). Hacim Hesaplarında İHA Kullanımı: Osmanbey Kampüsü Örneği. Photogrammetry Journal of Turkey; 1(1), 07-10.

Muammer S, Tiryakioğlu İ, & Uysal M (2017). Farklı veri toplama yöntemleriyle yapılan hacim hesaplarının karşılaştırılması. Geomatik, 2(2), 106-111.

Näsi R, Viljanen N, Kaivosoja J, Alhonoja K, Hakala T, Markelin L & Honkavaara E (2018). Estimating Biomass and Nitrogen Amount of Barley and Grass Using UAV and aircraft based spectral and photogrammetric 3D features. Remote Sensing 10(7), 1082.

Onitsuka K, Ninomiya K & Hoshino S (2018). Potential of 3D visualization for collaborative rural landscape planning with remote participants, Sustainability 10(9), 3059.

Polat N & Uysal M (2018). An experimental analysis of digital elevation models generated with Lidar Data and UAV photogrammetry. Journal of the Indian Society of Remote Sensing, 46(7), 1135-1142.

Remondino F (2011). Heritage recording and 3D modeling with photogrammetry and 3D scanning. Remote Sensing, 3(6), 1104–1138.

Toprak A S, Polat N & Uysal M (2019). 3D modeling of lion tombstones with UAV photogrammetry: a case study in ancient Phrygia (Turkey). Archaeological and Anthropological Sciences, 11(5), 1973-1976.

Tziavou O, Pytharouli S & Souter J (2018). Unmanned Aerial Vehicle (UAV) based mapping in engineering geological surveys: Considerations for optimum results. Engineering Geology, 232, 12-21.

Ulukavak M, Memduhoğlu A, Şenol H İ, Polat N, Çetin B & Demir M (2019). The Use of UAV in Archaeological Excavation: A Case Study in Şanlıurfa Historical Castle. International Journal of Environment and Geoinformatics, 6(3), 323-326.

Ulvi A (2018). Analysis of the Utility of the Unmanned Aerial Vehicle (UAV) in Volume Calculation by Using Photogrammetric Techniques. International Journal of Engineering and Geosciences, 3(2), 43-49.

Uslu A, Polat N, Toprak A S & Uysal M (2016). Kültürel Mirasın Fotogrametrik Yöntemle 3B Modellenmesi Örneği. Electronic Journal of Map Technologies, 8(2), 165-176.

Uysal M, Toprak A S & Polat N (2015). DEM generation with UAV Photogrammetry and accuracy analysis in Sahitler hill. Measurement, 73, 539-543.

Vacca A & Onishi H (2017). Drones: military weapons, surveillance, or mapping tools for environmental monitoring? The need for legal framework is required. Transportation Research Procedia, 25, 51–62.

Yakar M, Kabadayı A, Yiğit A Y, Çıkıkçı K & Catin S S (2016). Emir Saltuk Kümbeti Fotogrametrik Rölöve Çalışması ve 3 Boyutlu Modellenmesi. Geomatik1(1), 14-18.

Intercontinental Geoinformation Days

http://igd.mersin.edu.tr/2020/

# UAV BASED CROP MONITORING

**Mustafa Ozkan[1*], Nizar Polat[1]**

[1]Harran University, Engineering Faculty, Geomatic Engineering Department, Şanlıurfa, Turkey

**Keywords**
Crop tracking
UAV
Photogrammetry
Flooding
VARI

**ABSTRACT**

Today, UAV based monitoring considerably is being used in agriculture studies. The main reasons of this inevitable popularity are the advantages of UAV systems such as ease of use, speed, portability, and low operating costs. Besides, the UAV systems become more powerful with photogrammetric improvements. Photogrammetry allows us to create different topographic digital data such as digital elevation models and orthophotos. In this study, a photogrammetric UAV flight plan was prepared, and aerial images of a 22 ha. cornfield is collected in Şanlıurfa/Çamlıdere ''Fig. 2''. The main purpose of the study is to determine the deficit effects of excessive water. Therefore, the collected aerial images were photogrammetrically processed, and the affected area was automatically calculated as 1.5 ha.

## 1. INTRODUCTION

There is a strong relationship between the history of civilization and agriculture. That is, they depend on each other. Without precision agriculture applications, it was hard to track crops and fields.

The good news is that new digital technologies now make it possible to collect and process huge amounts of critical data at minimal costs—thus making a farm's field operations more insight-driven, and potentially more productive and efficient.

The agriculture ecosystem has already started to invest in these digital technologies. Multispectral satellite images are widely used for large fields, farms, and city-scale studies. In smaller areas, unmanned aerial vehicles (UAV) are popular. UAV systems bring new opportunities to all engineering fields as well as agriculture studies.

Depending on the mounted sensor, it is possible to produce different base products such as maps, digital elevation models, and orthophoto with the UAV. In an earlier study, (Uysal et al. 2015) generated a DEM with UAV photogrammetry and analyzed its accuracy. (Polat and Uysal 2017) generated digital terrain model from UAV based photogrammetric dense point cloud. (Ulukavak et al., 2019) used a UAV to model an archeological site. (Kaya et al. 2019) calculated an artificial pond volume with UAV and compared the results with terrestrial surveys.

Among all these engineering applications, vegetation purposed studies are also existing. Radoglou-Grammatikis et al. (2020) present a survey regarding the potential use of UAVs in precision agriculture. (Gao et al. 2020) try to design an agriculture framework to monitor plant diseases. A detailed study about UAV-based agricultural landscapes can be found in a previous study (Librán-Embid et al. 2019).

This study aimed to monitor the cornfield and detect the damaged area of overflowing water with a UAV. Moreover, it is also aimed to take measures by determining where the overflowing water flows and where it accumulates.

## 2. METHOD

This study map is made with the Structure from Motion (SFM) photogrammetry technic. SFM runs under the same basic conditions as stereoscopic Photogrammetry. It uses overlapping images in order to get a 3D structure of an interested object. Existing software can generate a 3D point cloud such as Pix4d mapper (commercial software) that has been used in this study.

The software advances in UAV applications and allows generating orthophoto in a willed coordinate system. For full performance of software, it is recommended to use a powerful computer due to the huge amount of data.

### 2.1 Preparation and Flight

The flight plan was prepared with Pix4d-Capture mobile application. The drone was set up in the field. All calibration settings were checked. Calibration settings must work properly. Big metal masses must be avoided

* **Corresponding Author**

*(surveyozkan0@gmail.com) ORCID ID 0000-0002-1476-9756
(nizarpolat@harran.edu.tr) ORCID ID 0000-0002-6061-7796

**Cite this study**

Ozkan M & Polat N (2020). UAV Based Crop Monitoring. Intercontinental Geoinformation Days (IGD), 256-258, Mersin, Turkey

throughout the calibration process since such masses locally affect Earth's magnetic field and satellite signals which is used for calibration by UAV.

The flight had two separate missions. All missions have 100 meters altitude and %80-%80 overlap. The drone was set up according to the pre-flight preparations in the field. The flight was performed with multiple batteries to avoid split operations which may cause deviation in RGB analysis with the change of sunlight and atmospheric conditions. The study took 35 minutes, and 310 images were collected. The date was 26 September 2020. The mission started at 1.40 pm. The flight was covered about a 22-hectare. The followed flight route and image overlaps are given in ''Fig.1''

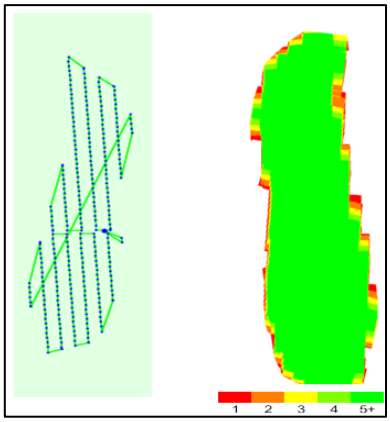


**Figure 1**. Flight route and image overlaps

### 2.2 VARI

VARI (The Visible Atmospherically Resistant Index) is an RGB index for leaf coverage. In other words, it stands for the average density of vegetation covering the ground. This index is used to estimate the fraction of vegetation in an image with low sensitivity to atmospheric effects.

Areas with abundant leaf coverage indicate that the biosphere is actively using hydrosphere for plant growth which is good (pix4d support). Therefore, the higher the value is, the better the optimum irrigation acquired.

VARI= (GREEN − RED) / (GREEN + RED − BLUE)

## 3. Study area and equipment

The study area is a corn field in Şanlıurfa/Çamlıdere. The area is located heading east 38 km from the city center of Şanlıurfa ''Fig.2''. The land has a streambed in the middle of the field. That means the land has a slopy character.

**Figure 2.** The location and shape of the interested corn field.

In this study, it is used DJI Mavic Pro as UAV system ''Fig. 3''. Mavic Pro drone is a pretty useful equipment for small areas. Mavic Pro has 25 minutes flight time. Mavic Pro is equipped with FC220 camera. FC220 has a 6.16mm*4.55 mm sensor size and has a 12.35 MP. We used pix4d capture flight planning and pix4d capture Works with ctrl+dji mobile application for android devices. Predefined settings of Pix4d capture provided us a quick and easy flight plan.

**Figure 3.** DJI Mavic Pro

## 4. RESULTS

All processes are made in Pix4d software. The ground sample distance (GSD) was calculated as 3.35 cm. The point cloud, triangle mesh, and orthomosaic map were created in the study.

The point cloud has 1540030 points. The orthomosaic map was generated with a 15 cm spatial resolution. The final product was VARI which is generated from orthomosaic ''Fig.4''.

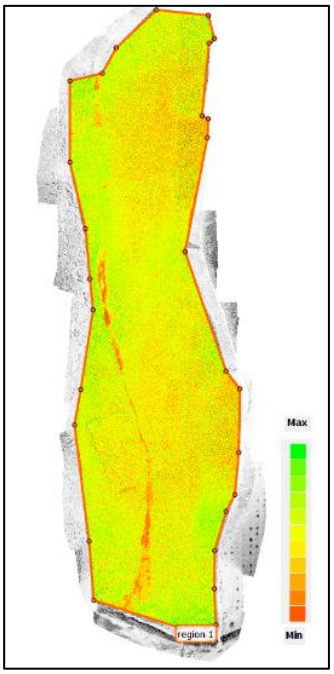


**Figure 4.** The generated VARI image.

The greener values indicate higher VARI values, where the corns' irrigation level is healthy. The damaged area is shown with reddish where the corns are over-irrigated. The area of interest was also calculated manually to be sure. In the end, the damaged area was calculated as 1.44 hectare manually and as 1.5 hectares automatically.

## 5. CONCLUSION

In this study, a 3D model of a corn farm was created with a process of aerial images obtained by UAV. The main purpose of the creation of this model is to detect damaged crop fields due to waterflood. In the end, a visible region vegetation index called VARI was generated and the damaged part of the cornfield was detected.

All processes took approximately 3 hours from flight to VARI generation thanks to the advantages of UAV and powerful computing. If this study was carried out with the traditional methods such as walking through the cornfield, it would have taken an entire day or more.

In future studies, it is planning to mount a multispectral camera that allows us to generate both VARI and normalized difference vegetation index to get more accurate crop monitoring.

## REFERENCES

Gao D., Sun Q., Hu B., Zhang S. (2020). A Framework for Agricultural Pest and Disease Monitoring Based on Internet-of-Things and Unmanned Aerial Vehicles. Sensors 2020, 20, 487; doi:10.3390/s20051487

ibrán-Embid F., Klaus F., Tscharntke T., Grass I. (2020). Unmanned aerial vehicles for biodiversity-friendly agricultural landscapes - A systematic review. Science of the Total Environment 732 ,139204. https://doi.org/10.1016/j.scitotenv.2020.139204

Kaya Y., Şenol H.İ., Memduhoğlu A., Akça Ş., Ulukavak M., Polat N. (2019). Hacim Hesaplarında İHA Kullanımı: Osmanbey Kampüsü Örneği. Türkiye Fotogrametri Dergisi– 2019; 1(1); 07-10

Pix4D Mapper website

Polat N., Uysal M, (2017). DTM GENERATION WITH UAV BASED PHOTOGRAMMETRIC POINT CLOUD. 4th International GeoAdvances Workshop, 14–15 October 2017, Safranbolu, Karabuk, Turkey

Radoglou-Grammatikis P., Sarigiannidis P., Lagkas T., Moscholiao I. (2020). A compiliation of UAV application for precision agriculture. Computer Network, 172 ,107148

Ulukavak M., Memduhoğlu A., Şenol H.İ., Polat N. (2019). The use of UAV and photogrammetry in digital documentation. Mersin Photogrammetry Journal – 2019; 1(1); 17-22

Uysal M, Toprak A.S., Polat N. (2015). DEM generation with UAV Photogrammetry and accuracy analysis in Sahitler hill. Measurement 73 (2015) 539–543

Intercontinental Geoinformation Days

http://igd.mersin.edu.tr/2020/

# Using of hybrid data acquisition techniques for cultural heritage: A case study of Pompeiopolis

**Seda Nur Gamze Hamal*[1], Binnaz Sarı [2], Ali Ulvi [3]**

[1] *Mersin University, Institute of Science, Remote Sensing and Geographical Information Systems, Mersin, Turkey*

**Keywords**
TLS
UAV
Photogrammetry
CrF
Hybrid

**ABSTRACT**

Various studies have been carried out on the documentation of cultural heritage using different methods. The method of collecting correct data is as important as the selection of the method to be used in the studies. Documentation studies focus on saving time and cost rather than the method of collecting data. However, obtaining accurate and complete data will increase the accuracy of the documentation work. In this way, projects prepared as a base for works such as a restoration will be designed correctly. At this point, image-based documentation studies such as photogrammetry provide important contributions to operators. As it is known, the photogrammetry method is basically classified into two as close-range and aerial photogrammetry according to the acquisition position of the image. Although a single data collection tool is preferred in most of the studies with the photogrammetry method, image acquisition from different locations (ground and air) was required for accurate and complete data. Recently, the term UAV photogrammetry has emerged with the use of unmanned aerial vehicles (UAV) in documentation studies. Thus, a complete model is created in documentation studies to be carried out by collecting both local and aerial data. In this study, three different data collection methods were used for documentation. The hybrid data collection approach is presented by selecting laser scanning (TLS) and Close range photogrammetry (CrF) and UAV photogrammetry techniques. The TLS, Crf, and UAV photogrammetry techniques used in the study were processed separately and the accuracy of 0,21-1,1-2,3 cm was calculated respectively. By combining the point clouds created from both data collection methods, 1.2 cm sensitivity was calculated. Finally, three-dimensional (3D) data of Soli-Pompeiopolis were created by combining these point clouds.

## 1. INTRODUCTION

Historical artifacts are damaged over time due to natural or unnatural reasons. In addition, archaeological sites are also affected by this situation, as well as the destruction of structural artifacts. The restoration, restitution, and excavation works of the destructions that have occurred contribute to the correct research and transfer of the artifacts or archaeological sites. The first step in the work to be done in an artifact or archaeological site is documentation studies.

Various studies are carried out on documentation studies using different methods. Ulvi et.al (2020) classified the documentation of cultural heritage into two titles as traditional and modern methods and included TLS, CrF, and UAV photogrammetry, which also includes the subject of this study, in modern methods. The photogrammetric method is one of the most often used techniques in documentation studies. The photogrammetric method is 100-130 times more efficient than traditional methods, 25 times more advantageous in terms of graphics, and 10 times more accurate in terms of accuracy (Sağıroğlu, 2004; Yakar et.al, 2016; Ulvi & Yiğit, 2019; Şenol and Kaya, 2019; Alptekin and Yakar, 2020). In addition, Yakar et.al (2015) stated that the photogrammetry technique saves time and cost compared to traditional documentation techniques. Especially in documentation studies, it is desired to save time and cost in collecting data (Çelik et.al, 2020; Yakar et.al, 2021;). However, while trying to save cost and time, choosing the wrong data collection method can push the operator to collect incomplete data. Collecting correctly and complete data is an important

* **Corresponding Author**

*(sedanurgamzehamal@gmail.com) ORCID ID 0000-0002-1050-3088
(binnaz452@gmail.com) ORCID ID 0000-0002-8240-9680
(aliulvi@mersin.edu.tr) ORCID ID 0000-0003-3005-8011

**Cite this study**

Hamal S N G, Sarı B & Ulvi A (2020). Using of hybrid data acquisition techniques for cultural heritage: A case study of Pompeiopolis. Intercontinental Geoinformation Days (IGD), 259-261, Mersin, Turkey

factor in method selection. For this reason, several data collection methods should be used to collect all data belonging to the study area. For this reason, in the study, data were collected using TLS, CrF, and UAV photogrammetry methods, which are among the modern methods.

The use of a single method in modeling complex structures, especially in the photogrammetry technique, in the documentation of cultural heritage does not allow accurate and complete documentation. Because, with ground-based systems (TLS and CrF), the data of the bottom part of the structure can be taken, but the top of the structure cannot be collected. The data deficiency arising from this situation can be overcome by changing the location where the device is installed or by using another data collection tool to collect the data of the upper fronts. UAVs, which have been used by many disciplines in recent years, have been integrated into this area and this problem has been overcome.

In the documentation made in this study, TLS, Crf, and UAV photogrammetry techniques, which are among the modern data collection and documentation techniques, were used. The hybrid data collection approach is presented by selecting laser scanning (TLS) and Close range photogrammetry (CrF) and UAV photogrammetry techniques. An accurate and dense set of 3D points belonging to all facets of the structure was acquired with hybrid data collection techniques. The TLS, Crf, and UAV photogrammetry techniques used in the study were processed separately and the accuracy of 0,4-1,1-1,3 cm was calculated respectively, and finally, three-dimensional (3D) data of Soli-Pompeiopolis were created by combining these point clouds.

## 2. METHOD

The methods used in the study and the chart of work-flow are given in Figure 1.

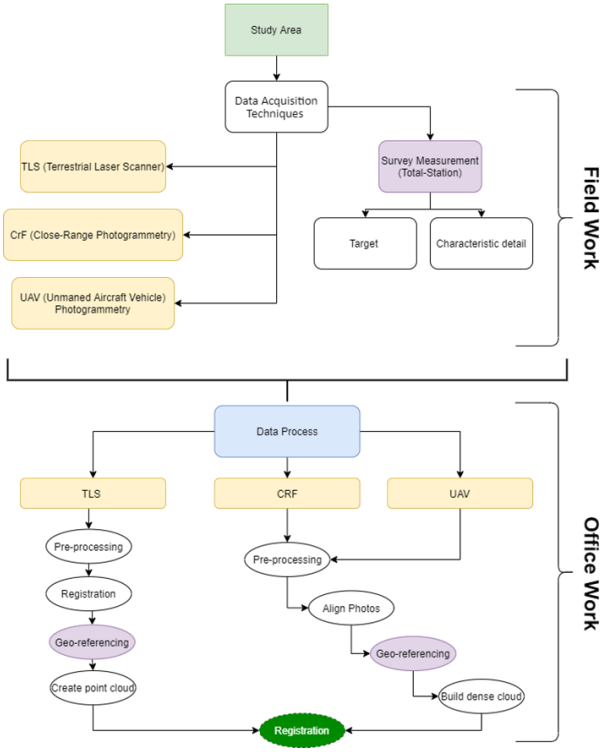


Figure 1. Workflow Chart

### 2.1. Study Area

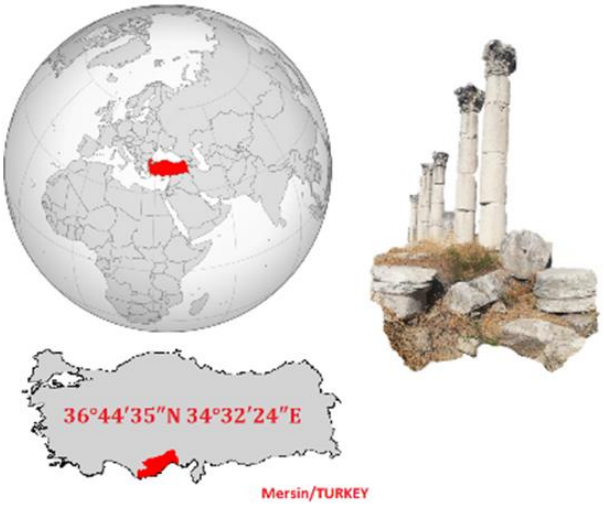


**Figure 2.** Study Area

Soli Pompeopolis located in Mersin / Turkey (Figure 2), it is one of the most important ruins of the province where it is located, and because it is close to the seashore, it is a large site with an ancient harbor (URL-1). According to the archaeological excavations started in 1999: BC. It has been among the important port cities of the Eastern Mediterranean since 2000.There are 33 giant columns on the site and the columns are in a complex structure with Corinthian type capitals (URL-2).

### 2.2. Data acquisition, Field-Work, and Office-Work

In the documentation made in the study, data were collected using TLS, Crf, and UAV photogrammetry techniques. For TLS, Crf and UAV, respectively; Faro Focus$^S$ 350 - Nikon D300 - Anafi Parrot devices are used.

Scans were made at 49 different station points determined in the study area. The number and location of the station points have been determined in a way that the area to be scanned can see one or more areas. Overlapping photographs were taken for CrF and UAV photogrammetry. For CrF 326 image data were collected for 78 UAV. Photo data were collected manually for CrF and autonomously for UAV. In addition, Total-stations and target and characteristic details are measured in order to transfer the result products created from different data collection methods both for registration and to the same scale and coordinate system.

In the process of data processing, firstly, pre-processing was performed for all data collection techniques. Then, the process steps shown in Figure 2 were applied for TLS, CrF and UAV Photogrammetry.

## 3. DİSCUSSİON AND CONCLUSİON

TLS, CrF, and UAV photogrammetry often have been used. By using these techniques together, complete data of the study area can be collected. In this study; Fast, high quality and resolution data can be collected at close-range with the TLS method. However, this method has two disadvantages due to its cost and ground-based data collection. Although the CrF method saves time and is a

low-cost data collection method, it has a disadvantage due to its ground-based data collection and not being able to be used effectively in large areas. UAV photogrammetry, on the other hand, has an advantage in terms of aerial data collection and cost, but it is affected by weather conditions and is not used in every area (prohibited area). For this reason, hybrid methods should be used as these methods are insufficient. TLS, Crf, and UAV photogrammetry techniques used in the study were evaluated separately and the accuracy of 0.4-1.1-1.3 cm, respectively, was calculated. Finally, by combining point clouds, the three-dimensional (3D) point cloud of Soli-Pompeiopolis was created correctly and completely.

**REFERENCES**


Alptekin, A, Yakar, M. (2020). Mersin Akyar Falezi'nin 3B modeli. Türkiye Lidar Dergisi, 2 (1), 5-9. Retrieved from https://dergipark.org.tr/en/pub/melid/issue/55648/697364

Çelik, M , Yakar, İ , Hamal, S. N. G. , Oğuz, G , Kanun, E . (2020). Sfm Tekniği ile Oluşturulan 3B Modellerin Kültürel Mirasın Belgelenmesi Çalışmalarında Kullanılması: Gözne Kalesi Örneği. Türkiye İnsansız Hava Araçları Dergisi, 2 (1) , 22-27 . Retrieved from https://dergipark.org.tr/en/pub/tiha/issue/54200/715377

Şanlıoğlu İ., Zeybek M., ve Karauğuz G. (2013). Photogrammetric Survey and 3D Modeling of Ivriz Rock Relief in Late Hittite Er. Mediterranean Arhaeology and Archaeometry, Vol. 13, No 2

Şenol, H, Kaya, Y. (2019). İnternet Tabanlı Veri Kullanımıyla Yerleşim Alanlarının Modellenmesi: Çiftlikköy Kampüsü Örneği. Türkiye Fotogrametri Dergisi, 1 (1), 11-16. Retrieved from https://dergipark.org.tr/en/pub/tufod/issue/50271/630438

Ulvi, A, Yiğit, A. (2019). Kültürel Mirasın Dijital Dokümantasyonu: Taşkent Sultan Çeşmesinin Fotogrametrik Teknikler Kullanarak 3b Modelinin Yapılması . Türkiye Fotogrametri Dergisi , 1 (1) , 1-6 . Retrieved from https://dergipark.org.tr/en/pub/tufod/issue/50271/629596

Ulvi, A., Yakar, M., Yiğit, A., & Kaya, Y. (2019). The Use of Photogrammetric Techniques in Documenting Cultural Heritage: The Example of Aksaray Selime Sultan Tomb. Universal Journal of Engineering Science, 7(3), 64-73.

ULVİ, A. &YAKAR, M. & YİĞİT, A.& KAYA, Y. (2020) İHA ve Yersel Fotogrametrik Teknikler Kullanarak Aksaray Kızıl Kilise'nin 3 Boyutlu Nokta Bulutu ve Modelinin Üretilmesi Geomatik Dergisi – 2020; 5(1); 19-26

Yakar, İ, Çelik, M, Hamal, S, Bilgi, S. (2021). Kültürel Mirasın Dokümantasyonu Çalışmalarında Farklı Yazılımların Karşılaştırılması: Dikilitaş (Theodosius Obeliski) Örneği. Geomatik, 6 (3), 217-226. DOI: 10.29128/geomatik.761475

Yakar, M., Kabadayı, A., Yiğit, A. Y., Çıkıkcı, K., Kaya, Y., & Catin, S. S. (2016). Emir Saltuk Kümbeti Fotogrametrik Rölöve Çalişmasi Ve 3Boyutlu Modellenmesi. Geomatik, 1(1), 14-18.

Yakar, M., Orhan, O., Ulvi, A., Yiğit, A. Y., & Yüzer, M. M. (2015). Sahip Ata Külliyesi Rölöve Örneği. TMMOB Harita ve Kadastro Mühendisleri Odası, 10.

URL-1http://www.solipompeiopolis.com/icerik/1/turkce.html

URL-2 https://tr.wikipedia.org/wiki/Soli,_Mersin

Intercontinental Geoinformation Days

http://igd.mersin.edu.tr/2020/

# Modeling of Adamkayalar Reliefs with current techniques

**İldeniz Leyla Öztürk*[1], Mehmet Özgür Çelik[1], Erkan Baygül[2]**

[1]*Mersin University, Engineering Faculty, Geomatics Engineering Department, Mersin, Turkey*
[2]*Geomatics Engineering, Ankara, Turkey*

**Keywords**
TLS
UAV
Documentation
3D Model

**ABSTRACT**

Throughout history, many civilizations with different ethnic and national values have lived in Anatolia. In many parts of Turkey's possible to encounter this civilization's cultural heritage. Cultural heritages in the world; Until today, it has been affected by natural events such as earthquakes, floods and fire. These have been completely or partially destroyed as a result of human activities. Cultural heritage is very precious to people and assurance. Quick and practical documentation is of great importance to this. Various methods are used for this documentation process. Among these methods, terrestrial laser scanning (TLS) and Unmanned Aerial Vehicle (UAV) photogrammetry are frequently preferred techniques in recent years. Both methods ensure recording cultural heritages and producing 3D realistic models. It is not always easy to collect data in places with cultural value because of their historical importance and location. At this juncture, the use of terrestrial laser scanners and UAVs makes an important contribution to the documentation of cultural heritage. This study aims to examine the Adamkayalar reliefs, by using TLS and UAV photogrammetry. By processing the data obtained from both methods, a 3D model of the study area was produced and the results were evaluated.

## 1. INTRODUCTION

Anatolian geography, which has hosted many different civilizations and cultures throughout history, contains numerous and unique heritages with historical, socio-economic and cultural values. It is extremely important to protect these cultural heritages, which offer clues about the life, traditions and customs of past societies. Studies conducted in recent years have focused on this issue in Turkey (Ulvi et al. 2020; Ulvi and Yiğit 2019; Çelik et al. 2019; Yakar et al. 2021). Within this scope, legislation has been created by taking into account the opinions and professional experiences of experts.

Efforts to identify, register, manage and preserve these cultural heritage works that mirror the past have gained momentum. Documentation has an important place in protecting cultural heritage and transferring it to future generations.

Documentation studies were done by traditional methods in the past, whereas today, terrestrial photogrammetry (Peña-Villasenín et al. 2017; Alshawabkeh and Haala 2004). Unmanned Aerial Vehicle (UAV) photogrammetry(Ulvi et al. 2019; Peña- et al. 2017; Döner et al. 2014; Westoby 2012; Bewley 2003), terrestrial laser scanning (TLS) method (Çelik et al. 2020; Noor et al. 2018; Baik 2017; Dore et al. 2015; Rüther et al. 2009; Doneus et al. 2008; Lambers et al. 2007; Freitas et al. 2007; Robson et al. 2001 and together(Lambers et al. 2007; Luis Lerma et al. 2010; Al-kheder et al. 2009; Yastikli 2009)modern techniques are preferred (Yakar et al. 2021).

In the study, the TLS method was preferred primarily because it provides a fast and high-resolution method and it allows the effective creation of surface geometries of cultural heritage elements (Deniz et al. 2017; Ulvi and Yakar, 2014; El-Hakim 2001; Barber et al. 2001). Scans were carried out in order to produce a 3D model of the Adamkayalar relief. Secondly, In addition to the YLT method, UAV photogrammetry was used. Photographs of the reliefs in different areas in the region were taken with UAV overlapping. The 3D model of the heritage was produced by processing the data obtained from both methods.

## 2. STUDY AREA

The working area, Adamkayalar BC. third century. and the fourth century AD. It is one of our cultural

* **Corresponding Author**

*(mozdurcelik@mersin.edu.tr) ORCID ID 0000-0003-4569-888X
(idenizleylaa@gmail.com) ORCID ID 0000-0003-0598-9316
(ebaygül@gmx.com) ORCID ID XXXX-XXXX-XXXX-XXXX

**Cite this study**

Ozturk I L, Çelik M Ö & Baygül E (2020). Modeling of Adamkayalar Reliefs with current techniques. Intercontinental Geoinformation Days (IGD), 262-265, Mersin, Turkey

heritages, which is thought to have been built in the period between 6th and 15th. It is located in Şeytan Deresi Valley, which is approximately 5 kilometers away from Kızkalesi District of Mersin Erdemli district (Kulturportalı 2020).The archaeological ruin known as Adamkayalar, which consists of large reliefs, is one of the important cultural heritage of Mersin city (Figure 1).

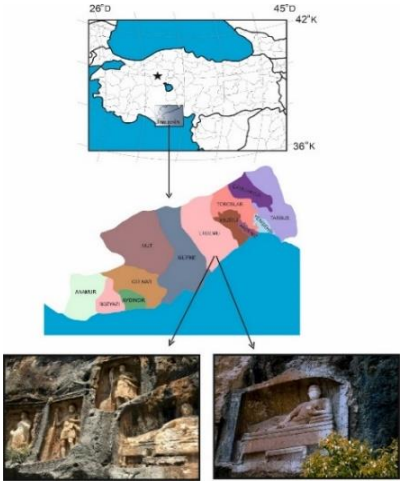

**Figure 1.** Study area

## 3. METHOD

Terrestrial photogrammetry has been used in 3D modeling of historical artifacts for many years, but it is insufficient alone (Uslu and Uysal 2017; Chandler et al. 2007). In this study, 3D modeling of Adamkayalar reliefs, one of the national assets, was carried out by using YLT and UAV photogrammetry in the documentation of historical artifacts that are cultural assets.

### 3.1. Terrestrial Laser Scanning (TLS)

The technique in which any object is scanned with the help of LIDAR (Light Detection and Ranging) technology is called laser scanning method (TLS). This technology is used in many fields such as cultural heritage recording, engineering projects and so on.

In this study, Faro focus$^S$ 350 instrument was used as a terrestrial scanner. This device works according to the phase comparison method.

In the phase comparison method, the length of the object and the device is found by the phase difference between the reflected and emitted waves. The mathematical interpretation of the method is shown in Equation 1.

$$D = \frac{c*\theta}{4\pi f} \quad (1)$$

*D: distance between device and object
**c: speed of light,
***f: frequency
****θ: phase difference

### 3.2. UAV Photogrammetry

Today, in photogrammetry, the Structure from Motion (SfM) technique is mostly used in UAV photogrammeters (Sarıtürk and Şeker 2017; Furukawa and Hernández 2013; westoby et al.2012). SfM is a method that aims to create a three-dimensional (3D) model from photographs taken with two-dimensional (2D) overlays (Snavely 2008; Dellaert et al. 2000). The main purpose of the method is 3D model production (Çelik et al.2020).

The SfM technique was preferred in the study due to its various features and advantages in creating 3D models. With the development of technology in the documentation and permanent documentation of cultural heritage, the 3D model has become a powerful option. In this context, aerial photos were taken with the SenseFly eBee UAV in order to obtain general information about the historical place. Images were taken by the Parrot Anafi UAV to better reveal the details of this work.

From these images obtained by UAV with different hardware and features, the 3D model of the work was created in the Agisoft Photoscan program, a commercial software using the SfM algorithm.

## 4. RESULTS

First of all, the LLS method, which is a fast and high-resolution technique and has become widely used in the documentation of cultural heritage assets, was preferred. 8 scans were carried out around the Adamkayalar reliefs with a local laser scanner (TLS) at suitable seating places. A land survey was made before the study in determining the residence locations. Care has been taken to ensure that the reliefs appear at the optimum level and have common details with the next scan. The data were transferred in Faro Scene software, where laser scanning data can be processed and used in 3D model production. The point cloud of the study area was created and a 3D model was produced from this point data set (Figure 2).

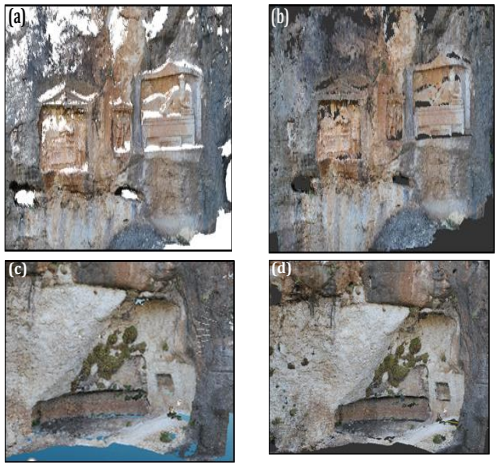


**Figure 2.** (a), (c) Point cloud obtained by TLS method (b), (d) 3D model.

As the second method; UAV photogrammetry was used together with the LLT method in order to make the 3D model more detailed. Two different UAVs were used in this method. First of all, the aerial (70 m height) images were taken with the eBee device in order to examine the study area as a whole and to obtain general information about the area. Then, photos were taken manually with the Parrot device in order to create clearly the facade and details of the reliefs in the 3D model. By processing the data obtained by both tools, point clouds and photo-

realistic 3D models of the heritage were produced (Figure 3, 4).

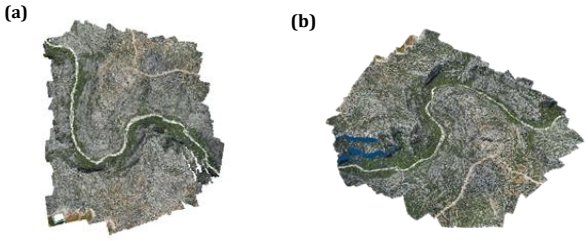


**Figure 3.** (a), (b) Point cloud obtained with SenseFly eBeee UAV

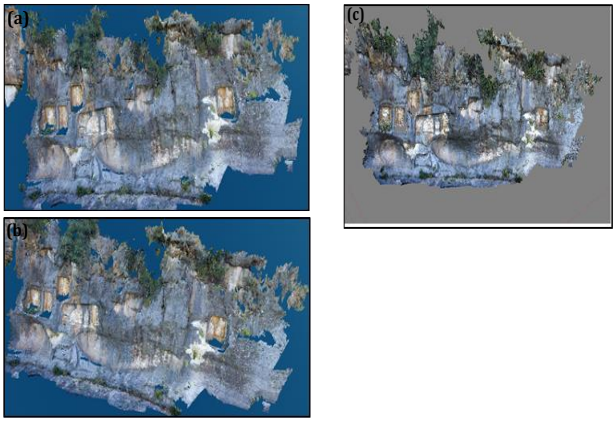


**Figure 4.** (a), (b) Point cloud obtained by Anafi Parrot UAV (c) 3D model

## 5. DISCUSSION AND CONCLUSION

The study area is the Adamkayalar relief, which has historical, sociological and cultural significance. In this heritage work, YLT and UAV photogrammetry methods, which have become widespread in documentation processes in parallel with the developing technological advances, were used. Although these techniques have advantages and disadvantages, each has its strengths.

With the work carried out, the positive and negative aspects of the techniques were tried to be determined. YLT method provides fast, high quality and resolution data in close range. In addition, accuracy and precision are extremely high. Although the positive features of this method are dominant, it also has some disadvantages. This method alone is insufficient for factors such as the relatively large size of the work or structure to be documented and the difficulty of access to the region.

The UAV photogrammetry method provides the opportunity to measure at close or far distances, without reaching the object. 3D model can be obtained directly or by means of point clouds by taking photographs of the object with overlapping. Within the framework of these features, this method can be used alone or in combination with different methods in the documentation of cultural heritage. This technique also has negative aspects. While the aerial view of the work to be modeled can be obtained easily, in some cases, facade photographs cannot be obtained properly. This problem causes the side surfaces and details to not be fully formed in the model of the work. In addition, it is not always possible to benefit from UAV photogrammetry due to factors such as the geography and geopolitical location of the study area

In the study, different methods were applied, measurements were made, and photo-realistic 3D models of the field were produced in a hybrid way. In this way, a permanent document belonging to the working area has been created. The historical work of this document; It is predicted that it will contribute to the transmission, protection, documentation and management of future generations. In addition, it is highly possible to use the 3D model as a base for possible interventions to the work. It is assumed that this study is important for adding this historical region bearing the traces of past cultures and civilizations to the national heritage records and can set an example for other similar studies.

## REFERENCES

Al-kheder, S., Al-shawabkeh, Y., Haala, N., (2009). Developing a documentation system for desert palaces in Jordan using 3D laser scanning and digital photogrammetry. Journal of Archaeological Science 36 (2), 537–546.

Al-Manasir, K., Fraser, C.S., (2006). Registration of terrestrial laser scanner data using imagery. The Photogrammetric Record 21 (115), 255–268.

Alshawabkeh, Y., Haala, N., (2004). Laser scanning and photogrammetry: a hybrid approach for heritage documentation. In: Third International Conference on Science & Technology in Archaeology & Conservation, The Hashimite University, Jordan.

Baik, A. (2017). From point cloud to Jeddah heritage BIM Nasif historical house- case study. Digital Applications in Archaeology and Cultural Heritage,.4, 1-18.

Barber D, Mills J & Bryan P G (2001). Laser Scanning and Photogrametry: 21st century metrology. 18-21 Semptember, 360-366. Potsdam, Germany.

Bewley, R.H., (2003). Aerial survey for archaeology. The Photogrammetric Record 18 (104), 273–292.

Çelik, M.Ö., Yakar, İ., Hamal, S.N.G., Oğuz, G.M. & Kanun, E. (2020). Sfm Tekniği ile Oluşturulan 3B Modellerin Kültürel Mirasın Belgelenmesi Çalışmalarında Kullanılması: Gözne Kalesi Örneği. Türkiye İnsansız Hava Araçları Dergisi, 2(1), 22-27.

Çelik, M.Ö., Yakar, İ., Hamal, S.N.G., (2020). Yersel lazer tarama (YLT) yönteminin kültürel mirasın dokümantasyonunda kullanımı: Alman Çeşmesi örneği. 2(1), 15-22.

Chandler, J.H., Bryan, P., Fryer, J.G., (2007). The development and application of a simple methodology for recording rock art using consumer-grade digital cameras. The Photogrammetric Record 22 (117), 10–21.

Dellaert, F. Seitz, S. M., Thorpe, C. E., & Thrun, S. (2000). Structure from motion without correspondence. Proceedings. IEEE Conference on Computer Vision and Pattern Recognition, CVPR 2000 (Cat. No.PR00662), Hilton Head Island, SC, 557-564 Vol. 2, doi:10.1109/CVPR.2000.854916

Deniz S, Öktem S, Kırbaş İ & Tarkan D (2017). Alansal/Yersel Lazer Tarayıcıların Arkeolojik Mekânların Fiziki Özelliklerinin Tespitinde Kullanılması: Kibrya Antik Kenti Odeon Yapısı Sahne Duvarı Örneği. Mehmet Akif Ersoy Üniversitesi Fen Bilimleri Enstitüsü Dergisi, 8(1), 211-217.

Doneus, M., Briese, C., Fera, M., Janner, M., (2008). Archaeological prospection of forested areas using full-waveform airborne laser scanning. Journal of Archaeological Science 35, 882–893.

Dore, C., Murphy, M., McCarthy, S., Brechin, F., Casidy, C., & Dirix, E. (2015). Structural simulations and conservation analysis - historic building Information model (HBIM). In 3D virtual reconstruction and visualization of complex architectures 2015 proceedings of the international conference in Avila, Spain.

Döner Fatih, Özdemir Samed, Ceylan Mustafa (2014) İnsansız Hava Aracı Sistemlerinin Veri Toplama Ve Haritalama Çalışmalarında Kullanımı, 5. Uzaktan Algılama-Cbs Sempozyumu (Uzal-Cbs 2014), İstanbul.

El-Hakim S F (2001). A flexible approach to 3D reconstruction from single images ACM Proceedings of SIGGRAPH '01, Technical Sketches, Los Angeles, California, 12th to 17th August 2001. 280 pages: 186.

Freitas, J.C., Abreu, M.A., Santos, P., Baptista, A.M., Zilha˜o, J., (2007). For a digital repository of rock art in Portugal. In: Figueiredo, A., Velho, G. (Eds.), The World is in Your Eyes. CAA Tomar, Portugal, pp. 193–196.

Furukawa, Y., ve Hernández, C. (2013). Multi-View Stereo: A Tutorial. Foundations and Trends® in Computer Graphics and Vision, Vol. 9, No. 1-2, 1-148

Kultur portalı (2020). https://www.kulturportali.gov.tr /turkiye/mersin/gezilecekyer/adamkayalar

L'udovít Kovani˘c. Surveying and High-Resolution Topography of the Ochtiná Aragonite Cave Based on TLS and Digital Photogrammetry

Lambers, K., Eisenbeiss, H., Sauerbier, M., Kupferschmidt, D., Gaisecker, T., Sotoodeh, S., Hanusch, T., (2007). Combining photogrammetry and laser scanning for the recording and modelling of the Late Intermediate Period site of Pinchango Alto, Palpa, Peru. Journal of Archaeological Science 34, 1702–1712.

Lerma L., Navarro S., Cabrelles M., Villaverde V. (2010) Terrestrial laser scanning and close range photogrammetry for 3D archaeological documentation: the Upper Palaeolithic Cave of Parpallo´ as a case study Jose, 37(3), 499-507.

Noor N. M., Kamaruddin Z. Abdullah A., Abdullah A. A., Eusoff S. S., & Mustafa H. M. (2018). Using terrestrial laser scanner for Malay heritage documentation: preliminary approach to Istana Balai Besar, Kelantan. International Journal of Development and Sustainability, 7(6), 1886-1897.

Peña-Villasenín S.; Gil-Docampo, M.; Ortiz-Sanz, J. (2017). 3-D Modeling of Historic Façades Using SFM Photogrammetry Metric Documentation of Dierent Building Types of a Historic Center. Int. J. Archit. Herit. 11, 871–890.

Robson Brown, K.A., Chalmers, A., Saigol, T., Green, C., d'Errico, F., (2001). An automatedlaser scan survey of the Upper Palaeolithic rock shelter of Cap Blanc. Journal of Archaeological Science 28, 283–289.

Rüther H., Chazan M., Schroeder R., Neeser R. Held C., Walker S. J., Matmon A., Horwitze L. K. (2009). Laser scanning for conservation and research of African cultural heritage sites: The case study of Wonderwerk Cave, South Africa, 36(9), 1847-1856.

Sabuncu A, Özener H., (2020). Mimari Dökümantasyonda Yersel Lazer Tarama Teknolojisi Kullanımı: Tarihi Sismoloji Binası Örneği,1(1): 45-52

Sarıtürk, B., ve Şeker D.Z. (2017). SFM Tekniği ile 3B Obje Modellenmesinde Kullanılan Ticari ve Açık-Kaynak Kodlu Yazılımların Karşılaştırılması. Afyon Kocatepe Üniversitesi Fen ve Mühendislik Bilimleri Dergisi, Özel Sayı, 126-131.

Snavely, N., 2008. Scene reconstruction and visualization from Internet photo collections, unpublished PhD thesis, University of Washington, USA.

ULVİ, A. & YİĞİT, A. (2019). Kültürel Mirasın Dijital Dokümantasyonu: Taşkent Sultan Çeşmesinin Fotogrametrik Teknikler Kullanarak 3B Modelinin Yapılması. Türkiye Fotogrametri Dergisi, 1 (1), 1-6.

Ulvi, A., Yakar, M. , Yiğit, A ., Kaya, Y. (2020) İHA ve Yersel Fotogrametrik Teknikler Kullanarak Aksaray Kızıl Kilise'nin 3 Boyutlu Nokta Bulutu ve Modelinin Üretilmesi Geomatik Dergisi – 2020; 5(1); 19-26

Ulvi, A., ve Yakar, M. (2014). Yersel Lazer Tarama Tekniği Kullanarak Kızkalesi'nin Nokta Bulutunun Elde Edilmesi ve Lazer Tarama Noktalarının Hassasiyet Araştırması. Electronic Journal of Map Technologies, 6 (1), 25-36.

Ulvi, A., Yakar, M., Yiğit, A., & Kaya, Y. (2019). The Use of Photogrammetric Techniques in Documenting Cultural Heritage: The Example of Aksaray Selime Sultan Tomb. Universal Journal Of Engineering Science, 7(3), 64-73, doi: 0.13189/ujes.2019.070303.

Uslu A., Uysal M. 2017. Arkeolojik Eserlerin Fotogrametri Yöntemi İle 3 Boyutlu Modellenmesi: Demeter Heykeli Örneği, ; 2(2);60-65

Westoby, M.J.; Brasington, J.; Glasser, N.F.; Hambrey, M.J.; Reynolds, J.M. (2012). 'Structure-from-Motion'photogrammetry: A low-cost, e ective tool for geoscience applications. Geomorphology, 179, 300–314.

Yakar i., hamal S. N. G., Çelik M. Ö., Bilgi S. (2021)Kültürel mirasın dokümantasyonu çalışmalarında farklı yazılımların karşılaştırılması: Dikilitaş (Theodosius Obeliski) Örneği

Yakar M., Ulvi A., Toprak A. S., Mutluoğlu Ö. Sandıklı Kültür ve Sanat Evinin Yersel Fotogrametrik ve İHA Teknikleri Kullanılarak Üç Boyutlu Modellenmesi.

Yastikli, N., (2007). Documentation of cultural heritage using digital photogrammetry and laser scanning. Journal of Cultural Heritage 8 (4), 423–427.

Intercontinental Geoinformation Days

http://igd.mersin.edu.tr/2020/

# Documentation of complex structure using unmanned aerial vehicle (UAV) photogrammetry method and terrestrial laser scanner (TLS)

**Binnaz Sarı*[1], Seda Nur Gamze Hamal[1], Ali Ulvi[1]**

[1]*Mersin University, Institute of Science, Remote Sensing and Geographical Information Systems, Mersin, Turkey*

**Keywords**
3D model
UAV
TLS
Photogrammetry
Structure

**ABSTRACT**

Modeling objects with different sizes and geometries and analyzing metric information is more difficult than regular geometric structures. The analysis and measurements of conical, spherical, and cylindrical structures such as minarets, domes, columns, statues, and monumental tombs cannot be accurate and precise with classical methods. Three-dimensional (3D) scanning technologies such as Terrestrial laser scanner (TLS) are an important tool for modeling complex structures. Undoubtedly, 3D scanners are well suited for measuring objects with irregular and complex surfaces and are probably one of the best methods for applications with similar structures. However, the biggest disadvantage of ground base scans such as TLS is that the data of the upper facades of the structure cannot be collected due to the scanning location. This problem can be overcome by collecting data on the upper fronts of the structure by platforms such as unmanned aerial vehicles (UAV). Therefore, in our study, the data were collected by TLS and UAV photogrammetry methods, and then the 3D model and analysis of the complex structures were made by combining the obtained data. As a result of the study, 0.21-2.3 cm accuracy was calculated for point clouds produced by TLS and UAV photogrammetry, respectively. By combining the point clouds created from both data collection methods, 1.2 cm sensitivity was calculated.

## 1. INTRODUCTION

3D model study of structure, analysis of attribute information, and integration with information systems; It is one of the common study areas of different disciplines. Especially structures subject to object deformation come at the beginning of analysis studies. Structures are subject to deformation due to many natural or unnatural reasons (Yakar et.al, 2015; Ulvi et.al, 2020). Analysis studies of the structures that are subject to deformation cannot be done completely with classical methods. Various analyses of these structures can be made with modern methods. At this point, 3D models can be produced with various data collection methods; analysis can be made quickly and easily.

Using 3D models to extract metric information of structures with different dimensions and geometries gives precise and accurate results (Yılmaz and Yakar, 2006; Ulvi and Yiğit, 2019). Especially conical, spherical, cylindrical; Modern methods should be used to analyze and measure similar structures such as minarets, domes, columns and statues. With the developing technology, UAV photogrammetry and laser scanning technology are used more effectively in 3D model studies. These systems, which are complementary to each other, are frequently used because they provide data and methods in a fast, efficient, economical and reliable manner. (Yakar and Yılmaz, 2008; Koruaz et.al, 2011; Şanlıoğlu et.al, 2013). These systems are preferred by various disciplines because of the ability to create accurately 3D models, to see the details on the object more clearly, to examine the changes, to present and store documents digitally (Karabörk et.al, 2009, Alptekin et.al, 2019).

Studies in the literature show that aboveground objects such as structures that make up the 3D city model can be created quickly from terrestrial laser scanning data (Yakar et.al, 2006; Çelik et.al, 2020).

In addition, with the integration of UAVs, the data belonging to the missing fronts has been collected.

In the study, considering the advantages of UAV photogrammetry and TLS system compared to each other, 3D models of cylindrical columns were created, accurate and accuracy analysis were made and various analyzes were obtained. Using UAV and TLS technologies together contributes to obtaining products with high accurate. The fact that the result obtained with these systems enables the product to be used in different application areas such as being digital, visualizing and managing 3D data and presenting them in a GIS

* **Corresponding Author**

* (binnaz452@gmail.com) ORCID ID 0000-0002-8240-9680
(sedanurgamzehamal@gmail.com) ORCID ID 0000-0002-1050-3088
(aliulvi@mersin.edu.tr) ORCID ID 0000-0003-3005-8011

**Cite this study**

Surname N, Surname N & Surname N (2020). Title of the study. Intercontinental Geoinformation Days (IGD), 266-268, Mersin, Turkey

environment is a base map for many studies. As a result of the study, 0.21-2.3 cm accurately was obtained for point clouds produced by TLS and UAV photogrammetry, respectively. By combining the point clouds obtained from data collection methods, 1.7 cm accurately was obtained.

## 2. METHOD

In the study, 3D analysis of complex structures was performed using TLS and UAV photogrammetry method. The working area is given in Figure 1, the plan for the 3D model is given in Figure 2 and the work flow chart is given in Figure 3.

### 2.1. Study Area

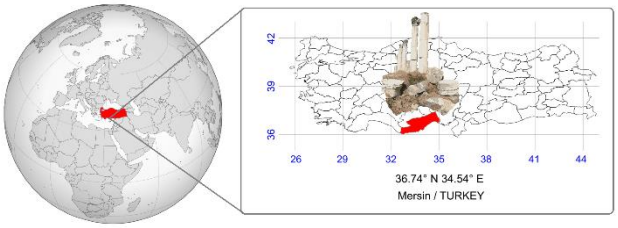


**Figure 1.** Study area

The study area is the Colonnaded street of the ancient city of Soli - Pompeiopolis in Mersin province.
In the study area, there are a total of 33 columns, 4 of which are in the west and 29 in the east.

### 2.2. 3D modeling and analysis

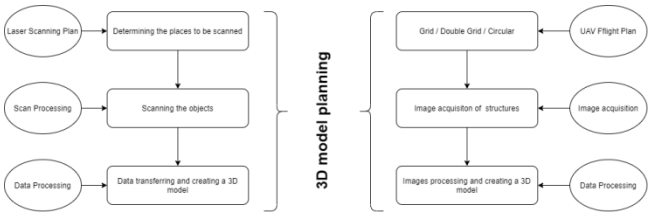


**Figure 2.** 3D model planning

TLS method; It is the system that is used to produce a point cloud with X, Y, Z coordinates belonging to the desired object with the object's LIDAR (Light Detection and Ranging) technology. TLS is used in studies such as documentation, restoration, restitution, reverse engineering, 3D modeling and analysis due to its features such as high accuracy, fast and short measurement, printing in digital form and forming a base for different studies.

UAV photogrammetry method, on the other hand, is basically a method of collecting data by taking overlap images using the photogrammetry method and obtaining a 3D model.

The data collection methods and work flow chart used in the study are shown in Figure 3.

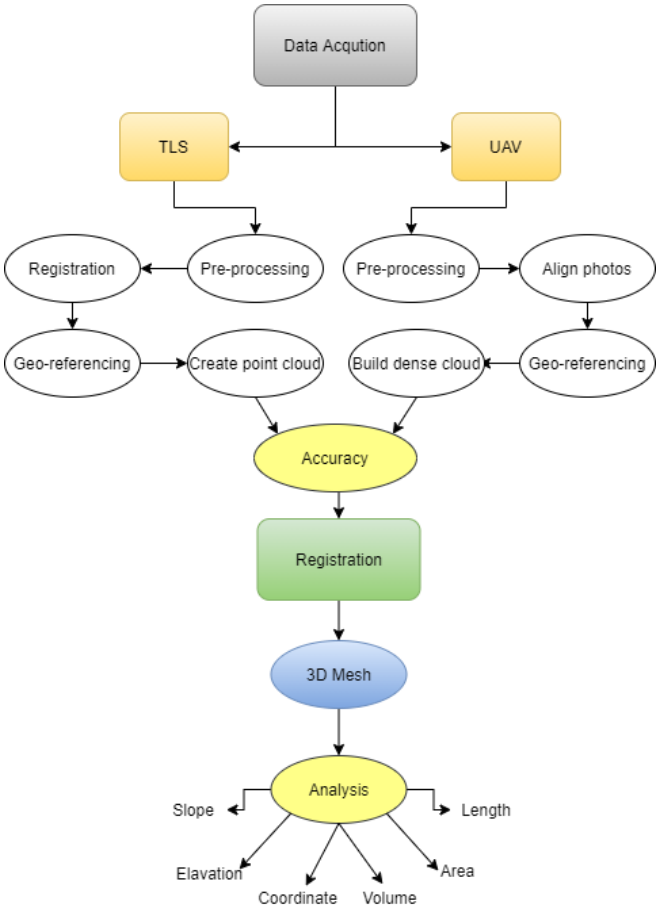


**Figure 3.** Work-flow chart

## 3. CONCLUSION

For the analysis of structures with different geometric shapes, their physical properties should be considered an appropriate evaluation tools should be selected. Rather than using a single method for spatial recording of structures, the use of hybrid methods provides significant contributions to an accurate analysis. For this purpose, firstly geodetic measurement techniques, laser scanning data collection methods such as UAV photogrammetry and TLS were used for the analysis of complex structures. However, field studies conducted with geodetic or traditional measurements cause excessive time, manpower and increase the cost. TLS and UAV photogrammetry come to the fore for faster and more accurate data collection, especially with time and cost savings.

The distance between TLS and the scanned surface directly affects the resolution of the point cloud data, and the rays coming from the laser scanning device to the surface to be scanned also affect the quality of the point cloud data. The TLS system also allows an object, structure or object to be scanned from horizontal and vertical directions to obtain a point cloud image. Therefore, it is the most preferred system in 3D modeling of structures. However, with such ground-centered systems, the data of the upper facades of the structures are missing. This problem was made by taking aerial pictures using carrier platforms such as UAVs, using the UAV photogrammetry method and producing a 3D point cloud of the structure. In this way, the data of the lower facades of the structure, UAV and upper facades were

collected with TLS. Complete 3D data of the structure was obtained with hybrid data collection methods and various analyzes were made.

## REFERENCES

Alptekin, A., Çelik, M. Ö., & Yakar, M. (2019). Anıtmezarın yersel lazer tarayıcı kullanarak 3B modellenmesi. Türkiye Lidar Dergisi, 1(1), 1-4.

Çelik, M, Yakar, İ, Hamal, S, Oğuz, G, Kanun, E. (2020). Sfm tekniği ile oluşturulan 3b modellerin kültürel mirasın belgelenmesi çalışmalarında kullanılması: Gözne Kalesi Örneği . Türkiye İnsansız Hava Araçları Dergisi, 2 (1), 22-27. Retrieved from https://dergipark.org.tr/en/pub/tiha/issue/54200/715377

Karabörk, H., Göktepe, A., Yılmaz, H.M., Mutluoğlu, Ö., Yıldız, F. and Yakar, M.,(2009). Tarihi ve kültürel varlıkların lazer tarama ve lazer nokta ölçme teknolojileri ile 3B modellenmesinde duyarlılık araştırması ve uygulama modelinin belirlenmesi. 12. Türkiye Harita Bilimsel ve Teknik Kurultayı, pp.11-15.

Korumaz, A.G., Dülgerler, O.N., & Yakar, M. (2011). Kültürel mirasın belgelenmesinde dijital yaklaşımlar. S.Ü. Mühendislik Mimarlık Fakültesi Dergisi, 26(3), 67-83.

Şanlıoğlu İ., Zeybek M., & Karauğuz G. (2013). photogrammetric survey and 3d modeling of Ivriz Rock Relief in late hittite era : Mediterranean Arhaeology and Archaeometry, 13(2).

ULVİ, A. & YİĞİT, A. (2019). Kültürel mirasın dijital dokümantasyonu: Taşkent Sultan Çeşmesinin Fotogrametrik Teknikler Kullanarak 3B Modelinin Yapılması. Türkiye Fotogrametri Dergisi, 1 (1), 1-6.

ULVİ, A.&YAKAR, M. & YİĞİT, A .& KAYA, Y. (2020) İHA ve yersel fotogrametrik teknikler kullanarak Aksaray Kızıl Kilise'nin 3 boyutlu nokta bulutu ve modelinin üretilmesi Geomatik Dergisi – 2020; 5(1); 19-26.

Yakar, M., & Yılmaz, H. M. (2008). Kültürel miraslardan tarihi Horozluhan'ın fotogrametrik rölöve çalışması ve 3 boyutlu modellenmesi.

Yakar, M., Kabadayı, A., Yiğit, A. Y., Çıkıkcı, K., Kaya, Y., & Catin, S. S. (2016). Emir Saltuk Kümbeti fotogrametrik rölöve çalışması ve 3boyutlu modellenmesi. Geomatik, 1(1), 14-18.

Yakar, M., Orhan, O., Ulvi, A., Yiğit, A. Y., & Yüzer, M. M. (2015). Sahip Ata Külliyesi Rölöve Örneği. TMMOB Harita ve Kadastro Mühendisleri Odası, 10.

YILMAZ, H. M., & YAKAR, M. (2006). Yersel lazer tarama Teknolojisi. Yapı Teknolojileri Elektronik Dergisi, 2(2), 43-48.